

**An Investigation into the Oxyturbine Power Cycles with
100% CO₂ Capture and Zero NO_x emission**

Hirbod Varasteh

A thesis submitted in partial fulfilment of the requirement of
Staffordshire University for the degree of Doctor of Philosophy

December 2020

Abstract

The world is facing serious issues related to global warming due to the massive use of fossil fuel sources. Global warming coupled with growing energy demand causes environmental concern. Carbon capture and storage (CCS) are promising technologies for achieving shortly to medium-term solution Green House Gas GHG emission reduction goals. The development of CCS for fossil fuel power generation can reduce carbon dioxide emission and produce electricity with lower capital cost (Capex), operating cost (Opex) in comparison with other renewable energies in the short and medium-term while reducing exergy destruction and increasing efficiency.

Oxy-fuel combustion technology is an effective way to increase the CO₂ capture ability of oxy-fuel combustion power plants. Also, its advantages in contrast to other CCS technologies include low fuel consumption, near-zero CO₂ emission, high combustion efficiency, flue gas volume reduction, and fewer nitrogen oxides (NO_x) formation. In this technology, the air is replaced with nearly pure oxygen as an oxidiser. The combustion exhaust is mainly the composition of CO₂ and H₂O. Then CO₂ can be separated from the water through lower-cost technologies such as the water condensation technology, which has lower power consumption. In this thesis, the major proposed oxy-combustion gas turbine power cycles (Oxyturbine cycles) have been investigated and compared by means of process simulation and techno-economic evaluation.

The investigated cycles in chapter 2 are SCOC-CC, COOPERATE Cycle, MATIANT, E-MATIANT, CC_MATIANT, Graz cycle, S-Graz cycle, Modified GRAZ, AZEP 85%, AZEP 100%, ZEITMOP Cycle, COOLCEP-S Cycle, Novel O₂/CO₂, NetPower, CES. These cycles were modelled with Aspen Plus based on the available cycle data from literature; then, parametric studies are performed after modelling validations. In this PhD thesis, a review of the Air Separation Unit (ASU) and the CO₂ Compression and Purification Unit (CPU) are presented. The Technology Readiness Level (TRL), Sensitivities and pilot industrial demonstration for oxy-combustion power cycle have also been studied.

In chapter 3, the methodology of the thesis and oxy-combustion cycles of process modelling is indicated. Also, the theories and thermodynamic formulas including mass, energy and exergy balances of Oxy combustion cycle were determined in the MATLAB code to calculate thermodynamic parameters in order to evaluate these cycles; the MATLAB codes are developed to link with Aspen Plus software to simulate the Oxy-fuel power cycle processes with the input data. In this chapter, techno-economic formulas were determined to calculate LCOE for oxy-combustion cycles.

In chapter 4, the exergy destruction in each component of the oxy-combustion power cycle is studied. Results indicate that the exergy destruction in combustion is more than other components and the heat exchanger is the second component with the highest exergy destruction; hence improving these two components are very important to reduce total exergy destruction.

In chapter 5, the Sensitivity and exergy analysis of the Semi-Closed Oxy-fuel Combustion Combined Cycle (SCOC-CC) and E-MATIANT are investigated in detail. TIT and efficiency of SCOC-CC cycle with respect to COP and fuel flowrate was drawn, and also a 3D plot of exergy destruction and TIT were indicated in this section. The Efficiency vs working flowrate for E-MATIANT was determined, and it indicates the maximum turbine efficiency is 46.9% at 290 kg/s based on the available technology for the E-MATIANT cycle.

In chapter 6, the sensitivity and exergy analysis of COOPERATE cycle is determined, and the sensitivity of the Efficiency vs working flowrate for COOPERATE cycle was plotted. Also, a pie chart for exergy destruction of equipment is determined. The exergy analysis indicates that the total exergy destruction in the COOPERATE cycle is minimum at 318 kg/s working flowrates; it is verified that the exergy efficiency and energy efficiency are maximum at this working flowrate.

In chapter 7, the simulation results of the NetPower cycle showed that the efficiency increases up to 1% with 2.5 °C reduction of ΔT_{min} in constant Combustion Outlet Temperature (COT) and constant recycled flow rates; however, the efficiency increases faster in constant flow rate compared to the constant COT. Also, NetPower cycle simulation indicates that COT and heat exchanger have a critical role in NetPower cycle performance and overall efficiency.

In chapter 8, the results of the TIT sensitivity for the S-CES cycle and the NetPower cycle indicates that the slope of cycle efficiency was higher in the NetPower cycle, which could be explained by the higher impact that the TIT produced in the turbine and the main heat exchanger for the NetPower cycle.

At the end, exergoeconomic, Techno-economic, Technology Readiness Level (TRL) and parametric comparison in Oxyturbine Power cycles are indicated in chapter 9 and the Radar chart for comparison of the oxy-combustion cycles were determined and the results were discussed more depth in this capture. Furthermore, Techno-economic analysis was conducted according to the oxy-combustion modelling and included performance, cost rate, Levelised Cost of Electricity (LCOE). The oxy-combustion cycles parameters were compared by means of TIT, TOT, CO₂/kWh, COP, Exergy, Thermal efficiency, Technology Readiness Level (TRL) bar diagrams and Multi-Criteria Decision Analysis (MCDA) with radar diagrams are provided to choose the best possible Oxyturbine cycles.

This PhD research provides a benchmark for comparing the oxy-combustion gas turbine power cycles and drew a road map for the development of these cycles for low carbon, high efficiency and low-cost energy in soon future.

Acknowledgements

I would like to express my deepest appreciation to my principal supervisor Professor Hamidreza Gohari Darabkhani, who has provided me with the opportunity to work under his supervision. Without his guidance and persistent help, this dissertation would not have been possible. His scientific feedback, Knowledge and expert advice made this research attainable. I also owe my gratitude to my second supervisor Professor Torfeh Sadat-Shafai for his support during this research.

I would like to thank my wife, Mrs Hamraz, and my daughter Tida for supporting me during my PhD. Also, thanks to my mother and my father, Mrs Shahnaz and Mr Mohammad Saeid, who have been there to help me at any stage of my life.

I would also like to acknowledge Staffordshire University for the provision of PhD studentship and sponsoring this research. I especially thank the Engineering department at Staffordshire University to support me.

Contents

Abstract	i
Acknowledgements	iv
Contents	v
List of Figures	xi
List of Tables	xvi
Abbreviations	xviii
Subscripts	xix
Symbols	xx
Chapter 1: Introduction	1
1.1 Aim of this research project	2
1.2 Objectives	3
1.3 Introduction to the gas turbine technology	5
1.4 Categories of gas turbines	6
1.5 Type of gas turbine	8
1.5.1 Single-shaft gas turbine	9
1.5.2 Dual shaft gas turbine with a power turbine	10
1.5.3 Triple shaft gas turbine with a power turbine	11
1.5.4 Open and closed thermodynamic cycles of gas turbine	13
1.6 Environmental impact	16
1.7 Summary	19
Chapter 2: Literature review of Oxyturbine power cycles and gas-CCS Technologies	20
2.1 Introduction	20
2.2 Main Technologies in CO ₂ Capture	21
2.2.1 Post-combustion capture	21
2.2.1.1 Physical Absorption	22
2.2.1.2 Selective exhaust gas recirculation (S-EGR) method	23
2.2.1.3 Chemical Absorption - Amine Absorption/Stripping Technology	25
2.2.1.4 Physical Adsorbent	26
2.2.1.5 Chemical Adsorbent (Amine-Based)	26
2.2.2 Pre-combustion capture	27
2.2.2.1 Chemical process	27
2.2.2.2 Membrane	28
2.2.2.3 Hydrogen production technologies	29

2.2.2.3.1	Steam Methane Reforming (SMR)	29
2.2.2.3.2	Autothermal Reforming (ATR).....	30
2.2.2.3.3	Vacuum pressure swing adsorption (VPSA) cycle	31
2.2.2.3.4	Renewable sources	32
2.2.3	Oxy-fuel combustion capture	33
2.2.3.1	Oxy-combustion classification.....	34
2.2.4	CO ₂ Capture technology conclusion	37
2.3	Oxygen production and Air Separation Units (ASU)	39
2.3.1	Cryogenic Air Separation Unit (ASU)	39
2.3.1.1	Pilot-scale	41
2.3.1.2	ASU development.....	41
2.3.2	Non-cryogenic Air Separation Unit (ASU).....	42
2.3.2.1	Adsorption	42
2.3.2.2	Pressure Swing Adsorption (PSA).....	42
2.3.2.2.1	Vacuum Pressure Swing Adsorption (VPSA).....	43
2.3.2.3	Chemical processes.....	44
2.3.2.4	Polymeric membranes.....	45
2.3.2.5	Ion Transport Membrane (ITM)	45
2.3.2.6	Chemical Looping Combustion (CLC).....	46
2.4	CO ₂ Compression and Purification Unit (CPU).....	46
2.5	Semi-Closed Oxy-Combustion Combined Cycle (SCOC-CC).....	49
2.5.1	SCOC-CC technologies.....	51
2.6	The COOPERATE cycle	51
2.6.1	The COOPERATE cycle technologies.....	53
2.7	The MATIANT cycle	54
2.8	The E-MATIANT cycle.....	55
2.9	CC-MATIANT cycle	57
2.9.1	CC-METIANT technologies	59
2.10	The Graz cycle	61
2.10.1	Graz cycle technologies	62
2.11	The S-Graz cycle.....	63
2.11.1	The S-Graz cycle technologies	64
2.12	The AZEP 100% cycle.....	65
2.12.1	The AZEP 100% cycle technologies	66
2.13	The AZEP 85% cycle.....	67
2.14	The ZEITMOP cycle.....	67
2.14.1	ZEITMOP technologies.....	69
2.15	The COOLCEP-S cycle	70
2.15.1	COOLCEP technologies.....	72
2.16	The COOLCEP-C cycle	72

2.16.1	COOLCEP-C technologies	73
2.17	Novel O ₂ /CO ₂ (Cao and Zheng, 2006)	74
2.17.1	The Novel O ₂ /CO ₂ technologies	75
2.18	NetPower cycle	76
2.18.1	NetPower demonstration	78
2.18.1.1	Turbine.....	79
2.18.1.2	Combustion.....	79
2.18.1.3	Heat exchanger	80
2.19	CES Cycle	81
2.19.1	The CES technologies	82
2.19.2	CES demonstration	82
2.19.2.1	Combustion.....	83
2.19.2.2	Turbine.....	84
2.20	Natural Gas Combined Cycle (NGCC)	85
2.21	The NGCC power plant with PCC	85
2.22	Summary	87
Chapter 3:	Methodology and Process modelling of the leading Oxyturbine cycles.....	89
3.1	Introduction.....	89
3.2	Oxy-combustion power cycle theories and calculations	90
3.2.1	Thermodynamic concept and equations	90
3.2.1.1	Continuity	90
3.2.1.2	Energy conservation	91
3.2.1.3	Energy quality (second law of thermodynamic)	91
3.2.1.4	Thermodynamic cycles	92
3.2.2	Exergy equations for the oxyfuel combustion cycle.....	93
3.2.3	Exergy destruction equations	97
3.2.4	EOS for gas turbine and steam turbine	94
3.3	Modelling and simulation	96
3.3.1	Plant simulation with a numerical approach.....	96
3.3.2	Aspen Plus pros and cons	96
3.3.3	Modelling equipment in Aspen Plus	97
3.3.3.1	Distillation column	97
3.3.3.2	Stripper (or desorption).....	97
3.3.3.3	Absorption (opposite of striping).....	98
3.3.3.4	Separator blocks in Aspen Plus.....	98
3.3.4	MATLAB Code link with Aspen Plus	99
3.4	Oxy combustion cycles modelling and simulation	99
3.4.1	The SCOC-CC cycle modelling and analysis.....	99
3.4.2	The COOPERATE cycle modelling and analysis	104

3.4.3	The E-MATIANT cycle modelling and analysis.....	108
3.4.4	The CC_MATIANT cycle modelling and analysis.....	112
3.4.5	The Graz cycle modelling and analysis.....	116
3.4.6	The S-Graz cycle modelling and analysis.....	120
3.4.7	The AZEP 100% cycle modelling and analysis.....	124
3.4.8	The ZEITMOP cycle modelling and analysis.....	128
3.4.9	The COOLCEP-S cycle modelling and analysis.....	132
3.4.10	The COOLCEP-C cycle modelling and analysis.....	136
3.4.11	The Novel O ₂ /CO ₂ (Cao and Zheng, 2006) modelling and analysis.....	140
3.4.12	The NetPower cycle modelling and analysis.....	145
3.4.13	The S-CES cycle modelling and analysis.....	151
3.5	Sensitivity comparison of CES and NetPower.....	159
3.6	Techno-economic analysis of oxy-combustion cycles.....	159
3.6.1	Cost rate.....	159
3.7	Summary.....	165
Chapter 4: Exergy analysis of leading oxy-combustion cycles.....		166
4.1	The SCOC-CC cycle modelling and analysis.....	166
4.2	The COOPERATE cycle modelling and analysis.....	168
4.3	The E-MATIANT cycle modelling and analysis.....	170
4.4	The CC_MATIANT cycle modelling and analysis.....	172
4.5	The Graz cycle modelling and analysis.....	174
4.6	The S-Graz cycle modelling and analysis.....	176
4.7	The AZEP 100% cycle modelling and analysis.....	178
4.8	The ZEITMOP cycle modelling and analysis.....	180
4.9	The COOLCEP-S cycle modelling and analysis.....	182
4.10	The COOLCEP-C cycle modelling and analysis.....	184
4.11	The Novel O ₂ /CO ₂ (Cao and Zheng, 2006) modelling and analysis.....	186
4.12	The NetPower cycle modelling and analysis.....	188
4.13	The S-CES cycle modelling and analysis.....	190
4.14	Summary.....	192
Chapter 5: Sensitivity and exergy analysis of Semi-Closed Oxy-fuel Combustion Combined Cycle (SCOC-CC) and E-MATIANT.....		194
5.1	Sensitivity analysis of Semi-Closed Oxy-fuel Combustion Combined Cycle (SCOC-CC). 194	
5.1.1	Introduction.....	194
5.1.2	Sensitivity analysis results.....	195
5.1.3	Summary.....	206
5.2	Sensitivity and exergy analysis of E-MATIANT cycle.....	207
5.2.1	Introduction.....	207
5.2.2	Sensitivity analysis results.....	208

5.2.3	Summary	210
Chapter 6:	Sensitivity and exergy analysis of COOPERATE cycle	211
6.1	Introduction.....	211
6.2	Sensitivity analysis results	211
6.3	Summary.....	220
Chapter 7:	Sensitivity analysis of the heat exchanger design in NetPower oxy-combustion cycle for carbon capture	221
7.1	Introduction.....	221
7.2	Analysing of NetPower cycle	222
7.2.1	NetPower cycle	222
7.2.2	NetPower simulation with Aspen Plus	224
7.2.2.1	Recovery Heat Exchanger:	224
7.2.2.2	Recovery Heat Exchanger modelling in Aspen Plus	225
7.2.2.3	CO ₂ Direct-fired Turbine	226
7.2.2.4	Turbine with cooling blades modelling in Aspen Plus	227
7.2.3	Turbine with cooling blade modelling in Aspen Plus by exergy analysis	228
7.2.3.1	Recycle gas compression loop	231
7.3	Evaluation of ΔT_{min} from the composite curve and grand compost curve of multi-stream heat exchanger.....	233
7.4	Heat exchanger design sensitivity analysis for NetPower cycle	234
7.4.1	Sensitivity analysis with a constant recycled flow rate	235
7.4.2	Sensitivity analysis with constant COT	237
7.5	Design and cost analysis of NetPower plant	239
7.6	Summary.....	241
Chapter 8:	Leading Oxy-combustion power cycles: NetPower and Supercritical CES	242
8.1	Introduction.....	242
8.1.1	CES supercritical cycle	243
8.1.2	CES supercritical plant modelling.....	247
8.1.3	Sensitivity analysis of TIT for Supercritical CES (S-CES) cycle	252
8.1.4	Sensitivity analysis of COP for Supercritical CES (S-CES) cycle	254
8.1.5	Sensitivity analysis of cooling water temperature in the heat exchanger	255
8.2	NetPower cycle	255
8.2.1	NetPower plant modelling.....	257
8.2.2	Sensitivity analysis of the TIT for the NetPower cycle	259
8.2.3	Sensitivity analysis of heat exchanger for NetPower cycle	259
8.3	Compare TIT sensitivity for CES and NetPower cycle	260
8.4	Pilot and industrial demonstration of Oxyturbine power cycles	261
8.4.1	Oxy combustion cycle demonstration	261

8.5	Summary.....	263
Chapter 9: Techno-economic, Technology Readiness Level (TRL) and parametric comparison in		
	Oxyturbine Power cycles	264
9.1	Introduction.....	264
9.2	TIT comparison of oxy-combustion cycles.....	264
9.3	TOT comparison of oxy-combustion cycles	267
9.4	COP (Combustion Outlet Pressure) comparison of oxy-combustion cycles.....	269
9.5	Exergy and thermal efficiency comparison of oxy-combustion cycles.....	271
9.6	CO ₂ /kWh for storage comparison of oxy-combustion cycles	273
9.7	TRL (Technology Readiness Level)	274
9.7.1	Combustion TRL.....	275
9.7.2	CO ₂ Compression and Purification Unit (CPU) TRL.....	276
9.7.3	SCOCC-CC TRL.....	277
9.7.4	Graze cycle TRL	278
9.7.5	CES TRL.....	278
9.7.6	NetPower TRL	278
9.8	Performance analysis	279
9.9	Techno-economic analysis of oxy-combustion cycles.....	281
9.9.1	Exergoeconomic.....	285
9.9.2	LCOE	290
9.10	Radar chart for comparison of the oxy-combustion cycles	294
9.11	Summary	298
Chapter 10: Conclusions and future works		
10.1	Conclusions.....	299
10.2	Future work and critical appraisal	302
Reference		304
Appendix (A) (MATLAB Code).....		315

List of Figures

Figure 1.1 Power generation in the UK for seven days from 08-Jan-2020 to 15-Jan-2020 (MyGridGB, 2020).....	1
Figure 1.2 Typical gas turbine cycle	6
Figure 1.3 Schematic of a single spool gas turbine with hot end drive (Tony Giampaolo, 2015).....	9
Figure 1.4 Schematic of a single spool gas turbine with a cold end drive (Tony Giampaolo, 2015)	9
Figure 1.5 GasTurb schematic of single shaft gas turbine (Gasturb, 2018)	10
Figure 1.6 GasTurb schematic of a dual-shaft gas turbine (Gasturb, 2018).....	11
Figure 1.7 GasTurb schematic of a triple gas turbine (Gasturb, 2018)	12
Figure 1.8 Triple shafts open cycle gas turbine with intercooler(Ying <i>et al.</i> , 2016).....	14
Figure 1.9 Single shaft closed cycle gas turbine with intercooler and recuperator (Soares, 2015)	14
Figure 2.1 Schematic diagram of Post-combustion capture (Ahmad, 2019).....	21
Figure 2.2 Schematic diagram of NGCC with S-EGR and CO ₂ capture unit (Merkel <i>et al.</i> , 2013).....	24
Figure 2.3 Schematic diagram of 100 kW pilot scale S-EGR with PDMS membrane (Russo <i>et al.</i> , 2018).....	25
Figure 2.4 Process Flow Diagram of a basic chemical absorption process for amine-based CO ₂ capture (MacDowell <i>et al.</i> , 2010)	25
Figure 2.5 Schematic diagram of pre-combustion capture (Jansen <i>et al.</i> , 2015).....	28
Figure 2.6 Schematic diagram of using membrane for pre-combustion capture (MTR, 2018).....	28
Figure 2.7 Schematic diagram of Autothermal Reforming (AR) (Antonini <i>et al.</i> , 2020)	31
Figure 2.8 Schematic diagram of VPSA hydrogen production (Antonini <i>et al.</i> , 2020).....	32
Figure 2.9 Schematic diagram of oxy-combustion capture	33
Figure 2.10 A cryogenic air separation unit with two-column distillation and compression of oxygen in a gaseous state (Manso and Nord, 2020)	40
Figure 2.11 ASU development.....	41
Figure 2.12 Pressure Swing Absorption (Kwon <i>et al.</i> , 2011).....	43
Figure 2.13 Vacuum Pressure Swing Adsorption (Laboo, 2020).....	44
Figure 2.14 Ion transport membrane (ITM)	45
Figure 2.15 Schematic diagram of CLC (Ingegneria <i>et al.</i> , 2012)	46
Figure 2.16 CO ₂ Compression and Purification Unit (Chaubey 2010)	47
Figure 2.17 Schematic Process Flow Diagram of CPU (Almås, 2012).....	48
Figure 2.18 Semi-closed oxy-combustion combined cycle (SCOC-CC) (Davison, 2015)	50
Figure 2.19 COOPERATE cycle Process flow diagram (Yantovski, 1996)	52
Figure 2.20 E-MATIANT schematic diagram (Manso and Nord, 2020)	55
Figure 2.21 T-S Diagram of E-MATIANT cycle (Mathieu, 2004).....	56
Figure 2.22 CC-MATIANT cycle (Mathieu and Nihart, 1999)	58
Figure 2.23 T-S diagram of CC-MATIANT (Mathieu and Nihart, 1999)	58
Figure 2.24 Modified CC-MATIANT cycle by (Zhao <i>et al.</i> , 2017).....	60
Figure 2.25 T-S diagram of modified MATIANT cycle by (Zhao <i>et al.</i> , 2017)	60

Figure 2.26 Graz cycle (ASME 2003, Atlanta) (Wolfgang Sanz <i>et al.</i> , 2005).....	62
Figure 2.27 High steam content Graz cycle (S- GC) schematic diagram (Jericha, Sanz and Göttlich, 2008a).....	64
Figure 2.28 The AZEPT 100% case (Sundkvist <i>et al.</i> , 2005)	66
Figure 2.29 The AZEP 85% case (Sundkvist <i>et al.</i> 2005b).....	67
Figure 2.30 ZEITMOP schematic diagram (Yantovski <i>et al.</i> , 2004)	68
Figure 2.31 T-S diagram of the ZEITMOP cycle (Yantovski <i>et al.</i> , 2004).....	69
Figure 2.32 COOLCEP-S cycle schematic (Liu <i>et al.</i> , 2017)	71
Figure 2.33 T-S diagram of the COOLCEP-S (Liu <i>et al.</i> , 2017).....	71
Figure 2.34 COOLCEP-C (Zhang <i>et al.</i> , 2010).....	73
Figure 2.35 T–S diagram in the COOLCEP-C system (Zhang <i>et al.</i> , 2010).....	73
Figure 2.36 Process Flow Diagram of novel O ₂ /CO ₂ cycle system (Cao and Zheng, 2006).....	75
Figure 2.37 NetPower cycle schematic diagram (Davison, 2015)	76
Figure 2.38 5MWth combustor operating at 300 bar (Allam <i>et al.</i> , 2017).....	79
Figure 2.39 Heatric Printed Circuit Heat Exchanger (Heatric, 2020)	80
Figure 2.40 CES schematic diagram (Davison, 2015)	81
Figure 2.41 20MWt Oxy-Fuel Combustor (Anderson <i>et al.</i> , 2008)	83
Figure 2.42 170 MWt Oxy-Fuel Combustor (Anderson <i>et al.</i> , 2008).....	84
Figure 2.43 Natural Gas Combined Cycle (NGCC) (Davison, 2015).....	85
Figure 2.44 Natural Gas with PCC (Dillon <i>et al.</i> , 2013).....	86
Figure 3.1 Different classifications of exergy (Marmolejo-Correa and Gundersen, 2015).....	94
Figure 3.2 New classification of the exergy for pressure-volume-temperature PVT systems (Quality, 2011).....	95
Figure 3.3 Aspen Plus modelling of SCOC-CC.....	101
Figure 3.4 Aspen Plus modelling of COOPERATE cycle	105
Figure 3.5 Aspen Plus modelling of E-MATIANT cycle	109
Figure 3.6 Aspen Plus modelling of CC-MATIANT cycle.....	113
Figure 3.7 Aspen Plus modelling of Graz cycle.....	117
Figure 3.8 Aspen Plus modelling of S-Graz cycle	121
Figure 3.9 Aspen Plus modelling of AZEP 100% cycle	125
Figure 3.10 Aspen Plus modelling of ZEITMOP cycle	129
Figure 3.11 Aspen Plus modelling of COOLCEP-S cycle.....	133
Figure 3.12 Aspen Plus modelling of COOLCEP-C cycle	137
Figure 3.13 Aspen Plus modelling of O ₂ /CO ₂ cycle	141
Figure 3.14 Aspen Plus modelling of NetPower cycle.....	146
Figure 3.15 Aspen Plus modelling of S-CES cycle.....	152
Figure 4.1 Exergy destruction for each equipment of SCOC-CC	167
Figure 4.2 Exergy destruction percentage of SCOC-CC.....	167
Figure 4.3 Exergy destruction per MWe for SCOC-CC	168
Figure 4.4 Exergy destruction of each equipment for COOPERATE cycle	169

Figure 4.5 Percentage of exergy distraction for each component.....	169
Figure 4.6 Exergy destruction per MWe for COOPERATE Cycle.....	170
Figure 4.7 Exergy destruction for each equipment of E-MATIANT	171
Figure 4.8 Exergy destruction percentage for E-MATIANT	171
Figure 4.9 Exergy destruction per MWe production for E-MATIANT	172
Figure 4.10 Exergy destruction for CC-MATIANT.....	173
Figure 4.11 Exergy destruction percentage of CC-MATIANT.....	173
Figure 4.12 Exergy destruction per MWe production for CC-MATIANT	174
Figure 4.13 Exergy destruction for Graz cycle	175
Figure 4.14 Exergy destruction percentage for Graz cycle	175
Figure 4.15 Exergy destruction per MWe for Graz cycle	176
Figure 4.16 Exergy destruction for S-Graz cycle.....	177
Figure 4.17 Exergy destruction percentage for S-Graz cycle.....	177
Figure 4.18 Exergy destruction per MWe for S-Graz cycle.....	178
Figure 4.19 Exergy destruction of AZEP 100%	179
Figure 4.20 Exergy destruction percentage for AZEP 100%	179
Figure 4.21 Exergy destruction per MWe for AZEP 100%	180
Figure 4.22 Exergy destruction of ZEITMOP.....	181
Figure 4.23 Exergy destruction percentage for ZEITMOP	181
Figure 4.24 Exergy destruction per MWe for ZEITMOP	182
Figure 4.25 Exergy destruction for COOLCEP-S.....	183
Figure 4.26 Exergy destruction percentage for COOLCEP-S.....	183
Figure 4.27 Exergy destruction per MWe for COOLCEP-S	184
Figure 4.28 Exergy destruction for COOLCEP-C	185
Figure 4.29 Exergy destruction percentage for COOLCEP-C	185
Figure 4.30 Exergy destruction per MWe for COOLCEP-C	186
Figure 4.31 Exergy destruction for Novel O ₂ /CO ₂ cycle	187
Figure 4.32 Exergy destruction percentage for NovelO ₂ /CO ₂ cycle	187
Figure 4.33 Exergy destruction MW/MWe for NovelO ₂ /CO ₂ cycle.....	188
Figure 4.34 Exergy destruction for NetPower.....	189
Figure 4.35 Exergy destruction percentage for NetPower.....	189
Figure 4.36 Exergy destruction MWe/MW for NetPower	190
Figure 4.37 Exergy destruction for S-CES.....	191
Figure 4.38 Exergy destruction percentage for S-CES.....	191
Figure 4.39 Exergy destruction MWe/MW for S-CES	192
Figure 5.1 Sensitivity of power cycle with Gas turbine pressure ratio.....	195
Figure 5.2 Sensitivity of Network to Pressure ratio	196
Figure 5.3 Efficiency with respect to Flowrate and COP.....	197
Figure 5.4 TIT with respect to COP and fuel flowrate.....	197
Figure 5.5 Efficiency respect to COP of a steam turbine for SCOC-CC.....	198

Figure 5.6 Efficiency with respect to COP of the steam turbine	198
Figure 5.7 Gas turbine work to TIT	199
Figure 5.8 Thermal efficiency with respect to TIT	200
Figure 5.9 Thermal efficiency with respect to TIT of gas turbine.....	201
Figure 5.10 Exergy destruction for each component SCOC-CC cycle	201
Figure 5.11 3D plot of exergy destruction with respect to flowrate and COP.....	202
Figure 5.12 3D TIT with respect to COP and flowrate	203
Figure 5.13 Stacked bar chart of exergy destruction	204
Figure 5.14 TIT respect to Specific work MW/kg	205
Figure 5.15 Efficiency vs working flowrate for E-MATIANT	208
Figure 5.16 Total exergy destruction, Network and efficiency for E-MATIANT	209
Figure 6.1 The sensitivity of Efficiency vs working flowrate for COOPERATE cycle.....	212
Figure 6.2 The sensitivity of Network vs working flowrate for COOPERATE cycle	212
Figure 6.3 Comparison of Energy efficiency and Exergy efficiency vs working flowrate	213
Figure 6.4 Exergy destruction of equipment for COOPERATE cycle.....	213
Figure 6.5 Pie chart for exergy destruction of equipment	214
Figure 6.6 Exergy destruction vs working flowrate for COOPERATE cycle.....	215
Figure 6.7 Exergy destruction vs min approach temperature and flowrate	216
Figure 6.8 Total exergy destruction vs efficiency of COOPERATE cycle	217
Figure 6.9 Efficiency Vs Working flowrate and Heat exchanger approach temperature	218
Figure 6.10 Exergy destruction vs flowrate and heat exchanger approach temperature	218
Figure 6.11 Exergy destruction per MWe for COOPERATE Cycle.....	219
Figure 7.1 Model of the improved continuous expansion model with N (number of cooled expansion steps) by Scaccabarozzi, Gatti (Scaccabarozzi, Gatti, and Martelli 2017, 551-560).....	227
Figure 7.2 Turbine block model in Aspen Plus	228
Figure 7.3 NetPower Turbine with a cooling blade.....	229
Figure 7.4 Aspen Plus model of NetPower cycle.....	232
Figure 7.5 Composite curve	233
Figure 7.6 Grand composite curve	234
Figure 7.7 Efficiency related to ΔT_{min} for constant recycled flow rate	235
Figure 7.8 COT related to ΔT_{min} for constant recycled flow rate.....	235
Figure 7.9 Overall heat transfer coefficient UA to ΔT_{min} for constant recycled flow rate	236
Figure 7.10 The required power for recycled compression loop relates to ΔT_{min} in a constant recycled flow rate (the power demand is approximately constant)	236
Figure 7.11 Turbine power output related to ΔT_{min} for constant recycled flow rate	237
Figure 7.12 Flow rate related to ΔT_{min} for constant COT 1150 °C	238
Figure 7.13 Required power of recycled compression loop against ΔT_{min} for constant COT 1150 °C	238
Figure 7.14 Efficiency related to ΔT_{min} with constant COT 1150 °C	239
Figure 8.1. Supercritical CES Schematic diagram (Ferrari <i>et al.</i> , 2017b).....	244

Figure 8.2. Aspen Plus modelling of Supercritical Oxyturbine cycle	250
Figure 8.3. Aspen Plus model flow diagram of Oxyturbine power island in a Supercritical cycle	250
Figure 8.4. Efficiency & TIT of Super-CES with respect to Natural gas flowrate in HP turbine	252
Figure 8.5. TIT (LP, MP, HP) Turbine with respect to Natural gas flowrate.....	253
Figure 8.6. the Sensitivity of natural gas flowrate (LPT, MPT, HPT) to efficiency	253
Figure 8.7. Efficiency vs recycle water pump pressure for S-CES cycle.....	254
Figure 8.8. Efficiency vs cooling water temperature in S-CES.....	255
Figure 8.9. Schematic modelling NetPower cycle with Aspen Plus	257
Figure 8.10. Oxyturbine cycle for NetPower cycle.....	258
Figure 8.11. The efficiency of NetPower cycle vs TIT	259
Figure 8.12. Efficiency related to ΔT_{min} for constant recycled flow rate	260
Figure 8.13. The sensitivity of cycle efficiency with respect to TIT for HPT of CES and NetPower cycle.....	261
Figure 9.1 TIT comparison of Oxy-combustion cycles.....	267
Figure 9.2 TOT Comparison of oxy-combustion cycle.....	269
Figure 9.3 COP Comparison of oxy-combustion cycles	271
Figure 9.4 Thermal Efficiency and Exergy Efficiency Comparison	273
Figure 9.5 Oxy-combustion cycles TRL comparison.....	277
Figure 9.6 Comparison of oxy-combustion cost rate in the bar chart.....	284
Figure 9.7 Comparison of exergoeconomic of oxy-combustion cycles	289
Figure 9.8 LCOE comparison of oxy-combustion cycles in the bar chart	293
Figure 9.9 Separate radar chart for each oxy-combustion cycle	295
Figure 9.10 Separate radar chart for each oxy-combustion cycle.....	296

List of Tables

Table 1.1 Chapters refer back to objectives and novelty	4
Table 1.2 Comparison of an industrial gas turbine with an aero-derivation gas turbine (Tony Giampaolo, MSME 2014).....	8
Table 1.3 Comparison of gas turbine based on the number of shafts (Forsthoffer, 2011)	13
Table 1.4 Comparison of the closed cycle a with open cycle gas turbine (Soares, 2015)	15
Table 2.1 Classification of oxy-combustion cycle	36
Table 2.2 The advantages and disadvantages of each technology (Figueroa <i>et al.</i> , 2008).....	37
Table 2.3 Comparison of different carbon capture technologies (Wall, 2007)	38
Table 2.4 Comparison of COOPERATE and Combined Cycle (Yantovski, 1996)	54
Table 2.5 Operating parameters for E-MATIANT Cycle (Mathieu, 2004).....	56
Table 3.1 Thermodynamic power cycle types.....	92
Table 3.2 Standard molar chemical exergy of different substances at $P_0=1.0$ atm and $T_0=298.15$ K (Ibrahim Dincer, 2013)	96
Table 3.3 Exergy balance equations for oxy-fuel combustion power cycle (Karaağaç, Kabul and Oğul, 2019).....	93
Table 3.4 Equation Of State (EOS).....	94
Table 3.5 Stream properties of SCOC-CC cycle from Aspen plus modelling	102
Table 3.6 Stream properties of SCOC-CC cycle from Aspen plus modelling	103
Table 3.7 Stream properties of COOPERATE cycle from Aspen plus modelling	106
Table 3.8 Stream properties of COOPERATE cycle from Aspen plus modelling	107
Table 3.9 Stream properties of E-MATIANT cycle from Aspen Plus modelling	110
Table 3.10 Stream properties of E-MATIANT cycle from Aspen Plus modelling	111
Table 3.11 Stream properties of CC-MATIANT cycle from Aspen Plus modelling	114
Table 3.12 Stream properties of CC-MATIANT cycle from Aspen Plus modelling	115
Table 3.13 Stream properties of Graz cycle from Aspen Plus modelling	118
Table 3.14 Stream properties of Graz cycle from Aspen Plus modelling	119
Table 3.15 Stream properties of S-Graz cycle from Aspen Plus modelling.....	122
Table 3.16 Stream properties of S-Graz cycle from Aspen Plus modelling.....	123
Table 3.17 Stream properties of AZEP 100% cycle from Aspen Plus modelling.....	126
Table 3.18 Stream properties of AZEP 100% cycle from Aspen Plus modelling.....	127
Table 3.19 Stream properties of ZEITMOP cycle from Aspen Plus modelling.....	130
Table 3.20 Stream properties of ZEITMOP cycle from Aspen Plus modelling.....	131
Table 3.21 Stream properties of COOLCEP-S cycle from Aspen Plus modelling	134
Table 3.22 Stream properties of COOLCEP-S cycle from Aspen Plus modelling	135
Table 3.23 Stream properties of COOLCEP-C cycle from Aspen Plus modelling	138
Table 3.24 Stream properties of COOLCEP-C cycle from Aspen Plus modelling	139
Table 3.25 Stream properties of O_2/CO_2 cycle from Aspen plus modelling	142
Table 3.26 Stream properties of O_2/CO_2 cycle from Aspen plus modelling	143

Table 3.27 Stream properties of O ₂ /CO ₂ cycle from Aspen plus modelling	144
Table 3.28 Stream properties of NetPower cycle from Aspen Plus modelling	147
Table 3.29 Stream properties of NetPower cycle from Aspen Plus modelling	148
Table 3.30 Stream properties of NetPower cycle from Aspen Plus modelling	149
Table 3.31 Stream properties of NetPower cycle from Aspen Plus modelling	150
Table 3.32 Stream properties of S-CES cycle from Aspen Plus modelling	153
Table 3.33 Stream properties of S-CES cycle from Aspen Plus modelling	154
Table 3.34 Stream properties of S-CES cycle from Aspen Plus modelling	155
Table 3.35 Stream properties of S-CES cycle from Aspen Plus modelling	156
Table 3.36 Stream properties of S-CES cycle from Aspen Plus modelling	157
Table 3.37 Stream properties of S-CES cycle from Aspen Plus modelling	158
Table 3.38 Equations for calculating the purchase cost (Z) for the components (Sahu and Sanjay, 2017) (Seyyedi, Ajam and Farahat, 2010).	160
Table 3.39 GT cost function (Carapellucci <i>et al.</i> , 2017)	161
Table 3.40 Estimated investment costs (W. Sanz <i>et al.</i> , 2005)	162
Table 3.41 Marshal and swift cost index at various years (Khaljani, Khoshbakhti Saray and Bahlouli, 2015).....	163
Table 5.1 The optimum design point of E-MATIANT Cycle.....	208
Table 7.1 NetPower cycle simulate result validated with IEA report	232
Table 8.1 The composition percentage of Supercritical CES cycle working fluid (IEAGHG, 2015) 245	
Table 8.2. The pressure of fuel gas and coolant temperature in each turbine (IEAGHG, 2015).....	245
Table 8.3. The natural gas mole fraction.....	248
Table 8.4. ASU Outlet mole fraction	249
Table 8.5. Comparing the results of the CES model with the IEA Report (IEAGHG, 2015).....	251
Table 8.6. Results of NetPower compared with the data published in the IEA 2015 report	258
Table 9.1 TIT of oxy-combustion cycles	266
Table 9.2 Turbine Outlet Temperature (TOT) of oxy-combustion cycle.....	268
Table 9.3 Combustion Outlet Pressure (COP) of Oxy-combustion cycle	270
Table 9.4 Thermal and exergy efficiency of oxy-combustion cycles.....	272
Table 9.5 CO ₂ /kWh for oxy-combustion cycles.....	274
Table 9.6 Technology Readiness Level (Oettinger 2015):.....	275
Table 9.7 Oxy-combustion and units TRL comparison	276
Table 9.8 Performance analysis of oxy combustions turbine by Aspen plus modelling analysis	280
Table 9.9 Cost analysis of each component for oxy-combustion cycles:.....	282
Table 9.10 Overall cost rate of oxy-combustion cycles	283
Table 9.11 Exergoeconomic analysis for oxy-combustion cycles.....	288
Table 9.12 Levelised Cost Of Electricity (LCOE) for oxy-combustion cycles.....	292
Table 9.13 Comparison parameters of Oxy-Combustion cycles	294
Table 9.14 Normalised parameters of Oxy-Combustion cycles.....	294

Abbreviations

AC	Avoidance Cost
ACC	Aker Clean Carbon
AFT	Adiabatic Flame Temperature
AR	Air Reactor
ASU	Air Separation Unit
AZEP	Advanced Zero-Emission Power cycle
CCGT	Combined Cycle Gas Turbine
CCS	Carbon Capture & Storage
CCS	Carbon Capture and Sequestration
CES	Clean energy system
CF	Capacity Factor
CI	Cost Index
CLC	Chemical Looping Combustion
COOLCEP	Cool Clean Efficient Power
COOPERATE	CO ₂ Prevented Emission Recuperative Advanced Turbine Energy Cycle
COP	Combustion Outlet Pressure
COT	Combustion Outlet Temperature
CRF	Capital Recovery Factor
DoE	Department of Energy
Eff	Efficiency
EO	Equation Oriented
EOR	Enhance Oil Recovery
EOS	Equation of State
FCF	Fixed Charge Factor
FGR	Flue Gas Recirculation
FOM	Fixed Operating Maintenance
FSC	Fixed-Site Carrier
FTT	Florida Turbine Technology
GHG	Global Greenhouse Gas
HPT	High-Pressure Turbine
HRSRG	Heat Recovery Steam Generator
HTT	Hight-Temperature Turbine
HX	Heat Exchanger
IEA	International Energy Agency
IGCC	Integrated Gasification Combined Cycle
IGCC-CCS	Integrated Gasification Combined Cycle - Carbon Capture & Storage
ITM	Ion Transport Membrane
LCOE	Levelized cost of electricity
LNG	Liquefied Natural Gas
MHE	Main Heat Exchanger
NGCC	Natural Gas Combined Cycle
OITM	Oxygen Ion Transport Membranes
Oxyturbine	Oxy-combustion
PCC	Post Combustion Capture

PDMS	Polydimethylsiloxane
PFD	Process Flow Diagram
RFG	Recycled Flue Gas
SCOC-CC	Semi-closed oxy-combustion combined cycle
S-EGR	Selective exhaust gas recirculation
SFC	Specific fuel consumption
SM	Sequential Modular
TBC	Thermal Barrier Coating
TCR	Total Capital Requirement
TIP	Turbine Inlet Pressure
TIT	Turbine Inlet Temperature
TOT	Turbine Outlet Temperature
TRL	Technology Readiness Level
UA	Overall Heat Coefficient
UNFCCC	United Nations Framework Convention on Climate Change
VOM	Variable Operating Maintenance
ZEITMOP	Zero Emission Ion Transport Membrane Oxygen Power
ZEPP	Zero Emission Power Plant

Subscripts

0	Environmental state
ch	Chemical
d	Destruction
f	Fuel
i	Inlet
k	Number of components
l	Loss
o	Outlet
p	Product
ph	Physical
T	Temperature
th	Thermal

Symbols

\dot{m}_i	Input mass flow rate
\dot{m}_o	Output mass flow rate
$\frac{\partial m}{\partial t}$	Mass rate of a control volume
ρ_i	Density of input flow
V_i	Volume of input flow
A_i	Area of input flow
ρ_o	Density of output flow
V_o	Volume of output flow
A_o	Area of output flow
\dot{E}_i	Energy rate of input flow
\dot{Q}	Heat rate
\dot{E}_o	Energy rate of output flow
\dot{W}	Work rate
$\frac{\partial S_{cv}}{\partial t}$	Entropy rate of a control volume
\dot{S}	Entropy rate of input flow
\dot{S}_{gen}	Entropy generation rate of a control volume
i	Numbers of input
e	Number of exits
o	Number of output
k	Number of heat rate
$\dot{E}x_i$	Exergy rate of input
\dot{Q}_k	Heat rate of a control volume
$\dot{E}x_o$	Exergy rate of output
$\dot{E}x_d$	Exergy destruction rate of a control volume
E_x^{CHE}	Chemical exergy
\dot{E}_x^T	Exergy rate of temperature
\dot{E}_x^P	Exergy rate of pressure
\dot{S}_i	Entropy rate of input flow
\dot{Q}_{cv}	Heat rate of a control volume
\dot{E}_x	Exergy rate of work
P	Pressure
T	Temperature
R	Ideal gas constant
c_p	Heat capacity of constant pressure

T_o	Temperature of reference
P_o	Pressure of reference
k	Specific heat ratio
ΔG_T^0	Standard Gibson free energy
\dot{W}_{net}	Net power output
\dot{m}_{fuel}	Mass flow rate of fuel
ΔH_T^0	Standard enthalpy of reaction
η	Efficiency
\dot{i}_{dest}	Exergy destruction rate
\dot{W}_{gt}	Work rate of gas turbine

Chapter 1: Introduction

Greenhouse gases are the main reason for the increase in the global mean temperature and climate change. Climate change is caused by the increased greenhouse effect; Carbon dioxide (CO₂) emissions from power plants and energy sectors are one of the GHG emissions, but it has major contributors to global greenhouse gas (GHG) emissions. The carbon budget for 2 °C scenarios have an upper limit on the cumulative CO₂ and is in the range of 800-1400 GtCO₂, and the carbon budget for 1.5 °C scenarios is in the range of 200-800 GtCO₂ (IEAGHG, 2019). Furthermore, Natural Gas(NG) demand is forecasted to increase 2.5% a year for the next ten years (IEAGHG, 2020).

Therefore, the reduction of carbon dioxide in the energy sector is the main part to mitigate climate change. The gas turbine is widely used to generate electrical power; Figure 1.1 shows the electricity generation in the UK for seven days.

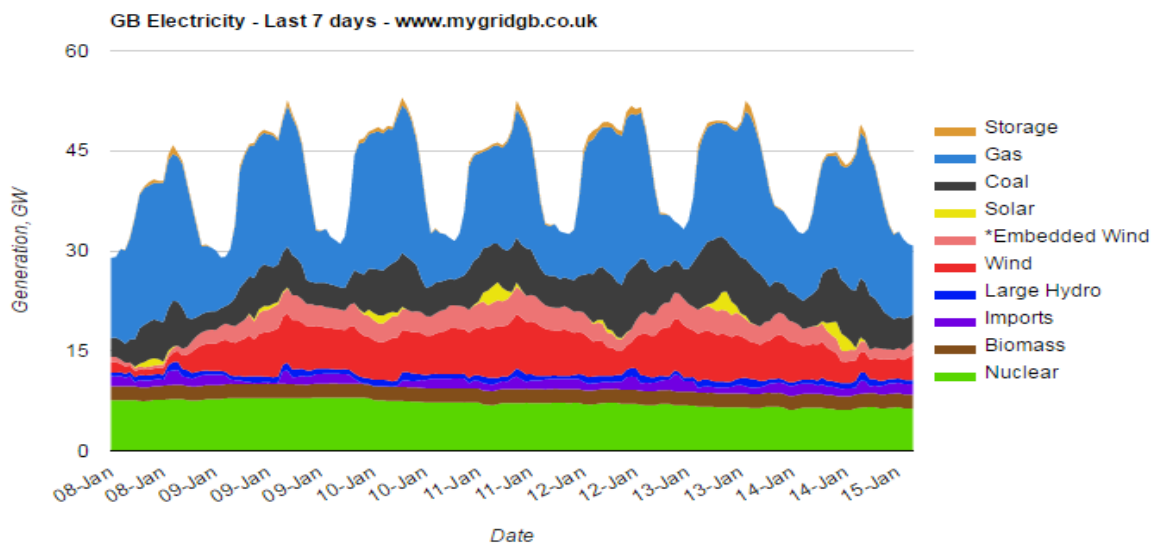


Figure 1.1 Power generation in the UK for seven days from 08-Jan-2020 to 15-Jan-2020 (MyGridGB, 2020)

The increasing concern for climate change has led to global efforts to reduce carbon dioxide (CO₂) in the atmosphere. It appears that by far the most significant contribution to the greenhouse effect stems from emissions of carbon dioxide CO₂. A large part of

the CO₂ emission is produced by combusting fossil fuels in conventional power plants and industrial processes (United State Environmental Protection Agency, 2018).

The gas turbine power generation is more flexible to respond to electrical demand, and this is the advantage of the gas turbine to renewable energy, however, conventional gas turbines burn fossil fuels and release a massive amount of CO₂ equivalent emission in the environment.

The power generation from fossil fuels is likely to continue in future to respond the energy demand and conventional power plants produce 74% in 2040 even under new policy scenario, The oil, gas and coal will resource 27%, 24% and 23% respectively of energy demand in 2040 (Gonzalez-Salazar, Kirsten and Prchlik, 2018).

In order to meet the electricity demand as well as the CO₂ mitigation targets, it is essential to increase the efficiency of fossil-fuel-based energy conversion systems along with the implementation of carbon capture and storage (CCS) technologies. There are three carbon capture technologies, including precombustion, oxyfuel combustion and post-combustion. Oxy-fuel combustion is one of the main carbon capture technologies that aim to provide zero NO_x emission and pure CO₂ streams ready for sequestration. The development of oxyfuel combustion technologies can lead to high-efficiency clean energy power plants.,the markets opportunity for this project is quite attractive, and the project dissemination in the energy industry is extensive.

1.1 Aim of this research project

This PhD project is aiming to provide a critical review of state of the art gas-fired oxy-turbine cycles with a key focus on the leading proposed cycles, including NetPower Cycle, CES Cycle, MATIANT Cycle, AZEP Cycle, and Graz Cycle. Also these cycle are compared based on the different aspect including exergoeconomic, LCOE, performance, TRL and exergy By the completion of this research, a platform for the process simulation and performance analysis of these type of cycles is provided using Aspen Plus software.

It is anticipated that as a result of this study, a road map for the development and deployment of the oxy-turbine power cycles as a clean replacement for the conventional power plants in the UK and worldwide is presented, which includes detailed technical information in these cycles. It is the first time several oxy-

combustion cycles technologies are investigated and compared together. Also, it is the first time these cycles are modelled with software and analysed with different parameters. The output of this PhD thesis will be a platform to develop the next generation of oxy-turbine power cycles.

1.2 Objectives

In order to achieve the aim stated in the section above, the following objectives must be reached:

- A. To investigate Carbon Capture, Air Separation Unit (ASU) and CO₂ Purification and Compression Unit (CPU) technologies.
- B. To investigate the oxy-combustion power cycles.
- C. To simulate the oxy-combustion cycles with Aspen Plus and tabulate the results of process modelling at each point.
- D. To assess the exergy destruction in components of the oxy-combustion cycles to compare the efficiency of the component to each other.
- E. To compare the parameters of oxy-combustion cycle including TIT, TOT, CO₂/kWh, COP, Exergy, Thermal efficiency, Technology Readiness Level (TRL) to provide a benchmark for comparing oxy-combustion cycles.
- F. To study the sensitivity of leading oxy-combustion cycles.
- G. To investigate pilot and industrial demonstration of Oxyturbine power cycles and comparison in terms of cost and efficiency.
- H. To evaluate the performance of the oxy-combustion cycles according to the Aspen plus modelling.
- I. To assess the cost rate and Levelized Cost Of Energy (LCOE) for oxy-combustion cycles.
- J. To compare several parameters on the radar diagram.

Table 1.1, indicates where these objectives are met and stating the novelty.

Table 1.1 Chapters refer back to objectives and novelty

Objectives	Novelty	Objectives meet in the chapters
A	Literature review of several oxy-combustion cycles.	Chapter 2
B	It is the first time several oxy combustions are investigated.	Chapter 2
C	It is the first time several oxy combustions are analysed with Aspen Plus and MATLAB Codes.	Chapter 3
D	It is the first exery destruction of components for several oxy-combustion cycles are calculated with Aspen Plus and MATLAB Codes.	Chapter 3
E	It is first these parameters of oxy-combustion cycles are compared.	Chapter 9
F	The heat exchanger sensitivity of the NetPower cycle was analysed, and the sensitivity of NetPower and CES are compared.	Chapter 7 and Chapter 8
G	The pilot and industrial demonstration of Oxyturbine powers are investigated, and updated information relates to equipment, cost, technology and efficiency are indicated.	Chapter 8. Chapter 9
H	Several oxy-combustion cycles performance are compared.	Chapter 9 and Chapter 3
I	Several oxy-combustion cycles cost are compared.	Chapter 9
J	Radar diagrams were used to compare several oxy-combustion cycles.	Chapter 9

1.3 Introduction to the gas turbine technology

The idea of the gas turbine goes back long ago, John Wilkins (1614-1672) used the motion of air that ascends the chimney to turn a rod (EAVES PSK, 1971), but the gas turbine goes back to Barber (1791) for the basic concept of power generation (Horlock and Bathie, 2004).

The gas turbine was used extensively 40 years ago in power generation and different industries. There are various types of the gas turbine with different fuels such as natural gas, diesel fuel, biomass gas.

The first generation gas turbine has major problems with the efficiency penalty of the compressor, and the compressor was driven independently in the early design of the gas turbine. Also, the turbine must be highly efficient to produce enough power to drive the compressor and generate the power network. One of the first gas turbines was developed by Armengaud and Lemae (French engineers) in 1904, the power network was about 10kW, and overall efficiency was approximately 3%. The first industrial gas turbine was produced by Brown Boveri in 1939; the network output was 4 MW. Whittle produced a gas turbine with enough power network for propulsion; The exhaust gas can produce a high-speed jet for aircraft propulsion in 1930.

The heavy gas turbine had been developed to produce electrical power by combined cycle gas turbine with a bottom cycle of the steam turbine (CCGT) (Horlock and Bathie, 2004). Gas turbine material technologies are developed during the last 20 years. The cooling method of the blade and new coating materials let the turbines work in the higher temperature such as NetPower cycle and CES cycle; in recent years, the development of compressor pressure ratio support increased turbine efficiency up to 60%.

Gas turbines convert the chemical energy of the fuel into whether mechanical energy or kinetic energy. There are two types of gas turbines, including power generation gas turbine that converts the chemical energy of the fuel to shaft power to produce electricity and gas turbine for aircraft which produce thrust to propel it (Schobeiri, 2018).

The main concept of gas turbine thermodynamics is receiving fuel energy at a high temperature at the combustor (C) to produce work at the gas turbine (A) and release

remaining energy to heat sink with the low temperature at the condenser (D), as shown in Figure 1.2.

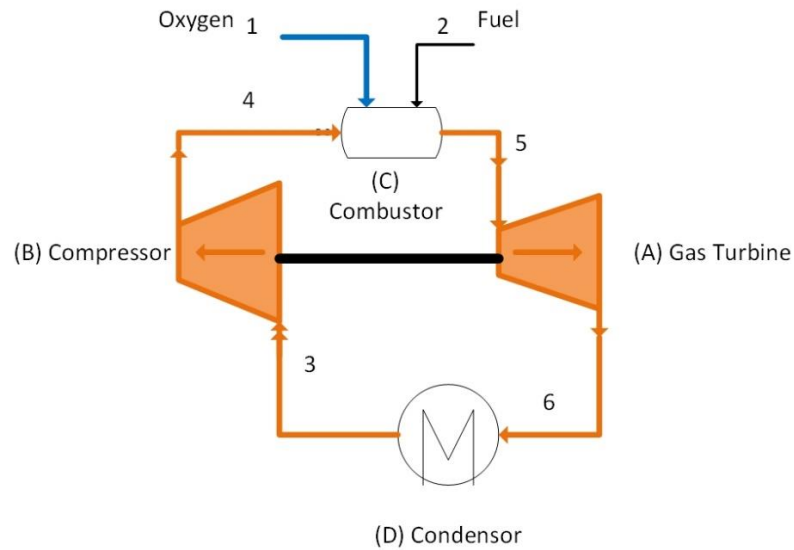


Figure 1.2 Typical gas turbine cycle

The power plants need to produce a network with minimum fuel consumption. However, the capital cost and operational cost need to be balanced to produce electricity with a lower cost (cost/ kW.h) (Horlock and Bathie, 2004).

In recent years, new technologies of the gas turbine have been developed to reduce greenhouse gas emissions.

1.4 Categories of gas turbines

There are seven categories for the gas turbine as below:

1- Heavy-Duty gas turbines:

The power generation units are larger, and they are between 3 MW to 480 MW, and the efficiencies are 30% - 46%.

2- Aircraft-Derivative:

These are aircraft gas turbines, which have been replaced fans with a turbine at the exhaust (Boyce, 2006), and power is between 2.5 MW to 50 MW with efficiencies of 35-45% (Boyce, 2006). They respond faster, lighter with up to 45% efficiency. The turbines are also popular due to their fuel flexibility (do Nascimento *et al.*, 2013).

3- Industrial gas turbine:

These types of gas turbines are used for medium-range power and are usually rated between 5–15 MW for the compressor of petrochemical plants with low efficiencies about 30% (Boyce, 2006).

One type of them is the Rolls-Royce Industrial Trent family gas turbine. This turbine produces high power with variable speed which is suitable for natural gas liquefaction, gas transportation, and gas injection for oil recovery. ALSTOM, General Electric, and Siemens-Westinghouse are the main manufacturer of the large single-shaft gas turbine with more than 250 MW per unit.

Industrial gas turbines can be used for different sectors because of their flexibility. These turbines can be used for mechanical drive systems, chemical industries, transportations, pump drives and power generation (Ahmed F. El-Sayed, 2017).

4- Small gas turbine:

The radial turbines with centrifugal compressors produce power between 0.5-2.5 MW with a very low efficiency of 15-25% (Boyce, 2006).

5- Micro-Turbine:

These turbines can produce power up to 300 kW, and they are used for industries and domestic clients. These gas turbines are open cycle gas turbines with different features such as high-speed operation, compact size, variable speed, low maintenance, easy installation, simple operability (Marco Antônio Rosa do Nascimento, 2005).

6- Gas turbines at sea:

The first successful boat with a gas turbine was Motor Gun Boat in 1947, and the first fast patrol boat with a gas turbine was fabricated by Rolls Royce Proteus. General electric fabricated LM services for U.S Navy Bruke Destroyer, Italian Lupo Farigate, AEGIS Gruiser. The advantages of the gas turbine for naive industries are compact size, low noise and high power density (Ahmed F. El-Sayed, 2017).

7- Gas turbines at the ground:

U.S. tank M1A1 Abram has used the AlliedSignal Lycoming AGT1500 gas turbine. Also, a gas turbine engine is used for Union Pacific in the United States to operate locomotives. The gas turbine produces electricity to the electric power motors of the locomotive (Union Pacific, 2020). Lightweight, reliability and compactness are the advantages of a gas turbine for road transportation. The gas turbine engine has a vibration-free operation compared with the reciprocating engine, and it has a lower

maintenance cost with low lubricating oil. The gas turbine engine can consume various fuels without redesigning combustion; furthermore, the micro gas turbine engine has lower carbon emission and is more environmentally friendly. Low efficiency during part-load and idle conditions is the gas turbine engine disadvantage for road transportation. Another disadvantage is the required time to reach full load from idle; the acceleration time depends on gas turbine characteristics (Cunha and Kyprianidis, 2012).

The project to fabricate Snow Plow with PT6 turboshaft gas turbine began in the early 1960s in collaboration with Pratt & Whitney Engines and the Department of Highways in British Columbia, Canada. The powerful Snow Plow was required to combat heavy snowfall, and it needs to be mobile enough to operate on the mountainous roads. The Snow Plow was used in British Columbia road for years (PT6Nation, 2018). Table 1.2 shows a comparison of the industrial gas turbine with an aero-derivation gas turbine.

Table 1.2 Comparison of an industrial gas turbine with an aero-derivation gas turbine

(Tony Giampaolo, MSME 2014)

Observation	Industrial Compared to Aero-Derivative
Shaft Speed	Slower
Air Flow	Higher
Maintenance Time	Longer
Maintenance lay-down space	Larger

1.5 Type of gas turbine

One of the classifications of gas turbines is the number of spools. The gas turbine can be single-spool, two-spool or three-spool. Also, the gas turbine can be a hot-end drive or cold end drive.

In the hot end drive, as shown in Figure 1.3, the output shaft is mounted at the turbine end, and the exhaust gas temperature is about 600°C. The disadvantages of this configuration are the high temperature affect bearing operation, and the assembly is difficult at the exhaust duct and maintenance accessibility (Tony Giampaolo, 2015).

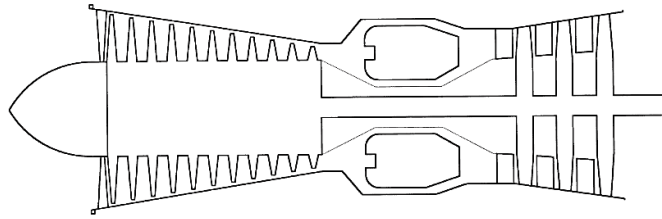


Figure 1.3 Schematic of a single spool gas turbine with hot end drive (Tony Giampaolo, 2015)

In the cold end drive, as shown in Figure 1.4, the output shaft is mounted at the front of the compressor. The advantages of this configuration are the accessibility of driven equipment, ease to service, maintenance, and work on ambient temperature (Tony Giampaolo, 2015).

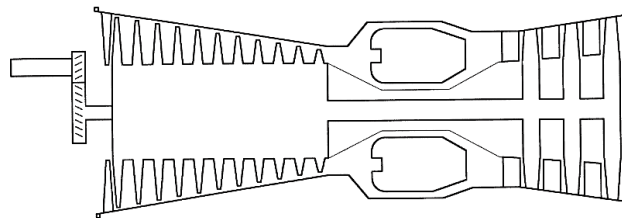


Figure 1.4 Schematic of a single spool gas turbine with a cold end drive (Tony Giampaolo, 2015)

1.5.1 Single-shaft gas turbine

In the single-shaft gas turbine, as shown in Figure 1.5, one shaft connects the compressor to the turbine. The air is drawn into the compressor to increase its pressure; then, high-pressure air burns with fuel to produce by-products at the high temperature. The hot output flue of combustion enters the turbine to produce power. Part of the power output is transferred through the shaft and absorbed by the compressor. The remaining power is used to drive a generator to produce electricity (Razak, 2007). As shown in Figure 1.5, the air enters and exits the compressor in the process between stage (2-3), the combustor process is between stage (31-4), the expansion process (turbine) is between stage (41-5).

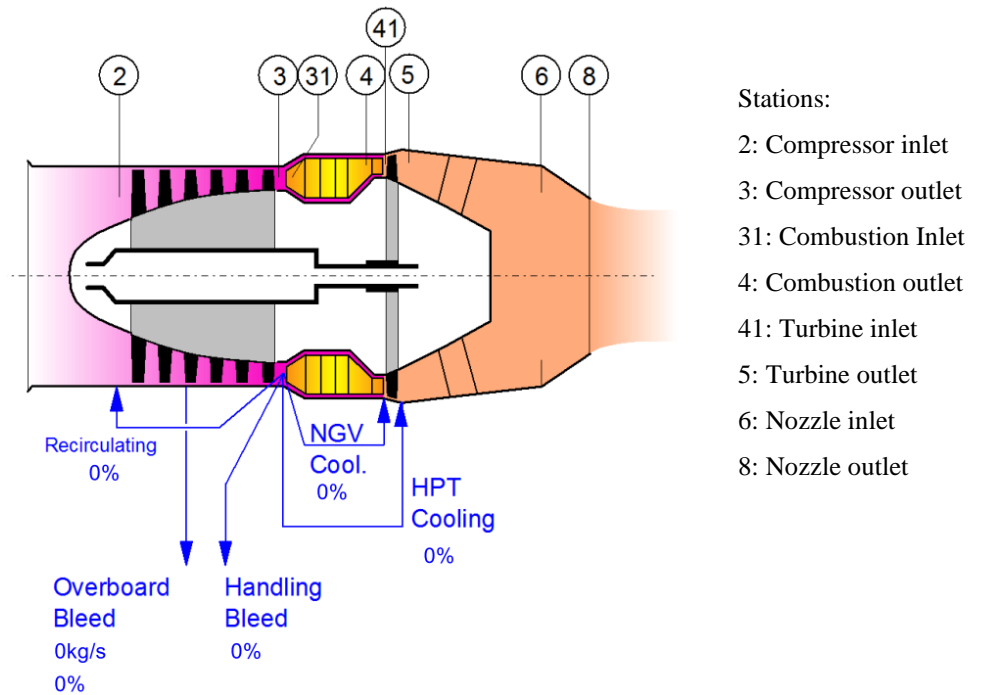


Figure 1.5 GasTurb schematic of single shaft gas turbine (Gasturb, 2018)

A single shaft gas turbine can be further classified based on the compressor type. The employed compressor can be the double and single compressor (Razak, 2007).

1.5.2 Dual shaft gas turbine with a power turbine

The first turbine is used to drive the compressor, and the second turbine is used to drive the load. The mechanically independent (free) turbine driving the load is called the power turbine. The remaining turbine or high-pressure turbine, compressor and combustor are called the gas generator.

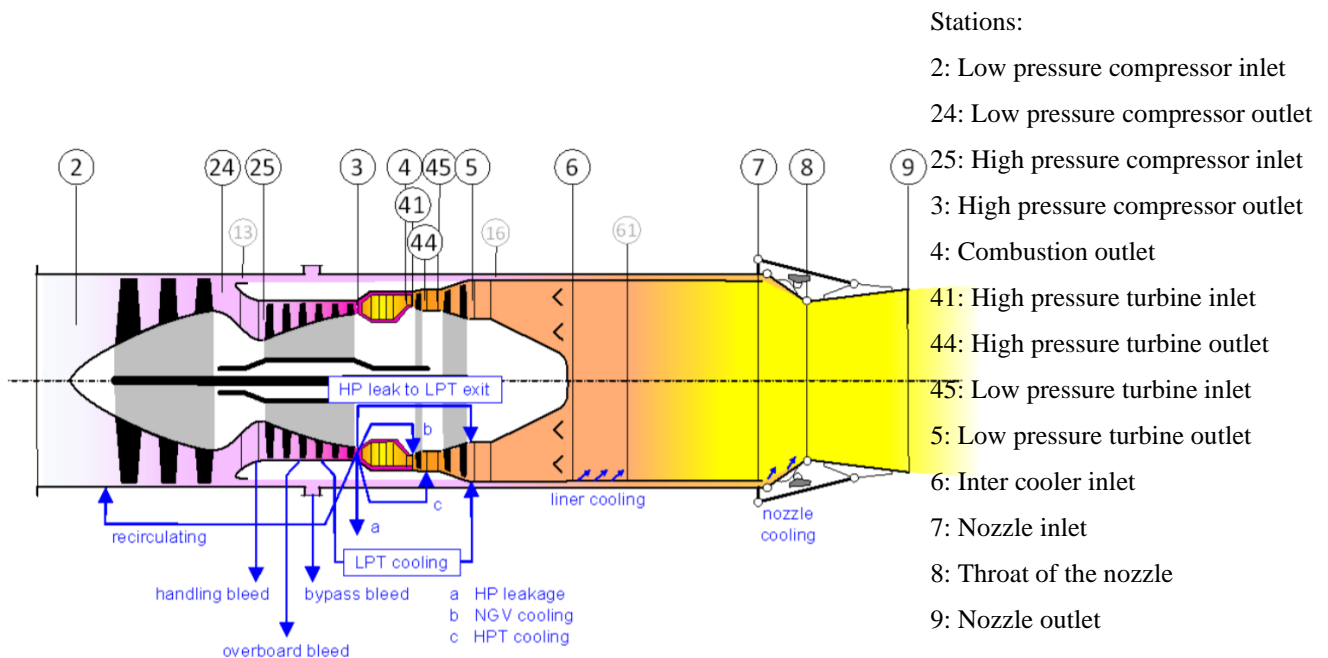


Figure 1.6 GasTurb schematic of a dual-shaft gas turbine (Gasturb, 2018)

As shown in Figure 1.6, the air enters and exits the low-pressure compressor process between stage (2-24), the high-pressure compressor process is between stage (25-3), the combustor process is between stage (3-4), the high-pressure expansion process (high-pressure turbine) is between stage (41-44), the low-pressure expansion process (low-pressure turbine) is between stage (45-5).

The first compressor is next to the intake, and it is identified as Low-Pressure Compressor (LPC), and it is connected to the Low-Pressure Turbine (LPT); it is driven with it. The High-Pressure Compressor (HPC) is connected to High-Pressure Turbine (HPT), and the shaft is concentric with the low-pressure shaft (Razak, 2007).

1.5.3 Triple shaft gas turbine with a power turbine

A three-shaft gas turbine includes a low-pressure, an intermediate-pressure, and a high-pressure shaft. Each shaft rotates at different speeds. The fan is connected to Low-Pressure Turbine (LPT) with the low-pressure shaft.

The intermediate shaft connects the intermediate-pressure compressor to the intermediate-pressure turbine, and the high-pressure shaft connects High-Pressure Compressor (HPC) and High-Pressure Turbine (HPT) (Ahmed F. El-Sayed, 2017).

As shown in Figure 1.7, the air enters and exits the low-pressure compressor process between stage (2-24), the high-pressure compressor process is between stage (25-3), the combustor process is between stage (3-4), the high-pressure expansion process (high-pressure turbine) is between stage (41-43), the Medium pressure expansion

process (medium pressure turbine) is between stage (45-47), the Low-pressure expansion process (low-pressure turbine) is between stage (48-5).

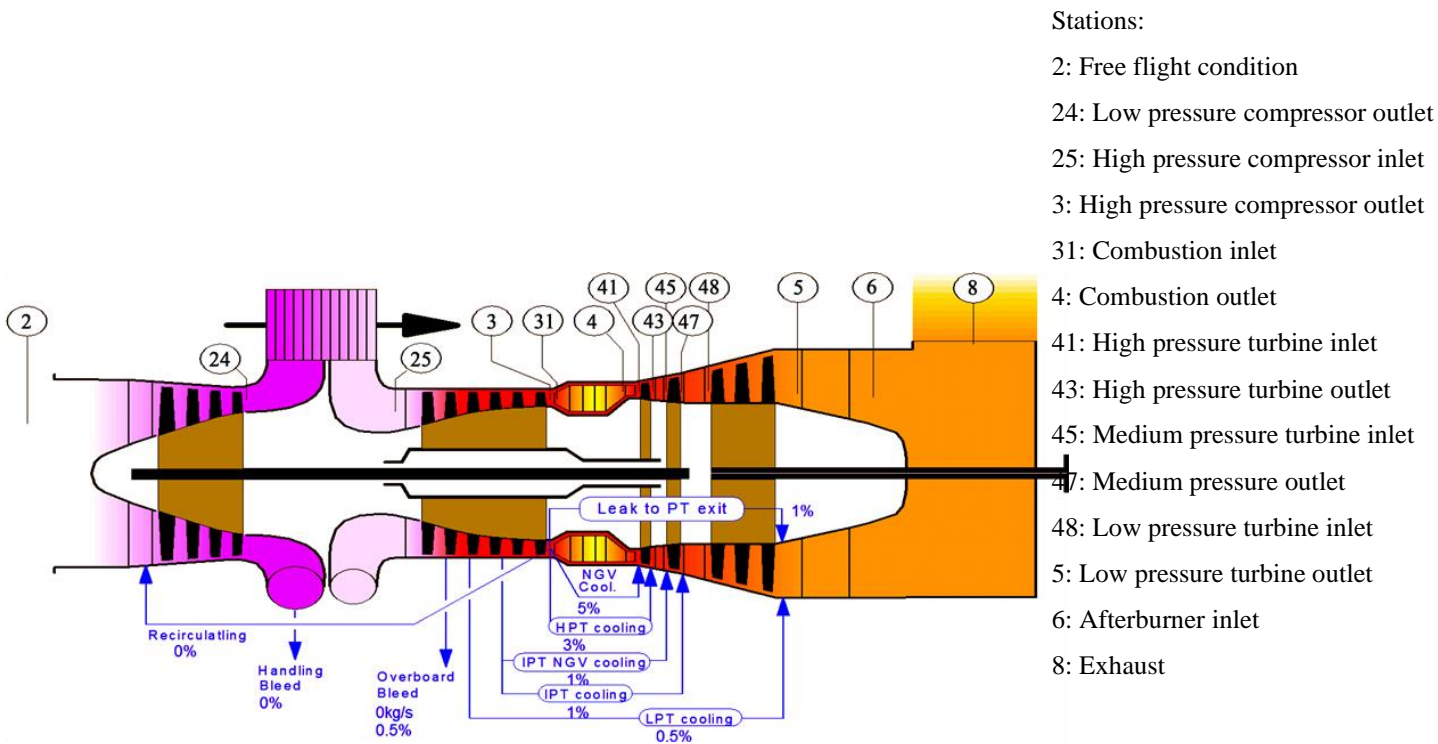


Figure 1.7 GasTurb schematic of a triple gas turbine (Gasturb, 2018)

Different types of gas turbines have advantages and disadvantages. Table 1.3 compares the single shaft, dual shaft and triple shaft gas turbine.

Table 1.3 Comparison of gas turbine based on the number of shafts (Forsthoffer, 2011)

Types	Advantages	Disadvantages
Single shaft gas turbine	<ul style="list-style-type: none"> • Simplest design • Lower maintenance • preventing over-speed conditions due to the high power required by the compressor and can act as an effective brake should the loss of electrical load occur 	<ul style="list-style-type: none"> • Requires large starting device • Limited Speed Range • Lower efficiency
Dual shaft gas turbine	<ul style="list-style-type: none"> • Higher Efficiency • Large speed range • Requires smaller starting device • the gas generator speed will vary with electrical load • smaller starting power requirements • better off-design performance 	<ul style="list-style-type: none"> • A more complex control system • Higher maintenance • shedding of the electrical load can result in over-speeding of the power turbine
Triple shaft gas turbine	<ul style="list-style-type: none"> • Higher efficiency • Large speed range • Requires smaller starting device • lower starting powers because only the high-pressure compressor and turbine in the gas generator need to be turned during starting • Aircraft gas turbines are referred to as aero-derivatives 	<ul style="list-style-type: none"> • A more complex control system • Higher maintenance

1.5.4 Open and closed thermodynamic cycles of gas turbine

In the open cycle gas turbine, the air enters from the atmosphere and passes through the compressor, combustor and turbine so the all working flow releases to the atmosphere.

In the closed-cycle gas turbine, the working flow is continuously recirculated through the gas turbine.

Figure 1.8 shows a triple shafts open cycle gas turbine with intercooler, as intercooler increases gas turbine efficiency. Triple shafts gas turbine includes Low-Pressure Compressor (LPC), High-Pressure Compressor (HPC), High-Pressure Turbine (HPT), Low-Pressure Turbine (LPT) and Power Turbine (PT). Combustor (B)

burns fuels with air, and PT is connected to the generator by gearbox for power production (Ying *et al.*, 2016).

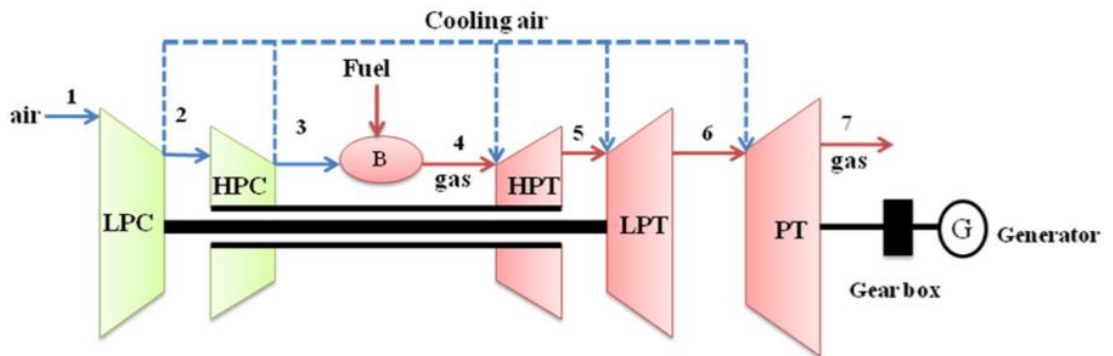


Figure 1.8 Triple shafts open cycle gas turbine with intercooler(Ying *et al.*, 2016)

Figure 1.9 shows a single shaft closed cycle gas turbine with intercooler and recuperator; the recuperator is used to receive heat instead of the combustor.

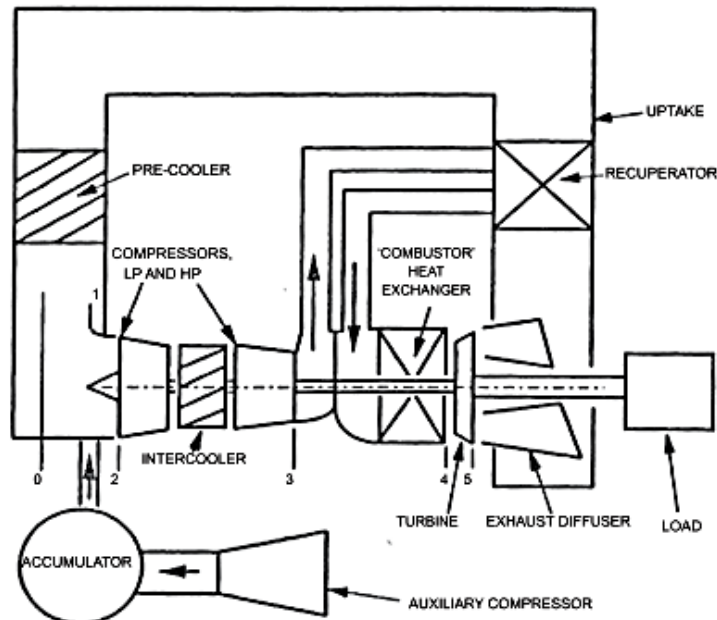


Figure 1.9 Single shaft closed cycle gas turbine with intercooler and recuperator (Soares, 2015)

The main benefit of closed-cycle is the high density of the working flow; it causes higher power output, and the pressure at the inlet to the gas turbine can be 20 times atmospheric pressure (Soares, 2015).

The high density of the working fluid at engine entry enables very high power output for a given size of the plant, which is the main benefit of the closed cycle. The pressure at the inlet to the gas turbine typically is around 20 times atmospheric pressure. In addition, varying the pressure level allows power regulation (Soares,

2015). Table 1.4 compares the advantages and disadvantages of closed and open cycle gas turbines.

Table 1.4 Comparison of the closed cycle a with open cycle gas turbine (Soares, 2015)

Gas turbine types	Advantages	Disadvantages
Closed cycle gas turbine	<ul style="list-style-type: none"> • Good thermal efficiency at low powers • Higher off-design performance • Cycle pressure is higher than atmospheric pressure • Smaller gas turbine size 	<ul style="list-style-type: none"> • Lower performance at the design point
Open cycle gas turbine	<ul style="list-style-type: none"> • Higher performance at the design point 	<ul style="list-style-type: none"> • Lower thermal efficiency at low powers • Lower off-design performance • Cycle pressure cannot be higher than atmospheric pressure • The bigger size of gas turbine

The Electrical generation gas turbine manufacturers include GE, Siemens, Mitsubishi Heavy Industries Ltd (MHI), Mitsui Engineering & Shipbuilding Company Ltd, Pratt & Whitney Canada, Pratt & Whitney Power Systems, ALSTOM, Solar Turbines Inc, Turbomeca, Vericor Power Systems Inc, Rolls-Royce, United Tech.

1.6 Environmental impact

When gas turbine combustion burns fuel with air, it produces byproducts, including oxides of nitrogen (NO_x), unburned hydrocarbons (UHC), carbon monoxide (CO), carbon dioxide (CO₂) and water (H₂O).

The result of high combustion pressure and temperatures of combustion is the oxidation of atmospheric nitrogen. NO_x also combines with UHC to produce toxic smog and CO, which is a toxic gas too. CO₂ and water vapour (H₂O) is produced as a result of the oxidation of hydrogen and carbon. CO₂ is not toxic but is a greenhouse gas and causes global warming (Razak, 2007). The regulations have changed to reduce greenhouse gases emission, and different technologies have recently been developed to avoid byproduct emission recently.

Zero Emission Power Plants (ZEPP) are the solution to produce energy from fossil fuels without carbon dioxide emission. There are many technologies related to these types of power plants (Foy and Yantovski, 2006). The ZEPP power plant needs to use Carbon Capture & Storage (CCS) technologies.

The carbon capture and storage (CCS) technologies, however, have been developed to minimize the CO₂ emission to the atmosphere. Three main capture technologies (pre-combustion, post-combustion and oxyfuel combustion) have been mainly developed for solid fuels (e.g., coal, biomass) combustion systems. However, there are many gas-fired power plants and industrial processes burning natural gas as a cleaner fuel. Although gas-fired plants emit less CO₂ but still to achieve the environmental goals of the Paris Agreement (Barston, 2019), it is essential to develop CCS technologies for the growing gas-fired systems.

Among the available technologies, turbine-based oxy-combustion cycles (Oxyturbine cycles) are one of the most suitable carbon capture technologies for gas-fired power plants. In this technology, natural gas is burned with pure oxygen, and temperature moderation is done by flue gas recirculation (FGR) so that the exhaust gas includes mainly CO₂ and water vapour ready for sequestration and storage.

The cost and readiness of capture technologies are important for carbon capture in the industrial process.

The CO₂ exhaust from the industrial process usually requires additional purification before compression, transport and storage. Also, CO₂ exhaust from boilers, turbines,

cement kilns, iron and steel furnaces and direct iron reduction processes require additional technologies to concentrate dilute streams to be economical for transportation and storage.

Carbon separation processes are similar to carbon capture for power plants and include chemical or physical adsorption, absorption, membrane and liquefaction or cryogenic separation. These processes can be divided into three main categories, including pre-combustion, post-combustion and oxyfuel combustion processes (OECD/IEA, 2011).

The increasing concern for climate change has led to global efforts to reduce carbon dioxide (CO₂) in the environment. It appears that by far the largest contribution to the greenhouse effect stems from emissions of carbon dioxide CO₂. A large part of the CO₂ emissions are produced by the combustion of fossil fuels in conventional power plants and industrial processes. However, Carbon Capture and Sequestration (CCS) technologies have been developed to minimise the CO₂ emission to the atmosphere.

Natural gas has the lowest CO₂ emissions per unit of energy of all fossil fuels at about 14 kg CO₂/GJ, compared to oil with about 20 kg CO₂/GJ and coal with about 25 kg CO₂/GJ. Although gas-fired plants emit less CO₂ but still to achieve the environmental goals of the Paris Agreement, it is essential to develop CCS technologies for the growing gas-fired systems. Among the available technologies, turbine-based oxy-combustion cycles (Oxyturbine cycles) are one of the most suitable carbon capture technologies for gas-fired power plants. In this technology, natural gas is burned with pure oxygen, and temperature moderation is done by Flue Gas Recirculation (FGR) so that the exhaust gas includes mainly CO₂ and water vapour ready for sequestration and storage. Recent developments in oxy-combustion technology have reduced the cost of capture and made it competitive with post-combustion technology.

Coal-fired power plants need to either implement costly carbon capture techniques or to switch to gas-fired power plants. Gas-fired power plants are the best replacement for the coal-fired power plant to decrease CO₂ emissions and increase power plant efficiency. The two Oxyturbine power cycles with maximum carbon capture and highest efficiencies were introduced by two companies, CES (Clean Energy System) and NetPower. These two cycles are recently have been developed to the demonstration phase.

Oxy-combustion is a thermodynamic cycle that burns fuel with pure oxygen. In a conventional plant, fuel burns with air which includes a significant amount of N_2 (Scaccabarozzi, Gatti and Martelli, 2017). CO_2 -rich and H_2O -rich are cycle fluids for a recent power cycle.

Oxy-combustion compared with post-combustion and pre-combustion methods have a lower capital cost and higher efficiency, which means lower carbon dioxide penalty. The advantages of Oxyturbine cycles are very low emission of nitrogen oxides, minimum chemical process and the ability to capture nearly 100% of carbon dioxide emissions (Chaudhry *et al.*, 2018). However, the disadvantages of Oxyturbine cycles are a high initial capital cost, ASU energy penalty and difficulties in retrofitting the old plants.

Over the last 30 years, different layouts have been proposed, including the Semi-Closed Oxy-Combustion Combined Cycle (SCOC-CC), the MATIANT cycle, the NetPower cycle, the Graz cycle, and the CES cycle. The SCOC-CC, MATIANT and NetPower cycles with CO_2 working fluid, while the Graz and the CES cycles have H_2O working fluid (Scaccabarozzi, Gatti and Martelli, 2017). In the former case, CO_2 capture is performed simply by splitting a part of the main flow, while in the second case water condensation produces a stream rich in carbon dioxide, which then can be easily captured via partial condensation (however, in both cases, a further purification step may be required depending on CO_2 purity specifications) (Scaccabarozzi, Gatti and Martelli, 2017).

The CES cycle is essentially an internal combustion steam cycle using the injection of steam and liquid water in the combustor to moderate the firing temperature. Pure oxygen is used as an oxygen and natural gas (or other fuels) as fuel. At the exit of the combustor, the mixture of H_2O and CO_2 expands in a turbine (eventually with reheat) and then it is cooled down in a water condenser (Scaccabarozzi, Gatti and Martelli, 2017). A further improvement of the cycle is presented, called Supercritical CES, employing a combustor operating at supercritical steam conditions (Mancuso *et al.*, 2015).

Complete reviews of the available Oxy-combustion cycle options can be found in the recent report published by the International Energy Agency (IEA) Green House Gas program and co-authored by AMEC-Foster Wheeler and Politecnico di Milano (Mancuso *et al.*, 2015).

1.7 Summary

In this chapter, the aim and objectives of the PhD thesis are discussed, then it has an introduction of the gas turbine. There are different types of gas turbines based on the number of the spool. Single shaft gas turbine is the simplest in design, but it has lower efficiency. Dual shaft gas turbines have higher efficiency and large speed range, but it needs more maintenance and complex control. Triple spool gas turbines has higher efficiency and can be used as an aircraft gas turbines, but it needs more maintenance and complex control too. Conventional gas turbines burn fuel with air and produce carbon dioxide as a byproduct. In the end, The byproducts of the gas turbine and the environmental impact are introduced.

Chapter 2: Literature review of Oxyturbine power cycles and gas- CCS Technologies

2.1 Introduction

Oxy-fuel combustion technology is an effective way of capturing CO₂ from power plants and industrial processes while increasing efficiency and reducing the cost. In this technology, the air is replaced with nearly pure oxygen as an oxidizer, the working flow will be enriched with CO₂ and H₂O, and then CO₂ can separate from the water with the condensation method. This has lower power consumption compared to other methods of carbon capture, such as pre-combustion and post-combustion technologies.

The oxy-combustion in gas turbine power plants (Oxyturbine power cycles) is seen as one of the best solutions to capture CO₂ from new and retrofitted gas-fired power stations. Therefore, studies to evaluate cycle configurations and flexibilities, process and performance simulations, sensitivity techno-economic analysis are highly essential to be carried out.

In this chapter, the following oxy-combustion power cycles are introduced, and the operational parameters are presented: SCOC-CC, COOPERATE Cycle, MATIANT, E-MATIANT, CC_MATIANT, Graz and S-Graz cycles, AZEP 85% and 100%, ZEITMOP, ZEITMOP Cycle, COOLCEP-S Cycle, Novel O₂/CO₂ (Cao and Zheng, 2006), NetPower and CES Cycles, then these cycles are modelled with Aspen Plus in next chapter (Chapter 3) based on these operational parameters from this chapter (Chapter 2), and also the simulation results and discussions will be presented in the next chapter (Chapter 3). The natural gas combined cycle with Post-combustion capture (NGCC-PCC or NGCC or CCGT) and Integrated Gasification Combined Cycle (IGCC), as reference cycles, are also investigated in order to compare with these oxy-combustion cycles.

2.2 Main Technologies in CO₂ Capture

The carbon capture and storage are capturing the CO₂ from a by-product of the combustion. The carbon capture technology can be applied for different industries such as power generation, hydrogen production, iron and steel, ammonia production, preparation of fossil fuels and natural gas processing. The carbon needs to transfer to a storage site to store under the ground (Freund, 2005).

The carbon capture technologies can be categorised into three categories (Horlock and Bathie, 2004):

1. Post-combustion capture
2. Pre combustion capture
3. Oxyfuel combustion capture

2.2.1 Post-combustion capture

Post-combustion capture is the process of capture the exhaust of a combustion-based. There are two methods for post-combustion capture, physical or chemical.

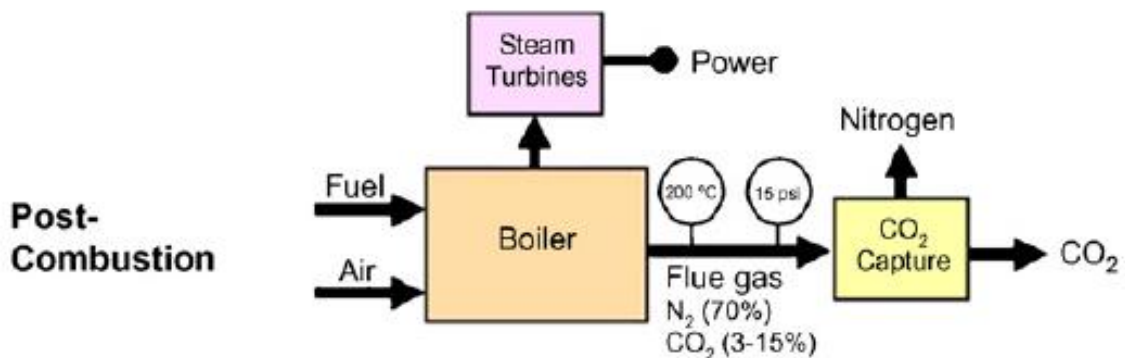


Figure 2.1 Schematic diagram of Post-combustion capture (Ahmad, 2019)

In the conventional power cycle, the fuel burns with air, and the byproduct releases to the environment after expansion in the turbine.

One of the technology to reduce emissions from the power cycle is using post-combustion CO₂ capture (PCC). This technology can be used to retrofit the power plant, and major changes at the power plant are not required. PCC can be used without

a major change in the design of the power plant components, including boiler, steam turbines, and/or gas turbines; however, separation of relatively low concentration of CO₂ from a large amount of nitrogen in the flue gas is one of the main challenges in post-combustion capture. Also, it involves unique challenges to applying carbon capture to various types of flue gas streams. The flue gases from coal plants include a CO₂ concentration of 12-15% in flue gases in comparison with flue gases from natural gas combined cycle (NGCC) plants typically contain ~4% CO₂ by volume (U.S. Department of Energy/NETL, 2019). This technology can be used with a limited investment in a new power plant, and it would be a quick response to avoid carbon emissions in a power plant (Feron, 2016).

The following integration with the conventional power plant is needed for retrofitting PCC for power plant (Feron, 2016):

- Supplying electricity to pumps and fans.
- Power plant control system for PCC.
- Providing heat for the capture process from the steam cycle if available.
- Flue gas path redesign for PCC.

However, it may have physical limitations to implement PCC and may need to redesign some parts, including redesign the HEN network (U.S. Department of Energy/NETL, 2019), the very last blade of the turbines need to be reinforce for retrofitting PPC to existing power plant because of floating pressure (Gibbins *et al.*, 2011), and old power plants are not suitable for retrofitting, so the new generation power plant is a more likely candidate for it (Feron, 2016).

2.2.1.1 Physical Absorption

In the physical absorption, this process is based on Henry's Law and the carbon dioxide is absorbed at low temperature and high pressure and then desorbed at high temperature and low pressure (Yu, Huang and Tan, 2012). The physical solvent absorbed CO₂ in the high pressure gas liquid contactor and then CO₂ flashed out in the low pressure flash tank. The advantage of physical absorption is that it captures CO₂ without any chemical reaction. Physical absorption technology has been widely

used in several industrial sectors with high CO₂ contents including nature gas, synthesis gas and hydrogen production (Yu, Huang and Tan, 2012).

2.2.1.2 Selective exhaust gas recirculation (S-EGR) method

Membranes have become more attractive in carbon capture technologies because they have a low environmental impact, low cost and high energy efficiency. Different types of membranes are organic polymers, common polymers and fixed-site carrier (FSC) nanocomposite (He, 2018). Post-combustion capture from the exhaust gas is complicated because of the low concentration of CO₂ in the flue gas. One of the methods to increase the performance of post-combustion capture is to increase CO₂ concentration in the flue gas.

A selective exhaust gas recycles (S-EGR) method can be used to increase the concentration of CO₂ before post-combustion capture. The S-EGR can reduce the minimum energy to capture CO₂ up to 40% (Merkel *et al.*, 2013).

In the S-EGR process, the combustion air is used to sweep CO₂ from a stream in a countercurrent membrane unit. The membrane strips CO₂ from flue gas and recycle it back to the power cycle (Merkel *et al.*, 2013). Figure 2.2 shows the schematic diagram of NGCC with S-EGR and CO₂ capture unit. The membrane increases CO₂ concentration in the working flow, and the capture unit can work in the higher performance and lower energy consumption.

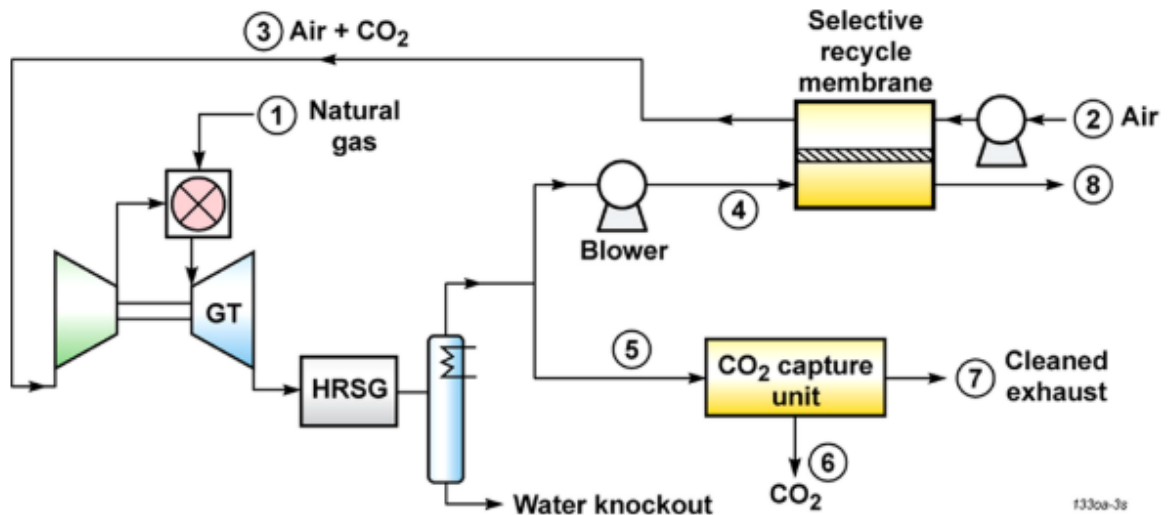


Figure 2.2 Schematic diagram of NGCC with S-EGR and CO₂ capture unit (Merkel *et al.*, 2013)

Air (2) sweeps CO₂ through the membrane, and the mixture of Air+CO₂ (3) is recycled back to the compressor and is burned with natural gas (1) in the combustion chamber. Working flow with a high concentration of CO₂ is separated into stream (4) and stream (5). Stream (4) enters the selective recycle membrane, CO₂ is absorbed in it, and the remaining byproduct (8) is released to the atmosphere. Stream (5) enters the CO₂ capture unit. CO₂ (6) is separated, and the remaining byproduct is released into the atmosphere as a cleaned exhaust (7).

One of the membranes that can be used for S-EGR method is Polydimethylsiloxane (PDMS). It includes a high-molecular polymer with semi-inorganic and semi-organic structures and can have the characteristics of both organic polymer and inorganic polymer. It has low transmission resistance and uses the common material of pervaporation membranes (Zhimin *et al.*, 2017).

Darabkhani *et al.* (2018) has investigated the selectivity/permeability of the PDMS membrane module in the S-EGR method (Darabkhani *et al.*, 2018). The performance of the 100 kW pilot-scale rig was studied by exploring the operating conditions of the PDMS membrane.

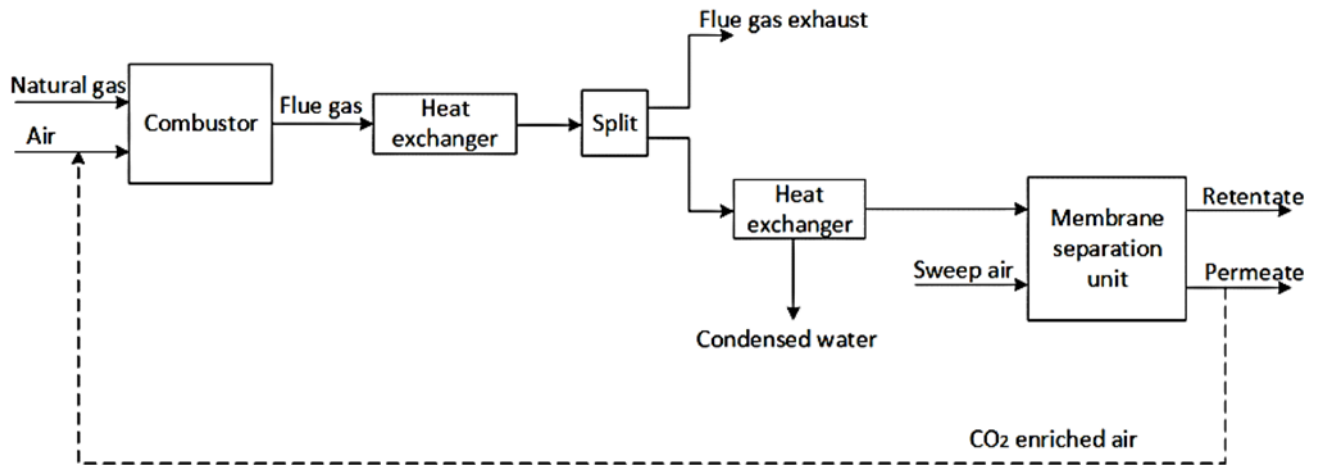


Figure 2.3 Schematic diagram of 100 kW pilot scale S-EGR with PDMS membrane (Russo *et al.*, 2018)

2.2.1.3 Chemical Absorption - Amine Absorption/Stripping Technology

The chemical absorption process includes absorber and stripper. The flue gas contains CO_2 that entered the absorber from the bottom and is contacted to absorbent, then CO_2 -rich absorbent flows go into a stripper for the thermal regeneration process (Yu, Huang and Tan, 2012).

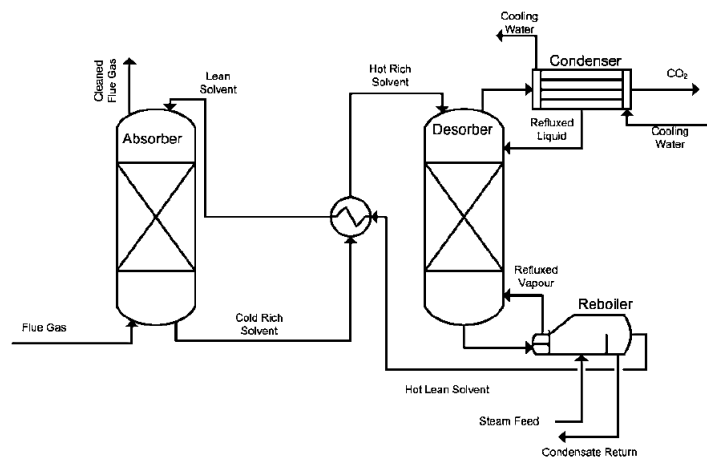


Figure 2.4 Process Flow Diagram of a basic chemical absorption process for amine-based CO_2 capture (MacDowell *et al.*, 2010)

2.2.1.4 Physical Adsorbent

Adsorption process are different from the absorption process; in the absorption process, molecules form fluid transfer to a solid surface, which produces a film of the adsorbate on the surface of the adsorbent. In the reversible process, which is called desorption, the molecule is separated from the surface, but in the absorption process, the adsorbate is dissolved (Artioli, 2008).

One of the carbonaceous adsorption, which is used widely, is activated carbon. It is used to capture carbon dioxide with low sensitivity to moisture, low cost and high thermal stability (Yu, Huang and Tan, 2012).

2.2.1.5 Chemical Adsorbent (Amine-Based)

In the chemical adsorption, acidic CO₂ molecules interact with the surface of the adsorbent with the formation of covalent bonding such as an amine (basic organic group).

Amine adsorbents are used widely, and it has low heat capacity and needs low heat for regeneration, but it has a high cost and low adsorption capacity of CO₂.

2.2.2 Pre-combustion capture

The pre-combustion capture is capturing CO₂ before the combustion takes place. The solid fossil fuel is gasified, or gaseous fuel is reformed in the reforming processes to produce syngas, and then the CO₂ is separated. The remaining exhaust includes hydrogen with a diluent such as steam and nitrogen.

In the gasification process, the syngas can be produced with partial oxidation of a carbon source (natural gas, biomass, coal). The by-products of syngas with oxygen are hydrogen, carbon monoxide, and carbon dioxide, or by-products can include nitrogen if the gasification is with air. There are different methods to remove CO₂ from syngas and produce hydrogen for power plants (MTR, 2018).

2.2.2.1 Chemical process

The integrated gasification combined cycle (IGCC) is one of the pre-combustion sample cycles, and this method is widely used for coal power plants (Nord, Anantharaman and Bolland, 2009). As shown in Figure 1.4, pre-combustion capture in both coal and natural gas applications is the same in principle; the overall plant can be divided into five different sections (Jansen *et al.*, 2015):

- Syngas island
- CO₂ separation
- CO₂ compression
- Power island
- Oxygen island (optional for NG cases)

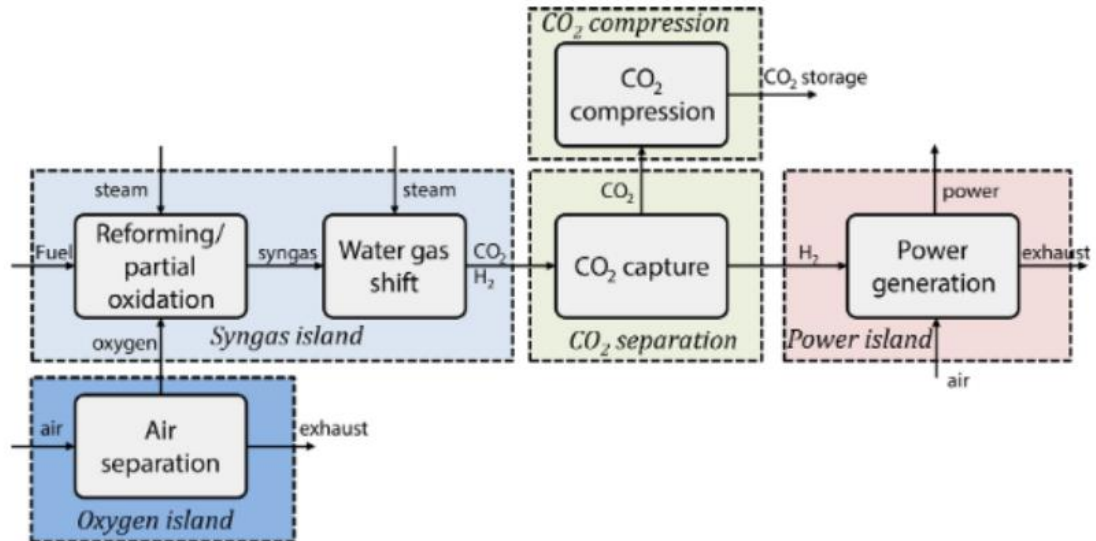


Figure 2.5 Schematic diagram of pre-combustion capture (Jansen *et al.*, 2015)

2.2.2.2 Membrane

The membranes can be used for the separation of CO_2 from syngas. The first commercially available membrane for syngas is MTR's unique Polaris membrane. It can be used to recover and purify CO_2 in the sequestration process.

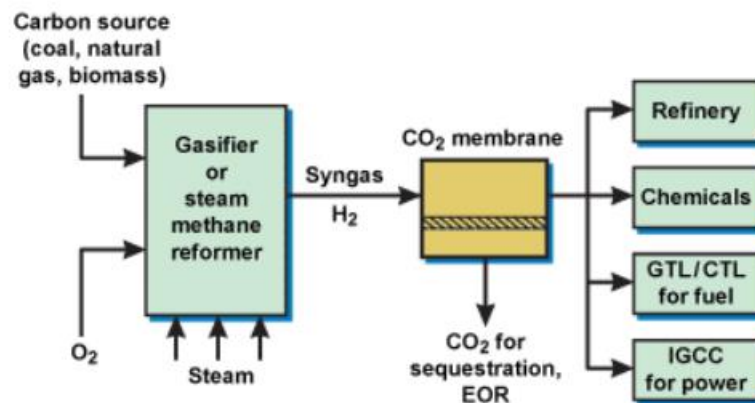


Figure 2.6 Schematic diagram of using membrane for pre-combustion capture (MTR, 2018)

2.2.2.3 *Hydrogen production technologies*

H₂ is the most common element in the world, but it doesn't freely exist in nature, and it combines with other elements to produce various components, including water (H₂O), hydrocarbons (C_nH_m) and Carbohydrates (C_m(H₂O)_n) (Folkson, 2014).

The hydrogen production process is the conversion of hydrogen-containing materials from fossil fuel, including methanol, gasoline, hydrocarbons, to the hydrogen-rich gas stream.

Hydrogen production from natural gas is the most popular commercial hydrogen production technology, and another fossil fuel contains more sulfur, and it requires a significant task to remove them; hence it consumes more energy and capital cost.

There are different technologies for hydrogen gas production as below:

- A. Steam methane reforming (SMR).
- B. Autothermal reforming (ATR).
- C. Vacuum pressure swing adsorption (VPSA).
- D. Renewable sources.

However, these technologies produce CO emission, and a chemical reactor is required to convert CO into CO₂, including preferential oxidation (PrOX) and water-gas shift (WGS) (Kalamaras *et al.*, 2013).

Another hydrogen production technology is Partial Oxidation (POX) and Catalytic Partial Oxidation (CPOX) of hydrocarbons. It is used for automobile fuel cells and other commercial applications.

2.2.2.3.1 *Steam Methane Reforming (SMR)*

One of the commercial technologies to produce H₂ is steam methane reforming (SMR). This process is less expensive and is widely used in industry. This technology has high efficiency and lower production and operational costs.

The process includes two reactions, namely;

- A. Reaction at the 700-1100 °C temperature with a metal catalyst to produce CO and H₂.

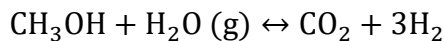
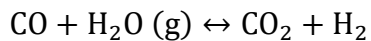
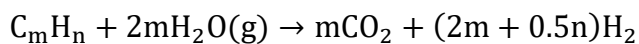
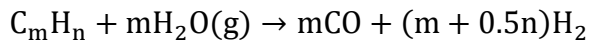
In this stage, the hydrocarbon and steam are mixed and then fed in the tubular catalytic reactor. The byproduct is syngas (H₂/CO gas mixture) with a low mole fraction of CO₂.

B. Lower temperature reaction to produce CO₂ and H₂.

In the second stage, the cooled syngas byproduct is fed into the CO catalyst converter. The catalyst converts carbon monoxide (CO) into carbon dioxide (CO₂) and hydrogen (H₂). The catalysts can be nonprecious metals, i.e. nickel or precious metals from Group VIII elements, i.e. platinum or rhodium.

The network of reforming reactions for hydrocarbons and methanol feedstocks are as Equation 2-1:

Equation 2-1



The hydrogen production heat efficiency by the SMR is around 70–85% for the methane process on an industrial scale. The disadvantage of SMR is the high production of CO₂, i.e. 7.05 kg CO₂/kg H₂ (Kalamaras *et al.*, 2013).

2.2.2.3.2 *Autothermal Reforming (ATR)*

Autothermal reforming (ATR) is one of the hydrogen production technology, as shown in Figure 2.7. The reaction heat is produced within the reaction vessel the contrary to a Steam Methane Reforming SMR plant which is required an external furnace. The Air Separation Unit (ASU) is used to produce oxygen to avoid the contamination of hydrogen with nitrogen. The syngas is moved with steam, and then it is purified in a Pressure Swing Absorber (PSA). The flue gas of PSA is burnt in the small fired heater, and the generated heat is recovered by the feed streams and secures some additional heat energy to the co-generation section.

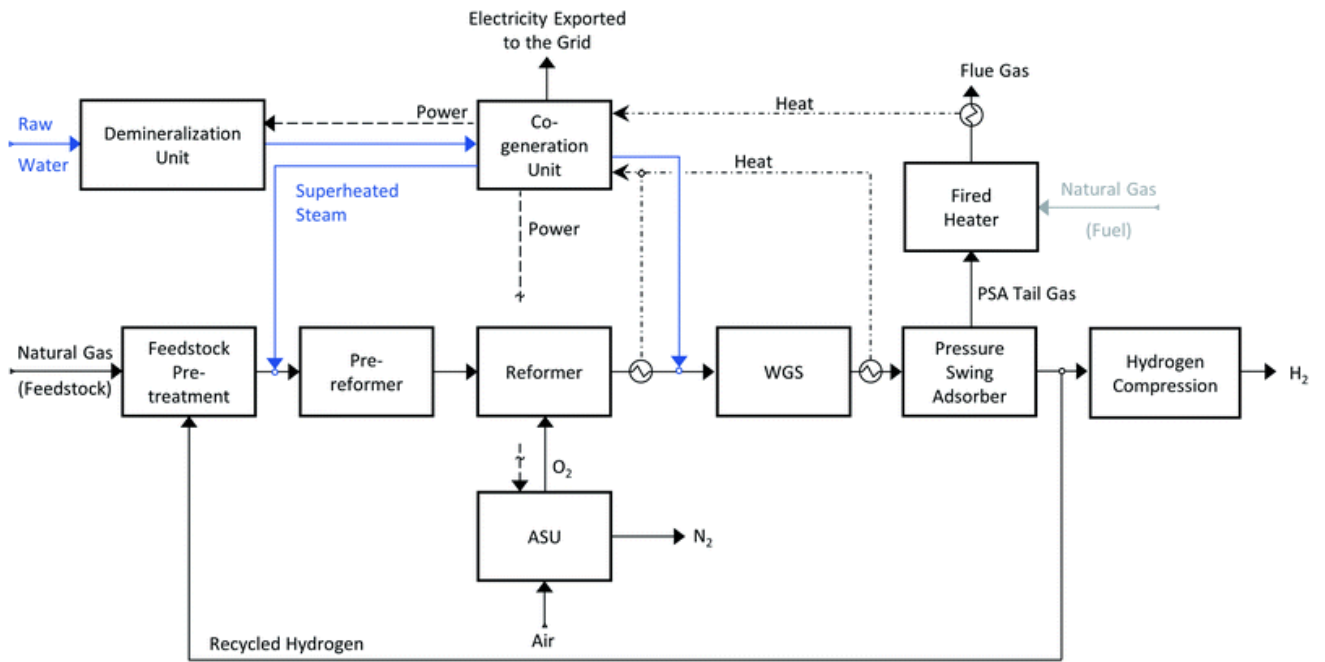


Figure 2.7 Schematic diagram of Autothermal Reforming (AR) (Antonini *et al.*, 2020)

The advantage of ART is the heating source; it does not require external heat and is less expensive than Steam Methane Reformer (SMR). Steam Methane Reforming is an endothermic process, and this reaction needs to take energy. Hence external heat source is required, but Autothermal reforming is the combination of endothermic reforming (demanding energy through steam reforming) and exothermic reforming (releasing energy through partial oxidation reactions). The second advantage of ART is shutting down and starting very fast, with a large amount of hydrogen production (Kalamaras *et al.*, 2013).

2.2.2.3.3 Vacuum pressure swing adsorption (VPSA) cycle

Vacuum pressure swing adsorption (VPSA) is shown in Figure 2.8. The hydrogen purification and CO₂ capture are combined in one process. This cycle includes a high-pressure adsorption stage (ads) and produces high purity H₂. The captured CO₂ is dehydrated and compressed, and flue gas is burned in the furnace (Antonini *et al.*, 2020). Another advantage of the VPSA unit is the flexibility of retrofitting existing hydrogen production equipment and partly uses it for H₂ production.

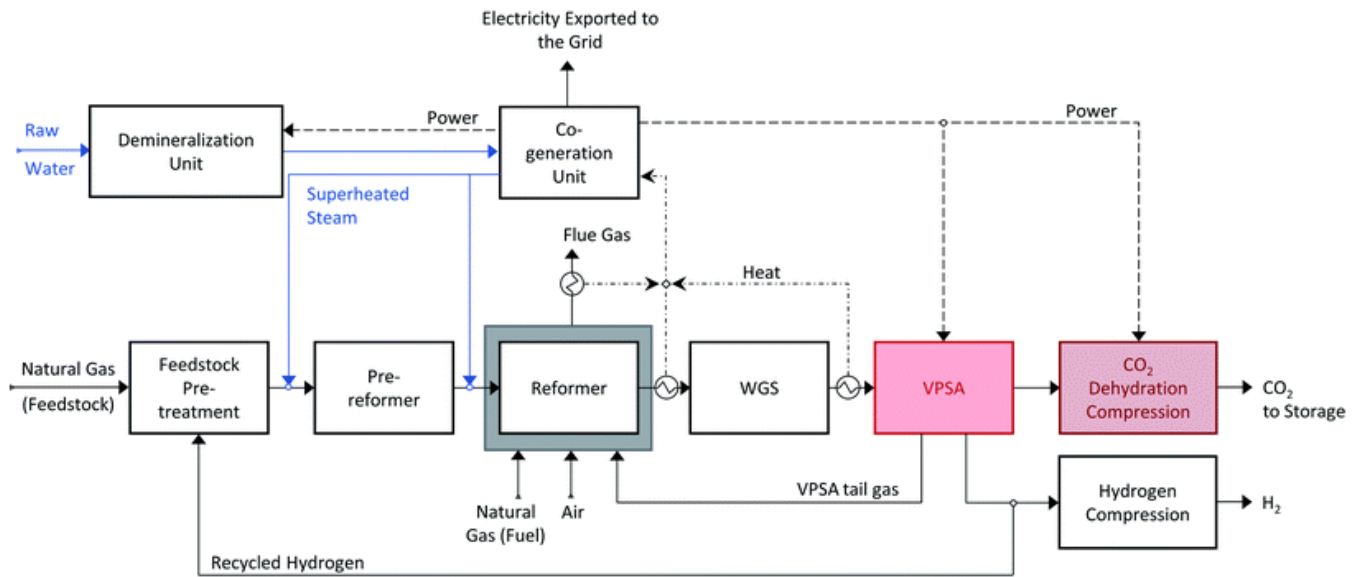
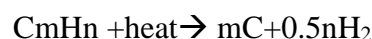


Figure 2.8 Schematic diagram of VPSA hydrogen production (Antonini *et al.*, 2020)

2.2.2.3.4 Renewable sources

There are renewable sources to produce hydrogen, which includes Biomass gasification, Pyrolysis, Aqueous Phase Reforming, Electrolysis, Photoelectrolysis, Thermochemical Water Splitting. In biomass gasification technology, renewable organic can be substituted for fossil fuel in gasification and hydrogen production.

Pyrolysis is another promising technology for hydrogen production. The raw organic material is heated up to 500-900 °C at 0.1-0.5 MPa pressure for the gasification process. This process is without air, oxygen or water; hence the carbon dioxide or carbon monoxide cannot be produced. The other equipment for the separation of carbon dioxide is eliminated in the process. The advantages of this process are relative simplicity, compactness, fuel flexibility and clean carbon product and reduction of CO₂ emission. The reaction formula is as below:



Aqueous Phase Reforming (APR) is one of the hydrogen production technology. The hydrogen is produced from biomass with oxygenated compounds such as sugar, glycerol, and sugar alcohols. The reaction temperature is 500K using a catalyst such

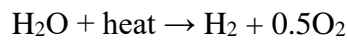
as a Pt-based catalyst. In this process, about 50% is hydrogen and the remaining is gaseous alkanes and carbon dioxide (Kaur *et al.*, 2019).

The low temperatures reaction in this process minimized undesirable decomposition reactions (Kalamaras *et al.*, 2013).

Electrolysis is another capable technology for hydrogen production. In water electrolysis, water is breaking into hydrogen and oxygen and already begin to be used commercially.

Photoelectrolysis is another renewable technology for hydrogen production with high efficiency and lower cost, and it is in the experimental development phase. In this process, a solar panel produces the necessary voltage for the direct decomposition of the water molecule into oxygen and hydrogen.

Thermochemical water splitting is another hydrogen production; in this process, heat is used to decompose water into hydrogen and oxygen as below chemical reaction.



One of the struggles of this process is the separation of H₂ and O₂ to avoid explosive mixture (Kalamaras *et al.*, 2013).

2.2.3 Oxy-fuel combustion capture

Oxy-fuel combustion technologies is an effective way to increase CO₂ capture ability while increasing efficiency and reducing the cost. In this technology, the air is replaced with nearly pure oxygen as an oxidiser (Climent Barba *et al.*, 2016a). The working flow will be enriched with CO₂ and H₂O, and then CO₂ can separate from the water with condensation method, which has lower power consumption compared with methods of carbon capture such as pre-combustion and post-combustion technology.

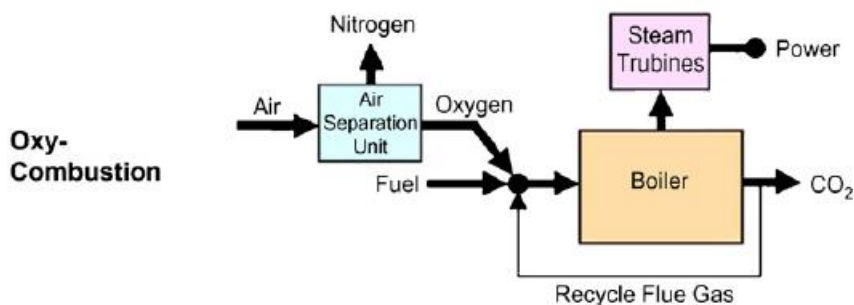


Figure 2.9 Schematic diagram of oxy-combustion capture

As shown in Figure 2.9, in the oxy-combustion process, fuel burns with pure oxygen instead of air and the by-products of combustion are CO₂ and H₂O.

The high purity oxygen needs to be mixed with the recycled flue gas (RFG) before combustion to provide a similar condition of air fired configuration for combustion (Figueroa *et al.*, 2008).

The CO₂ from the oxy-combustion stream can be separated by condensing water vapour. In the oxy-combustion process, the separation from CO₂ is very easy, but the problem moves to the Air Separation Unit (ASU) or other oxygen separation unit; this part consumes a large amount of energy which results in an efficiency penalty. (Matteo and Romano, 2019).

The oxy-combustion Adiabatic Flame Temperature (AFT) is higher than air combustion, and the recycled flue gas is required to reduce the temperature. Also, the furnace has higher gas emissivity because of the high concentration of CO₂ and H₂O.

Furthermore, the volume of the recycled gas in the oxy-combustion cycle is less than the air combustion cycle, and the density of the recycle flue is higher; the molecular weight of CO₂ is 44, but N₂ is 28 (Wall, 2007).

The fuel and pure oxygen of oxy-combustion need to be near stoichiometric for the best adjustment. The oxy-combustion allows the smaller size of equipment without a controller for NO_x, and the byproducts are mainly CO₂ and water. CO₂ can be easily separated from water by condensing and cooling process.

The oxy-combustion cycle is not entirely zero-emission, and it is near-zero-emission. Because some part of water vapour is recycled and the extra water vapour emits into the atmosphere, furthermore during the purification process of carbon dioxide, the extra contaminant is emitted into the atmosphere by flue gas.

The various zero-emission cycles for both water and CO₂ recirculation was presented by Yantovsky and Degtiarev (1993), and the results indicate recirculation of CO₂ has a much higher efficiency than H₂O recirculation (Manso, 2013).

2.2.3.1 Oxy-combustion classification

The oxy-combustion cycle can be categorized into five levels, as shown in Table 2.1:

1. Level 1 (Oxy-combustion oxygen production type)

The different oxy-combustion methods can be classified according to five levels of technologies. The first level is the separation of the oxygen if it is separated to an external device, like the cryogenics distillation, or it is separated inside the cycle. The internal separation can be done using metal oxide as an oxygen carrier or oxygen selective metal, which is loaded and regenerated in a cycled operation (Manso, 2013).

2. Level 2 (Oxy-combustion cycle type)

The second level refers to the main cycle type, a Rankine cycle or a Brayton cycle. For the Brayton cycle, the working fluid is always in a gaseous estate along with the expansion, compression, cooling, heat addition and rejection. On the other hand, in the Rankine cycle, the working fluid changes from the gaseous estate in the expansion to a liquid state in the compression along with a closed-loop. Normally the Rankine cycle uses water as working fluid and is used in coal-fired power plants, and the Brayton is used in conventional gas turbines cycles. Oxy-combustion cycles can use the pure Brayton cycle or the pure Rankine cycle, or a mixture of both cycles (Manso, 2013).

3. Level 3 (Oxy-combustion recycled flue gas composition)

The third level refers to the composition of the flue gas that is recycled for the control of the combustion temperature and the cool of the turbine in the gas turbine cycles. There are three possibilities for recycled flue gas. It can be pure water that has been condensed and separated from the flue gas, the pure CO₂ after the separation of the water or the flue gas without separation, water and CO₂ together. At that level, a separation can be made between the internally fired power cycles, which use the flue gas as a working fluid and the externally fired power cycles, which uses the flue gas to heat an external working fluid (Manso, 2013).

4. Level 4 (Oxy-combustion heat exchanger type)

Oxy combustion cycles have different types of heat exchanger to recover energy and increase efficiency, including network heat exchangers, printed circuit heat exchangers. NetPower cycle uses printed circuit heat exchanger and CES cycle tube heat exchanger.

5. Level 5 (Oxy-combustion CO₂ Compression and Purification Unit (CPU) type)

The CO₂ purification and compression unit consist of the following main sections:

- Raw gas compression.
- TSA unit.
- Auto-refrigerated Inerts Removal, including distillation column to meet the required oxygen specification in the CO₂ product.
- Final compression up to 110 bar (IEAGHG, 2015).

Table 2.1 Classification of oxy-combustion cycle

		Level 1 (Air separation)	Level 2 (Main cycle type)	Level 3 (Working fluid)	Level 4 (Heat Exchanger)	Level 5 (CPU)	Example
Oxyfuel power cycle	External Air Separation Unit		Bryton cycle	CO ₂	Plate heat exchanger	Compression and Purification Unit (CPU)	SCOC-GT E-Matiant CC- Matiant
			Mixed Bryton/Rankine cycle	CO ₂			Original MATiant cycle
				CO ₂ /H ₂ O			Graz cycle
			Rankine cycle	CO ₂ /H ₂ O			Atmospheric fired boilers
				H ₂ O			CES cycle
			Internal air separation Unit	Continuous operation for air separation			Bryton cycle
	Rankine cycle	CO ₂ /H ₂ O			Printed circuit heat exchanger	CLC integrated with CO ₂ Bryton cycle	
	Batch operation for air separation	Rankine cycle		CO ₂ /H ₂ O			CLC integrated with Rankine cycle
							CAR

2.2.4 CO₂ Capture technology conclusion

Each carbon capture method has an advantage and disadvantage in comparison with other carbon capture methods; Table 2.2 shows a comparison of post-combustion, pre-combustion, oxy-combustion technologies.

Table 2.2 The advantages and disadvantages of each technology (Figueroa *et al.*, 2008)

Capture Technologies	Advantages	Barriers to implementation
Post-Combustion	<ul style="list-style-type: none"> • It can be used for the majority of existing fossil fuel power plants • Option for retrofit technology 	<ul style="list-style-type: none"> • Dilute of CO₂ in flue gas • At ambient pressure of flue gas • Low CO₂ partial pressure causes lower performance or circulation volume and is not sufficiently high capture levels • Low CO₂ partial pressure causes lower pressure compared to sequestration requirements
Pre-Combustion	<ul style="list-style-type: none"> • Concentrated CO₂ in the synthesis gas • High-pressure synthesis gas increasing the driving force for separation • More technology is available for high-pressure separation <p>Reduction of compression cost</p> <ul style="list-style-type: none"> • Produced hydrogen can be store • Produced hydrogen can be used for different applications 	<ul style="list-style-type: none"> • The technology is applicable for a new plant; there are not many gasification plants in operations • Availability of equipment for commercial application • Cost of equipment • Extensive maintenance requirement
Oxy-combustion	<ul style="list-style-type: none"> • Very high CO₂ concentration in the flue gas • Retrofit technology option • Repowering technology option • Higher efficiency • Compact size than other technology • Reduction of electricity production cost with the new technology of oxygen production • It can be used for different sectors • Technology development causes reducing capital and operational cost 	<ul style="list-style-type: none"> • Cost of the large cryogenic air separation unit • Cooldown the recycled CO₂ to reduce the temperature of combustion, decreases cycle efficiency, and need more auxiliary equipment.

Post-combustion capture needs to develop technologies of materials for high-efficiency steam cycles, and chemical or physical solvent or different post-combustion techniques and it increases the electricity cost (Wall, 2007). The main disadvantage of the post-combustion chapter is the carbon capture at atmospheric pressure with quite big equipment. The reason for that is the high flue gas flowrate and low partial pressure of CO₂, so the process has low energy efficiency (RICARDO LLORENTE MANSO, 2013). Pre-combustion capture needs to develop technologies for oxygen production and longer life refractories (Wall, 2007).

The oxy-combustion power plant has a lower cost for capture CO₂ in comparison to other technologies because of the high concentration of CO₂ and low fuel gas volume; however, the cost of flue gas recirculation and air separation unit increase electricity cost (Acharya et al., 2005). In addition, combustion with oxygen has different characteristics than combustion with air, and it needs to redesign. Also, other equipment needs developed technologies, and it increases the cost of electricity. The cost of the electricity will be reduced by developing oxy-combustion power cycle equipment in the future (Matteo and Romano, 2019). Table 2.3 compares some of the characteristics of the PCC, IGCC-CCS and Oxy-fuel power plant.

Table 2.3 Comparison of different carbon capture technologies (Wall, 2007)

Technology	Combustion related			Technology related
	Fuel conversion	Emissions	Other	
PCC		NO _x , SO _x and Hg removal, consistent with solvent tolerance		Materials for high efficiency (temperature) steam cycles. CO ₂ capture by improved chemical and physical solvents, or by membrane and absorption techniques. Reduced energy for CO ₂ capture
IGCC-CCS	Improve and understand coal (particularly char) conversion	Ultra-low NO _x burners for H ₂ and syngas	Slag flow prediction	Oxygen production (with higher efficiency and lower cost, perhaps by ion transport and other novel systems). Longer life refractories. System design specific to local conditions and regulatory environment
Oxyf	Combustion characterisation in O ₂ /RFG environment	NO _x , SO _x , Hg and need for removal Burner development for ignition, avoiding external recirculation, and NO _x reduction	Deposition control of gas coolers Gas turbines for H ₂ and capable of operating at the higher pressures of IGCC-CCS gasifiers Radiative heat transfer prediction Corrosion and ash deposition Operability and dynamic behaviour Furnace design for reduced recycle CFD modeling of furnace design	Materials for high efficiency (as for PCC) Oxygen production (as for IGCC) Cycle optimisation and system thermal integration

2.3 Oxygen production and Air Separation Units (ASU)

The oxy-combustion cycle needs pure oxygen to burn with fuel. This producing oxygen is very energy-intensive and needs to develop to reduce the cost of oxy-combustion by reducing the cost of oxygen production (Figueroa *et al.*, 2008).

2.3.1 Cryogenic Air Separation Unit (ASU)

One of the economic air separation units is a cryogenic distillation of air. The purity of oxygen is 95-99%. The byproducts of the Air Separation Unit are nitrogen and argon with high purity. This nitrogen can be used in the gasifier or steam turbine to improve overall efficiency. The oxygen, nitrogen and argon have different boiling points; the boiling points at 1 atm are respectively -182.9, -195.8 and -185.9 °C.

In the air separation process, CO₂ and water need to be removed before the distillation of oxygen and nitrogen, the solid adsorbent pellets like alumina or molecular sieves can be used to remove them. When a high volume of oxygen is needed, deciding on cryogenic conditions is the best choice (Ham, 2011).

In the cryogenic ASU, the air is compressed, and water, carbon dioxide and other contaminants are removed from it. The output flue includes nitrogen, argon and oxygen and some small amount of other gases. Then the cleaned air enters the main heat exchanger (MHE) and is cooled to cryogenic conditions. The output of MHE enters the distillation unit to separate the air into a nitrogen stream, oxygen stream, and argon stream.

Finlay, The separated stream enters MHE to absorb heat from input air then compressed or pumped to the required pressure for downstream (Ham, 2011).

There are many different types of ASU; the difference is refrigeration, pressurizing, operating pressure and distillation section. The configuration in distillation can be two or three; it is dependent on the required output products.

Figure 2.10 shows a sample Air Separation Unit (ASU) with two-column distillation and compressor oxygen in the gaseous state. The refrigeration system is Main Heat Exchanger; the air is cooled down in the Main Heat Exchanger.

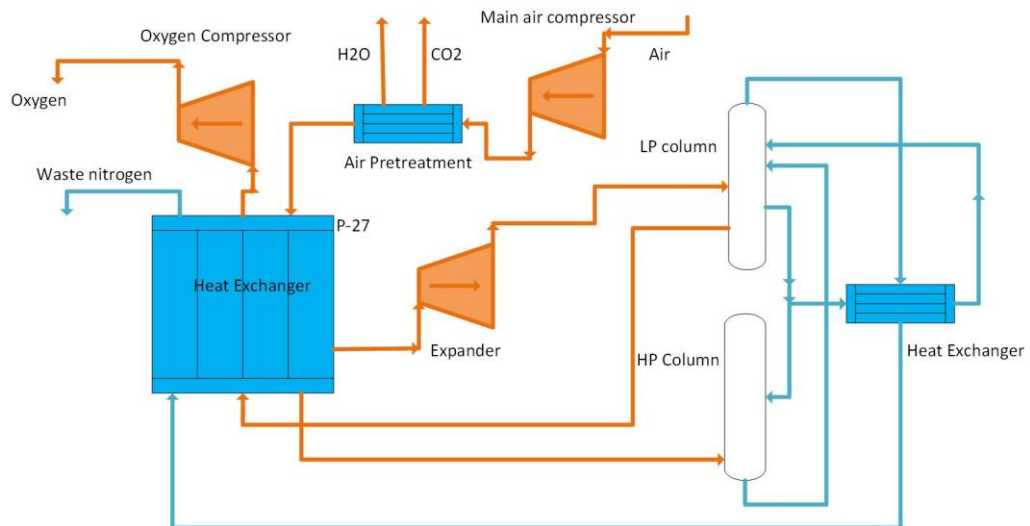


Figure 2.10 A cryogenic air separation unit with two-column distillation and compression of oxygen in a gaseous state (Manso and Nord, 2020)

Air is filtered and compressed up to 4-6 bar, then the output flue of the compressor is cooled. So in the air pretreatment unit, the water and CO₂ are extracted from the air. The clean air entered Main Heat Exchanger (MHE) and cooled up to the dew point, and is fed to high-Pressure column.

The pure vapour of nitrogen is separated from the liquid and goes to the top of the High Presser column and enters the low-pressure column, and then recycled. The liquid from the bottom of the column is recycled to the middle of a low-pressure column for the second distillation. The oxygen is extracted from the bottom of the LP column, and nitrogen is extracted from the top of the LP column.

The final products of the column enter again into the MHE to absorb the heat and increase the temperature before delivering downstream. The best cryogenic ASU can produce 3000 and 5000 ton O₂/day with a purity of 95% to 99.6% (Manso and Nord, 2020).

In other to receive oxygen with more purity, we need more stages, more energy and more drop pressure and energy waste. The high-pressure column is 4 to 7 bar, but the output oxygen stream from a low-pressure column is a little more than atmospheric pressure. The oxygen-based on the estate can be compressed to 75 bar before a feed to the power plant. In the power plant, the pressure of the oxygen can be adjusted based on the requirement (Manso and Nord, 2020).

2.3.1.1 Pilot-scale

Many oxy-combustion power plants have used the commercial supplier to secure the oxygen instead of producing oxygen from ASU in the plant. The small scale of ASU is impractical, but the large scale technology has been developed. However, Schwarze Pumpe pilot oxy-combustion plant with 30 MWth capacity has an ASU, and it shows how this unit can be coupled to the operation of the plant. Callide pilot oxy-combustion power plant with 100 MWth capacity has two ASU trains (Lockwood, 2014).

2.3.1.2 ASU development

The development of the oxy-combustion power cycle forces ASU manufacturers to develop technology and increase efficiency. Figure 2.11 shows the improvement in the bar chart. The cost of oxygen production was 200kWh/t O₂ in 2000, and it was developed by the industrial gas provider including Air Liquide, Air Products, Linde, and Praxair to produce 160 kWh/t O₂ with the heat integration and then optimized to 140–150 kWh/t in the next few years (Lockwood, 2014).

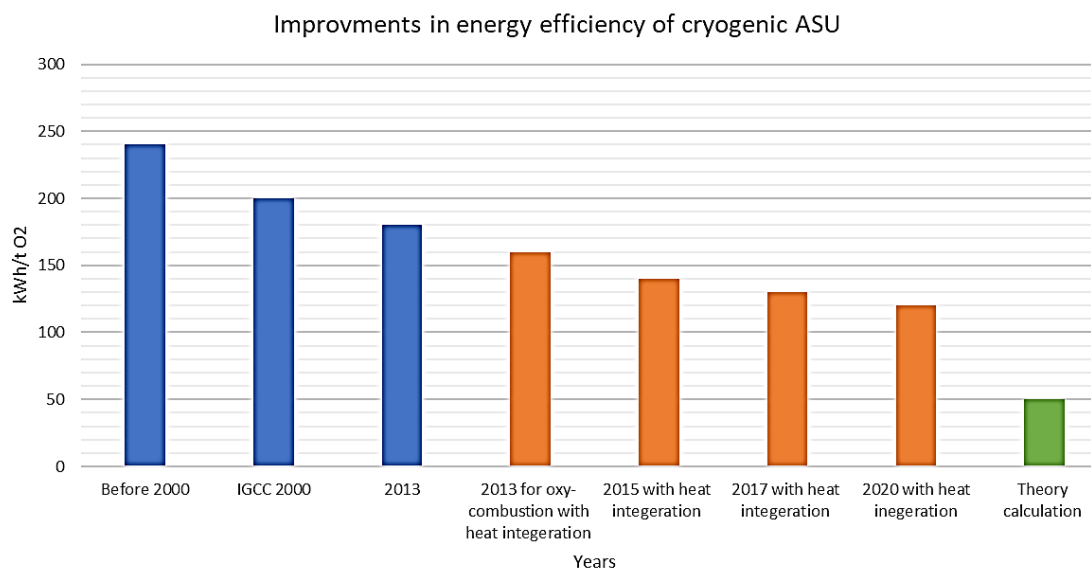


Figure 2.11 ASU development

Net efficiency can be higher with heat integration in the design of the CO₂ CPU. 140 kWh/t with heat integration was achieved in 2015, and 120 kWh/t was achieved

with further development by 2020. The energy consumption is expected to get reduced more and will be closer to the actual overall energy of separation. The theoretical energy consumption of an air separation unit is calculated 50 kWh/t (Perrin *et al.*, 2013). It can be closer to the theoretical energy consumption by the development and arrangement of combining compressor and waste heat recovery (Aneke and Wang, 2015).

2.3.2 Non-cryogenic Air Separation Unit (ASU)

The cryogenic ASU consume high energy and has a negative effect on the performance and efficiency of the power plant. There are several types of non-cryogenic air separation units:

2.3.2.1 Adsorption

In the adsorption process, synthetic or natural materials are used to adsorb nitrogen (Smith and Klosek, 2001). The adsorption process can be Pressure Swing Adsorption (PSA) or Temperature Swing Operation (TSA), but most of the commercial applicants use the PSA because longer cycle times are needed for TSA to heat up the bed of solid particles during regeneration of sorbent (Kelly (Kailai) Thambimuthu (Australia, 2005).

2.3.2.2 Pressure Swing Adsorption (PSA)

Pressure Swing Adsorption (PSA) process is based on the adsorptive separation of cycle character. The PSA cycles consist of two basic steps: adsorption and desorption.

In the adsorption process, the adsorbable elements are selectively removed from the gas. In the desorption (regeneration), the elements are removed from the adsorbent so that it is ready for the next cycle.

The main principle of the PSA process is to reduce pressure by less absorbable gas to clean the adsorbent bed, and then it can be prepared for the next cycle (Kelly (Kailai) Thambimuthu (Australia, 2005).

For oxygen production, as shown in Figure 2.12, the high-pressure air is passed through the vessel containing an adsorbent bed; this bed can attract nitrogen more than oxygen. Hence part or all of the nitrogen stays on the adsorbent bed, and the remaining oxygen enrichment gas comes out from the vessel. When the adsorbent bed reach the maximum capacity to adsorb nitrogen, it can be contacted by low-pressure gas to release the adsorbed nitrogen, and the bed is regenerated to the next cycle (Nexant, 2010).

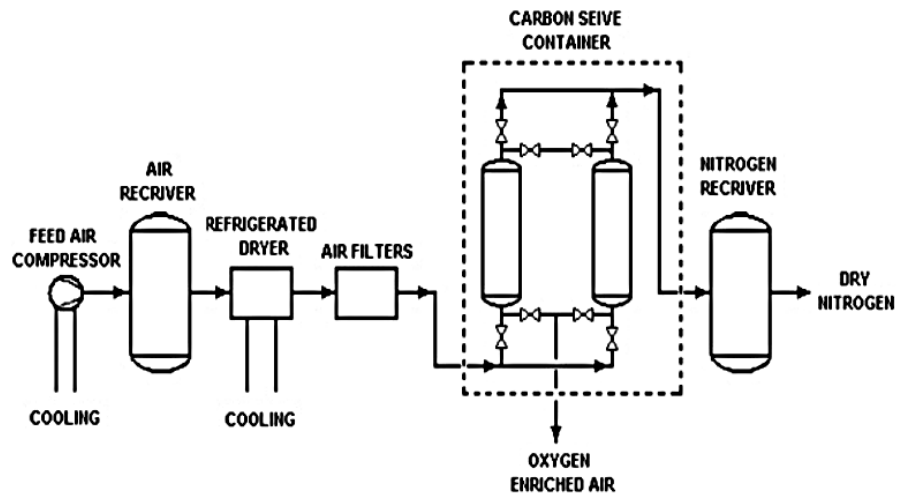


Figure 2.12 Pressure Swing Adsorption (Kwon *et al.*, 2011)

2.3.2.2.1 Vacuum Pressure Swing Adsorption (VPSA)

The Vacuum Pressure Swing Adsorption (VSA) is different from Pressure Swing Adsorption (PSA). VPSA systems input pressurised gas through the adsorbable bed and apply a vacuum to the purge gas (Nexant, 2010).

As shown in Figure 2.13, the vessel (A) in the adsorption phase is fed with compressed air. When the air valve is opened, then nitrogen molecules are adsorbed and separated from oxygen molecules, and the oxygen flow comes out from the vessel and stores in the buffer vessel.

2.3.2.4 Polymeric membranes

In the polymeric membrane for oxygen production, high pressure and low-pressure streams are separated by polymeric materials and oxygen, and nitrogen can transfer through it by different rates of diffusion. The size of an oxygen molecule is smaller than the size of nitrogen, so most of the polymeric membranes are more permeable to oxygen than nitrogen. This process increases the concentration of oxygen on the other side of the polymeric membranes.

2.3.2.5 Ion Transport Membrane (ITM)

On one side of the ITM gas mixture and the other side, hot air passes, then the oxygen ions penetrate through the membrane from the airside to another side, as shown in Figure 2.14. It is because of the oxygen partial pressure difference in the two sides of the membrane.

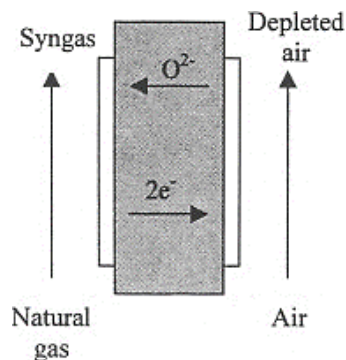


Figure 2.14 Ion transport membrane (ITM)

The ITM can operate at a temperature of about 1100 F. Oxygen molecules are changed into oxygen ions and then reform oxygen molecules at the other side of the membrane (Smith and Klosek, 2001). ITM for oxygen provide lower cost oxygen than cryogenic ASU. One of the methods to increase the efficiency of the Zero Emission Power Plant (ZEPP) is using an air turbine cycle at the exhaust of ITM for depleted air (Foy and Yantovski, 2006). Different types of ITM were developed by Praxair and BOC Group. The new ITM can have very high efficiency (Figuroa *et al.*, 2008).

2.3.2.6 Chemical Looping Combustion (CLC)

Chemical Looping Combustion (CLC) process separates oxygen from nitrogen. It includes combustion without direct contact with fuel and air. This cycle doesn't have a combustor, and the combustor converts into intermediate oxidation and reduction reactions near thermodynamic equilibrium (Manso, 2013).

Air enters the oxidising reactor to oxidise with metal such as nickel, iron and manganese, then the oxidised metal transfers to the fuel reactor to react with the fuel, and the by-products are CO₂ and H₂O (Manso, 2013). This process can be used instead of the air separation; The CLC cost is lower than ASU because of replacing the air compressors in ASU with fluidising blowers in CLC.

Figure 2.15 shows the schematic diagram of Chemical Looping Combustion CLC. As shown in the figure, the high-pressure air enters the Air Reactor (AR) and is oxidized with metal with the exothermic process. Then the high temperature O₂-depleted air which leaves the CLC island and enters the expander to generate power (Ingegneria *et al.*, 2012).

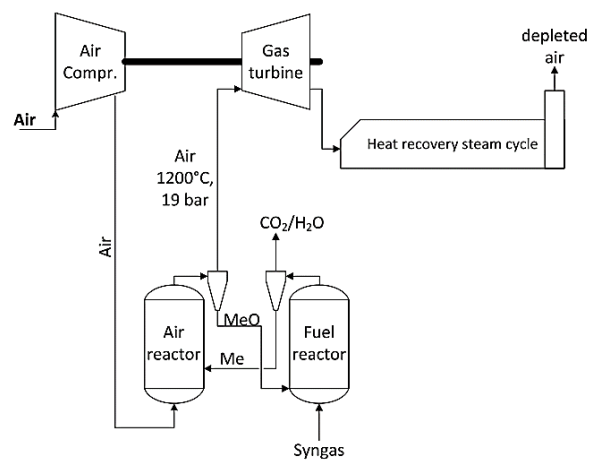


Figure 2.15 Schematic diagram of CLC (Ingegneria *et al.*, 2012)

2.4 CO₂ Compression and Purification Unit (CPU)

The CO₂ Compression and Purification Unit (CPU) is used to compress and capture CO₂ from oxy-combustion flue gases. The CPU components depend on the characteristic of CO₂ flue gas, which goes into the pipeline. Below are four major components for the CPU (Matuszewski, 2010).

1) Flue gas compression and drying:

In the first stage, flue gas with CO₂-rich composition is compressed to pressure up to 30 bar to separate water from CO₂. The water vapour of flue gas is compressed, hence condensed and can be separated from CO₂.

2) Partial condensation:

Some pipelines need further purification of CO₂ in the flue gas. The two-stage flash can be one of the options to purify CO₂ in the flue gas. The flue gas is cooled down to -59 °C, which is the critical point of CO₂. The cooled gas is flashed in the two-stage flash column, and CO₂ is separated from other gases.

3) Distillation:

High CO₂-rich flue gas includes an amount of O₂, which cannot be separated in the partial condensation process. Further distillation can be used to purify High CO₂-rich flue gas more than 99% and reduce the amount of O₂ content in the composition.

4) CO₂ final product compressor:

The final compression is required to reach the pressure of the CO₂ to the required level for the pipeline (Mantripragada and Rubin, 2019).

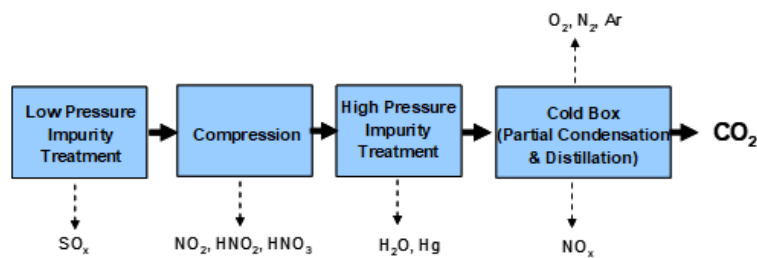


Figure 2.16 CO₂ Compression and Purification Unit (Chaubey 2010)

Figure 2.17 shows the schematic process flow diagram of CPU without further distillation and can produce CO₂-rich flue gas up to 96.3% (Almås, 2012). As shown in Figure 2.17, flue gas with CO₂-rich composition enters R-DCA to cool down, then flue gas is compressed in an R-P1 compressor; this process separates condensed water from flue gas. The remaining water is absorbed in the molecular sieve twin bed drier (R-S1). The dried flue gas enters a multi steam heat exchanger (RH-1) to cool down to -26 °C, then partially liquified gas enters a flash drum (RS-2). The flash drum separates the liquid from the gas.

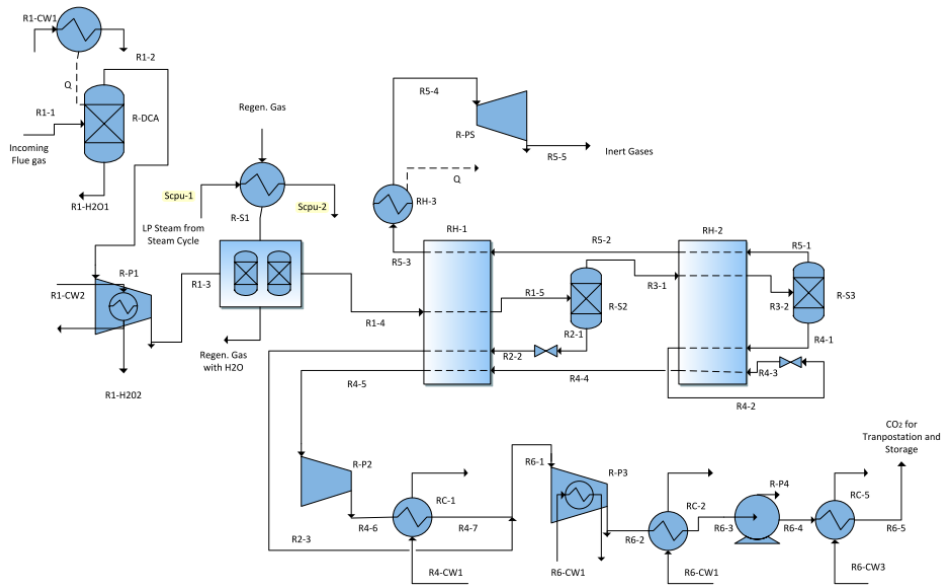


Figure 2.17 Schematic Process Flow Diagram of CPU (Almås, 2012)

The gas stream is cooled again to $-54\text{ }^{\circ}\text{C}$ in the multi stream heat exchanger (RH- 2) and then enters the flash drum (R-S3) to separate the liquid from inert gas. Then inert gas finally expands in the turbine (R-PS) and releases into the atmosphere. The liquid from the second flash drum (R-53) enters the Joule-Thomson valve to expand and reduce temperature to $-55.62\text{ }^{\circ}\text{C}$, and 9 bar (R4-3) then heats again in the multi-stream heat exchanger (RH-2), then compressed and cooled in the multi-stage compressor to reach 150 bar and $25\text{ }^{\circ}\text{C}$. This process produces 96.3 mol% CO_2 -rich flue gas (Almås, 2012).

2.5 Semi-Closed Oxy-Combustion Combined Cycle (SCOC-CC)

The semi-closed oxy-combustion combined cycle (SCOC-CC) is a usual oxy-turbine cycle. It is reassembled from the conventional combined cycle (Ferrari *et al.*, 2017a). The SCOC-CC is based on a Joule-Brayton combustion cycle. The recycled working flow can be set to obtain the required Turbine Outlet Temperature (TOT), and working flow chills the combustion.

The main composition of the working flow is CO₂ plus a small fraction of water. It depends on the pressure and temperature of the condenser to separate water from carbon dioxide then recycle it back. N₂ and Ar are derived from the air in Air Separation Unit (ASU). The pressure ratio can be set to maximize the efficiency of the SCOC-CC and acquire the useful TOT for the bottoming steam cycle in comparison to the air cycle with the same turbine inlet temperature. The air cycle requires a higher-pressure ratio to reach the same outlet temperature. The reason for this is the more complex composition in working flow and lower specific constant pressure heat capacity value of the working flow (Martelli, 2019).

The minimum pressure in the closed cycle can be higher than ambient pressure; the cycle which works on the higher pressure needs high-pressure facilities with more compact turbomachines and HRSG. The higher minimum pressure causes higher mechanical stress on the equipment, and the thicker parts are required for the equipment.

The cooling blades in the turbine reduce the surface needed for refrigeration, but it raises the heat transfer coefficients on the inside and outside of the turbine blades wall. Therefore, more working flow rate is required to cool down the outside turbine blade for the same turbine temperature (Scaccabarozzi, Gatti and Martelli, 2016).

Fuel burns with pure oxygen to produce CO₂ and water. The pure oxygen is provided by ASU, and carbon dioxide is recycled to moderate Turbine Inlet Temperature (TIT). All of the carbon dioxide production is captured in this cycle (Scaccabarozzi, Gatti and Martelli, 2016).

The gas flue of the condenser is mainly carbon dioxide. A part of carbon dioxide is extracted for compression and transportation to a storage unit, and the remaining carbon dioxide is recycled to the compressor (Chik, 2017). The schematic flow diagram is shown in Figure 2.18.

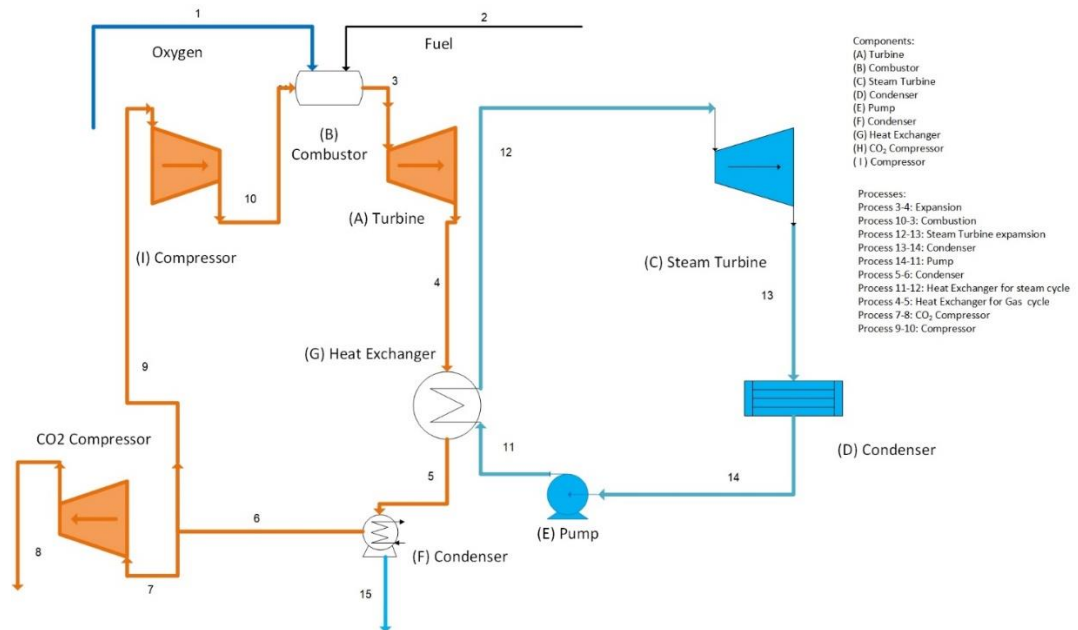


Figure 2.18 Semi-closed oxy-combustion combined cycle (SCOC-CC) (Davison, 2015)

The SCOC-CC was investigated in (Dahlquist *et al.*, 2013). It is shown that reducing the temperature of the recycled exhaust gases as much as possible could not increase the efficiency further, and the optimum heatsink temperature is calculated 60°C. The optimum pressure ratio is found 45 bar; however, the efficiency graph is rather flat, and at 34 bar pressure, the efficiency only reduces 0.16 efficiency point (Dahlquist *et al.*, 2013)

The lower pressure ratio increases the exhaust gas temperature to 620 °C. It can provide an excellent opportunity for easy upgrades turbine inlet temperature of the HP-Steam turbine towards 590-600 °C. The author mentioned that the gas properties of the oxy-combustion cycle are suitable for the bottoming cycle. The energy is more in the high-temperature region in comparison to the conventional combined cycle;

therefore, HRSG has better efficiency than a standard combined cycle (Dahlquist *et al.*, 2013).

Sundkvist *et al.* (2014) also investigated two alternatives of SCOC-CC with recirculation of the working fluid with the composition of CO₂ and H₂O, but the molar fraction of the H₂O is different due to different conditions for the condenser. The SCOC-CC plant with a high temperature (98°C) configuration for recycling working flow at the HRSG outlet has an efficiency of 41.9%. Still, the cycle with higher temperature and low steam content has a higher efficiency of 48%. Sundkvist *et al.* (2014) mentioned that the best design for SCOC-CC is an oxy-combustion cycle with a flue gas temperature of 630°C. The efficiency would be reduced by 0.2% by changing the flue gas temperature from 590°C to 630°C for entering HRSG, but it can be compensated by enhancement in the turbomachinery design (Sundkvist *et al.*, 2014).

Chiesa and Lozza estimated 39% efficiency for integrated gasification combined cycle (Chiesa and Lozza, 1999), but Lozza *et al.* estimated 46.17% efficiency (Lozza *et al.*, 2009). The turbine exhaust gas enters HRSG (heat recovery and steam generator), then flue gas enters the condenser, and water is condensed and separated from flue gas.

2.5.1 SCOC-CC technologies

One of the simplest oxy-combustion cycle configurations is SCOC-CC. But, the working flow has a composition of CO₂ and H₂O; hence the SCOC-CC power plant turbomachines are required to be designed and developed. The turbine blades and cooling channels need to be redesigned for working flow with the properties of CO₂-rich. The development of new equipment for CO₂-rich working flow is costly and needs R&D efforts (IEAGHG, 2015).

2.6 The COOPERATE cycle

A 10 MW Zero-Emission Power Plant (ZEPP) with liquid CO₂ cogeneration cycle with 48% is introduced by Yantovski *et al.* (1993, 1994a) and Wall *et al.* (1995), and

this was used for Enhanced Oil Recovery (EOR) later. The turbine inlet temperature is 1000 °C, and the pressure is 40 bar. This cycle was demonstrated by the Akar company in Norway 5 years later (Foy and Yantovski, 2006).

Yantovski et al. (1994b) described the ZEPP cycle with gas combustion in an O₂/CO₂ mixture and CO₂ recirculation. This cycle is called CO₂ Prevented Emission Recuperative Advanced Turbine Energy Cycle (COOPERATE) (Foy and Yantovski, 2006).

Yantovski et al. (1995) investigated the COOPERATE cycle and introduced internal combustion with triple turbine expansion and zero-emission CO₂, as shown in Figure 2.19 (Yantovski, 1996).

The main difference of COOPERATE cycle is that the exhaust stream from the high-pressure turbine enters directly to the combustor, and it does not pass in the regenerator (IEAGHG, 2015). The exhaust from the high-pressure turbine has a high heat capacity and would be suitable for regenerator.

The COOPERATE plant can work as a cogeneration plant, and the low-grade enthalpy can be used for district heating after recuperation (Yantovski, 1996). The author mentioned that the cycle could reach 60% efficiency if the Turbine Inlet Temperature (TIT) increases up to 1500° C. Still, the power consumption to produce oxygen is not considered in the efficiency and assumed the liquid oxygen is pumped to the plant and it was provided in the Air Products Company in Allentown (Yantovski, 1996).

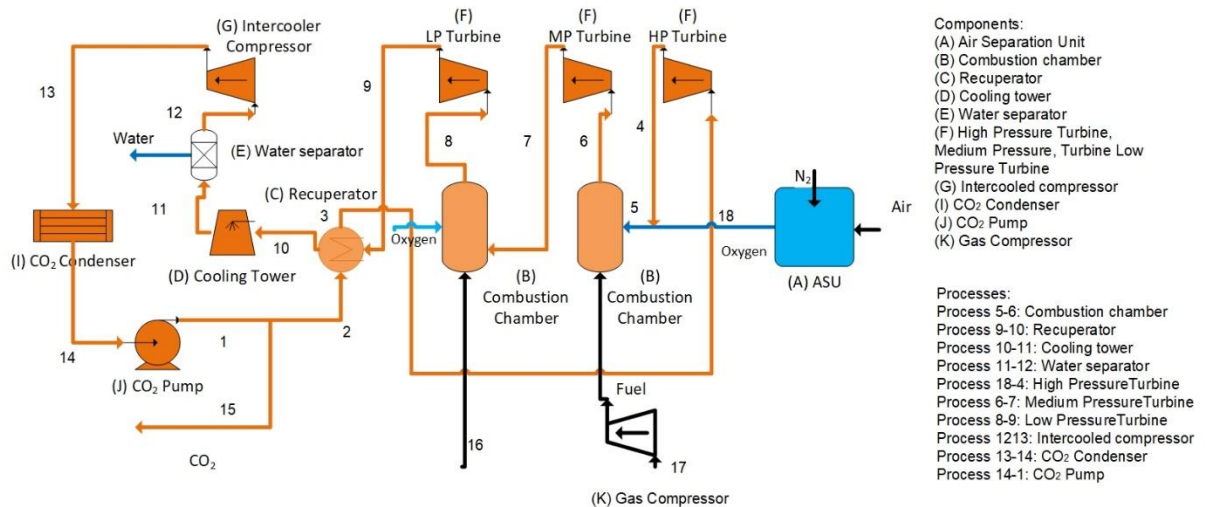


Figure 2.19 COOPERATE cycle Process flow diagram (Yantovski, 1996)

The COOPERATE cycle consists of Air Separation Unit (ASU), combustion from a mixture of fuel, oxygen and recycled carbon dioxide, three turbines, a carbon dioxide compressor, a condenser, and sequestration carbon dioxide. The maximum pressure and temperature of the turbine inlet working flow are 240 bar and 1250°C (Yantovski, 1996). The simple carbon dioxide internal combustion cycle is more suitable for increasing efficiency due to temperature increase (Yantovski, 1996).

2.6.1 The COOPERATE cycle technologies

Recuperation is a unique feature of the COOPERATE cycle. In the ordinary cycle, the amount of enthalpy (exergy) in the exhaust gas of the turbine is so great, and it cannot be transferred to the recycled working flow before combustion. Thus, the thermochemical recuperation with a catalyst is used to reform a fraction of fuel + CO₂ mixture to CO + H₂. This endothermic reaction takes extra enthalpy (exergy) of exhaust gases of the turbine.

In the COOPERATE cycle, the temperature of working flow declines in the turbine and the ordinary recuperation can be used to absorb the enthalpy (exergy) (Yantovski, 1996). The COOPERATE cycle presents 46.9% to 55.2% efficiency for TIT between 950 °C and 1350 °C and the pressure range between 4 and 240 bar (Foy and Yantovski, 2006). The pressure and temperature of turbine inlet gases in the COOPERATE cycle were not feasible for the turbine manufacturer before, but high pressure and temperature can be achieved in the new generation of the turbine.

Yantovski (1994c) developed a new cycle, and the cycle has 50% efficiency with feasible turbine inlet states of 600°C at 240 bar and 1300°C at 40 bar. This feasible cycle (COOPERATE-DEMO) is quasi-combined (Yantovski, 1996); this cycle includes two parts:

Rankine cycle with high pressure and working flue of CO₂

Brayton cycle with low pressure and working flue of CO₂

The cycle is compared with a standard combined cycle by (Yantovski, 1996), as shown in Table 2.4.

Table 2.4 Comparison of COOPERATE and Combined Cycle (Yantovski, 1996)

	Efficiency	Cost of electricity [c/kWh]	CO ₂ emissions [g/kWh]
Standard Combined Cycle	52.2%	4	360
COOPERATE	54.3%	5.55	0

The main challenge of the COOPERATE cycle is in the CO₂ condenser with non-condensable gases. In order to avoid CO₂ condensation, the working flue could be compressed immediately after exiting the cooling tower, and the compression process should not cross the saturation line. The developed version of the COOPERATE cycle is MATIANT cycle (Mathieu and Nihart, 1998).

2.7 The MATIANT cycle

Development of OCDOPUS project and the COOPERATE cycle lead to MATIANT cycle. This cycle has three expansion stages and two combustion stages with the reheating process. The cold carbon dioxide flow is recycled to the recuperator to absorb heat from the upper stream cycle and then enters the high-pressure turbine for expansion. The working flue pressure is reduced before entering combustors, so the combustors are conventional low-pressure combustors. The process is like COOPERATE cycle. The MATIANT cycle avoids the carbon dioxide condensation, the carbon dioxide is compressed after the exit of the cooling tower, but the COOPERATE cycle has a condenser (Manso, 2013). The reheating process causes to reduce wasted energy and increase cycle efficiency. There are variants of supercritical and combined cycle versions for MATIANT cycle (Zhao *et al.*, 2017). There are three types of the MATIANT cycle includes E-MATIANT, CC-MATIANT, and IGCC-MATIANT.

The MATIANT cycle is a developed version of COOPERATE cycle. This cycle is a Bryton cycle, and the condensation of the CO₂ is avoided. , and the Rankine cycle of COOPERATE is omitted.

The MATIANT cycle shows that efficiency loss from ASU is 11.5% to 14.5%. The

cycle includes a two-stage turbine with 45% efficiency when the fuel is natural gas. The turbine inlet temperature is 1300 °C with turbine exhaust gas of 700 °C. The efficiency can be increased up to 49% if the steam cycle is reheated by exhaust gases (Foy and Yantovski, 2006).

The MATIANT cycle efficiency has a technical limitation on the TIT and TOT of turbines. the cycle efficiency can increase from 44.3% to 46% If the upper pressure of cycle changes from 140 at TIT 1200 °C to 220 bar at TIT 1400 °C (Foy and Yantovski, 2006). (Mathieu and Van Loo, 2005) introduces an IGCC plant with an oxy-fuel MATIANT combined cycle. The efficiency is 44.8% at 120 bar and 1250 °C. In the study of (Mathieu and Desmaret, 2001), a solid oxide fuel cell (SOFC) was combined with the MATIANT cycle at a higher temperature (more than 700 °C) to improve the cycle efficiency.

2.8 The E-MATIANT cycle

Figure 2.20 shows the E-MATIANT cycle. This cycle design is very similar to a regenerative Ericsson-like cycle. It has nearly two isobaric processes, such as a regenerator and combustion chambers. Also, it contains two nearly isothermal processes, such as compression with intercoolers and expansion with a reheat (Manso and Nord, 2020). The Operating parameters of the design point for E-MATIANT Cycle is shown in Table 2.5 (Mathieu, 2004).

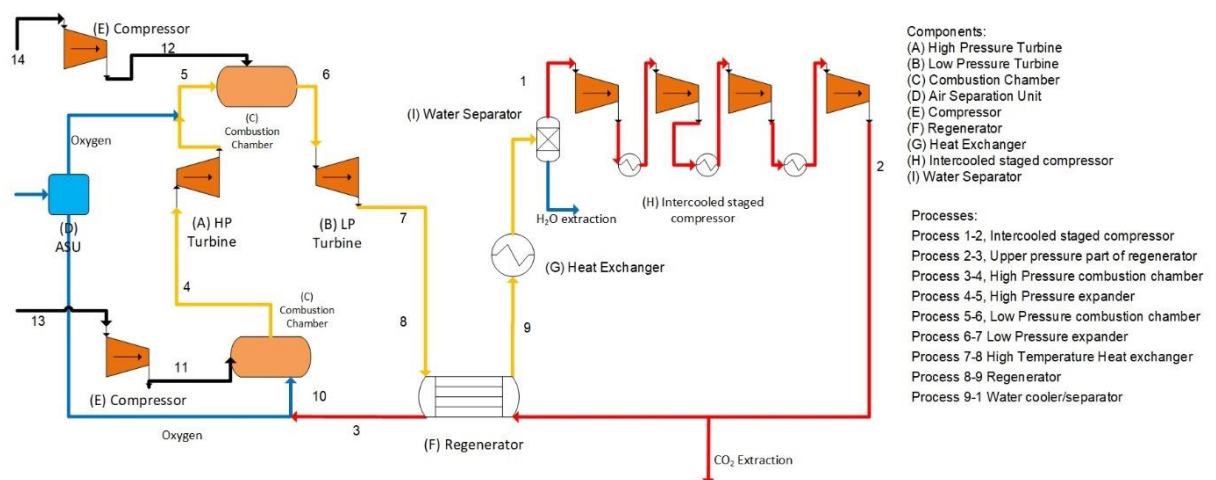


Figure 2.20 E-MATIANT schematic diagram (Manso and Nord, 2020)

Table 2.5 Operating parameters for E-MATIANT Cycle (Mathieu, 2004)

Upper cycle pressure	60 bar	Pinch-point at the regenerator outlet	20 °C
Lower cycle pressure	1 bar	Maximum inlet temperature in the regenerator	700 °C
Pressure drop in the combustion chamber	3%	Expander inlet temperature (TIT)	1300 °C
Isentropic efficiencies of the three expanders	0.87	Lower cycle temperature	30 °C
Isentropic efficiencies of oxygen compressor	0.75	Isentropic efficiencies of the fuel compressor	0.75
Isentropic efficiencies of the first three stages intercooled CO ₂ compressor	0.85		
Isentropic efficiencies of the last stage intercooled CO ₂ compressor	0.75		

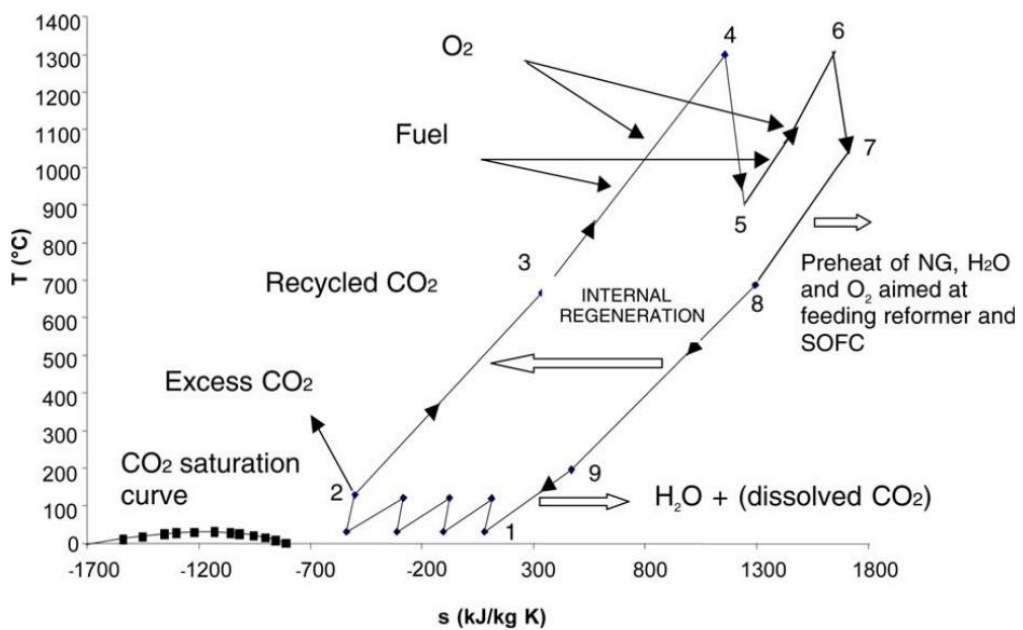


Figure 2.21 T-S Diagram of E-MATIANT cycle (Mathieu, 2004)

The working flue is condensed, and liquid water is separated from CO₂ at point 1. The CO₂ in the flue is compressed with intercooler up to 73 bar and 30°C. The cycle is a Brayton cycle, and it is in the supercritical position. The extra CO₂ is separated for sequestration at point 2, and the remaining CO₂ is recycled. The recycled CO₂ is heated in the regenerator up to 700 °C at point 3, and then it is premixed with the oxygen from ASU. The mixed stream of CO₂ and oxygen enters the combustion chamber and burn with compressed fuel.

The pressure of the combustion chamber is 60 bar, and the Combustion Outlet Temperature (COT) is 1300 °C. The combustion chamber temperature is controlled with the recycled CO₂ stream, and the flow rate of the recycled CO₂ can control the temperature of the combustion chamber to prevent exceeding the maximum possible temperature.

The combustion chamber exhaust gas is expanded in a High-Pressure Turbine, and the turbine exhaust pressure can be between 12 to 36 bar, which is dependent on the design of the cycle. The sensitivity analysis of the pressure can help to adapt exhaust pressure to the optimum point.

The exhaust of the High-pressure turbine is mixed with pure oxygen at point 5 and then enters the combustion chamber and burns with the pressurized fuel.

The working flue expands in the Low-Pressure turbine to 1 bar at point 7, then the exhaust of the low-pressure turbine cools down in the regenerator to heat the recycled CO₂ steam. The exhaust of the regenerator at point 9 condenses to near ambient temperature to separate water from steam before point 1 (Manso, 2013). Figure 2.21 shows the T-S diagram of the E-MATIANT cycle.

2.9 CC-MATIANT cycle

CC-MATIANT is an improvement for the E-MATIANT (Mathieu and Nihart, 1999) as shown in Figure 2.22. In the CC-MATINAT cycle, the new high-pressure expander is added to the CO₂ stream. The pressure can be higher than before, and it can be up to 300 bar (Manso, 2013).

The MATIANT cycle, as shown in Figure 2.22, has two parts 1) the supercritical part process through points (2,3,4,5,6), and 2) a regenerative CO₂ Brayton cycle process with reheat through points (6,7,8,9,10,11,12,1,2).

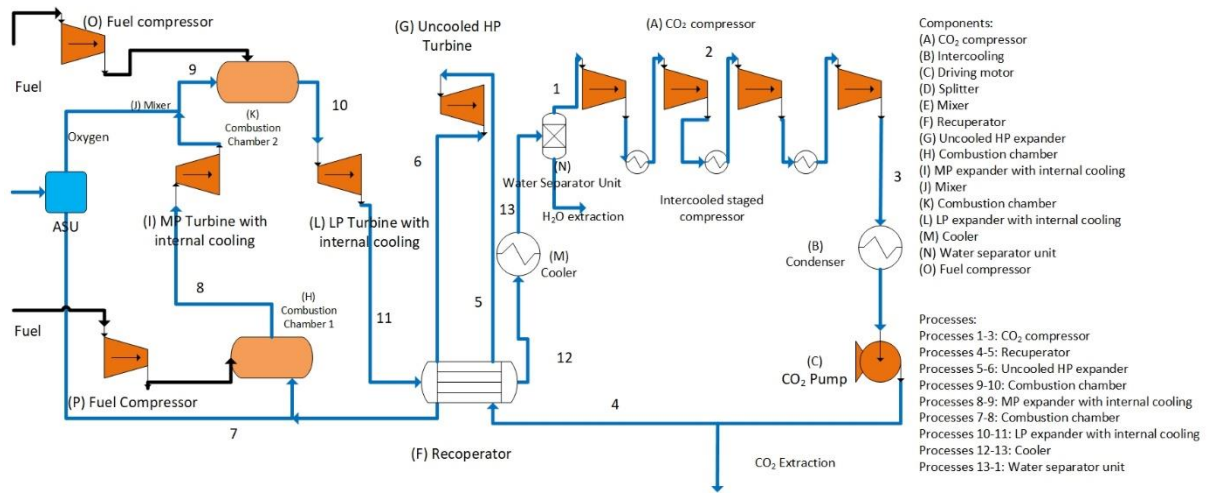


Figure 2.22 CC-MATIANT cycle (Mathieu and Nihart, 1999)

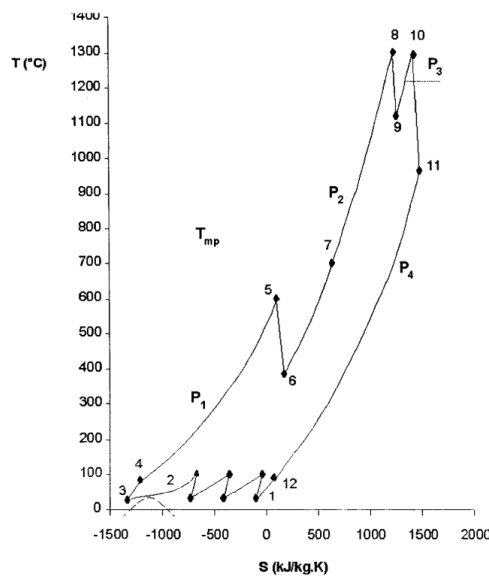


Figure 2.23 T-S diagram of CC-MATIANT (Mathieu and Nihart, 1999)

As it is shown in the T-S diagram of CC-MATIANT in Figure 2.23, The oxygen is mixed with the working flow of CO₂ at point 7, and the mixture enters the combustion chamber. Then the pressurized fuel at P₂ pressure burns with working flow in the combustion chamber. The process through the combustion chamber from 7-8 is isobar. COT (Combustion Outlet Temperature) is 1300 °C. The mixture of the CO₂/H₂O enters the turbine and expand through the process from point 8 to 9. The exhaust flue

enters the high-pressure turbine and mixes with oxygen, and then burns with fuel. The exhaust of the second combustion is combustion products with stoichiometric proportions. It includes 6% H₂O and 8% CO₂ with recycled CO₂.

The exhaust flue of the combustion enters the low-pressure turbine and expands through the process from point 10 to 11, and then the working flow enters the regenerator. In the regenerator, it heats high pressure working flow with pressure P1, and then it heats the exhaust gas from high-pressure turbine after high-pressure turbine expansion.

The outlet exhaust of the regenerator condenses in a cooler, and the water is extracted in a CO₂ /H₂O separator. The CO₂ stream is compressed and intercooled in four-stage compressors, and the cycle needs to be closer to the isothermal process for higher efficiency. The excess CO₂ in the cycle is extracted at point 4; the CO₂ can be in a liquid or supercritical state. The CO₂ can be extracted through the valve in a scrubber or membrane without any cost and energy consumption.

2.9.1 CC-METIANT technologies

The working flow of the cycle includes a small fraction of the Ar and N₂ from ASU; it also contains the extra O₂. The extra O₂ is available in the working flow because extra O₂ is required in practice to make the combustion complete without CO in the working flow.

The working flow impurity affects the cycle efficiency. The adiabatic exponent of the N₂ and Ar is higher than CO₂, so the compressor needs more electricity than pure CO₂ to compress the working flow, and also the working flow produces more power in the expanders, so it cannot significantly affect total network and efficiency (Mathieu and Nihart, 1999).

ASU in the cycle can produce O₂ at 5 bar with the purity of 99.5%, and the specific electricity consumption of ASU is 0.28 kWh/kg (Mathieu and Nihart, 1999).

The MATIANT cycle improvement in comparison to the previous cycle (COOPERATE) is in two areas. At the first one, the pressure increases from P1 to P4 without crossing the saturation line. At the second one, the condenser with two separate phases is removed (Mathieu and Nihart, 1999).

The net efficiency of the plant has been studied in several publications. Some of the obtained results of efficiency are 44.4%, 44.2%, or 47- 49% (Manso, 2013). (Zhao *et al.*, 2017) modified MATIANT cycle, as shown in Figure 2.24. The CO₂ compression process is changed with seven stages, the recompression and stream split added, the reheating process is omitted.

The efficiency of the modified cycle can reach 45.3%, and it is 0.35% less than CC-MATIANT cycle. The maximum efficiency can reach 48.63% by using the modern component with higher efficiency and constraints (Zhao *et al.*, 2017). T-S diagram of modified MATIANT cycle by (Zhao *et al.*, 2017) is shown in Figure 2.25.

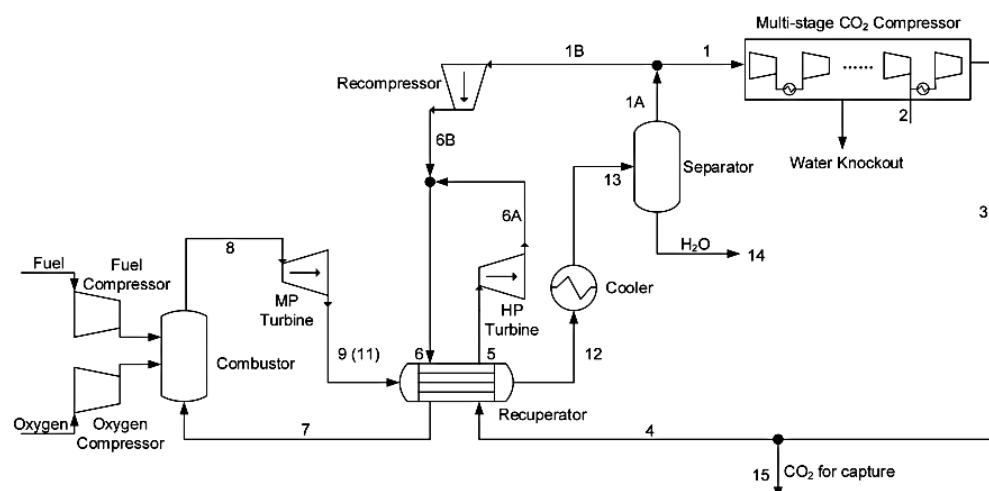


Figure 2.24 Modified CC-MATIANT cycle by (Zhao *et al.*, 2017)

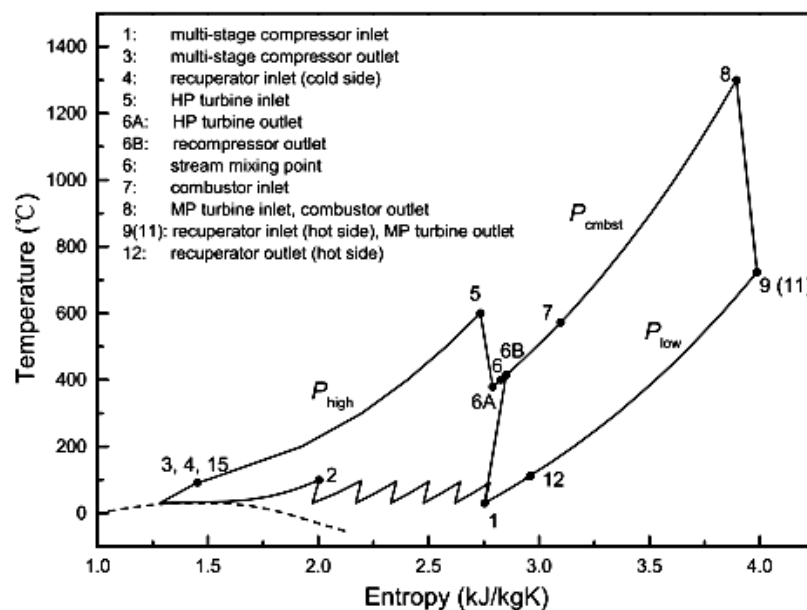


Figure 2.25 T-S diagram of modified MATIANT cycle by (Zhao *et al.*, 2017)

The MATIANT cycle was also adopted to an Integrated Coal Gasification Combined Cycle (IGCC) plant. This cycle is called IGCC-MATIANT.

2.10 The Graz cycle

Jericha (1985) introduces a hydrogen/oxygen power cycle without any emission. The cycle is the integration of a Rankine cycle at the bottom and a Bryton cycle. This cycle was developed, and Jericha (1995) introduces the Graz cycle (Foy and Yantovski, 2006). The Graz cycle, as shown in Figure 2.26, includes a low-temperature Rankine cycle and a high-temperature Brayton cycle.

Two streams are available for the Graz cycle. These include the flue gas and steam. The steam recovers heat in HRSG and expands in the high-pressure turbine. The flue gas cools down in the HRSG and then compresses and enters the combustion chamber. The fuel burns in the combustion chamber with a stoichiometric mass flow of oxygen at 40 bar.

The recycled CO₂ and steam are injected into the combustion chamber to moderate the temperature of combustion. The exhaust flue gas of combustion with 1400 °C expands in the High-Temperature Turbine (HTT) to 1 bar at 642 °C (Wolfgang Sanz *et al.*, 2005).

The exhaust gas of HTT needs to be condensed before further expansion to reach the condensation point. Hence the hot exhaust gas needs to be cooled in the HRSG, and then the heat is recovered from recycled steam from HRSG before entering HPT (Wolfgang Sanz *et al.*, 2005). Then the exhaust expands in the LPT to 0.25 bar, which is the pressure of the condenser.

The working flue in the condenser includes condensable (steam) and non-condensable (CO₂) components; hence the condenser temperature is related to the pressure of components. CO₂ and H₂O are separated in the condenser by condensing the water. The recycled water is preheated and vaporised before entering HPT. The steam enters HPT at 567 °C at 180 bar, and then after expansion, comes into the combustion chamber to moderate the temperature of combustion. It is also used to cool the first and second stages of HTT (Wolfgang Sanz *et al.*, 2005). The CO₂ is compressed to 1 bar (atmospheric pressure), and the excess CO₂ is separated.

2.11 The S-Graz cycle

The S-Graz cycle is similar to the initial design of the Graz cycle, but the carbon dioxide is not recycled back to the combustor. The exhaust gas for HRSG is separated into two parts, one part enters the Low-Pressure Turbine, and another part recycles back to the combustor.

Figure 2.27 shows the PFD (Process Flow Diagram) of the S-Graz cycle. The cycle is similar to the original Graz cycle. The fuel and oxygen with stoichiometric flowrates are fed into the combustion chamber. The combustion chamber pressure is 40 bar, and the Combustion Outlet Temperature (COT) is 1400 °C. The water steam and CO₂/H₂O mixture enter the combustion chamber to cool the burners and liner. The exhaust mixture of combustion is the mixture of 74% steam, 25.3% CO₂, 0.5% O₂ and 0.2% N₂ (mass fractions).

The working flow expands through the High-Temperature Turbine (HTT) to reach a pressure of 1.053 bar and 579 °C. The exhaust gas of the HTT is cooled in HRSG to around 180 °C (IEAGHG, 2015). But after the HRSG, only 45% of the cycle mass flow is further expanded in the LPT. The exhaust of LPT and condenser pressure would be 0.041 bar.

Liquid and gases are separated in the condenser. The CO₂ compresses in C3/C4 to reach atmospheric pressure for extraction with CO₂ extraction purity of 96%. The excess water is extracted during further compression for liquefaction. The recycled water is heated in the HRSG to reach the superheat state. The steam enters High-Pressure Turbine (HPT) at 549 °C at 180 bar.

The exhaust from HPT enters HTT to moderate the temperature, also recycled flow is compressed in C1/C2 after HRSG to reach the pressure of the combustion chamber at 600 °C (Jericha, Sanz and Göttlich, 2008a).

The realistic efficiency of the S-Graz cycle with natural gas by considering oxygen supply and mechanical, electrical, auxiliary losses and compression of CO₂ to 100 bar is 52.6%.

The efficiency of the cycle without the mechanical, electrical and auxiliary losses would be 54.6% (Wolfgang Sanz *et al.*, 2005). The initial investigation of the Graz cycle was done by the Statoil company.

2.12 The AZEP 100% cycle

Advanced zero-emission power cycle (AZEP) concept has Mixed Conductive Membrane (MCM) reactor. The function of this reactor includes membrane (separating O₂ from the air), burning fuel near stoichiometry, exchanging heat.

After air depleting in the MCM reactor, it expands in the gas turbine then enters the heat recovery steam generator (HRSG) to heat steam for the steam turbine.

ASU in the oxy-combustion cycle has a very negative effect on the net efficiency of the cycle. Oxygen Ion Transport Membranes (OITMs), in comparison with cryogenic ASU, has a less negative effect on efficiency and have a lower cost in comparison with cryogenic ASU (Foy and Yantovski, 2006).

The Advanced Zero Emission Power (AZEP) cycle includes a novel combustor integrated with a ceramic membrane and a heat exchanger. Figure 2.28 shows AZEP 100%. The MCM-reactor system is replaced with a combustion chamber in the AZEP cycle. The air is compressed before being heated in the MCM reactor. The outlet temperature of the reactor is 1200 °C, and 50% of the oxygen is transferred through the membrane and swept by CO₂ /H₂O gas. The sweep gas contains oxygen.

The sweep gas and natural gas react to generate heat in the combustion chamber. The excess sweep gas is extracted from the MCM reactor to keep the stable mass flow in the MCM. The extracted sweep gas contains heat. The CO₂/H₂O stream recovers the heat from HRSG to provide more steam and preheats the natural gas fuel (Sundkvist *et al.*, 2005). The exit gas from HRSG is condensed to separate water and CO₂; then, the CO₂ is compressed from 20 bar to 100 bar to be liquefied.

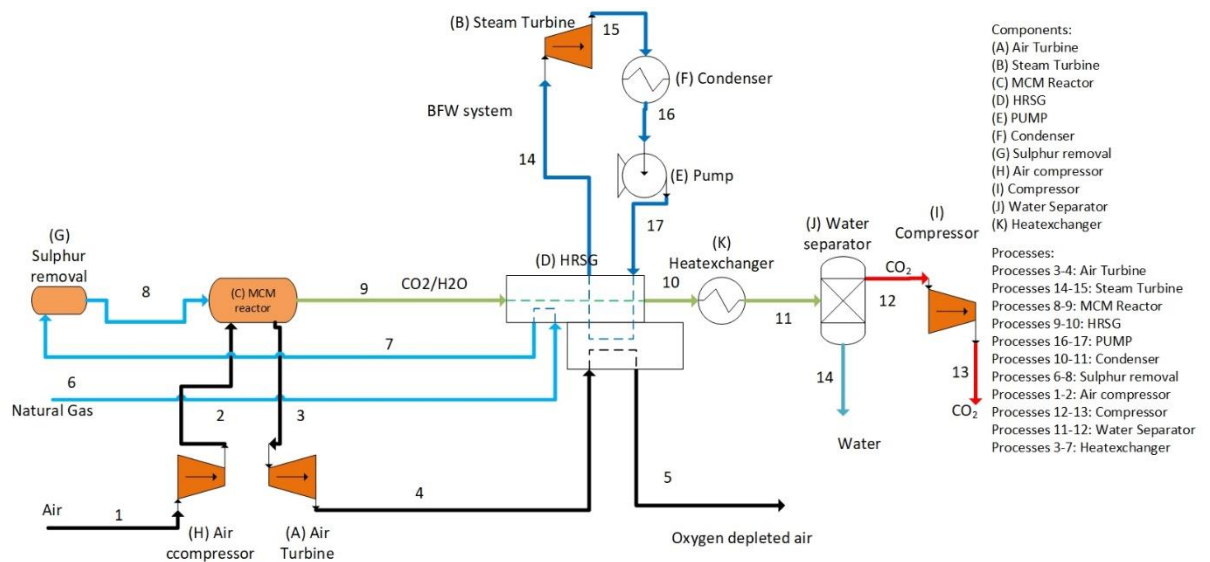


Figure 2.28 The AZEP 100% case (Sundkvist *et al.*, 2005)

2.12.1 The AZEP 100% cycle technologies

The air turbine with an air working flow at the bottoming cycle increases the efficiency of AZEP. Still, the maximum temperature of the AZEP cycle is restricted to 1200 °C, and it is far less than CCGT, which reduces the thermal efficiency.

The exhaust temperature is low, so the triple pressure steam turbine for 400 MWe is not feasible, but a dual pressure for 50 MWe and 400 MWe can be feasible in AZEP 100% (Sundkvist *et al.*, 2005).

The OITMs cannot provide high-temperature (TIT) for the turbine. Hence, it can limit the efficiency of the cycle. The AZEP 100% cycle efficiency is about 49.6% in comparison with the 57.9% efficiency of a V94.3A combined cycle power plant. It has an 8.3% penalty due to lower turbine inlet temperature (1200 °C) for both steam and gas turbines, and it reduces the efficiency in both turbines (Möller *et al.*, 2005).

Only tax intensive around €31 – €40/ton can make AZEP 100% cycle more attractive. An economic analysis of the AZEP cycle shows that a carbon emission tax of €31 – €40/ton would make the AZEP with 100% carbon capture as economically attractive as the V94.3A combined plant (Sundkvist and Eklund, 2004).

2.13 The AZEP 85% cycle

The efficiency of AZEP 100% cycle can be increased by adding the preheat combustion chamber before the gas turbine to preheat the air stream, as shown in Figure 2.29. The exhaust of the preheated combustion chamber is released into the air after recovering heat in HRSG, but in this cycle, 85% of the carbon dioxide is captured (Sundquist et al., 2004).

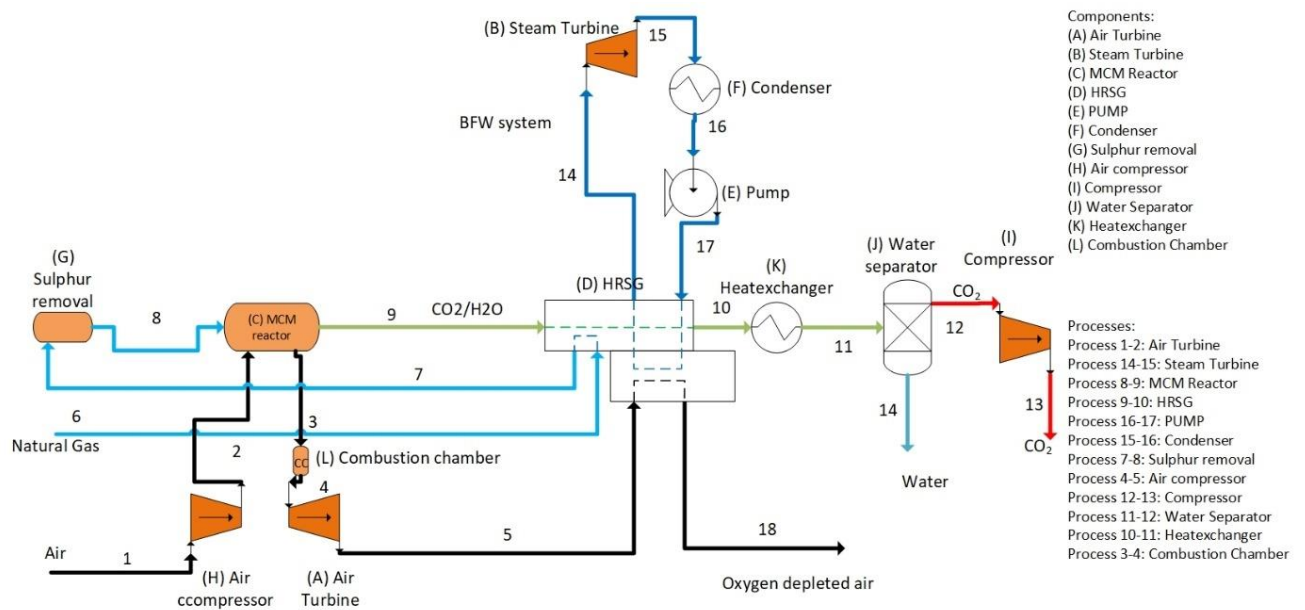


Figure 2.29 The AZEP 85% case (Sundkvist et al. 2005b)

The efficiency of AZEP 85% increases from 49.6% to 53.4%, and it has the same efficiency as the post-combustion CO₂ absorption cycle (Foy and Yantovski, 2006).

2.14 The ZEITMOP cycle

The Zero Emission Ion Transport Membrane Oxygen Power (ZEITMOP) is introduced by (Yantovski *et al.*, 2004). The main working flow of the cycle is CO₂, the carbon dioxide, which is enriched with O₂ in Oxygen Ion Transport Membranes (OITM), and CO₂/O₂ flow is an oxidant in natural/gas combustor (IEAGHG, 2015).

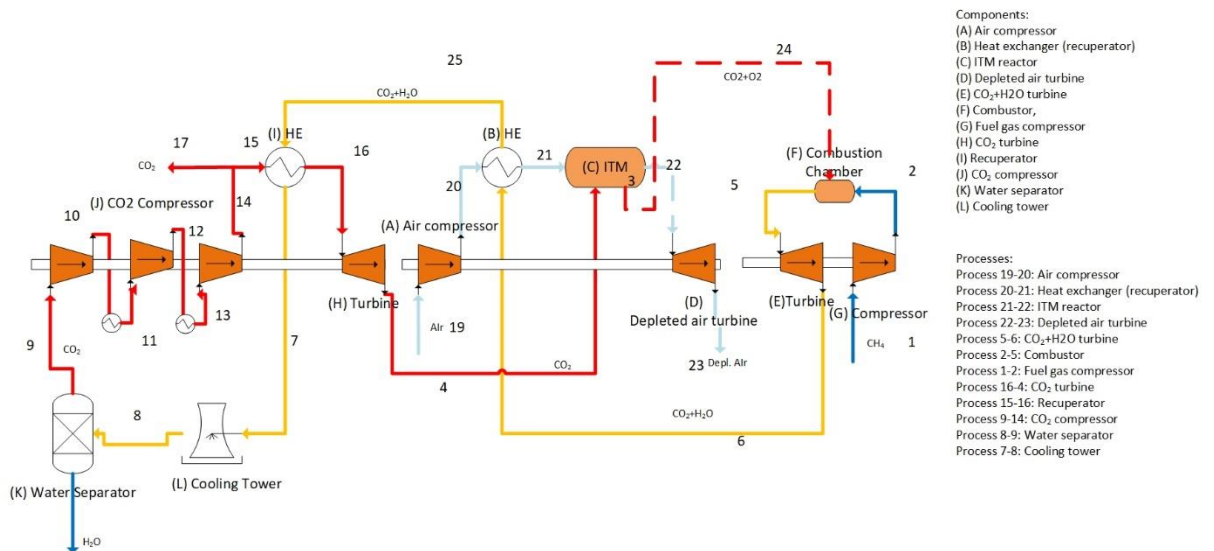


Figure 2.30 ZEITMOP schematic diagram (Yantovski *et al.*, 2004)

Figure 2.30 shows the simplest version of the ZEITMOP cycle. It is a gas-fired one, but the cycle can be used for pulverized coal and other fuel.

The ZEITMOP cycle consists of three main cycles:

1. The CO₂ cycle (7,9,10,11 and 12)
2. CO₂ /H₂O (3,6,7,10,12,13)
3. Air/O₂ -depleted and Air/O₂ branch (1,2,3,4,5,7)

The air with ambient conditions enters compressor (A), and it is heated up to 800-900 °C in the heat exchanger (B) by recovered heat from the turbine exhaust (E). The high temperature and pressure air enter ITM oxygen ceramic (C). The ITM (C) separates oxygen from the air, which penetrates the membrane. The other parts of the stream would be an oxygen-depleted air stream with high temperature and pressure.

The turbine exhaust (H) is carbon dioxide, and it sweeps the O₂ from ITM and then enters the combustion chamber (F). In the combustion chamber, the working flow burns with the pressurised natural gas.

The oxygen-depleted air has high pressure and temperature; it exits from ITM and enters the turbine (5). The oxygen-depleted air expanded through the turbine and then released to the atmosphere.

The exhaust of the combustion chamber (F) is a mixture of CO₂ and H₂O with a temperature about 1300-1600 °C. It expands through the low-pressure turbine (E), then

it is cooled in the HE (B), HE (I), and cooling tower (L). In the separator (K), the water is extracted from the cycle, and CO₂ is recycled back.

The nearly pure CO₂ enters the multi-staged compressor with an intercooler (J). The excess of CO₂ is extracted from the cycle in high pressure and liquid phase. The remaining CO₂ recovers the heat in HE (I) then expands in the high-pressure turbine (H) up to 15 bar. The exhaust of the turbine enters ITM (D) to sweep oxygen and then enters the combustion chamber (F).

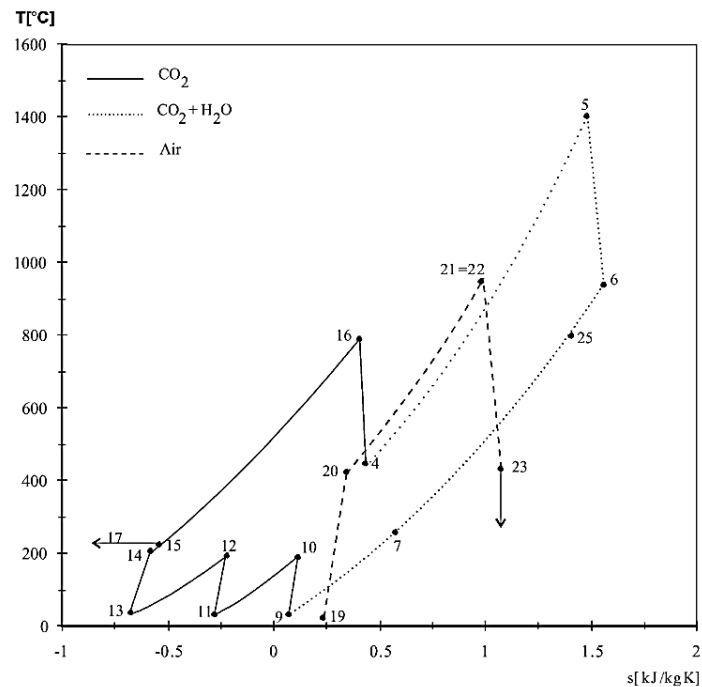


Figure 2.31 T-S diagram of the ZEITMOP cycle (Yantovski *et al.*, 2004)

Figure 2.31 shows the T-S diagram of the ZEITMOP cycle, the depleted oxygen air cycle is the Brayton cycle, the CO₂ cycle is the Brayton cycle, and it is a quasi-combined cycle with CO₂/H₂O is the steam cycle. The efficiency of this cycle is about 50% (Yantovski *et al.*, 2004).

2.14.1 ZEITMOP technologies

In the ZEITMOP cycle, the combustion chamber is separated from the ITM reactor; hence the TIT is independent of ITM maximum temperature and allows the cycle has a higher temperature and efficiency.

If the combustion temperature rises to 1500 °C, then the efficiency of the ZEITMOP cycle would be 56%, and if the TIT is 1300 °C, the efficiency would be around 46% (Foy and Yantovski, 2006).

The ZEITMOP cycle needs to be optimized, and it may reach higher efficiency through the optimisation and can be used for all types of fossil fuel. ZEITMOP cycle can be one of the best options for the power plant demonstration (Foy and Yantovski, 2006).

2.15 The COOLCEP-S cycle

The Cool Clean Efficient Power (COOLCEP) is used LNG as a heat sink because the temperature of LNG is about 110K and much lower than ambient air or water temperature. The cold exergy can be used to decrease the temperature of the heat sink of the cycle (Zheng, 2011). This process causes an increase in the Carnot efficiency of the cycle.

The COOLCEP power cycle is a zero CO₂ emission and highly efficient cycle. The fuel of the COOLCEP cycle is a novel Liquefied Natural Gas (LNG). The COOLCEP power plant is a supercritical CO₂ Rankine cycle. In the cold sink of the power plant, the LNG evaporation system provides refrigeration for the CO₂ subcritical evaporation process.

Figure 2.33 shows the PFD (Process Flow Diagram) of the COOLCEP-S. In the main cycle, the low-temperature CO₂ with the temperature of -50 °C in liquid phases (1) is pumped up to 30 bar. The output of the pump is heated through the EVA1. The pure oxygen from ASU is compressed and mixed with the working flow of CO₂ after the pump. The mixed working flow is heated through recuperator; the heat is recovered from the exhaust gas of the turbine. The outlet of the recuperator is injected into the combustion chamber and burns with natural gas, then the exhaust of the combustion chamber expands through the turbine. The turbine exhaust is cooled down in the recuperator to recover heat for downstream. It is cooled further in LNG-cooled heat exchanger HEX1 to condense water and separate it from CO₂.

The water is separated from CO₂ at the separator and extracted from the cycle (12). The remaining working flow, which is mainly CO₂, is condensed (14) by LNG evaporation and then recycled back. The remaining non-condensed gases are extracted

(15) and compressed (16), and cooled to provide the liquid CO₂ with mixed other compositions, and it is ready for capture. In the LNG cycle, LNG (18) is pumped up to 73.5 bar and then evaporated from the cycle heat sink, and also the LNG is used to cool the excess gases (19b) at HEX2. Two splits of the natural gases emerge before entering HEX1. The exit natural gas from HEX1 is split into two parts, one part is injected into the combustion chamber to burn, and another part is extracted from the cycle and send to the outside users (Liu *et al.*, 2017). Figure 2.33 shows the T-S diagram of the COOLCEP-S cycle.

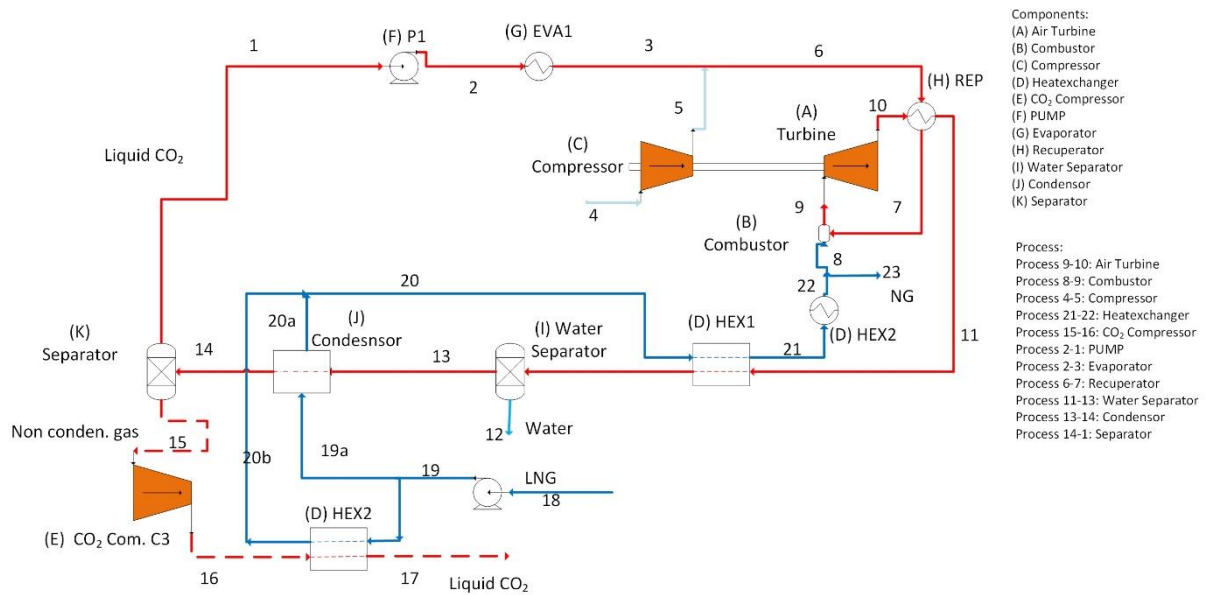


Figure 2.32 COOLCEP-S cycle schematic (Liu *et al.*, 2017)

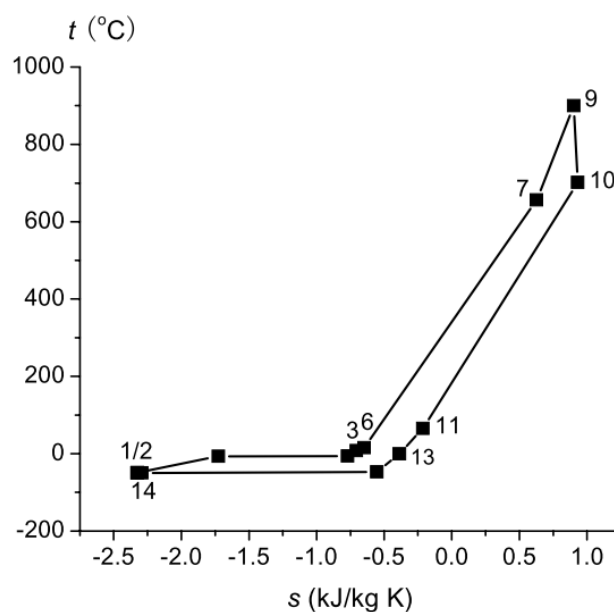


Figure 2.33 T-S diagram of the COOLCEP-S (Liu *et al.*, 2017)

2.15.1 COOLCEP technologies

LNG evaporation system is combined with the cycle. This cogeneration cycle has two main benefits:

1. In the condensation process, a lower temperature than ambient temperature can be achieved.
2. The liquid CO₂ with high pressure can be extracted from the cycle without a high-efficiency penalty.

The estimated capital cost for the optimized COOLCEP cycle is about 750 EUR/kWe with 8-9 years payback, and the electricity cost is about 0.031 EUR/kWh (Zhang *et al.*, 2010).

2.16 The COOLCEP-C cycle

There are two types of COOLCEP-S and COOLCEP-C available. The main difference between the two cycles is in the outlet pressure of the turbine.

In the COOLCEP-S cycle, the outlet pressure of the turbine is CO₂ condensation pressure. Still, the COOLCEP-C, the outlet pressure of the turbine is much lower pressure and expands in the near ambient pressure to produce more power (Zhang *et al.*, 2010). Furthermore, the TOT is much lower than COOLCEP-S, and a lower temperature heat exchanger is required. In the COOLCEP-C, a compressor (C2) is required to increase pressure to the condenser pressure of CO₂, as shown in Figure 2.34.

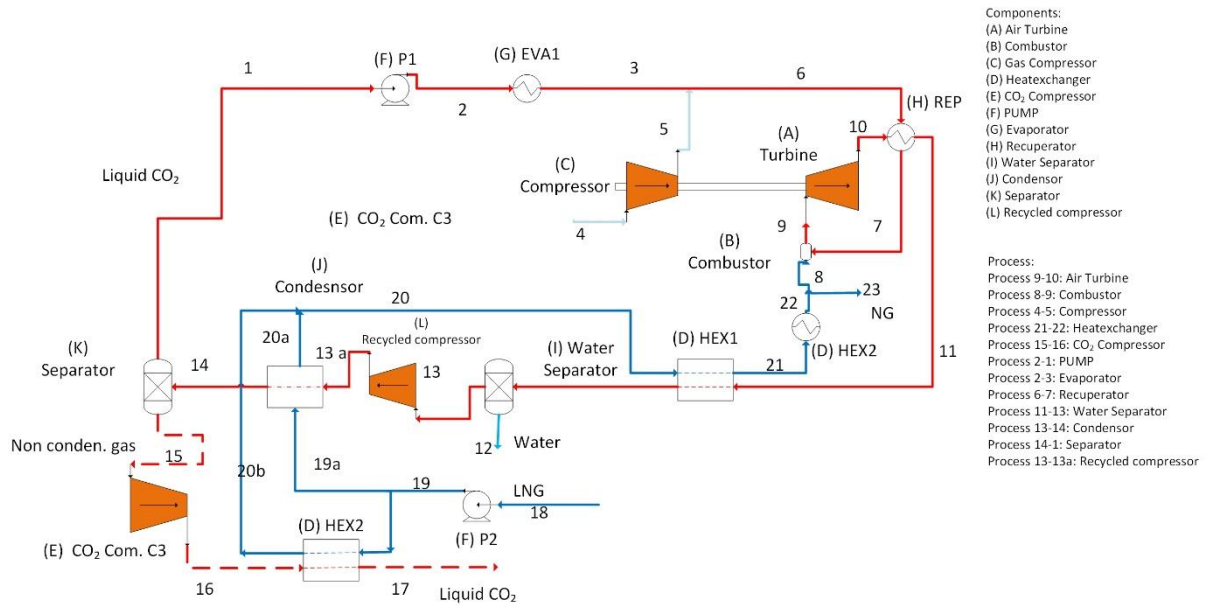


Figure 2.34 COOLCEP-C (Zhang *et al.*, 2010)

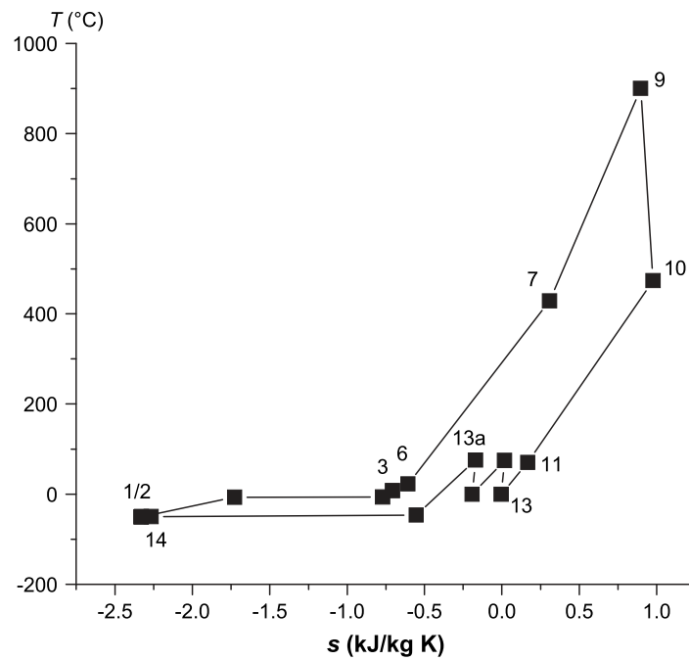


Figure 2.35 T-S diagram in the COOLCEP-C system (Zhang *et al.*, 2010)

2.16.1 COOLCEP-C technologies

The efficiency of the COOLCEP-S for 900 °C TIT is 59%, and it is higher than the efficiency of the COOLCEP-C, which is 52%.

The required compressor to increase the pressure up to CO₂ condenser pressure causes an efficiency penalty for COOLCEP-C cycle, and it reduces total efficiency.

However, the high temperature of turbine exhaust for COOLCEP-S causes the increase of capital cost for the special design of heat exchangers (Zhang *et al.*, 2010). T-s diagram of the COOLCEP-C system is shown in Figure 2.35.

2.17 Novel O₂/CO₂ (Cao and Zheng, 2006)

Figure 2.36 shows the Process Flow Diagram (PFD) diagram of the Novel O₂/CO₂ cycle. The natural fuel gas is compressed with the compressor (A) and mixed with compressed carbon dioxide in the mixer (G). The mixing flow is fed to the reformer (F) to reform methane fuel/carbon dioxide to CO, H₂, H₂O and excess CO₂. The reformed fuel (stream 4) and fuel-oxidiser (stream 5) are combusted and produce water and carbon dioxide with the high-temperature gases of 1573.15 K (stream 7) (Cao and Zheng, 2006).

The high-temperature exhaust from the combustion chamber enters the turbine (D). The turbine exhaust enters the reformer to cool and transfer heat to CO₂-NG reformer (stream 8); the exhaust working flow from the reformer enters the heat exchanger to heat saturated water for the ammonia absorption refrigeration system. The exhaust gas of the heat exchanger (stream 10) is condensed in the condenser (J), and then the mixture of the condensed water and CO₂ enters the separator (K) to extract water from the cycle.

The remaining composition is mainly CO₂. The working flow enters splitter (L) to divide CO₂ into two streams. One part of the CO₂ stream recycles and enters the cooler (M) to release heat, and the excess part of the CO₂ enters the three-stage compressor and cooler to compress the CO₂ up to 7.3 MPa and a final temperature of 303.5 K.

In the ammonia absorption refrigeration cycle, the low exergy heat waste from the turbine is used to generate chilled load in the heat sink of the cycle to cool the recycled working flow of the CO₂ (Cao and Zheng 2006).

2.18 NetPower cycle

The NetPower cycle is one of the novel oxy-combustion technologies, and it is developed recently with 8 Rivers Capital. The cycle is an oxy-combustion cycle with a working flow of carbon dioxide. NetPower cycle is also called the Allam cycle. The process flow diagram of the Allam cycle is presented in Figure 2.37.

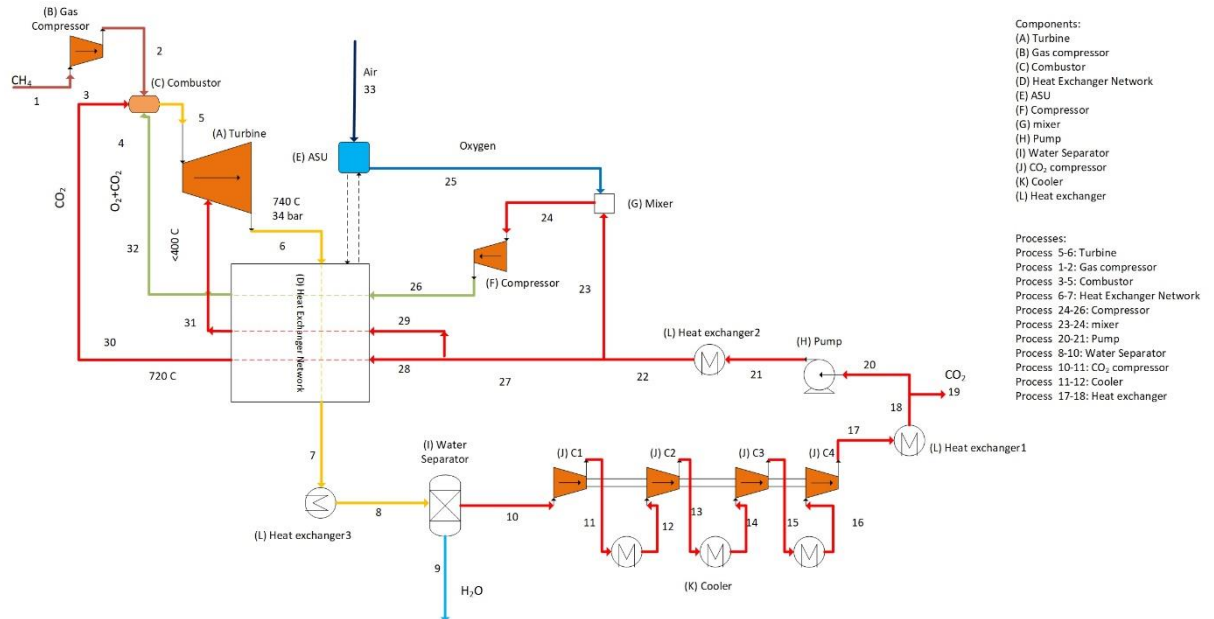


Figure 2.37 NetPower cycle schematic diagram (Davison, 2015)

NetPower cycle working flow is mainly carbon dioxide in a high-pressure. Turbine Inlet Pressure (TIP) is approximately 300 bar, and the low-pressure ratio is 10 bar. The direct-fired supercritical carbon dioxide (SCO_2) turbine is cooled with a cooling stream from the heat exchanger (Allam *et al.*, 2013).

The NetPower cycle is a Brayton cycle (Allam *et al.*, 2017). The NetPower cycle combustor burns natural gas with pure oxygen supplied from an ASU (Air Separation Unit) and high-pressure carbon dioxide stream inlets recycled from its power turbine. Recycled Fuel Gas (RFG) is heated with a recovery heat exchanger and flows to the combustor to reduce the Combustion Outlet Temperature (COT) by diluting the combustion products.

The RFG flowrate controls the temperature of combustion at an acceptable level. The direct-fired supercritical carbon dioxide (SCO_2) turbine is cooled with a cooling

stream from the heat exchanger (Allam *et al.*, 2013). The exhaust gas at 740 °C enters the recuperating heat exchanger that transfers heat from the hot outlet turbine exhaust gas to the three-cycle streams. This includes the carbon dioxide-rich stream recycled to the combustor for moderating the temperature of the combustor, the oxidant stream recycled to the combustor and the carbon dioxide-rich stream for cooling turbine blades. Also, the hot compressed air stream from the ASU enters the recuperating heat exchanger for recovering its heat. The cryogenic ASU provides the required oxygen for combustion.

The maximum pressure in the heat exchanger limit is 120 bar; therefore, oxygen cannot enter the heat exchanger at high pressure. The oxygen flow is mixed with part of the supercritical recycled CO₂ with oxygen concentrations in the range of 10–30% (molar basis), and then compressed to the required pressure by a dedicated O₂/CO₂ dense phase compressor. Before entering the combustor, the oxidant mixture is preheated in the regenerator (Scaccabarozzi, Gatti and Martelli, 2014).

The heat exchanger is one of the main parts of the NetPower cycle, and it has a main role in the efficiency of the NetPower cycle. The exhaust gas from the heat exchanger is cooled down, and the carbon dioxide is separated from the water. The water is sent to the wastewater treatment for recovery and treatment. A portion of the carbon dioxide stream from the water separation unit is fed for purification and compression unit. Most of the carbon dioxide is compressed and recycled back.

The recycled gas compression loop includes four stages inter-cooled compressor and two intercooled pumping stages. Inter-cooling is with cooling water. The carbon dioxide stream is divided into three parts; 45-50% of the flow rate is pumped to 305 bar and preheated in the recuperating heat exchanger. 10-12% of the flow rate is heated in the heat exchanger to 400 °C; then it is sent to the turbine for cooling the blade. The 32 to 45% of carbon dioxide stream is mixed with high purity oxygen. The oxidant stream is heated in the heat exchanger up to 720 °C , and it is sent to combustion to burn fuel (IEAGHG, 2015).

The critical features of the oxy turbine are 1) The inlet pressure is rather high. 2) The blades and shell are cooled because of the high Turbine Inlet Temperature (TIT). 3) The unconventional working fluid (Scaccabarozzi, Gatti and Martelli, 2014).

As for blade cooling, NetPower is proposed to use a classic open-circuit blade cooling system. Blades are cooled by the convection method, and there is a Thermal

Barrier Coating (TBC) on the blades to protect them from high temperature and corrosion. The heat transfer coefficient of CO₂ is significantly high; therefore, film cooling for the gas turbine is appropriate (Allam *et al.*, 2013).

One of the limitations of the Allam cycle is ASU operational parameters along with equipment constraints (Fernandes *et al.*, 2019); the cost of technology is another challenge of the NetPower. The NetPower equipment is required to redesign to overcome the limitations by using high pressure, highly recuperative, oxyfuel, supercritical CO₂ cycle (Power and Systems, 2017).

2.18.1 NetPower demonstration

The Allam cycle is one of the successful cycles, which is reached to the demonstration phase, 8 Rivers capital developed the Allam cycle for nearly seven years. NetPower company, which is owned by eight rivers, Exelon Generation and CB& I, developed the natural gas Allam cycle.

50 MW natural gas demonstration plant was completed in LA Porte, Texas, the USA by NetPower, and the first fire of plant had achieved success in May 2018. The plant is fully operational of the cycle with start-up, shut down, emergency operation, load following and partial load operation. 8 Rivers developed and designed the plant process and EPC (Engineering, Procurement and Construction) of the plant performed by CBI, and Exelon operates the plant.

The plant includes a novel supercritical CO₂ combustion Turbine, which is developed by Toshiba on a commercial scale. The 50 MWth demonstration plant was developed and simulated by 8 Rivers. All sizing and capacity are the actual design size.

Heatric company designed and fabricated the advanced high pressure printed circuit heat exchanger, which is one of the main parts of the power plant. The electrical output of the power plant is 25 MWe from 50MWth, and the power plant was built over a two-year period. 300 MWth NetPower plant is planned to demonstrate in 2022. The plant is based on natural gas (Flin, 2019).

2.18.1.1 Turbine

Novel turbine and combustion for NetPower demonstration have been developed by Toshiba. The hybrid design of the combustor and turbine cause operation in high temperature and pressure.

The turbine technology is a combination of steam turbine technology and gas turbine technology. The inner and outer pressure casing technology is from high-pressure steam turbine and technology of coating, internal cooling of turbine blades, and the inner casing is from demonstrated gas turbine technology (Allam *et al.*, 2017). Also, The turbine control system for NetPower has been developed by Toshiba.

2.18.1.2 Combustion

The NetPower cycle combustion needs novel technologies because of the working fluid present in the combustion region and high pressure. The stability of flame involves an additional challenge in the high-pressure range of 300 bar.

Figure 2.38 shows the 5MWth rig test; it was developed and proved in operation at full load combustion pressure of 300 bar.



Figure 2.38 5MWth combustor operating at 300 bar (Allam *et al.*, 2017)

The absence of nitrogen in the combustor is the beneficial aspect of Oxy-fuel combustion because one of the biggest challenges of design combustors is the reduction of the NO_x emission.

But the stable flame is the challenge of the premix oxy-fuel combustion; Toshiba developed a combustor with a very stable flame operation for the new Allam cycle (Allam *et al.*, 2017).

2.18.1.3 Heat exchanger

The main heart of the Net Power demonstration plant is a heat exchanger. It is one of the main parts to increase the efficiency of the cycle. A heat exchanger is supplied by Heatric company. This company designs Printed Circuit Heat Exchangers (PCHEs) with high performance and high-pressure specifications for NetPower plant, as shown in Figure 2.39.

Allam cycle high efficiency could not be possible with conventional heat transfer equipment. The close temperature approaches required can be achieved by diffusion bonded heat exchangers by Heatric company. The heat exchanger is made of 1.6 mm thick plates that are etched chemically; the geometry passes are designed in a complex pattern with maximum efficiency.

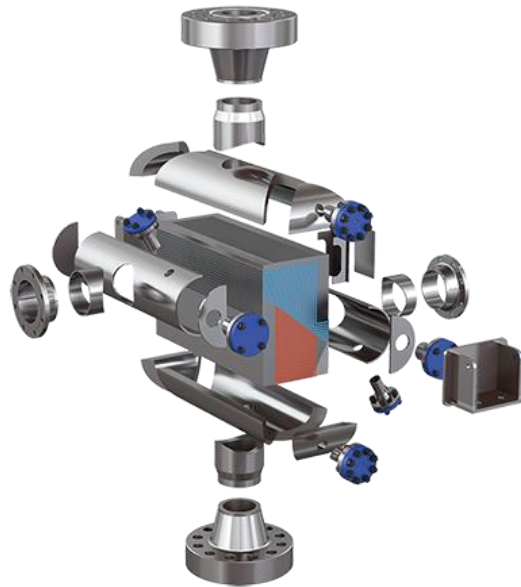


Figure 2.39 Heatric Printed Circuit Heat Exchanger (Heatric, 2020)

The Printed Circuit method causes flexibility to have separate flow streams on an individual plate, and the plates are diffusion bonded together. The heat exchanger package includes four joined multiple blocks to achieve the required duty. One block is the high-temperature block, which cools the turbine exhaust flow from 700 °C to 550 °C. The pressure is 300 bar, and it is required specifically to operate high pressure and temperature. This block is made from 6177 alloys.

The other block is low temperature, and the material is 316L stainless steel. The outlet temperature is about 60 °C (Allam *et al.*, 2017).

2.19 CES Cycle

Clean Energy System (CES) cycle is an oxy-combustion cycle that uses water (H_2O) as the main part of the working flow in the cycle. Bolland and Saether introduced the basic CES cycle, and then it is developed by Clean Energy Cycle Ltd (Zhao *et al.*, 2017).

Figure 2.40 shows the schematic Process Flow Diagram (PFD) of the Supercritical CES cycle. The CES cycle is essentially an internal combustion steam cycle using the injection of steam and liquid water in the combustor to moderate the firing temperature (Scaccabarozzi, Gatti and Martelli, 2014).

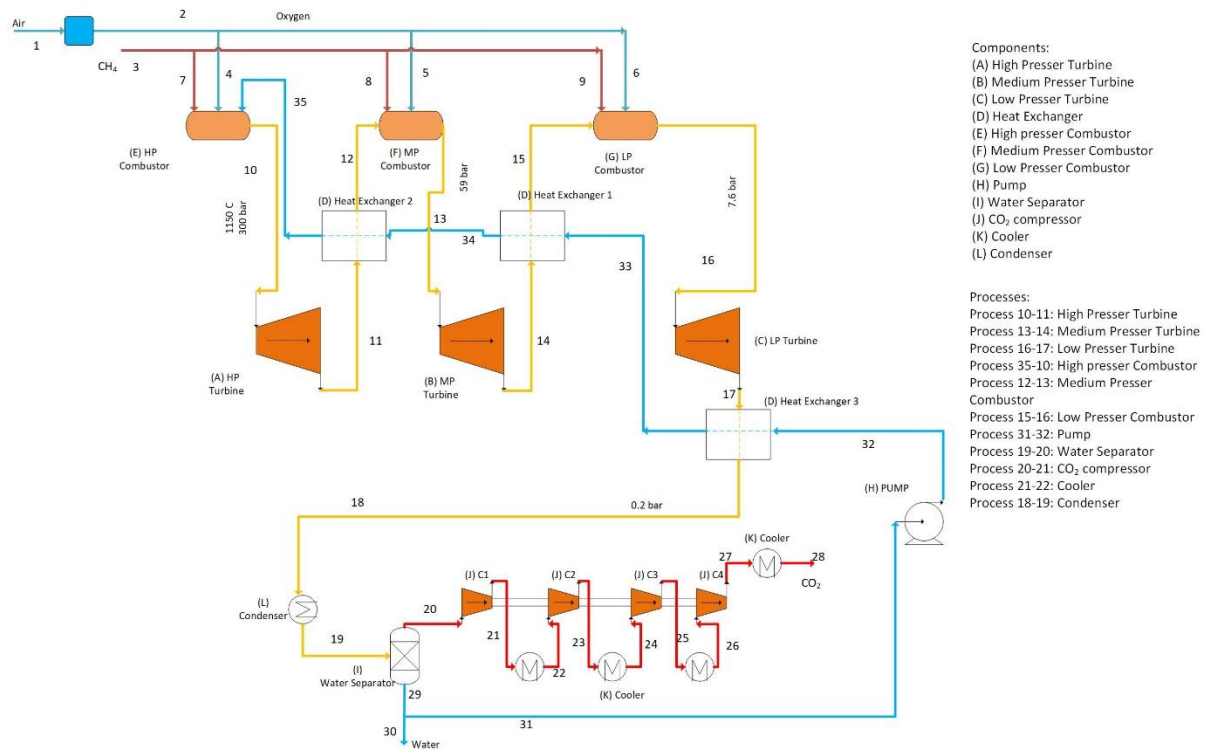


Figure 2.40 CES schematic diagram (Davison, 2015)

The supercritical CES is a further development of CES. It employs a combustor operating at supercritical steam conditions (Mancuso *et al.*, 2015). Complete reviews of the available oxy-combustion cycle options can be found in the recent report published by the International Energy Agency (IEA) Green House Gas program and co-authored by AMEC-Foster Wheeler and Politecnico di Milano (Mancuso *et al.*, 2015).

Supercritical CES Power cycle includes three turbines, compressor, and combustor. Natural gas is divided three-part, 23% of natural gas compressed to 310 bar is fed to the HP combustor, and 33% is fed to the MP, and the remaining is fed to the LP combustor. Fuel gases are preheated before feeding combustors. Pure oxygen is produced from ASU and compressed for HP combustor, and remaining are preheated before feeding to LP and MP combustor.

Exhaust gas from HPT is separated into two parts; one part is fed to the MP combustor and the remaining is directly fed to MPT for cooling the turbine to control blade metal temperature. Also, Exhaust gas from MPT is separated into two parts, one part is fed to the LP combustor, and the remaining is directly fed to LPT for the cooling turbine to control blade metal temperature.

There are four main units for supercritical CES cycle with carbon capture (IEAGHG, 2015): 1) Power Island 2) CO₂ purification and compression 3) Air Separation Unit (ASU) 4) Utility and of Site.

2.19.1 The CES technologies

During last decade, CES cycle efficiency is improved from 20% to 30% (50 MW J79/Deploy 2nd Generation Deploy), 35,45% (200 MW 3th Generation CES/Siemens/TriGen OFT900) and 50% (400MW CES/Siemens/TriGen) (Business and October, 2012). Clean Energy System (CES) demonstrates the project for testing, analyzing and design of modified Siemens SGT-900 gas turbine with the company of Siemens Energy and Florida Turbine Technology (FTT) and the US. Department of Energy (DoE) funding program (Climent Barba *et al.*, 2016b).

2.19.2 CES demonstration

The CES (Clean Energy System) power plant has main technical issues for designing the steam turbine with an inlet temperature of 1300 °C. The conventional steam turbine inlet temperature is 565 °C.

The 110 kW pilot project was proved at the University of California Davis by Clean Energy Systems in 2000. And the 20 MW power plant was operated in early 2003 for a few minutes test, and the 6MW power plant is operating now.

Also, a reheater was developed by the US Department of Energy's National Energy Technology Laboratory and tested by NASA. The power plant shows high efficiency and low-cost potential (Authors *et al.*, 2010).

2.19.2.1 Combustion

CES designed a 20 MWt combustor and integrated system after the acquisition of the Kimberlina power plant, as shown in Figure 2.41 (Anderson *et al.*, 2008).



Figure 2.41 20MWt Oxy-Fuel Combustor (Anderson *et al.*, 2008)

The second generation of CES combustion was the 170 MWt oxy-fuel combustion; it was designed in 2006 and fabrication completed in early 2008. The combustion with modified J79 gas turbine provides a power island, as shown in Figure 2.42.



Figure 2.42 170 MWt Oxy-Fuel Combustor (Anderson *et al.*, 2008)

2.19.2.2 Turbine

The first generation of the CES oxy-fuel turbine is from modified turbine. The modified GE79 gas turbine from an LMA1500 power system was utilized for a 50 MWe power plant. In this design, the compressor assembly is separated from the gas turbine unit (Anderson *et al.*, 2008).

The second generation of CES gas turbine is a modified intermediate pressure turbine (IPT) with a higher temperature (1180 °C). The selected gas turbine for modification was the Siemens SGT-900. CES redesigned SGT-900 by collaboration with Florida Turbine Technologies (FTT) and Siemens Energy and sponsored by the Department of Energy to create OFT-900 (Clean Energy System, 2020a).

The third generation of CES gas turbine is a similar new generation of Siemens gas turbine which is awarded by DOE. The inlet temperature is about 1760 °C and has high efficiency and low cost of electricity production (Anderson *et al.*, 2008).

2.20 Natural Gas Combined Cycle (NGCC)

The Natural Gas Combined Cycle (NGCC) or Combined Cycle Gas Turbine (CCGT) includes one Brayton and one Rankine cycle; natural gas burns with air to produce hot gas of CO_2 , H_2O and other byproducts, then expand in the gas turbine. The exhaust of the turbine enters the Heat Recovery Steam Generator (HRSG) to generate hot steam for the steam turbine. Carbon capture equipment can be added to the NGCC cycle during construction or as a retrofit. Figure 2.43 shows the schematic diagram of the NGCC.

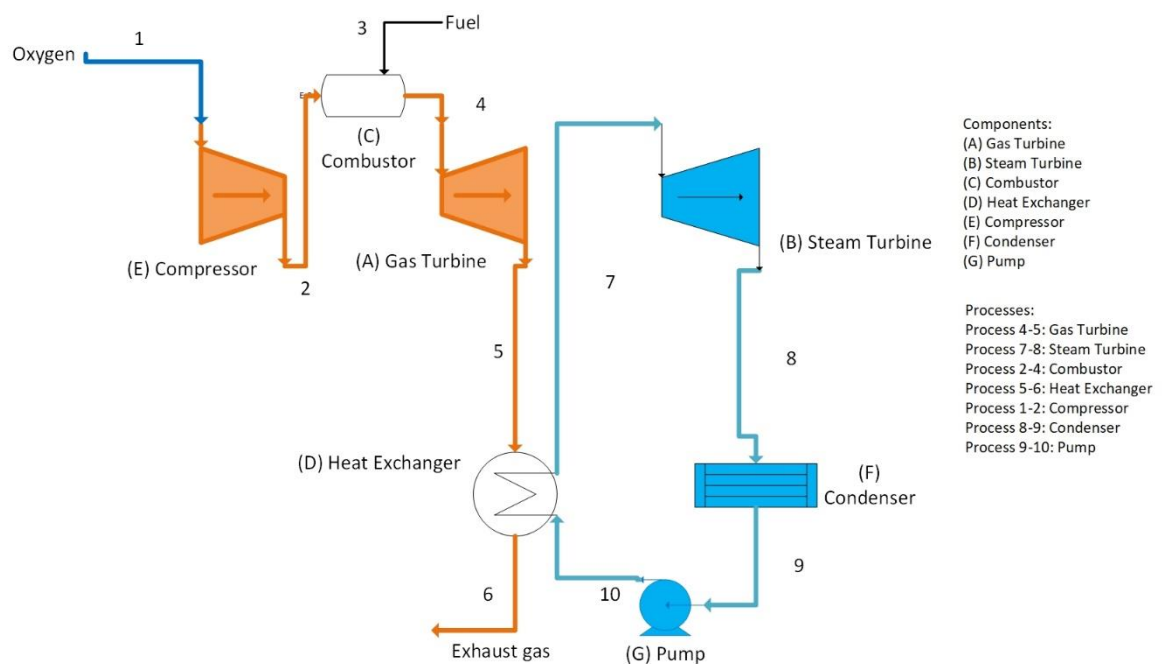


Figure 2.43 Natural Gas Combined Cycle (NGCC) (Davison, 2015)

2.21 The NGCC power plant with PCC

In the NGCC with Post Combustion Capture (PCC), an advanced amine solvents technology is used to capture CO_2 . This technology can be used to retrofit NGCC or used for near-term and large-scale power plants. The commercial PCC technology is developed by Aker Clean Carbon (ACC) of Norway, and it uses advanced amine solvent. The LHV efficiency for retrofit post-combustion capture technology is 49.8%, and for the newbuild plant, it increases up to 50.5%. Figure 2.44 shows a schematic diagram of the NGCC with PCC (Dillon *et al.*, 2013).

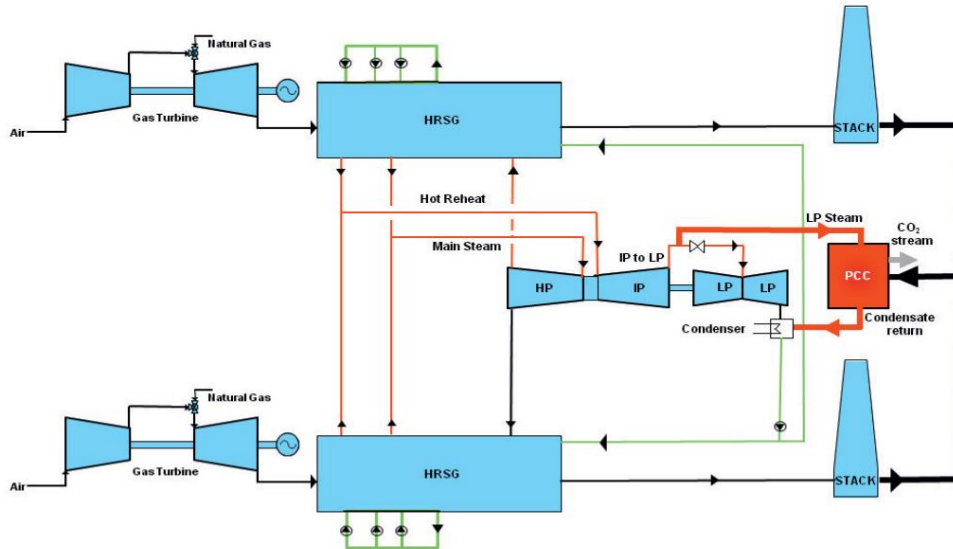


Figure 2.44 Natural Gas with PCC (Dillon *et al.*, 2013)

Other types of the oxy-combustion cycle are:

- Water-steam Rankine cycle with a steam-CO₂
- Recuperative reheat cycle (Gou *et al.*, 2006)
- Recuperative reheat cycle and a topping Brayton cycle (Gou *et al.*, 2006)
- LNG quasi-combined supercritical CO₂
- Rankine cycle (Zhang and Lior, 2006)
- ZE-SOLRGT (Luo and Zhang, 2011)

Although several Oxyturbine cycles are proposed and studied by thermodynamic analysis, only a few of them are currently in the demonstration phase.

2.22 Summary

This chapter has reviewed various technologies and issues related to main technologies of CO₂ capture, environmental impact, oxygen production and air separation unit and CO₂ compression and purification unit. Conventional gas turbines burn fuel with air and produce carbon dioxide as a byproduct. Zero Emission Power Plants (ZEPP) is the solution to avoid carbon dioxide emission. The ZEPP power plant needs to use Carbon Capture & Storage (CCS) technologies.

In this chapter, three main carbon capture technologies are investigated and compared in detail. An oxy-fuel combustion power cycle is a promising technology among other CCS technologies; it can produce very high CO₂ concentration in the flue gas with high efficiency. Recent technology development for oxy-fuel combustion causes reducing capital and operational cost. The air Separation Unit (ASU) is one of the challenges for oxy-fuel combustion technology and need to be improved for better cycle efficiency and have the main impact on the efficiency of the oxy-combustion cycle. Different methods of oxygen productions, including Cryogenic Air Separation (ASU), adoption, Pressure Swing Adsorption (PSA), Chemical processes and membranes, are investigated in this chapter.

Then, the oxy-combustion power cycles are investigated, and their main characteristics and parameters are presented. These oxy-combustion cycles are SCOC-CC, COOPERATE Cycle, MATIANT, E-MATIANT, CC_MATIANT, Graz and S-Graz cycles, AZEP 85% and 100%, ZEITMOP Cycle, COOLCEP-S Cycle, Novel O₂/CO₂ (Cao and Zheng, 2006), NetPower and CES Cycle. The oxy-combustion cycles offer high overall efficiencies for power generation while they offer high purity of CO₂ capture without producing NO_x; however, they need technically advanced components.

The Air Separation Unit (ASU) as an oxygen production unit requires high electricity consumption; this technology needs to develop to reduce auxiliary load. Other oxygen production technology also is used, including Ion Transport Membrane (ITM) in ZEITMOP cycle or Oxygen Ion Transport Membrane (OITM) in AZEP 100% and AZEP 80% cycle.

The highest efficiencies of oxy-combustion power cycles belong to S-Graze 57%, NetPower 55.1% and COOLCEP-S 59%. The S-CES cycle with steam working flow

is 48.9%, and ZEITMOP with ITM oxygen production technology is 51%, and AZEP 100% with OITM is 49.6%. Among these cycles, only NetPower and S-CES are recently in the demonstration stage, and these are investigated in detail in Chapters 7 and 8.

The recycled working flow for NetPower, E-MATIANT, CC-MATIANT are CO₂, and the recycled working flow for Graz, S-Graz, AZEP 100% and AZEP 85% cycles are a mixture of CO₂ and H₂O. The recycle working flow for the gas turbine cycle of SCOC-CC is CO₂, but the steam turbine cycle of SCOC-CC is H₂O. The recycled working flow for the ZEITMOP cycle is CO₂; however, it used air/oxygen depleted in its air cycle. The working recycled working flow for the S-CES cycle is H₂O. These cycles apply different technologies based on oxygen production methods and recycled working flow composition.

Chapter 3: Methodology and Process modelling of the leading Oxyturbine cycles

3.1 Introduction

Process simulation software can be used for four stages of a power plant design, including development, research, design and production. The software can be used to test specific designs under various design conditions without the need for running experiments. The process modelling can replace lab work and support research and development without the extensive cost of laboratory experiments and demonstration of the pilot plant. Also, the software can be used in the design stage for sizing the components of power cycles. In the production stage, the software can analyze the sensitivity of parameters without risk (Fogler and Gurmen, 2002).

Different types of process simulation software are developed recently, including ChemCad, AspenOne, gProms, BOAST, COMSOL, Eclipse, Thermoflex and ProSimplus software.

Among other software, the Aspen Plus is more user-friendly and can be used for real-world power plants from the research and development stage to monitoring full-scale power plants. Advanced System for Process Engineering (ASPEN) software was developed by researchers at MIT's laboratory in 1980. This software was commercialized with Aspen Tech company and has been developed for simulation of different types of processes (Uchechukwu Megwai, 2014).

Aveva's Pro II is cheaper than Aspen Plus software and leads in the mining industry; however, it's mostly designed for steady-state and can't change the converge method as easy as is Aspen Plus; also, Aspen Plus has a large database (ChemEngGuy, 2021). DWSIM is free and open-source software and performs similar tasks as Aspen plus commercial software. It can serve as an alternative process software for offshore petroleum production. Also, DWSIM has the same accuracy as Aspen Plus (Tangsriwong *et al.*, 2020).

3.2 Oxy-combustion power cycle theories and calculations

3.2.1 Thermodynamic concept and equations

Aspen Plus software uses the first principles of the thermodynamic to calculate parameters of the equipment, including turbine, compressor, heat exchanger, distillation and separator.

3.2.1.1 Continuity

The conservation of mass, along with conservation of energy and momentum, are the fundamental concept of physics. The thermodynamic and fluid mechanic problem can be solved with this fundamental concept. Conservation of mass is maintained by summation of input mass minus summation of output mass equal to change in mass in the control volume. The mass balance of control volume for the transient system is shown in Equation 3-1.

$$\sum_i \dot{m}_i - \sum_o \dot{m}_o = \frac{\partial m}{\partial t} \quad \text{Equation 3-1}$$

The mass in the turbomachine with the steady-state condition is constant over time, and it holds for all equipment in the steady-state. The mass balance for the steady-state process is shown in Equation 3-2.

$$\sum_i \dot{m}_i = \sum_o \dot{m}_o \quad \text{Equation 3-2}$$

The conservation of the mass can be written based on the velocity, density and area for a steady-state turbomachine, as shown in Equation 3-3.

$$\rho_i V_i A_i = \rho_o V_o A_o \quad \text{Equation 3-3}$$

3.2.1.2 Energy conservation

Another fundamental concept of physics is the first law of thermodynamic or energy conservation law. It means the amount of energy is constant, and energy is neither destroyed nor created. The energy can be converted from one form to another, but the total energy within the domain remains constant. The energy balance for steady-state control volume is shown in Equation 3-4.

$$\sum_i \dot{E}_i + \dot{Q} = \sum_o \dot{E}_o + \dot{W} \quad \text{Equation 3-4}$$

3.2.1.3 Energy quality (second law of thermodynamic)

The second law of thermodynamic is entropy balance. Entropy, same as energy and mass, is the extensive property and can be transferred into or out of control volume by mass streams. Since entropy is a property, it changes from one state to another. The entropy rate balance for the transient system is shown in Equation 3-5.

$$\frac{\partial S_{cv}}{\partial t} = \sum_i \frac{\dot{Q}}{T} + \sum_i \dot{S} - \sum_e \dot{S} + \dot{S}_{gen} \quad \text{Equation 3-5}$$

The \dot{S}_{gen} indicates the entropy generation rate due to irreversibility within the control volume. The entropy rate balance for the steady-state system is shown in Equation 3-6

$$\sum_i \dot{S} + \sum_i \frac{\dot{Q}}{T} + \dot{S}_{gen} = \sum_o \dot{S} + \sum_o \frac{\dot{Q}}{T} \quad \text{Equation 3-6}$$

3.2.1.4 Thermodynamic cycles

The thermodynamic concept of power cycles is based on the heat engine. The energy enters from the heat source at a high temperature, and part of it is converted to work, and the remaining energy exit into the heatsink at a low temperature. The power cycle's efficiency depends on the design parameters, including hot temperature source, the temperature of the heatsink, pressure ratio, the efficiency of compressor and turbine, heat exchanger min temperature of the power cycle. Different temperatures between heat source and heatsink can affect the efficiency based on the Carnot concept.

There are two main types of thermodynamic power cycles: external combustion engines or internal combustion engines. Thermodynamic cycles are categorised in Table 3.1.

Table 3.1 Thermodynamic power cycle types

Cycles	Engine type external or internal	Working flow phase
Rankine cycle (SHEPHERD, 2013)	External	Phase changes
Carnot Cycle (Zanzig, 1963)	External	Gas
Stirling (Zanzig, 1963)	External	Gas
Ericsson (Atkinson <i>et al.</i> , 2009)	External	Gas
Bell Coleman (Dinçer and Kanoğlu, 2010)	External	Gas
Hygroscopic (Rubio-Serrano, Soto-Pérez and Gutiérrez-Trashorras, 2019)	External	Gas
Malone engine (Vogel, 1992)	External	Liquid
Scuderi	External	Gas
Manson	External	Gas
Stoddard	External	Gas
Brayton cycle (SHEPHERD, 2013)	Internal	Gas
Otto Gasoline petrol	Internal	Gas
Diesel	Internal	Gas
Lenior	Internal	Gas

3.2.2 Exergy equations for the oxyfuel combustion cycle

Exergy analysis is a practical approach to evaluate the merit of energy conversion. Energy analysis can not evaluate energy conversion systems efficiently and precisely (Terzi, 2018).

Exergy analysis provides the causes and locations of thermodynamic losses more clearly than energy analysis. Hence, exergy analysis can assist in improving and optimizing designs (Dincer and Rosen, 2021) and find out which equipment in the system need to be improved.

The exergy balance can be extracted from the second thermodynamic law and entropy formula, as shown in Equation 3-7.

$$\sum_i \dot{E}x_i + \sum_k \left(1 - \frac{T}{T_k}\right) \dot{Q}_k = \sum_o \dot{E}x_o + \dot{W} + \dot{E}x_d \quad \text{Equation 3-7}$$

Also, it can be rearranged in Equation 3-8 (Javadzadeh and Hamedeyaz, 2014):

$$\begin{aligned} \dot{E}x^{CHE} + \left(\sum_{inlet} \dot{E}x^T - \sum_{outlet} \dot{E}x^T \right) + \left(\sum_{inlet} \dot{E}x^p - \sum_{outlet} \dot{E}x^p \right) \\ + T_o \left(\sum_{inlet} \dot{S}_i - \sum_{outlet} \dot{S}_i + \frac{\dot{Q}_{cv}}{T_o} \right) = \dot{E}x^w \end{aligned} \quad \text{Equation 3-8}$$

The exergy rate can be calculated as Equation 3-9:

$$\dot{E}x = \dot{m}(e_x) \quad \text{Equation 3-9}$$

Figure 3.1 the early classification of the exergy and Szargut et al. (1988) classified the total exergy include thermal, potential and kinetic exergy. Also, the thermal exergy includes chemical, physical, exergy.

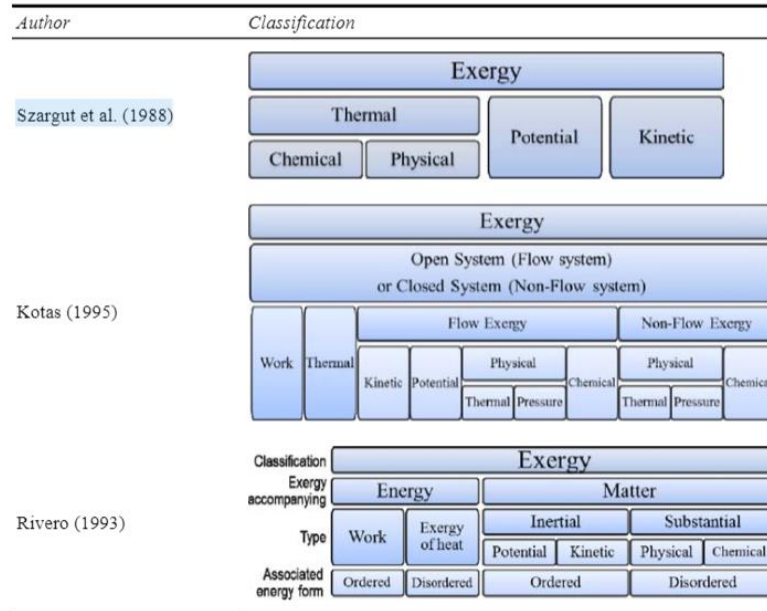


Figure 3.1 Different classifications of exergy (Marmolejo-Correa and Gundersen, 2015)

Figure 3.2 shows the new classification for exergy; this classification is used for the exergy analysis in this thesis. Total exergy includes chemical and physical exergy, and chemical exergy includes mixing and separation (molar fraction of components) and chemical reaction (chemical exergy inside the substance). The physical exergy includes thermo-mechanical and mechanical exergy.

Thermo-mechanical exergy is temperature and pressure based. These are used for most of the thermodynamic cycles. The mechanical exergy is kinetic and potential, which is usually considered constant in the thermodynamic cycle.

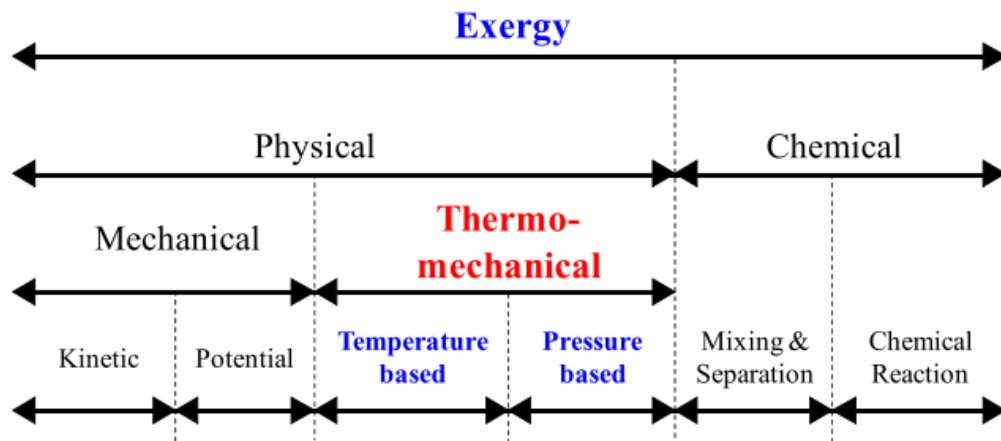


Figure 3.2 New classification of the exergy for pressure-volume-temperature PVT systems (Quality, 2011)

The total exergy can be calculated with Equation 3-10 (Sato, 2004):

$$E = \sum_i n_i \varepsilon_i^o + RT_o \sum_i n_i \ln \frac{P_i}{P_o} + \sum_i n_i C_{p,i} (T - T_o - T_o \ln \frac{T}{T_o}) + RT_o \sum_i (n_i \ln(\frac{n_i}{\sum_i n_i})) \quad \text{Equation 3-10}$$

The first part and last part of Equation 3-10 are the chemical exergy terms as shown in Equation 3-11 (Ibrahim Dincer, 2013):

$$ex_{ch,3} = \sum_k x_k ex_{ch}^k + RT_o \sum_k x_k \ln x_k \quad \text{Equation 3-11}$$

The second and third parts of Equation 3-10 are physical exergy terms as shown in Equation 3-12 (Ibrahim Dincer, 2013):

$$\begin{aligned}
 ex_{ph,3} &= (h_3 - h_o) - T_o(s_3 - s_o) && \text{Equation 3-12} \\
 &= C_p(T_3 - T_o) - T_o(C_p \ln \left(\frac{T_3}{T_o}\right) - R \ln \frac{P_3}{P_o})
 \end{aligned}$$

Also, the exergy of pressure and temperature can be rewritten as Equation 3-13 (Gundersen, 2009):

$$\begin{aligned}
 e_x^{(T)} &= c_p \left[T - T_o \left(1 + \ln \left(\frac{T}{T_o} \right) \right) \right] && \text{Equation 3-13} \\
 e_x^{(P)} &= T_o \cdot R \cdot \ln \frac{P}{P_o} = \frac{k-1}{k} \cdot c_p \cdot T_o \cdot \ln \frac{P}{P_o}
 \end{aligned}$$

Table 3.2 Shows chemical exergy for different substances (chemical reaction exergy) at P0=1.0 atm and T0=298.15 K:

Table 3.2 Standard molar chemical exergy of different substances at P0=1.0 atm and T0=298.15 K (Ibrahim Dincer, 2013)

Chemical exergy [KJ/Kmol]	
H ₂	236,100
O ₂	3970
N ₂	720
CH ₄	831,650
CO	275,100
CO ₂	19,860
C ₂ H ₆	14,95,840
C ₃ H ₈	21,54,000
C ₄ H ₁₀	28,05,800
H ₂ O liquid	900
H ₂ O vapour	9500

To calculate the total exergy of the flow, it requires to calculate physical exergy (temperature and pressure) and chemical exergy (chemical reaction and molar fraction).

3.2.3 Exergy destruction equations

The exergy B balance of a process gives:

$$B_{in} = B_{out} + B_{lost} + B_{destroyed} \quad \text{Equation 3-14}$$

With exergy efficiency defined as:

$$\eta_B = \frac{B_{out}}{B_{in}} = 1 - \frac{(B_{lost} + B_{destroyed})}{B_{in}} \quad \text{Equation 3-15}$$

For many engineering systems, this can be rephrased as:

$$\eta_B = \frac{\dot{W}_{net}}{\dot{m}_{fuel}\Delta G_T^0} \quad \text{Equation 3-16}$$

Where ΔG_T^0 is standard Gibbs (free) energy of reaction at temperature T and pressure $P_0 = 1$ bar (also known as the standard Gibbs function change). \dot{W}_{net} is the network output and \dot{m}_{fuel} is the mass flow rate of fuel.

The energy efficiency can be extracted from Equation 3-17 and Equation 3-18.

Equation 3-17

$$\eta_E = \frac{\dot{W}_{net}}{\dot{m}_{fuel}\Delta H_T^0}$$

Equation 3-18

$$\eta_B = \frac{\dot{W}_{net}}{\dot{m}_{fuel}\Delta G_T^0}$$

ΔH_T^0 is the standard enthalpy of reaction at temperature T and pressure $P_0 = 1$ bar, and always $\Delta G_T^0 < \Delta H_T^0$ so the energy efficiency must be smaller than the exergy efficiency. Sankey diagram can be used to show exergy flow in each oxy-combustion cycle. (Sharifzadeh, Meghdari and Rashtchian, 2017). The methane chemical energy per kg can be calculated by multiply 1.06 to LHV of Methane (Ahmadi, Dincer and Rosen, 2011). The total input exergy into the system is based on Equation 3-19:

Equation 3-19

$$\text{Chemical exergy fuel} = 802361 \frac{\text{J}}{\text{mol}} \times 1.06 \times m \frac{\text{mol}}{\text{s}} = \text{total chemical exergy}$$

$$\text{Total Chemical exergy fuel} + \text{physical exergy from oxygen} = \text{Total input exergy}$$

Table 3.3 shows the exergy balance for the oxy-combustion power cycle.

Table 3.3 Exergy balance equations for oxy-fuel combustion power cycle (Karaağaç, Kabul and Oğul, 2019)

System units	Mass balance equations	Energy balance equations	Exergy balance equations	Entropy balance equations	Exergy efficiency
Compressor	$\dot{m}_1 = \dot{m}_2$	$\dot{m}_1 \cdot h_1 + W_C = \dot{m}_2 h_2$	$E_{x1} + W_C = E_{x2} + E_{xdest}$	$\dot{m}_1 s_1 + S_{gen} = \dot{m}_2 s_2$	$\eta_{II} = \frac{E_{x2} - E_{x1}}{W_C}$
Combustion chamber	$\dot{m}_2 + \dot{m}_f = \dot{m}_3$	$\dot{m}_2 \cdot h_2 + \dot{m}_f \cdot h_f = \dot{m}_3 h_3$	$E_{x2} + E_{Y_{fuel}} = E_{x3} + E_{xdest}$	$\dot{m}_2 s_2 + S_{production} + \frac{Q_G}{T_K} = \dot{m}_3 s_3$	$\eta_{II} = \frac{E_{x3}}{E_{x2} + E_{fuel}}$
Gas turbine	$\dot{m}_3 = \dot{m}_4$	$\dot{m}_3 \cdot h_3 = \dot{m}_4 h_4 + W_T$	$E_{x3} = E_{x4} + W_T + E_{xdest}$	$\dot{m}_3 s_3 + S_{production} = \dot{m}_4 s_4$	$\eta_{II} = \frac{W_T}{E_{x3} - E_{x4}}$
HRSO	$\dot{m}_4 = \dot{m}_5$ $\dot{m}_7 = \dot{m}_8$ $\dot{m}_{18} = \dot{m}_{19} + \dot{m}_{20}$	$\dot{m}_4 h_4 + \dot{m}_7 h_7 +$ $\dot{m}_{18} h_{18} = \dot{m}_5 h_5 + \dot{m}_8 h_8 +$ $\dot{m}_{19} h_{19} + \dot{m}_{20} h_{20} + Q_L$	$E_{x4} + E_{x7} + E_{x18} = E_{x5} +$ $E_{x8} + E_{x19} + E_{x20} +$ $Q_L \left(1 - \frac{T_0}{T_K}\right) + E_{xdest}$	$\dot{m}_4 s_4 + \dot{m}_7 s_7 + \dot{m}_{18} s_{18} + S_{gen} =$ $\dot{m}_5 s_5 + \dot{m}_8 s_8 + \dot{m}_{19} s_{19} + \dot{m}_{20} s_{20} + \frac{Q_G}{T_K}$	$\eta_{II} = \frac{(E_{x8} - E_{x7}) + (E_{x19} - E_{x18})}{E_{x4} - E_{x5}}$
Pump LP	$\dot{m}_{17} = \dot{m}_{18}$	$\dot{m}_{17} \cdot h_{17} + W_{PLP} = \dot{m}_{18} h_{18}$	$E_{x17} + W_{PLP} = E_{x18} + E_{xdest}$	$\dot{m}_{17} s_{17} + S_{gen} = \dot{m}_{18} s_{18}$	$\eta_{II} = \frac{E_{x18} - E_{x17}}{W_P}$
Pump HP	$\dot{m}_6 = \dot{m}_7$	$\dot{m}_6 \cdot h_6 + W_{P2} = \dot{m}_7 h_7$	$E_{x6} + W_{PHP} = E_{x7} + E_{xdest}$	$\dot{m}_6 s_6 + S_{gen} = \dot{m}_7 s_7$	$\eta_{II} = \frac{E_{x7} - E_{x6}}{W_P}$
Pump 1	$\dot{m}_{12} = \dot{m}_{13}$	$\dot{m}_{12} \cdot h_{12} + W_{P1} = \dot{m}_{13} h_{13}$	$E_{x12} + W_{P1} = E_{x13} + E_{xdest}$	$\dot{m}_{12} s_{12} + S_{gen} = \dot{m}_{13} s_{13}$	$\eta_{II} = \frac{E_{x13} - E_{x12}}{W_P}$
HP	$\dot{m}_8 = \dot{m}_9$	$\dot{m}_8 \cdot h_8 = \dot{m}_9 h_9 + W_{HP}$	$E_{x8} = E_{x9} + W_{HP} + E_{xdest}$	$\dot{m}_8 s_8 + S_{gen} = \dot{m}_9 s_9$	$\eta_{II} = \frac{W_T}{E_{x8} - E_{x9}}$
LP	$\dot{m}_{10} = \dot{m}_{11}$	$\dot{m}_{10} \cdot h_{10} = \dot{m}_{11} h_{11} + W_{LP}$	$E_{x10} = E_{x11} + W_{LP} + E_{xdest}$	$\dot{m}_{10} s_{10} + S_{gen} = \dot{m}_{11} s_{11}$	$\eta_{II} = \frac{W_T}{E_{x10} - E_{x11}}$
Condenser	$\dot{m}_{11} = \dot{m}_{12}$ $\dot{m}_{21} = \dot{m}_{22}$	$\dot{m}_{11} h_{11} + \dot{m}_{21} h_{21} = \dot{m}_{12} h_{12} +$ $\dot{m}_{22} h_{22} + Q_L$	$E_{x11} + E_{x21} = E_{x12} + E_{x22} +$ $Q_{in} \left(1 - \frac{T_0}{T_K}\right) + E_{xdest}$	$\dot{m}_{11} s_{11} + \dot{m}_{21} s_{21} + S_{gen} = \dot{m}_{12} s_{12} +$ $\dot{m}_{22} s_{22} + \frac{Q_{in}}{T_K}$	$\eta_{II} = \frac{E_{x22} - E_{x21}}{E_{x11} - E_{x12}}$
Deaerator	$\dot{m}_{14} + \dot{m}_{20} = \dot{m}_{15}$	$\dot{m}_{14} h_{14} + \dot{m}_{20} h_{20} = \dot{m}_{15} h_{15} +$ Q_L	$E_{x14} + E_{x20} = E_{x15} +$ $Q_{in} \left(1 - \frac{T_0}{T_K}\right) + E_{xdest}$	$\dot{m}_{14} s_{14} + \dot{m}_{20} s_{20} + S_{gen} = \dot{m}_{15} s_{15}$	$\eta_{II} = \frac{E_{x15}}{E_{x14} + E_{x20}}$
Heat exchanger	$\dot{m}_{13} = \dot{m}_{14}$ $\dot{m}_{15} = \dot{m}_{16}$	$\dot{m}_{13} h_{13} + \dot{m}_{15} h_{15} = \dot{m}_{14} h_{14} +$ $\dot{m}_{16} h_{16} + Q_L$	$E_{x13} + E_{x15} = E_{x14} + E_{x16} +$ $Q_{in} \left(1 - \frac{T_0}{T_K}\right) + E_{xdest}$	$\dot{m}_{13} s_{13} + \dot{m}_{15} s_{15} + S_{gen} = \dot{m}_{14} s_{14} +$ $\dot{m}_{16} s_{16} + \frac{Q_{in}}{T_K}$	$\eta_{II} = \frac{E_{x15} - E_{x16}}{E_{x14} - E_{x13}}$

The energy efficiency can measure the quantity of the energy, but exergy can measure the quantity and quality of the energy. The exergy analysis especially helps to evaluate the waste and quality of the waste energy in each component. The exergy analysis enables us to find the emission of each component to the environment (Liao *et al.*, 2013).

The exergy destruction into the equipment can show the amount of heat release to the environment with each component. (Flanner, 2009) shows global warming is because of the waste heat and green gas emission. The heat waste of each component can be calculated by exergy analysis of the components.

The high thermal efficiency cannot cause high exergy efficiency (Shao *et al.*, 2018). Exergy analysis can provide the scale to find out which component has the highest destruction and heat loss and can be used to improve the efficiency of the cycle by indicating and revising the highest exergy lost equipment.

3.2.4 EOS for gas turbine and steam turbine

Equation of State (EOS) provides a mathematical formula to express the relation of physical states of matter. The Equation of State (EOS) usually relates pressure (P), volume (V), temperature (T) and the number of atoms to another. Table 3.4 shows the list of the equation of state (EOS) and specifications:

Table 3.4 Equation Of State (EOS)

Equation of State (EOS)	Type	Description
$pV = \text{constant}$	Linear	Boyle's law
$\frac{V_1}{T_1} = \frac{V_2}{T_2}$	Linear	Charles's law
$p_{\text{total}} = P_1 + P_2 + \dots + P_n = \sum_{i=1}^n p_i$	Linear	Dalton's law of partial pressures (1801)
$pV_m = R(T_C + 273.15 \text{ }^\circ\text{C})$	Linear	In 1834, Émile Clapeyron combined Boyle's Law and Charles' law into the first statement of the ideal gas law.

$(p + \frac{a}{V_m^2})(V_m - b) = RT$	Cubic $a = 3p_c V_c^2 \quad b = \frac{V_c}{3}$	Van der Waals equation of state (1873)
$p = \frac{RT}{V_m - b} - \frac{a}{\sqrt{T}V_m(V_m + b)}$	Cubic $a = 0.42748 \frac{R^2 T_c^5}{P_c}, \quad b = 0.08664 \frac{R T_c}{P_c}$	Redlich-Kwong equation of state
$p = \frac{RT}{V_m - b} - \frac{a \alpha}{V_m(V_m + b)}$ $\alpha = (1 + (0.48508 + 1.55171\omega - 0.15613\omega^2)(1 - T_r^{0.5}))^2$	Cubic $a = \frac{0.42747 R^2 T_c^2}{P_c}, \quad b = \frac{0.08664 R T_c}{P_c}$ $T_r = \frac{T}{T_c}$	Soave modification of Redlich-Kwong
$p = \frac{RT}{V_{m,SRK} - b} - \frac{a}{V_{m,SRK}(V_{m,SRK} + b)}$	Cubic $a = a_c \alpha$ $a_c = \frac{0.42747 R^2 T_c^2}{P_c}, \quad b = 0.08664 \frac{R T_c}{P_c}$	Volume translation of Peneloux et al. (1982)
$p = \frac{RT}{V_m - b} - \frac{a \alpha}{(V_m^2 + 2bV_m - b^2)}$	Cubic $a = 0.45724 \frac{R^2 T_c^2}{P_c}, \quad b = 0.07780 \frac{R T_c}{P_c}$ $\alpha = (1 + k(1 - T_r^{\frac{1}{2}}))^2$ $k = 0.37464 + 1.54226\omega - 0.26992\omega^2$ $T_r = \frac{T}{T_c}$	Peng–Robinson equation of state

In the oxy-combustion cycle simulation, the Peng-Robinson equation of state can be used for all modelling, including the Main cycle, ASU and CPU. This equation of state can give reasonable results at all temperatures and pressures. The steam tables can be used for the Rankine cycle and cooling water calculations (Almås, 2012). Sensitivity to PR equation of state is evaluated by Martelli et al., 2019, and the results indicate PR has the lowest gap with respect to REFPROP results, and the PR EoS is the best solution in the case of pure CO₂ (Martelli, 2019).

3.3 Modelling and simulation

3.3.1 Plant simulation with a numerical approach

There are two main numerical approach methods to calculate thermodynamic points and evaluation of thermodynamic properties for power plant components. These two methods are the sequential modular (SM) approach and the Equation Oriented (EO) approach.

In the Sequential Modular (SM) approach, the calculation is based on the subsequent block; the Output of each component is calculated based on the input and parameters of the block. The output result of each component will be the input of the following component.

In the equation oriented (EO) approach, The set of the equations are calculated based on the mass and energy balance and operation mode by simulation toolbox. It can easily simulate the thermodynamic cycle without the limitation of the SM strategy. However, the solution algorithm needs to be robust and reliable, and the solvers are more dependent on the initial point of iteration (Macchi, 2017).

3.3.2 Aspen Plus pros and cons

Aspen Plus software can be used for modelling power cycle and chemical processes. A large database of working fluids is available in Aspen Plus. Also, different EOSs can be selected for the calculation of the thermodynamic properties of the working fluid.

The Peng Robinson is a simple EOS, and it can be selected in Aspen Plus for modelling Gas turbine cycle. Also, advanced EOSs are available in Aspen Plus to be use for modelling of working fluid near saturation area or critical point. Besides, Aspen Plus can calculate mixed working fluid properties with two or more components to simulate a complex cycle.

One of the weaknesses of the Aspen Plus software is to define user-defined components and model actual turbines. The turbine block is a basic version of the turbine and can describe with isentropic efficiency. It cannot be linked to working fluid properties and other cycle and turbine parameters. Hence the accurate modelling of

turbine block required the definition of ad hoc models; the Aspen Plus software does not have a cooled turbine block, the combustor outlet temperature reached is higher than the maximum temperature allowed by the walls materials, but the cooling flow can not enter the expander block in different cooled step (Scaccabarozzi, Gatti and Martelli, 2014).

Also, Aspen Plus has limitations to model off-design and dynamic analysis because of fixed parameters of the blocks and the governing equations (Macchi, 2017). In the simulation, the efficiency penalty of vanes, cooling blades of turbine and walls of combustion or heat loss through the pipes are not taken into account and cycle efficiency penalty can be 2-3% of simulation efficiency (Cao and Zheng, 2006).

3.3.3 Modelling equipment in Aspen Plus

3.3.3.1 Distillation column

It is the general known process where multi-components are separated into pure components based on their difference in boiling points. This column typically consists of an enriching section where concentrated vapours are sent to the condenser and a stripping section where liquid/heavies are present.

The separation of components from a liquid mixture based on their vapour pressure or boiling point is called distillation.

The distillation has varied types as followings:

1. Flash evaporation
2. Fractional distillation
3. Steam distillation
4. Simple Distillation
5. Azeotropic distillation

3.3.3.2 Stripper (or desorption)

The opposite process to absorption is generally called stripping. The operation of removing absorbed solute from the solvent is called stripping. For example,

Ammonia is dissolved in water through the absorption process. The removal of absorbed Ammonia from the solvent (water) is called stripping. The stripping is also called a desorption process.

The flash stripper was used to model the separation of Carbon dioxide from water, It is essentially a distillation process where the heavy product is water/liquid, and the lighter product is generally a mixture of volatile organic materials. Generally, steam/air is used for heating purposes in the column. The separator simulates equilibrium phase separation (Haydary, 2019).

3.3.3.3 Absorption (opposite of striping)

In absorption (also called gas absorption, gas scrubbing, or gas washing), there is a transfer of one or more species from the gas phase to a liquid solvent. The species transferred to the liquid phase are referred to as solutes or absorbate. Absorption involves no change in the chemical species present in the system. Absorption is used to separate gas mixtures, remove impurities, or recover valuable chemicals. The operation of removing the absorbed solute from the solvent is called stripping. Absorbers usually are used with strippers to permit regeneration (or recovery) and recycling of the absorbent (Nguyen, 2012).

Absorption: gas is purified; solute is absorbed from the gas into the liquid stream

Stripping: liquid is purified; solute stripped from the liquid into a gas (Wankat, 1988)

3.3.3.4 Separator blocks in Aspen Plus

The Separator Blocks, Sep and Sep2, combine feed streams and then split the resulting stream based on your specifications. When the details of the separation are unknown or unimportant, you can use Sep and Sep2 instead of rigorous separation models (such as distillation or absorption models) to save computational time.

The flash blocks, Flash 2 and Flash 3, determine the thermal and phase conditions of a mixture with one or more inlet streams. You can generate heating or cooling curve tables for these models.

The flash blocks represent single-stage separators such as knock-out drums. They perform a phase equilibrium flash calculation based on the specifications. Adiabatic,

isothermal and isobaric flashes, and dew or bubble points, are among the calculations (Machner, 1958).

Decanter block can be used for the separation of two liquid phases but without a vapour phase (Machner, 1958). Decant process is used to draw off the liquid without disturbing the sediment.

3.3.4 MATLAB Code link with Aspen Plus

The MATLAB code is provided to link Aspen Plus software to MATLAB. The output data from Aspen Plus simulation input to the MATLAB software for further calculation of the other parameters of the cycle. Also, the MATLAB code allows to change design parameters of the power cycle and input them into the Aspen Plus software for simulation and output of the Aspen Plus simulation send back to the MATLAB (Appendix A).

The code in the MATLAB M file can create a local COM automation server to interface MATLAB with Aspen Plus and run the Aspen Plus software based on the MATLAB input (Tang, Boulter and Kitching, 2003). In this thesis, MATLAB code help to calculate the exergy of each component, cost and other parameters; hence the bar charts and graphs can be drawn with MATLAB. Furthermore, optimisation can be performed with MATLAB code in future papers.

3.4 Oxy combustion cycles modelling and simulation

3.4.1 The SCOC-CC cycle modelling and analysis

Figure 3.3 shows the Semi-Closed Oxy-Combustion Combined Cycle SCOC-CC cycle model in Aspen Plus software based on the schematic presented in Figure 2.18 of chapter 2; it has two parts steam cycle and gas turbine cycle.

The fuel and pure oxygen burn in the combustion and recycled CO₂ stream enter combustion to cool the combustion to 1517 °C, and the exhaust flow (Stream 2) from combustion enters to the Gas turbine for expanding from 45.8 bar to 1.07 bar pressure.

The gas turbine exhaust flue (Stream 3) enters HRSG for recovering heat for the steam cycle. Low pressure and temperature exhaust from HRSG (Stream 4) enters the condenser to condense water and separate from carbon dioxide. The part of carbon dioxide exhaust from the condenser (Stream 5) is compressed and recycled back to the combustion (Stream 1). The Schematic Process Flow Diagram of SCOC-CC is shown in Figure 3.3. Oxygen is fed from ASU to the cycle and thereby avoiding the post-combustion process for removing CO₂ in comparison with GT-CC with post-combustion capture (Bolland and Saether, 1992).

The Steam cycle working flow is mainly water, and High pressure and temperature water (Stream S4) enters the turbine for expansion. The exhaust flue from the steam turbine (Stream S6) enters the condenser and then pumped back to the HRSG (Stream S5). The stream properties are in Table 3.5.

Table 3.5 working flow properties at each stage for SCOC-CC cycle, the main working flow for the steam cycle is water, and recycled working flow for the gas turbine is carbon dioxide.

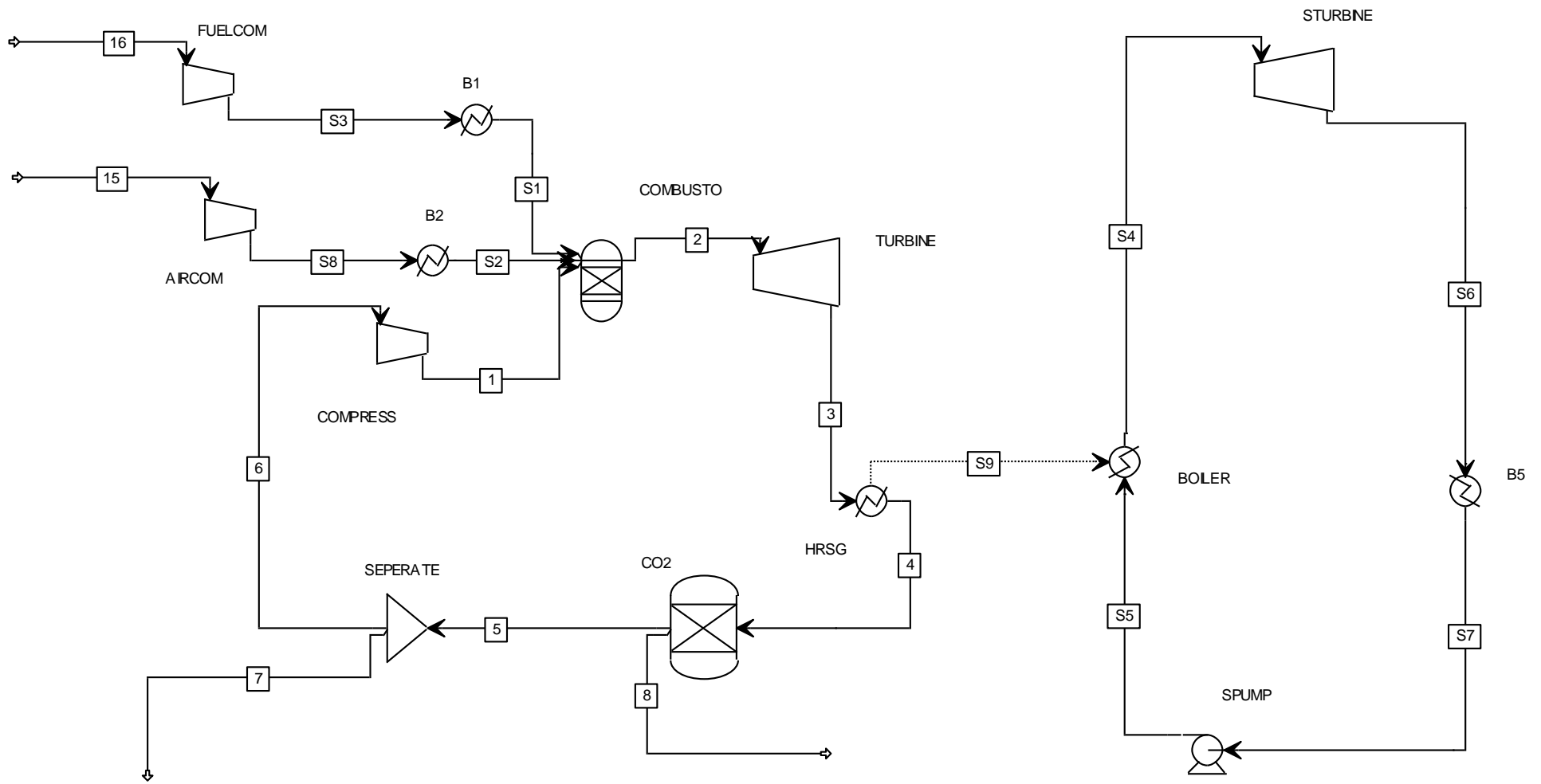


Figure 3.3 Aspen Plus modelling of SCOC-CC

Table 3.5 Stream properties of SCOC-CC cycle from Aspen plus modelling

Stream Name	Units	1.00	2.00	3.00	4.00	5.00	6.00	7.00	8.00
Description									
From		COMPRESS	COMBUSTO	TURBINE	HRSG	CO2	SEPERATE	SEPERATE	CO2
To		COMBUSTO	TURBINE	HRSG	CO2	SEPERATE	COMPRESS		
Phase		Vapor Phase	Liquid Phase						
Temperature	C	434.31	1517.56	870.22	66.90	28.00	28.00	28.00	66.90
Pressure	bar	45.80	45.80	1.07	1.03	1.03	1.03	1.03	1.03
Mass Enthalpy	MJ/kg	-8.54	-7.34	-8.26	-9.21	-8.94	-8.94	-8.94	-15.78
Mass Entropy	J/kg-K	189.01	1338.96	1488.44	97.42	68.80	68.80	68.80	-8728.61
Enthalpy Flow	MWatt	-5451.21	-5540.29	-6231.87	-6954.28	-6279.88	-5708.97	-570.91	-825.44
Mole Fractions									
CO2		1.00	0.85	0.85	0.85	1.00	1.00	1.00	0.00
O2		0.00	0.00	0.00	0.00	0.00	0.00	0.00	0.00
CH4		0.00	0.00	0.00	0.00	0.00	0.00	0.00	0.00
H2O		0.00	0.15	0.15	0.15	0.00	0.00	0.00	1.00
AR		0.00	0.00	0.00	0.00	0.00	0.00	0.00	0.00
N2		0.00	0.00	0.00	0.00	0.00	0.00	0.00	0.00
C2H4		0.00	0.00	0.00	0.00	0.00	0.00	0.00	0.00
C3H8		0.00	0.00	0.00	0.00	0.00	0.00	0.00	0.00
Mass Flows	kg/sec	638.60	754.79	754.79	754.79	702.46	638.60	63.86	52.30
Exergy flow rate	MWatt	235.47	1144.55	419.33	9.95	0.65	0.59	0.06	0.64
Mass exergy	kJ/kg	368.73	1516.39	555.56	13.19	0.93	0.93	0.93	12.21

Table 3.6 Stream properties of SCOC-CC cycle from Aspen plus modelling

Stream Name	Units	15.00	16.00	S1	S2	S3	S4	S5	S6	S7	S8
Description											
From				B1	B2	FUELCOM	BOILER	SPUMP	STURBINE	B5	AIRCOM
To		AIRCOM	FUELCOM	COMBUSTO	COMBUSTO	B1	STURBINE	BOILER	B5	SPUMP	B2
Phase		Vapor Phase	Liquid Phase	Vapor Phase	Liquid Phase	Vapor Phase					
Temperature	C	200.00	117.00	117.00	200.00	117.00	652.65	31.13	144.49	26.85	1130.23
Pressure	bar	1.00	46.00	46.00	45.80	46.00	142.00	142.00	0.04	0.04	45.80
Mass Enthalpy	MJ/kg	0.16	-4.46	-4.46	0.16	-4.46	4.01	0.13	2.74	0.11	1.16
Mass Entropy	J/kg-K	435.17	-6433.59	-6433.59	-569.02	-6433.59	8041.01	453.11	9025.50	393.91	587.02
Enthalpy Flow	MWatt	15.23	-103.87	-103.87	14.79	-103.87	746.77	24.36	510.65	21.02	107.85
Mole Fractions											
CO2		0.00	0.00	0.00	0.00	0.00	0.00	0.00	0.00	0.00	0.00
O2		1.00	0.00	0.00	1.00	0.00	0.00	0.00	0.00	0.00	1.00
CH4		0.00	1.00	1.00	0.00	1.00	0.00	0.00	0.00	0.00	0.00
H2O		0.00	0.00	0.00	0.00	0.00	1.00	1.00	1.00	1.00	0.00
AR		0.00	0.00	0.00	0.00	0.00	0.00	0.00	0.00	0.00	0.00
N2		0.00	0.00	0.00	0.00	0.00	0.00	0.00	0.00	0.00	0.00
C2H4		0.00	0.00	0.00	0.00	0.00	0.00	0.00	0.00	0.00	0.00
C3H8		0.00	0.00	0.00	0.00	0.00	0.00	0.00	0.00	0.00	0.00
Mass Flows	kg/sec	92.90	23.29	23.29	92.90	23.29	186.39	186.39	186.39	186.39	92.90
Exergy flow rate	MWatt	3.18	14.10	14.10	30.56	14.10	300.79	0.05	9.96	0.00	91.60
Mass exergy	kJ/kg	34.22	605.41	605.41	328.91	605.41	1613.82	0.26	53.44	0.02	985.98

3.4.2 The COOPERATE cycle modelling and analysis

Figure 3.3 shows the three stages COOPERATE cycle model in Aspen Plus based on the schematic of the cycle presented in Figure 2.19 of chapter 2. The cycle includes the main heat exchanger and two combustions. Table 3.5 shows the steam cycle properties of the modelled COOPERATE cycle; the recycled working flow is mainly carbon dioxide.

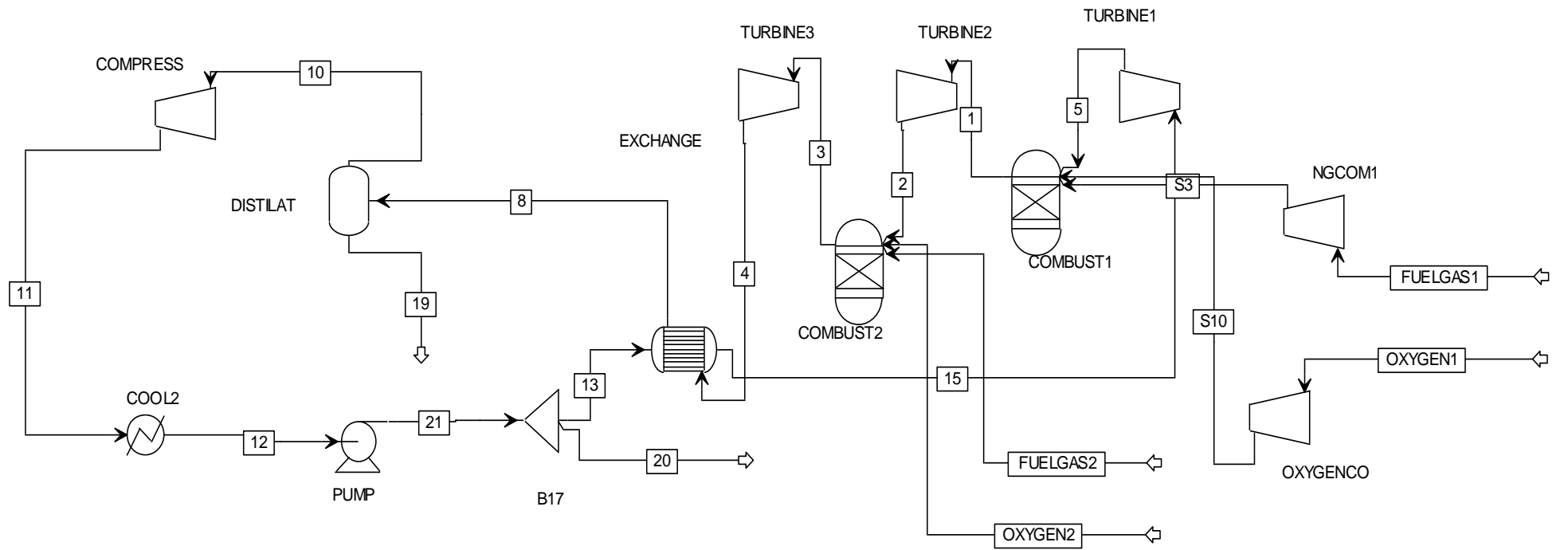


Figure 3.4 Aspen Plus modelling of COOPERATE cycle

Table 3.7 Stream properties of COOPERATE cycle from Aspen plus modelling

Stream Name	Units	1.00	2.00	3.00	4.00	5.00	8.00	10.00	11.00	12.00	13.00
Description											
From		COMBUST1	TURBINE2	COMBUST2	TURBINE3	TURBINE1	EXCHANGE	DISTILAT	COMPRESS	COOL2	B17
To		TURBINE2	COMBUST2	TURBINE3	EXCHANGE	COMBUST1	DISTILAT	COMPRESS	COOL2	PUMP	EXCHANGE
Phase		Vapor Phase	Liquid Phase	Vapor Phase							
Temperature	C	1495.59	1226.27	1650.06	1352.65	975.71	310.38	20.00	272.59	15.00	37.73
Pressure	bar	60.00	15.00	15.00	4.00	60.00	4.00	4.00	64.00	64.00	240.00
Mass Enthalpy	kJ/kg	-7284.65	-7664.61	-7150.29	-7585.13	-7874.38	-8962.61	-8957.72	-8731.41	-9218.44	-9193.53
Mass Entropy	kJ/kg-K	1.29	1.34	1.68	1.71	0.84	0.38	-0.22	-0.17	-1.55	-1.53
Enthalpy Flow	MWatt	-2526.06	-2657.82	-2685.15	-2848.45	-2504.05	-3365.73	-3132.48	-3053.34	-3223.65	-2923.54
Mole Fractions											
METHANE		0.00	0.00	0.00	0.00	0.00	0.00	0.00	0.00	0.00	0.00
ETHANE		0.00	0.00	0.00	0.00	0.00	0.00	0.00	0.00	0.00	0.00
PROPANE		0.00	0.00	0.00	0.00	0.00	0.00	0.00	0.00	0.00	0.00
BUTANE		0.00	0.00	0.00	0.00	0.00	0.00	0.00	0.00	0.00	0.00
PENTANE		0.00	0.00	0.00	0.00	0.00	0.00	0.00	0.00	0.00	0.00
CO2		0.91	0.91	0.84	0.84	0.99	0.84	0.99	0.99	0.99	0.99
NITROGEN		0.00	0.00	0.00	0.00	0.00	0.00	0.00	0.00	0.00	0.00
H2O		0.09	0.09	0.16	0.16	0.00	0.16	0.00	0.00	0.00	0.00
O2		0.00	0.00	0.00	0.00	0.00	0.00	0.00	0.00	0.00	0.00
Mass Flows	kg/sec	346.77	346.77	375.53	375.53	318.00	375.53	349.70	349.70	349.70	318.00
Exergy flow rate	MWatt	505.73	369.28	605.00	438.34	269.04	69.65	26.81	101.55	74.19	74.02
Molar exergy	MJ/kmol	60.75	44.36	64.34	46.61	37.12	7.41	3.36	12.74	9.31	10.21
Mass exergy	kJ/kg	1458.43	1064.92	1611.05	1167.25	846.03	185.48	76.68	290.39	212.16	232.76
Exergy flow rate	MWatt	505.73	369.28	605.00	438.34	269.04	69.65	26.81	101.55	74.19	74.02

Table 3.8 Stream properties of COOPERATE cycle from Aspen plus modelling

Stream Name	Units	15.00	19.00	20.00	21.00	FUELGAS1	FUELGAS2	OXYGEN1	OXYGEN2	S3	S10
Description											
From		EXCHANGE	DISTILAT	B17	PUMP					NGCOM1	OXYGENCO
To		TURBINE1			B17	NGCOM1	COMBUST2	OXYGENCO	COMBUST2	COMBUST1	COMBUST1
Phase		Vapor Phase	Liquid Phase	Vapor Phase	Liquid Phase	Vapor Phase					
Temperature	C	1202.65	20.00	37.73	37.73	15.00	15.00	15.00	15.00	161.45	176.61
Pressure	bar	240.00	4.00	240.00	240.00	15.00	15.00	15.00	15.00	75.00	60.00
Mass Enthalpy	kJ/kg	-7566.85	-15993.60	-9193.53	-9193.53	-4685.19	-4685.19	-13.82	-13.82	-4354.43	134.53
Mass Entropy	kJ/kg-K	0.79	-9.40	-1.53	-1.53	-6.54	-6.54	-0.74	-0.74	-6.42	-0.69
Enthalpy Flow	MWatt	-2406.26	-413.19	-291.40	-3214.94	-27.01	-27.01	-0.32	-0.32	-25.10	3.09
Mole Fractions											
METHANE		0.00	0.00	0.00	0.00	1.00	1.00	0.00	0.00	1.00	0.00
ETHANE		0.00	0.00	0.00	0.00	0.00	0.00	0.00	0.00	0.00	0.00
PROPANE		0.00	0.00	0.00	0.00	0.00	0.00	0.00	0.00	0.00	0.00
BUTANE		0.00	0.00	0.00	0.00	0.00	0.00	0.00	0.00	0.00	0.00
PENTANE		0.00	0.00	0.00	0.00	0.00	0.00	0.00	0.00	0.00	0.00
CO2		0.99	0.00	0.99	0.99	0.00	0.00	0.00	0.00	0.00	0.00
NITROGEN		0.00	0.00	0.00	0.00	0.00	0.00	0.00	0.00	0.00	0.00
H2O		0.00	1.00	0.00	0.00	0.00	0.00	0.00	0.00	0.00	0.00
O2		0.00	0.00	0.00	0.00	0.00	0.00	1.00	1.00	0.00	1.00
Mass Flows	kg/sec	318.00	25.83	31.70	349.70	5.77	5.77	23.00	23.00	5.77	23.00
Exergy flow rate	MWatt	371.02	0.01	7.38	81.40	2.38	2.38	4.78	4.78	4.08	7.85
Molar exergy	MJ/kmol	51.20	0.01	10.21	10.21	6.61	6.61	6.65	6.65	11.36	10.92
Mass exergy	kJ/kg	1166.74	0.55	232.76	232.76	412.08	412.08	207.95	207.95	708.09	341.17
Exergy flow rate	MWatt	371.02	0.01	7.38	81.40	2.38	2.38	4.78	4.78	4.08	7.85

3.4.3 The E-MATIANT cycle modelling and analysis

Figure 3.5 shows the E -MATIANT cycle model in Aspen Plus software based on the schematic presented in Figure 2.20 of chapter 2.; The gas turbine cycle including a High-Pressure Turbine (HPT) and Low-Pressure Turbine (LPT). Table 3.9 shows working flow properties at each stage for the E-MATIANT cycle, the main working flow for the steam cycle is water, and the recycled working flow for the gas turbine is carbon dioxide.

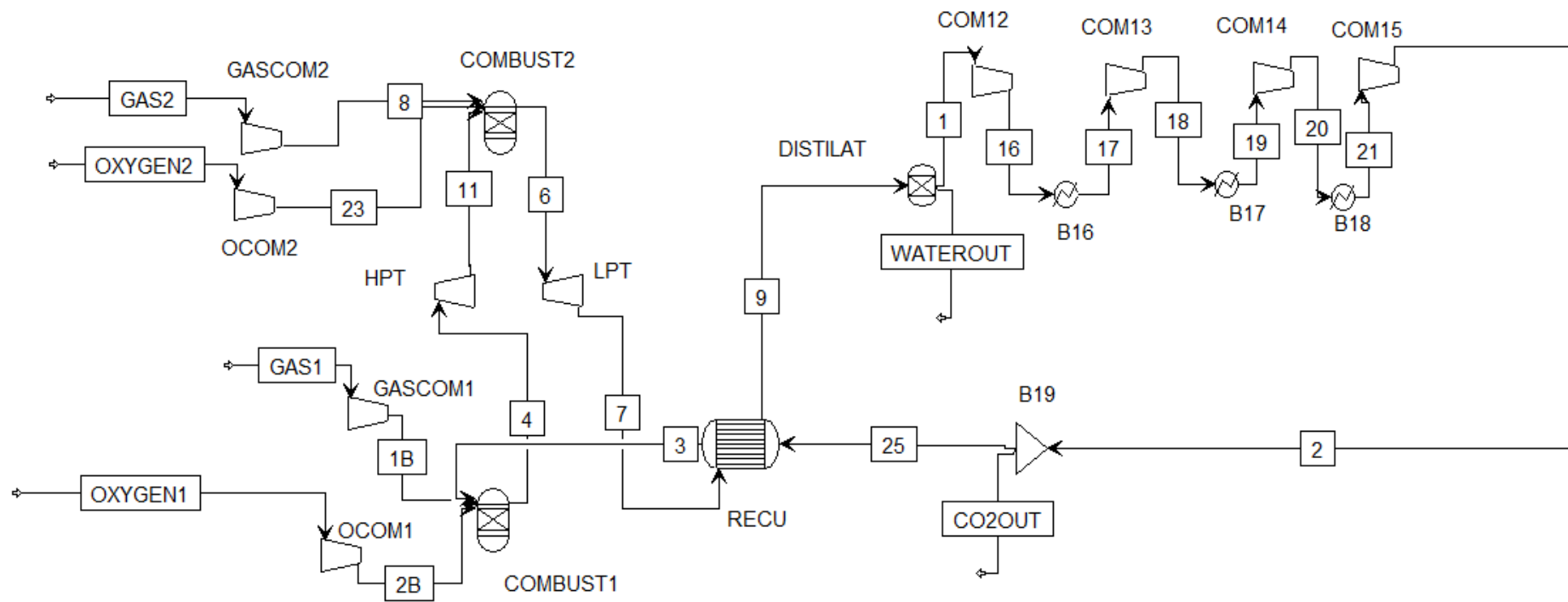


Figure 3.5 Aspen Plus modelling of E-MATIANT cycle

Table 3.9 Stream properties of E-MATIANT cycle from Aspen Plus modelling

Stream Name	Units	1.00	1B	2.00	2B	3.00	4.00	6.00	7.00	8.00	9.00	16.00	17.00	18.00
Description														
From		DISTILAT	GASCOM1	COM15	OCOM1	RECU	COMBUST1	COMBUST2	LPT	GASCOM2	RECU	COM12	B16	COM13
To		COM12	COMBUST1	B19	COMBUST1	COMBUST1	HPT	LPT	RECU	COMBUST2	DISTILAT	B16	COM13	B17
Phase		Vapor Phase												
Temperature	C	30.00	152.19	136.59	196.48	512.32	1131.21	1107.72	532.32	99.15	215.12	128.34	30.00	128.97
Pressure	bar	1.00	60.00	60.00	60.00	60.00	58.20	34.92	1.00	36.00	1.00	2.78	2.78	7.75
Mass Enthalpy	MJ/kg	-5.45	-5.91	-5.38	0.15	-4.97	-4.48	-4.54	-5.26	-6.01	-5.61	-5.36	-5.45	-5.37
Mass Entropy	kJ/kg-K	0.21	-4.14	-0.44	-0.65	0.26	0.95	1.04	1.18	-4.19	0.63	0.24	-0.02	0.02
Mole Fractions														
CH4		0.00	0.84	0.00	0.00	0.00	0.00	0.00	0.00	0.84	0.00	0.00	0.00	0.00
CO2		0.53	0.16	0.53	0.00	0.53	0.49	0.49	0.49	0.16	0.49	0.53	0.53	0.53
O2		0.47	0.00	0.47	1.00	0.47	0.43	0.43	0.43	0.00	0.43	0.47	0.47	0.47
H2O		0.00	0.00	0.00	0.00	0.00	0.08	0.09	0.09	0.00	0.09	0.00	0.00	0.00
Mass Flows	kg/sec	223.30	5.77	223.30	23.00	200.00	228.77	233.08	233.08	0.86	233.08	223.30	223.30	223.30
Mass exergy	kJ/kg	-0.81	521.24	270.25	348.12	468.58	1042.40	988.41	231.30	436.74	45.00	78.38	64.86	143.95
Molar exergy	MJ/kmol	-0.03	10.69	10.38	11.14	17.99	38.41	36.23	8.48	8.96	1.65	3.01	2.49	5.53
Exergy flow rate	MWatt	-0.18	3.01	60.35	8.01	93.72	238.46	230.38	53.91	0.38	10.49	17.50	14.48	32.14

Table 3.10 Stream properties of E-MATIANT cycle from Aspen Plus modelling

Stream Name	Units	19.00	20.00	21.00	23.00	CO2OUT	GAS1	GAS2	OXYGEN1	OXYGEN2	WATEROUT	11.00	25.00
Description													
From		B17	COM14	B18	OCOM2	B19					DISTILAT	HPT	B19
To		COM14	B18	COM15	COMBUST2		GASCOM1	GASCOM2	OCOM1	OCOM2		COMBUST2	RECU
Phase		Vapor Phase	Liquid Phase	Vapor Phase	Vapor Phase								
Temperature	C	30.00	129.63	30.00	122.27	136.59	15.00	15.00	15.00	15.00	15.00	1032.60	136.59
Pressure	bar	7.75	21.56	21.56	36.00	60.00	15.00	15.00	15.00	15.00	1.00	36.00	60.00
Mass Enthalpy	MJ/kg	-5.46	-5.37	-5.47	0.08	-5.38	-6.15	-6.15	-0.01	-0.01	-16.02	-4.60	-5.38
Mass Entropy	kJ/kg-K	-0.25	-0.21	-0.49	-0.68	-0.44	-4.29	-4.29	-0.74	-0.74	-9.48	0.96	-0.44
Mole Fractions													
CH4		0.00	0.00	0.00	0.00	0.00	0.84	0.84	0.00	0.00	0.00	0.00	0.00
CO2		0.53	0.53	0.53	0.00	0.53	0.16	0.16	0.00	0.00	0.00	0.49	0.53
O2		0.47	0.47	0.47	1.00	0.47	0.00	0.00	1.00	1.00	0.00	0.43	0.47
H2O		0.00	0.00	0.00	0.00	0.00	0.00	0.00	0.00	0.00	1.00	0.08	0.00
Mass Flows	kg/sec	223.30	223.30	223.30	3.45	23.30	5.77	0.86	23.00	3.45	9.78	228.77	200.00
Mass exergy	kJ/kg	130.11	208.01	193.53	286.91	270.25	321.64	321.64	207.95	207.95	0.78	909.91	270.25
Molar exergy	MJ/kmol	5.00	7.99	7.43	9.18	10.38	6.60	6.60	6.65	6.65	0.01	33.53	10.38
Exergy flow rate	MWatt	29.05	46.45	43.21	0.99	6.30	1.85	0.28	4.78	0.72	0.01	208.16	54.05

3.4.4 The CC_MATIANT cycle modelling and analysis

Figure 3.6 shows the CC-MATIANT cycle model in Aspen Plus software based on the schematic presented in Figure 2.22 of chapter 2. The gas turbine cycle including High-Pressure Turbine (HPT) and Low-Pressure Turbine (LPT).

Table 3.11 shows working flow properties at each stage for the CC-MATIANT cycle, the main working flow for the steam cycle is water, and the recycled working flow for the gas turbine is carbon dioxide.

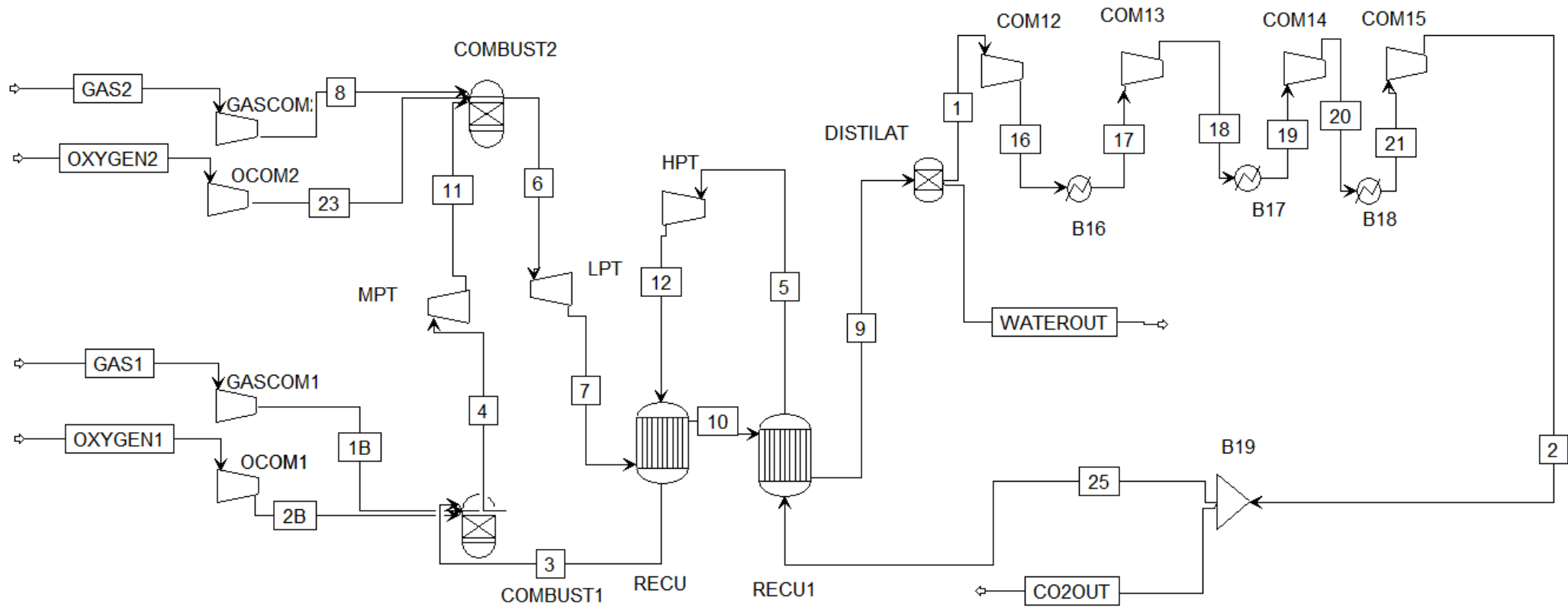


Figure 3.6 Aspen Plus modelling of CC-MATIANT cycle

Table 3.11 Stream properties of CC-MATIANT cycle from Aspen Plus modelling

Stream Name	Units	1.00	1B	2.00	2B	3.00	4.00	5.00	6.00	7.00	8.00	9.00	16.00	17.00	18.00
Description															
From		DISTILAT	GASCOM1	COM15	OCOM1	RECU	COMBUST1	RECU1	COMBUST2	LPT	GASCOM2	RECU1	COM12	B16	COM13
To		COM12	COMBUST1	B19	COMBUST1	COMBUST1	MPT	HPT	LPT	RECU	COMBUST2	DISTILAT	B16	COM13	B17
Phase		Vapor Phase													
Temperature	C	30.00	110.45	79.13	136.85	700.00	1497.72	600.00	1310.25	947.28	15.00	143.62	153.43	30.00	155.30
Pressure	bar	1.00	40.00	300.00	40.00	40.00	38.20	300.00	7.92	1.00	15.00	1.00	4.16	4.16	17.31
Mass Enthalpy	MJ/kg	-8.94	-4.47	-9.10	0.10	-8.22	-7.33	-8.35	-7.62	-8.12	-4.69	-9.10	-8.83	-8.94	-8.83
Mass Entropy	kJ/kg-K	0.08	-6.40	-1.30	-0.67	0.60	1.37	0.06	1.53	1.59	-6.54	0.32	0.12	-0.20	-0.16
Enthalpy Flow	MWatt	-4078.71	-51.58	-4153.17	4.50	-3451.20	-3498.28	-3507.83	-3702.94	-3948.82	-8.10	-4424.53	-4027.78	-4080.05	-4030.00
Mole Fractions															
CH4		0.00	1.00	0.00	0.00	0.00	0.00	0.00	0.00	0.00	1.00	0.00	0.00	0.00	0.00
CO2		1.00	0.00	1.00	0.00	1.00	0.88	1.00	0.86	0.86	0.00	0.86	1.00	1.00	1.00
O2		0.00	0.00	0.00	1.00	0.00	0.00	0.00	0.00	0.00	0.00	0.00	0.00	0.00	0.00
H2O		0.00	0.00	0.00	0.00	0.00	0.12	0.00	0.14	0.14	0.00	0.14	0.00	0.00	0.00
Mass Flows	kg/sec	456.38	11.53	456.38	46.00	420.00	477.53	420.00	486.16	486.16	1.73	486.16	456.38	456.38	456.38
Molar exergy	J/kmol	-0.03	9.33	10.89	9.55	24.89	59.44	26.01	46.42	25.21	6.61	1.03	4.35	3.46	7.77
Mass exergy	kJ/kg	-0.70	581.45	247.51	298.56	565.53	1456.35	591.11	1148.09	623.43	412.08	25.35	98.95	78.62	176.61
Exergy flow rate	MWatt	-0.32	6.70	112.96	13.73	237.52	695.45	248.27	558.16	303.09	0.71	12.32	45.16	35.88	80.60

Table 3.12 Stream properties of CC-MATIANT cycle from Aspen Plus modelling

Stream Name	Units	19.00	20.00	21.00	23.00	CO2OUT	GAS1	GAS2	OXYGEN1	OXYGEN2	WATEROUT	10.00	25.00	5.00	12.00	11.00	
Description																	
From		B17	COM14	B18	OCOM2	B19						DISTILAT	RECU	B19	RECU1	HPT	MPT
To		COM14	B18	COM15	COMBUST2		GASCOM1	GASCOM2	OCOM1	OCOM2		RECU1	RECU1	HPT	RECU	COMBUST2	
Phase		Vapor Phase	Vapor Phase	Liquid Phase	Vapor Phase	Liquid Phase	Vapor Phase										
Temperature	C	30.00	165.81	30.00	15.00	79.13	15.00	15.00	15.00	15.00	15.00	696.42	79.13	600.00	375.36	1209.10	
Pressure	bar	17.31	75.00	75.00	15.00	300.00	15.00	15.00	15.00	15.00	1.00	1.00	300.00	300.00	40.00	9.00	
Mass Enthalpy	MJ/kg	-8.95	-8.85	-9.14	-0.01	-9.10	-4.69	-4.69	-0.01	-0.01	-16.02	-8.45	-9.10	-8.35	-8.60	-7.74	
Mass Entropy	kJ/kg-K	-0.49	-0.46	-1.31	-0.74	-1.30	-6.54	-6.54	-0.74	-0.74	-9.48	1.29	-1.30	0.06	0.12	1.41	
Enthalpy Flow	MWatt	-4086.01	-4038.00	-4170.25	-0.10	-331.06	-54.02	-8.10	-0.64	-0.10	-477.00	-4110.25	-3822.11	-3507.83	-3612.62	-3694.74	
Mole Fractions																	
CH4		0.00	0.00	0.00	0.00	0.00	1.00	1.00	0.00	0.00	0.00	0.00	0.00	0.00	0.00	0.00	
CO2		1.00	1.00	1.00	0.00	1.00	0.00	0.00	0.00	0.00	0.00	0.86	1.00	1.00	1.00	0.88	
O2		0.00	0.00	0.00	1.00	0.00	0.00	0.00	1.00	1.00	0.00	0.00	0.00	0.00	0.00	0.00	
H2O		0.00	0.00	0.00	0.00	0.00	0.00	0.00	0.00	0.00	1.00	0.14	0.00	0.00	0.00	0.12	
Mass Flows	kg/sec	456.38	456.38	456.38	6.90	36.38	11.53	1.73	46.00	6.90	29.78	486.16	420.00	420.00	420.00	477.53	
Molar exergy	J/kmol	6.81	10.96	9.39	6.65	10.89	6.61	6.61	6.65	6.65	0.01	15.45	10.89	26.01	14.26	42.14	
Mass exergy	kJ/kg	154.75	249.07	213.26	207.95	247.51	412.08	412.08	207.95	207.95	0.78	382.10	247.51	591.11	324.00	1032.38	
Exergy flow rate	MWatt	70.63	113.67	97.33	1.43	9.00	4.75	0.71	9.57	1.43	0.02	185.76	103.95	248.27	136.08	493.00	

3.4.5 The Graz cycle modelling and analysis

Figure 3.7 shows the Graz cycle model in Aspen Plus software based on the schematic presented in Figure 2.26 of chapter 2; The cycle has two types of recycled working flow. The water is pumped back to the combustion, and carbon dioxide is compressed back to the combustion.

Table 3.13 shows working flow properties at each stage for the Graz cycle, the main working flow for the steam cycle is water, and the recycled working flow for the gas turbine is carbon dioxide.

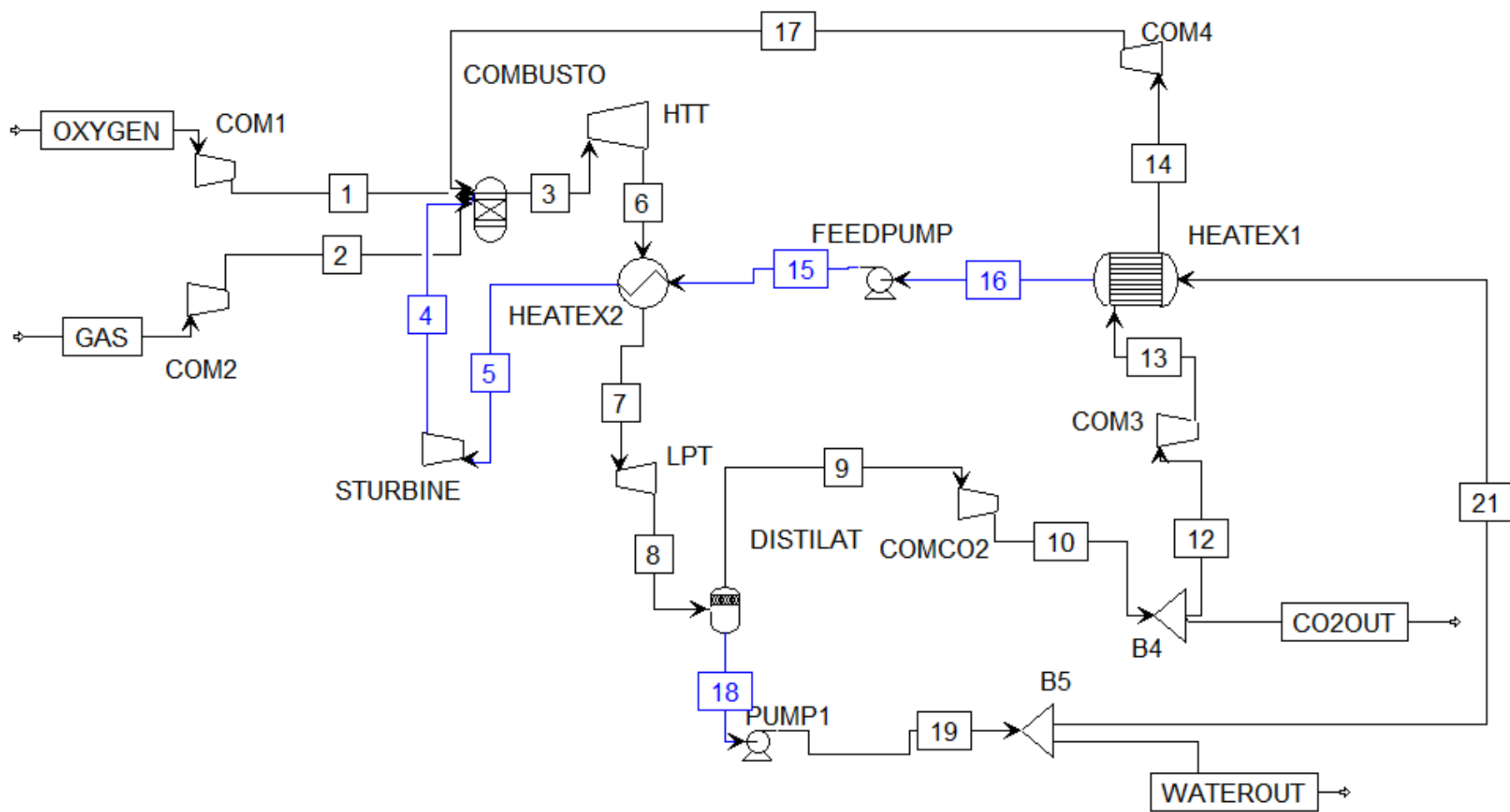


Figure 3.7 Aspen Plus modelling of Graz cycle

Table 3.13 Stream properties of Graz cycle from Aspen Plus modelling

Stream Name	Units	1.00	2.00	3.00	4.00	5.00	6.00	7.00	8.00	9.00	10.00	12.00
Description												
From		COM1	COM2	COMBUSTO	STURBINE	HEATEX2	HTT	HEATEX2	LPT	DISTILAT	COMCO2	B4
To		COMBUSTO	COMBUSTO	HTT	COMBUSTO	STURBINE	HEATEX2	LPT	DISTILAT	COMCO2	B4	COM3
Phase		Vapor Phase										
Temperature	C	141.61	112.82	1278.02	389.82	568.14	643.14	497.27	346.53	29.00	411.91	411.91
Pressure	bar	40.00	40.00	40.00	50.00	180.00	1.00	1.00	0.25	0.25	10.00	10.00
Mass Enthalpy	kJ/kg	108.35	-4439.06	-8001.61	-12681.90	-12305.70	-8940.91	-9137.51	-9330.42	-9260.82	-8850.49	-8850.49
Mass Entropy	kJ/kg-K	-0.65	-6.32	1.04	-2.69	-2.77	1.13	0.89	0.94	0.28	0.37	0.37
Enthalpy Flow	MWatt	0.31	-3.20	-264.82	-25.36	-24.61	-295.91	-302.41	-308.80	-274.30	-262.15	-243.39
Mole Fractions												
H2O		0.00	0.00	0.33	1.00	1.00	0.33	0.33	0.33	0.16	0.16	0.16
CO2		0.00	0.00	0.67	0.00	0.00	0.67	0.67	0.67	0.84	0.84	0.84
O2		1.00	0.00	0.00	0.00	0.00	0.00	0.00	0.00	0.00	0.00	0.00
CH4		0.00	1.00	0.00	0.00	0.00	0.00	0.00	0.00	0.00	0.00	0.00
Mass Flows	kg/sec	2.88	0.72	33.10	2.00	2.00	33.10	33.10	33.10	29.62	29.62	27.50
Molar exergy	kJ/kmol	9654.92	9527.03	48179.30	22700.10	29974.50	13972.60	9479.98	2154.38	-3113.04	12128.40	12128.40
Mass exergy	kJ/kg	301.73	593.85	1361.69	1254.65	1656.72	394.91	267.93	60.89	-78.12	304.34	304.34
Exergy flow rate	kWatt	867.47	427.96	45065.80	2509.31	3313.43	13069.60	8867.35	2015.16	-2313.79	9014.56	8369.44

Table 3.14 Stream properties of Graz cycle from Aspen Plus modelling

Stream Name	Units	13.00	14.00	15.00	16.00	17.00	18.00	19.00	21.00	CO2OUT	GAS	OXYGEN	WATEROUT
Description													
From		COM3	HEATEX1	FEEDPUMP	HEATEX1	COM4	DISTILAT	PUMP1	B5	B4			B5
To		HEATEX1	COM4	HEATEX2	FEEDPUMP	COMBUSTO	PUMP1	B5	HEATEX1		COM2	COM1	
Phase		Vapor Phase	Vapor Phase	Liquid Phase		Vapor Phase	Liquid Phase	Liquid Phase	Liquid Phase	Vapor Phase	Vapor Phase	Vapor Phase	Liquid Phase
Temperature	C	514.64	501.78	85.19	80.00	614.00	29.00	29.02	29.02	411.91	15.00	15.00	29.02
Pressure	bar	20.00	20.00	180.00	1.00	40.00	0.25	1.00	1.00	10.00	15.00	15.00	1.00
Mass Enthalpy	kJ/kg	-8726.60	-8742.36	-15559.10	-15581.50	-8602.50	-15798.30	-15798.20	-15798.20	-8850.49	-4667.21	-9.16	-15798.20
Mass Entropy	kJ/kg-K	0.40	0.38	-8.21	-8.28	0.40	-8.93	-8.93	-8.93	0.37	-6.50	-0.73	-8.93
Enthalpy Flow	MWatt	-239.98	-240.42	-31.12	-31.16	-236.57	-54.91	-54.91	-31.60	-18.76	-3.36	-0.03	-23.32
Mole Fractions													
H2O		0.16	0.16	1.00	1.00	0.16	1.00	1.00	1.00	0.16	0.00	0.00	1.00
CO2		0.84	0.84	0.00	0.00	0.84	0.00	0.00	0.00	0.84	0.00	0.00	0.00
O2		0.00	0.00	0.00	0.00	0.00	0.00	0.00	0.00	0.00	0.00	1.00	0.00
CH4		0.00	0.00	0.00	0.00	0.00	0.00	0.00	0.00	0.00	1.00	0.00	0.00
Mass Flows	kg/sec	27.50	27.50	2.00	2.00	27.50	3.48	3.48	2.00	2.12	0.72	2.88	1.48
Molar exergy	kJ/kmol	16782.70	16394.20	451.91	381.31	21684.30	3.73	3.76	3.77	12128.40	6686.48	6685.43	0.00
Mass exergy	kJ/kg	421.14	411.39	24.98	21.08	544.13	0.21	0.21	0.21	304.34	416.79	208.93	0.21
Exergy flow rate	kWatt	11581.20	11313.10	49.95	42.15	14963.60	0.72	0.72	0.42	645.12	300.36	600.67	0.31

3.4.6 The S-Graz cycle modelling and analysis

Figure 3.15 shows the S-Graz cycle model in Aspen Plus software based on the schematic presented in Figure 2.27 of chapter 2. Table 3.15 shows working flow properties at each stage for the S-Graz cycle, the recycled working flow is water, and it is pumped back to the combustion. The other recycled working flow is the exhaust of the turbine, and it is compressed back to the combustion, and composition is mainly water and carbon dioxide.

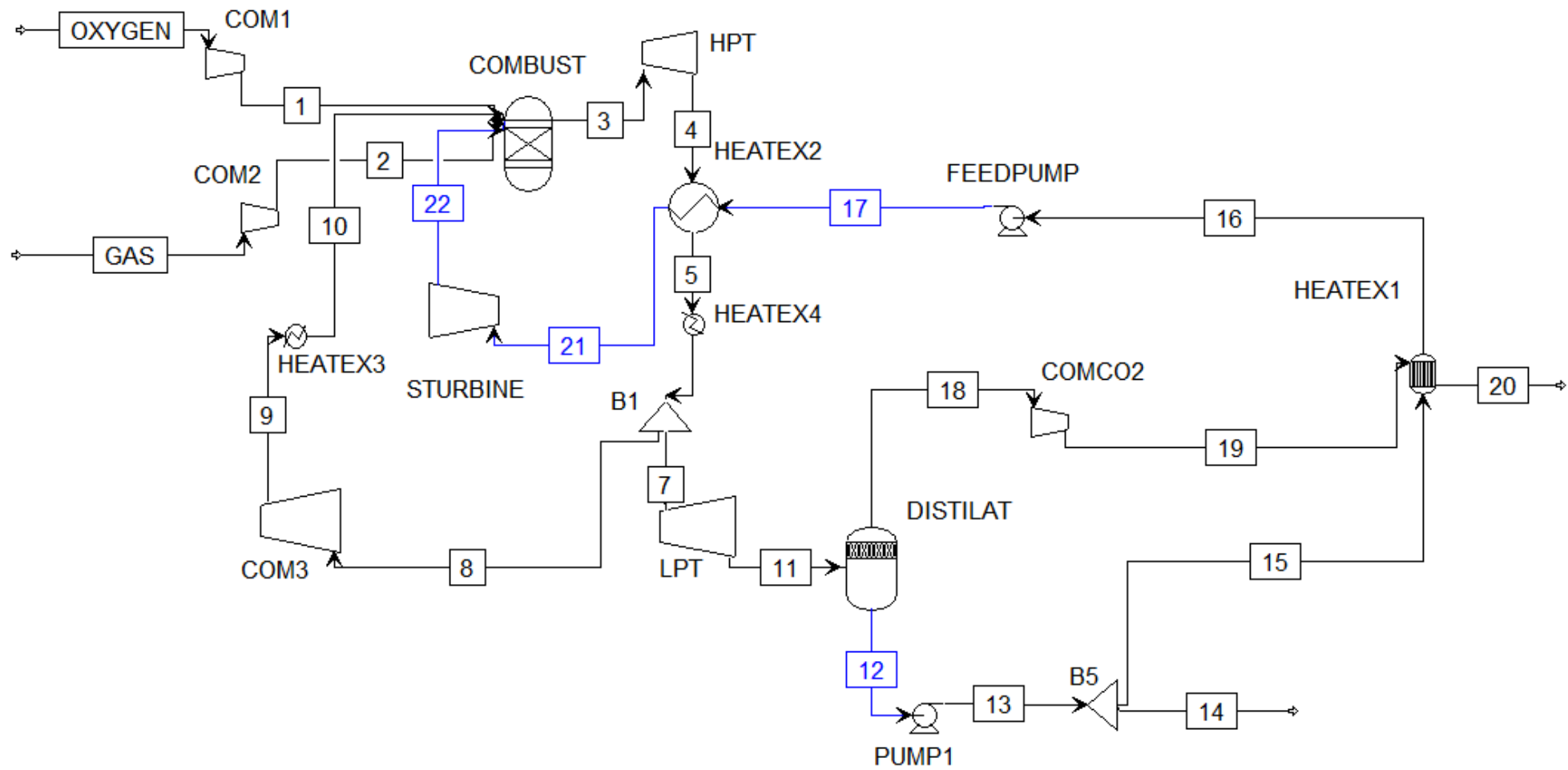


Figure 3.8 Aspen Plus modelling of S-Graz cycle

Table 3.15 Stream properties of S-Graz cycle from Aspen Plus modelling

Stream Name	Units	1.00	2.00	3.00	4.00	5.00	6.00	7.00	8.00	9.00	10.00	11.00	12.00
Description													
From		COM1	COM2	COMBUST	HPT	HEATEX2	HEATEX4	B1	B1	COM3	HEATEX3	LPT	DISTILAT
To		COMBUST	COMBUST	HPT	HEATEX2	HEATEX4	B1	LPT	COM3	HEATEX3	COMBUST	DISTILAT	PUMP1
Phase		Vapor Phase	Liquid Phase										
Temperature	C	141.61	112.82	1343.79	611.41	153.87	292.00	292.00	292.00	1148.26	622.00	77.19	29.00
Pressure	bar	40.00	40.00	40.00	1.00	1.00	1.00	1.00	1.00	40.00	40.00	0.09	0.09
Mass Enthalpy	kJ/kg	108.35	-4439.06	-9732.69	-11332.80	-12171.30	-11931.60	-11931.60	-11931.60	-10187.60	-11311.90	-12299.70	-15837.20
Molar Entropy	kJ/kmol-K	-20.75	-101.47	0.36	3.79	-23.81	-13.67	-13.67	-13.67	-5.89	-26.39	-10.23	-162.03
Mass Entropy	kJ/kg-K	-0.65	-6.32	0.02	0.18	-1.14	-0.66	-0.66	-0.66	-0.28	-1.26	-0.49	-8.99
Enthalpy Flow	MWatt	0.31	-3.20	-189.74	-220.93	-237.28	-232.60	-102.31	-130.29	-111.25	-123.53	-105.47	-93.08
Mole Fractions													
H2O		0.00	0.00	0.89	0.89	0.89	0.89	0.89	0.89	0.89	0.89	0.89	1.00
CO2		0.00	0.00	0.11	0.11	0.11	0.11	0.11	0.11	0.11	0.11	0.11	0.00
O2		1.00	0.00	0.00	0.00	0.00	0.00	0.00	0.00	0.00	0.00	0.00	0.00
CH4		0.00	1.00	0.00	0.00	0.00	0.00	0.00	0.00	0.00	0.00	0.00	0.00
Mass Flows	kg/sec	2.88	0.72	19.49	19.49	19.49	19.49	8.57	10.92	10.92	10.92	8.57	5.88
Molar exergy	MJ/kmol	9.65	9.53	51.24	16.83	7.56	9.54	9.54	9.54	43.61	26.26	0.83	0.00
Exergy flow rate	MWatt	0.87	0.43	47.87	15.72	7.06	8.91	3.92	4.99	22.82	13.74	0.34	0.00
Mass exergy	kJ/kg	301.73	593.85	2455.35	806.34	362.09	456.97	456.97	456.97	2089.81	1258.45	39.64	0.18

Table 3.16 Stream properties of S-Graz cycle from Aspen Plus modelling

Stream Name	Units	13.00	14.00	15.00	16.00	17.00	18.00	19.00	20.00	21.00	22.00	GAS	OXYGEN
Description													
From		PUMP1	B5	B5	HEATEX1	FEEDPUMP	DISTILAT	COMCO2	HEATEX1	HEATEX2	STURBINE		
To		B5		HEATEX1	FEEDPUMP	HEATEX2	COMCO2	HEATEX1		STURBINE	COMBUST	COM2	COM1
Phase		Liquid Phase	Vapor Phase										
Temperature	C	29.07	29.07	29.07	90.00	95.01	29.00	615.34	266.80	594.41	383.82	15.00	15.00
Pressure	bar	2.50	2.50	2.50	2.50	180.00	0.09	10.00	10.00	180.00	40.00	15.00	15.00
Mass Enthalpy	kJ/kg	-15836.90	-15836.90	-15836.90	-15575.90	-15553.40	-10135.00	-9364.55	-9846.48	-12270.80	-12717.70	-4667.21	-9.16
Molar Entropy	kJ/kmol-K	-162.02	-162.02	-162.02	-147.95	-146.86	7.41	11.74	-10.01	-49.25	-47.37	-104.21	-23.41
Mass Entropy	kJ/kg-K	-8.98	-8.98	-8.98	-8.21	-8.14	0.23	0.37	-0.32	-2.73	-2.63	-6.50	-0.73
Enthalpy Flow	MWatt	-93.08	-14.21	-78.87	-77.57	-77.46	-27.34	-25.26	-26.56	-61.11	-63.33	-3.36	-0.03
Mole Fractions													
H2O		1.00	1.00	1.00	1.00	1.00	0.47	0.47	0.47	1.00	1.00	0.00	0.00
CO2		0.00	0.00	0.00	0.00	0.00	0.53	0.53	0.53	0.00	0.00	0.00	0.00
O2		0.00	0.00	0.00	0.00	0.00	0.00	0.00	0.00	0.00	0.00	0.00	1.00
CH4		0.00	0.00	0.00	0.00	0.00	0.00	0.00	0.00	0.00	0.00	1.00	0.00
Mass Flows	kg/sec	5.88	0.90	4.98	4.98	4.98	2.70	2.70	2.70	4.98	4.98	0.72	2.88
Molar exergy	MJ/kmol	0.00	0.00	0.00	0.52	0.60	-3.75	19.42	10.61	30.69	22.07	6.69	6.69
Exergy flow rate	MWatt	0.00	0.00	0.00	0.14	0.17	-0.32	1.65	0.90	8.48	6.09	0.30	0.60
Mass exergy	kJ/kg	0.19	0.19	0.19	28.70	33.15	-118.06	611.74	334.05	1701.82	1223.75	416.79	208.93

3.4.7 The AZEP 100% cycle modelling and analysis

Figure 3.9 shows the CC-MATIANT cycle model in Aspen Plus software based on the schematic presented in Figure 2.28 of chapter 2. Table 3.17 shows stream properties at each stage for AZEP 100% cycle; there are three working flows in this cycle. In the air cycle, working flow is air, and air enters MCM after compression, then depleted hot air enters the turbine for expansion. In the steam cycle, water is working flow, and steam enters the turbine after recovery heat. In the gas turbine cycle, the working flow is a mixture of water and carbon dioxide, and the hot stream enters the gas turbine for expansion after the MCM unit.

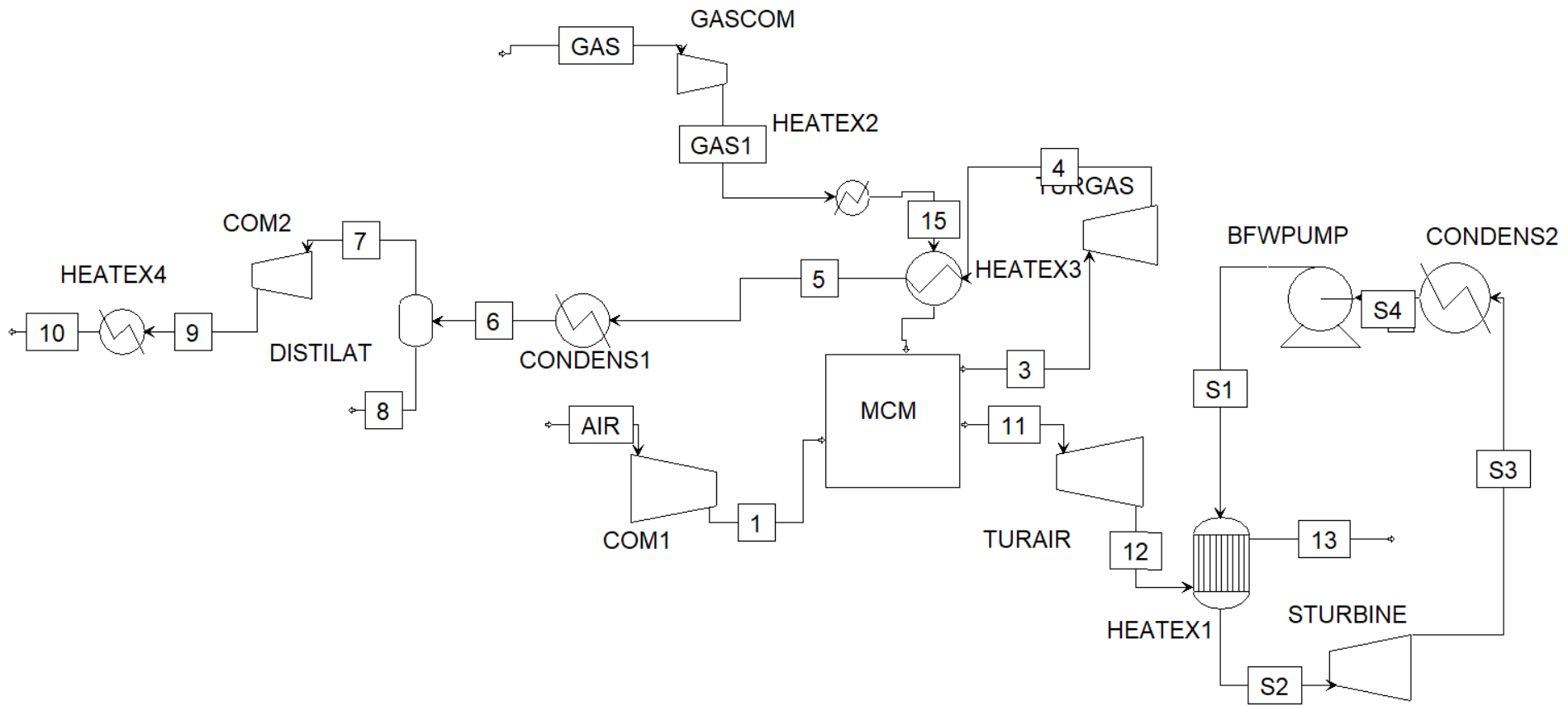


Figure 3.9 Aspen Plus modelling of AZEP 100% cycle

Table 3.17 Stream properties of AZEP 100% cycle from Aspen Plus modelling

Stream Name	Units	1.00	2.00	3.00	4.00	5.00	6.00	7.00	8.00	9.00	10.00
Description											
From		COM1	HEATEX3		TURGAS	HEATEX3	CONDENS1	DISTILAT	DISTILAT	COM2	HEATEX4
To				TURGAS	HEATEX3	CONDENS1	DISTILAT	COM2		HEATEX4	
Phase		Vapor Phase	Liquid Phase	Vapor Phase	Liquid Phase						
Temperature	C	401.81	250.00	1300.00	769.85	692.48	217.00	30.00	30.00	507.89	30.00
Pressure	bar	17.00	70.00	16.47	1.05	1.05	1.05	1.05	1.05	103.90	103.90
Molar Enthalpy	MJ/kmol	11.28	-65.61	-235.53	-261.49	-265.02	-284.89	-388.23	-287.34	-367.21	-399.40
Mass Enthalpy	kJ/kg	390.84	-4089.54	-8856.66	-9832.83	-9965.49	-10712.90	-9001.47	-15949.20	-8514.09	-9260.33
Mass Entropy	kJ/kg-K	0.18	-5.83	0.86	0.97	0.84	-0.22	0.06	-9.25	0.13	-1.53
Enthalpy Flow	MWatt	277.50	-57.25	-619.08	-687.32	-696.59	-748.83	-348.54	-497.29	-329.67	-358.56
Mole Fractions											
H2O		0.00	0.00	0.67	0.67	0.67	0.67	0.03	1.00	0.03	0.03
CO2		0.00	0.00	0.33	0.33	0.33	0.33	0.97	0.00	0.97	0.97
CH4		0.00	1.00	0.00	0.00	0.00	0.00	0.00	0.00	0.00	0.00
AIR		0.00	0.00	0.00	0.00	0.00	0.00	0.00	0.00	0.00	0.00
N2		0.79	0.00	0.00	0.00	0.00	0.00	0.00	0.00	0.00	0.00
O2		0.21	0.00	0.00	0.00	0.00	0.00	0.00	0.00	0.00	0.00
Mass Flows	kg/sec	710.00	14.00	69.90	69.90	69.90	69.90	38.72	31.18	38.72	38.72
Molar exergy	MJ/kmol	11.02	12.79	47.02	20.21	17.73	6.23	0.09	0.00	20.29	9.37
Mass exergy	kJ/kg	382.06	797.26	1768.27	760.13	666.87	234.33	2.14	0.19	470.41	217.27
Exergy flow rate	MWatt	271.26	11.16	123.60	53.13	46.61	16.38	0.08	0.01	18.21	8.41

Table 3.18 Stream properties of AZEP 100% cycle from Aspen Plus modelling

Stream Name	Units	11.00	12.00	13.00	15.00	AIR	GAS	GAS1	S1	S2	S3	S4
Description												
From			TURAIR	HEATEX1	HEATEX2			GASCOM	BFWPUMP	HEATEX1	STURBINE	CONDENS2
To		TURAIR	HEATEX1		HEATEX3	COM1	GASCOM	HEATEX2	HEATEX1	STURBINE	CONDENS2	BFWPUMP
Phase		Vapor Phase	Liquid Phase			Liquid Phase						
Temperature	C	1174.60	520.94	92.00	15.00	15.00	15.00	174.55	33.19	285.07	36.03	32.90
Pressure	bar	17.00	1.06	1.06	70.00	1.00	15.00	70.00	70.00	70.00	0.05	0.05
Molar Enthalpy	MJ/kmol	36.63	14.86	1.95	-76.23	-0.30	-75.16	-69.22	-286.96	-237.57	-254.04	-287.10
Mass Enthalpy	kJ/kg	1307.63	530.50	69.54	-4751.88	-10.41	-4685.19	-4314.61	-15928.60	-13187.10	-14101.10	-15936.40
Mass Entropy	kJ/kg-K	0.91	1.03	0.20	-7.50	0.12	-6.54	-6.30	-9.21	-3.60	-3.27	-9.21
Enthalpy Flow	MWatt	855.45	347.06	45.50	-66.53	-7.39	-65.59	-60.40	-1752.14	-1450.58	-1551.12	-1753.01
Mole Fractions												
H2O		0.00	0.00	0.00	0.00	0.00	0.00	0.00	1.00	1.00	1.00	1.00
CO2		0.00	0.00	0.00	0.00	0.00	0.00	0.00	0.00	0.00	0.00	0.00
CH4		0.00	0.00	0.00	1.00	0.00	1.00	1.00	0.00	0.00	0.00	0.00
AIR		0.00	0.00	0.00	0.00	0.00	0.00	0.00	0.00	0.00	0.00	0.00
N2		1.00	1.00	1.00	0.00	0.79	0.00	0.00	0.00	0.00	0.00	0.00
O2		0.00	0.00	0.00	0.00	0.21	0.00	0.00	0.00	0.00	0.00	0.00
Mass Flows	kg/sec	654.20	654.20	654.20	14.00	710.00	14.00	14.00	110.00	110.00	110.00	110.00
Molar exergy	MJ/kmol	29.00	6.28	0.30	10.15	-0.03	6.61	11.40	0.16	19.42	1.18	0.01
Mass exergy	kJ/kg	1035.27	224.04	10.83	632.84	-0.96	412.08	710.57	8.60	1077.70	65.78	0.35
Exergy flow rate	MWatt	677.28	146.57	7.09	8.86	-0.68	5.77	9.95	0.95	118.55	7.24	0.04

3.4.8 The ZEITMOP cycle modelling and analysis

Figure 3.10 shows the Zero Emission Ion Transport Membrane Oxygen Power (ZEITMOP) cycle model in Aspen Plus software based on the schematic presented in Figure 2.30 of chapter 2; ZEITMOP cycle is integrated to a high-temperature membrane for oxygen production (OTM). As the membrane requires a hot pressurized air stream to separate O₂, the externally heated air cycle can be present as a side cycle of the principal CO₂ cycle (ZEITMOP) or as the main power cycle (AZEP) (Ferrari *et al.*, 2017a). Table 3.19 shows stream properties at each stage for the ZEITMOP cycle; there are three types of working flow in the cycle.

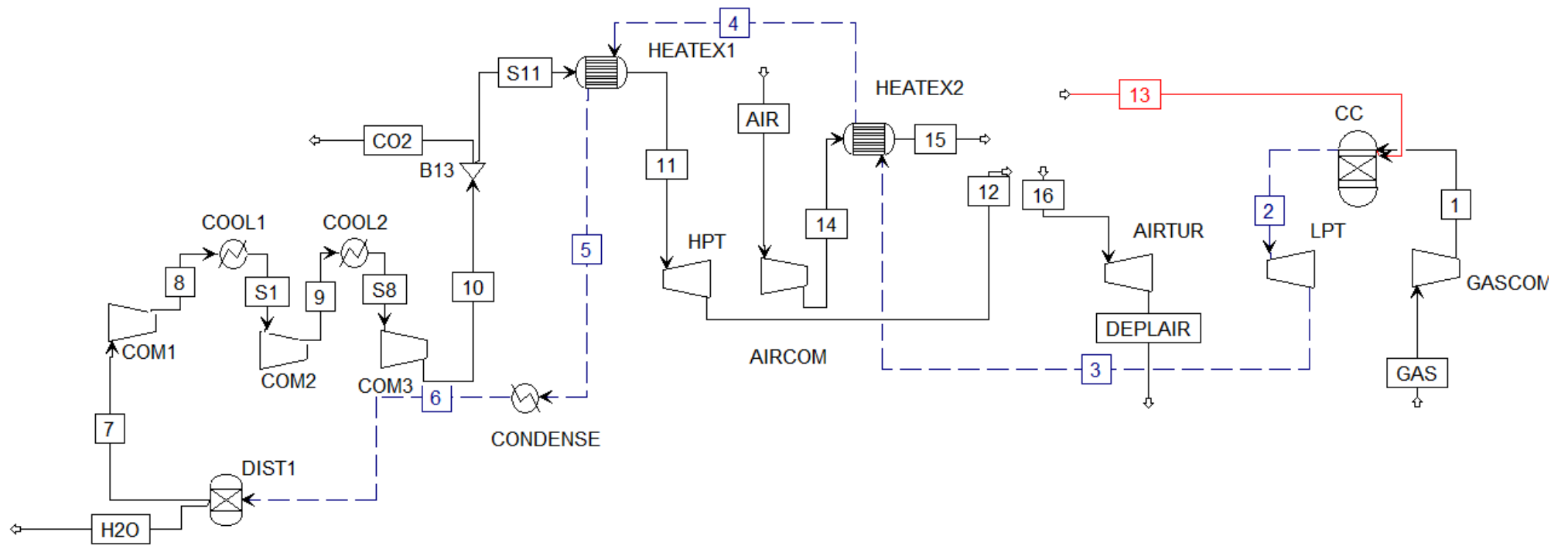


Figure 3.10 Aspen Plus modelling of ZEITMOP cycle

Table 3.19 Stream properties of ZEITMOP cycle from Aspen Plus modelling

Stream Name	Units	1.00	2.00	3.00	4.00	5.00	6.00	7.00	8.00	9.00	10.00	11.00
Description												
From		GASCOM	CC	LPT	HEATEX2	HEATEX1	CONDENSE	DIST1	COM1	COM2	COM3	HEATEX1
To		CC	LPT	HEATEX2	HEATEX1	CONDENSE	DIST1	COM1	COOL1	COOL2	B13	HPT
Phase		Vapor Phase		Vapor Phase								
Temperature	C	256.12	1156.86	724.23	610.39	213.91	30.00	30.00	181.60	186.06	198.75	600.39
Pressure	bar	15.00	15.00	1.00	1.00	1.00	1.00	1.00	5.95	35.33	210.00	210.00
Molar Enthalpy	MJ/kmol	-65.00	-321.11	-344.95	-350.88	-369.77	-380.56	-393.24	-387.14	-387.52	-389.77	-367.32
Mass Enthalpy	kJ/kg	-4.05	-7.78	-8.36	-8.50	-8.96	-9.22	-8.94	-8.80	-8.81	-8.86	-8.35
Molar Entropy	kJ/kmol-K	-79.64	52.24	54.96	48.66	20.52	-9.19	3.55	5.05	-10.29	-28.69	5.89
Mass Entropy	kJ/kg-K	-4.96	1.27	1.33	1.18	0.50	-0.22	0.08	0.11	-0.23	-0.65	0.13
Enthalpy Flow	MWatt	-64.82	-6068.05	-6518.69	-6630.60	-6987.57	-7191.53	-6646.79	-6543.74	-6550.09	-6588.20	-5840.42
Mole Fractions												
H2O		0.00	0.11	0.11	0.11	0.11	0.11	0.00	0.00	0.00	0.00	0.00
CO2		0.00	0.89	0.89	0.89	0.89	0.89	1.00	1.00	1.00	1.00	1.00
CH4		0.00	0.00	0.00	0.00	0.00	0.00	0.00	0.00	0.00	0.00	0.00
O2		0.00	0.00	0.00	0.00	0.00	0.00	0.00	0.00	0.00	0.00	0.00
N2		0.00	0.00	0.00	0.00	0.00	0.00	0.00	0.00	0.00	0.00	0.00
METHANE		1.00	0.00	0.00	0.00	0.00	0.00	0.00	0.00	0.00	0.00	0.00
Mass Flows	kg/sec	16.00	779.75	779.75	779.75	779.75	779.75	743.82	743.82	743.82	743.82	699.70
Molar exergy	MJ/kmol	9.24	41.11	16.45	12.41	1.91	-0.02	-0.03	5.62	9.82	13.05	25.19
Mass exergy	kJ/kg	576.17	996.38	398.75	300.78	46.35	-0.60	-0.70	127.68	223.09	296.50	572.39
Exergy flow rate	MWatt	9.22	776.93	310.93	234.53	36.14	-0.46	-0.52	94.97	165.94	220.54	400.50

Table 3.20 Stream properties of ZEITMOP cycle from Aspen Plus modelling

Stream Name	Units	12.00	13.00	14.00	15.00	16.00	AIR	CO2	DEPLAIR	GAS	H2O	S1	S8	S11
Description														
From		HPT		AIRCOM	HEATEX2			B13	AIRTUR		DIST1	COOL1	COOL2	B13
To			CC	HEATEX2		AIRTUR	AIRCOM			GASCOM		COM2	COM3	HEATEX1
Phase		Vapor Phase	Liquid Phase	Vapor Phase	Vapor Phase	Vapor Phase								
Temperature	C	311.40	365.00	382.31	714.23	714.00	15.00	198.75	256.15	15.00	30.00	30.00	30.00	198.75
Pressure	bar	15.00	15.00	15.00	15.00	15.00	1.00	210.00	1.00	1.00	1.00	5.95	35.33	210.00
Molar Enthalpy	MJ/kmol	-381.33	-335.38	10.67	21.33	21.10	-0.30	-389.77	6.78	-74.89	-287.33	-393.44	-394.87	-389.77
Mass Enthalpy	kJ/kg	-8.67	-7.86	0.37	0.74	0.75	-0.01	-8.86	0.24	-4.67	-15.95	-8.94	-8.97	-8.86
Molar Entropy	kJ/kmol-K	8.63	14.40	5.26	18.39	14.71	3.36	-28.69	17.88	-81.74	-166.62	-11.74	-29.89	-28.69
Mass Entropy	kJ/kg-K	0.20	0.34	0.18	0.64	0.52	0.12	-0.65	0.64	-5.10	-9.25	-0.27	-0.68	-0.65
Enthalpy Flow	MWatt	-6063.19	-6003.22	112.03	223.93	179.33	-3.15	-390.81	57.66	-74.69	-573.14	-6650.23	-6674.27	-6197.39
Mole Fractions														
H2O		0.00	0.00	0.00	0.00	0.00	0.00	0.00	0.00	0.00	1.00	0.00	0.00	0.00
CO2		1.00	0.89	0.00	0.00	0.00	0.00	1.00	0.00	0.00	0.00	1.00	1.00	1.00
CH4		0.00	0.00	0.00	0.00	0.00	0.00	0.00	0.00	0.00	0.00	0.00	0.00	0.00
O2		0.00	0.11	0.21	0.21	0.02	0.21	0.00	0.02	0.00	0.00	0.00	0.00	0.00
N2		0.00	0.00	0.79	0.79	0.98	0.79	0.00	0.98	0.00	0.00	0.00	0.00	0.00
METHANE		0.00	0.00	0.00	0.00	0.00	0.00	0.00	0.00	1.00	0.00	0.00	0.00	0.00
Mass Flows	kg/sec	699.70	763.75	302.93	302.93	238.93	302.93	44.12	238.93	16.00	35.93	743.82	743.82	699.70
Molar exergy	MJ/kmol	10.36	11.52	10.38	17.12	16.99	-0.03	13.05	1.74	-0.03	0.00	4.32	8.31	13.05
Mass exergy	kJ/kg	235.44	269.94	359.65	593.41	604.57	-0.96	296.50	61.74	-1.65	0.19	98.22	188.91	296.50
Exergy flow rate	MWatt	164.74	206.17	108.95	179.76	144.45	-0.29	13.08	14.75	-0.03	0.01	73.06	140.51	207.46

3.4.9 The COOLCEP-S cycle modelling and analysis

Figure 3.11 shows the Cool Clean Efficient Power (COOLCEP) -S cycle model in Aspen Plus software based on the schematic presented in Figure 2.32 of chapter 2; Table 3.21 shows stream properties and each stage for COOLCEP-S cycle, there are two main streams in this cycle.

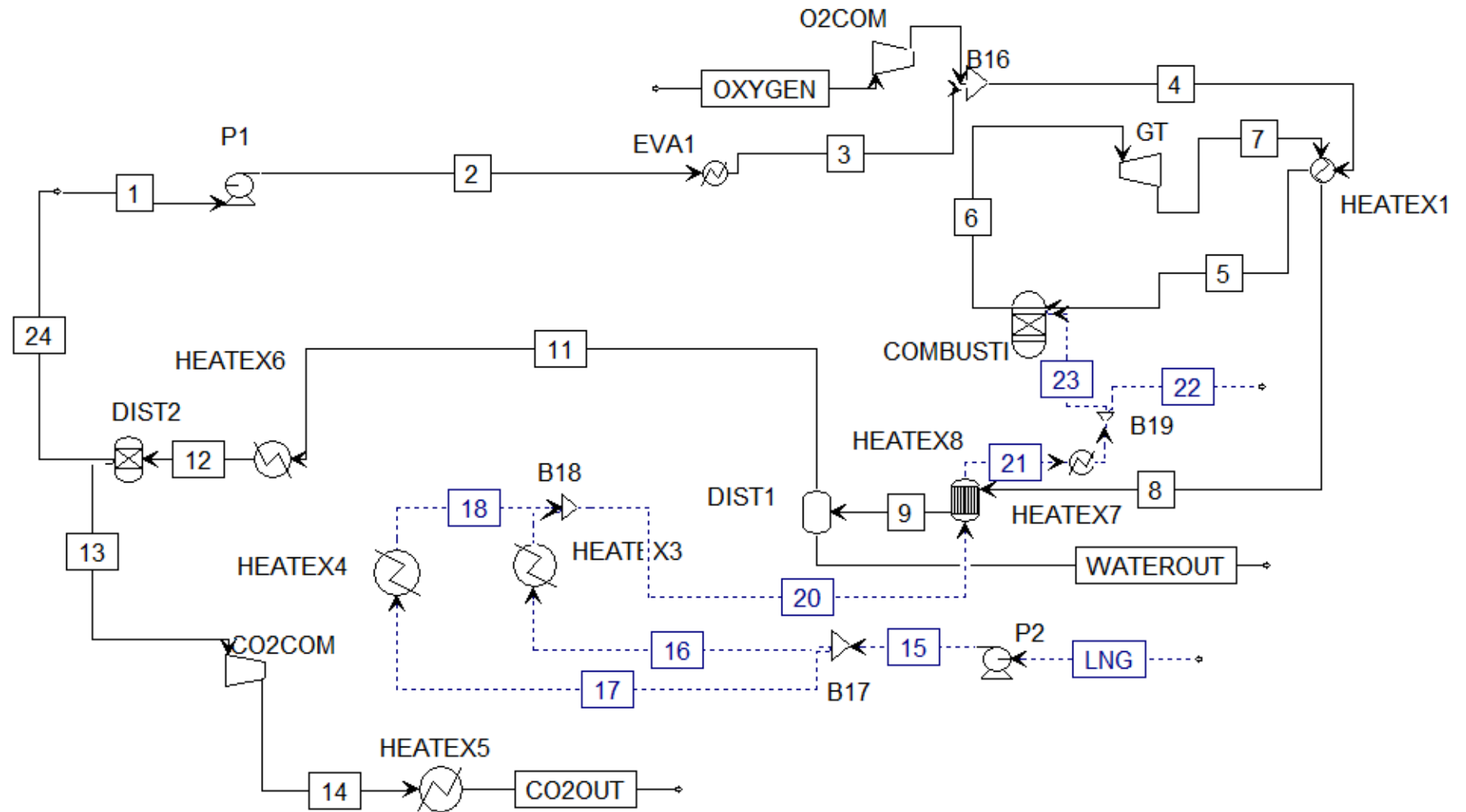


Figure 3.11 Aspen Plus modelling of COOLCEP-S cycle

Table 3.21 Stream properties of COOLCEP-S cycle from Aspen Plus modelling

Stream Name	Units	1.00	2.00	3.00	4.00	5.00	6.00	7.00	8.00	9.00	10.00	11.00	12.00	13.00	14.00
From			P1	EVA1	B16	HEATEX1	COMBUSTI	GT	HEATEX1	HEATEX8	O2COM	DIST1	HEATEX6	DIST2	CO2COM
To		P1	EVA1	B16	HEATEX1	COMBUSTI	GT	HEATEX1	HEATEX8	DIST1	B16	HEATEX6	DIST2	CO2COM	HEATEX5
Stream Class		CONVEN	CONVEN	CONVEN	CONVEN	CONVEN	CONVEN	CONVEN	CONVEN	CONVEN	CONVEN	CONVEN	CONVEN	CONVEN	CONVEN
Phase		Liquid Phase	Liquid Phase	Vapor Phase											
Temperature	C	-50.10	-48.84	8.00	27.16	650.41	898.80	696.41	105.36	74.00	596.04	0.00	-50.10	-50.10	20.30
Pressure	bar	6.97	29.68	29.40	29.12	29.12	29.12	7.15	7.15	7.15	29.12	7.15	7.15	7.15	60.00
Mass Enthalpy	MJ/kg	-9.34	-9.33	-8.96	-8.69	-8.03	-8.01	-8.27	-8.92	-8.95	0.57	-8.95	-9.32	-8.17	-8.06
Mass Entropy	kJ/kg-K	-2.03	-2.02	-0.62	-0.54	0.62	0.89	0.92	-0.10	-0.18	0.18	-0.37	-2.02	-1.13	-1.02
Enthalpy Flow	MWatt	-948.81	-948.52	-909.98	-908.35	-839.20	-842.47	-869.37	-938.51	-941.58	1.64	-919.40	-957.62	-8.89	-8.76
Mole Fractions															
H2O		0.00	0.00	0.00	0.00	0.00	0.04	0.04	0.04	0.04	0.00	0.00	0.00	0.06	0.06
CO2		1.00	1.00	1.00	0.96	0.96	0.96	0.96	0.96	0.96	0.00	1.00	1.00	0.78	0.78
CH4		0.00	0.00	0.00	0.00	0.00	0.00	0.00	0.00	0.00	0.00	0.00	0.00	0.00	0.00
O2		0.00	0.00	0.00	0.04	0.04	0.00	0.00	0.00	0.00	1.00	0.00	0.00	0.16	0.16
Mass Flows	kg/sec	101.61	101.61	101.61	104.49	104.49	105.18	105.18	105.18	105.18	2.88	102.71	102.71	1.09	1.09
Molar exergy	MJ/kmol	10.10	10.07	8.37	8.33	22.13	31.78	20.37	5.21	4.98	16.49	4.88	10.04	6.07	9.35
Mass exergy	kJ/kg	229.38	228.79	190.12	191.12	507.96	737.78	472.78	120.90	115.72	515.46	111.08	228.26	149.67	230.31
Exergy flow rate	Watt	23.31	23.25	19.32	19.97	53.08	77.60	49.73	12.72	12.17	1.48	11.41	23.44	0.16	0.25

Table 3.22 Stream properties of COOLCEP-S cycle from Aspen Plus modelling

Stream Name	Units	15.00	16.00	17.00	18.00	19.00	20.00	21.00	22.00	23.00	24.00	26.00	CO2OUT	LNG	OXYGEN	WATEROUT
From		P2	B17	B17	HEATEX4	HEATEX3	B18	HEATEX8	B19	B19	DIST2	HEATEX7	HEATEX5			
To		B17	HEATEX3	HEATEX4	B18	B18	HEATEX8	HEATEX7		COMBUSTI		B19		P2	O2COM	
Stream Class		CONVEN	CONVEN	CONVEN	CONVEN	CONVEN	CONVEN	CONVEN	CONVEN	CONVEN	CONVEN	CONVEN	CONVEN	CONVEN	CONVEN	CONVEN
Phase		Liquid Phase	Liquid Phase	Liquid Phase	Vapor Phase	Liquid Phase	Vapor Phase		Liquid Phase	Vapor Phase	Liquid Phase					
Temperature	C	-156.04	-156.04	-156.04	-49.80	-49.00	-49.44	-34.20	8.00	8.00	-50.10	8.00	-34.90	-162.00	15.00	0.00
Pressure	bar	72.10	72.10	72.10	72.10	72.10	72.10	72.10	70.30	70.30	6.97	70.30	60.00	1.00	1.00	7.15
Mass Enthalpy	MJ/kg	-5.53	-5.53	-5.53	-4.81	-4.80	-4.81	-4.77	-4.68	-4.68	-9.34	-4.68	-8.33	-5.55	-0.01	-13.35
Mass Entropy	kJ/kg-K	-11.47	-11.47	-11.47	-7.86	-7.85	-7.85	-7.71	-7.35	-7.35	-2.03	-7.35	-1.94	-11.67	-0.03	-6.18
Enthalpy Flow	MWatt	-525.87	-235.75	-290.12	-252.33	-204.96	-457.29	-454.23	-442.37	-3.22	-948.90	-445.59	-9.06	-528.15	-0.03	-32.98
Mole Fractions																
H2O		0.00	0.00	0.00	0.00	0.00	0.00	0.00	0.00	0.00	0.00	0.00	0.06	0.00	0.00	0.80
CO2		0.00	0.00	0.00	0.00	0.00	0.00	0.00	0.00	0.00	1.00	0.00	0.78	0.00	0.00	0.20
CH4		1.00	1.00	1.00	1.00	1.00	1.00	1.00	1.00	1.00	0.00	1.00	0.00	1.00	0.00	0.00
O2		0.00	0.00	0.00	0.00	0.00	0.00	0.00	0.00	0.00	0.00	0.00	0.16	0.00	1.00	0.00
Mass Flows	kg/sec	95.16	42.66	52.50	52.50	42.66	95.16	95.16	94.47	0.69	101.62	95.16	1.09	95.16	2.88	2.47
Molar exergy	MJ/kmol	16.69	16.69	16.69	10.96	10.95	10.96	10.81	10.53	10.53	10.10	10.53	9.57	17.25	-0.03	0.84
Mass exergy	kJ/kg	1040.28	1040.28	1040.28	683.16	682.60	682.91	673.60	656.21	656.21	229.38	656.21	235.95	1075.41	-0.86	35.95
Exergy flow rate	Watt	98.99	44.38	54.61	35.87	29.12	64.99	64.10	61.99	0.45	23.31	62.44	0.26	102.34	0.00	0.09

3.4.10 The COOLCEP-C cycle modelling and analysis

Figure 3.12 shows the Cool Clean Efficient Power (COOLCEP) -C cycle model in Aspen Plus software based on the schematic presented in Figure 2.34 of chapter 2; COOLCEP-C is similar with COOLCEP-S cycle; however, the working flow expands in the turbine up to near ambient pressure to produce more power and the turbine exhaust temperature; therefore regenerator hot stream inlet temperature is lower than COOLCEP-S. The COOLCEP-C needs a compressor to increase the CO₂ pressure to the condensation level.

Table 3.23 shows the steam properties of the COOLCEP-C cycle at each stage; there are two types of working flow in this cycle.

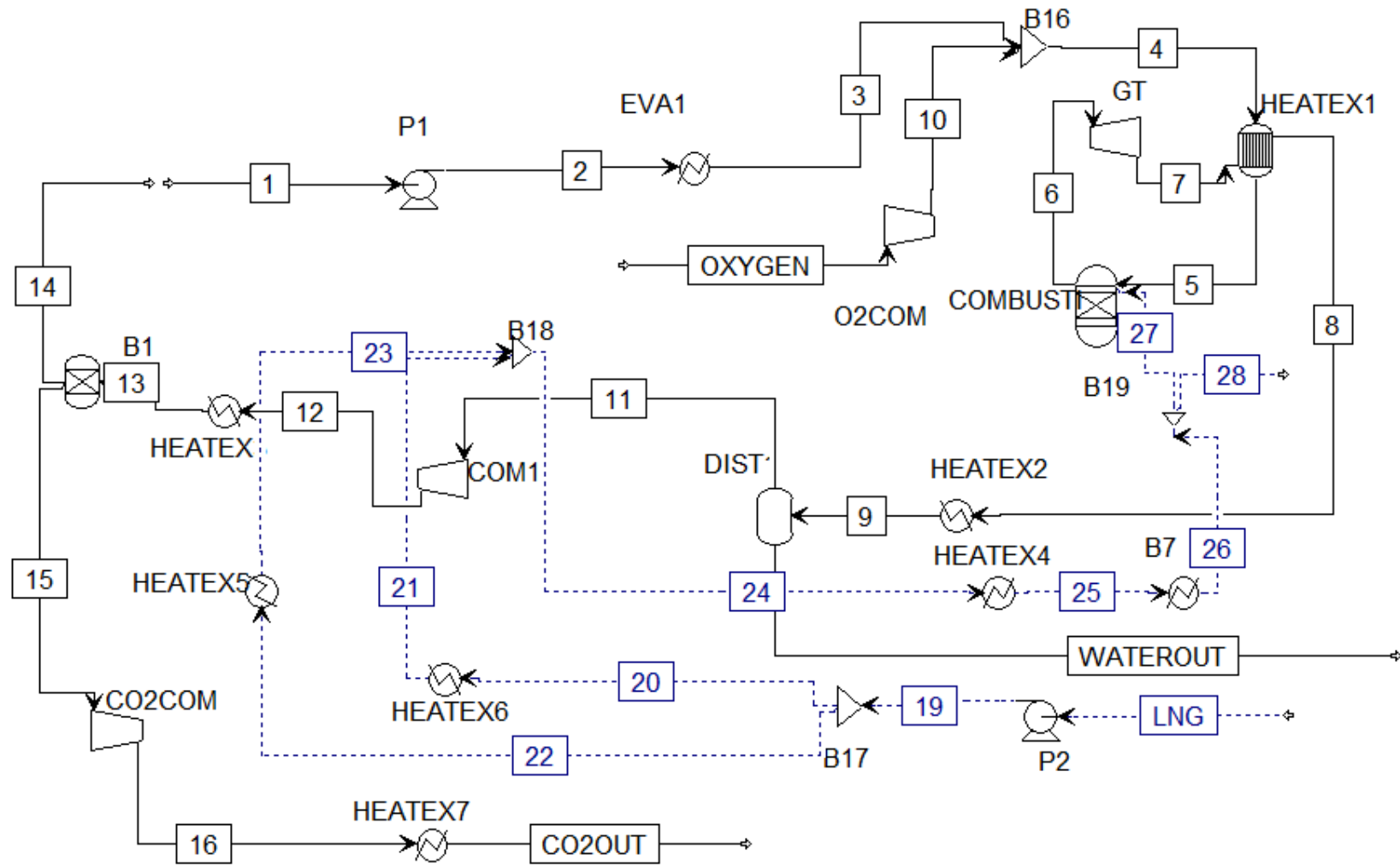


Figure 3.12 Aspen Plus modelling of COOLCEP-C cycle

Table 3.23 Stream properties of COOLCEP-C cycle from Aspen Plus modelling

Stream Name	Units	1.00	2.00	3.00	4.00	5.00	6.00	7.00	8.00	9.00	10.00	11.00	12.00	13.00	14.00	15.00
Description																
From			P1	EVA1	B16	HEATEX1	COMBUSTI	GT	HEATEX1	HEATEX2	O2COM	DIST1	COM1	HEATEX3	B1	B1
To		P1	EVA1	B16	HEATEX1	COMBUSTI	GT	HEATEX1	HEATEX2	DIST1	B16	COM1	HEATEX3	B1		CO2COM
Phase		Liquid Phase	Liquid Phase	Vapor Phase		Vapor Phase	Vapor Phase	Vapor Phase		Liquid Phase						
Temperature	C	-50.10	-49.10	8.00	34.91	439.79	915.11	472.18	70.20	14.00	596.64	0.00	157.58	-50.00	-50.10	-50.00
Pressure	bar	6.97	29.68	29.40	29.12	29.12	29.12	1.00	1.00	1.00	29.12	1.00	7.10	7.10	6.97	7.10
Molar Enthalpy	kJ/kmol	-411676.00	-411580.00	-395739.00	-366911.00	-348251.00	-339492.00	-362838.00	-380896.00	-385456.00	18209.10	-392534.00	-386410.00	-409427.00	-411676.00	-356052.00
Molar Enthalpy	kJ/kmol	-411.68	-411.58	-395.74	-366.91	-348.25	-339.49	-362.84	-380.90	-385.46	18.21	-392.53	-386.41	-409.43	-411.68	-356.05
Mass Enthalpy	kJ/kg	-9.35	-9.35	-8.99	-8.50	-8.07	-8.03	-8.58	-9.00	-9.11	0.57	-8.95	-8.81	-9.34	-9.35	-8.85
Mass Entropy	kJ/kg-K	-2.09	-2.09	-0.71	-0.57	0.32	0.90	0.99	0.17	-0.17	0.18	0.00	0.03	-2.06	-2.09	-1.03
Enthalpy Flow	MJ/sec	-565.46	-565.33	-543.57	-541.70	-514.15	-517.91	-553.53	-581.08	-588.03	1.87	-562.87	-554.09	-587.10	-565.46	-21.50
Mole Fractions																
H2O		0.00	0.00	0.00	0.00	0.00	0.06	0.06	0.06	0.06	0.00	0.00	0.00	0.00	0.00	0.11
CO2		1.00	1.00	1.00	0.93	0.93	0.93	0.93	0.93	0.93	0.00	0.99	0.99	0.99	1.00	0.81
CH4		0.00	0.00	0.00	0.00	0.00	0.00	0.00	0.00	0.00	0.00	0.00	0.00	0.00	0.00	0.00
O2		0.00	0.00	0.00	0.07	0.07	0.00	0.00	0.00	0.00	1.00	0.00	0.00	0.00	0.00	0.07
Mass Flows	kg/sec	60.45	60.45	60.45	63.74	63.74	64.53	64.53	64.53	64.53	3.29	62.88	62.88	62.88	60.45	2.43
Molar exergy	MJ/kmol	10.09	10.17	7.97	7.97	15.18	32.39	7.97	0.14	-0.01	16.53	0.01	5.70	9.96	10.09	4.75
Mass exergy	kJ/kg	229.19	230.97	181.10	184.52	351.71	765.67	188.31	3.31	-0.30	516.62	0.19	130.01	227.13	229.19	118.22
Exergy flow rate	MWatt	13.85	13.96	10.95	11.76	22.42	49.41	12.15	0.21	-0.02	1.70	0.01	8.18	14.28	13.85	0.29

Table 3.24 Stream properties of COOLCEP-C cycle from Aspen Plus modelling

Stream Name	Units	16.00	19.00	20.00	21.00	22.00	23.00	24.00	25.00	26.00	27.00	28.00	CO2OUT	LNG	OXYGEN	WATEROUT
Description																
From		CO2COM	P2	B17	HEATEX6	B17	HEATEX5	B18	HEATEX4	B7	B19	B19	HEATEX7			
To		HEATEX7	B17	HEATEX6	B18	HEATEX5	B18	HEATEX4	B7	B19	COMBUSTI			P2	O2COM	DIST1
Phase			Liquid Phase	Liquid Phase	Vapor Phase	Liquid Phase	Vapor Phase	Liquid Phase	Liquid Phase	Vapor Phase	Liquid Phase					
Temperature	C	76.23	-159.14	-159.14	-34.00	-159.14	-34.00	-34.00	1.00	8.00	8.00	8.00	-35.80	-162.00	15.00	0.00
Pressure	bar	60.00	72.10	72.10	72.10	72.10	72.10	72.10	72.10	70.30	70.30	70.30	60.00	1.00	1.00	1.00
Molar Enthalpy	kJ/kmol	-351828.00	-88831.20	-88831.20	-78724.10	-88831.20	-78724.10	-78724.10	-76918.30	-76556.20	-76556.20	-76556.20	-365462.00	-89130.90	-303.24	-289783.00
Molar Enthalpy	kJ/kmol	-351.83	-88.83	-88.83	-78.72	-88.83	-78.72	-78.72	-76.92	-76.56	-76.56	-76.56	-365.46	-89.13	-0.30	-289.78
Mass Enthalpy	kJ/kg	-8.75	-5.54	-5.54	-4.91	-5.54	-4.91	-4.91	-4.79	-4.77	-4.77	-4.77	-9.09	-5.56	-0.01	-16.09
Mass Entropy	kJ/kg-K	-1.00	-11.67	-11.67	-8.11	-11.67	-8.11	-8.11	-7.67	-7.58	-7.58	-7.58	-2.24	-11.71	-0.03	-9.72
Enthalpy Flow	MJ/sec	-21.25	-342.20	-110.74	-98.14	-231.45	-205.12	-303.26	-296.31	-294.91	-3.77	-291.15	-22.07	-343.35	-0.03	-26.55
Mole Fractions																
H2O		0.11	0.00	0.00	0.00	0.00	0.00	0.00	0.00	0.00	0.00	0.00	0.11	0.00	0.00	1.00
CO2		0.81	0.00	0.00	0.00	0.00	0.00	0.00	0.00	0.00	0.00	0.00	0.81	0.00	0.00	0.00
CH4		0.00	1.00	1.00	1.00	1.00	1.00	1.00	1.00	1.00	1.00	1.00	0.00	1.00	0.00	0.00
O2		0.07	0.00	0.00	0.00	0.00	0.00	0.00	0.00	0.00	0.00	0.00	0.07	0.00	1.00	0.00
Mass Flows	kg/sec	2.43	61.80	20.00	20.00	41.80	41.80	61.80	61.80	61.80	0.79	61.01	2.43	61.80	3.29	1.65
Molar exergy	MJ/kmol	8.61	17.50	17.50	10.56	17.50	10.56	10.56	10.26	10.18	10.18	10.18	9.85	17.37	-0.03	0.09
Mass exergy	kJ/kg	214.20	1091.09	1091.09	657.98	1091.09	657.98	657.98	639.24	634.35	634.35	634.35	244.88	1082.59	-0.86	5.03
Exergy flow rate	MWatt	0.52	67.43	21.82	13.16	45.61	27.50	40.66	39.51	39.20	0.50	38.70	0.59	66.90	0.00	0.01

3.4.11 The Novel O₂/CO₂ (Cao and Zheng, 2006) modelling and analysis

Figure 3.13 shows the Novel O₂/CO₂ cycle model in Aspen Plus software based on the schematic presented in Figure 2.36 of chapter 2. This cycle includes a gas turbine, CO₂-NG reformer and ammonia absorption refrigeration cycle. In this cycle, O₂ is the oxidizer of the fuel, and CO₂ is the working fluid (Cao and Zheng, 2006). The by-product of burning the fuel and O₂ in the combustion is H₂O and CO₂; the CO₂ is separated from H₂O through a cooling process. Table 3.14 shows steam properties at each stage for the O₂/CO₂ cycle; the recycled working flow is carbon dioxide.

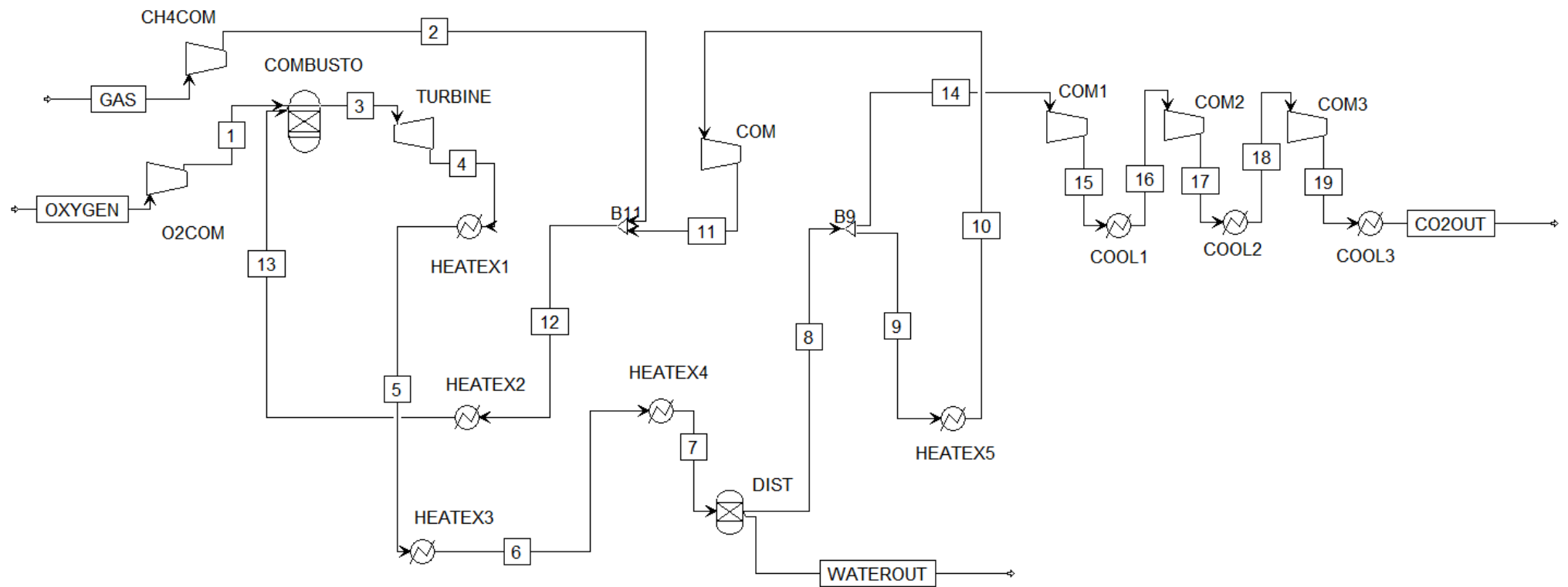


Figure 3.13 Aspen Plus modelling of O₂/CO₂ cycle

Table 3.25 Stream properties of O₂/CO₂ cycle from Aspen plus modelling

Stream Name	Units	1.00	2.00	3.00	4.00	5.00	6.00	7.00	8.00
Description									
From		O2COM	CH4COM	COMBUSTO	TURBINE	HEATEX1	HEATEX3	HEATEX4	DIST
To		COMBUSTO	B11	TURBINE	HEATEX1	HEATEX3	HEATEX4	DIST	B9
Phase		Vapor Phase		Vapor Phase					
Temperature	C	97.35	119.09	1139.93	787.07	224.75	144.95	29.95	29.95
Pressure	bar	11.00	10.00	10.00	1.03	1.03	1.03	1.03	1.03
Molar Enthalpy	MJ/kmol	2.14	-70.96	-328.73	-348.46	-376.44	-379.88	-385.26	-393.31
Mass Enthalpy	MJ/kg	0.07	-4.42	-7.74	-8.20	-8.86	-8.94	-9.07	-8.94
Mass Entropy	kJ/kg-K	-0.42	-5.57	1.34	1.41	0.53	0.36	-0.01	0.08
Enthalpy Flow	MWatt	0.27	-4.42	-700.72	-742.78	-802.44	-809.75	-821.23	-789.36
Mole Fractions									
H2O		0.00	0.00	0.06	0.06	0.06	0.06	0.06	0.00
CO2		0.00	0.00	0.94	0.94	0.94	0.94	0.94	1.00
CH4		0.00	1.00	0.00	0.00	0.00	0.00	0.00	0.00
O2		1.00	0.00	0.00	0.00	0.00	0.00	0.00	0.00
Mass Flows	kg/sec	3.99	1.00	90.57	90.57	90.57	90.57	90.57	88.32
Molar exergy	MJ/kmol	6.14	6.15	39.53	18.94	2.03	0.84	0.05	0.04
Mass exergy	kJ/kg	191.76	383.30	930.30	445.86	47.80	19.71	1.06	0.96
Exergy flow rate	kWatt	764.93	383.30	84256.40	40380.70	4329.10	1784.82	96.00	84.62

Table 3.26 Stream properties of O₂/CO₂ cycle from Aspen plus modelling

Stream Name	Units	9.00	10.00	11.00	12.00	13.00	14.00	15.00	16.00
Description									
From		B9	HEATEX5	COM	B11	HEATEX2	B9	COM1	COOL1
To		HEATEX5	COM	B11	HEATEX2	COMBUSTO	COM1	COOL1	COM2
Phase		Vapor Phase							
Temperature	C	29.95	0.00	190.45	188.31	741.35	29.95	148.41	30.00
Pressure	bar	1.03	1.03	10.00	10.00	10.00	1.03	4.21	4.21
Molar Enthalpy	MJ/kmol	-393.31	-394.41	-386.75	-376.94	-349.28	-393.31	-388.56	-393.31
Mass Enthalpy	MJ/kg	-8.94	-8.96	-8.79	-8.74	-8.10	-8.94	-8.83	-8.94
Mass Entropy	kJ/kg-K	0.08	-0.01	0.04	0.00	0.90	0.08	0.11	-0.19
Enthalpy Flow	MWatt	-764.84	-766.98	-752.08	-756.50	-700.99	-24.52	-24.22	-24.52
Mole Fractions									
H2O		0.00	0.00	0.00	0.00	0.00	0.00	0.00	0.00
CO2		1.00	1.00	1.00	0.97	0.97	1.00	1.00	1.00
CH4		0.00	0.00	0.00	0.03	0.03	0.00	0.00	0.00
O2		0.00	0.00	0.00	0.00	0.00	0.00	0.00	0.00
Mass Flows	kg/sec	85.58	85.58	85.58	86.58	86.58	2.74	2.74	2.74
Molar exergy	MJ/kmol	0.04	0.08	7.09	7.05	23.14	0.04	4.35	3.53
Mass exergy	kJ/kg	0.96	1.84	161.03	163.48	536.39	0.96	98.85	80.23
Exergy flow rate	kWatt	81.99	157.56	13780.80	14154.20	46440.70	2.63	271.17	220.07

Table 3.27 Stream properties of O₂/CO₂ cycle from Aspen plus modelling

Stream Name	Units	17.00	18.00	19.00	CO2OUT	GAS	OXYGEN	WATEROUT
Description								
From		COM2	COOL2	COM3	COOL3			DIST
To		COOL2	COM3	COOL3		CH4COM	O2COM	
Phase		Vapor Phase	Vapor Phase	Vapor Phase	Liquid Phase	Vapor Phase	Vapor Phase	Liquid Phase
Temperature	C	150.27	30.00	150.27	30.00	17.00	15.00	29.95
Pressure	bar	17.52	17.52	73.00	73.00	3.00	5.00	1.03
Molar Enthalpy	MJ/kmol	-388.48	-393.31	-388.48	-396.00	-74.80	-0.29	-285.43
Mass Enthalpy	MJ/kg	-8.83	-8.94	-8.83	-9.00	-4.66	-0.01	-15.84
Mass Entropy	kJ/kg-K	-0.15	-0.46	-0.42	-0.93	-5.65	-0.45	-8.99
Enthalpy Flow	MWatt	-24.22	-24.52	-24.22	-24.68	-4.66	-0.04	-35.58
Mole Fractions								
H2O		0.00	0.00	0.00	0.00	0.00	0.00	1.00
CO2		1.00	1.00	1.00	1.00	0.00	0.00	0.00
CH4		0.00	0.00	0.00	0.00	1.00	0.00	0.00
O2		0.00	0.00	0.00	0.00	0.00	1.00	0.00
Mass Flows	kg/sec	2.74	2.74	2.74	2.74	1.00	3.99	2.25
Molar exergy	MJ/kmol	7.91	7.07	11.45	10.53	2.69	3.96	0.00
Mass exergy	kJ/kg	179.75	160.60	260.12	239.26	167.97	123.82	0.25
Exergy flow rate	kWatt	493.09	440.55	713.56	656.35	167.97	493.91	0.56

3.4.12 The NetPower cycle modelling and analysis

The NetPower cycle is one of the novel oxy-combustion technologies, and it is developed recently with 8 Rivers Capital. The cycle is an oxy-combustion cycle with the working flow of carbon dioxide. The flow diagram of the Allam cycle is presented in Figure 2.37 and is described in detail in chapters 8 and 9.

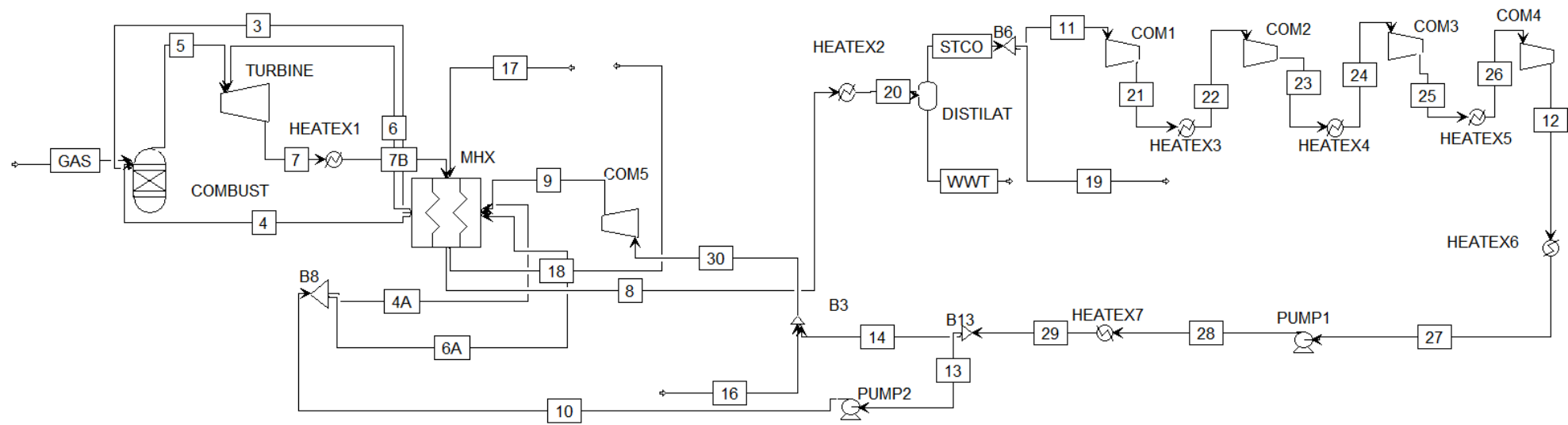


Figure 3.14 Aspen Plus modelling of NetPower cycle

Table 3.28 Stream properties of NetPower cycle from Aspen Plus modelling

Stream Name	Units	3.00	4.00	4A	5.00	6.00	6A	7.00	7B
Description									
From		MHX	MHX	B8	COMBUST	MHX	B8	TURBINE	HEATEX1
To		COMBUST	COMBUST	MHX	TURBINE	TURBINE	MHX	HEATEX1	MHX
Phase		Vapor Phase							
Temperature	C	714.41	714.41	50.77	1146.54	400.00	50.77	739.36	739.78
Pressure	bar	303.04	302.82	304.82	300.00	302.82	304.82	34.00	34.00
Molar Enthalpy	MJ/kmol	-303.55	-353.32	-394.87	-320.31	-370.90	-394.87	-344.10	-344.10
Mass Enthalpy	MJ/kg	-7.20	-8.08	-9.03	-7.60	-8.48	-9.03	-8.14	-8.14
Molar Entropy	MJ/kmol-K	0.01	0.01	-0.06	0.03	-0.01	-0.06	0.03	0.03
Mass Entropy	J/kg-K	249.56	227.24	-1455.39	683.60	-262.67	-1455.39	676.79	677.32
Molar Density	kmol/cum	3.44	3.43	19.78	2.39	5.21	19.78	0.40	0.40
Mass Density	kg/cum	144.89	149.99	864.93	100.66	227.74	864.93	16.96	16.95
Enthalpy Flow	MWatt	-4404.90	-5119.10	-5721.06	-9596.19	-1235.05	-1314.86	-11454.30	-11454.30
Mole Fractions									
AR		0.01	0.01	0.01	0.01	0.01	0.01	0.01	0.01
CO2		0.85	0.98	0.98	0.92	0.98	0.98	0.92	0.92
H2O		0.00	0.00	0.00	0.06	0.00	0.00	0.06	0.06
N2		0.01	0.01	0.01	0.01	0.01	0.01	0.01	0.01
O2		0.13	0.00	0.00	0.00	0.00	0.00	0.00	0.00
METHANE		0.00	0.00	0.00	0.00	0.00	0.00	0.00	0.00
ETHANE		0.00	0.00	0.00	0.00	0.00	0.00	0.00	0.00
PROPANE		0.00	0.00	0.00	0.00	0.00	0.00	0.00	0.00
BUTANE		0.00	0.00	0.00	0.00	0.00	0.00	0.00	0.00
PENTANE		0.00	0.00	0.00	0.00	0.00	0.00	0.00	0.00
Mass Flows	kg/sec	612.07	633.58	633.58	1262.16	145.61	145.61	1407.72	1407.72
Molar exergy	MJ/kmol	29.68	30.31	10.70	48.48	19.12	10.70	25.67	25.67
Mass exergy	MJ/kg	0.70	0.69	0.24	1.15	0.44	0.24	0.61	0.61
Exergy flow rate	Watt	430.75	439.20	155.09	1452.50	63.67	35.64	854.58	854.36

Table 3.29 Stream properties of NetPower cycle from Aspen Plus modelling

Stream Name	Units	8.00	9.00	10.00	11.00	12.00	13.00	14.00	16.00	17.00
Description										
From		MHX	COM5	PUMP2	B6	COM4	B13	B13		
To		HEATEX2	MHX	B8	COM1	HEATEX6	PUMP2	B3	B3	MHX
Phase			Vapor Phase	Liquid Phase	Vapor Phase	Vapor Phase	Liquid Phase	Liquid Phase	Vapor Phase	Vapor Phase
Temperature	C	55.00	45.47	50.77	29.00	42.51	25.50	25.50	15.00	275.00
Pressure	bar	33.00	305.04	304.82	33.00	79.95	119.91	119.91	120.00	7.50
Molar Enthalpy	MJ/kmol	-379.78	-342.74	-394.87	-386.81	-389.28	-396.12	-396.12	-1.38	4.87
Mass Enthalpy	MJ/kg	-8.98	-8.13	-9.03	-8.85	-8.90	-9.06	-9.06	-0.04	0.17
Molar Entropy	MJ/kmol-K	-0.03	-0.06	-0.06	-0.03	-0.04	-0.06	-0.06	-0.04	0.01
Mass Entropy	J/kg-K	-740.49	-1401.82	-1455.39	-644.11	-943.82	-1475.36	-1475.36	-1352.42	207.10
Molar Density	kmol/cum	1.48	19.18	10.74	1.62	5.65	14.83	14.83	5.47	0.16
Mass Density	kg/cum	62.51	808.95	469.49	70.65	247.20	648.64	648.64	175.17	4.74
Enthalpy Flow	MWatt	-12642.00	-4973.59	-7035.92	-11762.30	-11837.40	-7058.13	-4987.29	-2.66	46.64
Mole Fractions										
AR		0.01	0.01	0.01	0.01	0.01	0.01	0.01	0.00	0.01
CO2		0.92	0.85	0.98	0.98	0.98	0.98	0.98	0.00	0.00
H2O		0.06	0.00	0.00	0.00	0.00	0.00	0.00	0.00	0.01
N2		0.01	0.01	0.01	0.01	0.01	0.01	0.01	0.00	0.77
O2		0.00	0.13	0.00	0.00	0.00	0.00	0.00	1.00	0.21
METHANE		0.00	0.00	0.00	0.00	0.00	0.00	0.00	0.00	0.00
ETHANE		0.00	0.00	0.00	0.00	0.00	0.00	0.00	0.00	0.00
PROPANE		0.00	0.00	0.00	0.00	0.00	0.00	0.00	0.00	0.00
BUTANE		0.00	0.00	0.00	0.00	0.00	0.00	0.00	0.00	0.00
PENTANE		0.00	0.00	0.00	0.00	0.00	0.00	0.00	0.00	0.00
Mass Flows	kg/sec	1407.72	612.07	779.19	1329.76	1329.76	779.19	550.58	61.49	276.25
Molar exergy	MJ/kmol	7.86	11.26	10.70	8.19	9.63	9.72	9.72	11.62	7.00
Mass exergy	MJ/kg	0.19	0.27	0.24	0.19	0.22	0.22	0.22	0.36	0.24
Exergy flow rate	Watt	261.69	163.42	190.74	249.05	292.77	173.16	122.36	22.31	66.96

Table 3.30 Stream properties of NetPower cycle from Aspen Plus modelling

Stream Name	Units	18.00	19.00	20.00	21.00	22.00	23.00	24.00	25.00
Description									
From		MHX	B6	HEATEX2	COM1	HEATEX3	COM2	HEATEX4	COM3
To				DISTILAT	HEATEX3	COM2	HEATEX4	COM3	HEATEX5
Phase		Vapor Phase	Vapor Phase		Vapor Phase				
Temperature	C	55.00	29.00	29.00	48.26	25.00	44.27	25.00	44.07
Pressure	bar	7.30	33.00	33.00	41.18	41.17	51.37	51.36	64.08
Molar Enthalpy	MJ/kmol	-1.68	-386.81	-381.24	-386.26	-387.50	-387.00	-388.24	-387.80
Mass Enthalpy	MJ/kg	-0.06	-8.85	-9.01	-8.83	-8.86	-8.85	-8.88	-8.87
Molar Entropy	MJ/kmol-K	-0.01	-0.03	-0.04	-0.03	-0.03	-0.03	-0.04	-0.04
Mass Entropy	J/kg-K	-313.97	-644.11	-849.81	-638.27	-729.68	-724.33	-816.41	-811.65
Molar Density	kmol/cum	0.27	1.62	1.71	1.90	2.23	2.61	3.14	3.64
Mass Density	kg/cum	7.74	70.65	72.25	83.02	97.49	114.12	137.11	159.14
Enthalpy Flow	MWatt	-16.07	-392.22	-12690.50	-11745.70	-11783.40	-11768.30	-11806.00	-11792.60
Mole Fractions									
AR		0.01	0.01	0.01	0.01	0.01	0.01	0.01	0.01
CO2		0.00	0.98	0.92	0.98	0.98	0.98	0.98	0.98
H2O		0.01	0.00	0.06	0.00	0.00	0.00	0.00	0.00
N2		0.77	0.01	0.01	0.01	0.01	0.01	0.01	0.01
O2		0.21	0.00	0.00	0.00	0.00	0.00	0.00	0.00
METHANE		0.00	0.00	0.00	0.00	0.00	0.00	0.00	0.00
ETHANE		0.00	0.00	0.00	0.00	0.00	0.00	0.00	0.00
PROPANE		0.00	0.00	0.00	0.00	0.00	0.00	0.00	0.00
BUTANE		0.00	0.00	0.00	0.00	0.00	0.00	0.00	0.00
PENTANE		0.00	0.00	0.00	0.00	0.00	0.00	0.00	0.00
Mass Flows	kg/sec	276.25	44.34	1407.72	1329.76	1329.76	1329.76	1329.76	1329.76
Molar exergy	MJ/kmol	4.93	8.19	7.78	8.66	8.61	9.04	9.00	9.38
Mass exergy	MJ/kg	0.17	0.19	0.18	0.20	0.20	0.21	0.21	0.21
Exergy flow rate	Watt	47.17	8.30	259.07	263.32	261.94	274.84	273.70	285.20

Table 3.31 Stream properties of NetPower cycle from Aspen Plus modelling

Stream Name	Units	26.00	27.00	28.00	29.00	30.00	GAS	STCO	WWT
Description									
From		HEATEX5	HEATEX6	PUMP1	HEATEX7	B3		DISTILAT	DISTILAT
To		COM4	PUMP1	HEATEX7	B13	COM5	COMBUST	B6	
Phase		Vapor Phase	Liquid Phase	Liquid Phase	Liquid Phase	Vapor Phase	Vapor Phase	Vapor Phase	Liquid Phase
Temperature	C	25.00	26.00	35.55	25.50	17.04	145.00	29.00	29.00
Pressure	bar	64.07	79.94	119.91	119.91	120.00	305.00	33.00	33.00
Molar Enthalpy	MJ/kmol	-389.66	-394.99	-394.67	-396.12	-343.87	-78.74	-386.81	-287.39
Mass Enthalpy	MJ/kg	-8.91	-9.03	-9.03	-9.06	-8.15	-4.37	-8.85	-15.94
Molar Entropy	MJ/kmol-K	-0.04	-0.06	-0.06	-0.06	-0.06	-0.12	-0.03	-0.17
Mass Entropy	J/kg-K	-950.57	-1371.03	-1366.69	-1475.36	-1409.79	-6751.55	-644.11	-9257.99
Molar Density	kmol/cum	5.03	14.61	11.87	14.83	16.83	8.81	1.62	54.94
Mass Density	kg/cum	219.97	638.76	519.16	648.64	709.67	158.83	70.65	990.26
Enthalpy Flow	MWatt	-11849.20	-12011.20	-12001.50	-12045.40	-4989.94	-72.18	-12154.50	-536.01
Mole Fractions									
AR		0.01	0.01	0.01	0.01	0.01	0.00	0.01	0.00
CO2		0.98	0.98	0.98	0.98	0.85	0.02	0.98	0.00
H2O		0.00	0.00	0.00	0.00	0.00	0.00	0.00	1.00
N2		0.01	0.01	0.01	0.01	0.01	0.01	0.01	0.00
O2		0.00	0.00	0.00	0.00	0.13	0.00	0.00	0.00
METHANE		0.00	0.00	0.00	0.00	0.00	0.89	0.00	0.00
ETHANE		0.00	0.00	0.00	0.00	0.00	0.07	0.00	0.00
PROPANE		0.00	0.00	0.00	0.00	0.00	0.01	0.00	0.00
BUTANE		0.00	0.00	0.00	0.00	0.00	0.00	0.00	0.00
PENTANE		0.00	0.00	0.00	0.00	0.00	0.00	0.00	0.00
Mass Flows	kg/sec	1329.76	1329.76	1329.76	1329.76	612.07	16.52	1374.10	33.62
Molar exergy	MJ/kmol	9.33	9.48	9.75	9.72	10.24	14.00	8.19	0.07
Mass exergy	MJ/kg	0.21	0.22	0.22	0.22	0.24	0.78	0.19	0.00
Exergy flow rate	Watt	283.66	288.37	296.34	295.52	148.53	12.84	257.35	0.13

3.4.13 The S-CES cycle modelling and analysis

Figure 3.15 shows the S-CES cycle model in Aspen Plus software based on the schematic presented in Figure 2.40 of chapter 2; the S-CES is also described in detail in chapter 9. Table 3.16 shows steam properties at each stage for the S-CES cycle, and water is recycled as the working flow.

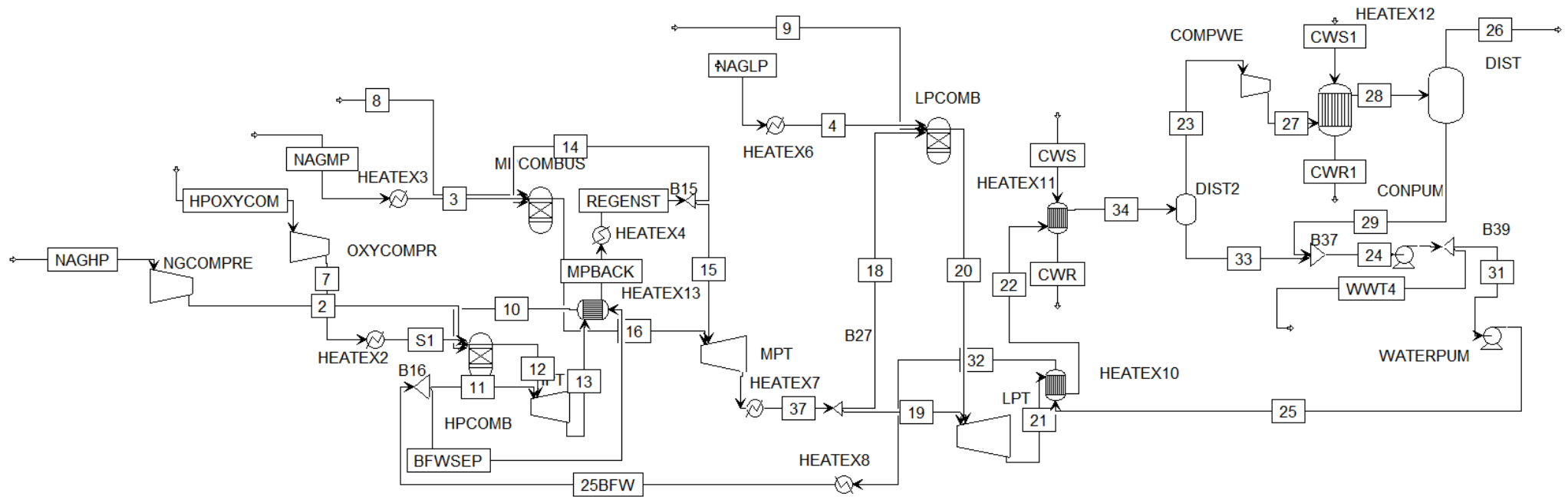


Figure 3.15 Aspen Plus modelling of S-CES cycle

Table 3.32 Stream properties of S-CES cycle from Aspen Plus modelling

Stream Name	Units	2.00	3.00	4.00	7.00	8.00	9.00	10.00	11.00
Description									
From		NGCOMPRES	HEATEX3	HEATEX6	OXYCOMPR			HEATEX13	B16
To		HPCOMB	MPCOMBUS	LPCOMB	HEATEX2	MPCOMBUS	LPCOMB	HPCOMB	HPT
Stream Class		CONVEN							
Phase		Vapor Phase							
Temperature	C	147.14	140.00	130.00	213.38	120.00	120.00	650.00	475.00
Pressure	bar	310.03	69.00	10.00	310.00	65.00	10.00	352.00	352.50
Mass Enthalpy	MJ/kg	-4.23	-4.25	-4.42	0.18	0.09	0.09	-12.13	-12.51
Molar Entropy	cal/mol-K	-27.91	-25.10	-21.61	-7.58	-6.01	-2.30	-12.46	-14.43
Mass Entropy	kJ/kg-K	-6.48	-5.83	-5.05	-0.99	-0.78	-0.30	-2.89	-3.34
Enthalpy Flow	MWatt	-16.32	-22.88	-23.65	2.66	1.83	2.46	-1285.01	-203.49
Mole Fractions									
AR		0.00	0.00	0.00	0.02	0.02	0.02	0.00	0.00
CO2		0.02	0.02	0.02	0.00	0.00	0.00	0.00	0.00
H2O		0.00	0.00	0.01	0.00	0.00	0.00	1.00	1.00
N2		0.01	0.01	0.00	0.01	0.01	0.01	0.00	0.00
O2		0.00	0.00	0.00	0.97	0.97	0.97	0.00	0.00
CH4		0.89	0.89	0.89	0.00	0.00	0.00	0.00	0.00
ETHAN-01		0.07	0.07	0.07	0.00	0.00	0.00	0.00	0.00
PROPA-01		0.01	0.01	0.01	0.00	0.00	0.00	0.00	0.00
N-BUT-01		0.00	0.00	0.00	0.00	0.00	0.00	0.00	0.00
N-PEN-01		0.00	0.00	0.00	0.00	0.00	0.00	0.00	0.00
Mass Flows	kg/sec	3.85	5.38	5.35	15.18	20.97	28.21	105.92	16.26
Molar exergy	MJ/kmol	15.01	11.20	6.29	15.46	10.69	6.05	33.81	29.40
Mass exergy	kJ/kg	833.02	621.35	350.89	481.42	332.71	188.24	1870.70	1627.12
Exergy flow rate	MWatt	3.21	3.34	1.88	7.31	6.98	5.31	198.14	26.46

Table 3.33 Stream properties of S-CES cycle from Aspen Plus modelling

Stream Name	Units	12.00	13.00	14.00	15.00	16.00	17.00	18.00	19.00
Description									
From		HPCOMB	HPT	B15	B15	MPCOMBUS	MPT	B27	B27
To		HPT	HEATEX13	MPCOMBUS	MPT	MPT	HEATEX7	LPCOMB	LPT
Stream Class		CONVEN							
Phase		Vapor Phase							
Temperature	C	1221.50	771.37	510.00	510.00	1557.87	790.47	420.00	420.00
Pressure	bar	310.00	62.00	62.00	62.00	62.00	8.74	8.74	8.74
Mass Enthalpy	MJ/kg	-10.39	-11.50	-12.06	-12.06	-9.13	-11.12	-11.87	-11.87
Molar Entropy	cal/mol-K	-6.28	-7.01	-9.80	-9.80	0.55	-2.17	-6.30	-6.30
Mass Entropy	kJ/kg-K	-1.38	-1.55	-2.17	-2.17	0.11	-0.46	-1.33	-1.33
Enthalpy Flow	MWatt	-1298.67	-1624.14	-901.44	-801.72	-922.49	-1862.49	-1198.29	-790.54
Mole Fractions									
AR		0.00	0.00	0.00	0.00	0.00	0.00	0.00	0.00
CO2		0.04	0.03	0.03	0.03	0.09	0.07	0.07	0.07
H2O		0.96	0.96	0.96	0.96	0.90	0.92	0.92	0.92
N2		0.00	0.00	0.00	0.00	0.00	0.00	0.00	0.00
O2		0.00	0.00	0.00	0.00	0.00	0.00	0.00	0.00
CH4		0.00	0.00	0.00	0.00	0.00	0.00	0.00	0.00
ETHAN-01		0.00	0.00	0.00	0.00	0.00	0.00	0.00	0.00
PROPA-01		0.00	0.00	0.00	0.00	0.00	0.00	0.00	0.00
N-BUT-01		0.00	0.00	0.00	0.00	0.00	0.00	0.00	0.00
N-PEN-01		0.00	0.00	0.00	0.00	0.00	0.00	0.00	0.00
Mass Flows	kg/sec	124.95	141.22	74.74	66.47	101.09	167.56	100.96	66.61
Molar exergy	MJ/kmol	51.83	32.46	25.34	25.34	60.99	27.73	17.88	17.88
Mass exergy	kJ/kg	2720.07	1714.17	1338.09	1338.09	2963.78	1393.84	898.60	898.60
Exergy flow rate	MWatt	339.88	242.07	100.01	88.95	299.61	233.56	90.72	59.85

Table 3.34 Stream properties of S-CES cycle from Aspen Plus modelling

Stream Name	Units	20.00	21.00	22.00	23.00	24.00	25.00	25BFW	26.00
Description									
From		LPCOMB	LPT	HEATEX10	DIST2	B37	WATERPUM	HEATEX8	DIST
To		LPT	HEATEX10	HEATEX11	COMPWE	CONPUM	HEATEX10	B16	
Stream Class		CONVEN	CONVEN	CONVEN	CONVEN	CONVEN	CONVEN	CONVEN	CONVEN
Phase		Vapor Phase	Vapor Phase		Vapor Phase	Liquid Phase	Liquid Phase	Vapor Phase	Vapor Phase
Temperature	C	1285.68	557.69	61.15	27.71	27.66	36.14	475.00	26.00
Pressure	bar	8.74	0.24	0.24	0.21	0.21	352.50	352.50	1.05
Mass Enthalpy	MJ/kg	-9.07	-10.91	-11.83	-7.59	-15.82	-15.78	-12.51	-7.13
Molar Entropy	cal/mol-K	3.40	3.45	-5.10	3.89	-38.72	-38.22	-14.43	1.83
Mass Entropy	kJ/kg-K	0.66	0.69	-1.02	0.44	-8.97	-8.85	-3.34	0.19
Enthalpy Flow	MWatt	-1219.48	-2194.82	-2379.51	-407.88	-2394.96	-1928.12	-1528.70	-354.23
Mole Fractions									
AR		0.00	0.00	0.00	0.03	0.00	0.00	0.00	0.03
CO2		0.11	0.09	0.09	0.60	0.00	0.00	0.00	0.71
H2O		0.85	0.87	0.87	0.18	1.00	1.00	1.00	0.03
N2		0.00	0.00	0.00	0.02	0.00	0.00	0.00	0.02
O2		0.04	0.03	0.03	0.18	0.00	0.00	0.00	0.21
CH4		0.00	0.00	0.00	0.00	0.00	0.00	0.00	0.00
ETHAN-01		0.00	0.00	0.00	0.00	0.00	0.00	0.00	0.00
PROPA-01		0.00	0.00	0.00	0.00	0.00	0.00	0.00	0.00
N-BUT-01		0.00	0.00	0.00	0.00	0.00	0.00	0.00	0.00
N-PEN-01		0.00	0.00	0.00	0.00	0.00	0.00	0.00	0.00
Mass Flows	kg/sec	134.52	201.13	201.13	53.75	151.42	122.18	122.18	49.71
Molar exergy	MJ/kmol	44.22	11.55	3.02	-3.47	0.00	0.02	29.40	0.09
Mass exergy	kJ/kg	2059.51	552.28	144.25	-93.96	0.11	1.09	1627.12	2.20
Exergy flow rate	MWatt	277.05	111.08	29.01	-5.05	0.02	0.13	198.80	0.11

Table 3.35 Stream properties of S-CES cycle from Aspen Plus modelling

Stream Name	Units	27.00	28.00	29.00	30.00	31.00	32.00	33.00	34.00
Description									
From		COMPWE	HEATEX12	DIST	CONPUM	B39	HEATEX10	DIST2	HEATEX11
To		HEATEX12	DIST	B37	B39	WATERPUM	HEATEX8	B37	DIST2
Stream Class		CONVEN	CONVEN	CONVEN	CONVEN	CONVEN	CONVEN	CONVEN	CONVEN
Phase		Vapor Phase		Liquid Phase					
Temperature	C	160.83	26.00	26.00	27.71	27.71	300.00	27.71	29.00
Pressure	bar	1.05	1.05	1.05	2.50	2.50	352.50	0.21	0.24
Mass Enthalpy	MJ/kg	-7.46	-7.77	-15.67	-15.82	-15.82	-14.27	-15.82	-13.62
Molar Entropy	cal/mol-K	3.89	-4.28	-38.46	-38.71	-38.71	-24.53	-38.72	-32.31
Mass Entropy	kJ/kg-K	0.44	-0.49	-8.79	-8.97	-8.97	-5.68	-8.98	-6.47
Enthalpy Flow	MWatt	-400.78	-417.57	-63.34	-2394.93	-1932.43	-1743.43	-2331.62	-2739.50
Mole Fractions									
AR		0.03	0.03	0.00	0.00	0.00	0.00	0.00	0.00
CO2		0.60	0.60	0.01	0.00	0.00	0.00	0.00	0.09
H2O		0.18	0.18	0.99	1.00	1.00	1.00	1.00	0.87
N2		0.02	0.02	0.00	0.00	0.00	0.00	0.00	0.00
O2		0.18	0.18	0.00	0.00	0.00	0.00	0.00	0.03
CH4		0.00	0.00	0.00	0.00	0.00	0.00	0.00	0.00
ETHAN-01		0.00	0.00	0.00	0.00	0.00	0.00	0.00	0.00
PROPA-01		0.00	0.00	0.00	0.00	0.00	0.00	0.00	0.00
N-BUT-01		0.00	0.00	0.00	0.00	0.00	0.00	0.00	0.00
N-PEN-01		0.00	0.00	0.00	0.00	0.00	0.00	0.00	0.00
Mass Flows	kg/sec	53.75	53.75	4.04	151.42	122.18	122.18	147.38	201.13
Molar exergy	MJ/kmol	1.41	0.08	0.00	0.00	0.00	10.25	0.00	-0.46
Mass exergy	kJ/kg	38.10	2.03	0.05	0.11	0.11	567.20	0.11	-21.92
Exergy flow rate	MWatt	2.05	0.11	0.00	0.02	0.01	69.30	0.02	-4.41

Table 3.36 Stream properties of S-CES cycle from Aspen Plus modelling

Stream Name	Units	37.00	BFWSEP	CWR	CWR1	CWS	CWS1	HPOXYCOM	MPBACK
Description									
From		HEATEX7	B16	HEATEX11	HEATEX12				HEATEX13
To		B27	HEATEX13			HEATEX11	HEATEX12	OXYCOMPR	HEATEX4
Stream Class		CONVEN	CONVEN	CONVEN	CONVEN	CONVEN	CONVEN	CONVEN	CONVEN
Phase		Vapor Phase	Vapor Phase	Liquid Phase	Liquid Phase	Liquid Phase	Liquid Phase	Vapor Phase	Vapor Phase
Temperature	C	420.00	475.00	12.76	11.08	11.00	11.00	120.00	641.08
Pressure	bar	8.74	352.50	1.00	1.00	1.00	1.00	150.00	62.00
Mass Enthalpy	MJ/kg	-11.87	-12.51	-15.91	-15.92	-15.92	-15.92	0.09	-11.79
Molar Entropy	cal/mol-K	-6.30	-14.43	-39.70	-39.80	-39.81	-39.81	-7.67	-8.33
Mass Entropy	kJ/kg-K	-1.33	-3.34	-9.23	-9.25	-9.25	-9.25	-1.00	-1.84
Enthalpy Flow	MWatt	-1988.83	-1325.21	-796399.00	-796742.00	-796759.00	-796759.00	1.32	-1664.34
Mole Fractions									
AR		0.00	0.00	0.00	0.00	0.00	0.00	0.02	0.00
CO2		0.07	0.00	0.00	0.00	0.00	0.00	0.00	0.03
H2O		0.92	1.00	1.00	1.00	1.00	1.00	0.00	0.96
N2		0.00	0.00	0.00	0.00	0.00	0.00	0.01	0.00
O2		0.00	0.00	0.00	0.00	0.00	0.00	0.97	0.00
CH4		0.00	0.00	0.00	0.00	0.00	0.00	0.00	0.00
ETHAN-01		0.00	0.00	0.00	0.00	0.00	0.00	0.00	0.00
PROPA-01		0.00	0.00	0.00	0.00	0.00	0.00	0.00	0.00
N-BUT-01		0.00	0.00	0.00	0.00	0.00	0.00	0.00	0.00
N-PEN-01		0.00	0.00	0.00	0.00	0.00	0.00	0.00	0.00
Mass Flows	kg/sec	167.56	105.92	50042.40	50042.40	50042.40	50042.40	15.18	141.22
Molar exergy	MJ/kmol	17.88	29.40	0.01	0.02	0.02	0.02	12.76	28.71
Mass exergy	kJ/kg	898.60	1627.12	0.79	1.06	1.08	1.08	397.25	1516.25
Exergy flow rate	MWatt	150.57	172.34	39.78	53.26	53.98	53.98	6.03	214.12

Table 3.37 Stream properties of S-CES cycle from Aspen Plus modelling

Stream Name	Units	NAGHP	NAGLP	NAGMP	REGENST	S1	WWT4
Description							
From					HEATEX4	HEATEX2	B39
To		NGCOMPRE	HEATEX6	HEATEX3	B15	HPCOMB	
Stream Class		CONVEN	CONVEN	CONVEN	CONVEN	CONVEN	CONVEN
Phase		Vapor Phase		Vapor Phase	Vapor Phase	Vapor Phase	Liquid Phase
Temperature	C	15.00	15.00	17.00	510.00	213.38	27.71
Pressure	bar	70.00	70.00	70.00	62.00	310.00	2.50
Mass Enthalpy	MJ/kg	-4.53	-4.70	-4.53	-12.06	0.18	-15.82
Molar Entropy	cal/mol-K	-28.56	-28.97	-28.50	-9.80	-7.58	-38.71
Mass Entropy	kJ/kg-K	-6.64	-6.76	-6.62	-2.17	-0.99	-8.97
Enthalpy Flow	MWatt	-17.46	-25.15	-24.35	-1703.16	2.66	-462.49
Mole Fractions							
AR		0.00	0.00	0.00	0.00	0.02	0.00
CO2		0.02	0.02	0.02	0.03	0.00	0.00
H2O		0.00	0.01	0.00	0.96	0.00	1.00
N2		0.01	0.00	0.01	0.00	0.01	0.00
O2		0.00	0.00	0.00	0.00	0.97	0.00
CH4		0.89	0.89	0.89	0.00	0.00	0.00
ETHAN-01		0.07	0.07	0.07	0.00	0.00	0.00
PROPA-01		0.01	0.01	0.01	0.00	0.00	0.00
N-BUT-01		0.00	0.00	0.00	0.00	0.00	0.00
N-PEN-01		0.00	0.00	0.00	0.00	0.00	0.00
Mass Flows	kg/sec	3.85	5.35	5.38	141.22	15.18	29.24
Molar exergy	MJ/kmol	10.51	10.45	10.50	25.34	15.46	0.00
Mass exergy	kJ/kg	583.03	582.72	582.90	1338.09	481.42	0.11
Exergy flow rate	MWatt	2.25	3.12	3.14	188.96	7.31	0.00

3.5 Sensitivity comparison of CES and NetPower

The supercritical CES power cycle is the best cycle of CES with respect to efficiency. Therefore, the supercritical CES power cycle is going to be compared with the recent NetPower cycle. The initial condition for supercritical CES and NetPower are equal. In order to calculate the efficiency of the turbines, it is required to calculate cooling blade parameters. In this paper, the turbine efficiency for both the CES cycle and the NetPower cycles are assumed constant.

In chapter 8, The NetPower and Supercritical CES cycle, modelling and simulation were carried out using Aspen Plus to study the efficiency of cycles on different parameters of Turbine Inlet Temperature (TIT), Combustion Outlet Pressure (COP), minimum approach temperature of the heat exchanger. The sensitivity of cycle efficiency on the TIT for the supercritical CES are compared with NetPower in one diagram.

3.6 Techno-economic analysis of oxy-combustion cycles

The economic feasibility of oxy-combustion cycles is the key to develop and commercialise these cycles. The cost of oxy-fuel combustion with CCS technologies depends on several factors, including Capital cost, operation cost, fuel price and maintenance costs (Hu, 2011). Techno-economic analysis needs to perform a cost evaluation and engineering study of oxy-combustion cycle; in this subchapter, the techno-economics of oxy-combustion cycles in terms of cost rate and levelised Cost of Electricity (LCOE) are studied.

3.6.1 Cost rate

The cost of power cycle equipment can be calculated from Table 3.38 & Table 3.39. The annual cost of the plant includes annual fuel cost, operating cost, and capital cost. The capital cost and maintenance cost of each equipment can be calculated from Equation 3-21 (Seyyedi, Ajam and Farahat, 2010), \dot{Z}_i unit is (\$/s)

$$\dot{Z}_i = \frac{Z_i \times \text{CRF} \times \varphi}{N \times 3600}$$

Equation 3-20

Z_i is purchase costs, it can be calculated from Table 3.38 and CFR is annual capital recovery factor (CRF=18.2%) and the number of the hours of plant operation per year (N= 8000 h), and φ is the maintenance factor (u=1.06).

The CRF can be calculated from Table 3.19 (Samanta and Ghosh, 2015).

$$\text{CRF} = \frac{d}{(1 - (1 + d)^{-n})}$$

Equation 3-21

D = Interest rate

n = Number of year

Table 3.38 Equations for calculating the purchase cost (Z) for the components (Sahu and Sanjay, 2017) (Seyyedi, Ajam and Farahat, 2010).

Compressor	$Z_C = \left(\frac{G_{11} \cdot \dot{m}_{a,i}}{G_{12} - \eta_{AC}}\right) \left(\frac{P_e}{P_i}\right) \ln\left(\frac{P_e}{P_i}\right)$
Intercooler	$Z_{IC} = G_{51} \left(\frac{\dot{m}_{a,i} \{(h_{IC,a})_i - (h_{IC,a})_e\}}{U(\Delta TLM)}\right)^{0.6}$
Recuperator	$Z_{RC} = G_{51} \left(\frac{\dot{m}_{g,i} \{(h_{RC,g})_i - (h_{RC,g})_e\}}{U(\Delta TLM)}\right)^{0.6}$
Combustion Chamber	$Z_{CC} = \left(\frac{G_{21} \cdot \dot{m}_{a,i}}{G_{22} - \frac{P_e}{P_i}}\right) (1 + \exp(G_{23} \cdot T_e - G_{24}))$
Gas Turbine	$Z_{GT} = \left(\frac{G_{31} \cdot \dot{m}_{g,e}}{G_{32} - \eta_{GT}}\right) \ln\left(\frac{P_i}{P_e}\right) (1 + \exp(G_{23} \cdot T_e - G_{24}))$
Heat recovery steam generator	$Z_{HRSG} = C_{51} \left[\left(\frac{\dot{Q}_{PH}}{\Delta TLM_{PH}}\right)^{0.8} + \left(\frac{\dot{Q}_{EV}}{\Delta TLM_{EV}}\right)^{0.8} \right] + C_{52} \dot{m}_{st} + C_{53} \dot{m}_g^{1.2}$

Compressor	$G_{11} = 39.5 \text{ \$/kg/s}$ $G_{12} = 0.9$
Intercooler	$G_{51} = 2290 \text{ \$/m}^{1.2}$ $U = 0.018 \text{ kW/m}^{1.2}\text{K}$
Recuperator	$G_{51} = 2290 \text{ \$/m}^{1.2}$ $U = 0.018 \text{ kW/m}^{1.2}\text{K}$
Combustion Chamber	$G_{21} = 25.65 \text{ \$/kg/s}$ $G_{22} = 0.995$ $G_{23} = 0.018 \text{ K}^{-1}$ $G_{24} = 26.4$
Gas Turbine	$G_{31} = 266.3 \text{ \$/kg/s}$ $G_{32} = 0.920$ $G_{33} = 0.036 \text{ K}^{-1}$ $G_{34} = 54.4$
Heat Recovery Steam Generator (HRSG)	$C_{51} = 3650 \text{ \$/}\left(\frac{\text{kW}}{\text{K}}\right)^{0.8}$ $C_{52} = 11820 \text{ \$/}\left(\frac{\text{kg}}{\text{s}}\right)$ $G_{53} = 658 \text{ \$/}(kg/s)^{1.2}$

Also, the gas turbine is the main cost of the power cycle can be calculated from Table 3.39 (Carapellucci *et al.*, 2017)

Table 3.39 GT cost function (Carapellucci *et al.*, 2017)

Power output	Aeroderivative gas turbine	Heavy duty gas turbine
Lower than 50MW	$2324P_{GT}^{0.85}$	$7113P_{GT}^{0.73}$
Higher than 50MW		$4424P_{GT}^{0.78}$

The capital cost of heat exchanger (HX) can be calculated from Equation 3-22 (Soltani *et al.*, 2013)

$$(COE_{CAP})_{HX} = 4122 \times A_{HX}^{0.6} \quad \text{Equation 3-22}$$

Where the overall heat transfer coefficient (U) of the heat exchanger is considered as 0.29 kW/m²k, assuming that the heat exchanger is made of stainless steel. The operation and maintenance cost is between 4% to 6% (Samanta and Ghosh, 2015) and is considered 6% in this research.

The cost of the equipment for the Rankine cycle (Khaljani, Khoshbakhti Saray and Bahlouli, 2015):

Pump:

$$Z_p = 3540(\dot{W}_p)^{0.71} \quad \text{Equation 3-23}$$

Evaporator:

$$Z_{eva} = 309.143(A_{area}) + 231.915 \quad \text{Equation 3-24}$$

Turbine:

$$Z_{\text{SteamTurbine}} = 6000(\dot{W}_T)^{0.7} \quad \text{Equation 3-25}$$

Condensor:

$$Z_{\text{cond}} = 1773(\dot{m}_{\text{steam}}) \quad \text{Equation 3-26}$$

Internal Heat Exchanger:

$$Z_{IHE} = 1.3(190 + 310A_{IHE}) \quad \text{Equation 3-27}$$

Table 3.40 shows the estimated investment cost of the Air Separation Unit (ASU), CO₂-Compression system (W. Sanz *et al.*, 2005).

Table 3.40 Estimated investment costs (W. Sanz *et al.*, 2005)

Air separation unit	O ₂ mass flow	\$(/kg O ₂ /s)	1 500 000
Other costs (Piping, CO ₂ -Recirc.)	CO ₂ mass flow	\$(/kg CO ₂ /s)	100 000
CO ₂ -Compression system	CO ₂ mass flow	\$(/kg CO ₂ /s)	450 000

Equation 3-28 needs to be used to calculate the cost of the base year to reference year:

$$\text{Cost at reference year} = \text{original Cost} \frac{\text{CI reference year}}{\text{CI original year}} \quad \text{Equation 3-28}$$

CI is the cost index, and the value is given in Table 3.41 Marshal and swift cost index at various years (Khaljani, Khoshbakhti Saray and Bahlouli, 2015) from 1990 to 2013. In the present work, to calculate the cost index, Marshal and swift index is used.

The purchasing cost of gas turbine cycle components is based on 1995, and purchasing costs of pump and condenser are based on 2011, and purchasing cost of the evaporator is based on 2006, purchasing cost of organic Rankine cycle turbine is based on 2013 and cost of the internal heat exchanger is based on 2010.

These purchasing costs were converted to equivalent expenses in 2013 by table index (Khaljani, Khoshbakhti Saray and Bahlouli, 2015).

Table 3.41 Marshal and swift cost index at various years (Khaljani, Khoshbakhti Saray and Bahlouli, 2015)

Year	Cost index
1990	915
1995	1027.5
1996	1039.2
1997	1056.8
1998	1061.9
1999	1068.3
2000	1089
2001	1092
2002	1100.2
2003	1109
2004	1115.6
2005	1129.6
2006	1143
2007	1156.6
2009	1170.2
2010	1194.77
2011	1242.56
2012	1256.23
2013	1267.53

Fuel cost can be calculated from the following formula (Sahu and Sanjay, 2017):

$$C_f = c_f \times \dot{m}_f \times \text{LHV} \quad \text{Equation 3-29}$$

The fuel cost per energy unit (on an LHV basis) is $c_f = 0.004 \text{ \$/MJ}$ (Sahu and Sanjay, 2016). The total capital cost of purchasing and maintenance is

$$\dot{Z}_T = \sum \dot{Z}_i \quad \text{Equation 3-30}$$

Total overall cost rate includes fuel cost, operating cost and purchasing cost, and can be calculated from the following formula:

$$\dot{C}_T = c_f \times \dot{m}_f \times \text{LHV} + \sum \dot{Z}_i \quad \text{Equation 3-31}$$

Cost of electricity consumption is 170 Euro/MWh and $170 \times 1.18 = 200.6 \text{ \$/MWh}$.

3.7 Summary

In this chapter, the oxy-combustion cycle theories for this PhD thesis are indicated; it includes the calculation method for the thermodynamic of oxy-combustion cycles, exergy analysis method are indicated, and EOS of the gas turbine and steam turbine for this PhD thesis has been defined. Furthermore, methodology for sensitivity analysis of oxy-combustion cycles are defined and CES, and NetPower sensitivity methodology is indicated. The techno-economic analysis formula and calculation method are explained for oxy-combustion cycles; these formulas are used for techno-economic calculation in chapter 9.

Then, The simulations of the oxy-combustions cycle were presented, the simulation process flow diagrams of each cycle were shown, and the detailed working flow properties were tabulated. These simulation data can be used for the oxy-combustion analysis of the next chapter.

Chapter 4: Exergy analysis of leading oxy-combustion cycles

4.1 The SCOC-CC cycle modelling and analysis

The amount of exergy destruction in each component is indicated in Figure 4.1, and Figure 4.2 shows the percentage of exergy destruction for each component, and furthermore, the exergy destruction per MWe of network output is indicated in Figure 4.3;

As shown in Figure 4.3, the higher exergy destruction is in the combustion of the gas turbine with 28.8% of total input exergy, the exergy loss in the combustor is caused by various reasons, including incomplete combustion in the chamber, the energy loss of the flue gas to the ambient, heat dissipation from the combustion (Fans, 2020) and mainly exergy loss due to chemical reaction and heat transfer occurs inside the combustion chamber (Pattanayak, 2015).

The second exergy destruction is in the HRSE; it is basically due to the severe mass and heat transfer process induced by a high difference of temperature in HRSE. As shown in Figure 4.1, the exergy destruction in the steam turbine is more than in the gas turbine because the working flow enters the gas turbine with a higher temperature in comparison with a steam turbine (Fans, 2020). The exergy destruction in turbines is because of their low isentropic efficiency, and it is due to their design parameters and wear of components.

The exergy destruction in the air compressor is higher than the gas turbine and steam turbine because of higher isentropic efficiency, and it is mainly due to design considerations.

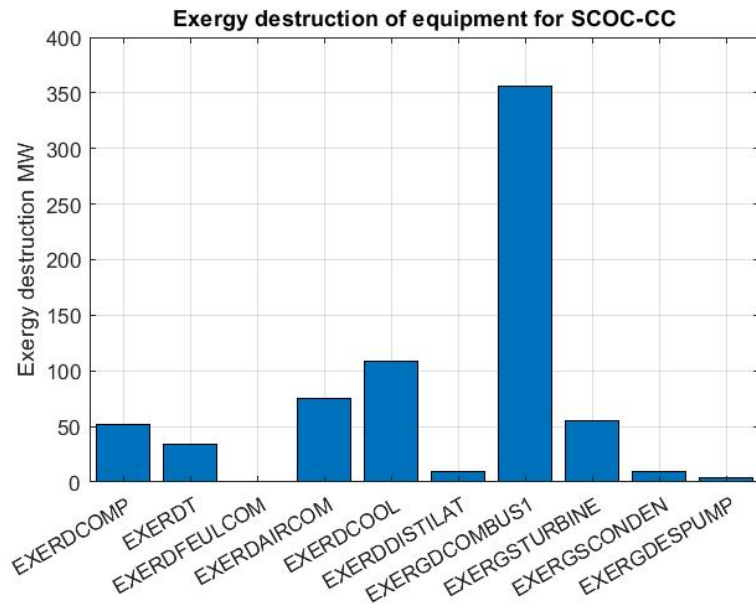


Figure 4.1 Exergy destruction for each equipment of SCOC-CC

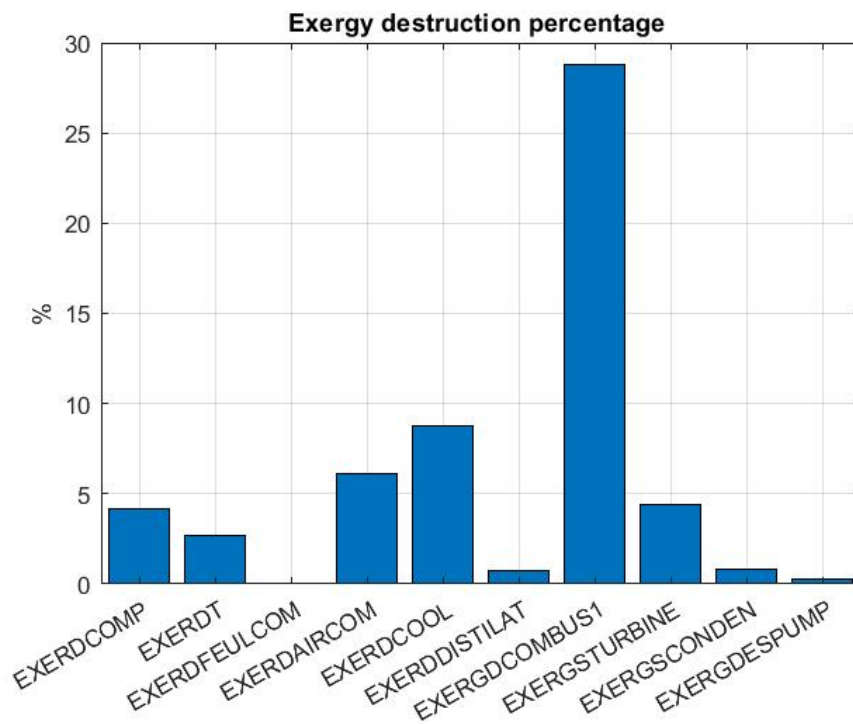


Figure 4.2 Exergy destruction percentage of SCOC-CC

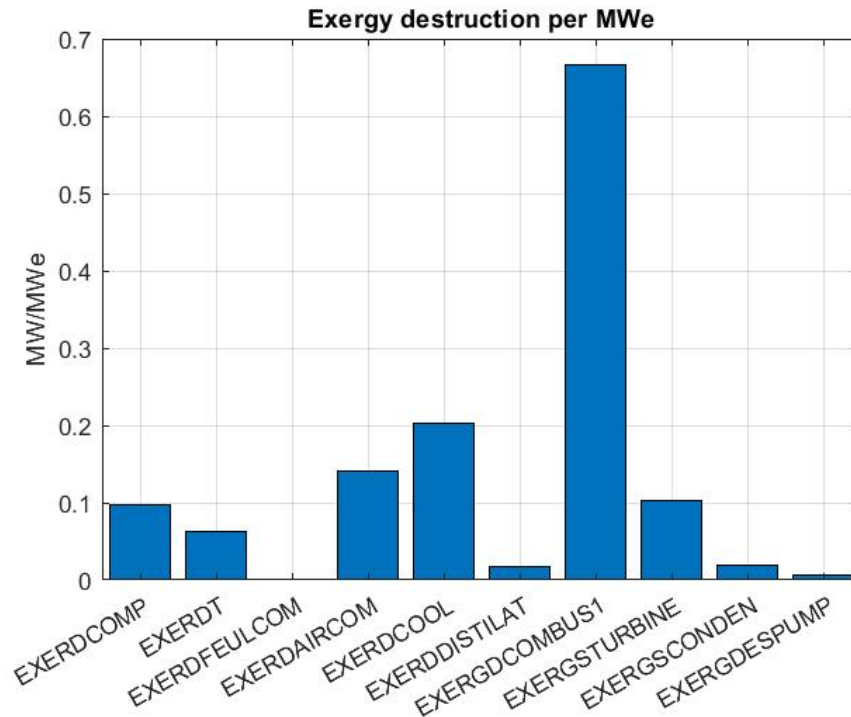


Figure 4.3 Exergy destruction per MWe for SCOC-CC

4.2 The COOPERATE cycle modelling and analysis

Figure 4.4 shows the amount of exergy destruction in each component, Figure 4.5 shows the percentage of exergy destruction for each component, and Figure 4.6 shows the exergy destruction per MWe of network output; the combustion with 24.4% of total exergy input and heat exchanger with 11.5% of total exergy input has higher exergy destruction. As discussed before, the exergy loss in the combustion is caused by various reasons, and mainly exergy loss due to chemical reaction and heat transfer occurs inside the combustion chamber (Pattanayak, 2015). The second exergy destruction is in the HRSE; it is basically due to the severe mass and heat transfer process induced by a high difference of temperature in HRSE. The exergy destruction in distillation with 6.9% of total input exergy is higher than other components after heat exchanger and combustions.

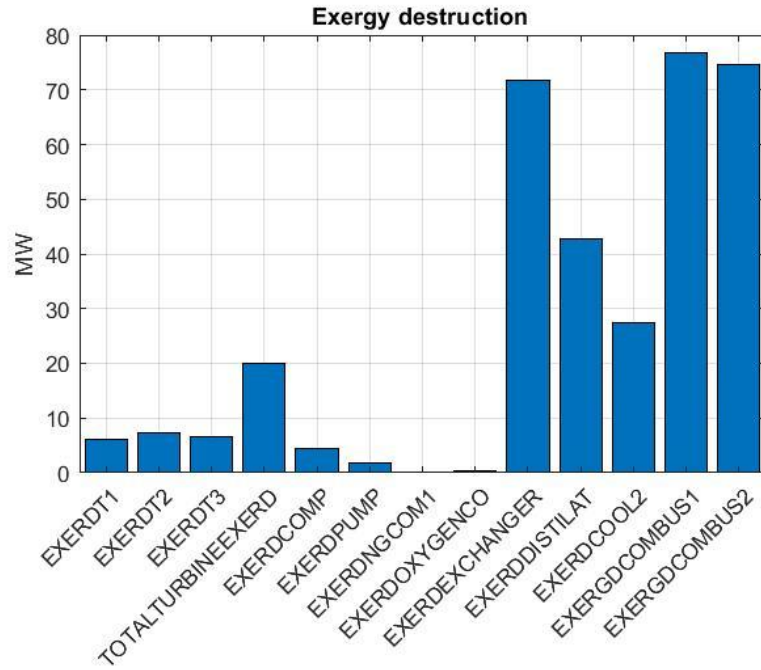


Figure 4.4 Exergy destruction of each equipment for COOPERATE cycle

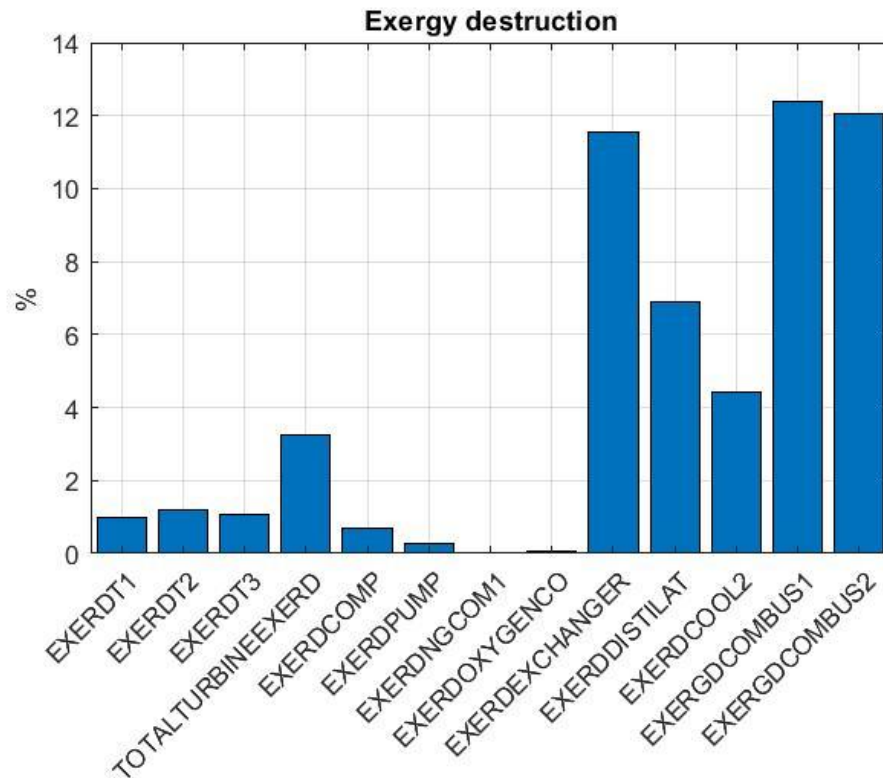


Figure 4.5 Percentage of exergy distraction for each component

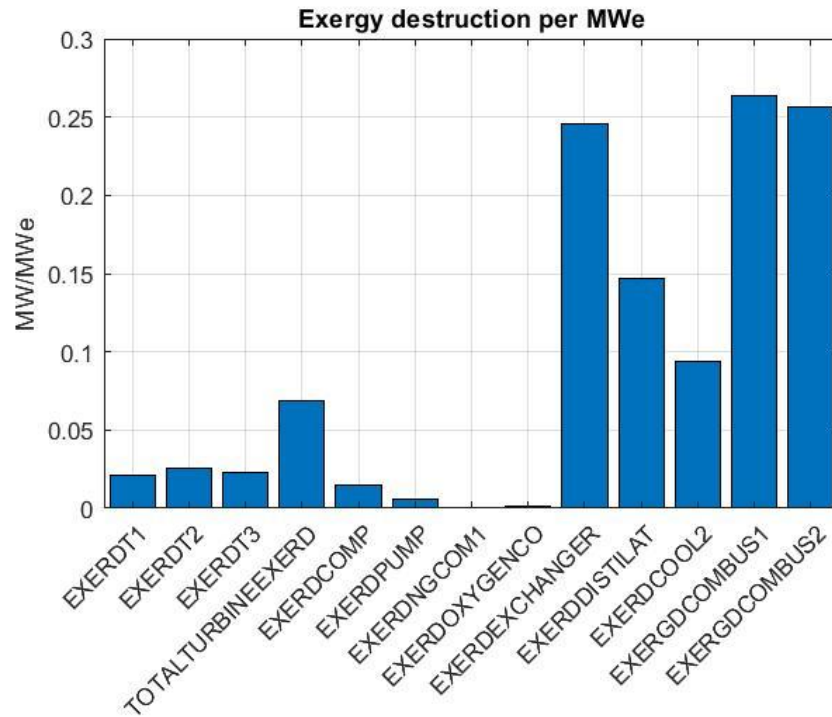


Figure 4.6 Exergy destruction per MWe for COOPERATE Cycle

4.3 The E-MATIANT cycle modelling and analysis

The amount of exergy destruction in each component is indicated in Figure 4.7, and Figure 4.8 shows the percentage of exergy destruction for each component, and Figure 4.9 shows the exergy destruction per MWe of network output.

Figure 4.8 shows exergy destruction percentage in E-MATIANT cycle; Exergy destruction in combustion with 30.85% is higher than other components. The second exergy destruction in the E-MATIANT cycle is recycled compressors with 8.8% of total input exergy.

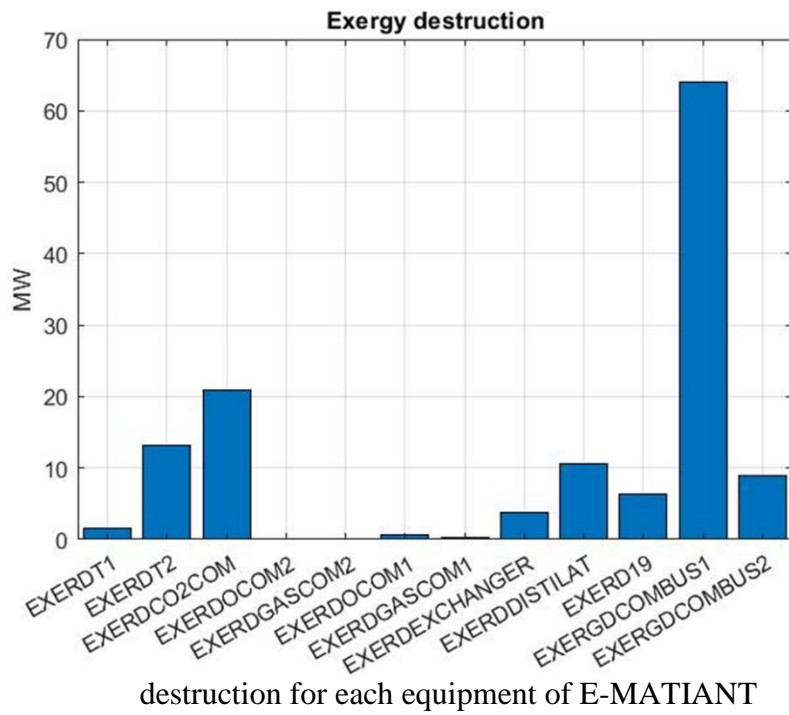


Figure 4.7
Exergy

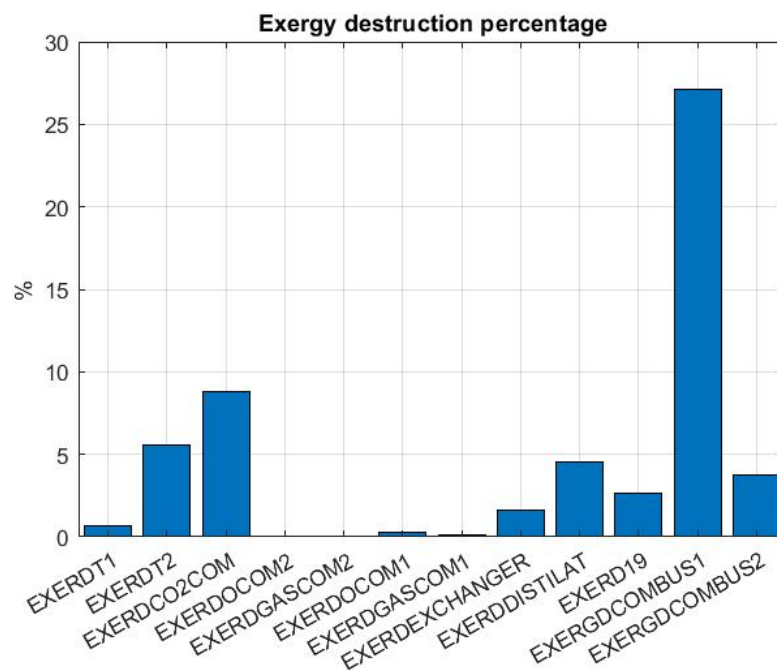


Figure 4.8 Exergy destruction percentage for E-MATIANT

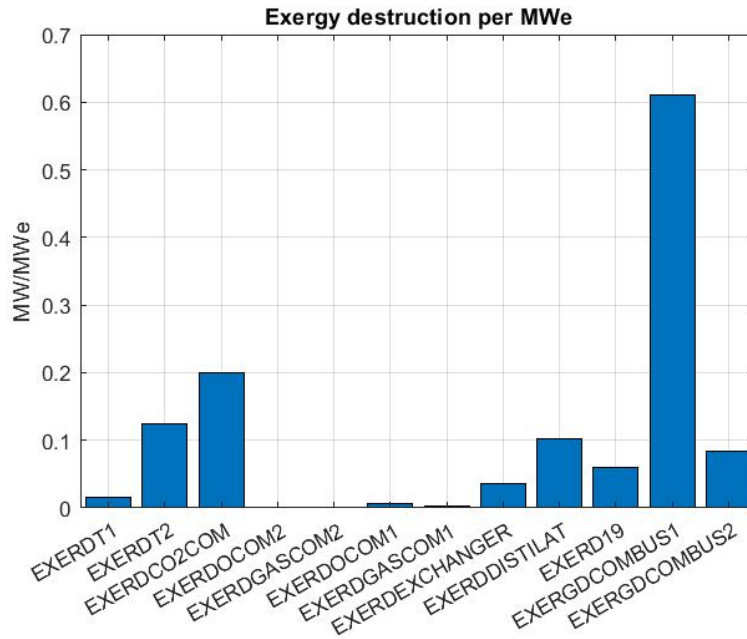


Figure 4.9 Exergy destruction per MWe production for E-MATIANT

4.4 The CC_MATIANT cycle modelling and analysis

The amount of exergy destruction in each component is indicated in Figure 4.10, and Figure 4.11 shows the percentage of exergy destruction for each component in the CC-MATIANT cycle, and Figure 4.12 shows the exergy destruction per MWe of network output;

Exergy destruction in the distillation is higher than other components, and the second main exergy destruction is combustion with 27.31 and then is the heat exchanger.

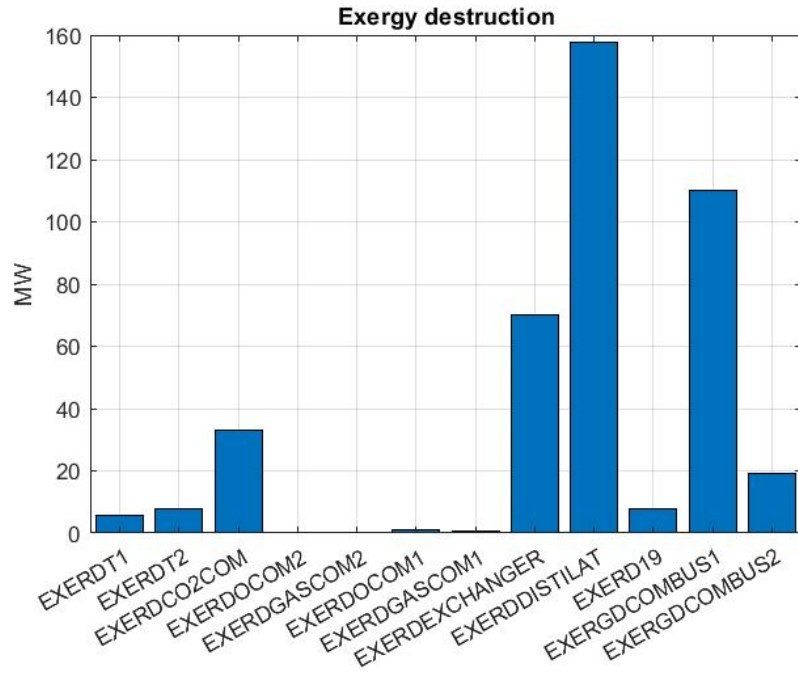


Figure 4.10 Exergy destruction for CC-MATIANT

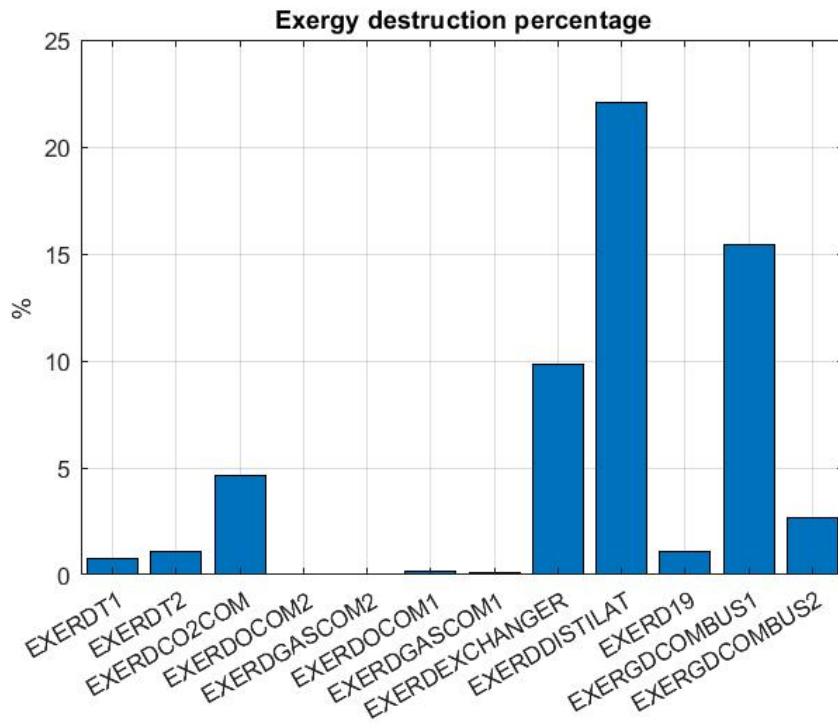


Figure 4.11 Exergy destruction percentage of CC-MATIANT

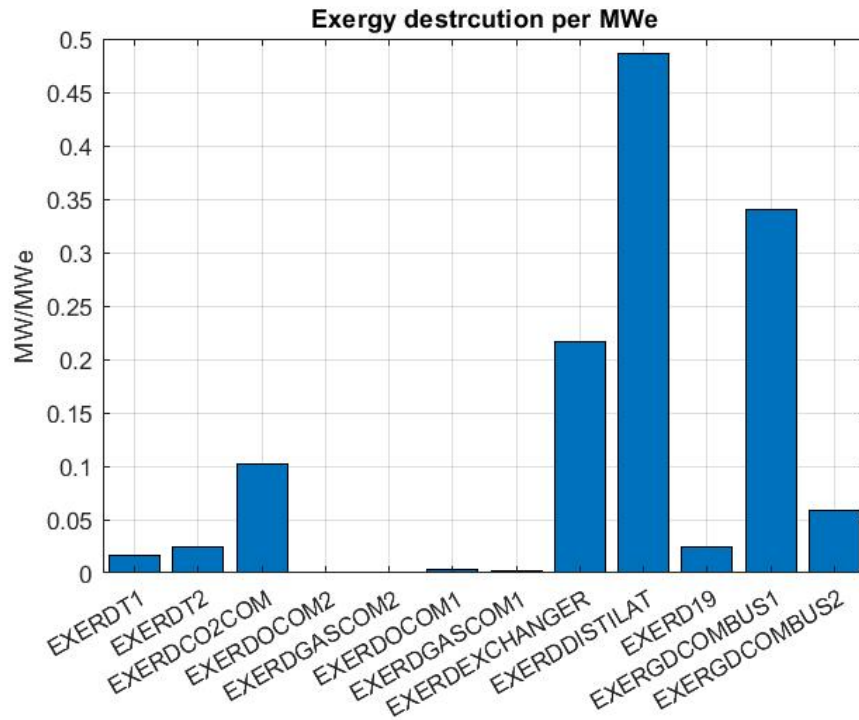


Figure 4.12 Exergy destrction per MWe production for CC-MATIANT

4.5 The Graz cycle modelling and analysis

Figure 4.13 shows the amount of exergy destruction in each component, Figure 4.14 shows the percentage of exergy destruction for each component in the Graz cycle, and Figure 4.15 shows the exergy destruction per MWe of network output; the exergy destruction in combustion with 29.5% is higher than other equipment in Graz cycle, and the second-high exergy destruction component is distillation with 11.15%.

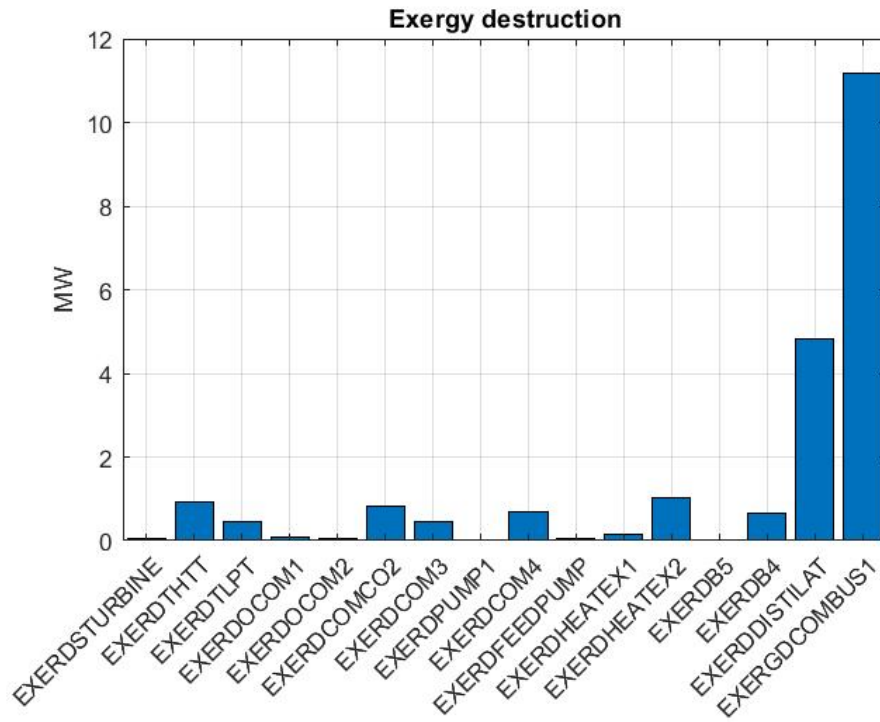


Figure 4.13 Exergy destruction for Graz cycle

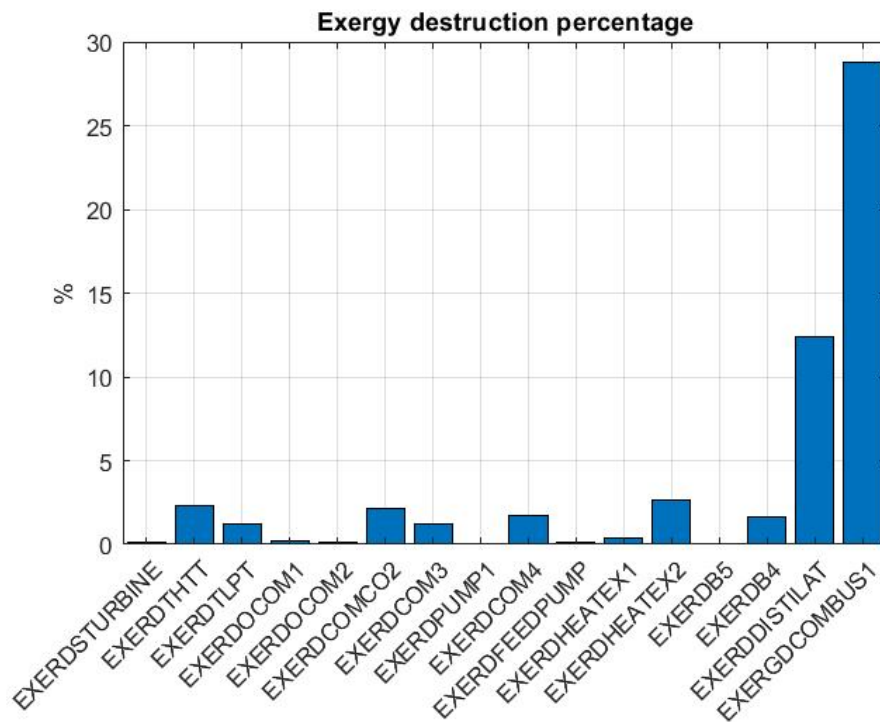


Figure 4.14 Exergy destruction percentage for Graz cycle

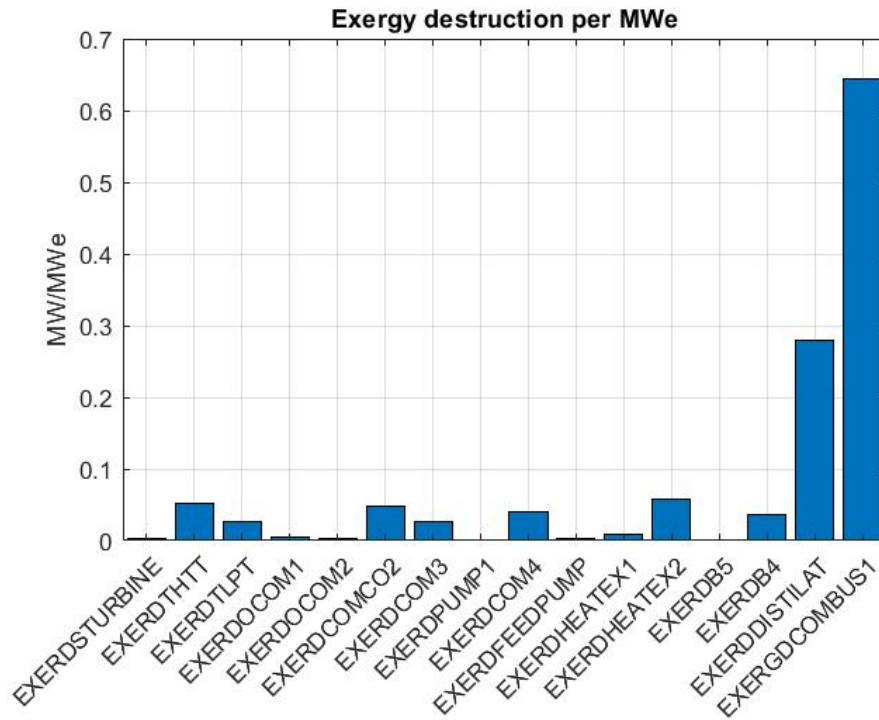


Figure 4.15 Exergy destruction per MWe for Graz cycle

4.6 The S-Graz cycle modelling and analysis

The amount of exergy destruction in each component is indicated in Figure 4.16, and Figure 4.17 shows the percentage of exergy destruction for each component, and Figure 4.18 shows the exergy destruction per MWe of network output.

Figure 4.17 shows the exergy destruction percentage for the S-Graz cycle; the combustion with 28.4% and heat exchanger with 18.6% have higher exergy destruction than other components.

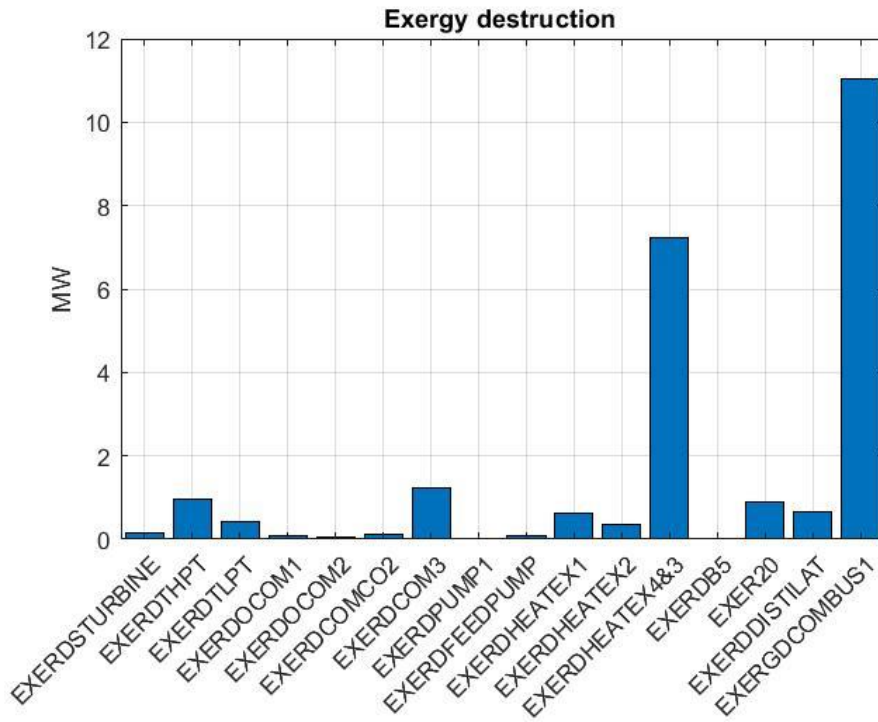


Figure 4.16 Exergy destruction for S-Graz cycle

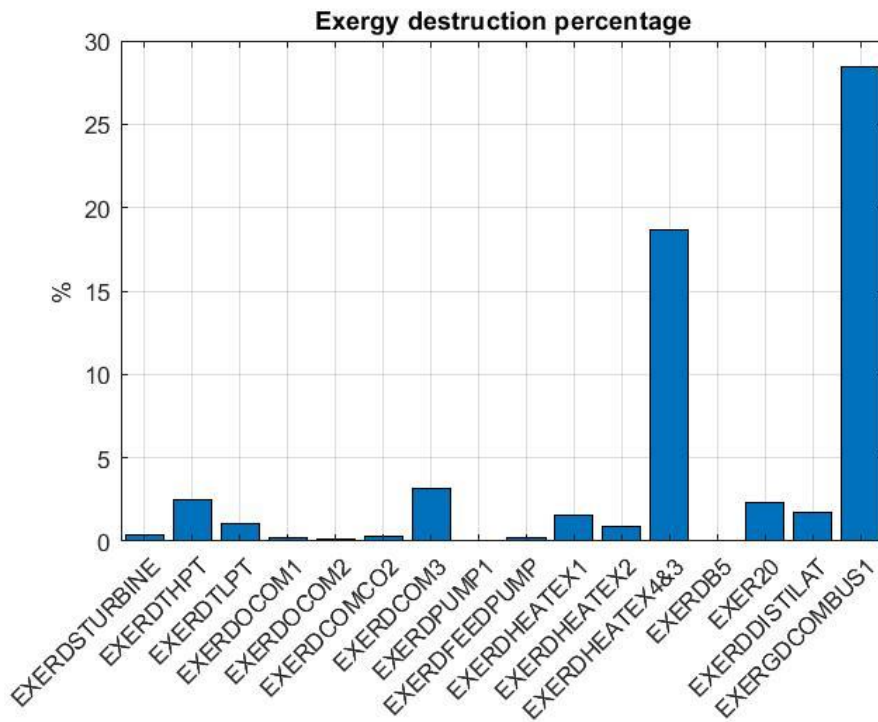


Figure 4.17 Exergy destruction percentage for S-Graz cycle

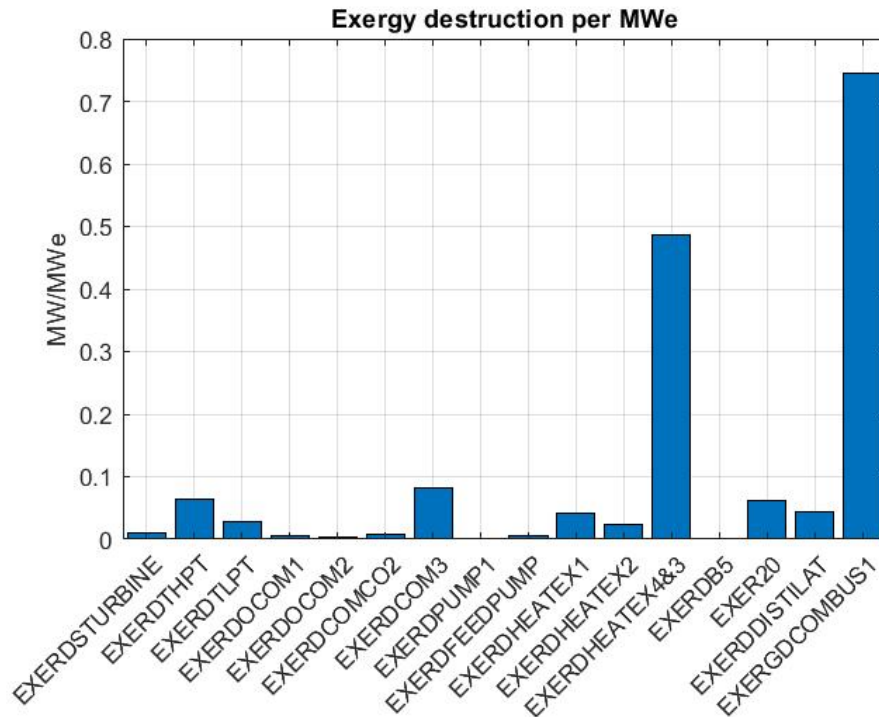


Figure 4.18 Exergy destruction per MWe for S-Graz cycle

4.7 The AZEP 100% cycle modelling and analysis

The amount of exergy destruction in each component is indicated in Figure 4.19, and Figure 4.20 shows the percentage of exergy destruction for each component, and Figure 4.21 shows the exergy destruction per MWe of network output.

Figure 4.20 shows the exergy destruction percentage in each component of AZEP 100% cycle; the main exergy destruction is in the MCM with 28.6% of total input exergy; the MCM technology development is important to increase the efficiency of the cycle.

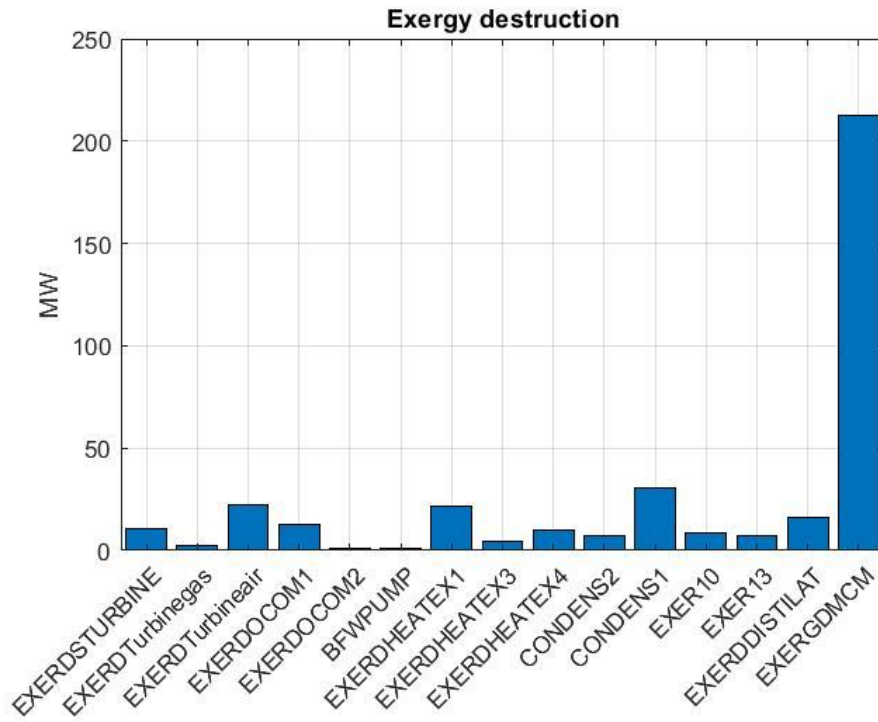


Figure 4.19 Exergy destruction of AZEP 100%

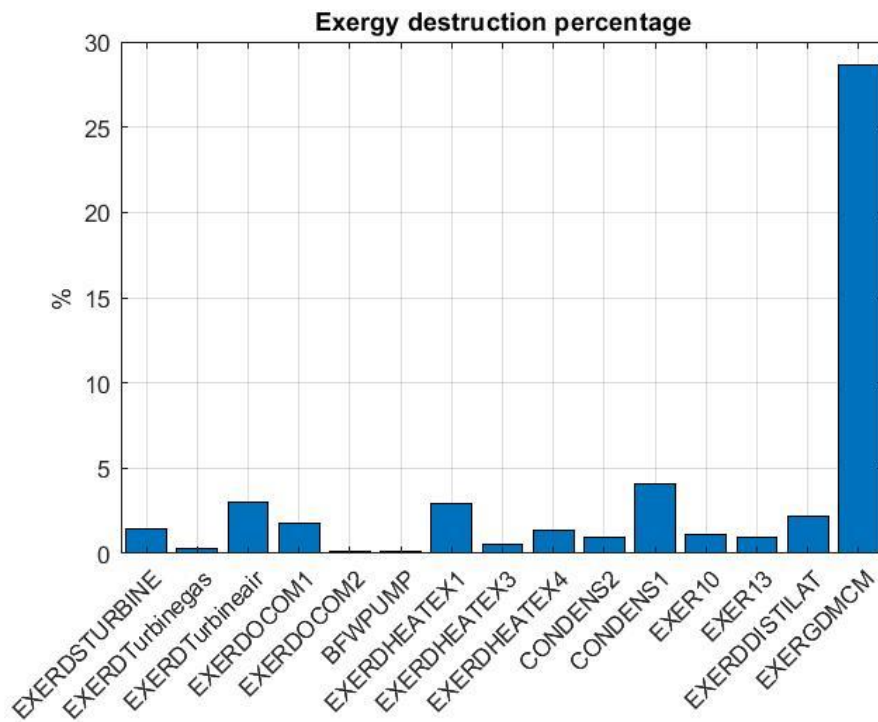


Figure 4.20 Exergy destruction percentage for AZEP 100%

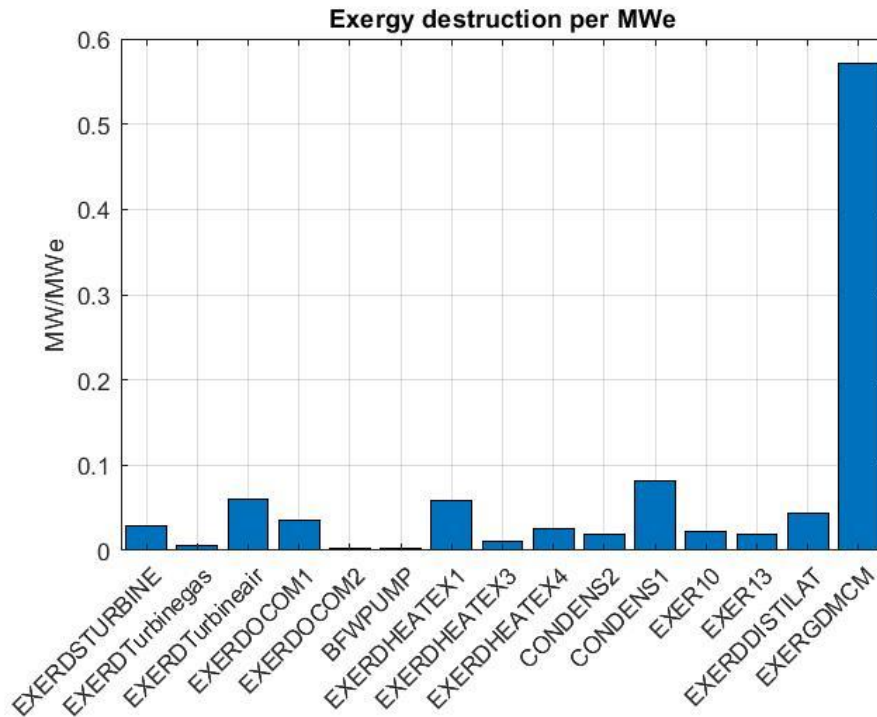


Figure 4.21 Exergy destruction per MWe for AZEP 100%

4.8 The ZEITMOP cycle modelling and analysis

The amount of exergy destruction in each component is indicated in Figure 4.22, Figure 4.23 shows the percentage of exergy destruction for each component, and Figure 4.24 shows the exergy destruction per MWe of network output; The combustion is the highest exergy destruction component, and ITM has the same exergy destruction as HPT and LPT.

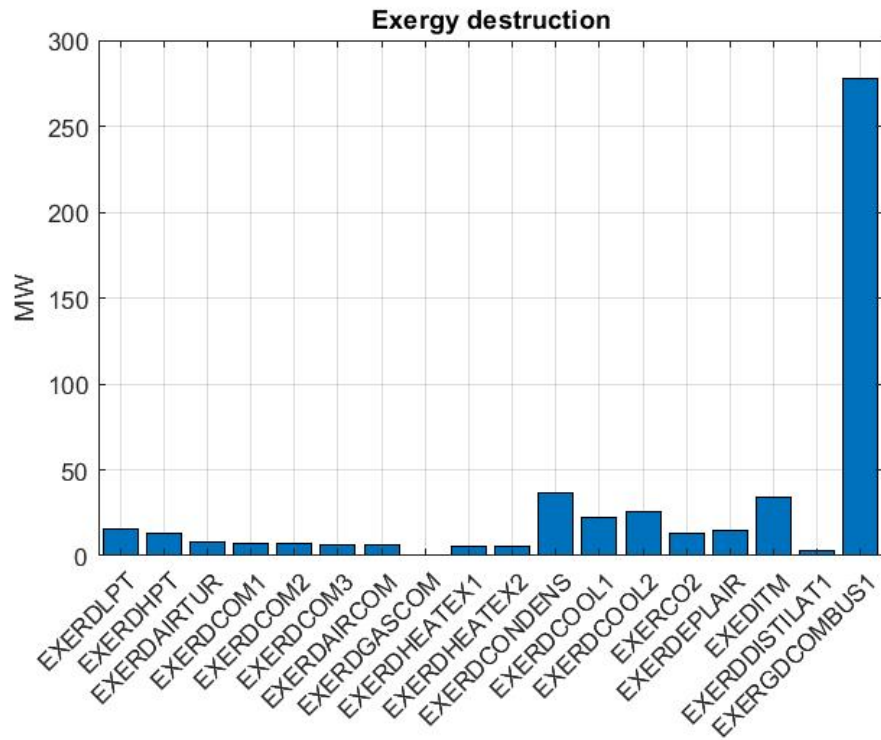


Figure 4.22 Exergy destruction of ZEITMOP

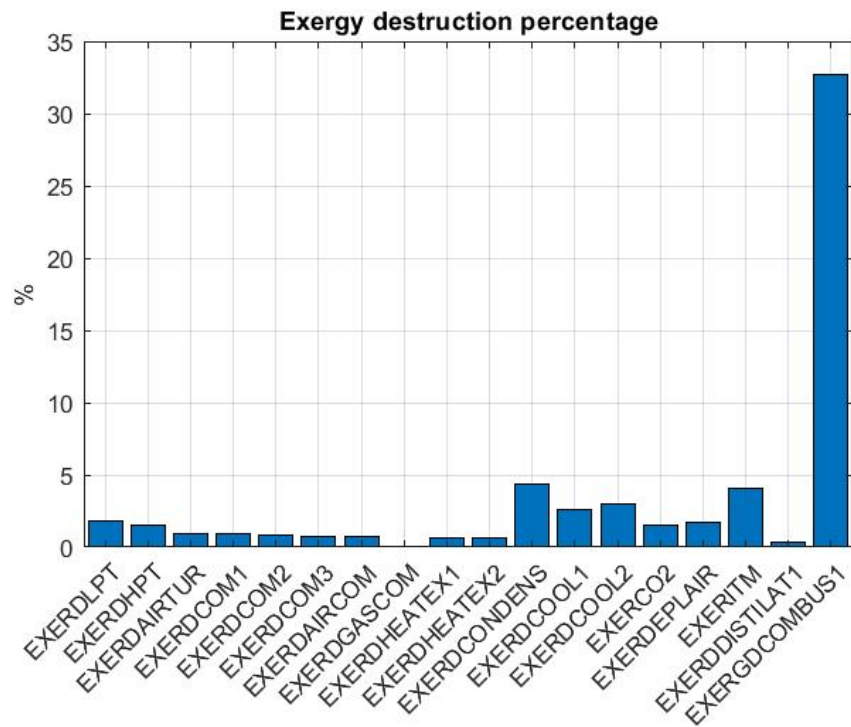


Figure 4.23 Exergy destruction percentage for ZEITMOP

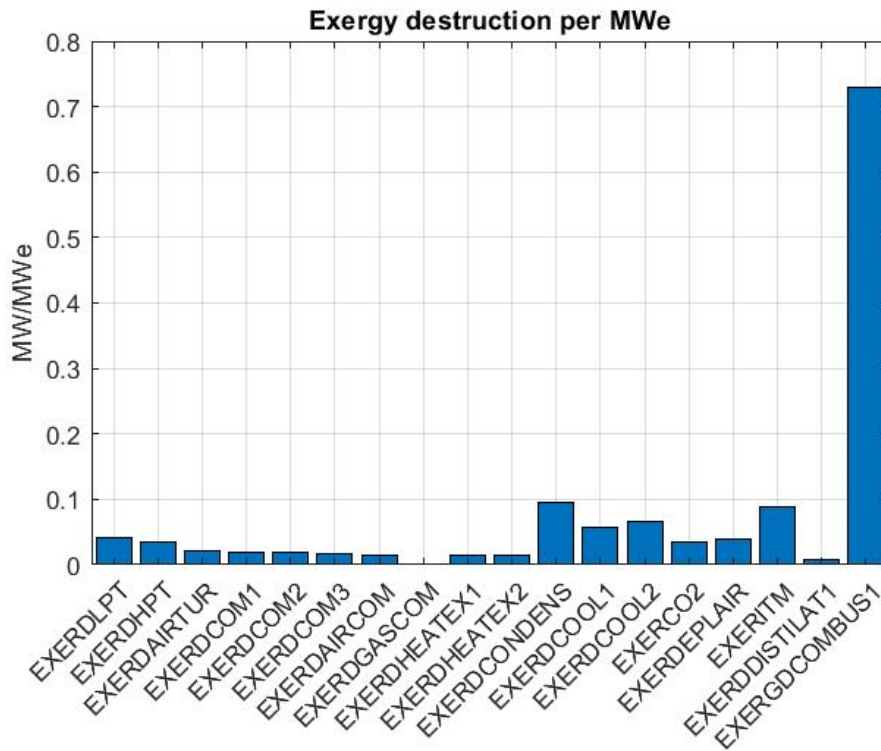


Figure 4.24 Exergy destruction per MWe for ZEITMOP

4.9 The COOLCEP-S cycle modelling and analysis

The amount of exergy destruction in each component is indicated in Figure 4.25, and Figure 4.26 shows the percentage of exergy destruction for each component, and Figure 4.27 shows the exergy destruction per MWe of network output; The main exergy destruction is in the combustion, and negative exergy destruction shows the exergy input from LNG working flow with very low temperature.

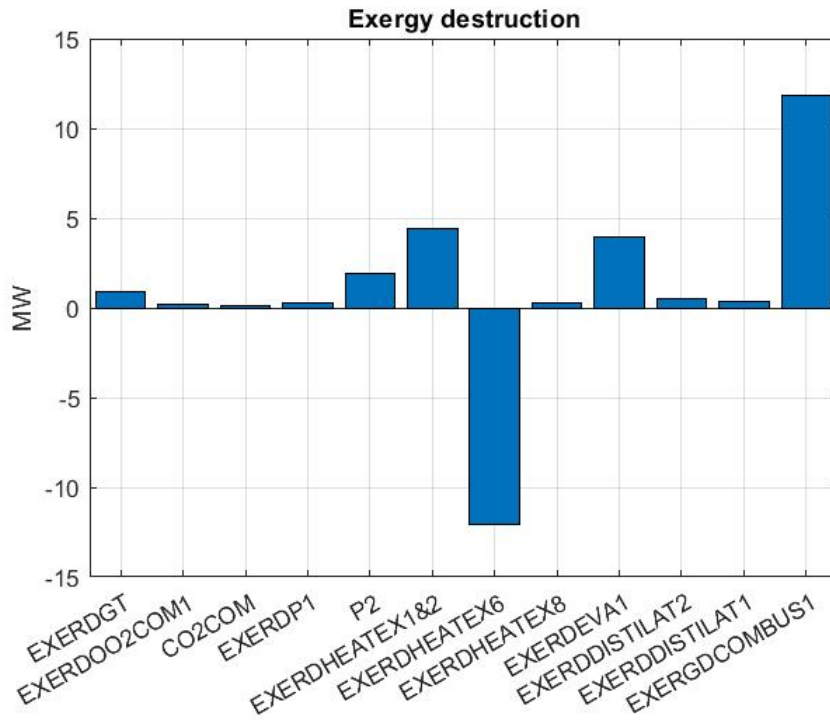


Figure 4.25 Exergy destruction for COOLCEP-S

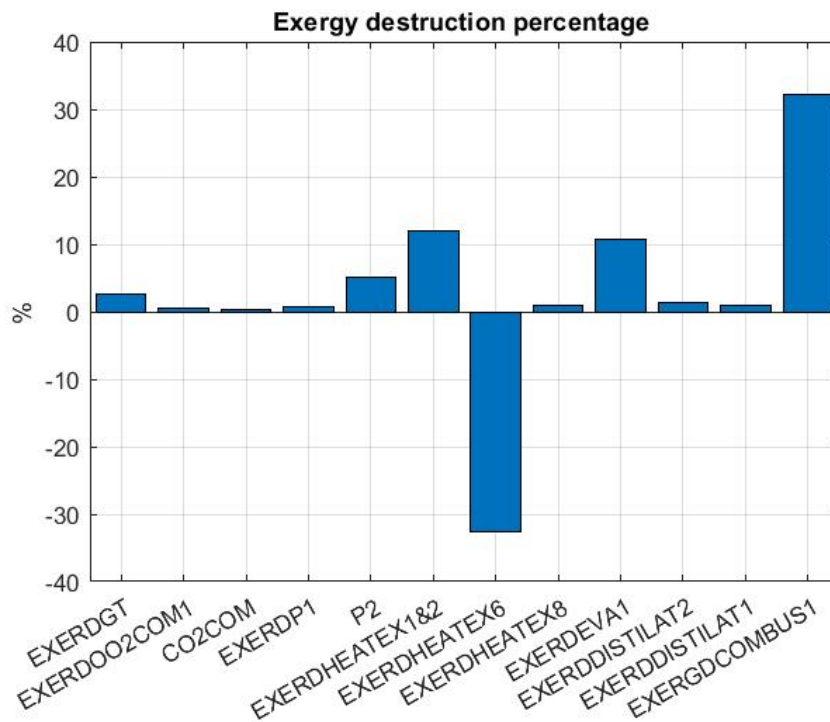


Figure 4.26 Exergy destruction percentage for COOLCEP-S

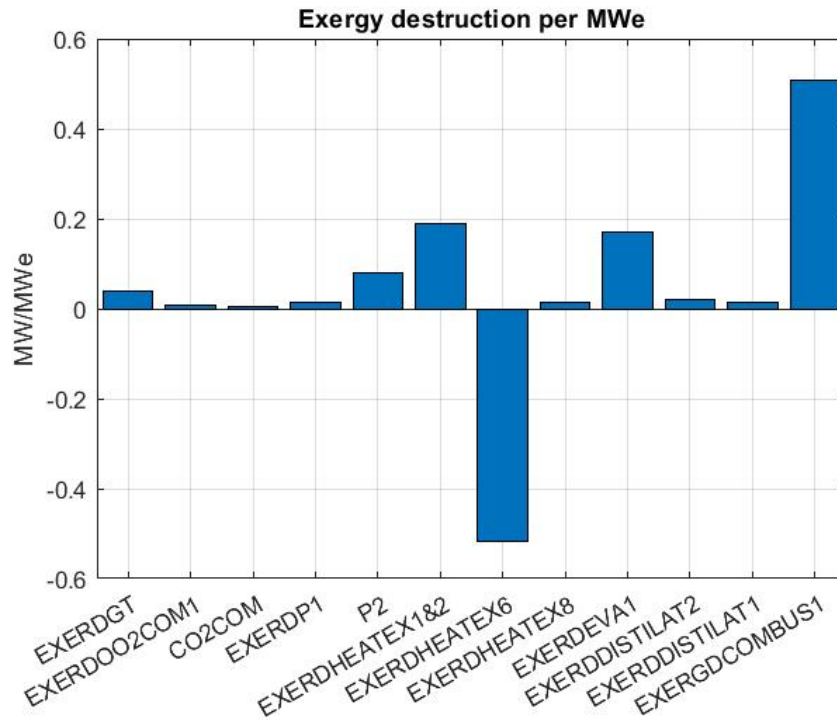


Figure 4.27 Exergy destruction per MWe for COOLCEP-S

4.10 The COOLCEP-C cycle modelling and analysis

The amount of exergy destruction in each component is indicated in Figure 4.28, and Figure 4.29 shows the percentage of exergy destruction for each component, and Figure 4.30 shows the exergy destruction per MWe of network output;

The main exergy destruction is in the combustion with 35% . The negative exergy destruction indicates the exergy input from LNG working flow with lower than environment temperature.

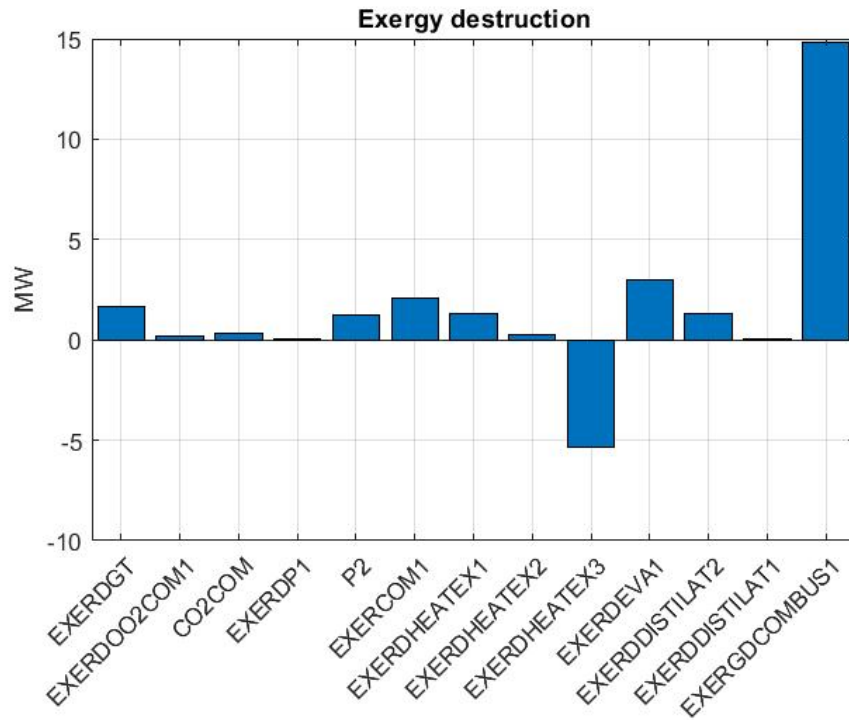


Figure 4.28 Exergy destruction for COOLCEP-C

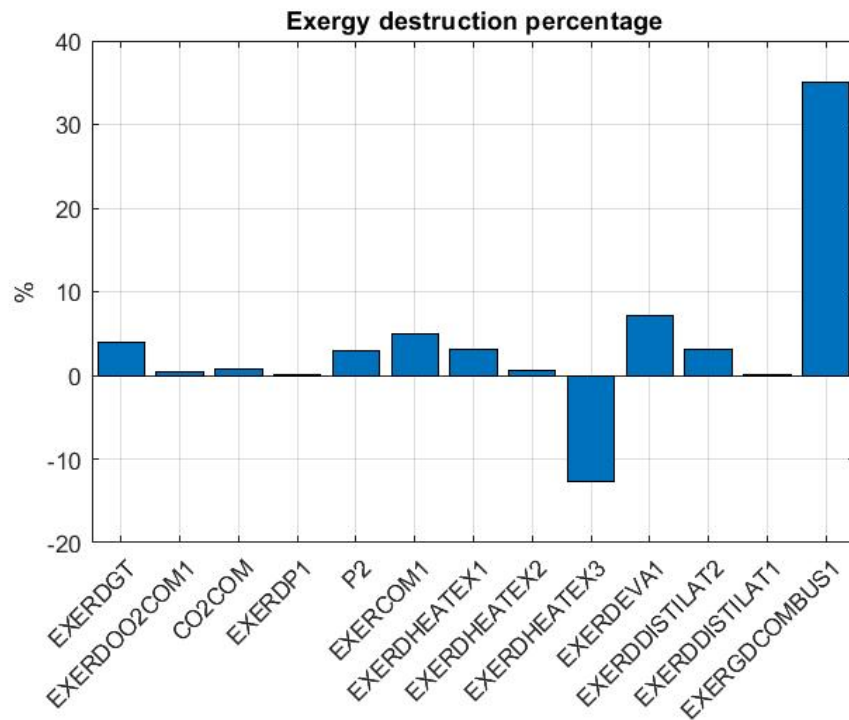


Figure 4.29 Exergy destruction percentage for COOLCEP-C

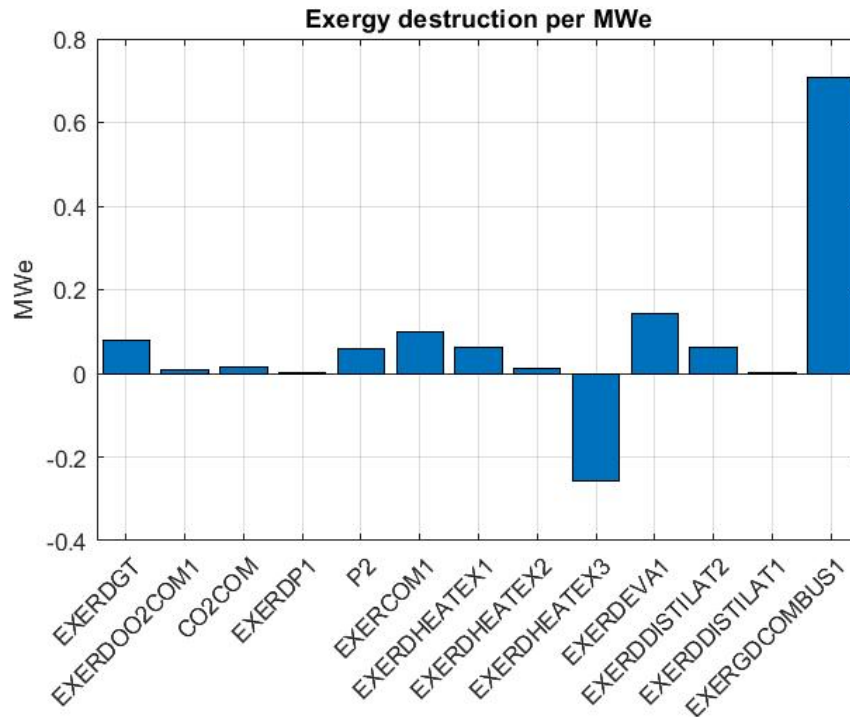


Figure 4.30 Exergy destruction per MWe for COOLCEP-C

4.11 The Novel O₂/CO₂ (Cao and Zheng, 2006) modelling and analysis

Figure 4.31 shows the amount of exergy destruction in each component, Figure 4.32 shows the percentage of exergy destruction for each component, and Figure 4.33 shows the exergy destruction per MWe of network output; The highest exergy destruction is in the combustion with 29.8%, and the second main exergy destruction is in the heat recovery unit with 7%.

The reformer is the major location of loss (Cao and Zheng, 2006) after combustion. The exergy destruction caused by the combustion reaction is significantly higher than the exergy destruction due to the reforming reaction. The exergy destruction associated with the reforming reaction can be reduced by preheating the hydrocarbon and the steam and by mixing the reactants at equal temperature and pressure. Friction and heat losses also contribute to thermodynamic inefficiencies (Tsatsaronis and Czielsa, 2003).

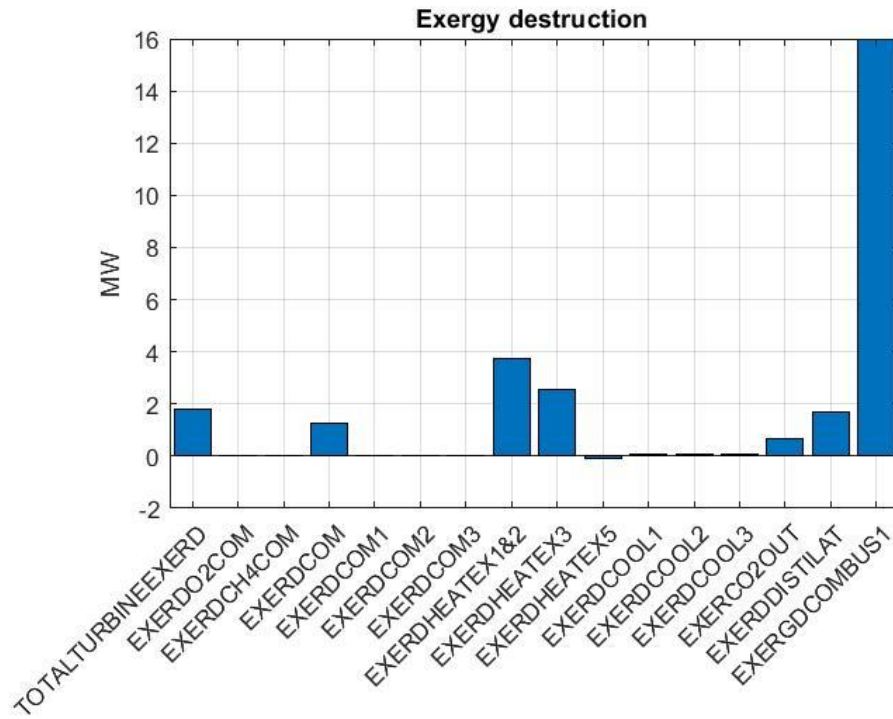


Figure 4.31 Exergy destruction for Novel O₂/CO₂ cycle

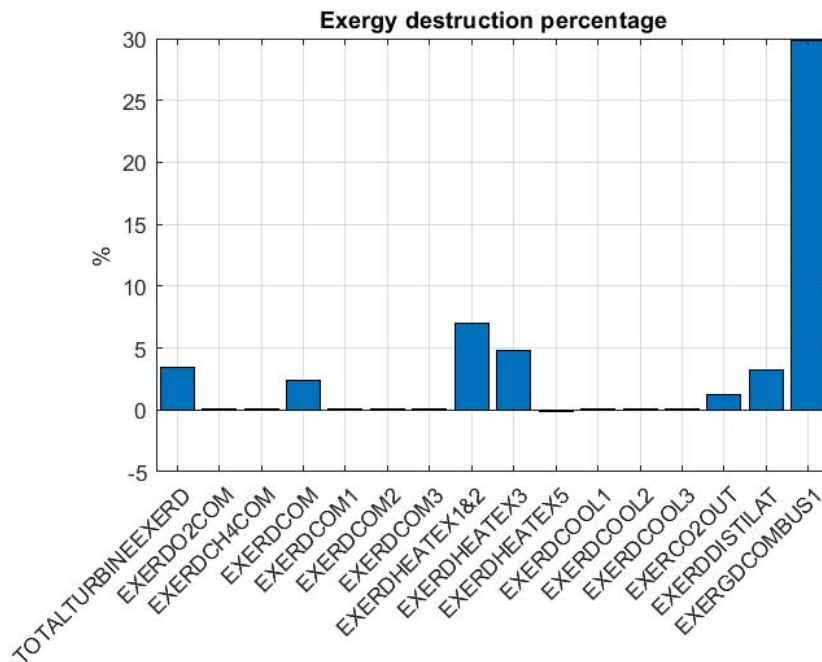


Figure 4.32 Exergy destruction percentage for Novel O₂/CO₂ cycle

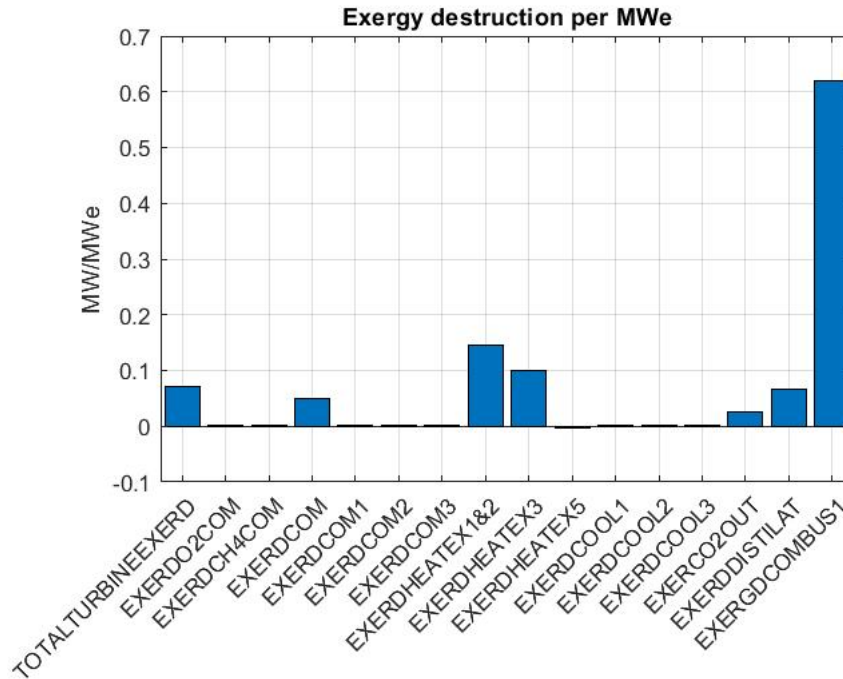


Figure 4.33 Exergy destruction MW/MWe for NovelO₂/CO₂ cycle

4.12 The NetPower cycle modelling and analysis

Steam properties at each stage for the NetPower cycle are explained in Table 3.28 of chapter 3; the recycled working flow is carbon dioxide. The heat exchanger is the main part of the cycle to increase overall efficiency. Figure 4.34 shows the amount of exergy destruction in each component for the NetPower cycle, Figure 4.35 shows the percentage of exergy destruction for each component, and Figure 4.36 shows the exergy destruction per MWe of network output;

The highest exergy destruction is in combustion, and it is 15.24%. Also, the Turbine has high exergy destruction with 4.58%, the ASU with 5.3% and the main heat exchanger with 4% have higher exergy destruction in comparison with other components. The NetPower cycle needs to develop a Turbine, combustion, ASU and Main Heat Exchanger to increase efficiency.

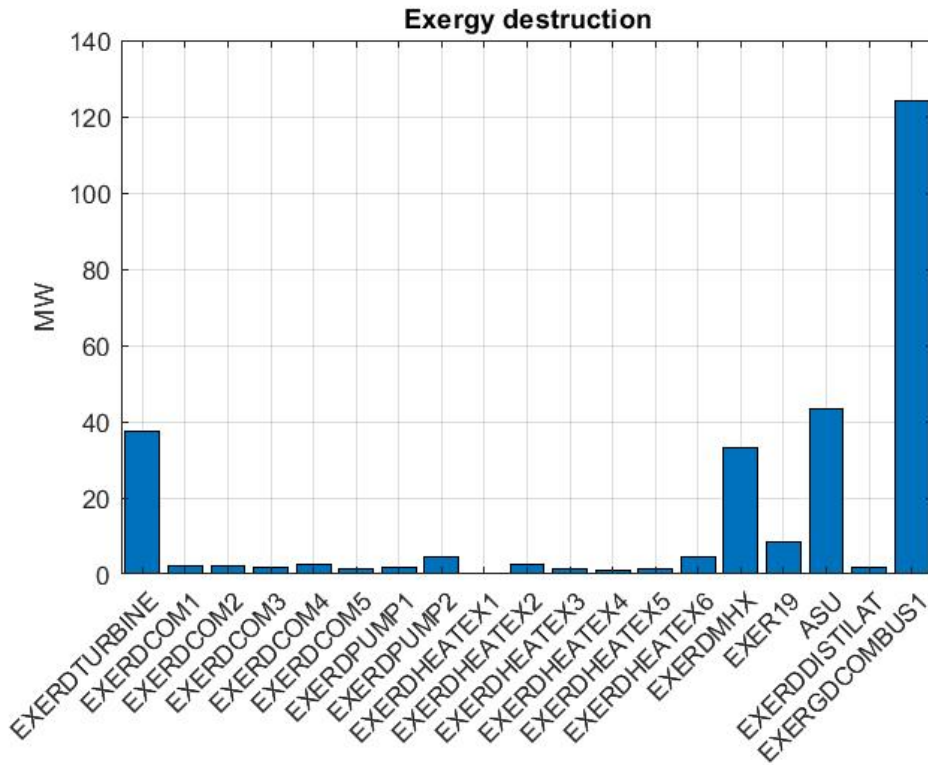


Figure 4.34 Exergy destruction for NetPower

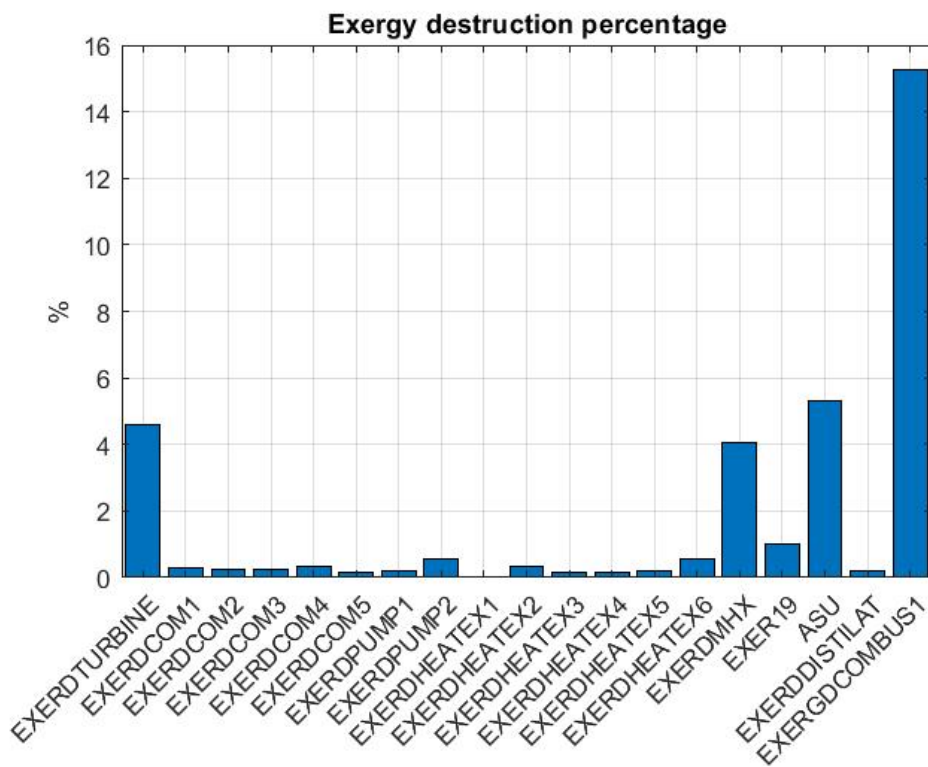


Figure 4.35 Exergy destruction percentage for NetPower

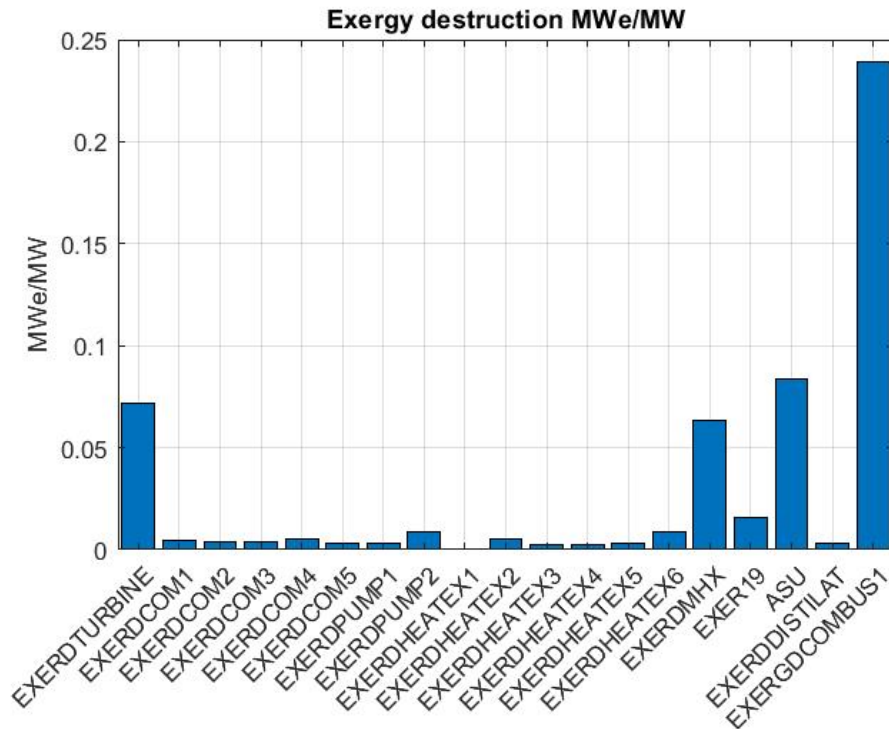


Figure 4.36 Exergy destruction MWe/MW for NetPower

4.13 The S-CES cycle modelling and analysis

Figure 4.37 shows the amount of exergy destruction in each component in the S-CES cycle, Figure 4.38 shows the percentage of exergy destruction for each component, and Figure 4.39 shows the exergy destruction per MWe of network output; The main exergy destructions are in High Pressure, Medium Pressure, and Low-Pressure combustions with 8.1%, 10.5%, 11.78% exergy destruction respectively and also ASU with 8.3% and turbines with total 8.3% exergy destruction have the highest exergy destruction after combustions in comparison with other components. S-CES needs to develop combustions, turbine and ASU technology to increase efficiency.

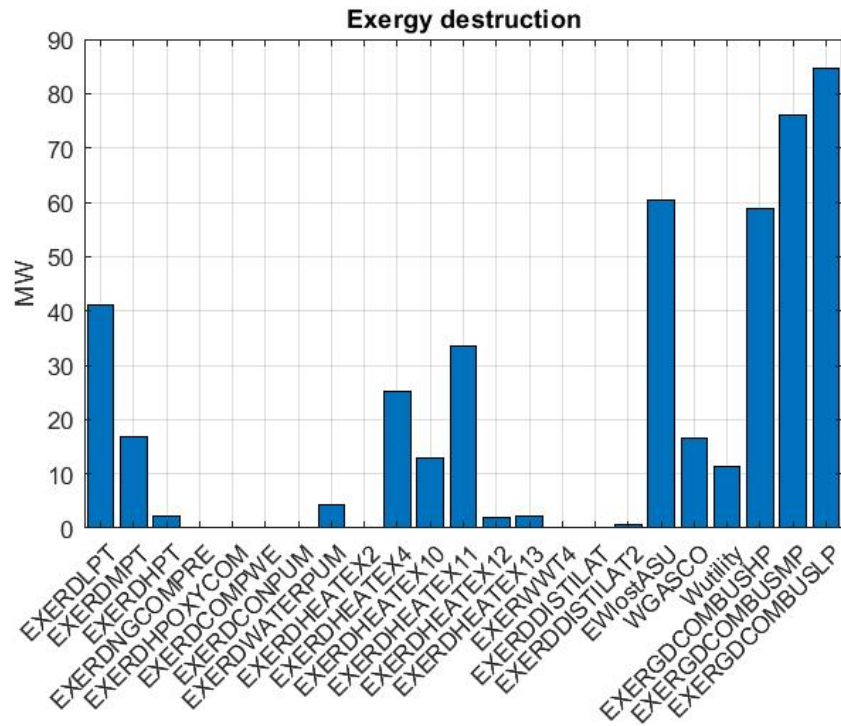


Figure 4.37 Exergy destruction for S-CES

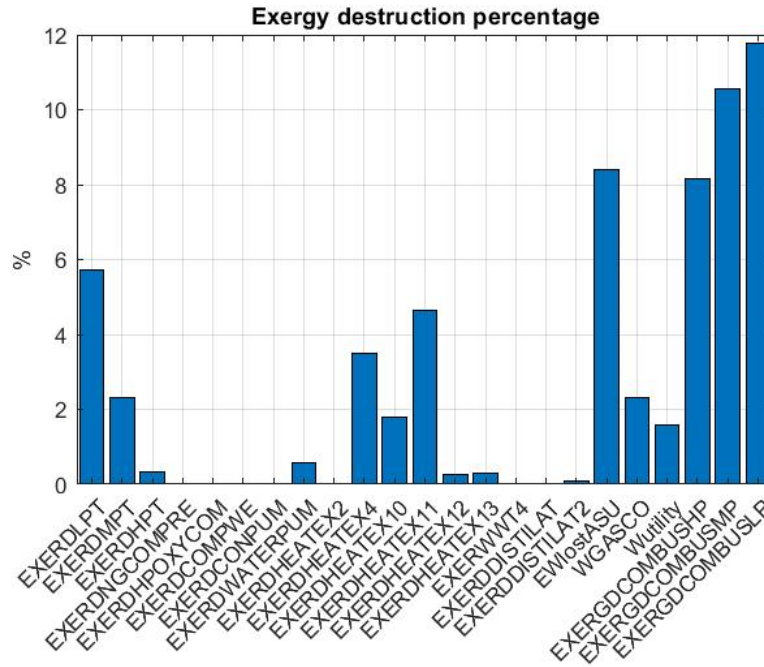


Figure 4.38 Exergy destruction percentage for S-CES

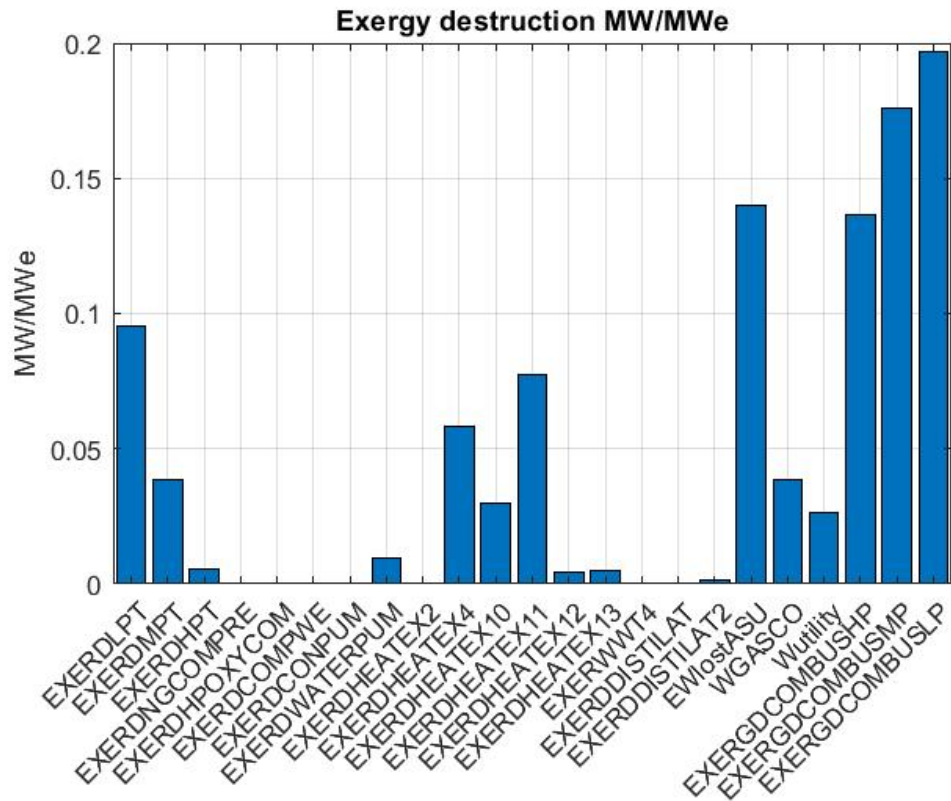


Figure 4.39 Exergy destruction MWe/MW for S-CES

4.14 Summary

In this chapter, the exergy analysis of the oxy-combustion power cycle had been conducted. The exergy destruction or irreversibility of each component were calculated with MATLAB code and compared in the bar diagrams. The irreversibility of each component is due to various reasons. Reduction of exergy destruction in each component can enhance the overall performance.

The exergy destruction analysis of the oxy-combustion power cycle is a powerful tool to determine the main exergy loss through the cycle and potential components for improvement. Reduction of exergy destruction in each component can improve the overall efficiency of the oxy-combustion power cycle. The following points can determine from the analysis:

- Combustion has higher irreversibility and exergy destruction in oxy-combustion cycles due to the chemical reaction process, and heat transfer

occurs in the combustion chambers. One of the ways to reduce exergy loss in combustion is preheating the reactants in the combustion chamber (Oyedepo *et al.*, 2015). Improving combustion technologies is one of the critical points to increase the overall efficiency of the oxy-combustion power cycle, and this component needs to develop in future for the oxy-combustion power cycle.

- The second main exergy loss in oxy-combustions are HRSG or heat exchanger due to heat transfer between two-stream. Therefore, improving the efficiency of HRSG can reduce exergy destruction and improve overall efficiency. The efficiency of HRSG and heat exchangers can be increased by increasing the temperature of inlet gas (Bunyamanid *et al.*, 2016) or reducing the min approach temperature with proper design.
- The higher turbine inlet temperature causes lower exergy destruction, and increasing the TIT will cause more turbine output work. To increase the turbine inlet temperature, turbine blade coating need to develop to resist high temperature (Oyedepo *et al.*, 2015). Development in blade cooling technology and blade coating can reduce exergy destruction in the turbine and increase the overall efficiency of the oxy-combustion cycle.
- Improving turbine and compressor isentropic efficiency can reduce exergy destruction in these components. The design parameters of turbomachinery have a higher effect on the isentropic efficiency, including the aerodynamic surface of the blade and main body.
- Recovering heat from turbine exhaust can recover exergy from downstream and use it again. The combined cycle is one of the best technology to recover exergy from the exhaust of the gas turbine.
- The reformer has better application in the oxy-combustion cycle due to the quantity a duality of heat load; for example, the CO₂-NG reforming technology can recover exergy from turbine exhaust effectively due to the endothermic nature of the process.

Chapter 5: Sensitivity and exergy analysis of Semi-Closed Oxy-fuel Combustion Combined Cycle (SCOC-CC) and E-MATIANT

5.1 Sensitivity analysis of Semi-Closed Oxy-fuel Combustion Combined Cycle (SCOC-CC)

5.1.1 Introduction

Oxy-fuel combustion is one of the promising technologies for zero-emission in power cycles. The Semi-closed oxy-fuel combustion combined cycle (SCOC-CC) is an oxy-combustion cycle with high efficiency, and it is similar to the conventional gas turbine combined cycle (GTCC).

In this chapter, the SCOC-CC cycle is modelled with Aspen Plus, and sensitivity analysis was performed based on the modelling. The sensitivity of TIT, Network and efficiency were analysed for gas turbine and steam turbine pressure. The network is net power output from the cycle, and efficiency is calculated by divide Network to LHV. The optimum pressure point for efficiency was determined from the analysis. Furthermore, the cycle sensitivity analysis was performed, and the map graph has been produced.

The exergy of the SCOC-CC cycle that presents in chapter 4 was analysed, and the exergy destruction of the components was calculated in the design point, and the bar graph extracted. Also, the exergy destruction sensitivity of the working flowrate was analysed.

In the end, the Capital and operating cost of the cycle were calculated for SCOC-CC, and the Levelised Cost of Electricity (LCOE) was calculated. SCOC-CC includes

one Bryton cycle and one Rankine cycle similar to the conventional Combined cycle (Ferrari *et al.*, 2017a), so the design and development of the components are easier than other oxy-fuel combustions. SCOC-CC cycle includes one Brayton cycle and one Rankine cycle. In the Gas turbine cycle, fuel burns with pure oxygen and produce carbon dioxide and water, the gas flue after HRSG enters the condenser and water is separated from flue gas. The remaining composition is carbon dioxide, and part of it is recycled back to the cycle while the rest is separated for compressing and transporting to the storage site (Thorbergsson and Grönstedt, 2016).

5.1.2 Sensitivity analysis results

Figure 5.1 indicates the total network relative to the power ratio of the gas turbine without changing steam turbine parameters. In this case study, the sensitivity of the power network related to the pressure ratio is evaluated to find out the optimum point for the pressure ratio. This figure shows that the network increases when the pressure ratio increases from 20 bar to 40 bar. Then the net power output decreases from 40 bar to 100 bar because the required work of pump and compressors increase, so the total network reduces. This curve indicates a maximum point of pressure ratio. Increasing pressure ratio can increase network and performance up to a maximum point; then, there is not any benefit to increasing pressure ratio more.

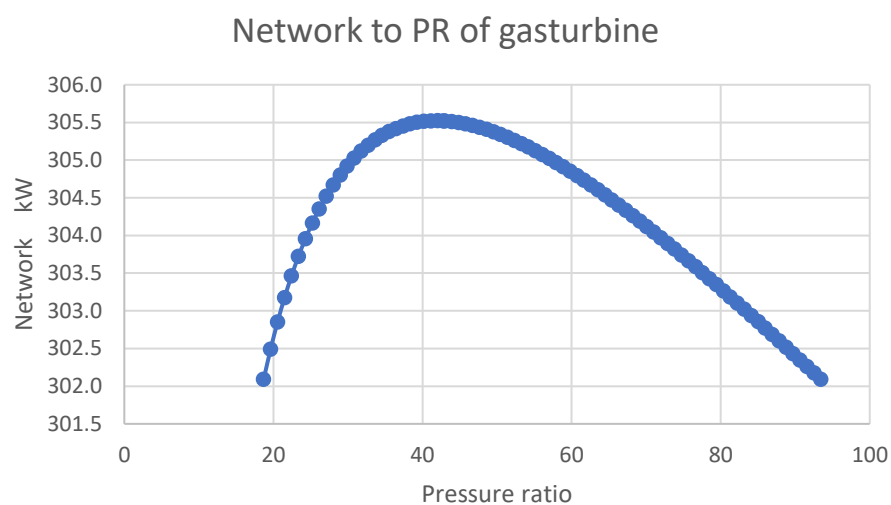


Figure 5.1 Sensitivity of power cycle with Gas turbine pressure ratio

Figure 5.2 shows the total NetPower sensitivity to the pressure ratio between 100 to 500 bar. This diagram can be used to compare the sensitivity of the network to pressure ratio with another oxy-combustion power cycle.

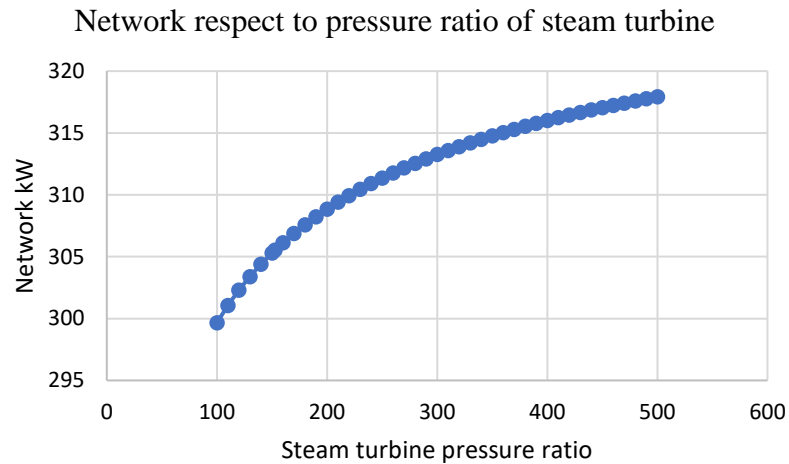


Figure 5.2 Sensitivity of Network to Pressure ratio

Figure 5.3 shows the efficiency relative to fuel flowrate and COP (Combustion Outlet Pressure). By increasing pressure, total efficiency increases to the maximum point and then decreases because the compressor requires more power when increasing pressure, so the total network reduces; also, it should be related to specific volume; in the steady-state flow, expansion or compression work is equal to the specific volume of the fluid multiple to change of pressure. Hence, the specific volume of the working fluid needs to be as low as possible during a compression process and as high as possible during an expansion process.

The figure shows that by increasing the fuel flow rate, the efficiency goes down. It is because more fuel is burning, and the ratio of network W_{net} to heat input Q_H reduces.

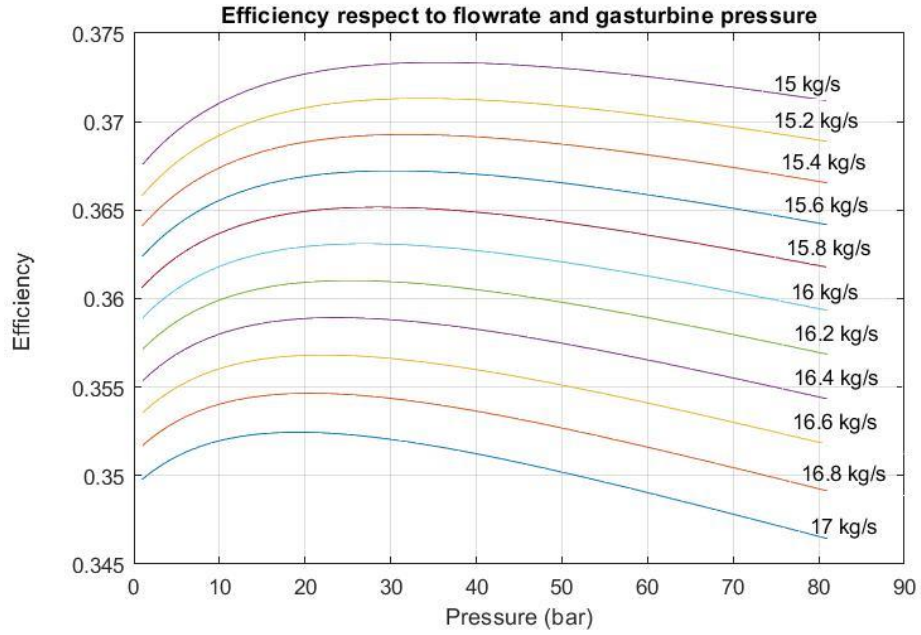


Figure 5.3 Efficiency with respect to Flowrate and COP

Figure 5.4 shows the TIT (Turbine Inlet Temperature) increases when fuel flowrate grows because of burring more fuel with Stoichiometry ratio. Also, the figure indicates the changing COP (Combustion Outlet Pressure). The TIT does not change too much, and TIT is not so sensitive to COP. It is important to consider the minimum point for designing a power cycle and choosing another pressure to have higher TIT.

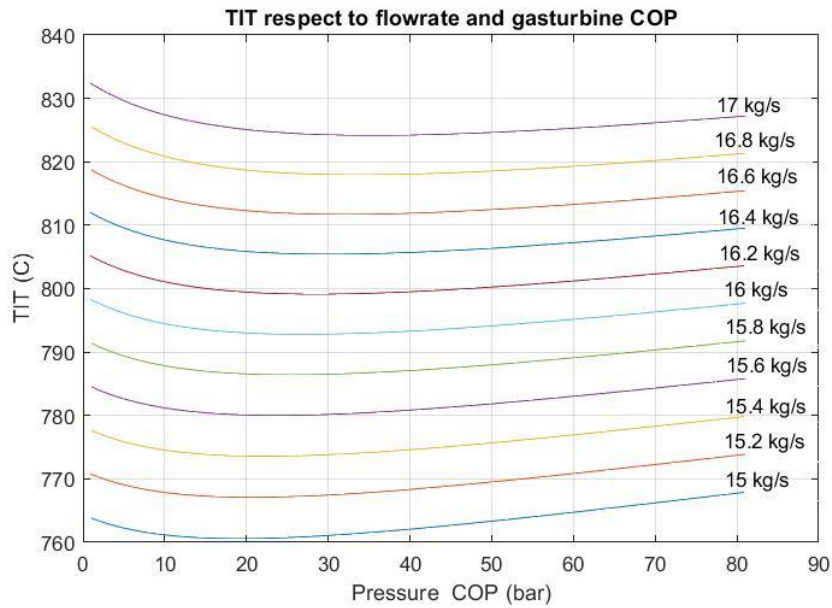


Figure 5.4 TIT with respect to COP and fuel flowrate

Figure 5.5 shows the efficiency rises with growing pressure from 5 bar to 20 bar, but the efficiency does not change excessively and is not very sensitive with respect to pressure. This is because the pressure of the steam cycle can only affect the network of the steam turbine and cannot increase the network of the gas turbine. The gas turbine produces the main power output in the combined cycle. Hence, increasing efficiency in the steam cycle has a lower effect on the overall efficiency.

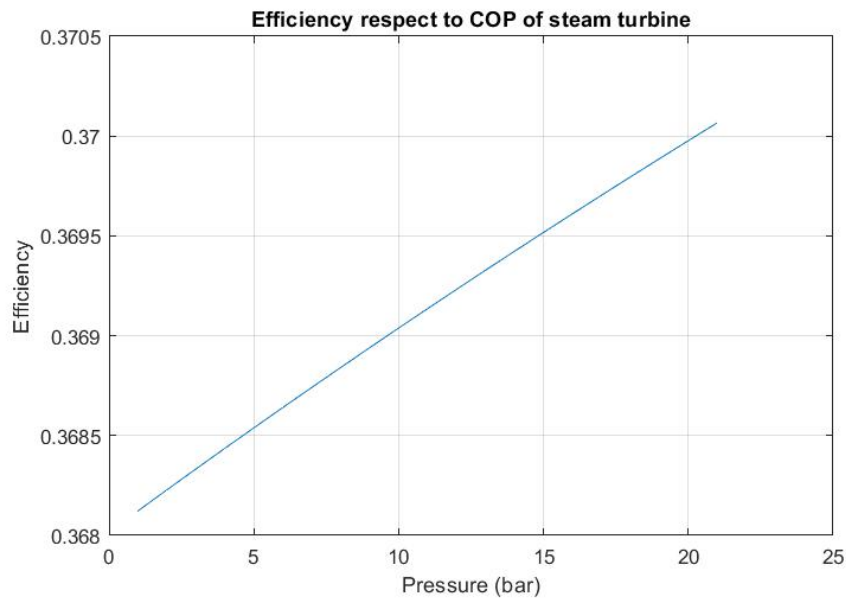


Figure 5.5 Efficiency respect to COP of a steam turbine for SCOC-CC

For evaluating efficiency relative to pressure, the efficiency is calculated for a large range of pressure. Figure 5.6 shows the efficiency increases slightly up to 38%.

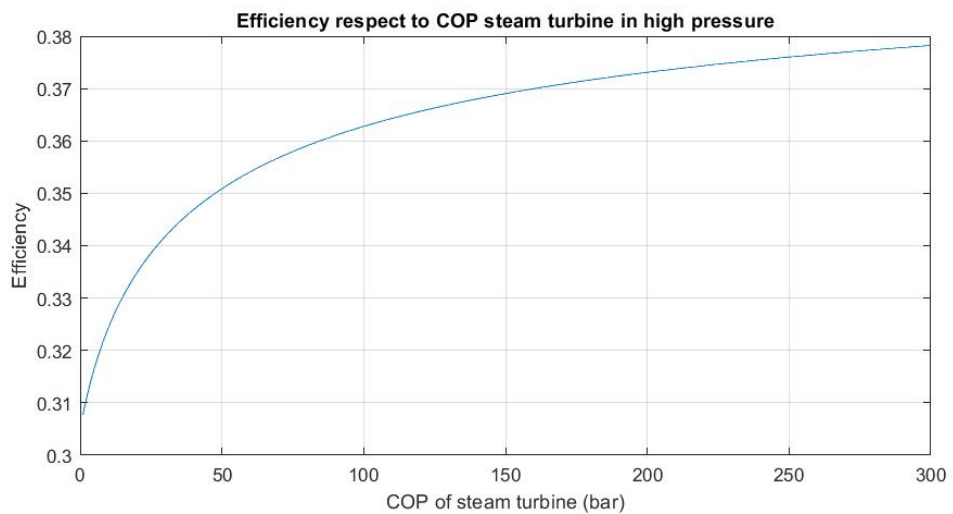


Figure 5.6 Efficiency with respect to COP of the steam turbine

The gas turbine work is negative because it is a workout from the cycle and the absolute value of gas turbine work grows by rising pressure and fuel flowrate rate.

As shown in Figure 5.7, the maximum gas turbine work is 5100 KJ. The results approve that the turbine work is higher when the pressure, TIT and fuel flow rate are higher.

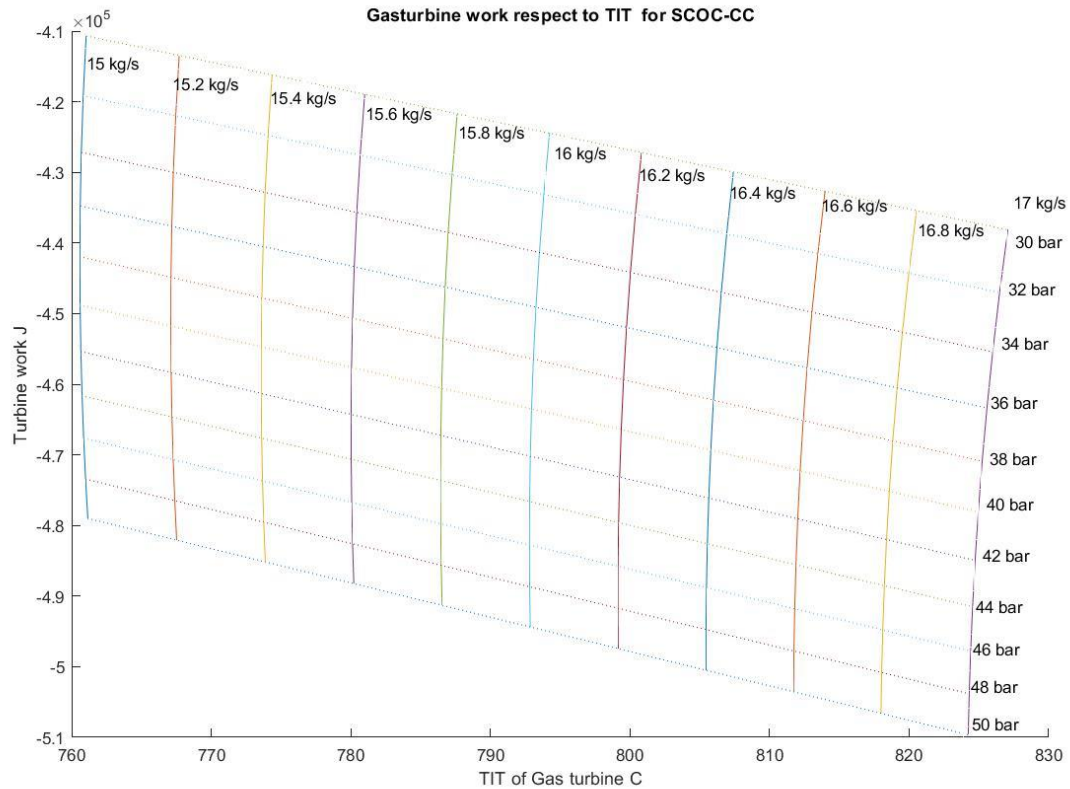


Figure 5.7 Gas turbine work to TIT

Thermal efficiency climbs by increasing TIT at constant pressure, as shown in Figure 5.8, but the thermal efficiency goes up with reducing TIT at constant flow rate with changing the pressure from 30 bar to 50 bar.

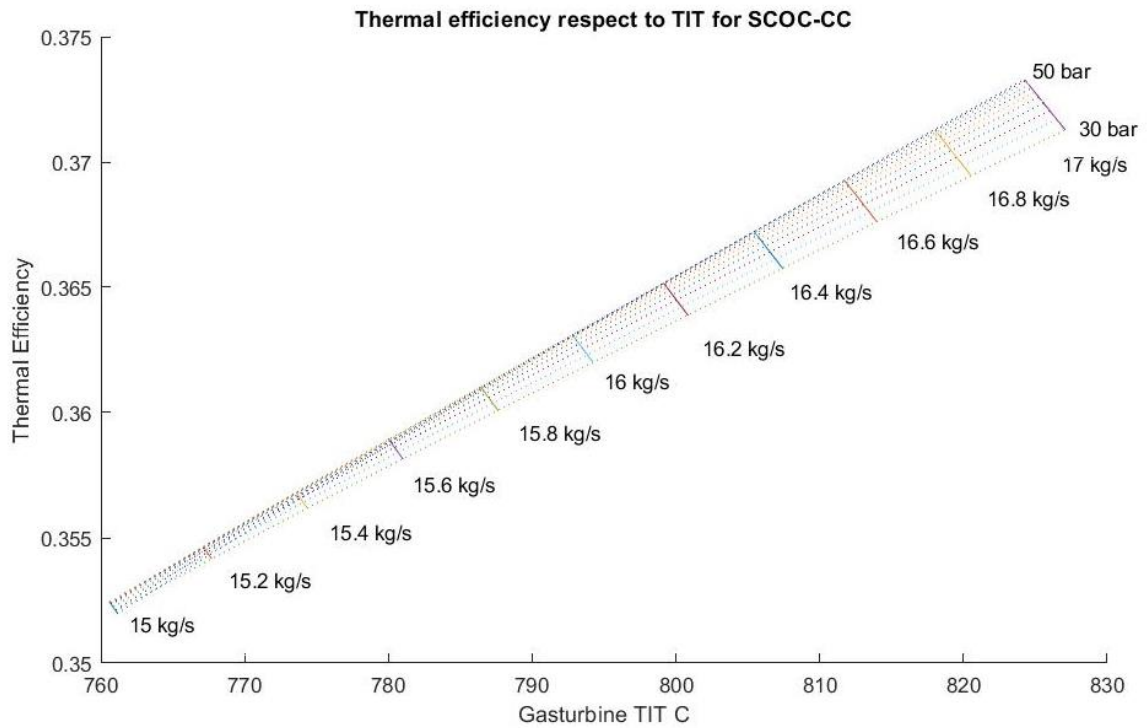


Figure 5.8 Thermal efficiency with respect to TIT

Figure 5.9 shows thermal efficiency is maximum at the maximum pressure of the turbine and steam turbine.

Thermal efficiency has a linear relation with the pressure of the gas turbine and steam turbine. The figure also shows that in the constant gas turbine pressure by changing steam turbine pressure, the temperature of TIT is changed very slightly.

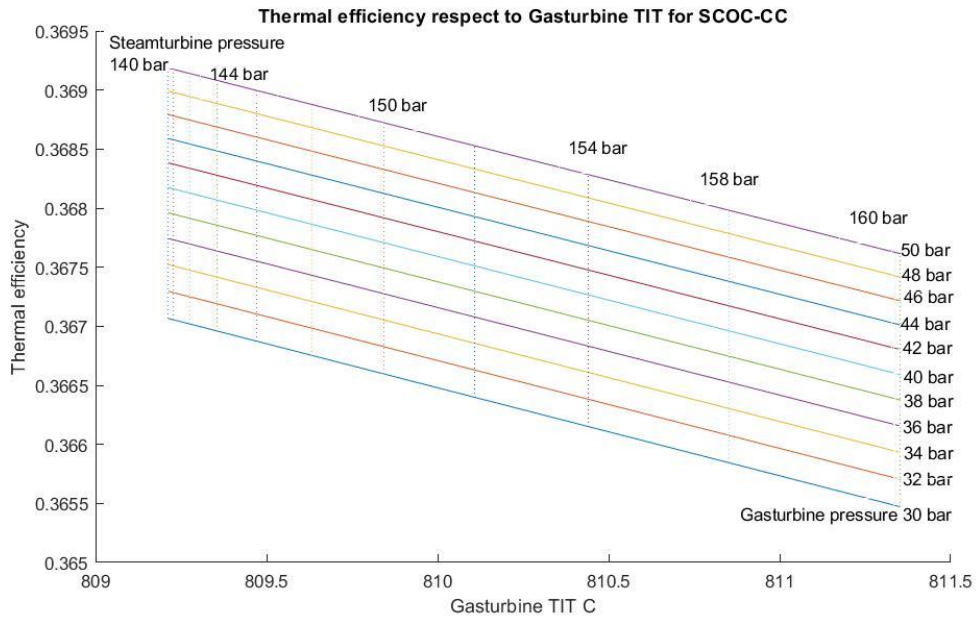


Figure 5.9 Thermal efficiency with respect to TIT of gas turbine

The exergy destruction is calculated for each component, as shown in Figure 5.10. The bar chart shows that combustion has the highest exergy destruction in the power cycle and the second-highest exergy destruction is in the heat exchanger. These two components are very important to reduce exergy destruction in the power cycle and increase efficiency. Gas and Steam turbines have the highest exergy destruction after combustion and heat exchanger.

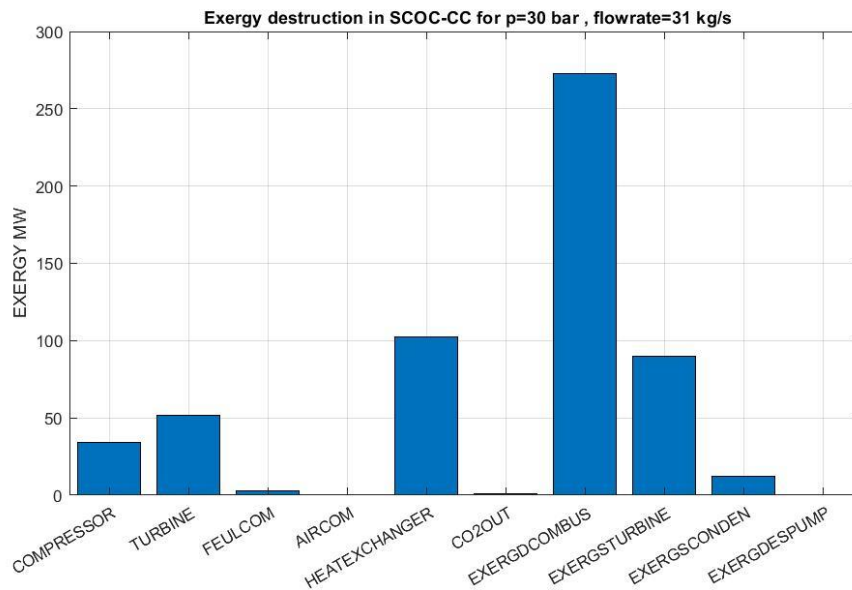


Figure 5.10 Exergy destruction for each component SCOC-CC cycle

The 3D plot of exergy destruction in Figure 5.11 shows that total exergy destruction grows by increasing the fuel flow rate and pressure. The highest exergy destruction is at 60 pressure bar and 80 kg/s fuel flow rate, because higher fuel flow rate can cause higher exergy destruction in equipment, including turbine and combustion.

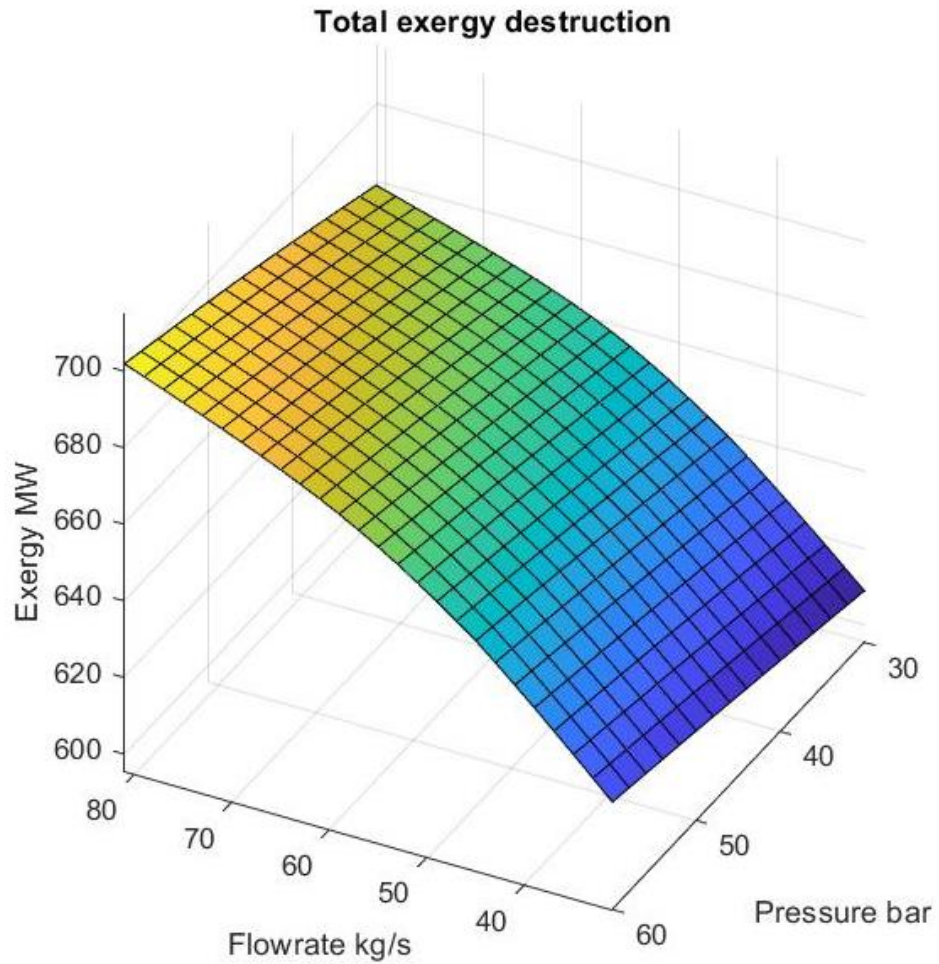


Figure 5.11 3D plot of exergy destruction with respect to flowrate and COP

The 3D plot of TIT to the pressure and flow rate is shown in Figure 5.12. The graph shows a minimum point of TIT related to the pressure of the turbine, and there is a maximum point of TIT related to optimum flowrate.

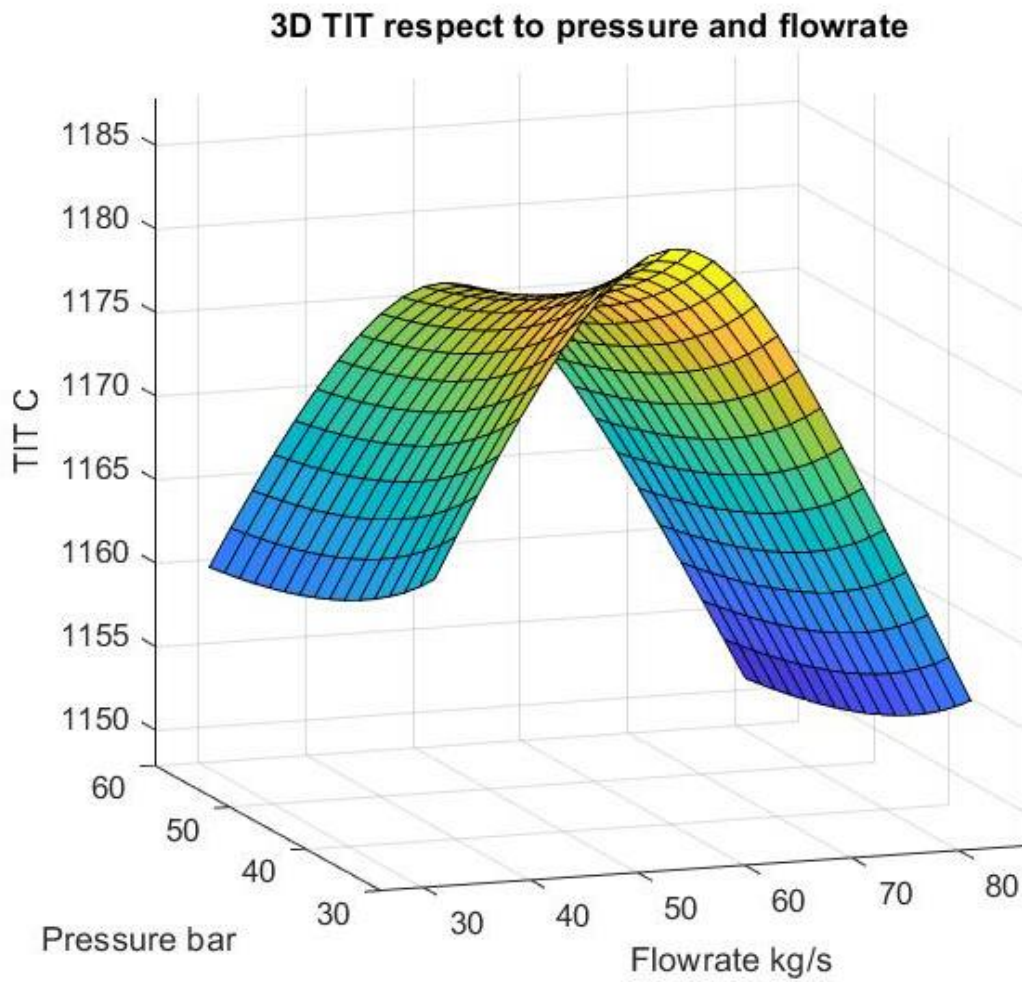


Figure 5.12 3D TIT with respect to COP and flowrate

Figure 5.13 shows the stacked bar chart of exergy destruction for the SCOC-CC cycle. This diagram compares stacked bar chart of exergy for different pressures and flow rates; the diagram shows that by increasing the fuel flow rate, the exergy destruction of combustion rises. The stacked bar chart of exergy destruction is a very good benchmark to compare the exergy destruction of different oxy-combustion cycles.

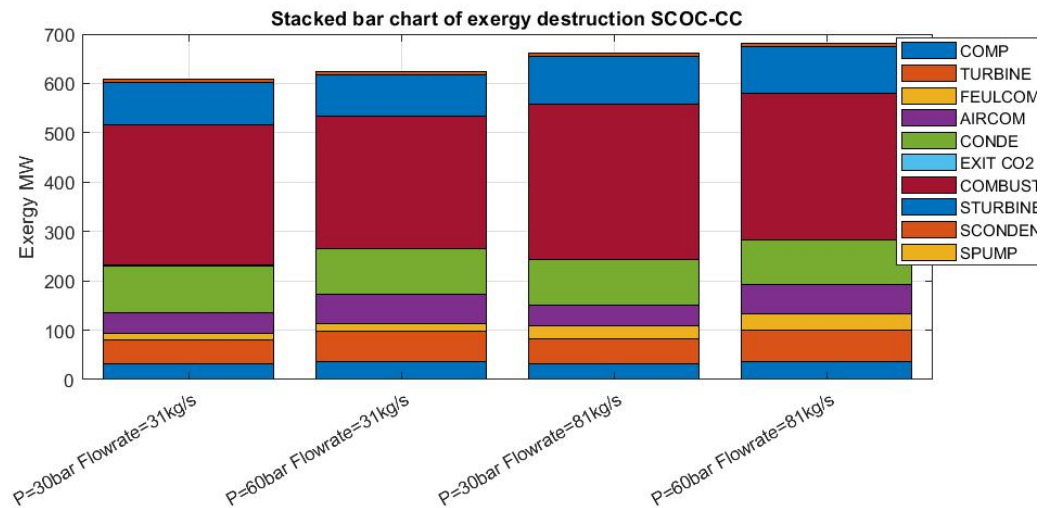


Figure 5.13 Stacked bar chart of exergy destruction

Total specific work with respect to TIT for different pressure and fuel flow rate is calculated, as shown in Figure 5.14. Both TIT and Specific work of SCOC-CC cycle increase in higher pressure and flow rate. The relation of TIT to specific work is linear in constant pressure with changing the fuel flow rate, but it is nonlinear in constant flowrate with changing pressure, it is because of the nonlinear relation of temperature and pressure for compressible flow based on Equation 5-1(NASA, 2017).

Equation 5-1

$$T = T_0 \left(\frac{P}{P_0} \right)^{\frac{k-1}{k}}$$

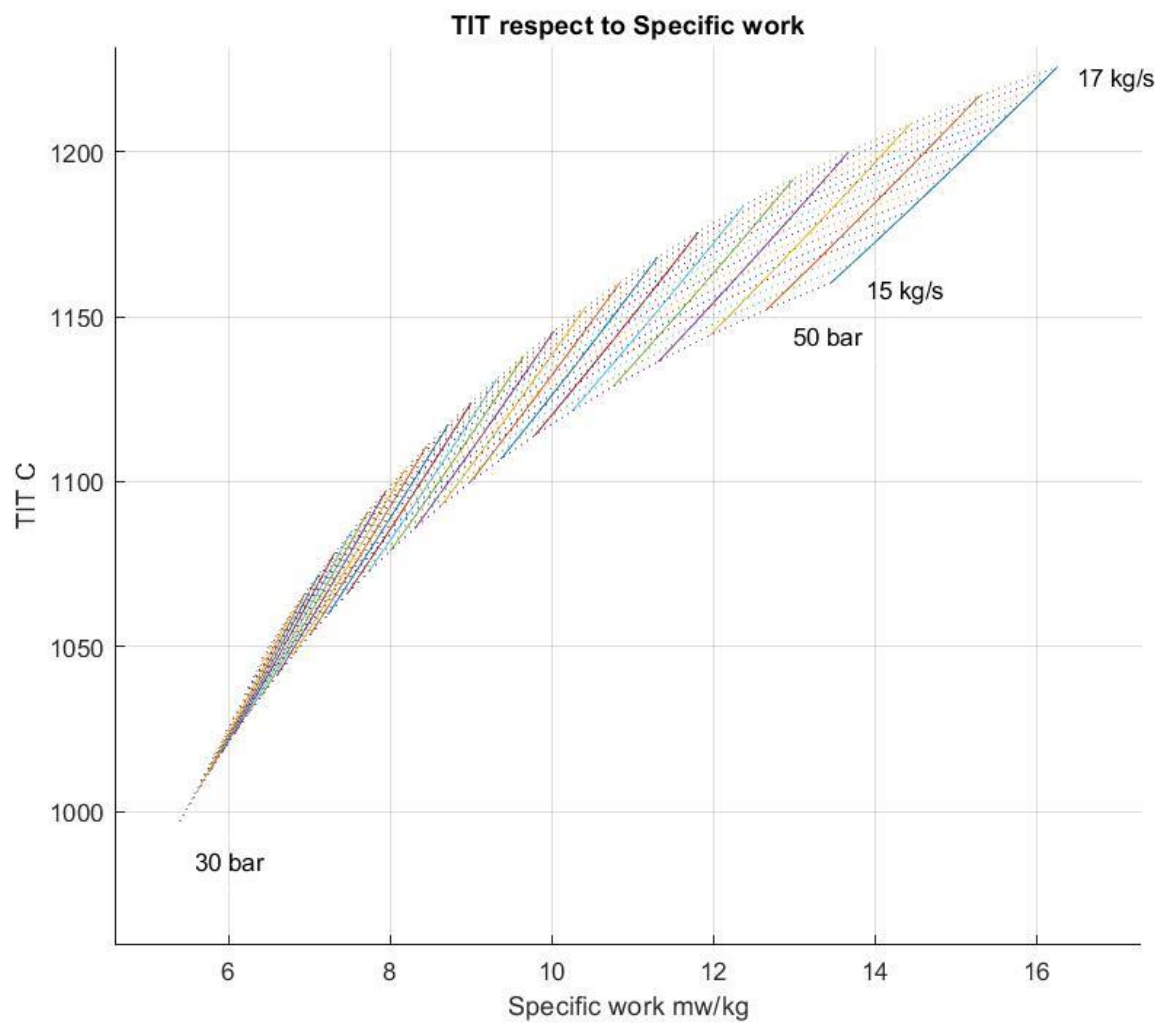


Figure 5.14 TIT respect to Specific work MW/kg

5.1.3 Summary

SCOC-CC is one of the promising oxy-combustion cycles with high efficiency, and technology development of equipment for this cycle can increase the cycle efficiency. The full sensitivity analysis of the cycle was performed for different flowrate, TIT and pressure. Also, the exergy destruction of components was calculated, and the bar chart was extracted; it is shown that exergy destruction in combustion and HRSG are higher in comparison to other components. The performance analysis of the SCOC-CC cycle and Techno-economic analysis of the cycle was calculated.

In this chapter, the sensitivity of Network with respect to the gas turbine pressure ratio was analysed for SCOC-CC, and it indicates that the maximum work is at 40 pressure ratio. The sensitivity of efficiency with respect to the flowrate and Combustion Outlet Pressure (COP) indicates that reduction of working flow from 15 kg/s to 17 kg/s can grow the efficiency from 35% to 37%; the overall efficiency of the cycle increases by increasing the cycle pressure (COP), however, it is shown that the efficiency of the cycle by increasing COP from 400 bar to 600 bar, increases less than 1%, and it does not have the benefit to the cycle by considering the capital cost. The results indicate the TIT of the power cycle is changing with respect to fuel flowrate because the best fuel flowrate is stoichiometry ratio, and the maximum TIT occurs in the stoichiometry ratio, but the TIT is nearly constant with respect to the pressure. The overall exergy destruction grows from 600 MW to 700 MW by increasing the fuel flow rate from 31 kg/s to 81 kg/s and Combustion Outlet Pressure (COP) from 30 bar to 60 bar.

5.2 Sensitivity and exergy analysis of E-MATIANT cycle

5.2.1 Introduction

In this chapter, E-MATIANT Oxy-fuel combustion is investigated. The cycle includes one supercritical Rankine like cycle and a Bryton cycle. The Aspen Plus modelling of the cycle was provided for analysing the thermodynamics parameters of the E-MATIANT cycle. The sensitivities of cycle parameters were analysed. Then the graphs of exergy, efficiency, Network vs working flow rates were extracted. Likewise, exergy destruction of the component at the design point was calculated and shown in a bar graph. The exergy bar graph can show the most exergy destruction of components in the cycle and help the designer to develop these components.

The increasing concern about climate change has addressed the efforts of researchers and scientists to develop the power cycles with CCS (Carbon Capture and Storage). The oxy-fuel combustion power cycle is one of the promising technologies to separate and sequester CO₂. The by-product of oxy-combustion is CO₂ and H₂O. Hence, the CO₂ can be separated from H₂O by cooling the flue below the dew point.

The isentropic efficiencies are 85% for a three-stage compressor and 80% for one stage compressor. The fuel is assumed to feed the combustion at 17 °C and 3 bar. The cycle sensitivity is minimal to the temperature and pressure of the fuel. The fuel pressure depends on the network, and it can be as high as 40 or 60 bar (Mathieu and Nihart, 1999).

The required fuel pressure depends on the combustion pressure. The compression can be low or zero. If the pressure is lower than the network, it would be possible to recover from the expander. In this case, preheating of the fuel is required before injection to the combustion (Mathieu and Nihart, 1999). Table 5.1 indicates the optimum design point of the E-MATIANT cycle with the maximum possible TIT of 1300 °C.

Table 5.1 The optimum design point of E-MATIANT Cycle

Maximum efficiency	46.9%
Working flow rate	290 kg/s
TIT	1300 °C
Pressure	60 bar

5.2.2 Sensitivity analysis results

Figure 5.15 shows the sensitivity of efficiency, exergy destruction and network with respect to the working flow rate. It indicates that when the exergy destruction is minimum at 160 kg/s working flowrate, the network and efficiency are maximum. The exergy destruction indicates the thermodynamic inefficiencies in the power plant. Hence the maximum inefficiencies cause a reduction of Network power output and thermal efficiency.

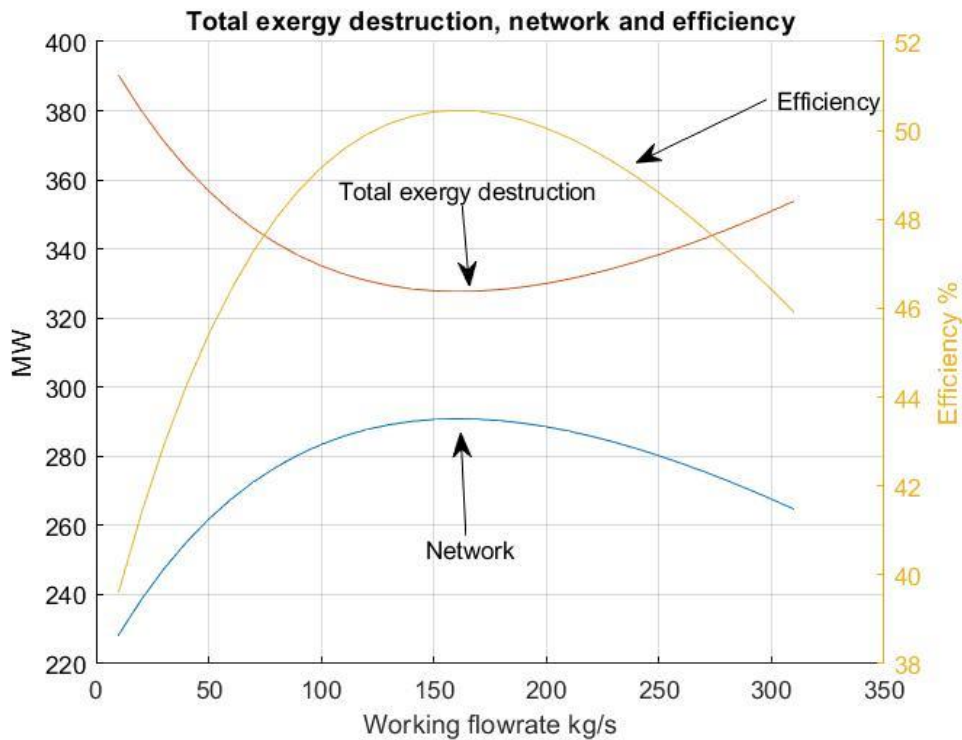


Figure 5.15 Efficiency vs working flowrate for E-MATIANT

Figure 5.16 shows the sensitivity of TIT and efficiency with respect to the working flow rate kg/s. It indicates that the maximum efficiency is 50% at 160 kg/s, but the

TIT temperature is nearly 2000 C, and it is very high for the turbine. The TIT can reach the maximum temperature of 1300° C based on the power cycle technology. Hence the maximum turbine efficiency is 46.9% at 290 kg/s based on the available technology. The required fuel pressure depends on the combustion pressure. The compression can be low ratio or zero if input fuel pressure is closer or equal to combustion pressure.. If its pressure is lower than Network, it will be possible to recover from the expander; in this case, the preheat of the fuel is required before injection to the combustion (Mathieu and Nihart, 1999).

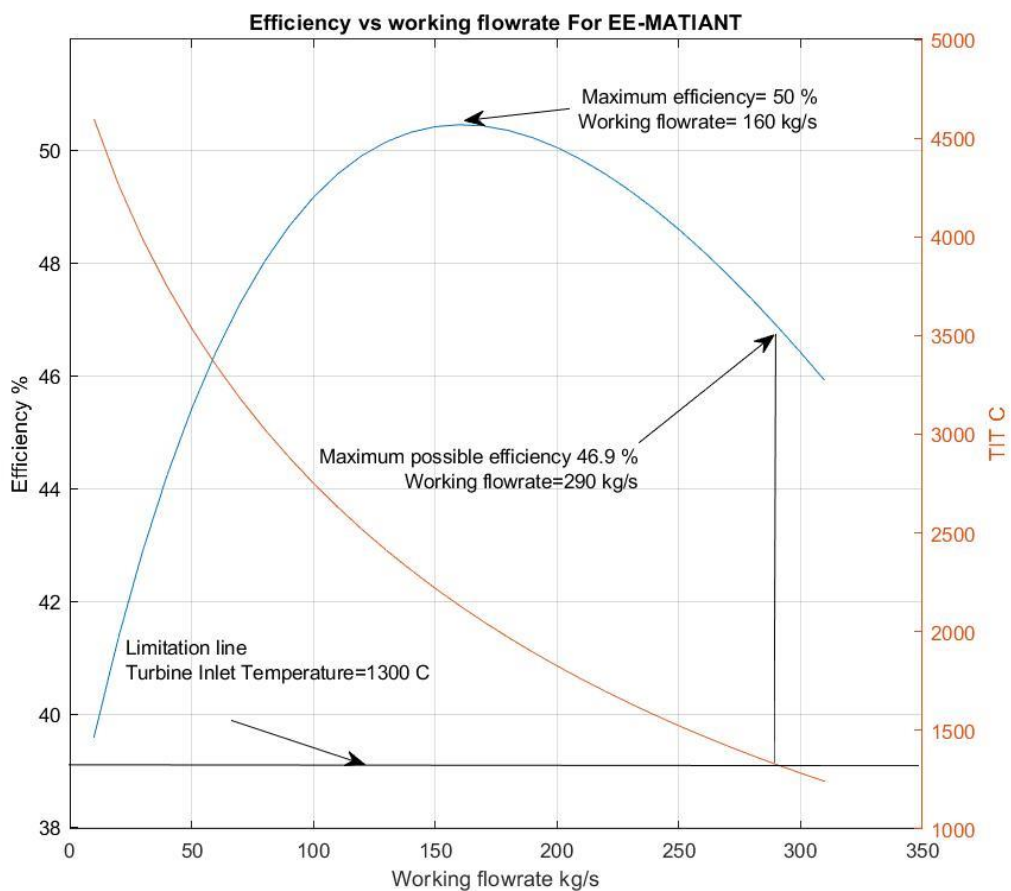


Figure 5.16 Total exergy destruction, Network and efficiency for E-MATIANT

5.2.3 Summary

The exergy analysis shows that the highest exergy destruction is in the first combustion, and the combustion design needs to develop to reduce exergy destruction in combustion and increase the overall efficiency of the power cycle.

The sensitivity analysis of the cycle shows that the overall efficiency of the cycle can be increased by more than 50% without temperature limitation. Developing a turbine with a high inlet temperature causes higher efficiency in the cycle. The overall efficiency of the E-MATIANT cycle at a maximum of 1300 °C is 46.9%; this efficiency can be achieved at 290 kg/s recycled working flow.

Furthermore, the optimum efficiency is at working flow with minimum exergy destruction and maximum Network. The results indicate that the maximum efficiency is 50% that when the exergy destruction is minimum at 160 kg/s working flowrates, however, the TIT is too high, and it is more than the limitation point. The maximum efficiency is 46.9% at 290 kg/s working flow with TIT of 1300 °C.

Chapter 6: Sensitivity and exergy analysis of COOPERATE cycle

6.1 Introduction

One of the first designs of Zero Emission Power Plant ZEPPs is (COOPERATE) power cycle, and the cycle was investigated and analysed. The Aspen Plus model of the cycle was developed, and the steam properties, including temperature, pressure and exergy, were tabulated for each stage.

The bar chart of the exergy destruction for each component was extracted to compare exergy destruction in components. Also, the sensitivities of the cycle efficiency and exergy destruction based on the recycled working flow rate were analysed. The performance analysis of the cycle on the design point was calculated and tabulated, and finally, the results of the techno-economic analysis for the COOPERATE cycle were presented.

COOPERATE is a highly efficient ZEPP cycle, which is introduced by Yantovski (Yantovski, 1996); the COOPERATE cycle is (CO₂ Prevented Emission Recuperative Advanced Turbine Energy), and in this cycle, the CO₂ is recycled back as shown in Figure 2.19. In this cycle, Natural gas is burned with pure oxygen in the combustion, and H₂O/CO₂ mixture is the by-product of the combustion, and water can be separated from CO₂ through the condensing process.

The cycle efficiency is related to the combustion temperature and can be between 46.9% to 55%, and this can be for TIT between 950 to 1350 °C. The turbine inlet pressure for LP, MP and HP turbine is 15, 60, 240 bar, respectively.

6.2 Sensitivity analysis results

The oxygen flow rate is 46 kg/s for a 300 MW Power plant; it is assumed to burn Stoichiometry with methane; it is assumed to achieve complete combustion under Stoichiometry; however, there is an excess of oxygen for the proper burning process in real combustion figures in chapter 3 shows which equipment has more exergy destruction and causes to reduce total exergy efficiency or efficiency.

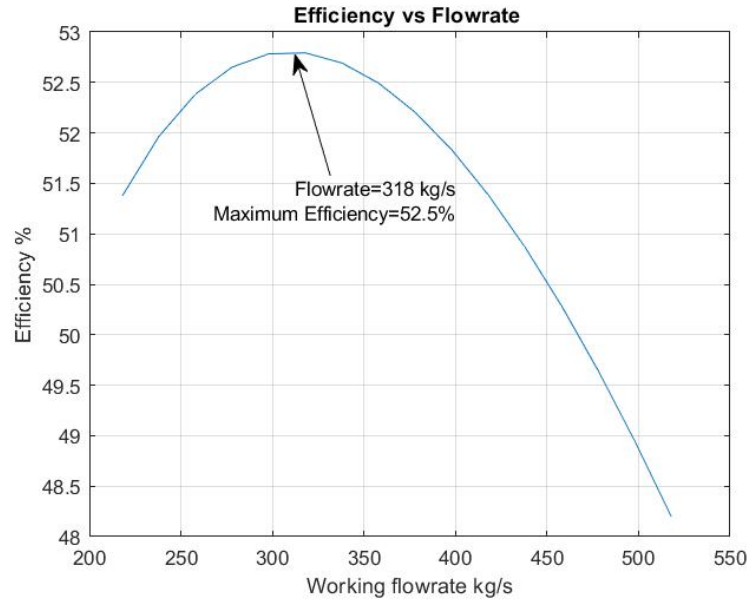


Figure 6.1 The sensitivity of Efficiency vs working flowrate for COOPERATE cycle

In order to evaluate the best working flowrate for COOPERATE cycle, the sensitivity of efficiency with respect to working flowrate is analysed, the Figure 6.1 shows the maximum efficiency is 52.5% at 318 kg/s working flow the other cycle parameters are assumed constant.

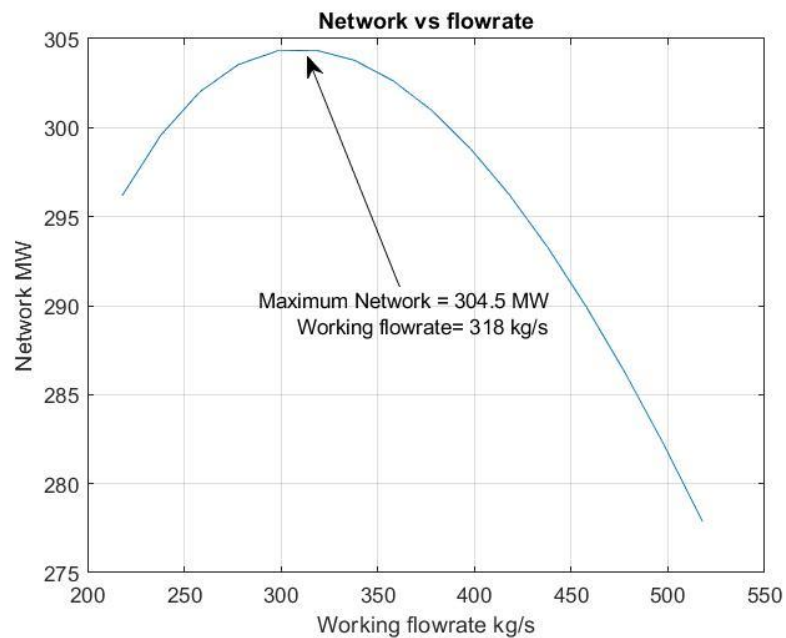


Figure 6.2 The sensitivity of Network vs working flowrate for COOPERATE cycle

Figure 6.2 shows the maximum Network is 304.5 MW at 318 kg/s working flowrates; the result can be confirmed by the literature of the 300 MW COOPERATE

cycle demonstrated by E. I. Yantovski (Yantovski, 1996), and it indicates that with 46 kg/s of oxygen, working flow rate needs to be 318 kg/s.

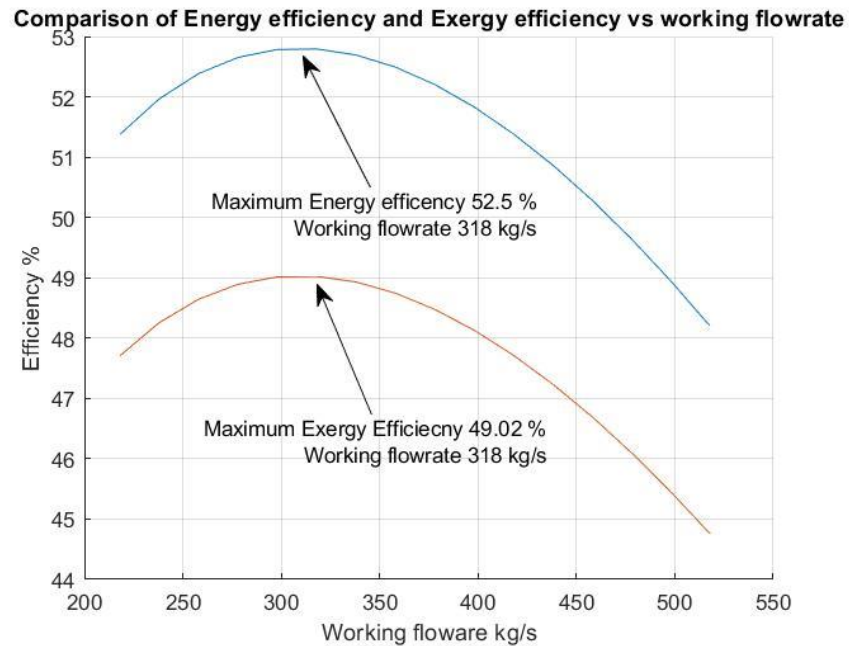


Figure 6.3 Comparison of Energy efficiency and Exergy efficiency vs working flowrate

The exergy efficiency is less than energy efficiency; Figure 6.3 shows the maximum exergy efficiency is 49.02%, and the energy efficiency is 3.48% more than it. Total Chemical exergy fuel is 611.28 MW, and total physical exergy from oxygen is 9.56 MW. Hence, the total exergy input to the system is 620.84 MW. The physical exergy of fuel is negligible.

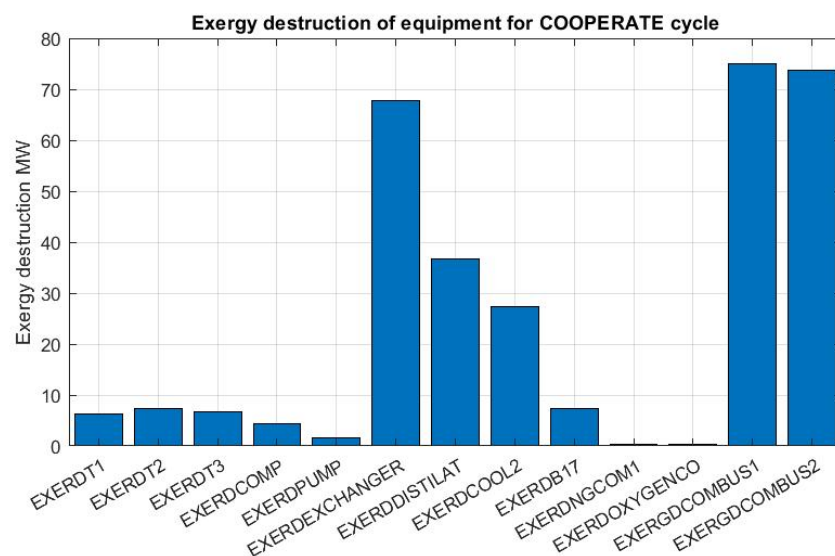


Figure 6.4 Exergy destruction of equipment for COOPERATE cycle

The exergy destruction can be used to compare irreversibility in the equipment and find the source of exergy waste in the power plant. Figure 6.4 shows combustions and heat exchangers have the highest exergy destruction in the COOPERATE cycle. The exergy destructions in the turbines are lower than other components; this is because of the high efficiency of turbines. The other sources of exergy destructions are condenser (EXERCOOL2) and distillation (EXERDESTILAT).

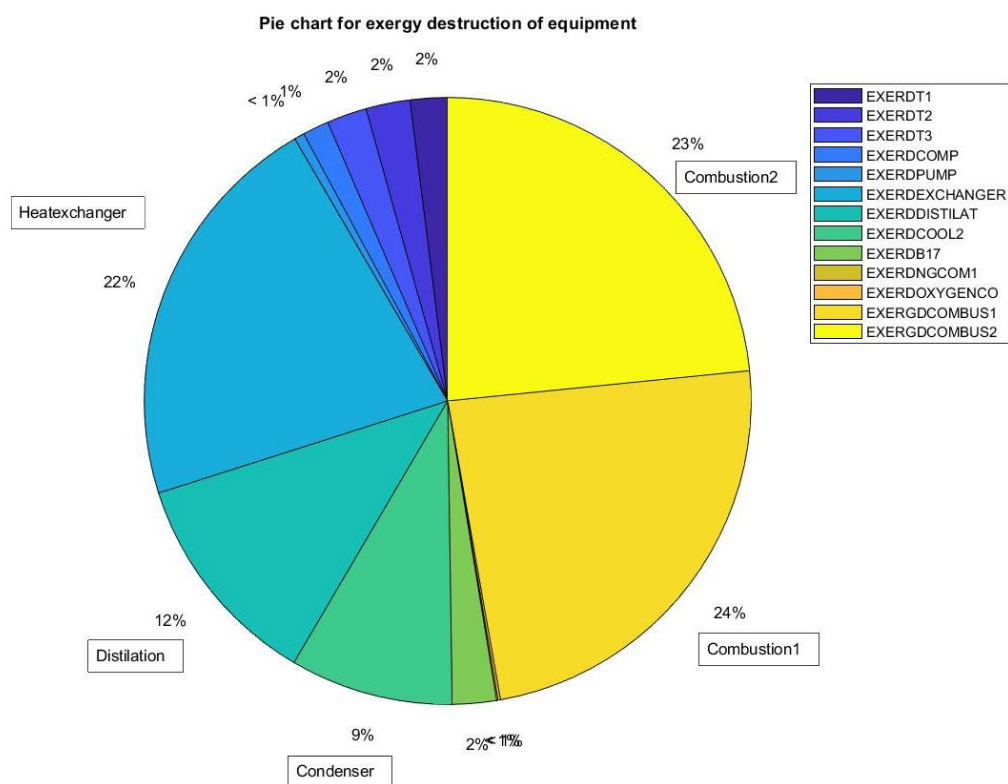


Figure 6.5 Pie chart for exergy destruction of equipment

47% of exergy destruction is in two combustions. The heat exchanger, distillation, and condenser exergy destructions are 22%, 12% and 9%, respectively. Figure 6.5 shows the pie chart of exergy destructions in the equipment.

Figure 6.6 shows, the total exergy destruction in the COOPERATE cycle is minimum at 318 kg/s working flowrates; it is verified that the exergy efficiency and energy efficiency are maximum at 318 kg/s working flowrate.

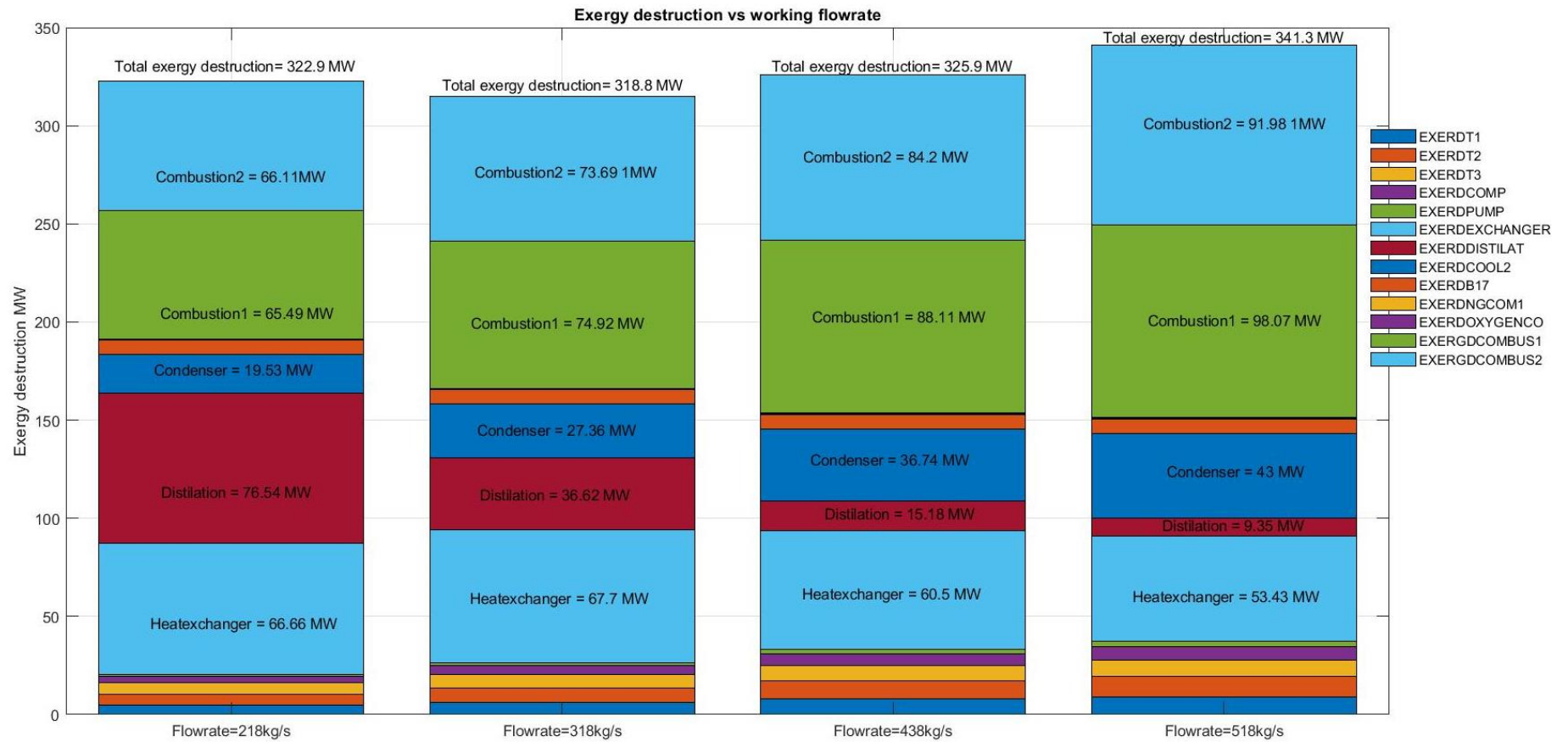


Figure 6.6 Exergy destruction vs working flowrate for COOPERATE cycle

The bar chart shows that the exergy destructions of combustion and condenser are increased by going up working flowrate. Still, exergy destruction of the heat exchanger and distillation are decreased by increasing the working flowrate. The minimum exergy destruction is at 318 kg/s working flowrate, the comparison of exergy destruction in working flowrate of 218 kg and 318 kg/s; it can realise that the main destruction is in distillation from 76.54 MW to 38.52 MW. The exergy analysis of the components demonstrates exergy destruction and waste in each equipment and the effect of exergy destruction of each equipment in total efficiency.

Figure 6.7 shows the total exergy destruction increases when the min approach temperature of the heat exchanger increases, but the exergy destruction has a minimum point at the specific point of the working flow rate.

The 3D plot of exergy destruction vs min approach temperature and flowrates demonstrate the flowrate at the minimum exergy destruction point decreases when min approach temperature increases. The sensitivity analysis of exergy destruction demonstrate that to reach the minim point of the exergy destruction need less flowrate in the higher min approach temperature of the heat exchanger.

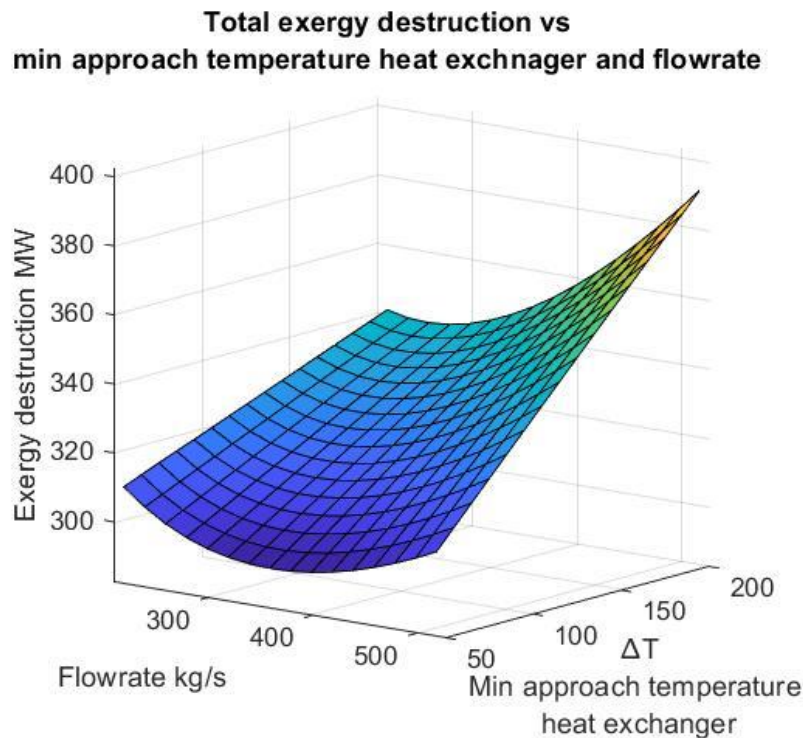


Figure 6.7 Exergy destruction vs min approach temperature and flowrate

Figure 6.8 shows the sensitivity of efficiency vs exergy destruction. The figure shows that by increasing flowrate, the exergy destruction increases and thermal efficiency decreases.

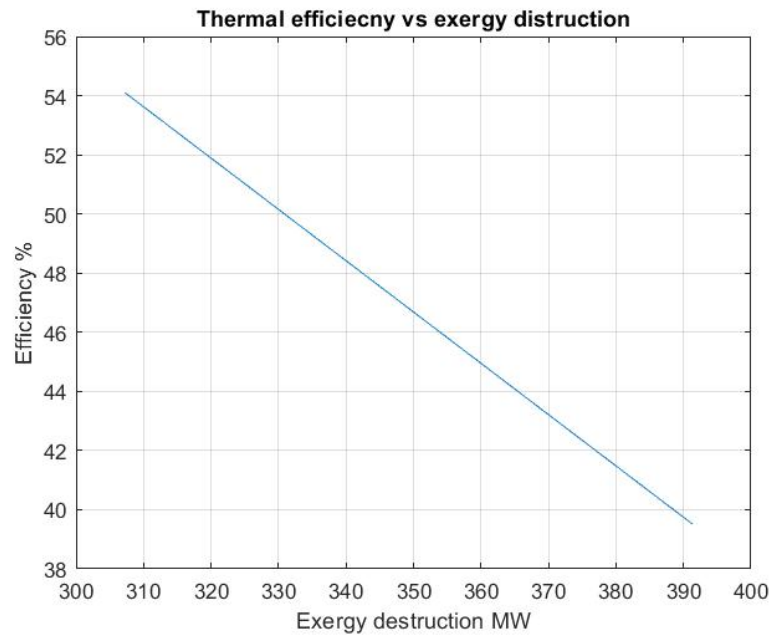


Figure 6.8 Total exergy destruction vs efficiency of COOPERATE cycle

Figure 6.9 shows the maximum efficiency increases with reducing ΔT of the heat exchanger. The maximum efficiency is 52.79% for $\Delta T=110$ at 318 kg/s flowrate. Figure 6.10 shows the minimum exergy destruction is 314.8 MW at 319 kg/s, which is maximum efficiency.

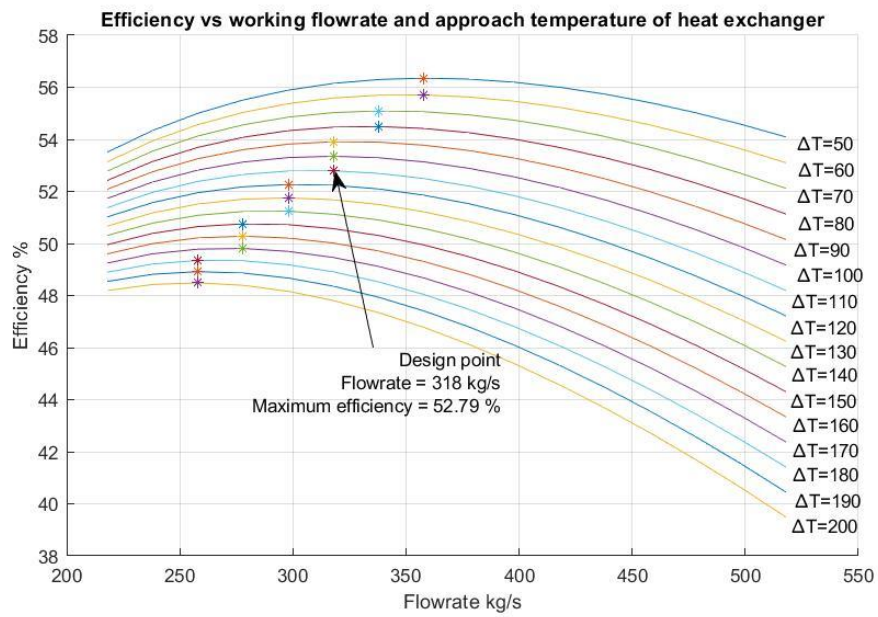


Figure 6.9 Efficiency Vs Working flowrate and Heat exchanger approach temperature

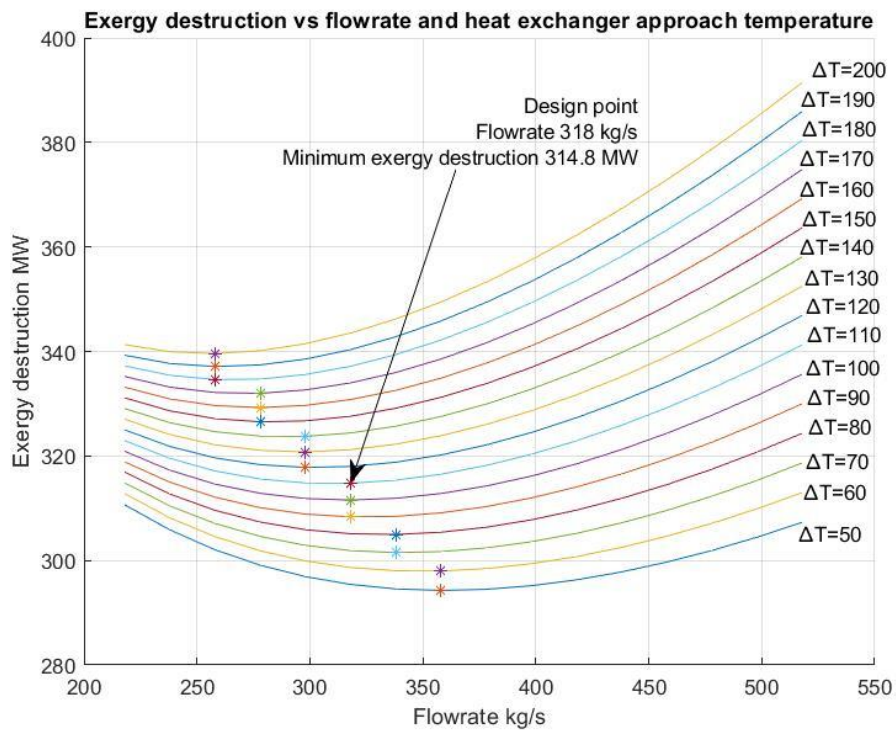


Figure 6.10 Exergy destruction vs flowrate and heat exchanger approach temperature

As shown in Figure 6.11, the maximum exergy destructions are at heat exchangers and combustions. Total exergy destruction of the turbine is less than heat exchanger, combustions, distillation and condenser. The results indicate technologies of these components need to be developed to improve efficiency instead of improving turbine technologies.

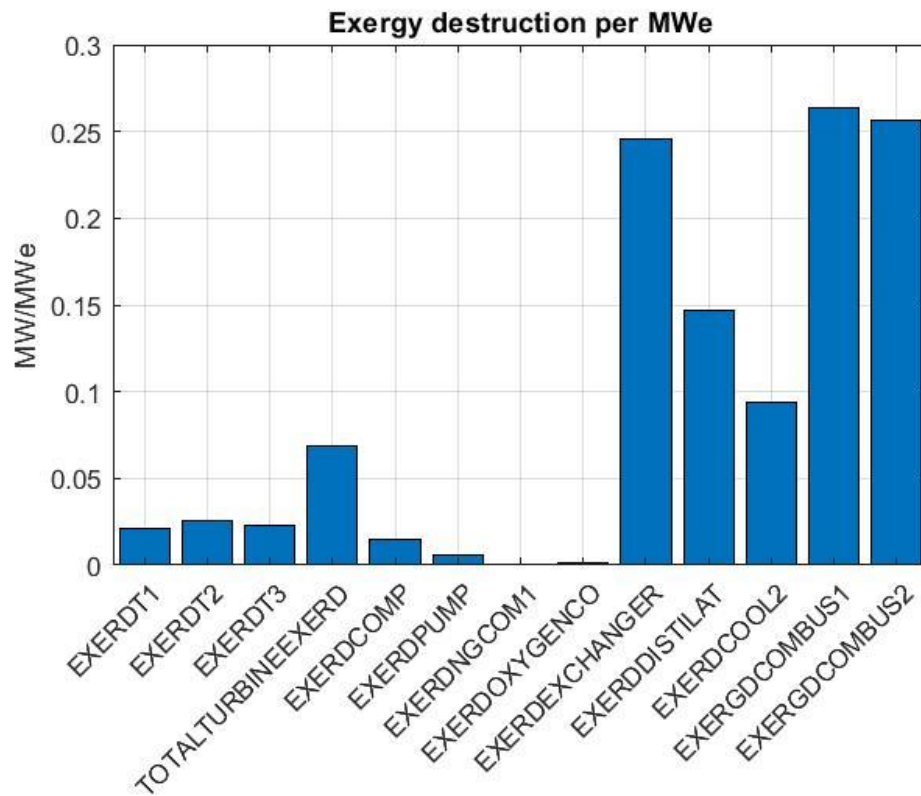


Figure 6.11 Exergy destruction per MWe for COOPERATE Cycle

6.3 Summary

The analysis shows the heat exchanger approach temperature has a high effect on the COOPERATE cycle efficiency, and it can be increased from 48% to 58%. Also, the total exergy destruction of the cycle vs working flow rate and heat exchanger approach temperature is shown.

The analysis shows that the heat exchanger causes high exergy destruction in the cycle, and technology development of heat exchanger can increase efficiency, and this cycle will be a promising cycle in the future. The techno-economic analysis shows that gas turbines, heat exchangers and Air Separation Unit have the highest cost in the cycle.

The result indicates that exergy destruction in distillation has more variation by working flow rate for COOPERATE cycle and is one of the main causes of the exergy destruction in high working flow rate.

The maximum efficiency is 52.79% for $\Delta T=110$ at 318 kg/s flowrates, with the minimum exergy destruction is about 314.8 MW. The exergy destruction in combustions grow by increasing flowrate from 218 kg/s to 518 kg/s because of the high rate of the chemical reaction and increasing the turbulent flow inside the combustions.

Chapter 7: Sensitivity analysis of the heat exchanger design in NetPower oxy-combustion cycle for carbon capture

7.1 Introduction

For gas turbines, several Oxy-combustion power cycles (Oxyturbine cycles) have been investigated by means of thermodynamic analysis. NetPower cycle is one of the leading oxyturbine power cycles with almost full carbon capture capability from the natural gas-fired power plant. In this chapter, sensitivity analysis of the heat exchanger design in NetPower cycle is completed by means of process modelling. The heat capacity variation and supercritical carbon dioxide with gaseous admixtures are considered for multi-zone analysis with Aspen Plus software. It is found that the heat exchanger design has a major role in increasing the efficiency of NetPower cycle. The pinch-point analysis is done to extract the composite and grand composite curve for the heat exchanger. In this paper, the relationship between the cycle efficiency and the minimum approach temperature (ΔT_{min}) of the heat exchanger has also been evaluated. An increase in ΔT_{min} causes a decrease in the temperature of the recycled flue gases (RFG) and an overall decrease in the required power for the recycled gas compressor. The main challenge in the design of heat exchangers in power plants is a tradeoff between Capital and Operational costs. To achieve lower ΔT_{min} , a larger size of a heat exchanger is required. This means a higher capital cost but leading to better heat recovery and lower operational costs. To achieve this, ΔT_{min} is selected from the minimum point in the diagrams of capital and operational costs.

This study provides an insight into the NetPower Oxy-combustion cycle's performance analysis and operational condition based on its heat exchanger design. Greenhouse gases are the main reason for warming the atmosphere temperature and climate change. Several oxyturbine cycles are proposed and studied by thermodynamic

analysis; only two cycles of CES and Allam (NetPower) are currently in the demonstration phase, both funded by DOE in the US.

The Allam cycle is one of the novel oxy-combustion technologies, and it is developed recently with 8 Rivers Capital. The 8 Rivers, Exelon Generation, and CB&I are owners of NetPower. NetPower develops the natural gas Allam cycle, and it is currently building a 50 MWth natural gas demonstration power plant in La Porte, Texas (Allam *et al.*, 2017). This article presents the latest results of our investigation on the effects of heat exchanger design on the NetPower oxyturbine cycle with full carbon capture.

7.2 Analysing of NetPower cycle

7.2.1 NetPower cycle

NetPower cycle was introduced by Rodney Allam. NetPower cycle working flow is mainly carbon dioxide in a high-pressure and turbine inlet pressure (TIP) is approximately 300 bar and low-pressure-ratio of 10. It is a highly recuperated Bryton cycle (Allam *et al.*, 2017). NetPower cycle combustor burns natural gas with pure oxygen supplied from an Air Separation Unit (ASU) and high-pressure carbon dioxide stream inlets recycled from its power turbine. Recycle Fuel Gas (RFG) is heated with a recovery heat exchanger and flows to the combustor to reduce the Combustion Outlet Temperature (COT) by diluting the combustion products. The RFG flowrate controls the temperature of combustion at an acceptable level. The direct-fired supercritical carbon dioxide (SCO₂) turbine is cooled with a cooling stream from the heat exchanger (Allam *et al.*, 2013).

The exhaust gas with 740°C enters recuperating heat exchanger that transfers heat from hot outlet turbine exhaust gas to the three-cycle streams. It includes the carbon dioxide-rich stream recycled to the combustor (to the moderate temperature of combustor), the oxidant stream recycled to the combustor and the carbon dioxide-rich

stream for cooling turbine blades. Also, the hot compressed air stream from ASU (Air Separation Unit) enters recuperating heat exchanger for recovering its heat.

The heat exchanger is one of the main parts of NetPower cycle, and it has a main role in NetPower cycle efficiency. The exhaust gas from the heat exchanger is cooled down, and the carbon dioxide is separated from the water. The water is sent to the wastewater treatment for recovery and treatment. A portion of carbon dioxide stream from water separation units sent for purification and compression unit. Most carbon dioxide is compressed and recycled back.

Recycle gas compression loop includes four stages intercooled compressor and two intercooled pumping stages. Inter cooling is with cooling water. The carbon dioxide stream is divided into three parts; 45-50% of flow rate is pumped to 305 bars and preheated in the recuperating heat exchanger. 10-12% of the flowrate after heated in the heat exchanger up to a maximum of 400 °C, then it is sent to the turbine for the cooling blade.

The 32 -45% of carbon dioxide stream is mixed with high purity oxygen the oxidant stream is heated in heat exchanger up to 720 °C and It is sent to combustion to burn fuel (IEAGHG, 2015).

NetPower Plant includes three main parts:

1. NetPower cycle
2. Recycle compression loop
3. Carbon dioxide purification and compression

The Air Separation Unit, CO₂ purification compression unit, utility and offside units are extracted from the IEA report 2015, and these are considered constant in this model (IEA 2015 report).

7.2.2 NetPower simulation with Aspen Plus

7.2.2.1 Recovery Heat Exchanger:

The heat exchanger on NetPower cycle can be a compact multi-channel plate-fin design or printed circuit in Nickel-alloy (e.g. Alloy 617)(IEAGHG, 2015).

Heatric Company supplies four printed circuit heat exchangers (PCHEs) for NetPower to commission the 50 MW demonstration plant in Texas (Heatric 2016). PCHEs is a multi-stream heat exchanger type. The PCHEs is replaced with conventional Heat Exchanger Network (HEN) on NetPower Cycle. Therefore the total annual cost (TAC) is decreased. A Multi-Stream Heat Exchanger (MSHE) enables a simultaneous heat exchange between more than two streams in a single unit (Joda *et al.*, 2011). The multi-stream heat exchanger is a special case of a Heat Exchanger Network without external utilities. Therefore, classical pinch analysis can be performed on a Multi-stream heat exchanger (Watson and Barton, 2016).

Heatric PCHEs are manufactured by diffusion bonding; these are fabricated with no joints, welds or points of failure, resulting in units combining exceptional strength and integrity with high efficiency. PCHEs are smaller and lighter than conventional heat exchangers; their specifications are high-pressure capabilities, high range temperature, small size, higher structural integrity (Diffusion bonding technology 2016).

The heat exchanger cost effects strongly on the final plant cost. A smaller minimum temperature approach ΔT_{min} for heat exchanger increases efficiency but also increases the capital cost (CAPEX). Therefore, it is required to optimise between capital cost, operational cost (OPEX) and efficiency. CAPEX vs OPEX studies is required to find an optimum operating point of the system. The cost of heat exchange affects significantly by minimum approach temperature (ΔT_{min}) and pressure drop. The cold streams include two high-rich recycled carbon dioxide streams and one oxidant stream. The high-rich recycled carbon dioxide stream includes one Recycled Flue Gas RFG, which is heated and enters to combustion; another stream is cooling turbine stream, which is heated and enters turbine for the cooling blade. Oxidant stream is heated and enters combustion for burning fuel.

The hot streams include an exhaust stream from the turbine and hot gas from ASU. The huge difference between the heat capacity of carbon dioxide in hot and cold streams causes a significant imbalance. In order to avoid imbalance in heat transfer, first, the cold streams are heated up with heat from the operation of the CO₂ recycle compressor outside the multi-stream heat exchanger and hot air from ASU compressors inside the multi-stream heat exchanger. Then, they are heated with exhaust gas from the turbine (Allam et al. 2017).

7.2.2.2 Recovery Heat Exchanger modelling in Aspen Plus

The recovery heat exchanger is modelled with multi-stream heat exchanger MHeatX block in Aspen Plus; this calculates heat duty between multi hot and cold streams. Furthermore, this block calculates the overall UA (overall heat transfer coefficient) for the exchanger, minimum approach temperature ΔT_{min} , Number of Transfer Units (NTU), analyses a detailed zone analysis and composite curve (AspenTech).

The design parameters of multi-stream heat exchanger for NetPower cycle are dependent on the following items:

1. Flow rate composition
2. Heat capacities
3. Temperatures of stream

In order to calculate design parameters of multi-stream heat exchanger for a power plant, it requires all material of energy balance, design of combustion and turbine to be done. Energy integration can be considered the last step of the design for the power plant. After calculation of design parameters such as UA (overall heat transfer coefficient) and ΔT_{min} . In order to design an efficient multi-seam heat exchanger with minimum size and cost, the following parameters should be considered:

1. Temperature difference
2. Conducting material
3. Fluid turbulence (more turbulent more heat exchange)
4. Fluid velocity
5. Surface area
6. Direction of Flow

The main issue in heat exchanger design for the power plant cycle is a pinch point. During partial load or unsteady state circumstances, sometimes pinch point or temperature crossover might happen in the multi-stream heat exchanger. In these conditions, the heat exchanger will not perform effectively.

7.2.2.3 *CO₂ Direct-fired Turbine*

The turbine is one of the important parts of a power plant cycle. The turbine cooling causes difficulties in calculations to find the efficiency of CO₂ Direct-fired turbine. In our simulation, the efficiency of the turbine for NetPower cycle is considered constant.

First Supercritical CO₂ (S-CO₂) turbine is supplied with Toshiba for the plant build in Texas, USA (Toshiba 2016). NetPower cycle turbine is intercooling turbine, and it requires the following developments.

NetPower turbine has higher inlet pressure than a conventional turbine, so the shell requires adoption. Blades and shells require cooling because of the TIT of the NetPower cycle. Working flow in NetPower cycle is carbon dioxide, so it is necessary that the conventional facilities are redesigned for carbon dioxide working flow. The blades in the NetPower turbine are cooling with the open circuit blade cooling method, and they are protected with cooling film and cooled by convection.

Higher Inlet turbine temperature (TIT) causes higher efficiency in NetPower cycle. The metal working temperature of turbine blades is a barrier to increase turbine temperature. The efficiency of the power turbine will increase by increasing its metalworking temperature. Furthermore, the heat transfer coefficient of the cooling flow, which is almost pure carbon dioxide is very high compared to conventional cooling flow.

The exergy of a system is the maximum energy that is available to be used. Increasing gas turbine inlet temperature decreases in combustion chamber exergy destruction (Kaviri, Jaafar and Lazim, 2012). This is due to the fact that this increase leads to decreasing entropy destruction. On the other side, TIT in power turbines is required to be of a higher value to avoid exergy destruction (Sanjay, 2011). Increasing TIT increases both efficiency and specific work output (Sanjay, 2011) significantly. In NetPower cycle, TIT (Turbine Inlet Temperature) or COT (Combustion Outlet Temperature) is controlled with Recycle Gas Flow (RGF), while multi-flow heat

exchanger recovers heat from turbine exhaust gases (Scaccabarozzi, Gatti, and Martelli, 2017).

7.2.2.4 Turbine with cooling blades modelling in Aspen Plus

Modelling a turbine with a cooling blade system is challenging in Aspen Plus, but other components such as compressor, pump, combustion and separator are available in the software blocks, and they are not required to use an ad-hoc block or to provide separate code to model them. This means a simulation of the turbine block with cooling blades is not straightforward modelling in this software.

There are different methods to simulate a turbine with a cooling blade system. One of the methods to simulate a turbine with cooling blades is assuming that working fluid is an ideal mixture of ideal gas species. This method has been used in some commercial simulation codes (e.g. GT Pro) and private simulation codes (e.g. GE simulation code by Politecnico di Milano) (Scaccabarozzi, Gatti, and Martelli, 2016).

Another method that is modelled with EL-Maris is the cooled expansion model (M. A. El-Masri). This model is improved by Roberto Scaccabarozzi for simulation of the turbine with a cooling blade in Aspen Plus as shown in Figure 7.1; the turbine is split to infinite expansion steps and used a correlation to improve the accuracy of the model (Scaccabarozzi, Gatti, and Martelli, 2017). This method is required to calculate correction factors to correct results and limited to a specific range of temperature.

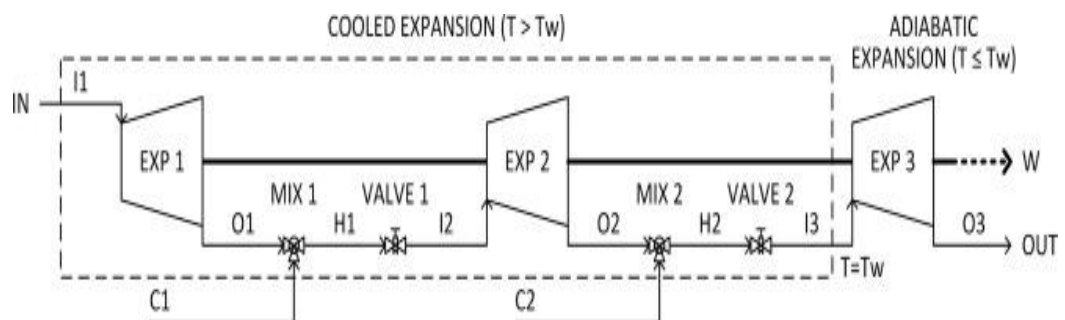


Figure 7.1 Model of the improved continuous expansion model with N (number of cooled expansion steps) by Scaccabarozzi, Gatti (Scaccabarozzi, Gatti, and Martelli 2017, 551-560)

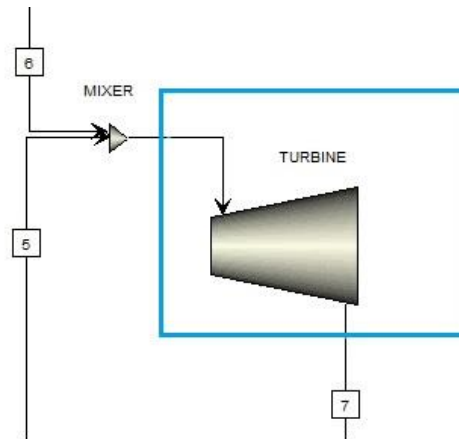


Figure 7.2 Turbine block model in Aspen Plus

In this article, a new method is offered to simulate a turbine with a cooling blade as shown in Figure 7.2; It is a conventional turbine in Aspen Plus with a mixer before, however difference efficiency is considered to have model closer to the actual model. In order to simulate and calculate turbine parameters, the energy balance and exergy is also evaluated using this method.

7.2.3 Turbine with cooling blade modelling in Aspen Plus by exergy analysis

The general exergy formula is calculated based on Equation 7-1:

Equation 7-1

$$\dot{E}_{x,heat} + \sum_i m\dot{e}_{x,i} = \sum_e m\dot{e}_{x,e} + \dot{E}_{x,w} + \dot{I}_{dest}$$

The following formula can be extracted for NetPower turbine with cooling blades in Figure 7.3.

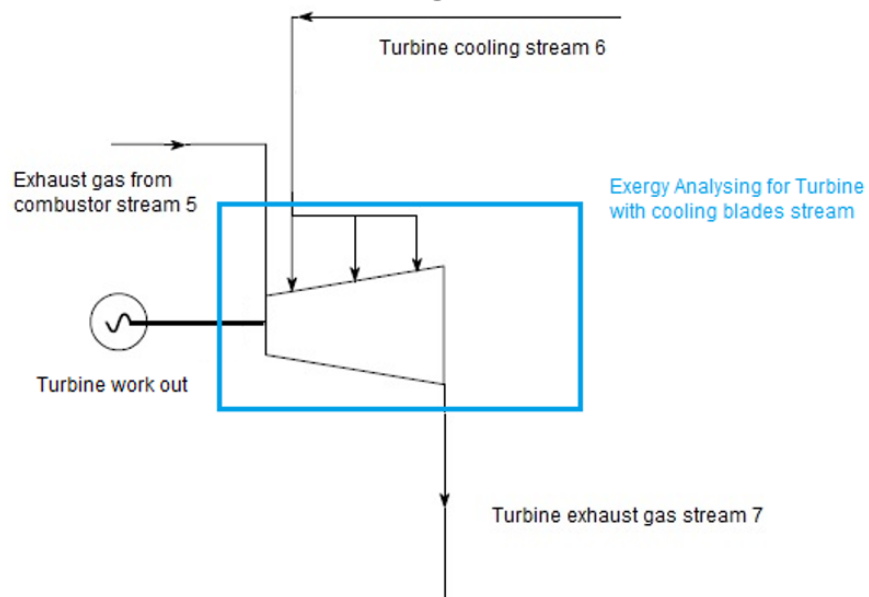


Figure 7.3 NetPower Turbine with a cooling blade

Equation 7-2

$$A) \sum_i \dot{m} e_{x,i} = \sum_e \dot{m} e_{x,e} + \dot{E}_{x,w} + \dot{I}_{dest}$$

$$B) \sum_i \dot{m} e_{x,i} = \dot{E}_{x,5} + \dot{E}_{x,6}$$

$$C) \sum_e \dot{m} e_{x,e} = \dot{E}_{x,7}$$

$$D) \dot{E}_{x,w} = \dot{W}_{gt}$$

$$E) \dot{I}_{dest} = \dot{I}_{dest \text{ Turbine with cooling}}$$

$$F) \dot{E}_{x,5} + \dot{E}_{x,6} = \dot{E}_{x,7} + \dot{W}_{gt} + \dot{I}_{dest \text{ Turbine with cooling}}$$

The diagram presented in Figure 7.3 is used to model NetPower Turbine with cooling blades in Aspen Plus:

If we consider flow gases are mixed before entering Aspen Plus turbine block, then the following formula can be extracted.

Equation 7-3

$$A) \dot{E}_{x,heat} + \sum_i m \dot{e}_{x,i} = \sum_e m \dot{e}_{x,e} + \dot{E}_{x,w} + \dot{I}_{dest}$$

$$B) \sum_i m \dot{e}_{x,i} = \dot{E}_{x,5} + \dot{E}_{x,6}$$

$$C) \sum_e m \dot{e}_{x,e} = \dot{E}_{x,7}$$

$$D) \dot{E}_{x,w} = W_{gt}$$

$$E) \dot{I}_{dest \text{ aspen model}} = \dot{I}_{dest \text{ Turbine aspen}} + \dot{I}_{mixer}$$

$$F) \dot{E}_{x,5} + \dot{E}_{x,6} = \dot{E}_{x,7} + W_{gt} + \dot{I}_{dest \text{ aspen model}}$$

hence the following equation is extracted:

Equation 7-4

$$A) 0 = \dot{I}_{aspen \text{ model}} - \dot{I}_{dest \text{ Turbine with cooling}}$$

$$B) \dot{I}_{dest \text{ Turbine aspen}} + \dot{I}_{mixer} = \dot{I}_{dest \text{ Turbine with cooling}}$$

$$C) \dot{I}_{dest \text{ Turbine aspen}} = \dot{I}_{dest \text{ Turbine with cooling}} - \dot{I}_{mixer}$$

The equation shows that in order to model the turbine with the cooling system in Aspen Plus, the recycled cooling stream and exhaust gas of combustion can be mixed, and exergy destructs in the mixer before entering turbine block.

The equation shows that destruction in the Aspen Plus model turbine is less than the turbine with a cooling system. Therefore, the entropy generation in the Aspen Plus model is less than the turbine with cooling blades, and it is extracted from the equation

Equation 7-4 (C) and in the aspen model, isentropic efficiency should be more than turbine cooling blades, it can be shown with Aspen Plus turbine model.

Equation 7-5

$$\dot{I}_{dest\ Turbine\ aspen} = T_0 \dot{S}_{gen}$$

In this article, the isentropic efficiency is considered constant for simulation. The entropy map of the turbine with cooling blades is required for accurate calculation.

The exergy analysis for a turbine with cooling blades will be developed for accurate modelling of NetPower cycle in the future.

7.2.3.1 *Recycle gas compression loop*

The exhaust gas exits the heat exchanger after heat recovery and loss its temperature. The flowing gas enters the separation unit with water cooling to separate water from carbon dioxide. Water is sent to a water treatment unit, and it can be recycled to reuse in the power cycle.

The carbon dioxide is separated into two parts, one part as a cycle by-product for cycle stability exit to sequestration unit. The other part is recycled through a four-stage intercooled compressor and two intercooled pumping stages, and all intercooling is with cooling water and cooling tower. The cooling water temperature is dependent on the environmental condition, and it is cooled on a natural draft cooling tower. Table.1 show the condition of cooling water for the NetPower cycle.

Table.1 Condition of cooling water for NetPower

Cooling water approach temperature	7°C
Supply temperature	Normal 15°C Maximum 36°C

The recycle stream is divided into three streams: 10-12% of carbon dioxide recycled flow is sent to the turbine for cooling turbine blades. It is pumped in the final pumping stage and preheated in a heat exchanger before entering the turbine to increase turbine

efficiency. 45-50% of carbon dioxide flow is recycled and sent to combustion to absorb heat from combustion and control the flame temperature. 38-45% of carbon dioxide recycle flow is mixed with high purity oxygen and produce an oxidant stream, and it is compressed and preheated before entering combustion for burning fuel.

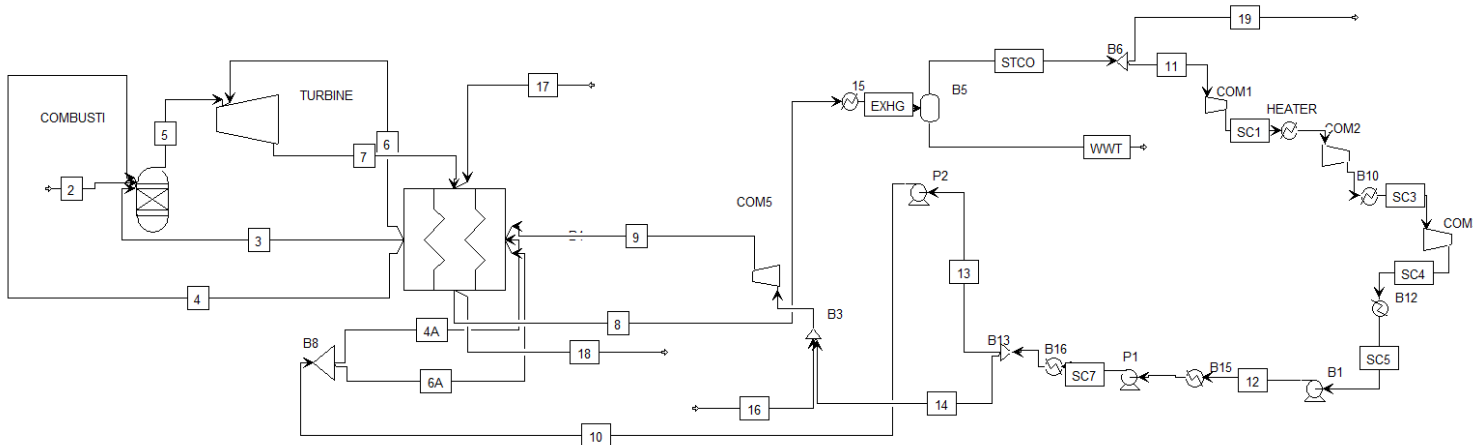


Figure 7.4 Aspen Plus model of NetPower cycle

Table 7.1 NetPower cycle simulate result validated with IEA report

Pressure bar (IEA)	Pressure bar	Temp C (IEA)	Temp C	Total Flow Mmol/hr (IEA)	Total Flow Mmol/hr	Composition (% mole)										Stream
						O2 (IEA)	O2	N2 (IEA)	N2	H2O (IEA)	H2O	CO2 (IEA)	CO2	AR (IEA)	AR	
303.00	303.04	720.00	720.00	52.30	52.30	13.34	13.37	1.05	1.05	0.13	0.13	84.94	84.92	0.53	0.53	3
303.00	303.08	720.00	720.00	52.30	52.30	0.21	0.24	1.18	1.18	0.15	0.15	97.88	97.86	0.57	0.57	4
300.00	300.00	1150.00	1150.82	108.05	108.00	0.20	0.23	1.11	1.11	6.36	6.35	91.80	91.78	0.53	0.53	5
303.00	303.08	<400	398.00	11.93	11.93	0.21	0.24	1.18	1.18	0.15	0.15	97.88	97.86	0.57	0.57	6
34.00	33.99	740.00	739.98	119.99	120.00	0.20	0.23	1.12	1.12	5.74	5.73	92.41	92.39	0.54	0.54	7
33.00	33.99	55.00	59.04	119.99	120.00	0.20	0.23	1.12	1.12	5.74	5.73	92.41	92.39	0.54	0.54	8
305.00	305.04	45.00	45.65	52.30	52.30	13.34	13.37	1.05	1.05	0.13	0.13	84.94	84.92	0.53	0.53	9
305.00	305.08	50.00	50.92	64.23	64.23	0.21	0.24	1.18	1.18	0.15	0.15	97.88	97.86	0.57	0.57	10
33.00	33.99	29.00	29.00	109.62	110.00	0.21	0.24	1.18	1.18	0.15	0.15	97.88	97.86	0.57	0.57	11
80.00	82.35	43.00	41.41	109.62	110.00	0.21	0.24	1.18	1.18	0.15	0.15	97.88	97.86	0.57	0.57	12
100-120	123.51	26.00	26.00	64.23	64.23	0.21	0.24	1.18	1.18	0.15	0.15	97.88	97.86	0.57	0.57	13
100-120	123.51	26.00	26.00	45.39	45.39	0.21	0.24	1.18	1.18	0.15	0.15	97.88	97.86	0.57	0.57	14
100-120	120.00	15.00	15.00	6.92	6.92	99.50	99.50	0.20	0.20	0.00	0.00	0.00	0.00	0.30	0.30	16
7.50	7.50	275.00	275.00	34.46	34.46	20.75	20.75	77.32	77.32	0.97	0.97	0.04	0.04	0.92	0.92	17
7.30	7.50	55.00	59.04	34.46	34.46	20.75	20.75	77.32	77.32	0.97	0.97	0.04	0.04	0.92	0.92	18
33.00	33.99	29.00	29.00	3.65	3.65	0.21	0.24	1.18	1.18	0.15	0.15	97.88	97.86	0.57	0.57	19

The percentage of oxidant and fuel gas should be stoichiometric to achieve the best efficiency of the plant. In order to evaluate our Aspen Plus model, the results have been compared to the results of NetPower cycles presented in 2015 IEA report. Figure

7.4 shows the NetPower modelling with stream numbers, and Table 7.1 shows the results from our model in comparison with the data published in the IEA 2015 report. As the table shows, the result is matched to the IEA report, and it generally validates our simulation approach and model.

There is 7.3% error in the temperature of stream eight, which is cold exhaust flow from the heat exchanger, this model temperature is 59.04 °C, and the IEA report is 55 °C. There is also a 4.4% error in temperature and 2.94% error in pressure of stream 12, which is the total recycle stream from the compressor; this model temperature and pressure is 41.41 °C, and 82.35 bar and IEA report is 43 °C and 80 bars. These small variations are mainly because of the differences between the efficiencies of pumps and compressors in our simulation with the IEA report as we don't have access to real pumps and compressors data for the NetPower cycle.

7.3 Evaluation of ΔT_{min} from the composite curve and grand compost curve of multi-stream heat exchanger

The composite curve of the multi-stream heat exchanger is extracted for the Aspen Plus MHeatX block. Figure 7.5 shows the composite curve. The minimum vertical distance between the hot curve and a cold curve is ΔT_{min} . ΔT_{min} in this simulation is 5.3 °C, and this is consistent with the ΔT_{min} 5 °C in IEA report (IEA 2015 report).

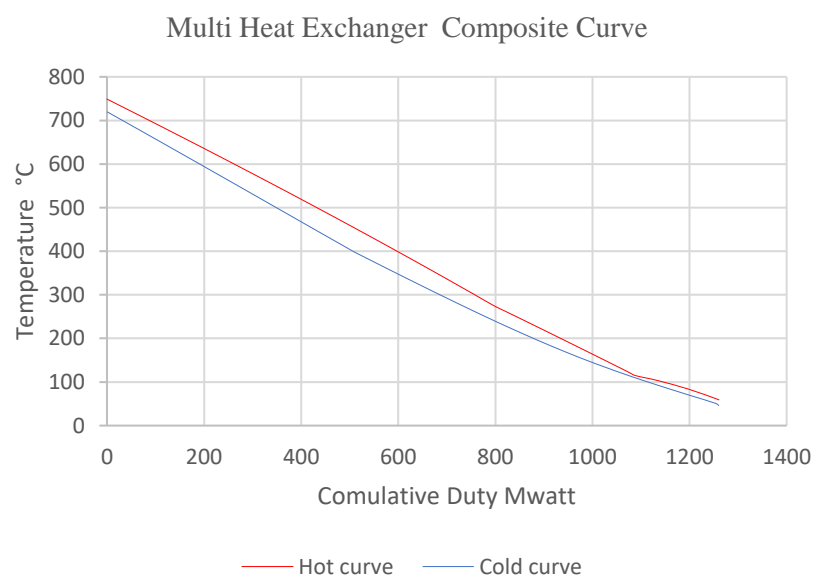


Figure 7.5 Composite curve

Zone analysis for the MheatX Aspen Plus block shows that the pinch temperature is at 112.13 °C. The heat duty between the hot and cold curves in the pinch temperature is zero. Therefore, the grand composite curve in the pinch temperature is zero. Figure 7.6 is the Grand Composite Curve (GCC) of the multi-stream heat exchanger. It is the graphical representation of the heat cascade, and it presents the excess heat available to a process within each temperature interval.

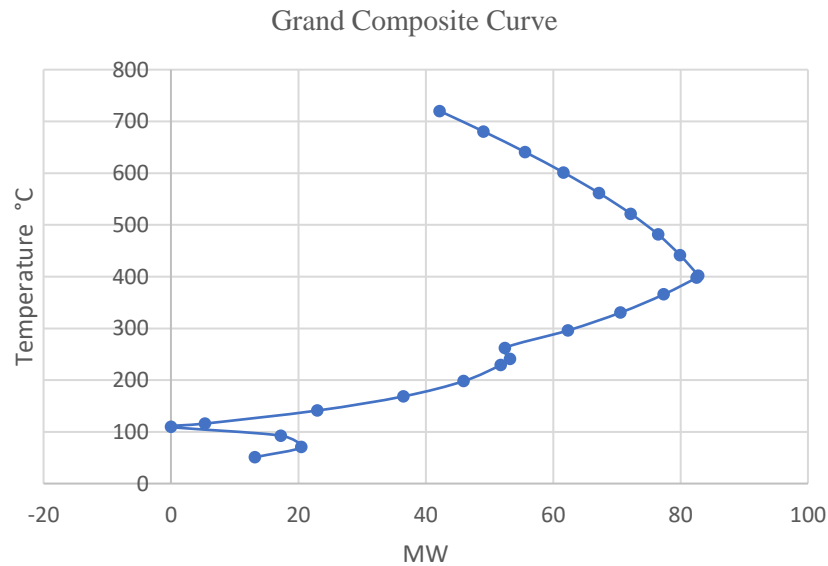


Figure 7.6 Grand composite curve

7.4 Heat exchanger design sensitivity analysis for NetPower cycle

In order to analyse the sensitivity of NetPower cycle related to design parameters of the heat exchanger, the following assumption is considered:

- A) Changing heat exchanger parameters with constant recycled flow rate and difference COT (combustion outlet temperature).
- B) Changing heat exchanger parameters with constant COT (combustion outlet temperature) and difference recycled flow rate.

In order to simplified simulations, the isentropic efficiency of the cycle is considered constant for all simulations. It is necessary to add a turbine with a cooling blade efficiency map, compressor and pump efficiency maps for accurate simulation.

7.4.1 Sensitivity analysis with a constant recycled flow rate

The ΔT_{min} for the heat exchanger is changed from 0 °C to 20 °C, and a diagram for power cycle efficiency related to ΔT_{min} is extracted Figure 7.7. The recycled flow rate is constant so that the combustion outlet temperature (COT) is increased with decreasing the minimum approach temperature of the heat exchanger. Figure 7.8 shows COT related to ΔT_{min} for constant flow rate.

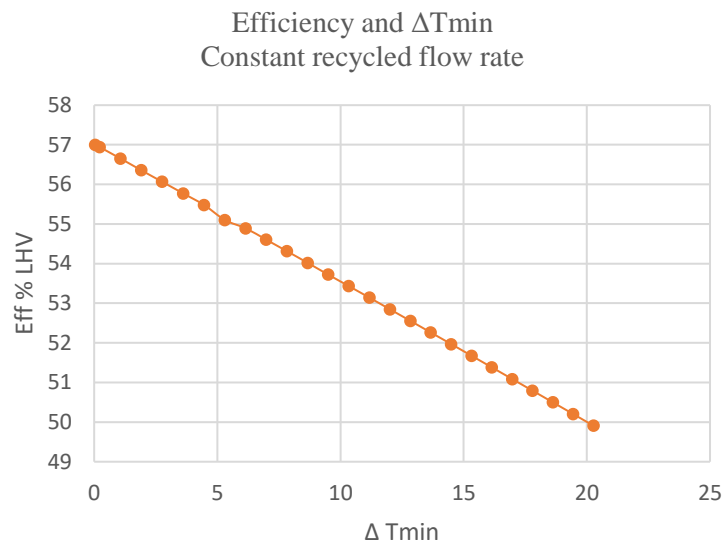


Figure 7.7 Efficiency related to ΔT_{min} for constant recycled flow rate

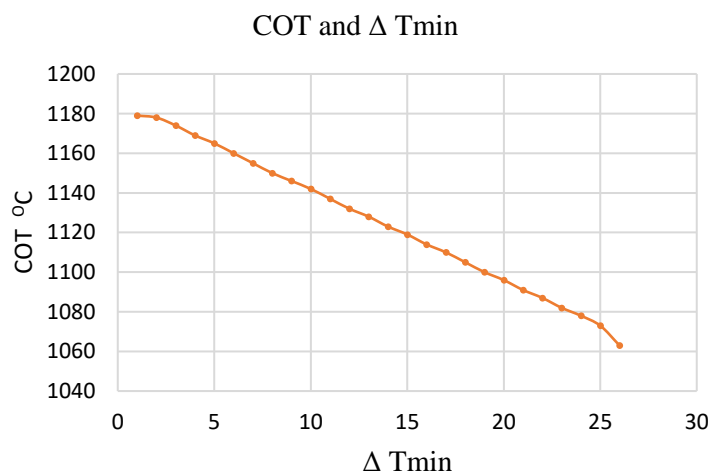


Figure 7.8 COT related to ΔT_{min} for constant recycled flow rate

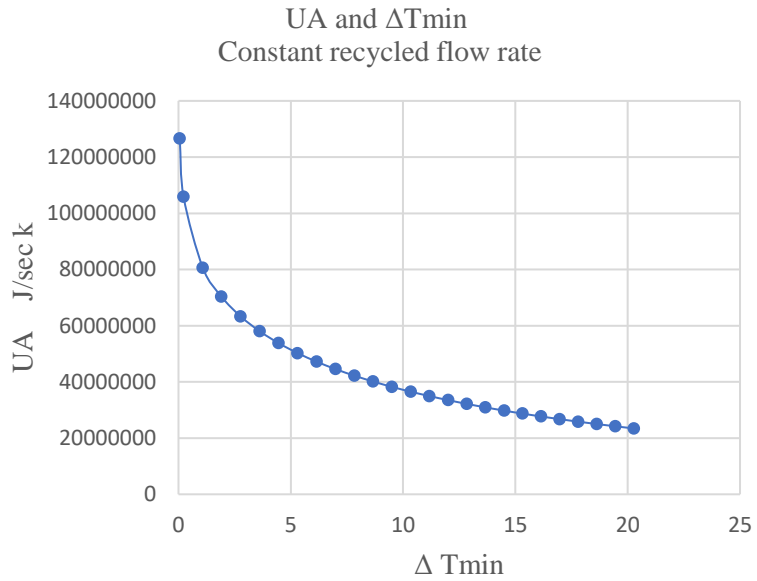


Figure 7.9 Overall heat transfer coefficient UA to ΔT_{min} for constant recycled flow rate

Figure 7.9 shows the overall heat transfer coefficient (UA) related to ΔT_{min} for constant flowrate. In order to decrease the minimum approach temperature ΔT_{min} a heat exchanger with a higher overall coefficient, UA needs to be designed, resulting in higher capital cost (CAPEX). The diagram shows that decreasing ΔT_{min} to near-zero increases the UA exponentially; therefore, capital cost will highly increase. The required power for the compressor recycle loop is constant because the recycle flow rate is constant, as shown in Figure 7.10.

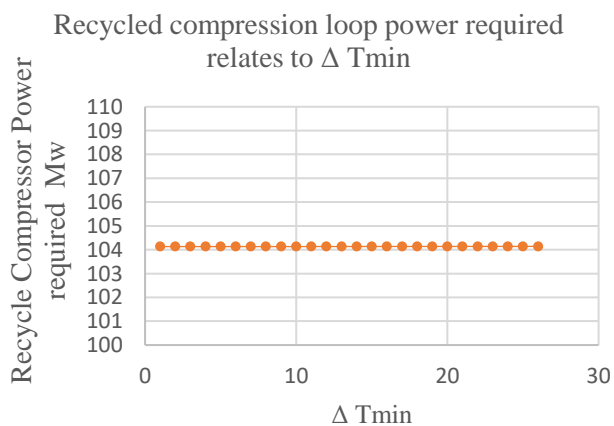


Figure 7.10 The required power for recycled compression loop relates to ΔT_{min} in a constant recycled flow rate (the power demand is approximately constant)

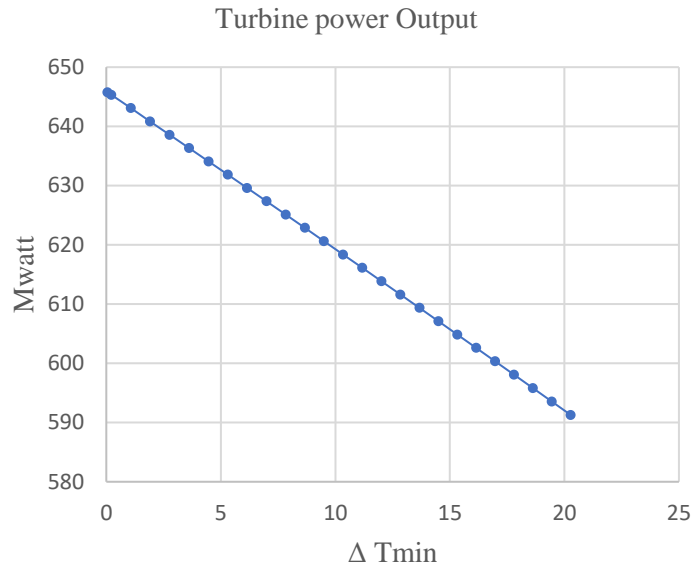


Figure 7.11 Turbine power output related to ΔT_{min} for constant recycled flow rate

Figure 7.11 shows turbine power output is increased related to lower ΔT_{min} for constant flowrate. This analysis shows that with lower ΔT_{min} without decreasing COT with more recycled flow rate, the temperature of flow gas in the turbine is increased, so the turbine power increased. Furthermore, the required recycle compressor loop power is constant, so the cycle efficiency is increased.

The material property in turbine blades is a critical point of temperature design in a gas turbine. Increasing maximum allowed turbine metal temperature from 860 °C to 950 °C causes allowing the COT increases from 1150 °C to 1120 °C (IEA 2015 report).

7.4.2 Sensitivity analysis with constant COT

In the constant Combustion Outlet Temperature (COT) simulations, the recycled flow rate will need to change related to the minimum approach temperature (ΔT_{min}) of the heat exchanger. For lower ΔT_{min} , the recycled flow rate has to increase to compensate for the increasing temperature of recycled flow and prevent increasing of COT. Figure 7.12 shows recycle flow rate versus ΔT_{min} .

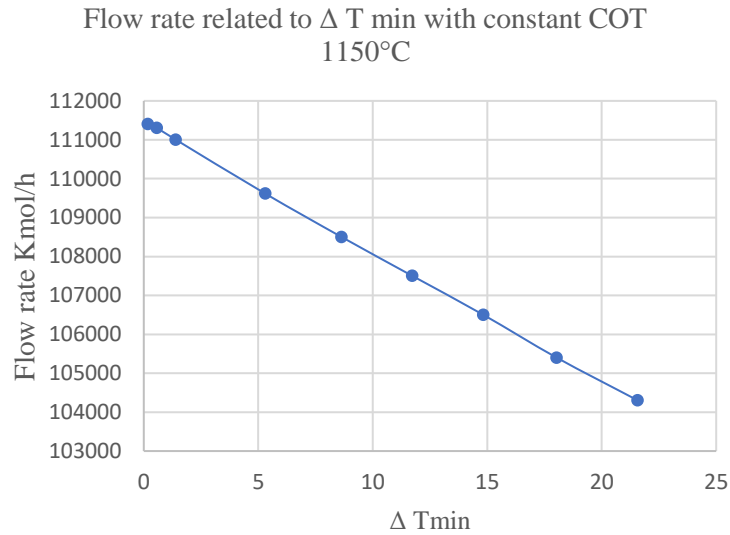


Figure 7.12 Flow rate related to ΔT_{min} for constant COT 1150 °C

The power of the compression loop is dependent on the working flow rate, so that it is required more power to compress the working flow by increasing the working flow.

Figure 7.13 shows recycled compression loop required power related to ΔT_{min} . These recycle data are in agreement with the IEA report regarding minimum approach temperature (IEA 2015 report).

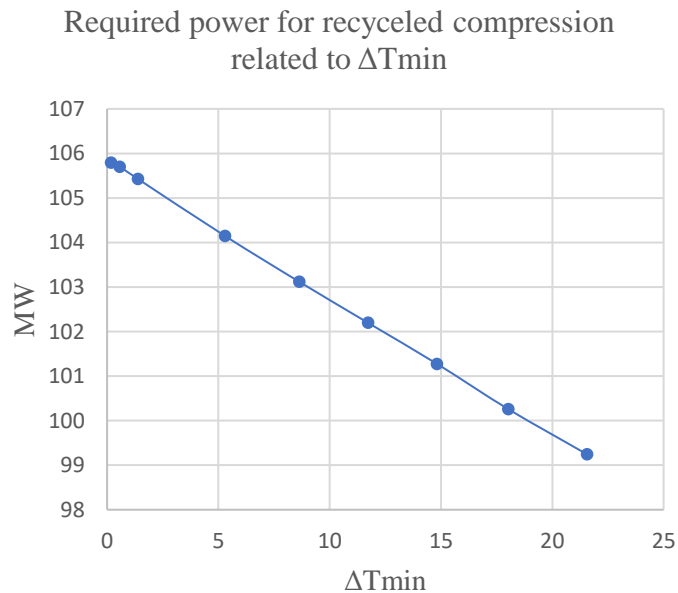


Figure 7.13 Required power of recycled compression loop against ΔT_{min} for constant COT 1150 °C

The higher the ΔT_{min} causes, the lower recycle final temperature and flow rate and power generation for the turbine. On the other hand, the recycle gas compressor power

is decreased (IEA 2015 report), but the overall power cycle efficiency is decreased. The following diagram approves the above discussion with the IEA report.

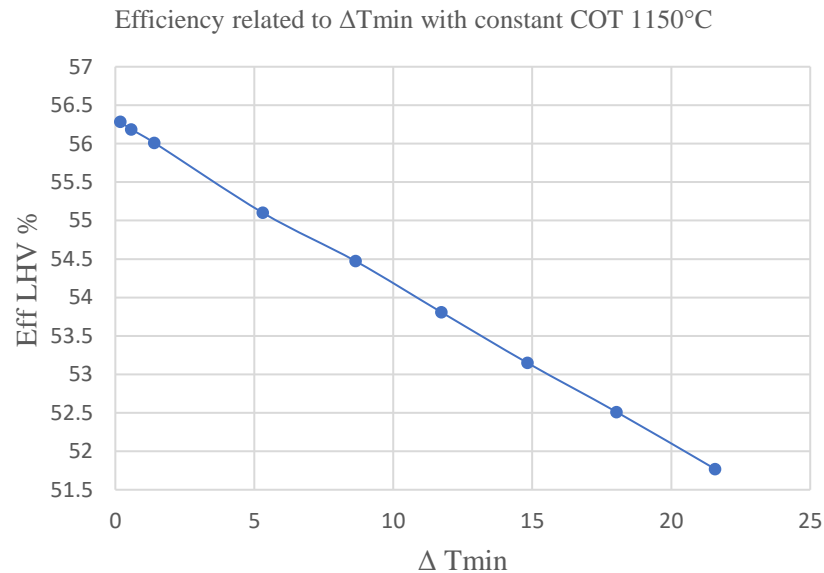


Figure 7.14 Efficiency related to ΔT_{min} with constant COT 1150 °C

7.5 Design and cost analysis of NetPower plant

The results show that to achieve higher cycle efficiency; lower ΔT_{min} is also needed a higher overall heat coefficient (UA).

The following parameters are suggested for decreasing ΔT_{min} and increasing overall heat coefficient (UA) for multi-stream heat exchanger in the NetPower cycle:

- Increasing size of the recovery heat exchanger and heat transfer area
- Using higher conductive material to increase the overall heat coefficient
- High efficient design of heat exchanger and consider more effective direction of flow, e.g. concurrent flow
- Using new manufacturing technologies such as printed circuit heat exchanger PCHE (as used in NetPower cycle)
- Avoiding crossover and pinch point in multi-stream heat exchanger in evaporation and condensation condition.
- Analysing composite curve and grand composite curve

- Implementation of the above items (to achieve lower ΔT_{min}) increases the cost of the multi heat exchanger component in the power cycles.

The following parameters should be considered to design and evaluate the cost of heat exchange for the NetPower plant: Heat recovery with multi-stream heat exchanger saves energy cost by reducing hot and cold utilities. The capital cost (CAPEX) of utilities and operational cost (OPEX) of utilities are reduced. The capital cost of heat exchanger price will increase by lower ΔT_{min} . In order to reduce pressure drop in the multi-stream heat exchanger, the CAPEX will increase, but energy cost and OPEX will drop.

The efficiency is increased, and operational energy cost is reduced by lower ΔT_{min} . In order to design a multi-stream heat exchanger for the NetPower plant, it is required to tradeoff between capital cost (CAPEX) and operational cost (OPEX) for specifying ΔT_{min} .

7.6 Summary

In this chapter, the sensitivity of the NetPower oxyturbine cycle is analysed by means of process modelling in Aspen Plus software. The results show that heat exchanger design has important effects on the efficiency, capital cost, saving energy and operational cost of the cycle.

The simulation results show that the efficiency increases with lower ΔT_{\min} in both constant COT and constant recycled flow rates. The COT shows an increase by decreasing ΔT_{\min} with a constant recycled flow rate. The efficiency increases faster in constant flow rate compared to the constant COT.

The power demand for the recycling compression loop was found to be highly dependent on the recycle flow rate, and with a constant flow rate, the recycle compression loop power demand is constant. The higher ΔT_{\min} with constant COT causes lower recycle final temperature, lower flow rate and lower turbine power output. The modelling shows that the power demand of the recycle compression loop was decreased, and in total, the efficiency decreased by more than 1%. These results are consistent with the results presented in the IEA 2015 report (IEA, 2015).

The overall heat coefficient (UA) diagram of the heat exchanger related to ΔT_{\min} shows that decreasing ΔT_{\min} near-zero causes an exponentially increase in the capital cost. The tradeoff between the capital cost and efficiency in the NetPower cycle is very critical and will be justified by selecting an efficient ΔT_{\min} .

In order to reach higher cycle efficiencies, COT will need to be increased. This shows that the material property of turbine blades or turbine blades cooling strategies have a critical role in increasing the efficiency of the NetPower Cycle. Furthermore, designing heat exchangers with higher overall heat coefficient (UA) and lower ΔT_{\min} results in higher efficiencies in the NetPower cycle. This means heat exchanger has a critical role in NetPower cycle performance and overall efficiency, and therefore it is very important to invest in new heat exchanger manufacturing technologies, materials and design methods resulting in lower capital and operational cost of the cycle in the near future.

Chapter 8: Leading Oxy-combustion power cycles: NetPower and Supercritical CES

8.1 Introduction

Several oxyturbine cycles have been introduced by means of thermodynamic analysis. However, only NetPower and Supercritical CES cycles have recently proceeded to the demonstration phase. The NetPower cycle recirculates only carbon dioxide as the working fluid, and the Supercritical CES cycle uses water as its working fluid. The Supercritical CES cycle that has the best efficiency among other types of CES cycles includes high, medium and low-pressure turbines (HP, MP, and LP) and the exhaust gas from the high-pressure turbine is reheated and expanded in an MP and LP. Pure oxygen is produced in an Air Separation Unit (ASU) and directly injected into the combustion chamber. The NetPower cycle includes a single turbine with high inlet pressure and a main multi-stream heat exchanger. Pure oxygen is produced in the ASU and mixed with the recycled carbon dioxide before being introducing to the combustion chamber. Both cycles include recycling loops and carbon dioxide purification sections. These novel cycles reduce the cost for power generation with complete CO₂ capture and sequestration with nearly zero-emission.

In this chapter, The NetPower and Supercritical CES Cycles are investigated by means of process simulation and the technologies and utilised facilities compared using sensitivity analysis. Both cycles are simulated with Aspen Plus software with the same initial conditions, and the simulation results are compared with the IEA 2015 report for validation. The sensitivity of both cycles are analysed with respect to the Turbine Inlet Temperature (TIT), Combustion Outlet Pressure (COP) and Heat Exchanger Approach Temperature (HET). The efficiencies are extracted for both the NetPower and CES cycles, and the partial load behaviour of the cycles are investigated. The initial results show that the NetPower cycle is more sensitive to the Turbine Inlet Temperature (TIT) variations in comparison with the S-CES cycle. The

results of this paper provide a platform for a comprehensive techno-economical and sensitivity analysis of the NetPower and Supercritical CES Cycles as the leading Oxy-combustion power cycles with full carbon capture.

In this chapter, these two cycles are compared in terms of the sensitivity of cycles with respect to Turbine Inlet Temperature (TIT), Combustion Outlet Pressure (COP) and heat exchanger approach temperature. Between the available technologies for carbon capture, turbine-based oxy-combustion cycles seem to be a hopeful carbon-free solution for the production of electricity.

In this chapter, NetPower and Supercritical CES Cycles are investigated by means of process simulation and the technologies and utilized facilities are compared using sensitivity analysis. In order to make a fair comparison between these cycles, each cycle has been modelled, and its thermodynamic and economic performances have been estimated on a common design basis. The results of the thermodynamic calculations indicate a net electric efficiency of 55.1% for the NetPower cycle and 48.9% for the supercritical CES. The economic analysis shows that the NetPower cycle has the lowest Cost of Electricity (COE), equal to 88.3 €/MWh, and the other cycles are in the range of 93–95 €/MWh (Mancuso *et al.*, 2015).

8.1.1 CES supercritical cycle

The Clean Energy System (CES) cycle is an oxy-combustion cycle that uses water (H₂O) as the main part of the working flow in the cycle. Bolland and Saether introduced a basic CES Cycle which was developed by Clean Energy Cycle Ltd (Zhao *et al.*, 2017). During the last decade, CES cycle efficiency has improved from 20% to 30% (50 MW J79/Deploy 2nd Generation Deploy) to 35,45% (200 MW 3th Generation CES/Siemens/TriGen OFT900) and 50% (400MW CES/Siemens/TriGen) (Business and October, 2012).

Clean Energy System (CES) demonstrate project for testing, analyzing and design of modified Siemens SGT-900 gas turbine with the company of Siemens Energy and Florida Turbine Technology (FTT) and the US. Department of Energy (DOE) funding program (Climent Barba *et al.*, 2016a). Figure 8.1 shows the schematic process flow diagram (PFD) of the Supercritical CES cycle.

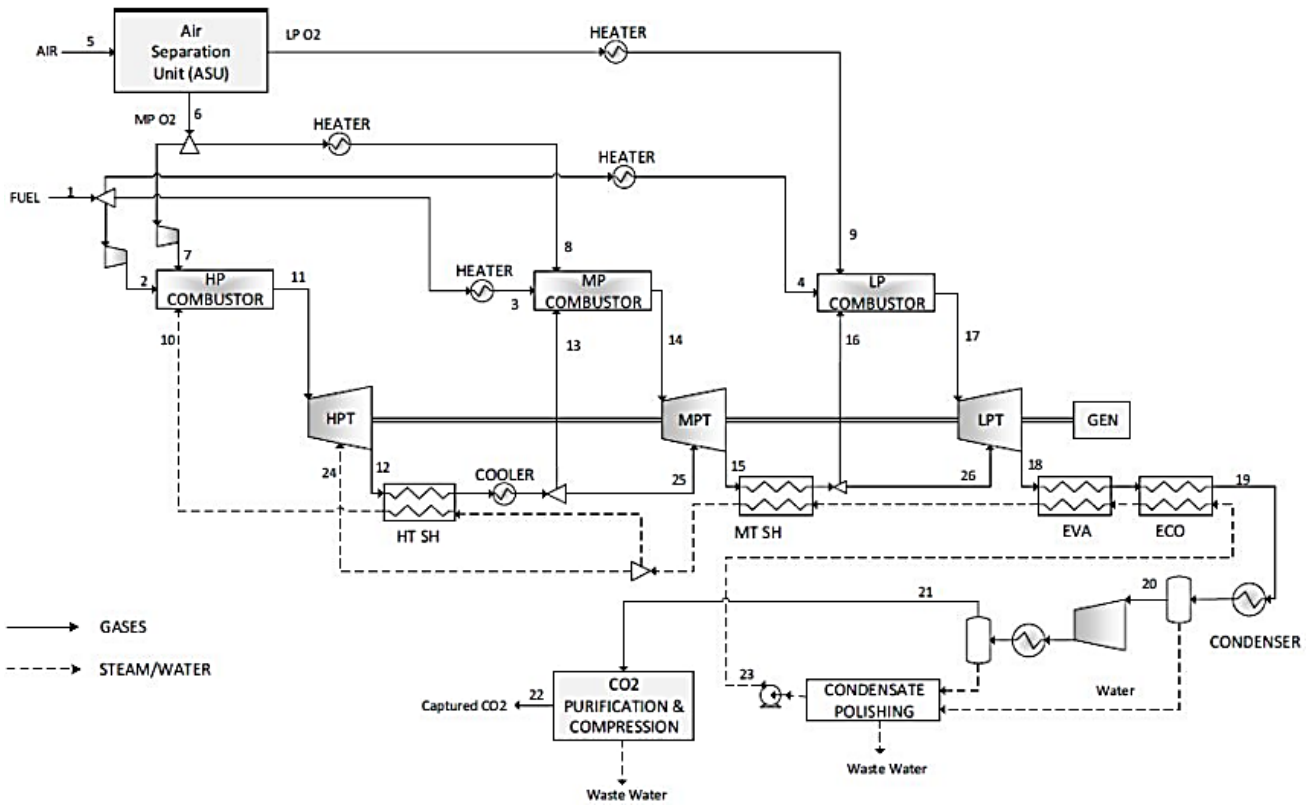


Figure 8.1. Supercritical CES Schematic diagram (Ferrari *et al.*, 2017b)

The Supercritical CES power cycle includes three turbines, compressor, and combustor. Natural gas is divided three-part, 23% of natural gas is compressed to 310 bar and is fed to the HP combustor, and 33% is fed to the MP, and the remaining is fed to the LP combustor. Fuel gases are preheated before feeding combustors. Pure oxygen is produced from the ASU and compressed for the HP combustor, with the remainder being preheated before feeding to LP and MP combustor.

Exhaust gas from HPT is separated into two parts. One part is fed to the MP combustor, and the remaining is directly fed to the MPT for the cooling turbine to control blade metal temperature. Also, exhaust gas from the MPT is separated into two parts, one part is fed to the LP combustor, and the remainder is directly fed to the LPT for the cooling turbine to control blade metal temperature.

There are four main units for supercritical CES cycle with carbon capture (IEAGHG, 2015):

1. Power Island
2. CO₂ purification and compression

3. Air Separation Unit (ASU)

4. Utility and of Site

Table 8.1 The composition percentage of Supercritical CES cycle working fluid (IEAGHG, 2015)

Composition	Exhaust Gas HPT %	Exhaust Gas MPT %	Exhaust Gas LPT%
Ar	0.13%	0.27%	0.43%
CO ₂	3.11%	6.6%	10.23%
H ₂ O	96.5%	92.65%	88.72%
N ₂	0.09%	0.19%	0.29%
O ₂	0.18%	0.29%	0.36%

The working fluid in the CES cycle is about 90% water (H₂O) and around 10% carbon dioxide. Table 8.1 shows that CO₂ percentage is increased in working flow from HPT to MPT and then LPT and water (H₂O) is decreased, it is because the gas product is cumulated through the cycle from HPT to MPT and then LPT.

CES Supercritical Power Island has an F-class oxy-combustion gas turbine; an F-class gas turbine is the commonly used gas turbine in the supercritical CES cycle. The H-class gas turbine has recently been introduced, and it is cutting edge technology with higher performance. This kind of turbine can be used for the next-generation supercritical CES power cycle. Gas turbine package includes HP turbine (HPT) with two cooling stages, MP turbine (MPT) with four cooling stages, LP turbine (LPT) with three cooling stages followed by an uncooled section, Oxy turbine generator, HP, MP, LP combustor, and NG Compressor.

Table 8.2. The pressure of fuel gas and coolant temperature in each turbine (IEAGHG, 2015)

Composition	HPT		MPT		LPT	
	Inlet flue gas	Coolant Stream	Inlet flue gas	Coolant Stream	Inlet flue gas	Coolant Stream
Temperature (°C)	1150	475	1533	510	1533	420
Pressure bar	300	340	58.5	59.5	7.6	8
Mass flow (kg/h)	448670	58330	363190	238665	490385	239255

HPT (Coolant stream) / (Inlet flue gas) ratio = $58330/448670 = 0.13$

MPT (Coolant stream) / (Inlet flue gas) ratio = $238665/363190 = 0.657$

LPT (Coolant stream) / (Inlet flue gas) ratio = $239255/490385 = 0.488$

Table 8.2 shows that TIT in HPT is 1150° C less than TIT in MPT and LPT; therefore, the ratio of coolant stream to inlet fuel gas is higher than HPT. Turbine efficiencies of MPT and LPT are highly affected by the coolant stream, and it needs to be considered in the simulation and modelling of the CES cycle. The heat recovery section and BFW system include BFW economizer, Steam superheater, Inert gas heater, Regenerator heater, BWF pump, Deaerator drum. The Fuel gas condenser package and compressor package includes condenser package, fuel gas condensate pump, wet fuel gas compressors, and condensate separators intercooler. The CO₂ purification and compression section includes CO₂-rich gas compression, condensate separator, intercoolers, TSA (Temperature Swing Adsorption).

An ASU (Air Separation Unit) uses a substantial amount of oxyturbine plant energy. There are several methods to separate oxygen from the air, such as the cryogenic distillation process, membrane technology, and pressure swing adsorption. The ASU for the supercritical CES cycle is a cryogenic distillation process. In this process, the air is cooled to liquify then selectively distil nitrogen, oxygen, argon and other rare inert gases at their various boiling temperatures. The output of the ASU is oxygen with 97% purity and which is fed directly to the MP and LP combustor and compressed for the HP combustor.

The utility unit uses part of the energy of the cycle to provide an operation for the power plant; it includes a cooling system, natural gas receiving system, raw material system, demineralized water system, firefighting system and others.

8.1.2 CES supercritical plant modelling

The CES supercritical cycle is modelled with Aspen Plus software. Modelling of the CES supercritical power cycle requires the modelling of different components of the cycle.

A list of the main components for CES supercritical are below:

1. Supercritical carbon dioxide Oxyturbine cycle
2. Condenser and wet gas compressor
3. ASU (Air Separation Unit)
4. The natural gas receiving system
5. Carbon dioxide purification and compressor

A supercritical carbon dioxide Oxyturbine cycle unit, condenser unit and wet gas compressor unit are modelled. The ASU, natural gas receiving system and carbon dioxide purification and compressor are not modelled and data is collected from an IEA 2015 report (Mancuso *et al.*, 2015).

To model a supercritical carbon dioxide Oxyturbine cycle unit, the following list of components requires simulation and evaluation; HP, MP and LP Turbines, Compressors, BWF Pumps, Heat exchangers, Deaerator Drum.

Modelling a turbine with a cooled blade cannot be modelled directly with Aspen Plus blocks. An accurate model of turbine performance and output fluid specification is required to evaluate different parameters, including cooled flow temperature, cooled flowrate, blade design, cooling internal channels, cooling effectiveness, cooled flow pressure and heat exchange effectiveness. Cooled turbine efficiency is calculated by J.H Harlock (Horlock and Torbidoni, 2008a), and El-Marisi introduced a continued expansion model of the cooled turbine (El-Masri, 1986), and recently, Roberto Scaccabarozzi defined the adapted model of El-Marisi (Scaccabarozzi, Gatti and Martelli, 2016).

The turbine efficiency is assumed constant, and pressure drop of cooled blade turbine is not considered in turbine efficiency (Scaccabarozzi, Gatti and Martelli, 2014) Other components of the CES Power cycle can be modelled accurately with

Aspen Plus software blocks. The Peng Robinson Equation of State (EOS) is chosen for the Oxyturbine cycle model (Scaccabarozzi, Gatti and Martelli, 2017), and Lee-Kesler-Plocker Equation Of State (EOS) is preferred for Carbon Dioxide recompression modelling (Penkuhn and Tsatsaronis, 2016).

Figure 8.1 shows that natural gas fuel and the air is fed into the cycle, then water and carbon dioxide is produced as a by-product from the cycle. Table 8.3 shows the gas fuel composition of natural gas fuel, which is used in this simulation (Mancuso *et al.*, 2015):

Table 8.3. The natural gas mole fraction

The natural GAS mole fraction	
Ethan	0.89
Methane	0.07
Propane	0.01
Butane	0.1
Pentane	0.0001
Carbone Dioxide	0.002
Nitrogen	0.0089
Total	1
Gas fuel properties	
Temperature	15°C
Pressure	70 bars
LHV	46.502 MJ/kg

Oxygen is purified in the ASU; the outlet flow of the ASU composition and properties are in Table 8.4.

In this research, ASU is considered as a black box that is not modelled here:

Table 8.4. ASU Outlet mole fraction

ASU OUTLET mole fraction	
Oxygen	0.97
N ₂	0.01
AR	0.02
Properties	
Temperature	15°C
Pressure	30 bars

In this model, cold temperature for the condenser is 29 °C and COT (Combustion Outlet Temperature) of HPT is 1150 °C and MPT and LPT are 1533 °C so the Carnot efficiency can be calculated based on Equation 8-1.

Equation 8-1

$$\eta_c = 1 - \frac{T_C}{T_H} = 1 - \frac{302K}{1806K} = 0.832$$

The maximum efficiency (Carnot efficiency) of the CES cycle with the above condition is 83.2%. To increase Carnot efficiency, it is required to increase the maximum temperature or decrease the cold temperature of the condenser. Process Flow Diagram

(PFD) of a Supercritical Cycle with Aspen Plus is in Figure 8.2. Figure 8.3 shows full details of the Aspen Plus model flow diagram of the Oxyturbine power island in the Supercritical cycle showed in Figure 8.2.

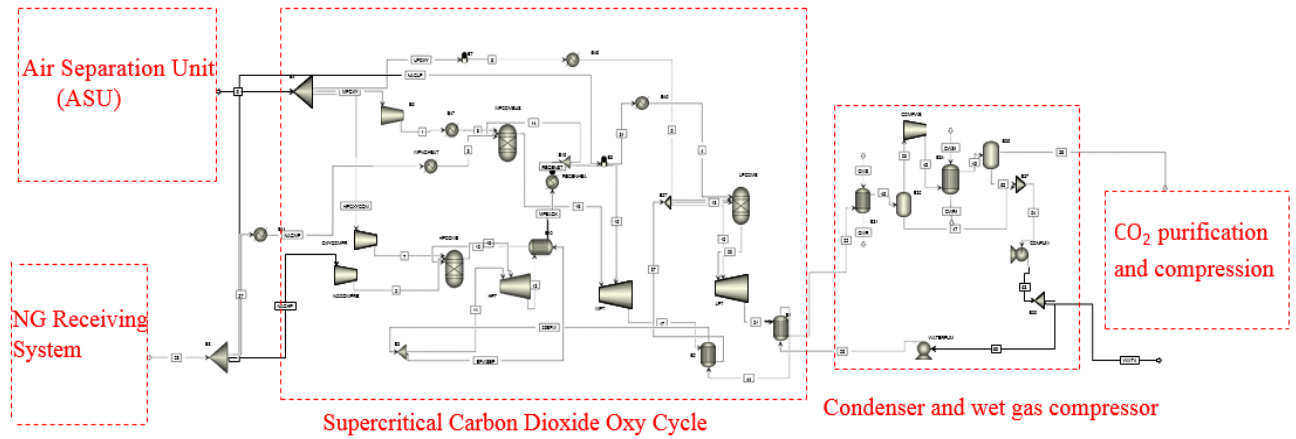


Figure 8.2. Aspen Plus modelling of Supercritical Oxyturbine cycle

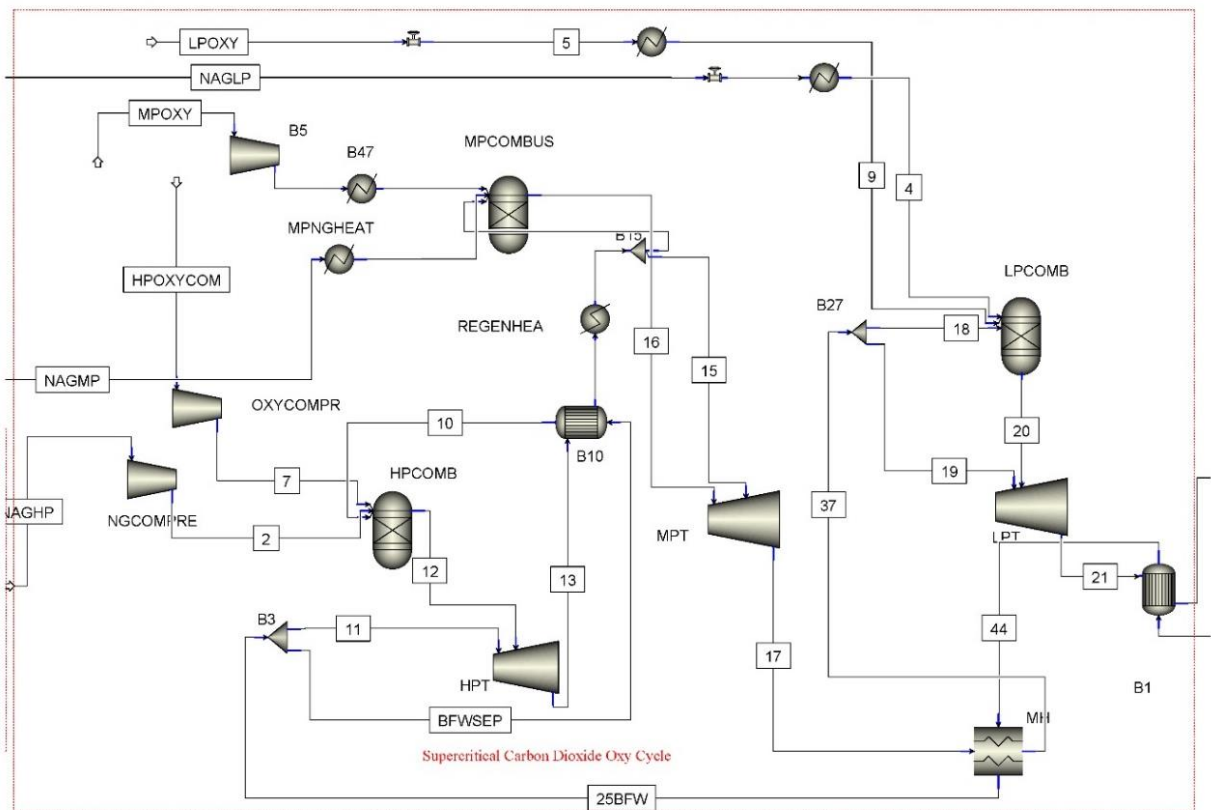


Figure 8.3. Aspen Plus model flow diagram of Oxyturbine power island in a Supercritical cycle

Table 8.5 shows the results of the simulation based on the assumption in this work in comparison with the IEA report data (IEAGHG, 2015).

Table 8.5. Comparing the results of the CES model with the IEA Report (IEAGHG, 2015)

STREAM	TEMPERATURE (C)		PRESSURE (BAR)		MOLE FRACTION OF CO ₂	
	[IEA report]	This work	[IEA report]	This work	[IEA report]	This work
2	28	30.85	112.2	112.20	0	0.00
4	15	15.00	5	5.00	0	0.00
5	506.2	525.03	106.6	106.60	0	0.00
7	394.7	406.90	106.6	106.60	0	0.00
9	509	518.00	9.9	9.90	0.061	0.14
10	15	15.00	5	5.00	0	0.00
11	96.6	99.87	9.9	9.90	0	0.00
12	15	15.00	3	3.00	0	0.00
13	131.2	135.55	9.9	9.90	0	0.00
15	493.3	505.19	0.11	0.11	0.099	0.20
16	58	58.00	0.105	0.11	0.099	0.20
17	27	27.00	0.1	0.10	0.707	0.64
18	249.4	252.58	1.05	1.05	0.707	0.64
19	27	27.00	1	1.00	0	0.00
20	27	27.00	1	1.00	0.97	0.97
21	221.8	221.75	8.88	8.88	0.97	0.97

An accurate model needs to access all databases from previous literature to obtain the best comparison. The reason for the difference between the model and the IEA report is the unknown efficiency of the cooled turbine, compressor, and pump, which are assumed by the author.

The sensitivity analysis of the cycles was carried out to study the effect of the following parameters on cycle efficiency.

1. TIT (Turbine Inlet Temperature)
2. COP (Combustion Outlet Pressure)
3. Heat exchanger effectiveness

8.1.3 Sensitivity analysis of TIT for Supercritical CES (S-CES) cycle

Natural gas burns in combustion with nearly pure oxygen, and Recycle Water Flow (RWF) controls the temperature of combustion. It is required to change both natural gas rate and Oxygen flow rates to change the temperature of combustion. If the natural gas flow rate is increased, but the oxygen flowrate is not changed, then the temperature will be decreased because natural fuel gas is burned with oxygen at a stoichiometry rate.

The TIT diagram of the Supercritical cycle for HPT is shown in Figure 8.4. The diagram shows that the TIT is increased when the natural gas fuel rate for the HP Turbine and oxygen fuel rate increase simultaneously, and the stoichiometry ratio is constant. Therefore efficiency is increased, as shown in Figure 8.4.

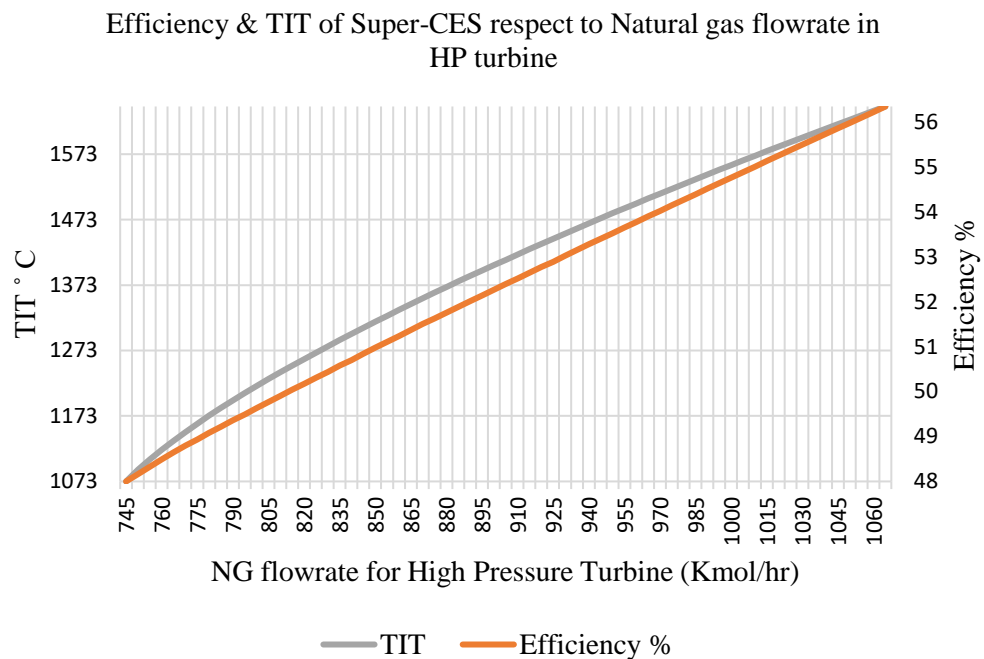


Figure 8.4. Efficiency & TIT of Super-CES with respect to Natural gas flowrate in HP turbine

TIT (LP,MP,HP) Turbine vs Natural gas flowrate

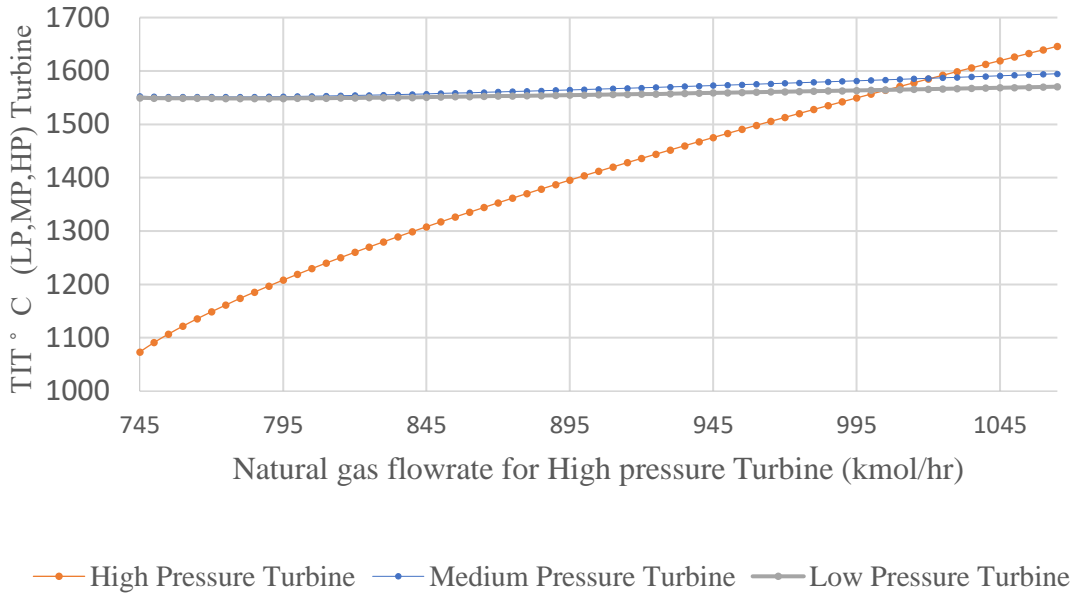


Figure 8.5. TIT (LP, MP, HP) Turbine with respect to Natural gas flowrate

TIT diagram of the Supercritical cycle for MPT is shown in Figure 8.5; the diagram shows that TIT is increased when the natural gas fuel rate for the HP Turbine and oxygen fuel rate is increased simultaneously. Therefore, the cycle efficiency is increased, as shown in Figure 8.6.

Sensitivity of natural gas flowrate (LPT,MPT,HPT) to efficiency

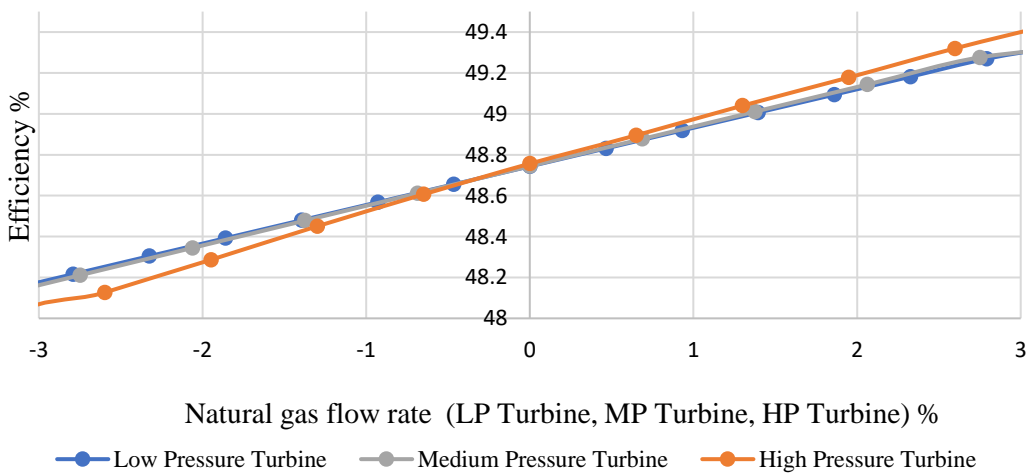


Figure 8.6. the Sensitivity of natural gas flowrate (LPT, MPT, HPT) to efficiency

This can be explained that by increasing TIT, the network of the cycle will increase despite increasing pump and cooling losses. The metallurgical limitation of the turbine cooled blade causes a constant maximum value of the TIT (A K Tiwari, 2012). The results shown most recently by (Kaviri, Jaafar and Lazim, 2012) are the combustion chamber exergy destruction can be reduced with increasing the TIT. Energy destruction and entropy are increased at lower TIT. Total exergy destruction in the cycle with TIT of 1527 °C is about 45% lower than a cycle with TIT=1427 °C. The specific network efficiency is increasing significantly with increasing TIT. Furthermore, the best coolant is steam cooling for a TIT higher than 1427 °C, and it is better than other cooling methods such as air cooling (A K Tiwari, 2012).

8.1.4 Sensitivity analysis of COP for Supercritical CES (S-CES) cycle

Another important parameter of the power plant cycle is pressure; The supercritical CES cycle pressure can be increased with the increasing pressure of Recycle Water Pump (RWP) Figure 8.7.

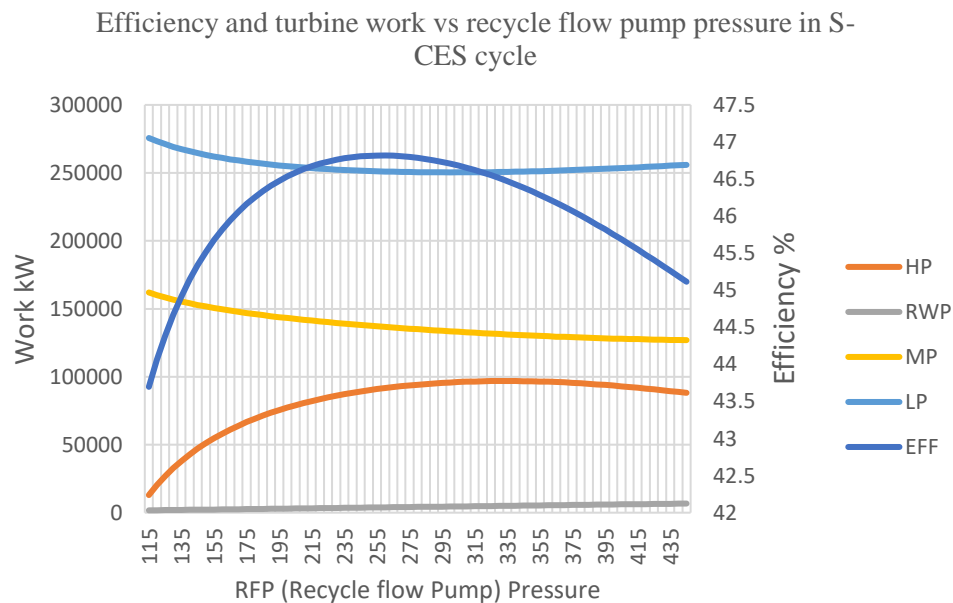


Figure 8.7. Efficiency vs recycle water pump pressure for S-CES cycle

Currently, Kaviri shows that an increase in the compressor pressure ratio decreases the cost of exergy destruction (A K Tiwari, 2012). The reason is that by increasing the compressor ratio, the outlet temperature is increased. So, the temperature difference

decreases because the cost of exergy destruction is a direct function of exergy destruction.

8.1.5 Sensitivity analysis of cooling water temperature in the heat exchanger

Cooling water temperature affects the minimum temperature of the cycle, so the Carnot efficiency of the cycle is related to cooling water temperature. However, increasing the cooling water temperature causes a higher temperature for Recycle Water Flow (RWF), combustion temperature and Turbine Inlet Temperature (TIT). Figure 8.8 shows that when the cooling water temperature is increased from 5 °C to 29 °C, the efficiency of the cycle is increased. Efficiency is decreased rapidly for cooling water temperature more than 29 °C. It's because of the design point of the cooling water heat exchanger, and high temperature cannot cool the stream in the heat sink.

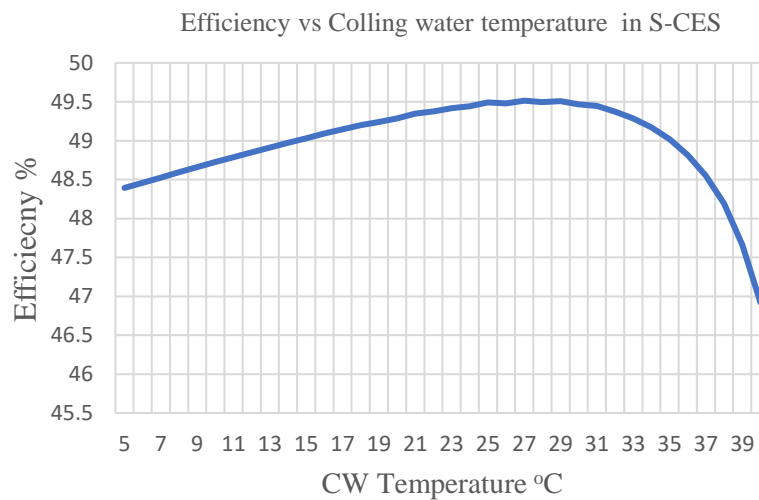


Figure 8.8. Efficiency vs cooling water temperature in S-CES

8.2 NetPower cycle

The NetPower cycle (Allam cycle) has supercritical CO₂ as a working fluid providing integrated high-efficiency Brayton cycle. NetPower cycle is introduced with Rodney Allam. The cycle is an oxy-combustion cycle with a working fluid of Carbon dioxide. The NetPower cycle working flow is mainly carbon dioxide in a high-

pressure, and Turbine Inlet Pressure (TIP) is approximately 300 bar. It is highly recuperated.

The NetPower cycle is a Bryton cycle (Allam *et al.*, 2013). The NetPower cycle combustor burns natural gas with pure oxygen supplied from an ASU (Air Separation Unit) and high-pressure carbon dioxide stream inlets recycled from its power turbine. Recycle Fuel Gas (RFG) is heated with a recovery heat exchanger and flows to the combustor to reduce the Combustion Outlet Temperature (COT) by diluting the combustion products. The RFG flowrate controls the temperature of combustion at an acceptable level. The direct-fired supercritical carbon dioxide (SCO₂) turbine is cooled with a cooling stream from the heat exchanger. The exhaust gas at 740°C enters the recuperating heat exchanger that transfers heat from the hot outlet turbine exhaust gas to the three-cycle streams. This includes the carbon dioxide-rich stream recycled to the combustor for moderating the temperature of the combustor, the oxidant stream recycled to the combustor and the carbon dioxide-rich stream for cooling turbine blades. Also, the hot compressed air stream from the ASU enters the recuperating heat exchanger for recovering its heat.

The cryogenic ASU provides the required oxygen for combustion. The Heat exchanger's maximum pressure limit is 120 bar; therefore, oxygen cannot enter the heat exchanger at high pressure. The oxygen flow is mixed with part of the supercritical recycled CO₂ with oxygen concentrations in the range of 10–30% (molar basis) and then compressed to the required pressure by a dedicated O₂/CO₂ dense phase compressor. Before entering the combustor, the oxidant mixture is preheated in the regenerator (Scaccabarozzi, Gatti and Martelli, 2016).

The heat exchanger is one of the main parts of the NetPower cycle, and it has a main role in the NetPower cycle's efficiency. The exhaust gas from the heat exchanger is cooled down, and the carbon dioxide is separated from the water. The water is sent to the wastewater treatment for recovery and treatment. A portion of the carbon dioxide stream from the water separation unit is fed for purification and compression unit. Most of the carbon dioxide is compressed and recycled back.

The recycled gas compression loop includes four stages inter-cooled compressors and two inter-cooled pumping stages. Inter-cooling is with cooling water. The carbon dioxide stream is divided into three parts; 45-50% of the flow rate is pumped to 305

bar and preheated in the recuperating heat exchanger. 10-12% of the flow rate is heated in the heat exchanger to 400 °C, then it is sent to the turbine for cooling the blade.

The 32% to 45% of carbon dioxide stream is mixed with high purity oxygen. The oxidant stream is heated in the heat exchanger up to 720 °C , and it is sent to combustion to burn fuel (Mancuso *et al.*, 2015).

The critical features of the oxy turbine are:

1. The inlet pressure is rather high.
2. The blades and shell are cooled because of the high TIT (Turbine Inlet Temperature).
3. Unconventional working fluid. (Scaccabarozzi, Gatti and Martelli, 2017)

As for blade cooling, NET Power is proposed to use a classic open-circuit blade cooling system. Blades are cooled by the convection method, and there is a Thermal Barrier Coating (TBC) on the blades to protect them from high temperature and corrosion (Allam *et al.*, 2013). The heat transfer coefficient of CO₂ is significantly high; therefore, film cooling for today’s gas turbine is appropriate (Allam *et al.*, 2013).

8.2.1 NetPower plant modelling

The NetPower cycle is modelled with Aspen Plus software, The PFD of the NetPower cycle modelled with Aspen Plus is shown in Figure 8.9 and Figure 8.10.

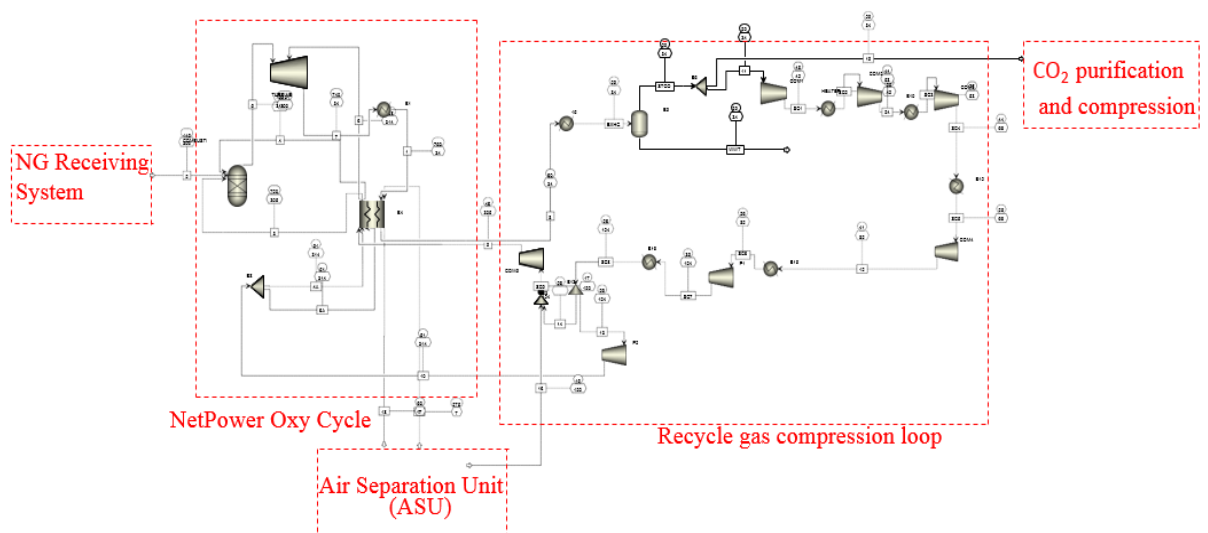


Figure 8.9. Schematic modelling NetPower cycle with Aspen Plus

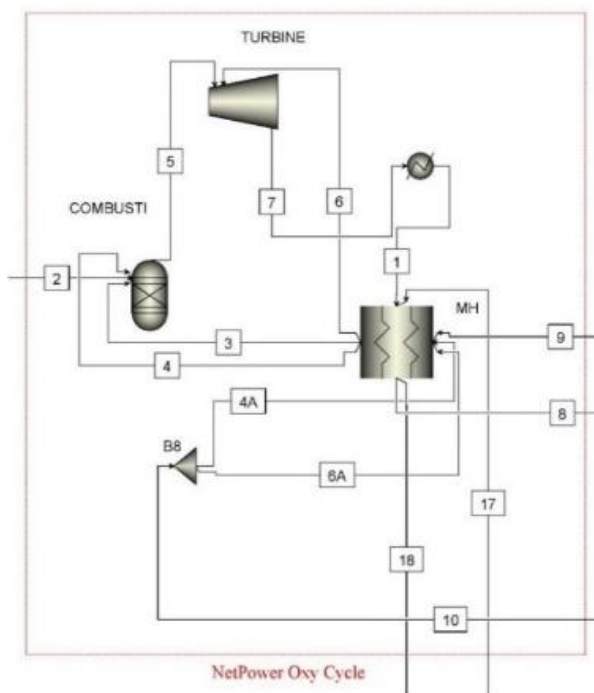


Figure 8.10. Oxyturbine cycle for NetPower cycle

Table 8.6 shows the comparison of the NetPower cycle modelled in Aspen Plus with IEA 2015 report. The calculated efficiency is 55.1% in Aspen Plus Model, which is approved by the IEA report.

Table 8.6. Results of NetPower compared with the data published in the IEA 2015 report

Stream	Composition (% mole)										Total Flow Mmol/hr	Total Flow Mmol/hr (IEA)	Temp C	Temp C (IEA)	Pressure bar	Pressure bar (IEA)
	AR	AR (IEA)	CO ₂	CO ₂ (IEA)	H ₂ O	H ₂ O (IEA)	N ₂	N ₂ (IEA)	O ₂	O ₂ (IEA)						
3	0.53	0.53	84.92	84.94	0.13	0.13	1.05	1.05	13.37	13.34	52.30	52.30	720.00	720.00	303.04	303.00
4	0.57	0.57	97.86	97.88	0.15	0.15	1.18	1.18	0.24	0.21	52.30	52.30	720.00	720.00	303.08	303.00
5	0.53	0.53	91.78	91.80	6.35	6.36	1.11	1.11	0.23	0.20	108.00	108.05	1150.82	1150.00	300.00	300.00
6	0.57	0.57	97.86	97.88	0.15	0.15	1.18	1.18	0.24	0.21	11.93	11.93	398.00	<400	303.08	303.00
7	0.54	0.54	92.39	92.41	5.73	5.74	1.12	1.12	0.23	0.20	120.00	119.99	739.98	740.00	33.99	34.00
8	0.54	0.54	92.39	92.41	5.73	5.74	1.12	1.12	0.23	0.20	120.00	119.99	59.04	55.00	33.99	33.00
9	0.53	0.53	84.92	84.94	0.13	0.13	1.05	1.05	13.37	13.34	52.30	52.30	45.65	45.00	305.04	305.00
10	0.57	0.57	97.86	97.88	0.15	0.15	1.18	1.18	0.24	0.21	64.23	64.23	50.92	50.00	305.08	305.00
17	0.92	0.92	0.04	0.04	0.97	0.97	77.32	77.32	20.75	20.75	34.46	34.46	275.00	275.00	7.50	7.50
18	0.92	0.92	0.04	0.04	0.97	0.97	77.32	77.32	20.75	20.75	34.46	34.46	59.04	55.00	7.50	7.30

8.2.2 Sensitivity analysis of the TIT for the NetPower cycle

The Recycle flow of the supercritical CO₂ controls the temperature of the combustor. The recycled stream is preheated in the multi-stream heat exchanger before the inlet to the combustor. By increasing the pressure of the RGF compressor, the combustion outlet pressure (COP) is increased. Figure 8.11 shows increasing the COP causes an increased efficiency of the NetPower cycle.

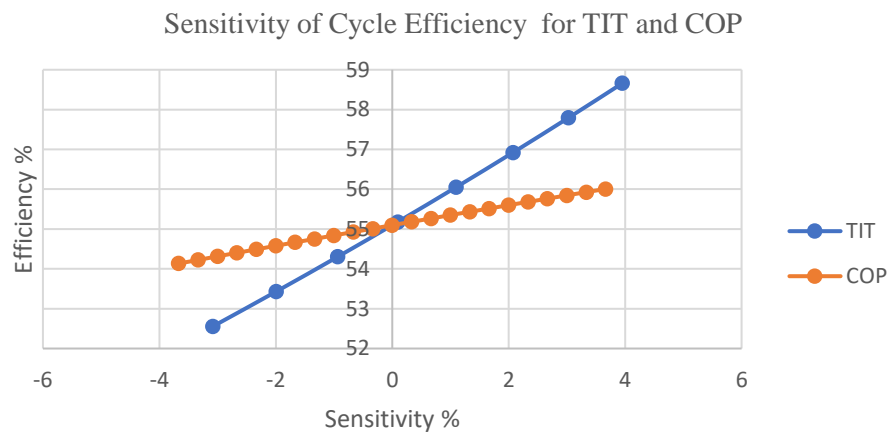


Figure 8.11. The efficiency of NetPower cycle vs TIT

8.2.3 Sensitivity analysis of heat exchanger for NetPower cycle

The heat exchanger on the NetPower cycle is a compact multi-channel plate-fin design or a printed circuit in Nickel-alloy (e.g., Alloy 617) (Mancuso *et al.*, 2015). Heatric company has supplied four Printed Circuit Heat Exchangers (PCHEs) for NetPower to commission the 50 MW demonstration plant in Texas (Heat, 2018).

The recovery heat exchanger is modelled with a multi-stream heat exchanger MHeatX block in Aspen Plus. This block calculates heat duty between multi hot and cold streams. Furthermore, it calculates the overall UA (overall heat transfer coefficient) for the exchanger, minimum approach temperature ΔT_{min} , Number of Transfer Units (NTU), analyses a detailed zone analysis and composite curve (Machner, 1958). The heat exchanger is an important component in the NetPower cycle to affect efficiency. The ΔT_{min} for the heat exchanger is changed from 0°C to

20°C, and the diagram of power cycle efficiency related to ΔT_{min} is shown in Figure 8.12 (Varasteh and Darabkhani, 2018).

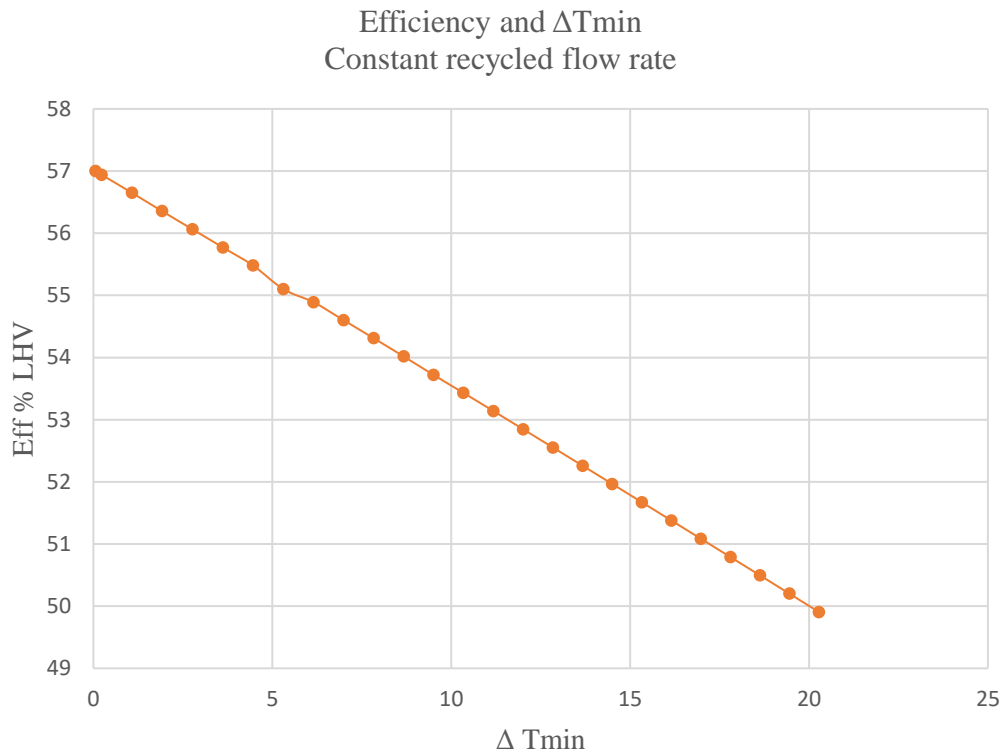


Figure 8.12. Efficiency related to ΔT_{min} for constant recycled flow rate

8.3 Compare TIT sensitivity for CES and NetPower cycle

The results of the TIT sensitivity for the S-CES cycle and the NetPower cycle were shown in Figure 8.13. The slope of cycle efficiency was higher in the NetPower cycle, which could be explained by the higher impact that the TIT produced in the turbine and the main heat exchanger for the NetPower cycle.

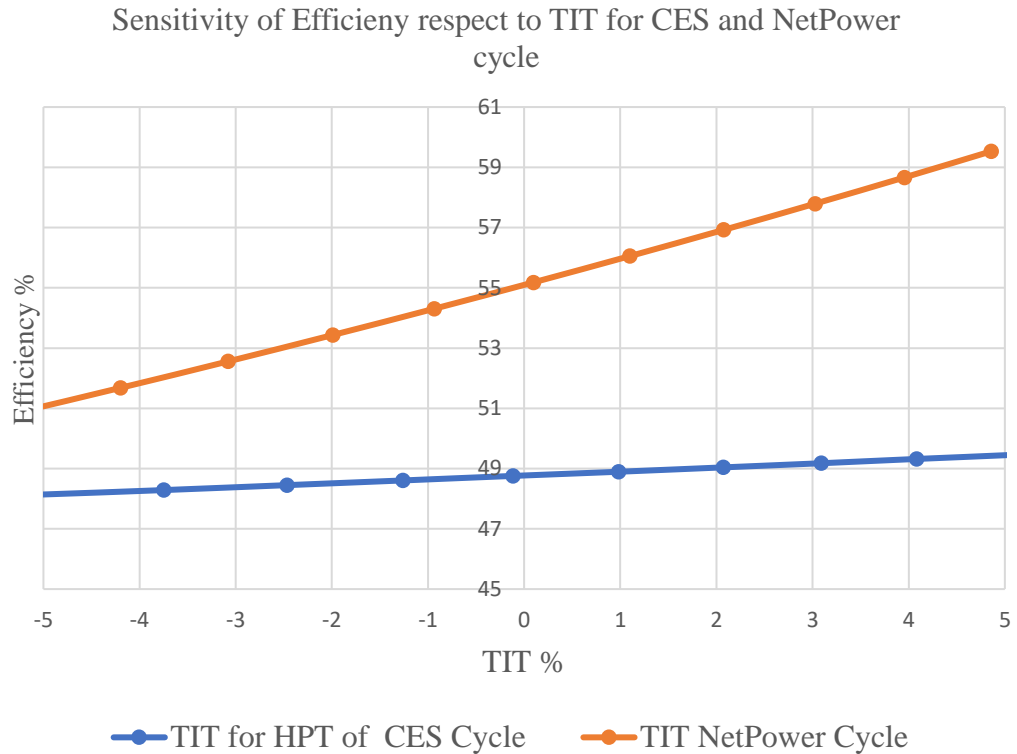


Figure 8.13. The sensitivity of cycle efficiency with respect to TIT for HPT of CES and NetPower cycle

8.4 Pilot and industrial demonstration of Oxyturbine power cycles

8.4.1 Oxy combustion cycle demonstration

Although the technologies are developed for oxy-fuel combustion equipment, there are gaps in the knowledge for practical and commercial demonstration of the power plant. The cost of the carbon dioxide capture, storage and utilization are essential for demonstration. In the operating stage, the higher efficiency, control strategies, capture process with optimism operation, reducing energy requirement for carbon dioxide capture and system reliability need to be tested and improved.

The life cycle and environmental problems of the carbon dioxide capture, transportation, storage or utilization should be reevaluated and needed to investigate more for oxy-fuel combustion power plants (Authors *et al.*, 2010).

The main two leading oxy-combustion plants are NetPower and CES power plants which are in the demonstration phase.

The NetPower cycle has established a 50 MW demonstration power plant in Texas, and the power plant is under operation now; and NetPower has planned to bring a 300 MW plant online in 2022 (Patel, 2019).

Clean energy system company developed CES cycle, 5MW CES Power plant established at the CES test site in Kimberlina, CA in August 2003. CES company has planned to construct a 50 MW oxy-combustion power plant in southern California.

8.5 Summary

Based on the analysis of the CES and the NetPower cycles, real plant investment decisions are affected by technology and regional characteristics as below:

- The results of the TIT sensitivity for the S-CES cycle and the NetPower cycle indicate that the slope of cycle efficiency was higher in the NetPower cycle, which could be explained by the higher impact that the TIT produced in the turbine and the main heat exchanger for the NetPower cycle.
- Increasing recycle flow pressure increases efficiency in the NetPower cycle, but efficiency is decreased in the S-CES cycle because more work is required for the RWF.
- Cooling water temperature affects the minimum temperature of the S-CES cycle; this leads to an increase in efficiency until it reaches the maximum point and then decreases.
- The main heat exchanger (Network Heat Exchanger) of the NetPower cycle has a significant effect on efficiency. Decreasing ΔT_{min} causes an increase in cycle efficiency.
- The analysis also indicates that TIT, COP, and heat exchanger effectiveness are the main parameters affecting cycle efficiency. To evaluate cycle parameters more accurately, an ad-hoc model of cooled turbine and heat exchanger is required instead of using a simplified block of Aspen Plus software.

As future work, An accurate model of a cooled blade turbine and heat exchanger need also be developed for precise sensitivity analysis and optimization of the power cycle parameters. The NetPower is more flexible in operation than a combined cycle, and it is projected to be more economical without tax on carbon (Flin, 2019).

CES company modified a traditional gas turbine to operate with Steam/CO₂ drive gas rather than an air-based drive gas. CES technology enables the turbine to extract three times more power than a conventional gas turbine (CES, 2020b).

Chapter 9: Techno-economic, Technology Readiness Level (TRL) and parametric comparison in Oxyturbine Power cycles

9.1 Introduction

Oxy-combustion cycles are necessary to especially advance the technologies (van der Spek, Ramirez and Faaij, 2017); during last two decades, the oxy-combustion cycles technologies are developed, and some of the technologies have proceeded to commercial state, (Van Der Spek *et al.*, 2017); however, there is a gap in comparison of available oxy-combustion technologies.

This chapter aims to compare the oxy-combustion cycles in term of parameters, technology readiness level (TRL), performance and economy. The cycle parameters, including Turbine Inlet Temperature (TIT), Turbine Outlet Temperature (TOT), Combustion Outlet Pressure (COP), thermal and exergy efficiency, carbon dioxide per KWh of electricity, are studied and compared in detail. Also, the Technology Readiness Level (TRL) are assessed in detail and compared. Then, the performance, cost rates and LCOE for oxy-combustion cycles are analysed and compared, and the radar diagram is drawn to compare all deliberated parameters.

9.2 TIT comparison of oxy-combustion cycles

Turbine Inlet Temperature (TIT) is an important parameter of the oxy-combustion cycle; TIT can affect oxy-combustion cycle performance, Higher TIT can increase the net power output of the cycle and increase the efficiency (Calli, Colpan and Gunerhan, 2018); however, higher TIT can be achieved by the development of gas turbine technologies including development of cooling blade system, new materials for

thermal barrier coating (TBC) for turbine blade, blade construction and layering (Higher temperatures in turbines - Kraftwerk Forschung, 2020)

The turbine blade cooling system is one of the technology to increase Turbine Inlet Temperature (TIT); however, it causes energy losses in the turbines and lower aerodynamic efficiency; hence it has a negative impact to efficiency (Horlock and Torbidoni, 2008b)

Table 9.1 shows TIT for each oxy-combustion cycle, It's combined from modelling and data extracted from literature, and the TIT of S-CES is high (1533°C). Hence, this cycle need developed technology for a gas turbine blade. Clean energy system company with collaboration by Siemens Energy and Florida Turbine Technologies (FTT) and sponsored by the Department of Energy recently developed OFT-900 oxy-fuel turbine and can reach to highest temperature up to 1976°C (Clean Energy System, 2020b) and CES Power cycle is in the demonstration stage. The Novel O₂/CO₂ (Cao and Zheng, 2006) cycle also has 1573 °C TIT, this cycle is not in the demonstration stage, and more development of technologies is required. NetPower cycle TIT temperature is 1150 °C, and Toshiba ESS delivered the turbine and combustor, which are the system's crucial components.

As shown in Figure 9.1, the highest TIT s belongs to the S-CES and Novel O₂/CO₂; the gas turbine with high TIT needs blade-cooling and developed technology. The efficiency of the turbine can be increased by developed technologies for cooling blade and blade thermal barrier coating.

NetPower TIT is lower than S-CES and this can be the advantage of the cycle in comparison with S-CES, and it has less dependency on the new technology for cooling blade and blades thermal barrier coating; however, the gas turbine needs new technology for high purity CO₂ working flow.

AZEP 100% and 80% have lower TIT in comparison with other cycles, so the technology development in the cooling blade and blade thermal coating barrier cannot increase the efficiency of the cycle considerably.

Table 9.1 TIT of oxy-combustion cycles

Oxy-Combustion cycle	TIT °C (ref) (Turbine Inlet Temperature)
SCOC-CC (Sammak <i>et al.</i> , 2012)	Steam Turbine=600 Gas Turbine= 1400
COOPERATE (Yantovski, 1996)	High-Pressure Turbine=800 Medium-Pressure Turbine=1250 Low-Pressure Turbine=1250
E-MATIANT (Mathieu, 2005)	1300
CC_MATIANT	High-Pressure Turbine=600 Intermediate-Pressure Turbine=1300 Low-Pressure Turbine=1300
Graz cycle (Wolfgang Sanz <i>et al.</i> , 2005)	High-Temperature Turbine = 1400 High-Pressure turbine= 567 Low-Pressure turbine=160
S-Graz cycle (Jericha, Sanz and Göttlich, 2008a)	High-Temperature Turbine = 1400 High-Pressure turbine= 549 Low-Pressure turbine= 544
Modified-Graz Cycle (Jericha, Sanz and Göttlich, 2008a)	High-Temperature Turbine = 1400 High-Pressure turbine= 550 Low-Pressure turbine=175
AZEPT 100% (Möller <i>et al.</i> , 2005)	MCM outlet Temperature =1200 Air Gas Turbine=700(Foy and Yantovski, 2006) 3 Stages Steam Turbine=510/485/240
AZEP 85% (Möller <i>et al.</i> , 2005)(Petrapoulou <i>et al.</i> , 2010)	MCM outlet Temperature =1200 Air Gas Turbine=1327 3 Stages Steam Turbine=510/485/240
ZEITMOP	High-Pressure Turbine=678 Low-Pressure Turbine=1400 Air Turbine=841
COOLCEP-S (Zhang <i>et al.</i> , 2010)	Gas Turbine= 900
COOLCEP-C (Zhang <i>et al.</i> , 2010)	Gas Turbine= 900
Novel O ₂ /CO ₂ (Cao and Zheng, 2006)	Gas Turbine=1573
NetPower cycle (IEAGHG, 2015)	Gas Turbine=1150
S-CES (IEAGHG, 2015)	High-Pressure Turbine=1150 Medium-Pressure Turbine=1533 Low-Pressure Turbine=1533
NGCC with post-combustion (Mondino <i>et al.</i> , 2019)	GT Temperature=1504.5 High-Pressure Steam turbine=600 Intermediate-Pressure Steam Turbine=600 Low-Pressure Steam Turbine=72.32

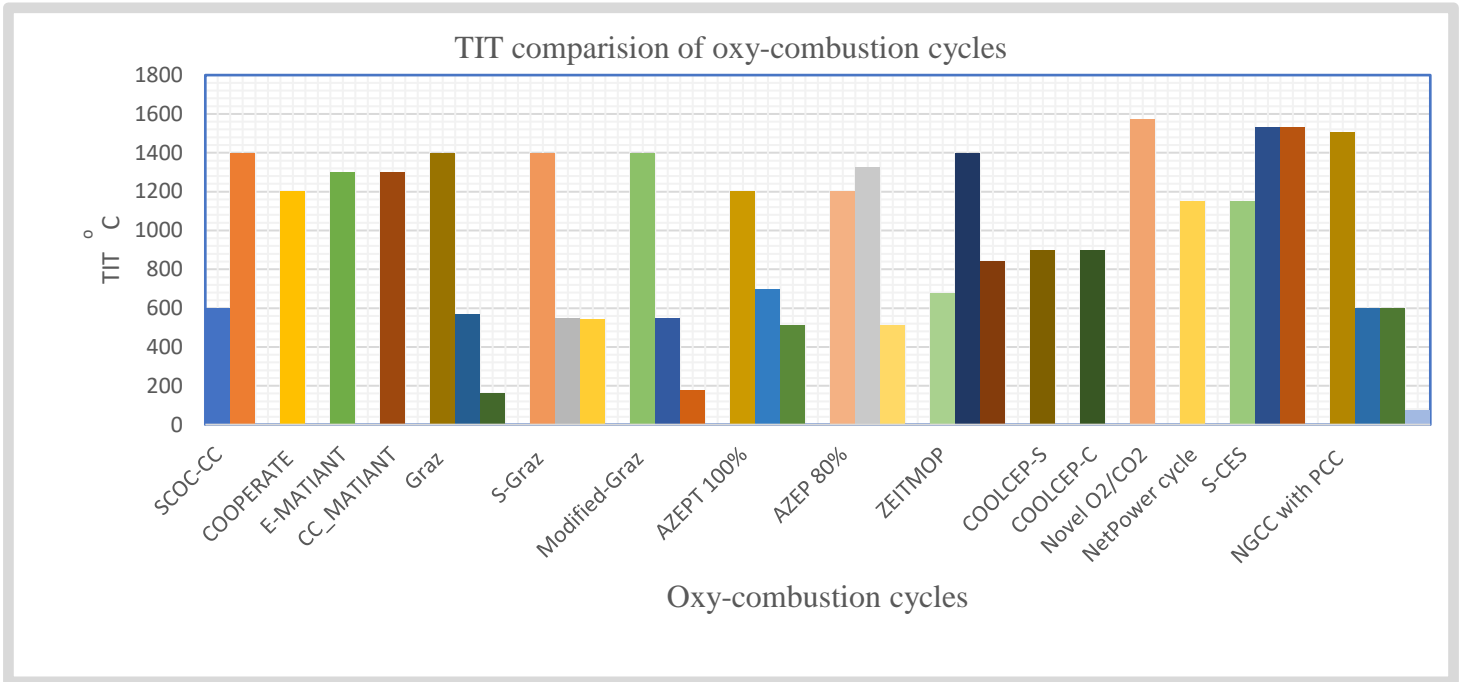


Figure 9.1 TIT comparison of Oxy-combustion cycles

9.3 TOT comparison of oxy-combustion cycles

The TOT of the gas turbine depends on TIT and turbine efficiency. The highest turbine efficiency causes the lowest Turbine Outlet Temperature (TOT).

Table 9.2 shows the TOT of the oxy-combustion cycle. TOT of the high-pressure turbine for S-CES is 740 °C, and the exhaust of the turbine reheat and expand in the medium-pressure turbine, and TOT of the Low-pressure Turbine for S-CES is 560 °C, and the working flow of exhaust of LPT has proper temperature for recovering. Hence the heat exchanger is used after LPT. Novel O₂/CO₂ has 1192 °C TOT, hence working flow has a high quality of energy, and the reformer is used to recover energy.

TOT of the NetPower cycle is 740 °C, the working flow of the turbine exhaust also has high-quality energy, and the energy is recovered in the main heat exchanger (Network Heat Exchanger).

Table 9.2 Turbine Outlet Temperature (TOT) of oxy-combustion cycle

Oxy-Combustion cycle	TOT (Turbine Outlet Temperature) °C
SCOC-CC (Sammak <i>et al.</i> , 2012)	Steam Turbine=29 Gas Turbine= 619
COOPERATE (Yantovski, 1996)	High-Pressure Turbine=500 Medium-Pressure Turbine=1000 Low-Pressure Turbine=900
E-MATIANT (Mathieu, 2005)	High-Pressure Turbine= 900 Low-Pressure Turbine =1100
CC_MATIANT (Mathieu and Nihart, 1999)	High-Pressure Turbine=350 Intermediate-Pressure Turbine=1100 Low-Pressure Turbine=950
Graz cycle (Wolfgang Sanz <i>et al.</i> , 2005)	High-Temperature Turbine =579 High-Pressure turbine= 330
S-Graz cycle (Jericha, Sanz and Göttlich, 2008a)	High-Temperature Turbine = 584
Modified-Graz Cycle (Jericha, Sanz and Göttlich, 2008a)	High-Temperature Turbine = 573
AZEPT 100% (Gicquel, 2018)	Gas Turbine=770 Air Turbine=521 3 Stages Steam Turbine=36
AZEP 85% (Petraokopoulou, 2010)	Air Gas Turbine=578.8 3 Stages Steam Turbine=315/315/44
ZEITMOP	High-Pressure Turbine= 375 Low-pressure Turbine =856 Air Turbine=241
COOLCEP-S (Zhang <i>et al.</i> , 2010)	Gas Turbine= 700
COOLCEP-C (Zhang <i>et al.</i> , 2010)	Gas Turbine= 500
Novel O ₂ /CO ₂ (Cao and Zheng, 2006)	Gas Turbine= 1192
NetPower cycle (IEAGHG, 2015)	Gas Turbine=740
S-CES (IEAGHG, 2015)	High-Pressure Turbine=740 Medium-Pressure Turbine=790 Low-Pressure Turbine=560
NGCC with post-combustion (Mondino <i>et al.</i> , 2019)	GT Temperature=646.9

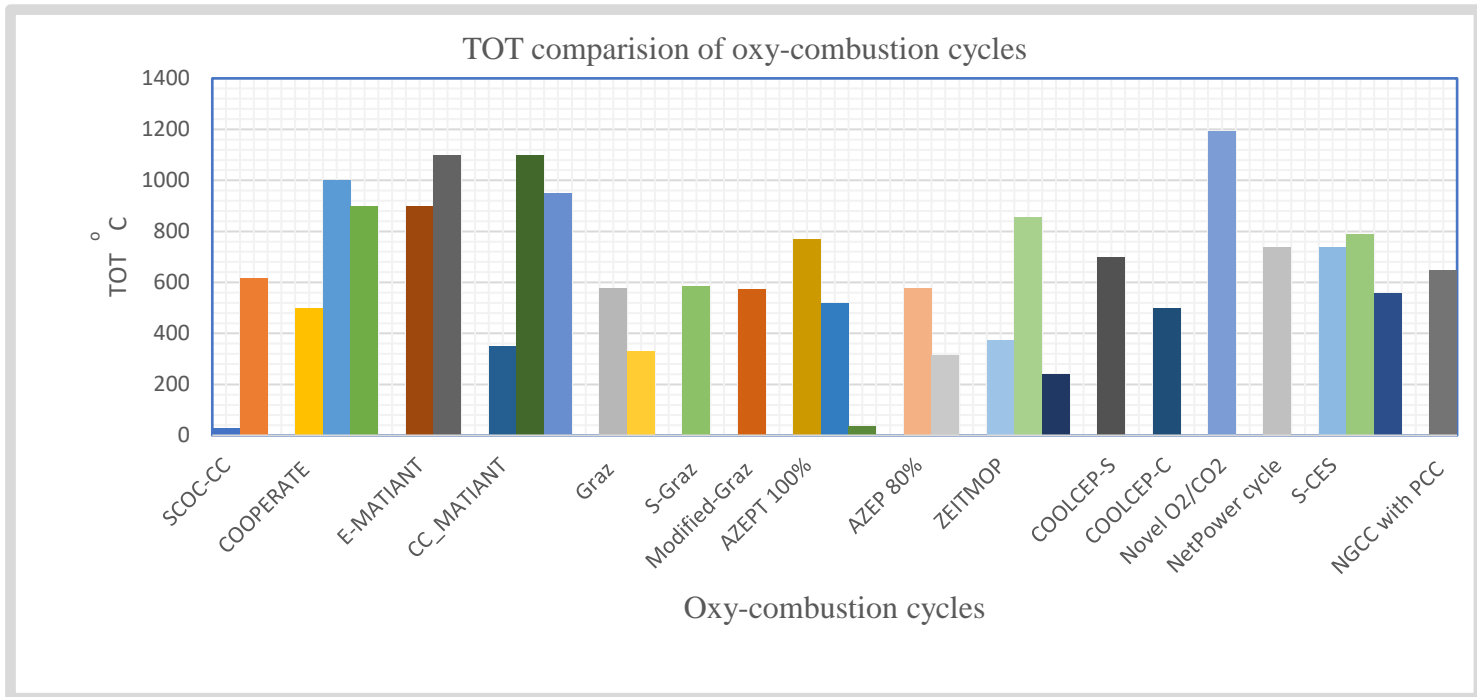


Figure 9.2 TOT Comparison of oxy-combustion cycle

As shown in Figure 9.2, the SCOC-CC, NetPower and S-CES have high turbine efficiency and lower TOT, but the Novel O₂/CO₂, E-MATIANT, CC-MATIANT, and COOPERATE cycle need to develop their turbine technology and efficiency to reduce their TOT. However, the high TOT is useful for heat recovery downstream; high temperature can raise the heat exchanger efficiency, and these cycles are useful for heat exchanger and heat recovery and steam generation (HRSG).

9.4 COP (Combustion Outlet Pressure) comparison of oxy-combustion cycles

The overall efficiency of the oxy-combustion cycle can be improved by increasing the pressure ratio, increasing turbine inlet temperature and reducing condensation temperature (Boyce and Chen, 1974). In addition, combustion efficiency significantly increases in the higher pressure. The high pressure and temperature in the combustion can reduce CO emission. However, it may increase NO_x emission (Yan *et al.*, 2018), but nitrogen is not available in oxy-fuel combustions, so it would be another advantage for them for working in high pressure and temperature. Table 9.3 shows the

Combustion Outlet Pressure COP of the oxy-combustion cycle. S-CES has COP of 300 bar for high-Pressure Combustor; CES developed technology for high-pressure combustion, including Direct Steam Gas Generator (CES, 2020a). COP of NetPower cycle is 300 bar, and this cycle was demonstrated recently, and Toshiba developed the combustion technology.

Table 9.3 Combustion Outlet Pressure (COP) of Oxy-combustion cycle

Oxy-Combustion cycle	COP (bar)
SCOC-CC (Thorbergsson and Grönstedt, 2016)	Gas Turbine= 44.5
COOPERATE (Yantovski, 1996)	High-Combustion Pressure =210 bar Medium-Combustion Pressure =60 bar Low-Combustion Pressure =15 bar
E-MATIANT (Mathieu, 2004)	High-Combustion Pressure = 60 Reheat Pressure= 12
CC_MATIANT (Mathieu and Nihart, 1999)	High-Combustion Pressure=300 Intermediate-combustion pressure=40 Reheat Pressure=9.7
Graz cycle (Jericha, Sanz and Göttlich, 2008b)	High-Temperature Turbine = 40 High-Pressure turbine= 180 Low-Pressure turbine=1
S-Graz cycle (Jericha, Sanz and Göttlich, 2008a)	High-Temperature Turbine =40 High-Pressure turbine= 180 Low-Pressure turbine=1.05
Modified-Graz Cycle (Jericha, Sanz and Göttlich, 2008a)	High-Temperature Turbine = 40 High-Pressure turbine= 180 Low-Pressure turbine=
AZEPT 100% (Möller <i>et al.</i> , 2005)	Air Gas Turbine=17 3 Stages Steam Turbine=70
AZEP 85% (Petrakopoulou, 2010)	Air Gas Turbine=16.81 3 Stages Steam Turbine=124/134.56/4.1
ZEITMOP (Foy and McGovern, 2007)	High-Pressure Turbine= 210 Low-pressure Turbine =15 Air Turbine=15
COOLCEP-S (Zhang <i>et al.</i> , 2010)	Gas Turbine= 70
COOLCEP-C (Zhang <i>et al.</i> , 2010)	Gas Turbine= 70
Novel O ₂ /CO ₂ (Cao and Zheng, 2006)	Gas Turbine= 10
NetPower cycle (IEAGHG, 2015)	Gas Turbine=300
S-CES (IEAGHG, 2015)	High-Pressure Turbine=300 Medium-Pressure Turbine=59.5 Low-Pressure Turbine=7.6
NGCC with post-combustion (Mondino <i>et al.</i> , 2019)	GT Temperature=39.29 High-Pressure Steam turbine=186 Intermediate-Pressure Steam Turbine=30 Low-Pressure Steam Turbine=0.3447

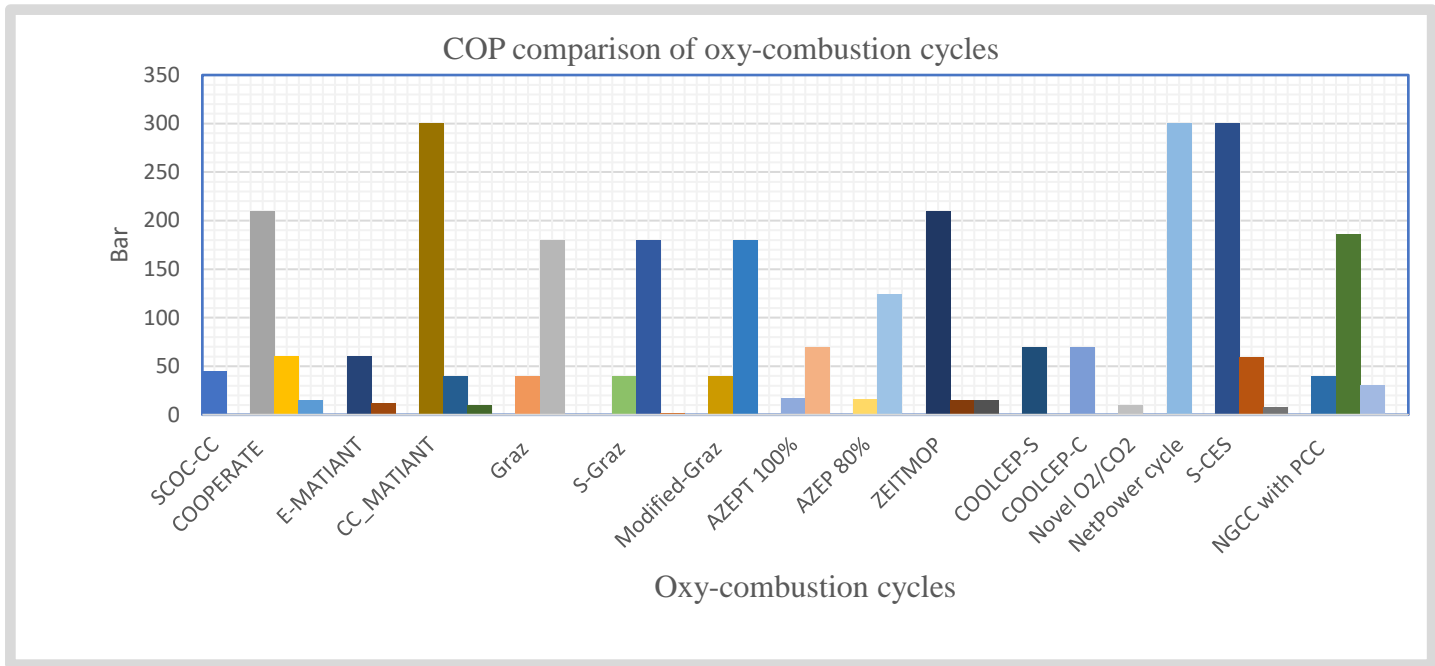


Figure 9.3 COP Comparison of oxy-combustion cycles

As shown in Figure 9.3, the S-CES, NetPower and CC-MATIANT cycles have the highest COP; this cycle needs developed technologies of combustions. The Graz, S-Graz have lower COP than these cycles. ZEITMOP has lower pressure for combustion, so combustion technologies are available; however, this cycle needs to develop technology for oxygen production with ITM technology. AZEP 100% and AZEP85% has COP than ZEITMOP; however, they also need to develop oxygen production with OITM technology. The SCOC-CC has very low COP. Hence, these cycles can improve efficiency with rising combustion pressure and COP.

9.5 Exergy and thermal efficiency comparison of oxy-combustion cycles

As shown in Table 9.4, The thermal efficiency of the oxy-combustion cycle can be up to 53.12% for the Graz cycle or 59% for COOLCEP-S based on the reference. Thermal efficiency for demonstration cycles is 55.1% for NetPower and 48.9% for the S-CES cycle based on the reference. These cycles were simulated with Aspen plus

software base on working flow properties in chapter 3, and the calculated thermal and exergy efficiencies are shown in Table 9.4.

Table 9.4 Thermal and exergy efficiency of oxy-combustion cycles

Oxy-Combustion cycle	Thermal efficiency (ref)	Exergy efficiency (modelling)
SCOC-CC (Rogalev, Kindra and Osipov, 2018)	46.16%	43.2%
COOPERATE (Yantovski, 1996)	52%	49.02%
E-MATIANT (Mathieu, 2004)	40–47%	44%
CC_MATIANT (Mathieu and Nihart, 1999)	45-49%	45.39%
Graz cycle (Jericha, Sanz and Göttlich, 2008b)	53.12%	44.65%
S-Graz cycle (Jericha, Sanz and Göttlich, 2008a)	52.5%	38.24%
AZEPT 100% (Möller <i>et al.</i> , 2005)	49.6%	40.6%
ZEITMOP (Foy and McGovern, 2007)	51%	44.91%
COOLCEP-S (Zhang <i>et al.</i> , 2010)	59%	40.9%
COOLCEP-C (Zhang <i>et al.</i> , 2010)	52%	37.95%
Novel O ₂ /CO ₂ (Cao and Zheng, 2006)	48.9%	47.34%
NetPower cycle (IEAGHG, 2015)	55.1%	51.03%
S-CES (IEAGHG, 2015)	48.9%	45.15
NGCC with post-combustion capture (Ferrari <i>et al.</i> , 2017c)	52%	--

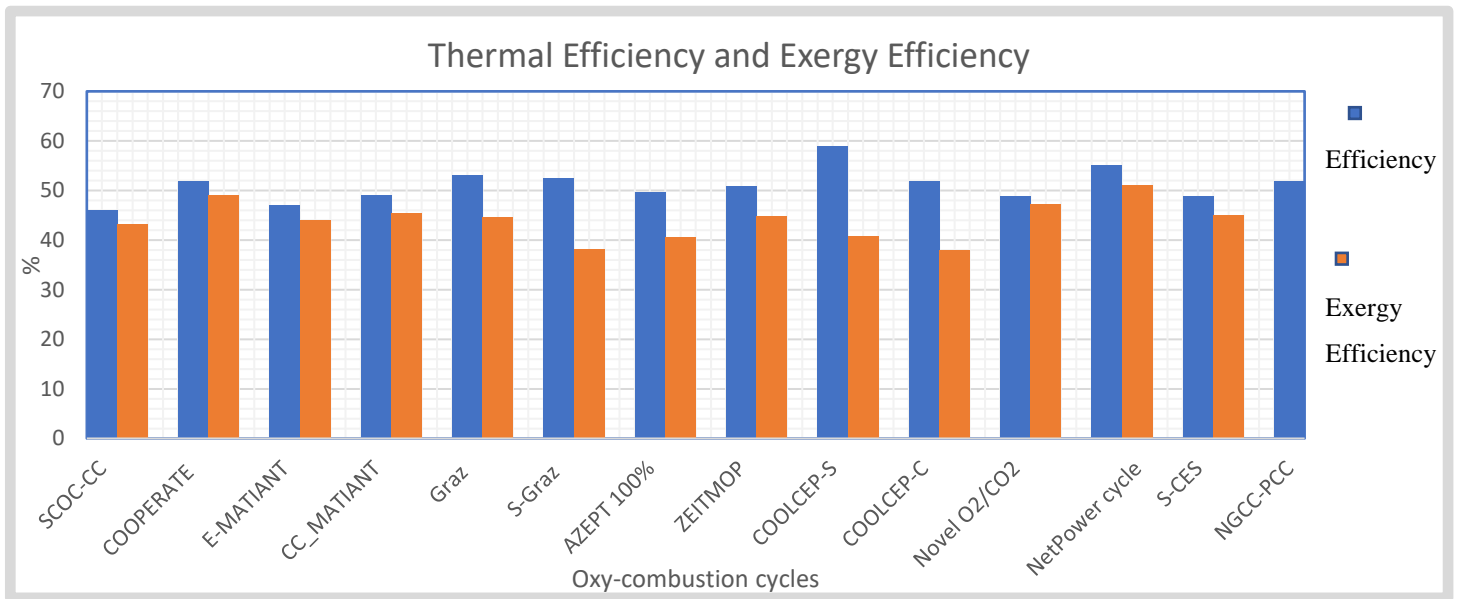


Figure 9.4 Thermal Efficiency and Exergy Efficiency Comparison

Figure 9.4 compares exergy and thermal efficiencies of the oxy-combustion cycle, and the highest efficiency belongs to COOLCEP-S; however, this cycle receives benefits from low-temperature LNG. The S-Graze cycle is the second high-efficiency cycle. However, this cycle needs to be developed before the demonstration stage.

The NetPower cycle efficiency is 55.1%, and it has higher efficiency among demonstration cycles. S-CES efficiency is 48.9%; however, CES is going to improve efficiency with a new product of combustion and turbine in the future demonstration cycle. The exergy efficiency is lower than thermal efficiency due to the amount of exergy input into cycles is higher than thermal energy input into cycles.

9.6 CO₂/kWh for storage comparison of oxy-combustion cycles

Table 9.5 shows the Carbon footprint of each oxy-combustion cycle. The carbon footprint for the NetPower cycle is calculated 0.30 CO₂ kg/kWh; however, this carbon footprint can be virtually zero because the NetPower cycle produces high-pressure CO₂ that can be transferred through the pipeline and utilised for Enhanced Oil Recovery (EOR) for underground storage or chemical feedstock (Fernandes *et al.*, 2019). The carbon emission for another demonstration cycle which is the S-CES cycle

is 0.32 CO₂ kg/kWh; however, the by-product CO₂ has lower pressure, and it needs to be compressed before transferring through the pipe for unitization.

Table 9.5 CO₂/kWh for oxy-combustion cycles

Oxy-Combustion cycles	CO ₂ kg/kWh (Modelling in this work)
SCOC-CC	0.43
COOPERATE	0.39
E-MATIANT	0.48
CC_MATIANT	0.40
Graz cycle	0.40
S-Graz cycle	0.47
AZEPT 100%	0.36
ZEITMOP	0.41
COOLCEP-S	0.45
COOLCEP-C	0.37
Novel O ₂ /CO ₂	0.38
NetPower cycle	0.30
S-CES	0.32

As shown in Table 9.5, the lowest carbon footprint belongs to NetPower. S-CES has a higher carbon footprint than NetPower; however, it is still lower than other oxy-combustion cycles.

9.7 TRL (Technology Readiness Level)

Technology Readiness Level (TRL) is a ranking technology based on development. The TRL can be divided into three main levels: TRL1-3 for research at lab-scale, TRL 4-6 for technology development and small scale demonstration and TRL 7-9 for large-scale operational demonstration and commercialization of the full system (Contributing *et al.*, 2020).

The Technology Readiness Level for the oxy-combustion cycle is categorised in detail in Table 9.6.

Table 9.6 Technology Readiness Level (Oettinger 2015):

Development Stage	TRL	Description
System operation	9	The actual system operates a full range
System Commissioning	8	Actual system test and demonstrate
	7	Full-scale prototype demonstration
Technology Demonstration	6	Pilot Scale
Technology Development	5	Laboratory Scale
	4	Validation in the Laboratory environment
System Operations	3	Proof-of-Concept Demonstrated, Analytically and/or Experimentally
	2	Technology concept application formulates
Basic Technology Research	1	Basic Principles Observed and Reported

9.7.1 Combustion TRL

By product of the oxy-combustion contains a higher mole fraction of H₂O and CO₂ than air combustion. The different air compositions affect the combustion technologies in terms of radiative and convective characteristics, corrosion properties and impacts on boiler materials constructions (Oettinger, 2015). Hence, the combustion TRL is 2 for another oxy-combustion cycle. However, the combustion TRL for NETPower cycle and CES cycle are 9.

9.7.2 CO₂ Compression and Purification Unit (CPU) TRL

The CPU includes a compression and scrubbing unit to provide pure CO₂ for transport and storage (Oettinger, 2015); there are different types of technologies to remove impurities. The TRL for a warm gas clean up unit is 6-7, Inert removal unit is 8, and recovery from the vent is 7, Boiler unit TRL is 9, and Oxygen production unit TRL are ASU:9, ITM:7 OTM:4, The oxy-combustion cycles comparison base on the overall TRL and Oxygen production unit as shown in Table 9.7.

Table 9.7 Oxy-combustion and units TRL comparison

Oxy-Combustion cycle	Oxygen Production Unit (IEAGHG, 2014)	Overall Oxy-combustion Power cycle (Ferguson, 2018)
SCOC-CC	ASU 9	2
COOPERATE	ASU 9	2
E-MATIANT	ASU 9	2
CC_MATIANT	ASU 9	2
Graz cycle	ASU 9	2
S-Graz cycle	ASU 9	2
Modified-Graz Cycle	ASU 9	2
AZEPT 100%	OITM 4	2
AZEP 85%	OITM 4	2
ZEITMOP	ITM 7	2
COOLCEP-S	ASU 9	2
COOLCEP-C	ASU 9	2
Novel O ₂ /CO ₂	ASU 9	2
NetPower cycle	ASU 9	7
CES	ASU 9	5

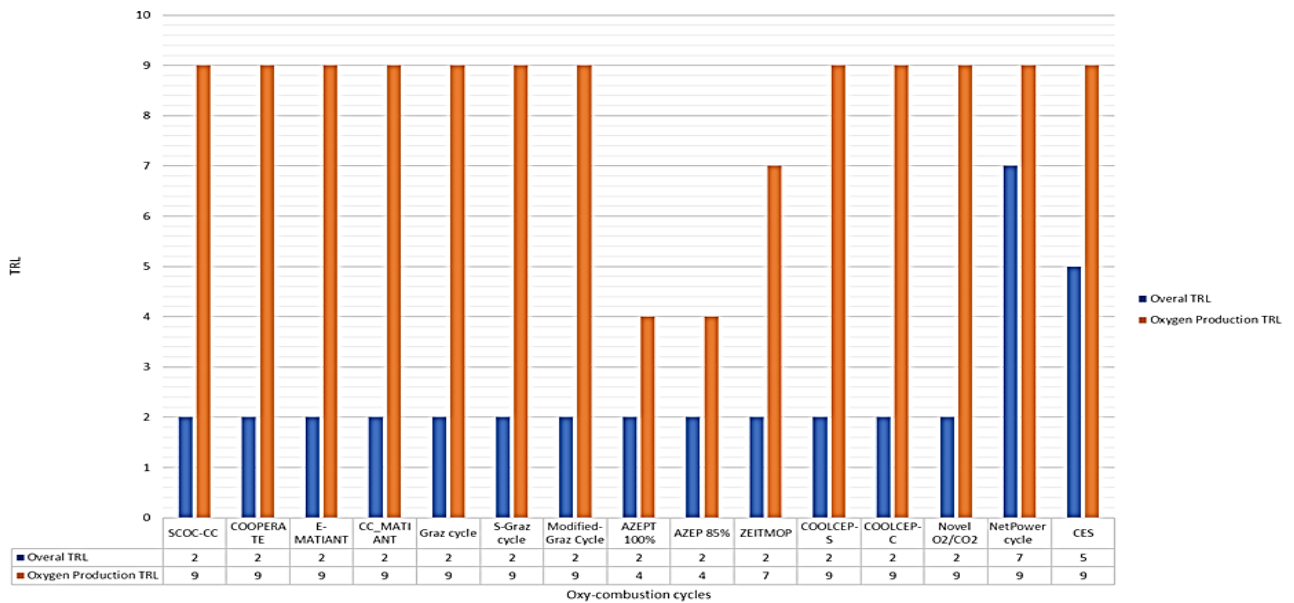


Figure 9.5 Oxy-combustion cycles TRL comparison

As shown in Figure 9.5, TRL of oxy-combustion cycles are compared in the bar chart; Oxy-combustion cycles with Air Separation Unit (ASU) oxygen production have TRL 9, the ASU technology developed and is used in actual operation. ZEIMOP cycle uses ITM technology to produce oxygen, and this technology is on the full-scale demonstration stage with TRL 7, and AZEP 100% and AZEP 85% use Oxygen Ion Transfer Membrane OTIM, and this technology is in the validation and laboratory experiment stage with TRL 4.

Among the oxy-combustion cycles, the NetPower cycle is in the full-scale demonstration stage with overall TRL 7, and S-CES is in the laboratory stage with overall TRL 5, and other oxy-combustion cycles are in the technology concept and application formulas with overall TRL 2.

9.7.3 SCOC-CC TRL

Even though it is the simplest form of the oxy-combustion cycle, with similar features to a conventional combined cycle, the unusual working fluid in the gas turbine cycle turbo-machinery of the SOCC-CC plant needs to be developed from first principles, requiring huge investment for the R&D efforts (Ferguson, 2018).

9.7.4 Graze cycle TRL

The Graz cycle has been studied by various institutes and has been modified to improve efficiency. The predicted net efficiency has been reported as 48.6%. Particular attention has been given to the development of the turbo-machinery, especially the high-temperature turbine, which requires a completely new design. Another important issue is related to the use of an H₂O-rich stream being used for turbine blade cooling. Overall, the cycle is still immature and needs to be developed further (Ferguson, 2018).

9.7.5 CES TRL

The above announcement on the CES website indicates that it is undertaking a feasibility study into using biomass-derived syngas in its own oxy-fuel Gas Generator followed by its gas cycle to produce carbon-negative power and that it plans to deploy a small scale commercial demonstration “BioCCS” plant at the Kimberlina Facility.

9.7.6 NetPower TRL

Considering that a 50 MWth demonstration plant is undergoing commissioning at this time, Wood judges the TRL level of the Net Power system to be TRL-7. NetPower successfully achieved the first supercritical carbon dioxide power plant with carbon capture in La Porte, TX and test facilities including 50MWth Toshiba Energy Systems & Solutions Corporation (Toshiba) and combustor. The combustor is integrated with the turbine, and power is generated, NetPower has planned the global development 300MWe, and this power plant will be commercially deployed in 2022 (TMI Staff & Contributors, 2018).

9.8 Performance analysis

The performance comparison of oxy-combustion cycles is made in Table 9.8, the oxy-combustion cycle was modelled in the chapter by modelling the oxy-combustion cycles in chapter 3. The results are used for a performance comparison of oxy-combustion cycles.

Table 9.8 shows performance analysis of oxy-combustion cycles for each equipment, fuel consumption, maintenance cost and purchasing cost. The performance analysis of oxy-combustion cycles indicates the energy consumption for each component and the relationship between the performance and each component of oxy-combustion cycles. The table also shows the efficiency of each oxy-combustion cycle with Air Separation Unit (ASU) and CO₂ compression and Purification Unit (CPU) and without them. The comparison indicates an efficiency penalty due to ASU and CPU.

Table 9.8 Performance analysis of oxy combustions turbine by Aspen plus modelling analysis

	SCOC-CC	COOPERATE	E-MATIANT	CC_MATIANT	Graz cycle	S-Graz cycle	AZEPT 100%	ZEITMOP	COOLCEP-S	COOLCEP-C	Novel O ₂ /CO ₂	NetPower cycle	CES
Turbine Output (MW)	927.70	385.00	192.10	393.70	39.40	36.60	677.20	795.10	26.90	35.61	42.01	624.25	445.10
Recycled compressor or pump (MW)	290.11	88.00	81.42	62.13	21.57	21.30	19.80	289.26	0.42	9.19	15.80	116.43	29.94
Natura gas compressor (MW)	0.00	1.90	1.60	2.40	0.16	0.16	5.18	9.87	2.29	1.15	0.24	6.95	16.55
Oxygen compressor (MW)	102.91	3.50	4.30	5.10	0.34	0.34	284.90	115.18	1.70	1.90	0.30	0.00	0.00
Air Seperation Unit (MW) (ref)	75.43	37.35	21.48	42.95	2.33	2.33	0.00	0.00	2.33	2.67	3.24	85.45	78.75
CO2 Purification Unit CPU (MW) (ref)	28.77	14.21	5.44	16.43	0.89	0.85	17.29	19.77	0.85	0.97	1.24	6.20	16.67
Network output (MW) (without ASU and CPU)	534.68	291.50	104.80	324.10	17.30	14.80	367.35	380.80	20.20	20.72	25.70	415.47	324.70
Gas flowrate kg/s	23.29	11.50	4.40	13.30	0.72	0.72	14.00	16.00	0.69	0.79	1.00	16.52	14.60
Oxygen Flow rate kg/s	92.90	46.00	26.45	52.90	2.88	2.88	710.00	302.90	2.88	3.29	3.99	61.50	64.40
LHV MW	1164.40	576.50	217.73	663.00	36.00	36.00	700.00	800.00	34.40	39.45	50.00	768.08	678.40
Efficiency % (without ASU and CPU)	45.92	50.60	48.10	48.90	48.08	41.17	52.50	47.60	58.70	52.50	51.43	54.09	47.90
Efficiency % (with ASU and CPU)	36.97	41.64	35.76	39.92	39.18	32.26	50.00	45.13	56.15	50.00	42.39	53.28	44.69
Recycled compressor or pump/Turbine Output	31.27	20.78	37.96	11.56	52.54	52.46	0.13	34.22	1.08	24.12	35.47	16.82	2.57
Natura gas compressor/Turbine Output	0.00	0.49	0.83	0.61	0.41	0.44	0.76	1.24	8.51	3.23	0.57	1.11	3.72
Oxygen compressor/Turbine Output	11.09	0.91	2.24	1.30	0.86	0.93	42.07	14.49	6.32	5.34	0.72	0.00	0.00
Air Seperation Unit/Turbine Output	8.13	9.70	11.18	10.91	5.93	6.38	0.00	0.00	8.66	7.50	7.71	13.69	17.69
Co2 Purification Unit CPU/Turbine Output	3.10	1.53	0.59	1.77	0.10	0.09	1.86	2.13	0.09	0.11	0.13	0.67	1.80
Network output(without ASU and CPU)/Turbine Output	57.64	75.71	54.55	82.32	43.91	40.44	54.25	47.89	75.09	58.19	61.18	66.56	72.95

The results indicate that COOLCEP, AZEP 100% and NetPower cycle have higher efficiency with ASU and CPU unit; however, the NetPower cycle is in the demonstration stage among them. NetPower has 54.09% efficiency without ASU and CPU penalties, and the efficiency reduces to 53.8% with considering these units. The NetPower efficiency is higher than Natural Gas Combined Cycle with Post Combustion Capture (NGCC-PPC) as a reference power cycle with 52% efficiency (Ferrari *et al.*, 2017c).

The S-CES is another oxy-combustion in the demonstration stage, the efficiency without the ASU and CPU penalties is 47.9%, and the efficiency reduces to 44.69% with considering these units; however, CES new technologies can improve the efficiency in future CES power plant (Clean Energy System, 2020b).

9.9 Techno-economic analysis of oxy-combustion cycles

The cost analysis of each equipment for oxy-combustion cycles are calculated based on the formula and are shown in Table 3.38 with details, and the calculated overall cost rate of oxy-combustion cycles are shown in Table 9.10

Figure 9.6 shows a comparison of cost rate (\$/h) for oxy-combustion cycles in the bar chart. The cost rates are converted to equivalent expenses in 2013 by table index (Khaljani, Khoshbakhti Saray and Bahlouli, 2015).

The capital cost rate is calculated from the Purchase Equipment Cost (PEC) of each equipment Equation 3-20, then the overall cost rate is calculated from the summation of capital cost rate, fuel cost rate and maintenance cost. The energy consumption cost in Table 9.4 shows the cost of the energy consumption for auxiliary equipment of oxy-combustion power plant.

SCOC-CC, COOPERATE and CC-MATIANT have the highest overall cost rate due to higher turbine and combustion cost rates; the two demonstration cycles, NetPower and S-CES, have lower overall cost rates than these cycles. The NetPower cycle and S-CES also have lower fuel cost rates than CC-MATIANT. ZEIPTMOP has a higher overall cost rate than AZEP 100% due to turbine, fuel cost rate and maintenance cost rate.

Table 9.9 Cost analysis of each component for oxy-combustion cycles:

Oxy-combustion equipment	SCOC-CC	COOPERATE	E-MATIANT	CC_MATIANT	Graz cycle	S-Graz cycle	AZEPT 100%	ZEITMOP	COOLCEP-S	COOLCEP-C	Novel O ₂ /CO ₂	NetPower cycle	S-CES
Gas turbine output cost (\$)	9.91E+07	4.04E+07	3.61E+06	8.51E+07	1.00E+06	1.27E+07	1.54E+07	1.80E+07	5.70E+05	3.46E+05	8.17E+05	1.21E+07	2.45E+07
Recycled compressor cost (\$)	2.47E+07	3.40E+06	5.60E+05	7.12E+05	1.29E+05	3.32E+05	4.10E+06	5.66E+06	4.45E+03	9.81E+03	4.43E+05	6.41E+05	2.08E+05
Natura gas compressor cost (\$)	0.00E+00	1.02E+04	7.41E+03	6.62E+03	4.14E+02	4.14E+02	2.21E+04	1.43E+05	8.59E+05	5.29E+05	8.81E+02	2.22E+05	5.57E+03
Oxygen compressor cost (\$)	3.59E+06	2.80E+04	2.96E+04	2.64E+04	1.65E+03	1.65E+03	7.50E+06	2.70E+06	6.17E+04	7.05E+04	1.52E+03	0.00E+00	0.00E+00
Air Separation Unit cost (\$)	7.30E+07	6.90E+07	3.97E+07	7.94E+07	4.31E+06	4.31E+06	0.00E+00	0.00E+00	4.32E+06	4.94E+06	5.98E+06	9.23E+07	9.66E+07
Combustion cost (\$)	1.48E+08	8.36E+08	3.34E+05	6.65E+07				6.74E+05	6.03E+04	3.66E+04	2.71E+04	4.07E+06	4.17E+07
Recuperate cost (\$)		3.27E+07	5.76E+07	1.22E+09			6.45E+05	6.81E+08	2.83E+07	1.72E+07			
Steam Turbine cost (Rankine) (\$)	3.46E+07				6.34E+05	1.32E+06	1.90E+07						
Recycled pump cost (Rankine) (\$)	1.21E+06	2.25E+06			5.42E+04	1.06E+05	4.31E+05		1.97E+05	1.14E+05		6.71E+06	1.39E+06
condenser cost (Rankine) (\$)	3.30E+05												3.57E+05
heat exchanger steam cost (Rankine) (\$)	3.19E+08				1.29E+04	1.00E+05							1.38E+06
Evaporator cost (Rankine) (\$)													
Updated cost based on Marshal and swift cost index 2013													
Gas turbine output cost (\$)	1.22E+08	4.98E+07	4.45E+06	1.05E+08	1.24E+06	1.57E+07	1.89E+07	2.21E+07	7.04E+05	4.26E+05	1.01E+06	1.49E+07	3.03E+07
Recycled compressor cost (\$)	3.04E+07	4.20E+06	6.91E+05	8.78E+05	1.59E+05	4.10E+05	1.76E+05	6.98E+06	1.06E+06	6.52E+05	5.47E+05	7.91E+05	2.57E+05
Natura gas compressor cost (\$)	0.00E+00	1.26E+04	9.14E+03	8.16E+03	5.10E+02	5.10E+02	2.72E+04	1.76E+05	1.06E+06	6.52E+05	1.09E+03	2.74E+05	6.87E+03
Oxygen compressor cost (\$)	4.43E+06	3.45E+04	3.65E+04	3.26E+04	2.04E+03	2.04E+03	9.26E+06	3.33E+06	7.61E+04	8.70E+04	1.87E+03		0.00E+00
Air Separation Unit cost (\$)	7.30E+07	6.90E+07	3.97E+07	7.94E+07	4.31E+06	4.31E+06			4.32E+06	4.94E+06	5.98E+06	9.23E+07	9.66E+07
Co2 Purification Unit CPU cost (\$)							0.00E+00		0.00E+00	0.00E+00	0.00E+00		0.00E+00
Heat Recovery Steam Generator cost (\$)													
Combustion cost (\$)	1.83E+08	1.03E+09	4.12E+05	8.20E+07				8.32E+05	7.43E+04	4.51E+04	3.35E+04	5.02E+06	5.14E+07
Recuperate cost (\$)		4.04E+07	7.11E+07	1.50E+09			7.96E+05	8.40E+08	3.49E+07	2.12E+07			
Steam Turbine cost (Rankine) (\$)	3.46E+07				6.34E+05	1.32E+06	1.90E+07						
Recycled pump cost (Rankine) (\$)	1.23E+06	2.30E+06			5.53E+04	1.08E+05	4.40E+05		2.01E+05	1.16E+05		6.84E+06	1.42E+06
condenser cost (Rankine) (\$)	3.37E+05												3.64E+05
Heat exchanger steam cost (Rankine) (\$)	3.37E+08				1.36E+04	1.06E+05							1.46E+06

Table 9.10 Overall cost rate of oxy-combustion cycles

Cost rate	SCOC-CC	COOPERATE	E-MATIANT	CC_MATIANT	Graz cycle	S-Graz cycle	AZEPT 100%	ZEITMOP	COOLCEP-S	COOLCEP-C	Novel O ₂ /CO ₂	NetPower cycle	S-CES
Total PEC (\$)	7.86E+08	1.20E+09	1.16E+08	1.77E+09	6.41E+06	2.20E+07	4.85E+07	8.74E+08	4.14E+07	2.75E+07	7.57E+06	1.20E+08	1.82E+08
Total Capital cost rate (\$/h)	1.63E+04	2.49E+04	2.42E+03	3.67E+04	1.33E+02	4.56E+02	1.01E+03	1.81E+04	8.59E+02	5.71E+02	1.57E+02	2.49E+03	3.77E+03
Fuel cost rate (\$/h)	1.68E+04	8.30E+03	3.14E+03	9.55E+03	5.18E+02	5.18E+02	1.01E+04	1.15E+04	4.95E+02	5.68E+02	7.20E+02	1.11E+04	9.77E+03
Maintenance cost (\$/h)	9.80E+02	1.49E+03	1.45E+02	2.20E+03	7.99E+00	2.74E+01	6.04E+01	1.09E+03	5.15E+01	3.43E+01	9.44E+00	1.50E+02	2.26E+02
Energy consumption cost (\$/h)	5.69E+08	1.68E+08	1.41E+08	1.38E+08	3.38E+07	3.34E+07	2.51E+08	5.22E+08	5.78E+06	1.81E+07	2.64E+07	2.39E+08	1.24E+08
Overall Cost rate \$/h	3.E+04	3.E+04	6.E+03	5.E+04	7.E+02	1.E+03	1.E+04	3.E+04	1.E+03	1.E+03	9.E+02	1.E+04	1.E+04

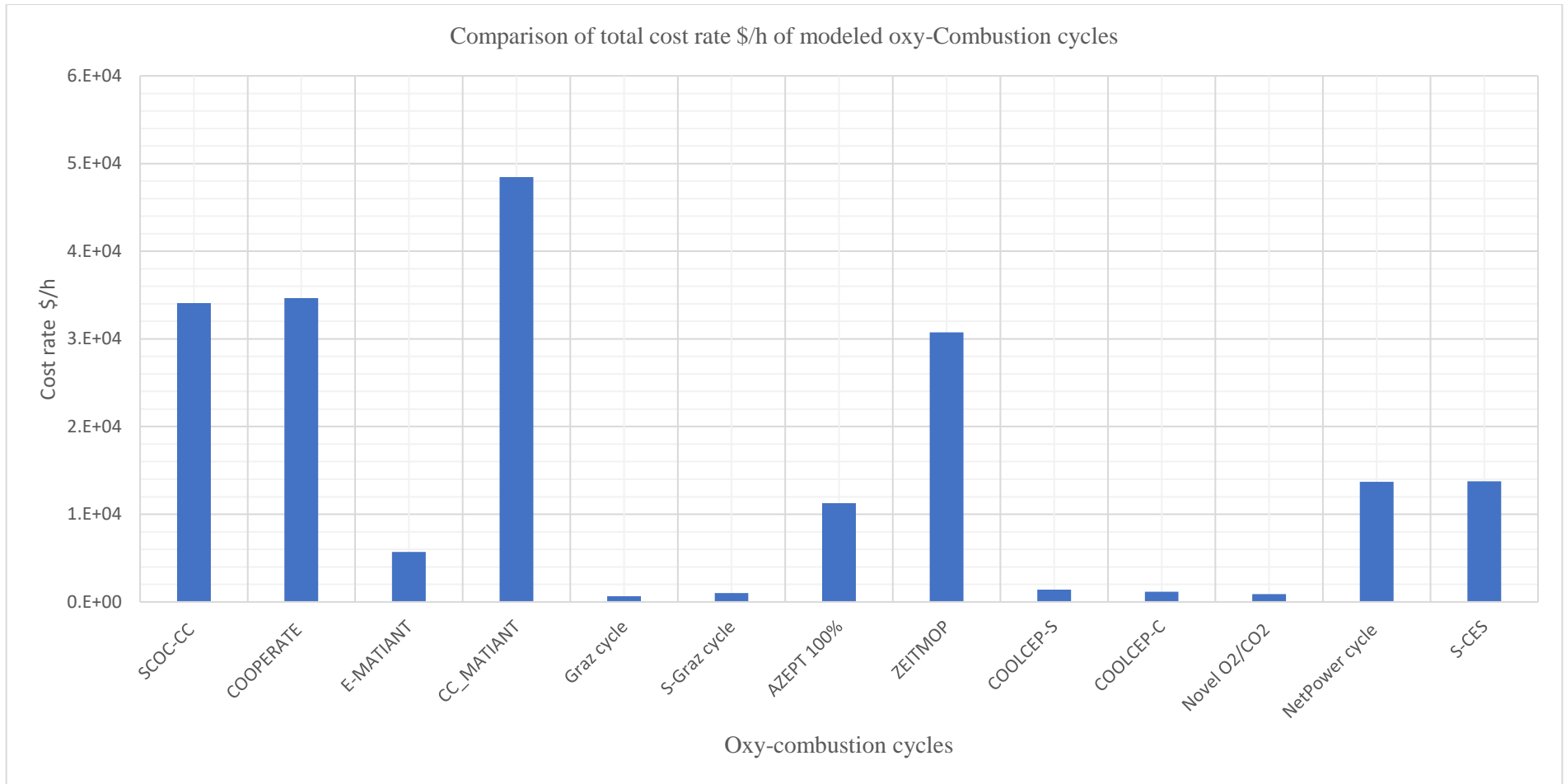


Figure 9.6 Comparison of oxy-combustion cost rate in the bar chart

9.9.1 Exergoeconomic

Cost rate can be defined with the exergy terms in Equation 9-1, Equation 9-2 (Moran, 1948).

$$\dot{C}_i = c_i \cdot \dot{E}_i = c_i \cdot (\dot{m}_i \cdot e_i) \quad \text{Equation 9-1}$$

$$\dot{C}_e = c_e \cdot \dot{E}_e = c_e \cdot (\dot{m}_e \cdot e_e) \quad \text{Equation 9-2}$$

E_i, E_e is exergy rate (kW or MW), and e_i, e_e is specific exergy (kJ/kg or MJ/kg) and m_i, m_e flow rate (kg/s or Kg/h) and c_i, c_e is the average cost per unit of exergy (\$/MJ or \$/KJ). C_e, C_i in cost rate (\$/s or \$/h).

General equation of cost rate for each component is under Equation 9-2 (Moran, 1948)

$$\sum_i \dot{C}_i + \dot{Z}_k = \sum_e \dot{C}_e \quad \text{Equation 9-3}$$

The exergoeconomic parameters can be calculated from the following equations, the output exergy of component is product exergy, and the input exergy of component is fuel exergy.

$$\varepsilon = \frac{\dot{E}_P}{\dot{E}_F} \times 100 \text{ exergetic efficiency} \quad \text{Equation 9-4}$$

Average fuel cost per exergy unit of component $C_{F,k}$

$$c_{F,k} = \frac{\dot{C}_{F,k}}{\dot{E}_{F,k}} \quad \text{Equation 9-5}$$

Average product cost per exergy unit of component $c_{p,k}$

$$c_{p,k} = \frac{\dot{C}_{p,k}}{\dot{E}_{p,k}} \quad \text{Equation 9-6}$$

$$\dot{C}_{D,k} = c_{F,k} \cdot \dot{E}_{D,k} \quad \text{Cost rate of exergy destruction} \quad \text{Equation 9-7}$$

$$\dot{C}_{L,k} = c_{F,k} \cdot \dot{E}_{L,k} \quad \text{Cost rate of exergy loss,} \quad \text{Equation 9-8}$$

$$f_k = \frac{\dot{Z}_k}{\dot{Z}_k + \dot{C}_{D,k} + \dot{C}_{L,k}} \quad \text{Exergoeconomic factor} \quad \text{Equation 9-9}$$

$$r_k = \frac{c_{F,k} - c_{P,k}}{c_{F,k}} \quad \text{Relative cost difference} \quad \text{Equation 9-10}$$

The subscript of F is fuel, P is a product, D is exergy destruction, L is exergy loss, and k is component (Moran, 1948) (Soltani *et al.*, 2013). Table 9.11 shows the exergoeconomic analysis for oxy-combustion cycle, the exergy destructions are calculated by Aspen Plus software, and the Cost rate of Fuel C_f is considered 11.15 (\$/GJ) (Petrakopoulou, Tsatsaronis and Morosuk, 2011). A lower value of exergoeconomic factor indicates that cost saving in the entire system might be

achieved by reducing exergy destruction in components and improving component efficiency, even by increasing capital investment, on another side, when the value of exergoeconomic factor is high the investment cost can be decreased with the expense of increasing exergy destruction in the component (Moran, 1948).

Figure 9.7 compares the exergoeconomic factor for different oxy-combustion cycles; the highest exergoeconomic factors belong to COOPERATE cycle with $f = 72.4\%$ and CC-MATIANT with $f = 75.5\%$, hence these cycles are not required more capital investment to reduce exergy destruction in component, and the investment cannot have more benefit for the cycle efficiency.

The exergoeconomic factors of NetPower are $f=46.1\%$, and S-CES is $f= 46.5\%$; hence, these cycles have a capacity for additional capital investment to reduce exergy destruction in components and increase the overall efficiency.

Table 9.11 Exergoeconomic analysis for oxy-combustion cycles

	Total Input Exergy (MW)	Network (MW)	C_f (\$/GJ)	Total exergy destruction+ loss (MW)	Exergy destruction cost (\$/h)	Overall Cost rate (\$/h)	Overall Cost rate + Exergy destruction cost (\$/h)	Exergoeconomic factor f %
SCOC-CC	1237.80	534.68	11.15	703.12	28223.24	34072.39	62295.63	54.69
COOPERATE	620.84	291.54	11.15	329.30	13218.27	34655.62	47873.89	72.39
E-MATIANT	236.24	104.81	11.15	131.43	5275.62	5695.69	10971.31	51.91
CC_MATIANT	713.97	322.69	11.15	391.27	15705.77	48459.62	64165.39	75.52
Graz cycle	38.81	18.27	11.15	20.54	824.34	659.56	1483.89	44.45
S-Graz cycle	38.81	14.84	11.15	23.97	962.07	1001.84	1963.91	51.01
AZEPT 100%	741.53	367.35	11.15	374.17	15019.35	11147.63	26166.98	42.60
ZEITMOP	847.92	380.77	11.15	467.15	18751.45	30749.77	49501.22	62.12
COOLCEP-S	36.47	20.20	11.15	16.27	653.12	1405.79	2058.91	68.28
COOLCEP-C	42.33	20.72	11.15	21.61	867.43	1173.29	2040.72	57.49
Novel O ₂ /CO ₂	53.51	25.72	11.15	27.79	1115.47	886.69	2002.15	44.29
NetPower cycle	814.17	415.48	11.15	398.69	16003.47	13703.56	29707.03	46.13
S-CES	719.10	324.70	11.15	394.41	15831.50	13769.56	29601.06	46.52

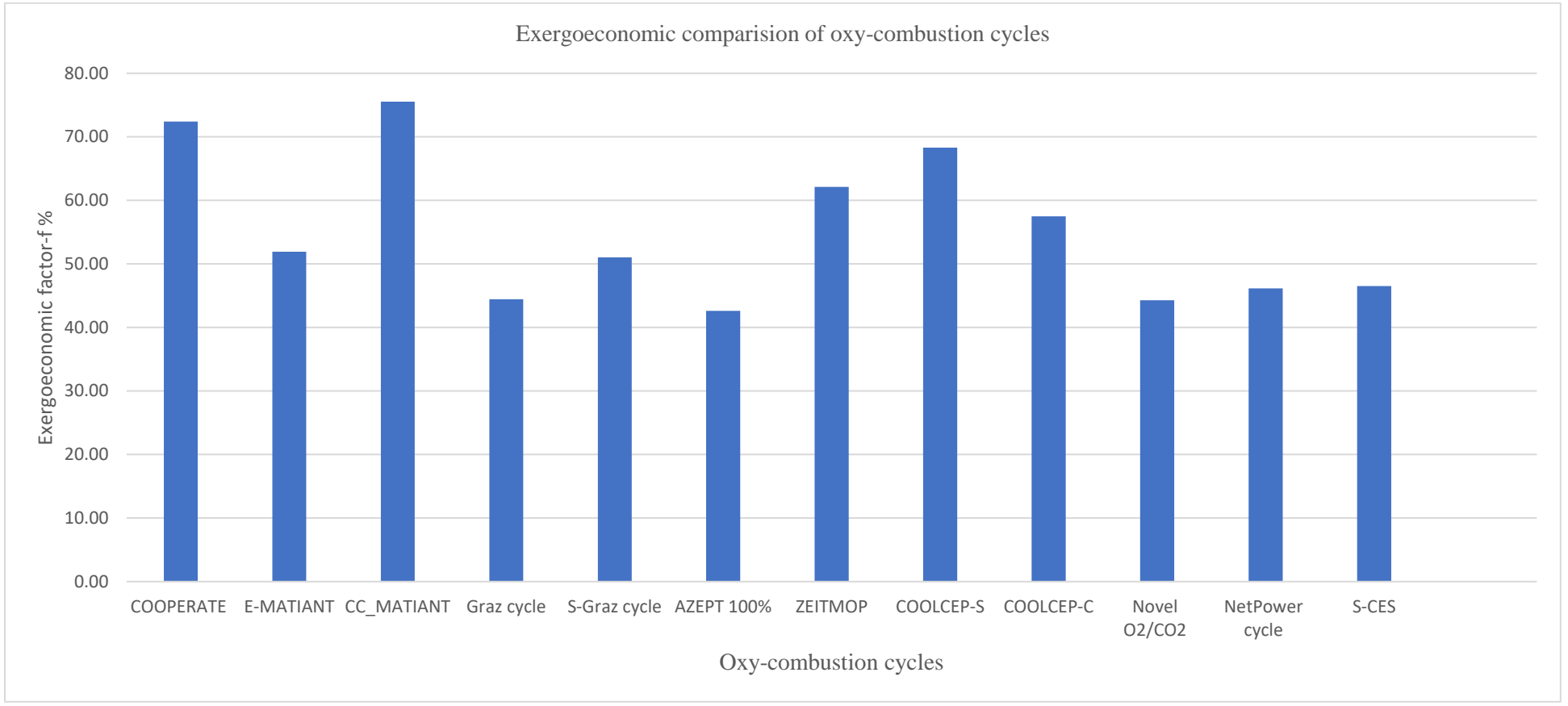


Figure 9.7 Comparison of exergoeconomic of oxy-combustion cycles

9.9.2 LCOE

Levelised cost of electricity can be calculated from Equation 9-11 (Hanak, Powell and Manovic, 2017).

$$\text{LCOE} = \frac{\text{TCR} \times \text{FCF} + \text{FOM}}{\dot{W}_{\text{net}} \times \text{CF} \times 8760} + \text{VOM} + \frac{\text{SFC}}{\eta_{\text{th}}} \quad \text{Equation 9-11}$$

The parameters are the following:

η_{th} net thermal efficiency

CF Capacity factor

TCR total capital requirement

FOM Fixed operating maintenance

VOM Variable operating maintenance

SFC fuel cost

FCF Fixed charge factor

The cost of avoided carbon dioxide can be calculated from Equation 9-12:

$$\text{AC} = \frac{\text{LCOE}_{\text{capture}} - \text{LCOE}_{\text{ref}}}{e_{\text{CO2 ref}} - e_{\text{CO2 capture}}} \quad \text{Equation 9-12}$$

Cost of CO₂ captured can be calculated from Equation 9-13 (Rubin, Davison and Herzog, 2015)

$$\begin{aligned} \text{Cost of CO2 captured } \left(\frac{\$}{\text{tCO2}} \right) & \qquad \text{Equation 9-13} \\ & = \frac{\text{LCOE}_{\text{cc}} - \text{LCOE}_{\text{ref}}}{\left(\frac{\text{tCO2}}{\text{MWh}} \right)_{\text{captured}}} \end{aligned}$$

$\left(\frac{\text{tCO2}}{\text{MWh}} \right)_{\text{captured}}$ = total mass of CO2 captured per net MWh for the plant with capture (It is equal to CO2 produced minus emitted). Also, the energy penalty can be calculated from Equation 9-14 (Budinis *et al.*, 2018).

$$\begin{aligned} \text{Energy penalty} & \qquad \text{Equation 9-14} \\ = 100 \left(\frac{\text{Power output without CCS} - \text{Power output with CCS}}{\text{Power output without CCS}} \right) \end{aligned}$$

$$\begin{aligned} \text{Efficiency penalty} & \\ & = \text{Efficiency without CCS (\%)} \\ & - \text{Efficiency with CCS (\%)} \end{aligned}$$

The results of LCOE for modelled oxy-combustion cycles are shown in Table 9.12, and Figure 9.8 shows a comparison of LCOE in the bar chart. CC-MATIANT has the highest LCOE due to the highest total levelised capital cost rate. NetPower cycle and AZEP 100% have lower LCOE; however, NetPower has the lowest LCOE for the demonstration cycle. S-CES has 44 \$/MWh LCOE, and it is higher than the NetPower cycle due to higher Purchased Equipment Cost (PEC) and levelised maintenance cost.

Table 9.12 Levelised Cost Of Electricity (LCOE) for oxy-combustion cycles

LCOE	SCOC-CC	COOPERATE	E-MATIANT	CC_MATIANT	Graz cycle	S-Graz cycle	AZEPT 100%	ZEITMOP	COOLCEP-S	COOLCEP-C	Novel O ₂ /CO ₂	NetPower cycle	S-CES
Total PEC (\$)	7.86E+08	1.20E+09	1.16E+08	1.77E+09	6.41E+06	2.20E+07	4.85E+07	8.74E+08	4.14E+07	2.75E+07	7.57E+06	1.20E+08	1.82E+08
Total Levelised Capital cost rate (\$/h)	1.81E+04	2.76E+04	2.68E+03	4.08E+04	1.48E+02	5.07E+02	1.12E+03	2.02E+04	9.54E+02	6.34E+02	1.75E+02	2.77E+03	4.19E+03
Fuel cost rate (\$/h)	1.68E+04	8.30E+03	3.14E+03	9.55E+03	5.18E+02	5.18E+02	1.01E+04	1.15E+04	4.95E+02	5.68E+02	7.20E+02	1.11E+04	9.77E+03
Levelised Maintenance cost (\$/h)	1.09E+03	1.66E+03	1.61E+02	2.45E+03	8.88E+00	3.04E+01	6.71E+01	1.21E+03	5.73E+01	3.81E+01	1.05E+01	1.66E+02	2.52E+02
Energy consumption cost (\$/h)	5.69E+08	1.68E+08	1.41E+08	1.38E+08	3.38E+07	3.34E+07	2.51E+08	5.22E+08	5.78E+06	1.81E+07	2.64E+07	2.39E+08	1.24E+08
Net Work output (MW)	5.35E+02	2.92E+02	1.05E+02	3.24E+02	1.73E+01	1.48E+01	3.67E+02	3.81E+02	2.02E+01	2.07E+01	2.57E+01	4.15E+02	3.25E+02
LCOE \$/MWh	67	129	57	163	39	71	31	86	75	60	35	34	44

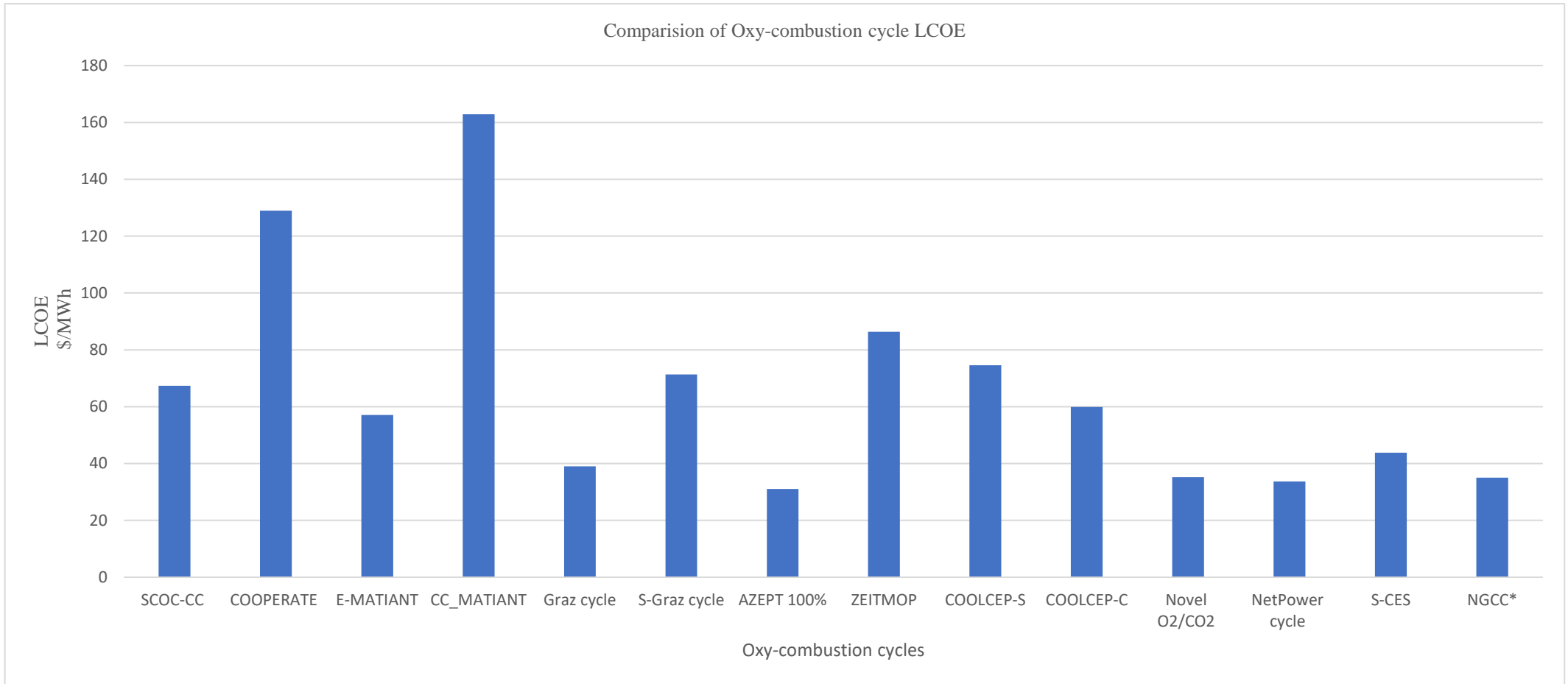


Figure 9.8 LCOE comparison of oxy-combustion cycles in the bar chart

* LCOE of NGCC is 34.51 \$/MWh based on reference (Energy Information Administration, 2021).

9.10 Radar chart for comparison of the oxy-combustion cycles

Table 9.13 shows the comparison parameter of ox combustion cycles, and data were normalised in Table 9.14 shows the comparison of oxy-combustion cycle parameters in the radar (spider) chart. Figure 9.9 and Figure 9.10 present separate radar charts for each oxy-combustion cycle.

Table 9.13 Comparison parameters of Oxy-Combustion cycles

Oxy-Combustion cycle	TIT	TOT	COP	Eff	Exergy Eff	LCOE	Oxygen Production (TRL)	Overall TRL	CO ₂ /kWh	Exergoeconomic f %
SCOC-CC	1400	619	44.50	46.16	43.20	67.32	9	2	0.43	54.7
COOPERATE	1200	500	210.00	52.00	49.02	128.93	9	2	0.39	72.4
E-MATIANT	1300	900	15.00	47.00	44.00	57.06	9	2	0.49	51.9
CC_MATIANT	1300	1100	60.00	49.00	45.39	162.86	9	2	0.40	75.5
Graz	1400	350	300.00	53.12	44.65	39.03	9	2	0.41	44.4
S-Graz	1400	579	180.00	52.50	38.24	71.32	9	2	0.48	51
AZEPT 100%	1200	770	180.00	49.60	40.60	31.01	4	2	0.37	42.6
ZEITMOP	1400	856	210.00	51.00	44.91	86.36	7	2	0.42	62.1
COOLCEP-S	900	700	15.00	59.00	40.90	74.61	9	2	0.15	68.3
COOLCEP-C	900	1192	70.00	52.00	37.95	59.89	9	2	0.37	57.5
Novel O ₂ /CO ₂	1573	500	70.00	48.90	47.34	35.22	9	2	0.38	44.3
NetPower	1150	1192	1.00	55.10	51.03	33.69	9	7	0.30	46.1
S-CES	1533	790	300.00	48.90	45.15	43.78	9	5	0.32	46.5

Table 9.14 Normalised parameters of Oxy-Combustion cycles

Oxy-Combustion cycle	TIT	TOT	COP	Eff	Exergy Eff	LCOE	Oxygen Production (TRL)	Overall TRL	CO ₂ /kWh	Exergoeconomic
SCOC-CC	0.89	0.52	0.15	0.78	0.85	0.46	1	0.29	0.35	0.78
COOPERATE	0.76	0.42	0.7	0.88	0.96	0.24	1	0.29	0.38	0.59
E-MATIANT	0.83	0.76	0.2	0.8	0.86	0.54	1	0.29	0.31	0.82
CC_MATIANT	0.83	0.92	1	0.83	0.89	0.19	1	0.29	0.38	0.56
Graz	0.89	0.29	0.6	0.9	0.87	0.79	1	0.29	0.37	0.96
S-Graz	0.89	0.49	0.6	0.89	0.75	0.43	1	0.29	0.31	0.84
AZEPT 100%	0.76	0.65	0.23	0.84	0.8	1	0.44	0.29	0.41	1
ZEITMOP	0.89	0.72	0.7	0.86	0.88	0.36	0.78	0.29	0.36	0.69
COOLCEP-S	0.57	0.59	0.23	1	0.8	0.42	1	0.29	1.00	0.62
COOLCEP-C	0.57	1	0.23	0.88	0.74	0.52	1	0.29	0.41	0.74
Novel O ₂ /CO ₂	1	0.42	0.03	0.83	0.93	0.88	1	0.29	0.39	0.96
NetPower	0.73	1	1	0.93	1	0.92	1	1	0.50	0.92
S-CES	0.97	0.66	1	0.83	0.88	0.71	1	0.71	0.47	0.92

Figure 9.9 Separate radar chart for each oxy-combustion cycle

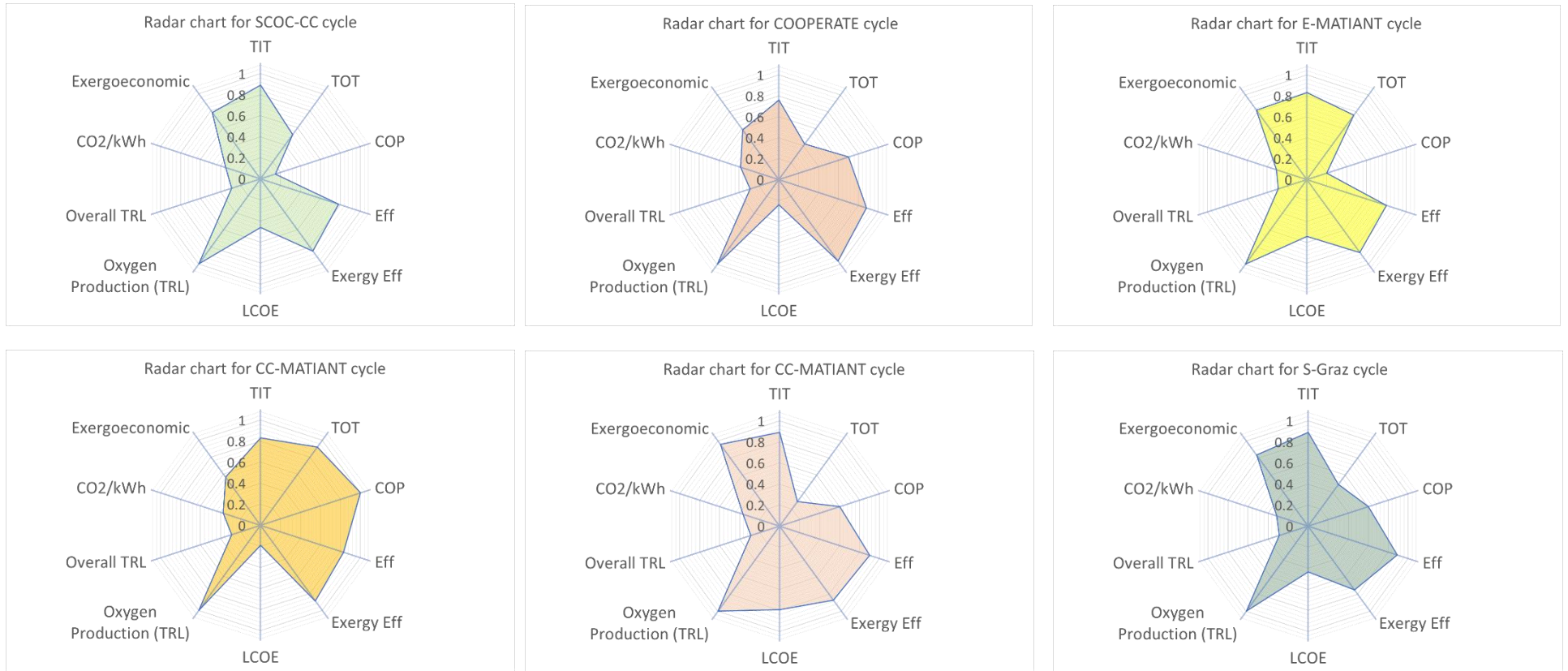
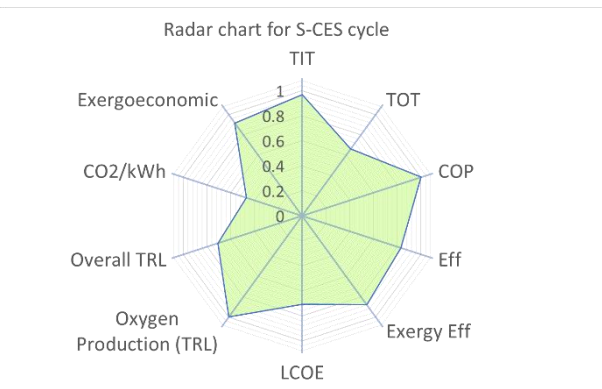
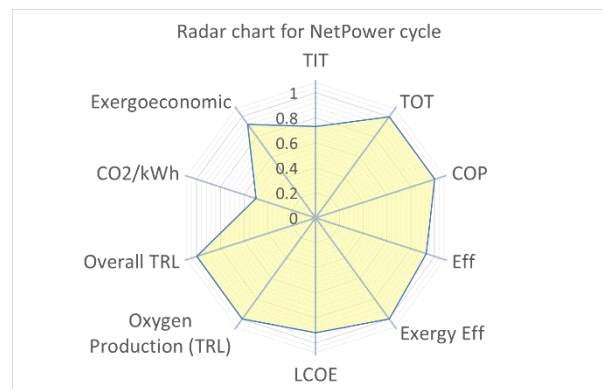
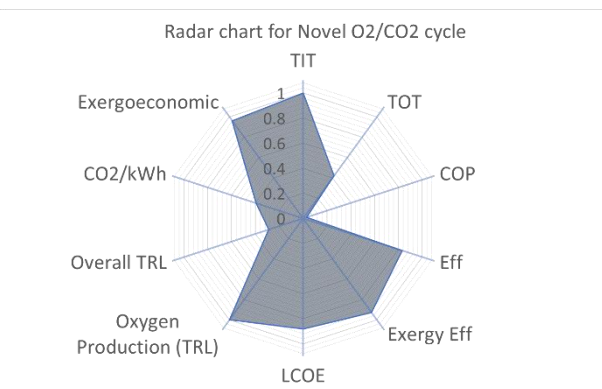
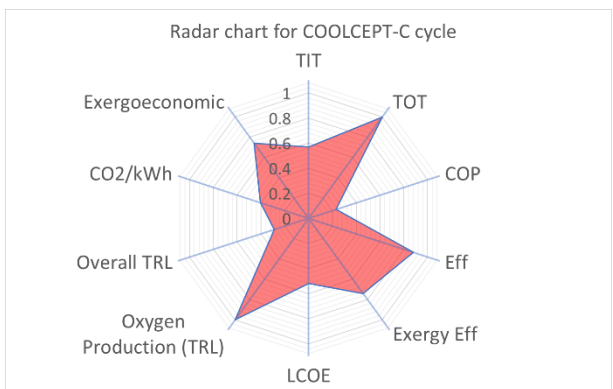
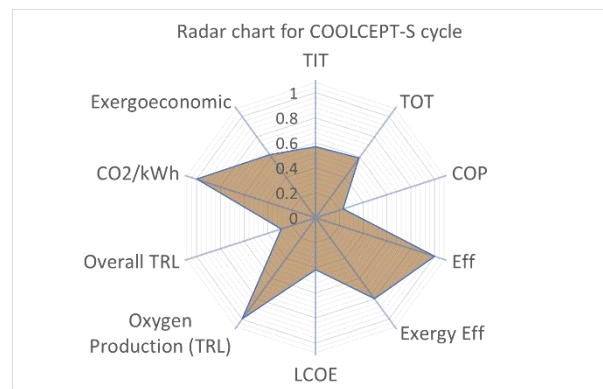
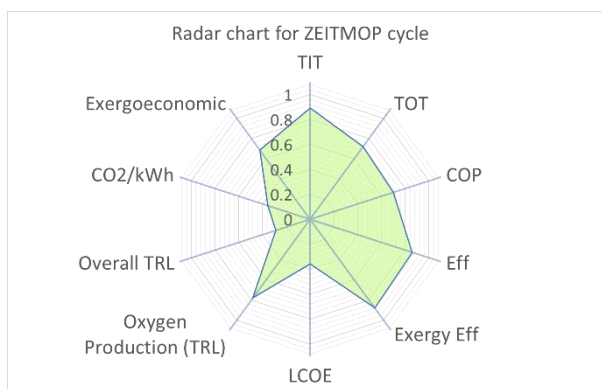
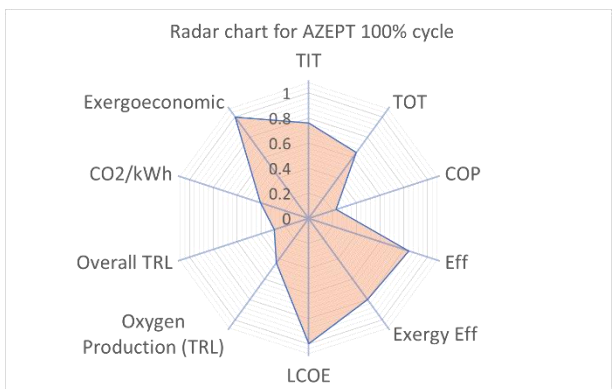


Figure 9.10 Separate radar chart for each oxy-combustion cycle



The normalised parameters of oxy-combustion cycles are presented in Table 9.14, and the TIT, TOT, COP, Eff, Exergy Eff, LCOE, Oxygen Production (TRL), Overall TRL, CO₂/kWh, Exergoeconomic f % parameters of the oxy-combustion cycle are compared.

Based on Figure 9.9, Figure 9.10, it can be concluded COOLCEP-S, NetPower, AZEPT 100% have better thermal, exergy efficiency than other oxy-combustion cycles; however, COOLCEP-S, AZEPT 100% have lower COP, TIT and TRL. In addition, NetPower has lower LCOE; hence, the electricity price of NetPower is lower than COOLCEP-S, AZEPT 100%.

The exergoeconomic factor for NetPower, S-CES, Novel O₂/CO₂, Graz, AZEPT 100% are far from ideal, so these cycles can be improved by more capital investment, and the capital investment can reduce exergy destruction in the component and reduce electricity cost. In terms of carbon emission production, COOLCEP-S, NetPower, S-CES cycles present lower emissions than other cycles, however, the COOLCEP-S needs to develop technologies based on the TRL, and it has higher electricity cost than NetPower and S-CES.

CC-MATIANT present better overall parameters, including thermal, exergy efficiency, COP, TIT in comparison with other cycles; however, it needs to develop because of lower TRL and the cost of electricity, LCOE, is high.

ZEITMOP cycle also presents better efficiency and parameters, including TIT, TOT, COP; however, it has Low overall TRL and Oxygen production TRL, and the Oxygen production technology needs to develop for this cycle. Also, it shows a higher levelised cost of electricity LCOE in comparison with other cycles.

S-CES and NetPower cycles present proper efficiency with lower carbon emission, and they have the highest TRL among other oxy-combustion cycles. These two cycles are only demonstration cycles with very low cost of electricity in comparison with other cycles; however, the NetPower cycle has higher TIT, TOT and TRL. The NetPower cycle can get more benefit than the S-CES cycle from high-efficiency heat recovery because of higher Turbine Outlet Temperature (TOT), but the TIT of the S-CES cycle is higher than NetPower, so it needs more developed technology for combustion and cooling blade system, which CES company recently developed.

9.11 Summary

This PhD thesis concludes most of the oxy-combustion cycles are studied from cycle performance and parameters including TIT, TOT, COP, Eff, Exergy Eff, LCOE, Oxygen Production (TRL), Overall TRL, CO₂/kWh, Exergoeconomic f % parameters of oxy-combustion.

The results indicate that the NetPower and S-CES are developed in technologies to have higher TIT in comparison with other cycles, TIT of NetPower is 1150 °C, and S-CES is 1553 °C; however, these cycles need to develop in exergoeconomic factor and more capital investment can benefit cycle with lower exergy destruction in component and reduce the cost of electricity.

The NetPower, COOLCEP-C, and CC-MATIANT cycles have high Turbine Outlet Temperatures with TOT of 790 °C, 1192 °C, 1100 °C, respectively which aid the heat recovery efficiency from the turbine exhaust gas and these cycles are proper options to use heat exchanger equipment.

The highest Combustion Outlet Pressures (COP) belong to NetPower, S-CES and CC-MATIANT, which are 300 bar. Hence, these cycles need to have developed combustion and turbine technologies. Among this cycle, the NetPower and S-CES were developed as high-pressure components.

Also, NetPower with 0.3 CO₂ kg/kWh and S-CES with 0.32 CO₂ kg/kWh present a more environment-friendly oxy-combustion power plant, with a lower Carbon dioxide emission per electricity production.

The COOPERATE cycle with $f = 72.4\%$ and CC-MATIANT with $f = 75.5\%$ have high exergoeconomic factors, and more capital investment cannot reduce the more exergy destruction in the component to benefit efficiency; however, the NetPower with $f=46.1\%$ and S-CES with $f= 46.5\%$ need more capital investment to benefit efficiency from reducing exergy destruction in cycle components, in addition, these cycles present better LCOE.

Chapter 10: Conclusions and future works

10.1 Conclusions

In this chapter, the summary of the concluded results and discussion through the research chapters are presented. The thesis objectives are met through the chapters as follows. The Carbon Capture, Air Separation Unit (ASU) and CO₂ Purification and Compression Unit (CPU) technologies, and the oxy-combustion power cycles are investigated in detail in chapter 2. Also, pilot and industrial demonstration of Oxyturbine power cycles and comparison in terms of cost and efficiency are investigated in this chapter. The exergy destruction in components of the oxy-combustion cycles to compare the efficiency of the component to each other are accessed in chapter 4, and the sensitivity of leading oxy-combustion cycles was studied in chapter 5 and 6. the parameters of the oxy-combustion cycle, including TIT, TOT, CO₂/kWh, COP, Exergy, Thermal efficiency, Technology Readiness Level (TRL) to provide a benchmark for comparing oxy-combustion cycles are compared in chapter 9, and performance, LCOE, and exergoeconomic of the oxy-combustion cycles according to the Aspen plus modelling in this chapter. In the end, the radar diagrams to compare oxy-combustion cycles were determined in chapter 9.

Following the conclusion, the key point of future works is outlined. In chapter 1, Gas turbines, the main technologies of CCS (Carbon Capture & Storage), Oxygen production, including cryogenic and non-cryogenic Air Separation Unit (ASU) and CO₂ Compression and Purification Unit (CPU) were investigated. The thermodynamic cycles of post-combustion capture, pre-combustion capture and oxy-combustion capture were studied and described in detail; also advantages and disadvantages of CCS technologies were tabulated and explained in detail in the conclusion of Chapter 1. The main disadvantage of the post-combustion capture is the carbon capture at atmospheric pressure. Pre-combustion capture technologies need to develop oxygen production and long life refractories. The oxy-combustion power plant shows a lower cost for capturing CO₂ in comparison with other technologies because of the high concentration of CO₂ and low fuel gas volume; however, the cost of flue gas recirculation and air separation unit increase the electricity cost.

The thermodynamic of oxy-combustion cycle including SCOC-CC, COOPERATE Cycle, MATIANT, E-MATIANT, CC_MATIANT, Graz and S-Graz cycles, AZEP 85% and 100%, ZEITMOP, ZEITMOP Cycle, COOLCEP-S Cycle, Novel O₂/CO₂ (Cao and Zheng, 2006), NetPower and CES Cycles were investigated with details in chapter 2. The thermodynamic cycle of the oxy-combustion cycles was extracted from the literature, and process flow diagrams of the oxy-combustion cycles were drawn in this chapter. The process flow diagrams were explained in detail, and each process was clarified in the diagrams. Furthermore, in chapter 2, the technologies of each oxy-combustion cycle were discussed in detail. The advantages, disadvantages and cost of each of the cycle technologies were mentioned in this chapter.

In chapter 3, the modelling of the oxy-combustion cycles was provided by using Aspen Plus software. Also, the software of process modelling was considered, and the pros and cons of Aspen plus software were mentioned in the first part of the chapter. The oxy-combustions cycles were simulated based on the modelled cycles with Aspen plus software. The stream parameters, including temperature, pressure, flow rate, composition, were calculated and tabulated in this chapter. The results are a reference for the oxy-combustion power cycles calculation; also, the exergy flowrates of streams were calculated for the cycles. The results indicate that the combustion has higher irreversibility and exergy destruction in oxy-combustion cycles due to the chemical reaction process, and heat transfer occurs in the combustion chambers such as SCOC-CC with 28.8% and COOPERATE with 24.4% of total input exergy.

The second main exergy loss in oxy-combustions are HRSG or heat exchanger due to heat transfer between two-stream; therefore, improving the efficiency of HRSG can reduce exergy destruction and improve overall efficiency.

Furthermore, the exergy destruction in each component was shown in bar charts for oxy-combustion cycles to compare irreversibilities and inefficiencies in each component of the cycle. The exergy destruction can be used to find the most exergy destructive component, and it shows that for improving the cycle efficiency and reducing energy penalties in the oxy-combustion power plant, these components need to be developed.

Thermodynamics theory formula, exergy analysis equations, Equation of State (EOS) for oxy-combustion cycle were discussed in chapter 3; These equations are

fundamental equations for the analysis of oxy-combustion; they are a reference for thermodynamic analysis of oxy-combustion cycles.

Techno-economic, sensitivity and exergy analysis of main oxy-combustion cycle including SCOC-CC, E-MATIANT, and COOPERATE cycles were studied in chapters 5 and 6. These chapters were prepared and written up into three papers for high-rank journals. The sensitivity and 3D graphs of the exergy destruction vs flow rate and pressure for the SCOC-CC cycle were plotted, and the thermal and exergy efficiency sensitivity vs working flow rate for the E-MATIANT cycle was presented in chapter 5. The sensitivity analysis of SCOC-CC indicates that the maximum work is at 40 pressure ratio. The sensitivity of efficiency with respect to the flowrate and Combustion Outlet Pressure (COP) indicates that reduction of working flow from 15 kg/s to 17 kg/s can grow the efficiency from 35% to 37%; The overall efficiency of the E-MATIANT cycle at a maximum of 1300 °C is 46.9%; this efficiency can be achieved at 290 kg/s recycled working flow.

In chapter 6, the exergy destruction sensitivity of the COOPERATE cycle was presented in the bar chart. Also, the 3D plot of exergy destruction vs min approach temperature and flowrates were demonstrated; The results indicate the flowrate at the minimum exergy destruction point decreases when the min approach temperature increases. The results indicate that the maximum efficiency of COOPERATE cycle is 52.79% for $\Delta T=110$ at 318 kg/s flowrates with the minimum exergy destruction is about 314.8 MW. The exergy destruction in combustions grow by increasing flowrate from 218 kg/s to 518 kg/s because of the high rate of the chemical reaction and increasing the turbulent flow inside the combustions.

The sensitivity of the heat exchanger design of NetPower was analysed by Aspen plus software in chapter 7. The sensitivity of efficiency vs ΔT_{min} with constant COT and the constant flow rate was plotted; also, the design and cost analysis of heat exchanger were discussed. The result was published as a peer-reviewed journal paper. In Chapter 8, NetPower and CES, two leading oxy-combustion cycles were compared. The efficiency sensitivity vs TIT for CES and NetPower cycle were compared. The results of the TIT sensitivity for the S-CES cycle and the NetPower cycle indicates that the slope of cycle efficiency was higher in the NetPower cycle, which could be explained by the higher impact that the TIT produced in the turbine and the main heat

exchanger for the NetPower cycle. The results were presented at the GHG-14 conference and in SSN peer-review procedia.

The pilot and industrial demonstration of the Oxyturbine power cycles were investigated in chapter 8. In this chapter, demonstration cycles including CES and NetPower were analysed in detail, and the technologies of turbine, heat exchanger and combustor for each cycle were assessed.

Techno-economic, Risk, Technology Readiness Level (TRL) and parametric comparison in Oxyturbine Power Cycles were analysed in chapter 9. In this chapter, TIT, TOT, COP, exergy and thermal efficiency, carbon emission per kWh, TRL of the oxy-combustion cycle were compared in tables and bar charts. The performance analysis of the oxy-combustion cycle was compared, and techno-economic analysis was compared in terms of cost rate and LCOE; these were also presented in bar charts and, the radar diagram of parameters for comparing the oxy-combustion cycles was presented. The results indicate that that the NetPower and S-CES are developed in technologies to have higher TIT in comparison with other cycles, TIT of NetPower is 1150 °C, and S-CES is 1553 °C; however, the NetPower with $f=46.1\%$ and S-CES with $f=46.5\%$ need more capital investment to benefit efficiency from reducing exergy destruction in cycle components, in addition, these cycles present better LCOE.

This PhD research is presenting the comparison of the proposed or demonstrated oxy-combustion cycles. It can be used to draw a road map for the development and deployment of low carbon, higher efficiency and low-cost energy, and it would be a reference for future researchers in oxy-combustion cycles.

10.2 Future work and critical appraisal

The future extensions of this research are outlined briefly as follows:

- **Multi-objective optimisation of Oxy-combustion cycles in respect to design parameters:** The design parameters of the oxy-combustion cycle need to consider the production of electricity with minimum exergy destruction, minimum cost and minimum impact on the environment. In order to design the oxy-combustion power cycle with high efficiency at low cost, the trade-off between efficiency and cost is needed to be considered. Multi-objective optimization is used to find the best trade-off between cycle

design parameters. The optimised cycle will have lower exergy destruction, minimum fuel consumption, minimum capital cost and minimum impact on the environment.

- **Thermochemical analysis of the working flow composition for oxy-combustion cycles:** The working flow composition has the main impact on the efficiency of the combustion, turbine and heat exchanger. Thermochemical optimisation of the oxy-combustion cycle needs to be studied to indicate the composition with higher overall efficiency for oxy-combustion cycles.

Reference

- A K Tiwari, M. M. H. and M. I. (2012) 'Effect of Operating Parameters on the Performance of Combined Cycle Power Plant', *Journal of Industrial Microbiology and Biotechnology*. doi: 10.1007/s10295-007-0291-8.
- Ahmad, F. (2019) *Dynamic Scheduling and Control of MEA Absorption Processes for CO₂ Capture Using gProms*.
- Ahmadi, P., Dincer, I. and Rosen, M. A. (2011) 'Exergy, exergoeconomic and environmental analyses and evolutionary algorithm based multi-objective optimization of combined cycle power plants', *Energy*, 36(10), pp. 5886–5898. doi: 10.1016/j.energy.2011.08.034.
- Ahmed F. El-Sayed (2017) *Aircraft Propulsion and Gas Turbine Engines, Second Edition*.
- Allam, R. *et al.* (2017) 'Demonstration of the Allam Cycle: An Update on the Development Status of a High Efficiency Supercritical Carbon Dioxide Power Process Employing Full Carbon Capture', *Energy Procedia*, 114(November 2016), pp. 5948–5966. doi: 10.1016/j.egypro.2017.03.1731.
- Allam, R. J. *et al.* (2013) 'High efficiency and low cost of electricity generation from fossil fuels while eliminating atmospheric emissions, including carbon dioxide', *Energy Procedia*, 37, pp. 1135–1149. doi: 10.1016/j.egypro.2013.05.211.
- Almås, K. (2012) 'Coal-fired Power Plants based on Oxy-combustion with Carbon Capture : Combustion Conditions and Water Consumption', pp. 13–100.
- Anderson, R. E. *et al.* (2008) 'Adapting gas turbines to zero emission oxy-fuel power plants', *Proceedings of the ASME Turbo Expo*, 2, pp. 781–791. doi: 10.1115/GT2008-51377.
- Aneke, M. and Wang, M. (2015) 'Potential for improving the energy efficiency of cryogenic air separation unit (ASU) using binary heat recovery cycles', *Applied Thermal Engineering*, 81, pp. 223–231. doi: 10.1016/J.APPLTHERMALENG.2015.02.034.
- Antonini, C. *et al.* (2020) 'Hydrogen production from natural gas and biomethane with carbon capture and storage - A techno-environmental analysis', *Sustainable Energy and Fuels*, 4(6), pp. 2967–2986. doi: 10.1039/d0se00222d.
- Artioli, Y. (2008) 'Adsorption', in *Encyclopedia of Ecology, Five-Volume Set*. Elsevier Inc., pp. 60–65. doi: 10.1016/B978-008045405-4.00252-4.
- Atkinson, J. *et al.* (2009) *Design and operation*. Available at: <https://www.ncbi.nlm.nih.gov/books/NBK143274/>.
- Authors, C. L. *et al.* (2010) 'Capture of CO₂', *Energy & fuels*, 24(MAIJUN), pp. 3687–3697.
- Barston, R. P. (2019) 'The Paris agreement', in *Modern Diplomacy*, pp. 492–505. doi: 10.4324/9781351270090-20.
- Bolland, O. and Saether, S. (1992) 'New Concepts for Natural Gas Fired Power Plants', *Energy Conversion and Management*, 33(5–8), pp. 467–475.
- Boyce, M. P. (2006) *Gas Turbine Third Edition Engineering*.
- Boyce, M. P. and Chen, M. S. (1974) 'OPTIMIZATION OF VARIOUS GAS TURBINE CYCLES.', in, pp. 91–100.
- Budinis, S. *et al.* (2018) 'An assessment of CCS costs, barriers and potential', *Energy Strategy Reviews*, 22(May), pp. 61–81. doi: 10.1016/j.esr.2018.08.003.
- Bunyamanid, Y. *et al.* (2016) 'An Analysis of Energy and Carbon Intensities and Exergy Efficiency in Natural Gas Combined-Cycle Power Plants: A Case Study of Thailand', *MATEC Web of Conferences*, 68, pp. 6–11. doi:

- 10.1051/mateconf/20166814001.
- Business, W. and October, M. (2012) ‘Advanced Turbine Developments for Oxy-Combustion TriGen™ Plants 2012 WESTCARB Business Meeting’.
- Calli, O., Colpan, C. O. and Gunerhan, H. (2018) ‘Performance Assessment of a Biomass-Fired Regenerative ORC System Through Energy and Exergy Analyses’, in *Exergetic, Energetic and Environmental Dimensions*. Elsevier Inc., pp. 253–277. doi: 10.1016/B978-0-12-813734-5.00015-9.
- Cao, W. and Zheng, D. (2006) ‘Exergy regeneration in an O₂/CO₂ gas turbine cycle with chemical recuperation by CO₂ reforming of methane’, *Energy Conversion and Management*, 47(18–19), pp. 3019–3030. doi: 10.1016/j.enconman.2006.03.010.
- Carapellucci, R. *et al.* (2017) ‘IMECE2013-63492’, pp. 1–12.
- CES (2020a) *Direct Steam Gas Generators — Clean Energy Systems*. Available at: <http://www.cleanenergysystems.com/gas-generators> (Accessed: 3 December 2020).
- CES (2020b) *Oxy-Fuel Turbines — Clean Energy Systems*. Available at: <http://www.cleanenergysystems.com/oxy-fuel-turbines> (Accessed: 2 December 2020).
- Chaudhry, G. *et al.* (2018) ‘Analysis of oxy-fuel combustion power cycle utilizing a pressurized coal combustor The MIT Faculty has made this article openly available . Please share how this access benefits you . Your story matters . Citation Elsevier License Publisher Version Access’.
- ChemEngGuy (2021) *What is PRO/II from Schneider Electric / AVEVA ? – ChemEngGuy*. Available at: <https://www.chemicalengineeringguy.com/the-blog/process-simulation/what-is-pro-ii-from-schneider-electric-aveva/> (Accessed: 25 July 2021).
- Chiesa, P. and Lozza, G. (1999) ‘CO₂ emission abatement in igcc power plants by semiclosed cycles: Part a with oxygen-blown combustion’, *Journal of Engineering for Gas Turbines and Power*, 121(4), pp. 635–641. doi: 10.1115/1.2818519.
- Chik, M. N. (2017) ‘Journal of Energy’, pp. 1–12.
- Clean Energy System (2020a) *Oxy-Fuel Turbines — Clean Energy Systems*. Available at: <http://www.cleanenergysystems.com/oxy-fuel-turbines> (Accessed: 3 June 2020).
- Clean Energy System (2020b) *Oxy-Fuel Turbines — Clean Energy Systems*. Available at: <http://www.cleanenergysystems.com/oxy-fuel-turbines> (Accessed: 3 December 2020).
- Climent Barba, F. *et al.* (2016a) ‘A technical evaluation, performance analysis and risk assessment of multiple novel oxy-turbine power cycles with complete CO₂ capture’, *Journal of Cleaner Production*, 133, pp. 971–985. doi: 10.1016/j.jclepro.2016.05.189.
- Climent Barba, F. *et al.* (2016b) ‘A technical evaluation, performance analysis and risk assessment of multiple novel oxy-turbine power cycles with complete CO₂ capture’, *Journal of Cleaner Production*, 133, pp. 971–985. doi: 10.1016/j.jclepro.2016.05.189.
- Contributing, T. N. *et al.* (2020) *A survey of key technological innovations for the low-carbon economy*.
- Cunha, H. E. and Kyprianidis, K. G. (2012) ‘Investigation of the potential of gas turbines for vehicular applications’, *Proceedings of the ASME Turbo Expo*, 3(June 2012), pp. 51–64. doi: 10.1115/GT2012-68402.
- Dahlquist, A. *et al.* (2013) ‘Optimization of an oxyfuel combined cycle regarding performance and complexity level’, *Proceedings of the ASME Turbo Expo*, 2(July 2016). doi: 10.1115/GT2013-94755.
- Darabkhani, H. G. *et al.* (2018) ‘Design, process simulation and construction of a 100 kW pilot-scale CO₂ membrane rig: Improving in situ CO₂ capture using selective

- exhaust gas recirculation (S-EGR)', *Journal of Natural Gas Science and Engineering*, 50(September 2017), pp. 128–138. doi: 10.1016/j.jngse.2017.09.012.
- Davison, J. (2015) 'Techno-Economic Assessment of Oxy- Combustion Turbine Power Plants with CO₂ Capture Outline of Presentation Background and scope of the study', (October).
- Dillon, D. *et al.* (2013) 'Post-combustion capture on natural gas combined cycle plants: A technical and economical evaluation of retrofit, new build, and the application of exhaust gas recycle', *Energy Procedia*, 37, pp. 2397–2405. doi: 10.1016/j.egypro.2013.06.121.
- Dinçer, I. and Kanoğlu, M. (2010) *Refrigeration Systems and Applications, Second Edition, Refrigeration Systems and Applications, Second Edition*. doi: 10.1002/9780470661093.
- Dincer, I. and Rosen, M. A. (2021) 'Exergy and energy analyses', *Exergy*, pp. 23–35. doi: 10.1016/B978-0-12-824372-5.00002-6.
- EAVES PSK (1971) *Gas turbines for power generation, Electronics and Power*. doi: 10.1049/ep.1971.0241.
- El-Masri, M. A. (1986) 'On thermodynamics of gas-turbine cycles: Part 2—A model for expansion in cooled turbines', *Journal of Engineering for Gas Turbines and Power*, 108(1), pp. 151–159. doi: 10.1115/1.3239862.
- Energy Information Administration, U. (2021) 'Levelized Costs of New Generation Resources in the Annual Energy Outlook 2021'.
- Fans, T. (2020) 'Energy , Exergy and Economic Analyses of a'.
- Ferguson, S. (2018) 'Assessing the Cost Reduction Potential and Competitiveness of Novel (Next Generation) UK Carbon Capture Technology Benchmarking State-of-the-art and Next Generation Technologies', (February).
- Fernandes, D. *et al.* (2019) 'Process and Carbon Footprint Analyses of the Allam Cycle Power Plant Integrated with an Air Separation Unit', *International Journal of Chemical Engineering*, 2019, pp. 325–340. doi: 10.1155/2019/6035856.
- Feron, P. H. M. (2016) *Absorption-Based Post-Combustion Capture of Carbon Dioxide (Woodhead Publishing Series in Energy)*.
- Ferrari, N. *et al.* (2017a) 'Oxy-turbine for Power Plant with CO₂ Capture', *Energy Procedia*, 114(November 2016), pp. 471–480. doi: 10.1016/j.egypro.2017.03.1189.
- Ferrari, N. *et al.* (2017b) 'Oxy-turbine for Power Plant with CO₂ Capture', *Energy Procedia*, 114(November 2016), pp. 471–480. doi: 10.1016/j.egypro.2017.03.1189.
- Ferrari, N. *et al.* (2017c) 'Oxy-turbine for Power Plant with CO₂ Capture', *Energy Procedia*, 114, pp. 471–480. doi: 10.1016/j.egypro.2017.03.1189.
- Figueroa, J. D. *et al.* (2008) 'Advances in CO₂ capture technology-The U.S. Department of Energy's Carbon Sequestration Program', *International Journal of Greenhouse Gas Control*, 2(1), pp. 9–20. doi: 10.1016/S1750-5836(07)00094-1.
- Flanner, M. G. (2009) 'Integrating anthropogenic heat flux with global climate models', *Geophysical Research Letters*, 36(2), pp. 1–5. doi: 10.1029/2008GL036465.
- Flin, D. (2019) *First fire for La Porte carbon capture demo | Gas Turbine World*. Available at: <https://gasturbineworld.com/first-fire-for-la-porte-carbon-capture-demo/> (Accessed: 26 May 2020).
- Folkson, R. (2014) *Alternative fuels and advanced vehicle technologies for improved environmental performance: Towards zero carbon transportation, Alternative Fuels and Advanced Vehicle Technologies for Improved Environmental Performance: Towards Zero Carbon Transportation*. doi: 10.1533/9780857097422.
- Forsthoffer, W. E. (2011) *Forsthoffers Best Practice Handbook for Rotating Machinery by William E Forsthoffer (z-lib.org)*.

- Foy, K. and McGovern, J. (2007) ‘Analysis of the effects of combining air separation with combustion in a zero emissions (ZEITMOP) cycle’, *Energy Conversion and Management*, 48(11), pp. 3046–3052. doi: 10.1016/j.enconman.2007.06.041.
- Foy, K. and Yantovski, E. (2006) ‘History and state-of-the-art of fuel fired zero emission power cycles’, *International Journal of Thermodynamics*, 9(2), pp. 37–63. doi: 10.5541/ijot.1034000170.
- Freund, P. (2005) ‘IPCC Special Report on Carbon dioxide Capture and Storage Contents’, *IPCC Special Report on Carbon dioxide Capture and Storage*, (En línea), pp. 52–71.
- Gasturb (2018) *GasTurb 13 Design and Off-Design Performance of Gas Turbines*.
- Gibbins, J. et al. (2011) ‘2 th Meeting of the International Post-Combustion CO₂ Capture Network 2 p Retrofitting Post Combustion Capture Retrofitting Post Combustion Capture to Existing Power Plant Acknowledgements: DECC, RCUK, IEA GHG’. Available at: <https://www.netl.doe.gov/coal/carbon-capture/post-combustion> (Accessed: 25 July 2021).
- Gicquel, R. (2018) *Online course and simulator for engineering thermodynamics*. Available at: <https://direns.mines-paristech.fr/Sites/Thopt/en/co/cycles-combines.html%0Adirens.mines-paristech.fr/Sites/Thopt/en/co/chambres-combustion.html> (Accessed: 21 July 2020).
- Gonzalez-Salazar, M. A., Kirsten, T. and Prchlik, L. (2018) ‘Review of the operational flexibility and emissions of gas- and coal-fired power plants in a future with growing renewables’, *Renewable and Sustainable Energy Reviews*, 82(July 2017), pp. 1497–1513. doi: 10.1016/j.rser.2017.05.278.
- Gundersen, T. (2009) *THE CONCEPT OF EXERGY AND ENERGY QUALITY*.
- Ham, L. van der (2011) *Improving the Second law efficiency of a cryogenic air separation unit Thesis for the degree of Philosophiae Doctor*.
- Hanak, D. P., Powell, D. and Manovic, V. (2017) ‘Techno-economic analysis of oxy-combustion coal-fired power plant with cryogenic oxygen storage’, *Applied Energy*, 191, pp. 193–203. doi: 10.1016/j.apenergy.2017.01.049.
- Haydary, J. (2019) *Chemical Process Design and Aspen Plus and Aspen HYSYS Applications*.
- He, X. (2018) ‘The Latest Development on Membrane Materials and Processes for Post-combustion CO₂ Capture: A Review OPEN ACCESS Citation: He X. The Latest Development on Membrane Materials and Processes for Post-combustion CO₂ Capture: A Review’, *ScienceForecast Publications LLC., |. SF J Material Chem Eng*, 1(1), p. 1009. Available at: <https://scienceforecastoa.com/> (Accessed: 24 August 2020).
- Heat, C. (2018) ‘News : Heatric supplies Circuit Heat advanced recuperator for NET Power ’ s first- Heatric supplies advanced recuperator for NET Power ’ s first-of-a-kind supercritical CO₂ power plant’.
- Heatric (2020) *Printed Circuit Heat Exchangers - High-Integrity Equipment | Heatric*. Available at: <https://www.heatric.com/heat-exchangers/> (Accessed: 3 June 2020).
- Higher temperatures in turbines - Kraftwerk Forschung* (2020). Available at: <http://kraftwerkforschung.info/en/higher-temperatures-in-turbines/> (Accessed: 3 December 2020).
- Horlock, J. H. and Bathie, W. W. (2004) *Advanced Gas Turbine Cycles*, *Journal of Engineering for Gas Turbines and Power*. doi: 10.1115/1.1789994.
- Horlock, J. H. and Torbidoni, L. (2008a) ‘Calculations of cooled turbine efficiency’, *Journal of Engineering for Gas Turbines and Power*, 130(1), p. 011703. doi: 10.1115/1.2771250.
- Horlock, J. H. and Torbidoni, L. (2008b) ‘Calculations of cooled turbine efficiency’, *Journal*

- of Engineering for Gas Turbines and Power*, 130(1). doi: 10.1115/1.2771250.
- Hu, Y. (2011) *CO₂ capture from oxy-fuel combustion power plants*.
- Ibrahim Dincer, M. A. R. (2013) *Chemical Exergy, Chemical Exergy*.
- IEAGHG (2014) ‘ASSESSMENT OF EMERGING CO₂ CAPTURE TECHNOLOGIES AND THEIR POTENTIAL TO Report : 2014 / TR4 December 2014’, (December).
- IEAGHG (2015) ‘Oxy-Combustion Turbine Power Plants’, 2015/05, August, 2015, (August).
- IEAGHG (2019) ‘IEA GREENHOUSE GAS R&D PROGRAMME CCS in Energy and Climate Scenarios’. Available at: www.ieaghg.org (Accessed: 25 July 2021).
- IEAGHG (2020) *Future Role of CCS Technologies in the Power Sector*. Available at: <https://ieaghg.org/publications/technical-reports/reports-list/9-technical-reports/1046-2020-08-future-role-of-ccs-technologies-in-the-power-sector> (Accessed: 25 July 2021).
- Ingegneria, F. *et al.* (2012) ‘Politecnico di milano’, pp. 1–11.
- Jansen, D. *et al.* (2015) ‘Pre-combustion CO₂ capture’, *International Journal of Greenhouse Gas Control*, 40, pp. 167–187. doi: 10.1016/j.ijggc.2015.05.028.
- Javadzadeh, Y. and Hamedeyaz, S. (2014) ‘Floating Drug Delivery Systems for Eradication of Helicobacter pylori in Treatment of Peptic Ulcer Disease’, *Trends in Helicobacter pylori Infection*, i(tourism), p. 13. doi: 10.5772/57353.
- Jericha, H. and Fesharaki, M. (1995) ‘Graz cycle - 1500°C max temperature potential H₂ - O₂ fired CO₂ capture with CH₄ - O₂ firing’, *American Society of Mechanical Engineers (Paper)*.
- Jericha, H. and Göttlich, E. (2002) ‘Conceptual design for an industrial prototype GRAZ CYCLE power plant’, *American Society of Mechanical Engineers, International Gas Turbine Institute, Turbo Expo (Publication) IGTI, 2 A*, pp. 413–420. doi: 10.1115/GT2002-30118.
- Jericha, H., Sanz, W. and Göttlich, E. (2008a) ‘Design concept for large output Graz Cycle gas turbines’, *Journal of Engineering for Gas Turbines and Power*, 130(1). doi: 10.1115/1.2747260.
- Jericha, H., Sanz, W. and Göttlich, E. (2008b) ‘Design concept for large output Graz Cycle gas turbines’, *Journal of Engineering for Gas Turbines and Power*, 130(1), pp. 1–10. doi: 10.1115/1.2747260.
- Joda, F. *et al.* (2011) ‘Improving multi-stream heat exchanger design by reducing the number of sections’, *2011 4th International Conference on Modeling, Simulation and Applied Optimization, ICMSAO 2011*. doi: 10.1109/ICMSAO.2011.5775470.
- Kalamaras, C. M. *et al.* (2013) ‘Conference Paper Hydrogen Production Technologies: Current State and Future Developments’, *Conference Papers in Energy*, 2013. doi: 10.1155/2013/690627.
- Karaağaç, M. O., Kabul, A. and Oğul, H. (2019) ‘First- and second-law thermodynamic analyses of a combined natural gas cycle power plant: Sankey and Grossman diagrams’, *Turkish Journal of Physics*, 43(1), pp. 93–108. doi: 10.3906/fiz-1809-9.
- Kaur, R. *et al.* (2019) ‘Thermochemical Route for Biohydrogen Production’, in *Biohydrogen*. Elsevier, pp. 187–218. doi: 10.1016/b978-0-444-64203-5.00008-3.
- Kaviri, A. G., Jaafar, M. N. M. and Lazim, T. M. (2012) ‘Modeling and multi-objective exergy based optimization of a combined cycle power plant using a genetic algorithm’, *Energy Conversion and Management*, 58, pp. 94–103. doi: 10.1016/j.enconman.2012.01.002.
- Kelly (Kailai) Thambimuthu (Australia (2005) ‘Capture of CO₂’.
- Khaljani, M., Khoshbakhti Saray, R. and Bahlouli, K. (2015) ‘Comprehensive analysis of energy, exergy and exergo-economic of cogeneration of heat and power in a

- combined gas turbine and organic Rankine cycle', *Energy Conversion and Management*, 97, pp. 154–165. doi: 10.1016/j.enconman.2015.02.067.
- Kwon, S. *et al.* (2011) 'CO₂ Sorption', in *Coal Gasification and Its Applications*. Elsevier, pp. 293–339. doi: 10.1016/b978-0-8155-2049-8.10010-5.
- Laboo (2020) *Vacuum Pressure swing adsorption oxygen*. Available at: [http://www.laboogas.net/Products/pressure swing adsorption/49.html](http://www.laboogas.net/Products/pressure%20swing%20adsorption/49.html) (Accessed: 15 October 2020).
- Liao, M. *et al.* (2013) 'Decomposition of embodied exergy flows in manufactured products and implications for carbon tariff policies', *Asia Europe Journal*, 11(3), pp. 265–283. doi: 10.1007/s10308-013-0357-3.
- Liu, M. *et al.* (2017) 'IMECE2008-66467', pp. 1–12.
- Lockwood, T. (2014) 'Developments in oxyfuel combustion of coal', *IEA Clean Coal Centre, CCC/240, London, United Kingdom*, (10), pp. 1–122.
- Lozza, G. *et al.* (2009) *CO₂ Capture from Natural Gas Combined Cycles, 1st International Conference ...* Available at: [http://www.co2club.it/agenda/full paper/Lozza_full paper.pdf](http://www.co2club.it/agenda/full%20paper/Lozza_full%20paper.pdf) (Accessed: 6 December 2018).
- Macchi, E. (2017) 'Organic Rankine Cycle (ORC) Power Systems', *Organic Rankine Cycle (ORC) Power Systems*. doi: 10.1016/c2014-0-04239-6.
- MacDowell, N. *et al.* (2010) 'An overview of CO₂ capture technologies', *Energy and Environmental Science*, 3(11), pp. 1645–1669. doi: 10.1039/c004106h.
- Machner, K. (1958) 'Die Mikrobestimmung von Hippursäure im Urin', *Fresenius' Zeitschrift für Analytische Chemie*, 163(1), p. 69. doi: 10.1007/BF00447266.
- Mancuso, L. *et al.* (2015) 'Oxy-combustion turbine power plants. Report: 2015/05', *Ieaghg*, (August).
- Manso, R. L. (2013) 'CO₂ capture in power plants-using the oxy-combustion principle', (July), p. 93. Available at: <http://www.diva-portal.org/smash/get/diva2:652833/FULLTEXT01.pdf>.
- Manso, R. L. and Nord, L. O. (2020) *CO₂ capture in power plants-using the oxy-combustion principle*.
- Mantripragada, H. C. and Rubin, E. S. (2019) *IECM Technical Documentation: CO₂ Purification Unit (CPU) Models*. Available at: www.iecm-online.com (Accessed: 14 October 2020).
- Marco Antônio Rosa do Nascimento (2005) 'Micro gas turbine engine', *Tribology and Lubrication Technology*, 61(1), pp. 12–13. doi: 10.1007/978-0-387-48998-8_967.
- Marmolejo-Correa, D. and Gundersen, T. (2015) 'A new efficiency parameter for exergy analysis in low temperature processes', *International Journal of Exergy*, 17(2), pp. 135–170. doi: 10.1504/IJEX.2015.069988.
- Martelli, E. (2019) *POLITECNICO DI MILANO Thermodynamic Analysis and Numerical Optimization of the NET Power oxycombustion cycle*.
- Mathieu, P. (2004) 'Towards the hydrogen era using near-zero CO₂ emissions energy systems', *Energy*, 29(12-15 SPEC. ISS.), pp. 1993–2002. doi: 10.1016/j.energy.2004.03.007.
- Mathieu, P. (2005) 'Zero Emission Technologies: An Option for Climate Change Mitigation', *International Journal of Green Energy*, 2(2), pp. 193–199. doi: 10.1081/ge-200058979.
- Mathieu, P. and Van Loo, F. (2005) 'Modeling of an IGCC plant based on an oxy-fuel combustion combined cycle', *ECOS 2005 - Proceedings of the 18th International Conference on Efficiency, Cost, Optimization, Simulation, and Environmental Impact of Energy Systems*, pp. 651–658. Available at: https://www.researchgate.net/publication/290188450_Modeling_of_an_IGCC_plant

- _based_on_an_oxy-fuel_combustion_combined_cycle (Accessed: 18 April 2020).
- Mathieu, P. and Nihart, R. (1998) 'Zero emission MATIANT cycle', *American Society of Mechanical Engineers (Paper)*, 111111(GT). doi: 10.1115/98-gt-383.
- Mathieu, P. and Nihart, R. (1999) 'Sensitivity analysis of the MATIANT cycle', *Energy Conversion and Management*, 40(15), pp. 1687–1700. doi: 10.1016/S0196-8904(99)00062-X.
- Matteo, R. : and Romano, C. (2019) *POLITECNICO DI MILANO Post-combustion CO₂ Capture from a Natural Gas Combined Cycle with CO₂ membranes*.
- Matuszewski, M. (2010) 'Cost and Performance for Low-Rank Pulverized Coal Oxycombustion Energy Plants', (September), p. 442.
- Merkel, T. C. *et al.* (2013) 'Selective exhaust gas recycle with membranes for CO₂ capture from natural gas combined cycle power plants', *Industrial and Engineering Chemistry Research*, 52(3), pp. 1150–1159. doi: 10.1021/ie302110z.
- Möller, B. F. *et al.* (2005) *AZEP gas turbine combined cycle power plants - Thermo-economic analysis, ECOS 2005 - Proceedings of the 18th International Conference on Efficiency, Cost, Optimization, Simulation, and Environmental Impact of Energy Systems*.
- Mondino, G. *et al.* (2019) 'Moving bed temperature swing adsorption for CO₂ capture from a natural gas combined cycle power plant', *International Journal of Greenhouse Gas Control*, 85(June), pp. 58–70. doi: 10.1016/j.ijggc.2019.03.021.
- Moran, B.-G. T.-M. J. (1948) 'Thermal design and optimization By Adrian', p. 58.
- MTR (2018) *CO₂ Removal from Syngas - Membrane Technology and Research*, MTR Membrane Technology and Research. Available at: <https://www.mtrinc.com/our-business/refinery-and-syngas/co2-removal-from-syngas/> (Accessed: 25 August 2020).
- MyGridGB (2020) *MyGridGB – Charting British electricity*. Available at: <http://www.mygridgb.co.uk/> (Accessed: 8 December 2020).
- NASA (2017) 'Isentropic Flow Equations', (M), pp. 1–4. Available at: <https://www.grc.nasa.gov/www/k-12/VirtualAero/BottleRocket/airplane/isentrop.html> (Accessed: 30 July 2021).
- do Nascimento, M. A. R. *et al.* (2013) 'Micro Gas Turbine Engine: A Review', in *Progress in Gas Turbine Performance*. InTech. doi: 10.5772/54444.
- Nexant (2010) 'Air Separation Technology Cryogenic air separation units (ASU), membrane , and adsorption (PSA , VSA) technologies are discussed . Cost estimates for producing oxygen , nitrogen (and argon) from air using an ASU and producing oxygen using a VSA are', (February).
- Nguyen, T. K. (2012) *Chapter 5 Absorption and Stripping, Solutions*. Available at: http://www.cgscgs.com/ga_tt.htm (Accessed: 8 March 2020).
- Nord, L. O., Anantharaman, R. and Bolland, O. (2009) 'Design and off-design analyses of a pre-combustion CO₂ capture process in a natural gas combined cycle power plant', *International Journal of Greenhouse Gas Control*, 3(4), pp. 385–392. doi: 10.1016/j.ijggc.2009.02.001.
- OECD/IEA (2011) *Technology Roadmap Carbon Capture and Storage in Industrial Applications UNITED, SpringerReference*. doi: 10.1007/springerreference_7300.
- Oettinger, M. (2015) 'Capture 1 – Oxy-Combustion Capture', pp. 1–37. *Oxygen generation* (2020).
- Oyedepo, S. O. *et al.* (2015) 'Exergy costing analysis and performance evaluation of selected gas turbine power plants', *Cogent Engineering*, 2(1). doi: 10.1080/23311916.2015.1101048.
- Patel, S. (2019) '300-MW Natural Gas Allam Cycle Power Plant Targeted for 2022', *Power*.

- Available at: <https://www.powermag.com/300-mw-natural-gas-allam-cycle-power-plant-targeted-for-2022/> (Accessed: 2 December 2020).
- Pattanayak, L. (2015) 'Thermodynamic modeling and exergy analysis of gas turbine cycle for different boundary conditions', *International Journal of Power Electronics and Drive Systems*, 6(2), pp. 205–215. doi: 10.11591/ijpeds.v6.i2.pp205-215.
- Penkuhn, M. and Tsatsaronis, G. (2016) 'Exergy Analysis of the Allam Cycle', *The 5th International Symposium - Supercritical CO2 Power Cycles*, pp. 1–18. Available at: <http://sco2symposium.com/www2/sco2/papers2016/OxyFuel/040paper.pdf>.
- Perrin, N. *et al.* (2013) 'Oxycombustion for carbon capture on coal power plants and industrial processes: Advantages, innovative solutions and key projects', *Energy Procedia*, 37, pp. 1389–1404. doi: 10.1016/j.egypro.2013.06.015.
- Petrakopoulou, F. (2010) 'Comparative Evaluation of Power Plants with CO2 Capture: Thermodynamic, Economic and Environmental Performance', p. 230.
- Petrakopoulou, F. *et al.* (2010) 'Exergy-based analyses of an advanced zero emission plant', *International Journal of Low-Carbon Technologies*, 5(4), pp. 231–238. doi: 10.1093/ijlct/ctq028.
- Petrakopoulou, F., Tsatsaronis, G. and Morosuk, T. (2011) 'Exergoeconomic analysis of an advanced zero emission plant', *Journal of Engineering for Gas Turbines and Power*, 133(11). doi: 10.1115/1.4003641.
- Power, N. E. T. and Systems, M. P. (2017) 'NET Power ' s CO2 cycle : the breakthrough that CCS needs', pp. 2–4. Available at: <https://www.modernpowersystems.com/features/featurenet-powers-co2-cycle-the-breakthrough-that-ccs-needs/> (Accessed: 25 July 2021).
- PT6Nation (2018) *The PT6 Nation - From the Archives: Early Rumbblings of the PT6-powered Snowplow*. Available at: <http://www.pt6nation.com/en/community/story/from-the-archives-early-rumbli/> (Accessed: 17 October 2020).
- Quality, E. (2011) 'A N I N T R O D U C T I O N T O T H E C O N C E P T O F E X E R G Y', (March), pp. 1–26.
- Razak, A. M. Y. (2007) *Industrial gas turbines Performance and operability*.
- RICARDO LLORENTE MANSO (2013) *CO2 capture in power plants-using the oxy-combustion principle*. Norwegian University of Science and Technology.
- Rogalev, A., Kindra, V. and Osipov, S. (2018) 'Modeling methods for oxy-fuel combustion cycles with multicomponent working fluid', *AIP Conference Proceedings*, 2047(November). doi: 10.1063/1.5081653.
- Rubin, E. S., Davison, J. E. and Herzog, H. J. (2015) 'The cost of CO2 capture and storage', *International Journal of Greenhouse Gas Control*, 40, pp. 378–400. doi: 10.1016/j.ijggc.2015.05.018.
- Rubio-Serrano, F. J., Soto-Pérez, F. and Gutiérrez-Trashorras, A. J. (2019) 'Influence of cooling temperature increase in a hygroscopic cycle on the performance of the cooling equipment', *Energy Conversion and Management*, 200, p. 112080. doi: 10.1016/j.enconman.2019.112080.
- Russo, G. *et al.* (2018) 'Selective-exhaust gas recirculation for CO2 capture using membrane technology', *Journal of Membrane Science*, 549(March), pp. 649–659. doi: 10.1016/j.memsci.2017.10.052.
- Sahu, M. K. and Sanjay (2016) 'Investigation of the effect of air film blade cooling on thermoeconomics of gas turbine based power plant cycle', *Energy*, 115, pp. 1320–1330. doi: 10.1016/j.energy.2016.09.069.
- Sahu, M. K. and Sanjay (2017) 'Thermoeconomic investigation of power utilities: Intercooled recuperated gas turbine cycle featuring cooled turbine blades', *Energy*,

- 138, pp. 490–499. doi: 10.1016/j.energy.2017.07.083.
- Samanta, S. and Ghosh, S. (2015) ‘A techno-economic analysis of partial repowering of a 210 MW coal fired power plant’, *Advances in Energy Research*, 3(3), pp. 167–179. doi: 10.12989/eri.2015.3.3.167.
- Sammak, M. *et al.* (2012) ‘Conceptual mean-line design of single and twin-shaft oxy-fuel gas turbine in a semi-closed oxy-fuel combustion combined cycle’, *Proceedings of the ASME Turbo Expo*, 3(8), pp. 289–297. doi: 10.1115/GT2012-69470.
- Sanz, W. *et al.* (2005) ‘A further step towards a graz cycle power plant for CO₂ capture’, *Proceedings of the ASME Turbo Expo*, 5, pp. 181–190. doi: 10.1115/GT2005-68456.
- Sanz, Wolfgang *et al.* (2005) ‘Thermodynamic and economic investigation of an improved Graz Cycle power plant for CO₂ capture’, *Journal of Engineering for Gas Turbines and Power*, 127(4), pp. 765–772. doi: 10.1115/1.1850944.
- Sato, N. (2004) *Chemical Energy and Exergy: An Introduction to Chemical Thermodynamics for ... - Norio Sato - Google Books*. Available at: https://books.google.co.uk/books?hl=en&lr=&id=HMZd9OqejYIC&oi=fnd&pg=PP9&ots=FsmDziZ90A&sig=IkJzgHCpzk55uVXVhU617g9JT4U&redir_esc=y#v=onepage&q&f=false (Accessed: 31 March 2020).
- Scaccabarozzi, R., Gatti, M. and Martelli, E. (2014) *Thermodynamic Analysis and Numerical Optimization of the NET Power oxycombustion cycle*, *Politecnico Di Milano*.
- Scaccabarozzi, R., Gatti, M. and Martelli, E. (2016) ‘Thermodynamic analysis and numerical optimization of the NET Power oxy-combustion cycle’, *Applied Energy*, 178, pp. 505–526. doi: 10.1016/j.apenergy.2016.06.060.
- Scaccabarozzi, R., Gatti, M. and Martelli, E. (2017) ‘Thermodynamic Optimization and Part-load Analysis of the NET Power Cycle’, *Energy Procedia*, 114(November 2016), pp. 551–560. doi: 10.1016/j.egypro.2017.03.1197.
- Schobeiri, M. T. (2018) *Design* .,
- Seyyedi, S. M., Ajam, H. and Farahat, S. (2010) ‘A new approach for optimization of thermal power plant based on the exergoeconomic analysis and structural optimization method: Application to the CGAM problem’, *Energy Conversion and Management*, 51(11), pp. 2202–2211. doi: 10.1016/j.enconman.2010.03.014.
- Shao, Y. *et al.* (2018) ‘Comparison and analysis of thermal efficiency and exergy efficiency in energy systems by case study’, in *Energy Procedia*. Elsevier Ltd, pp. 161–168. doi: 10.1016/j.egypro.2018.10.081.
- Sharifzadeh, M., Meghdari, M. and Rashtchian, D. (2017) ‘Multi-objective design and operation of Solid Oxide Fuel Cell (SOFC) Triple Combined-cycle Power Generation systems: Integrating energy efficiency and operational safety’, *Applied Energy*, 185(1), pp. 345–361. doi: 10.1016/j.apenergy.2016.11.010.
- SHEPHERD, P. J. (2013) *Fundamentals of Thermodynamics, A Course in Theoretical Physics*. doi: 10.1002/9781118516911.ch5.
- Smith, A. R. and Klosek, J. (2001) ‘A review of air separation technologies and their integration with energy conversion processes’, *Fuel Processing Technology*, 70(2), pp. 115–134. doi: 10.1016/S0378-3820(01)00131-X.
- Soares, C. (2015) *Gas Turbines : A Handbook of Air, Land and Sea Applications*.
- Soltani, S. *et al.* (2013) ‘A comparative exergoeconomic analysis of two biomass and co-firing combined power plants’, *Energy Conversion and Management*, 76, pp. 83–91. doi: 10.1016/j.enconman.2013.07.030.
- Van Der Spek, M. *et al.* (2017) ‘Techno-economic Performance of State-of-the-Art Oxyfuel Technology for Low-CO₂ Coal-fired Electricity Production’, *Energy Procedia*, 114(November 2016), pp. 6432–6439. doi: 10.1016/j.egypro.2017.03.1779.

- van der Spek, M., Ramirez, A. and Faaij, A. (2017) ‘Challenges and uncertainties of ex ante techno-economic analysis of low TRL CO₂ capture technology: Lessons from a case study of an NGCC with exhaust gas recycle and electric swing adsorption’, *Applied Energy*, 208, pp. 920–934. doi: 10.1016/j.apenergy.2017.09.058.
- Sundkvist, S. G. *et al.* (2005) ‘Azep gas turbine combined cycle power plants - Thermal optimisation and LCA analysis’, *Greenhouse Gas Control Technologies*, pp. 263–271. doi: 10.1016/B978-008044704-9/50027-6.
- Sundkvist, S. G. *et al.* (2014) ‘Concept for a combustion system in oxyfuel gas turbine combined cycles’, *Journal of Engineering for Gas Turbines and Power*, 136(10). doi: 10.1115/1.4027296.
- Tang, Y., Boulter, S. L. and Kitching, R. L. (2003) ‘Heat and smoke effects on the germination of seeds from soil seed banks across forest edges between subtropical rainforest and eucalypt forest at Lamington National Park, south-eastern Queensland, Australia’, *Australian Journal of Botany*, 51(3), pp. 227–237. doi: 10.1071/BT02091.
- Tangsriwong, K. *et al.* (2020) ‘IOP Conference Series: Earth and Environmental Science Modeling of chemical processes using commercial and open-source software: A comparison between Aspen Plus and DWSIM Modeling of chemical processes using commercial and open-source software: A comparison’, 463, p. 12057. doi: 10.1088/1755-1315/463/1/012057.
- Terzi, R. (2018) ‘Application of Exergy Analysis to Energy Systems’, *Application of Exergy*. doi: 10.5772/INTECHOPEN.74433.
- Thorbergsson, E. and Grönstedt, T. (2016) ‘A Thermodynamic Analysis of Two Competing Mid-Sized Oxyfuel Combustion Combined Cycles’, *Journal of Energy*, 2016, pp. 1–14. doi: 10.1155/2016/2438431.
- TMI Staff & Contributors (2018) *First fire of 50 MW combustor in CO₂-based power plant - Turbomachinery Magazine*. Available at: <https://www.turbomachinerymag.com/first-fire-of-50-mw-combustor-in-co2-based-power-plant/> (Accessed: 4 December 2020).
- Tony Giampaolo, M. P. E. (2015) *Gas Turbine Handbook: Principles and Practice, Fifth Edition*. Available at: <https://books.google.co.uk/books?id=NcVUCAAAQBAJ>.
- Tsatsaronis, G. and Czesla, F. (2003) ‘EXERGY ANALYSIS OF SIMPLE PROCESSES’, I.
- U.S. Department of Energy/NETL (2019) *Post-Combustion CO₂ Capture | netl.doe.gov*. Available at: <https://www.netl.doe.gov/coal/carbon-capture/post-combustion> (Accessed: 25 July 2021).
- Union Pacific (2020) *UP: Gas Turbine Locomotives*. Available at: https://www.up.com/aboutup/special_trains/gas-turbine/index.htm (Accessed: 17 October 2020).
- United State Environmental Protection Agency (2018) ‘Sources of Greenhouse Gas Emissions | Greenhouse Gas (GHG) Emissions | US EPA’, *Greenhouse Gas Emissions*. Available at: <https://www.epa.gov/ghgemissions/sources-greenhouse-gas-emissions> (Accessed: 17 July 2021).
- Varasteh, H. and Darabkhani, H. G. (2018) ‘Sensitivity Analysis of the Heat Exchanger Design in NetPower Oxy- Combustion Cycle for Carbon Capture’, (May), p. 103. doi: 10.1999/1307-6892/85218.
- Vogel, E. F. (1992) ‘Plantwide Process Control Simulation’, *Practical Distillation Control*, pp. 86–95. doi: 10.1007/978-1-4757-0277-4_6.
- Wall, T. F. (2007) ‘Combustion processes for carbon capture’, *Proceedings of the Combustion Institute*, 31 I(1), pp. 31–47. doi: 10.1016/j.proci.2006.08.123.
- Wankat, P. C. (1988) *Absorption and stripping*.

- Watson, H. A. J. and Barton, P. I. (2016) ‘Simulation and Design Methods for Multiphase Multistream Heat Exchangers’, *IFAC-PapersOnLine*, 49(7), pp. 839–844. doi: 10.1016/j.ifacol.2016.07.294.
- Yan, Y. *et al.* (2018) ‘Effects of Inlet Parameters on Combustion Performance in Gas Turbine Combustor’, *International Journal of Turbo and Jet Engines*, 35(4), pp. 339–350. doi: 10.1515/tjj-2016-0058.
- Yantovski, E. *et al.* (2004) ‘Zero-emission fuel-fired power plants with ion transport membrane’, *Energy*, 29(12-15 SPEC. ISS.), pp. 2077–2088. doi: 10.1016/j.energy.2004.03.013.
- Yantovski, E. I. (1996) ‘The COOPERATE — Demo power cycle’, *Fuel and Energy Abstracts*, 37(3), p. 209. doi: 10.1016/0140-6701(96)88930-2.
- Ying, Y. *et al.* (2016) ‘Study on gas turbine engine fault diagnostic approach with a hybrid of gray relation theory and gas-path analysis’, *Advances in Mechanical Engineering*, 8(1). doi: 10.1177/1687814015627769.
- Yu, C. H., Huang, C. H. and Tan, C. S. (2012) ‘A review of CO₂ capture by absorption and adsorption’, *Aerosol and Air Quality Research*, 12(5), pp. 745–769. doi: 10.4209/aaqr.2012.05.0132.
- Zanzig, J. (1963) *The stirling cycle engine*, *SAE Technical Papers*. doi: 10.4271/630315.
- Zhang, N. *et al.* (2010) ‘COOLCEP (cool clean efficient power): A novel CO₂-capturing oxy-fuel power system with LNG (liquefied natural gas) coldness energy utilization’, *Energy*, 35(2), pp. 1200–1210. doi: 10.1016/j.energy.2009.04.002.
- Zhao, Y. *et al.* (2017) ‘Thermodynamic study of an improved MATIANT cycle with stream split and recompression’, *Applied Thermal Engineering*, 125, pp. 452–469. doi: 10.1016/j.applthermaleng.2017.05.023.
- Zheng, L. (2011) *Oxy-fuel combustion for power generation and carbon dioxide (CO₂) capture*, *Oxy-Fuel Combustion for Power Generation and Carbon Dioxide (CO₂)*. Woodhead. doi: 10.1533/9780857090980.
- Zhimin, H. *et al.* (2017) ‘Study on Polydimethylsiloxane Desorption Membrane of CO₂-Dimethyl carbonate System’, in *Energy Procedia*. Elsevier Ltd, pp. 210–215. doi: 10.1016/j.egypro.2017.07.024.

Appendix (A) (MATLAB Code)

```
%-----Combustion1-----
MOLFLOW3(i,j)=(a.Tree.FindNode("\Data\Streams\3\Output\MOLEFLMX\MIXED").value*1000/3600)
EXER3PH(i,j)=MOLFLOW3(i,j)*(a.Tree.FindNode("\Data\Streams\3\Output\STRM_UPP\EXERGYML\MIXED\TOTAL").value)
EXER3TOTAL(i,j)=EXER3PH(i,j)

MOLFLOW4(i,j)=(a.Tree.FindNode("\Data\Streams\4\Output\MOLEFLMX\MIXED").value*1000/3600)
EXER4PH(i,j)=MOLFLOW4(i,j)*(a.Tree.FindNode("\Data\Streams\4\Output\STRM_UPP\EXERGYML\MIXED\TOTAL").value)
EXER4TOTAL(i,j)=EXER4PH(i,j)

MOLFLOWGAS(i,j)=(a.Tree.FindNode("\Data\Streams\GAS\Output\MOLEFLMX\MIXED").value*1000/3600)
CHEMEXERGYGASMETHANE(i,j)=802361*1.06*a.Tree.FindNode("\Data\Streams\GAS\Output\MOLEFRAC\MIXED\METHANE").value
EXERGASCHTOTAL(i,j)=MOLFLOWGAS(i,j)*CHEMEXERGYGASMETHANE(i,j)
MOLFLOWGAS(i,j)=(a.Tree.FindNode("\Data\Streams\GAS\Output\MOLEFLMX\MIXED").value*1000/3600)
EXERGASPTOTAL(i,j)=MOLFLOWGAS(i,j)*(a.Tree.FindNode("\Data\Streams\GAS\Output\STRM_UPP\EXERGYML\MIXED\TOTAL").value)
EXERGASTOTAL(i,j)=EXERGASCHTOTAL(i,j)+EXERGASPTOTAL(i,j)

MOLFLOWGAS(i,j)=(a.Tree.FindNode("\Data\Streams\GAS\Output\MOLEFLMX\MIXED").value*1000/3600)
EXERGASPTOTAL(i,j)=MOLFLOWGAS(i,j)*(a.Tree.FindNode("\Data\Streams\GAS\Output\STRM_UPP\EXERGYML\MIXED\TOTAL").value)

MOLFLOW5(i,j)=(a.Tree.FindNode("\Data\Streams\5\Output\MOLEFLMX\MIXED").value*1000/3600)
EXER5PH(i,j)=MOLFLOW5(i,j)*(a.Tree.FindNode("\Data\Streams\5\Output\STRM_UPP\EXERGYML\MIXED\TOTAL").value)
EXER5TOTAL(i,j)=EXER5PH(i,j)

EXERGD COMBUS1(i,j)=EXER3TOTAL(i,j)+EXER4TOTAL(i,j)+EXERGASTOTAL(i,j)-EXER5TOTAL(i,j)
```

```
function Zcombustion=combustioncost(pe,pi,Te,m)

clear Zrecuperator

%Pe=5.6227Aih
%Pi=1.0132
%effc=a.Tree.FindNode("\Data\Blocks\WATERPUM\Input\EFF").value
%effc=0.88
%Mai=a.Tree.FindNode("\Data\Streams\31\Output\MASSFLMX\MIXED").value/3600
%Mai=1
%-----
%G11=39.5
%G12=0.9
G21=25.65
G22=0.995
G23=0.018
G24=26.4
Zcombustion=(G21*m)/(G22-(pe/pi))*(1+exp(G23*Te-G24))

%-----
%CRF=0.12*((1+0.12)^20)/((1+0.12)^20-1)
%-----
CRF=0.182
N=8000
Q=1.06

%-----
Zcombustionr=Zcombustion*CRF*Q/N

end
```

```
function ZC=comcost (Pe, Pi, Mai)

clear ZC

%Pe=5.6227
%Pi=1.0132
%effc=a.Tree.FindNode("\Data\Blocks\WATERPUM\Input\EFF").value
effc=0.72
%Mai=a.Tree.FindNode("\Data\Streams\31\Output\MASSFLMX\MIXED").value/3600
%Mai=1
%-----
G11=39.5
G12=0.9
ZC=(G11*Mai)/(G12-effc)*(Pe/Pi)*log(Pe/Pi)

%-----
CRF=0.12*((1+0.12)^20)/((1+0.12)^20-1)
%-----
CRF=0.182
N=8000
Q=1.06

%-----
ZCr=ZC*CRF*Q/N

end
```

```
function Zcond=condcost (Mstream)

clear Zp

%Pe=5.6227
%Pi=1.0132
%effc=a.Tree.FindNode("\Data\Blocks\WATERPUM\Input\EFF").value
%effc=0.88
%Mai=a.Tree.FindNode("\Data\Streams\31\Output\MASSFLMX\MIXED").value/3600
%Mai=1
%-----
%G11=39.5
%G12=0.9
Zcond=1773* (Mstream)

%-----
%CRF=0.12* ((1+0.12)^20)/((1+0.12)^20-1)
%-----
CRF=0.182
N=8000
Q=1.06

%-----
Zcondr=Zcond*CRF*Q/N

end
```

```
function Zeva=evacost(Aarea)

clear Zp

%Pe=5.6227
%Pi=1.0132
%effc=a.Tree.FindNode("\Data\Blocks\WATERPUM\Input\EFF").value
%effc=0.88
%Mai=a.Tree.FindNode("\Data\Streams\31\Output\MASSFLMX\MIXED").value/3600
%Mai=1
%-----
%G11=39.5
%G12=0.9
Zeva=309.143*(Aarea)+231.915

%-----
%CRF=0.12*((1+0.12)^20)/((1+0.12)^20-1)
%-----
CRF=0.182
N=8000
Q=1.06

%-----
Zeval=Zeva*CRF*Q/N

end
```

```
function Zihe=Heatxsteamcost(AIHE)

clear Zp

%Pe=5.6227Aih
%Pi=1.0132
%effc=a.Tree.FindNode("\Data\Blocks\WATERPUM\Input\EFF").value
%effc=0.88
%Mai=a.Tree.FindNode("\Data\Streams\31\Output\MASSFLMX\MIXED").value/3600
%Mai=1
%-----
%G11=39.5
%G12=0.9
Zihe=1.3*(190+310*AIHE)

%-----
%CRF=0.12*((1+0.12)^20)/((1+0.12)^20-1)
%-----
CRF=0.182
N=8000
Q=1.06

%-----
Ziher=Zihe*CRF*Q/N

end
```

```
function Zhrsg=hrsgcost (Qph,Qev,TLMph,TLMeV,Msteam,Mgas)

clear Zrecuperator

%Pe=5.6227Aih
%Pi=1.0132
%effc=a.Tree.FindNode("\Data\Blocks\WATERPUM\Input\EFF").value
%effc=0.88
%Mai=a.Tree.FindNode("\Data\Streams\31\Output\MASSFLMX\MIXED").value/3600
%Mai=1
%-----
G61=3650;
G62=11820;
G63=658;
Zhrsg=G61*((Qph/TLMph)^0.8+(Qev/TLMeV)^0.8)+G62*Msteam+G63*Mgas;

%-----
%CRF=0.12*((1+0.12)^20)/((1+0.12)^20-1)
%-----
CRF=0.182;
N=8000;
Q=1.06;

%-----
Zhrsgr=Zhrsg*CRF*Q/N;

end
```

```
function Zintercool=intercoolcost (hi,he,TLM,m)

clear Zintercool

%Pe=5.6227Aih
%Pi=1.0132
%effc=a.Tree.FindNode("\Data\Blocks\WATERPUM\Input\EFF").value
%effc=0.88
%Mai=a.Tree.FindNode("\Data\Streams\31\Output\MASSFLMX\MIXED").value/3600
%Mai=1
%-----
%G11=39.5
%G12=0.9
U=
Zintercool=G51*(m*(hi-he)/(U*TLM))^0.6

%-----
%CRF=0.12*((1+0.12)^20)/((1+0.12)^20-1)
%-----
CRF=0.182
N=8000
Q=1.06

%-----
Zintercoolr=Zintercool*CRF*Q/N

end
```

07/12/20 01:27 C:\PHD\OneDrive - Staffords...\Pumpcost.m 1 of 1

```
function Zp=pumcost (pumpwork)

clear Zp

%Pe=5.6227
%Pi=1.0132
%effc=a.Tree.FindNode("\Data\Blocks\WATERPUM\Input\EFF").value
effc=0.88
%Mai=a.Tree.FindNode("\Data\Streams\31\Output\MASSFLMX\MIXED").value/3600
%Mai=1
%-----
G11=39.5
G12=0.9
Zp=3540*(pumpwork)^0.71

%-----
%CRF=0.12*((1+0.12)^20)/((1+0.12)^20-1)
%-----
CRF=0.182
N=8000
Q=1.06

%-----
Zpr=Zp*CRF*Q/N

end
```

07/12/20 01:28 C:\PHD\OneDrive - St...\Recuperatorcost.m 1 of 1

```
function Zrecuperator=recuperatorcost (hi,he,TLM,m)

clear Zrecuperator

%Pe=5.6227Aih
%Pi=1.0132
%effc=a.Tree.FindNode("\Data\Blocks\WATERPUM\Input\EFF").value
%effc=0.88
%Mai=a.Tree.FindNode("\Data\Streams\31\Output\MASSFLMX\MIXED").value/3600
%Mai=1
%-----
%G11=39.5
%G12=0.9
G51=2290
U=0.018
Zrecuperator=G51*(m*(hi-he)/(U*TLM))^0.6

%-----
%CRF=0.12*((1+0.12)^20)/((1+0.12)^20-1)
%-----
CRF=0.182
N=8000
Q=1.06

%-----
Zrecuperatorr=Zrecuperator*CRF*Q/N

end
```

07/12/20 01:28 C:\PHD\OneDrive - Staff...\Sturbinecost.m 1 of 1

```
function Zsturbine=sturbine(sturbinework)

clear Zp

%Pe=5.6227
%Pi=1.0132
%effc=a.Tree.FindNode("\Data\Blocks\WATERPUM\Input\EFF").value
%effc=0.88
%Mai=a.Tree.FindNode("\Data\Streams\31\Output\MASSFLMX\MIXED").value/3600
%Mai=1
%-----
%G11=39.5
%G12=0.9
Zsturbine=6000*(sturbinework)^0.7

%-----
%CRF=0.12*((1+0.12)^20)/((1+0.12)^20-1)
%-----
CRF=0.182
N=8000
Q=1.06

%-----
Zsturbiner=Zsturbine*CRF*Q/N

end
```

```
function Zturbine=turbinecost(pe,pi,Ti,m)

clear Zrecuperator

%Pe=5.6227Aih
%Pi=1.0132
%effc=a.Tree.FindNode("\Data\Blocks\WATERPUM\Input\EFF").value
efft=0.85
%Mai=a.Tree.FindNode("\Data\Streams\31\Output\MASSFLMX\MIXED").value/3600
%Mai=1
%-----
%G11=39.5
%G12=0.9
G31=266.3
G32=0.92
G33=0.036
G34=54.4
Zturbine=(G31*m)/(G32-efft)*log(pi/pe)*(1+exp(G33*Ti-G34))

%-----
%CRF=0.12*((1+0.12)^20)/((1+0.12)^20-1)
%-----
CRF=0.182
N=8000
Q=1.06

%-----
Zturbiner=Zturbine*CRF*Q/N

end
```

```
clear
clc
global AspenEngine a
AspenVersion = 'apwn.document.36.0'
Aspenpath=('C:\PHD\OneDrive - Staffordshire
University\Modeling\12Netpower\netpowerfinal64.bkp')
a=actxserver(AspenVersion)
AspenEngine = a.Application.Engine;
a.invoke('InitFromFile2',Aspenpath)
a.Visible=0

get(a)

clear Twork B3work B2work B8work Network x

%a.Tree.FindNode("\Data\Streams\AIRR\Input\TOTFLOW\MIXED").value=0.1292;
%a.Tree.FindNode("\Data\Streams\FUELL\Input\TOTFLOW\MIXED").value=0.00307;
%flowrate1=a.Tree.FindNode("\Data\Streams\GAS\Output\MASSFLOW\MIXED\METHANE").
value/3600
flowrate1=a.Tree.FindNode("\Data\Streams\GAS\Output\MASSFLMX\MIXED").value/3600
%flowrate2=a.Tree.FindNode("\Data\Streams\GAS2\Input\TOTFLOW\MIXED").value

i=1

%for DELTEXCH=20:1:20
    %a.Tree.FindNode("\Data\Blocks\RECU\Input\VALUE").value=DELTEXCH;
    %for per=30:2:60
%30:2:60
        j=1
        %for workingflowrate=290:1:330
            %a.Tree.FindNode("\Data\Blocks\B19\Input\BASIS_FLOW\25").value=workingflowrate
            %for flowrate=15:0.2:17
%31:2:81
                %for per2=140:2:160

%a.Tree.FindNode("\Data\Streams\16\Input\TOTFLOW\MIXED").value=flowrate
%a.Tree.FindNode("\Data\Blocks\COMPRESS\Input\PRES").value=per
%a.Tree.FindNode("\Data\Blocks\FUELCOM\Input\PRES").value=per
%a.Tree.FindNode("\Data\Blocks\AIRCOM\Input\PRES").value=per
%a.Tree.FindNode("\Data\Blocks\SPUMP\Input\PRES").value=per2

Run2(AspenEngine);
while (get(AspenEngine,'IsRunning'))==1
pause(1)
end
pause(1)

error_check(i,j)=a.Application.Tree.FindNode('\Data\Results Summary\Run-
```

```

Status\Output\UOSSSTAT').value
error_check2(i,j)=a.Application.Tree.FindNode('\Data\Results Summary\Run-
Status\Output\UOSSSTAT2').value
%name(i,j)=a.Application.Tree.FindNode('\Data\Results Summary\Run-
Status\Output\RUNID').Value;

Turbine(i,j)=a.Tree.FindNode("\Data\Blocks\TURBINE\Output\WNET").value

Totalturbine(i,j)=Turbine(i,j)

COM1(i,j)=a.Tree.FindNode("\Data\Blocks\COM1\Output\WNET").value
COM2(i,j)=a.Tree.FindNode("\Data\Blocks\COM2\Output\WNET").value
COM3(i,j)=a.Tree.FindNode("\Data\Blocks\COM3\Output\WNET").value
COM4(i,j)=a.Tree.FindNode("\Data\Blocks\COM4\Output\WNET").value
COM5(i,j)=a.Tree.FindNode("\Data\Blocks\COM5\Output\WNET").value
%GASCOM(i,j)=a.Tree.FindNode("\Data\Blocks\GASCOM\Output\WNET").value
PUMP1(i,j)=a.Tree.FindNode("\Data\Blocks\PUMP1\Output\WNET").value
PUMP2(i,j)=a.Tree.FindNode("\Data\Blocks\PUMP2\Output\WNET").value

Utility(i,j)=103750000

Network(i,j)=Totalturbine(i,j)+COM1(i,j)+COM2(i,j)+COM3(i,j)+COM4(i,j)+COM5(i,j)
+PUMP1(i,j)+PUMP2(i,j)

LHV1(i,j)=46502*1000*flowrate1;
%LHV2(i,j)=50*1000000*flowrate2;
Eff(i,j)=(-Network(i,j)*100)/LHV1(i,j);
Effwithlost=(-Network(i,j)-Utility)*100/LHV1(i,j)
%TurbineHPTOT4(i,j)=a.Tree.FindNode("\Data\Streams\4\Output\TEMP_OUT\MIXED").value
%TurbineHPCIT13(i,j)=a.Tree.FindNode("\Data\Streams\3\Output\TEMP_OUT\MIXED").value
%TurbineLPTTOT6(i,j)=a.Tree.FindNode("\Data\Streams\6\Output\TEMP_OUT\MIXED").value
%TurbineLPTTOT11(i,j)=a.Tree.FindNode("\Data\Streams\11\Output\TEMP_OUT\MIXED").value

EXER6(i,j)=a.Tree.FindNode("\Data\Streams\6\Output\STRM_UPP\EXERGYFL\MIXED\TOTAL").
value
EXER5(i,j)=a.Tree.FindNode("\Data\Streams\5\Output\STRM_UPP\EXERGYFL\MIXED\TOTAL").
value
EXER7(i,j)=a.Tree.FindNode("\Data\Streams\7\Output\STRM_UPP\EXERGYFL\MIXED\TOTAL").
value

EXERDTURBINE(i,j)=EXER6(i,j)+EXER5(i,j)-EXER7(i,j)+Turbine(i,j)

TOTALTURBINEEXERD(i,j)=EXERDTURBINE(i,j)

EXER11(i,j)=a.Tree.FindNode("\Data\Streams\11\Output\STRM_UPP\EXERGYFL\MIXED\TOTAL").
value
EXER21(i,j)=a.Tree.FindNode("\Data\Streams\21\Output\STRM_UPP\EXERGYFL\MIXED\TOTAL").
value
EXERDCOM1(i,j)=EXER11(i,j)-EXER21(i,j)+COM1(i,j)

```

```
EXER22(i,j)=a.Tree.FindNode("\Data\Streams\22\Output\STRM_UPP\EXERGYFL\MIXED\TOTAL").value
EXER23(i,j)=a.Tree.FindNode("\Data\Streams\23\Output\STRM_UPP\EXERGYFL\MIXED\TOTAL").value
EXERDCOM2(i,j)=EXER22(i,j)-EXER23(i,j)+COM2(i,j)

EXER24(i,j)=a.Tree.FindNode("\Data\Streams\24\Output\STRM_UPP\EXERGYFL\MIXED\TOTAL").value
EXER25(i,j)=a.Tree.FindNode("\Data\Streams\25\Output\STRM_UPP\EXERGYFL\MIXED\TOTAL").value
EXERDCOM3(i,j)=EXER24(i,j)-EXER25(i,j)+COM3(i,j)

EXER26(i,j)=a.Tree.FindNode("\Data\Streams\26\Output\STRM_UPP\EXERGYFL\MIXED\TOTAL").value
EXER12(i,j)=a.Tree.FindNode("\Data\Streams\12\Output\STRM_UPP\EXERGYFL\MIXED\TOTAL").value
EXERDCOM4(i,j)=EXER26(i,j)-EXER12(i,j)+COM4(i,j)

EXER30(i,j)=a.Tree.FindNode("\Data\Streams\30\Output\STRM_UPP\EXERGYFL\MIXED\TOTAL").value
EXER9(i,j)=a.Tree.FindNode("\Data\Streams\9\Output\STRM_UPP\EXERGYFL\MIXED\TOTAL").value
EXERDCOM5(i,j)=EXER30(i,j)-EXER9(i,j)+COM5(i,j)

EXER27(i,j)=a.Tree.FindNode("\Data\Streams\27\Output\STRM_UPP\EXERGYFL\MIXED\TOTAL").value
EXER28(i,j)=a.Tree.FindNode("\Data\Streams\28\Output\STRM_UPP\EXERGYFL\MIXED\TOTAL").value
EXERDPUMP1(i,j)=EXER27(i,j)-EXER28(i,j)+PUMP1(i,j)

EXER13(i,j)=a.Tree.FindNode("\Data\Streams\13\Output\STRM_UPP\EXERGYFL\MIXED\TOTAL").value
EXER10(i,j)=a.Tree.FindNode("\Data\Streams\10\Output\STRM_UPP\EXERGYFL\MIXED\TOTAL").value
EXERDPUMP2(i,j)=EXER13(i,j)-EXER10(i,j)+PUMP2(i,j)

%EXERGAS(i,j)=a.Tree.FindNode
("\Data\Streams\GAS\Output\STRM_UPP\EXERGYFL\MIXED\TOTAL").value
%EXER1(i,j)=a.Tree.FindNode("\Data\Streams\1\Output\STRM_UPP\EXERGYFL\MIXED\TOTAL").value
%EXERDGASCOM(i,j)=EXERGAS(i,j)-EXER1(i,j)+GASCOM(i,j)

EXER7(i,j)=a.Tree.FindNode("\Data\Streams\7\Output\STRM_UPP\EXERGYFL\MIXED\TOTAL").value
EXER7B(i,j)=a.Tree.FindNode("\Data\Streams\7B\Output\STRM_UPP\EXERGYFL\MIXED\TOTAL").value
```

```
EXERDHEATEX1(i,j)=EXER7(i,j)-EXER7B(i,j)

EXER8(i,j)=a.Tree.FindNode("\Data\Streams\8\Output\STRM_UPP\EXERGYFL\MIXED\TOTAL").↵
value
EXER20(i,j)=a.Tree.FindNode("\Data\Streams\20\Output\STRM_UPP\EXERGYFL\MIXED\TOTAL").↵
value
EXERDHEATEX2(i,j)=EXER8(i,j)-EXER20(i,j)

EXER21(i,j)=a.Tree.FindNode("\Data\Streams\21\Output\STRM_UPP\EXERGYFL\MIXED\TOTAL").↵
value
EXER22(i,j)=a.Tree.FindNode("\Data\Streams\22\Output\STRM_UPP\EXERGYFL\MIXED\TOTAL").↵
value
EXERDHEATEX3(i,j)=EXER21(i,j)-EXER22(i,j)

EXER23(i,j)=a.Tree.FindNode("\Data\Streams\23\Output\STRM_UPP\EXERGYFL\MIXED\TOTAL").↵
value
EXER24(i,j)=a.Tree.FindNode("\Data\Streams\24\Output\STRM_UPP\EXERGYFL\MIXED\TOTAL").↵
value
EXERDHEATEX4(i,j)=EXER23(i,j)-EXER24(i,j)

EXER25(i,j)=a.Tree.FindNode("\Data\Streams\25\Output\STRM_UPP\EXERGYFL\MIXED\TOTAL").↵
value
EXER26(i,j)=a.Tree.FindNode("\Data\Streams\26\Output\STRM_UPP\EXERGYFL\MIXED\TOTAL").↵
value
EXERDHEATEX5(i,j)=EXER25(i,j)-EXER26(i,j)

EXER12(i,j)=a.Tree.FindNode("\Data\Streams\12\Output\STRM_UPP\EXERGYFL\MIXED\TOTAL").↵
value
EXER27(i,j)=a.Tree.FindNode("\Data\Streams\27\Output\STRM_UPP\EXERGYFL\MIXED\TOTAL").↵
value
EXERDHEATEX6(i,j)=EXER12(i,j)-EXER27(i,j)

EXER28(i,j)=a.Tree.FindNode("\Data\Streams\28\Output\STRM_UPP\EXERGYFL\MIXED\TOTAL").↵
value
EXER29(i,j)=a.Tree.FindNode("\Data\Streams\29\Output\STRM_UPP\EXERGYFL\MIXED\TOTAL").↵
value
EXERDHEATEX7(i,j)=EXER28(i,j)-EXER29(i,j)

EXER17(i,j)=a.Tree.FindNode("\Data\Streams\17\Output\STRM_UPP\EXERGYFL\MIXED\TOTAL").↵
value
EXER7B(i,j)=a.Tree.FindNode("\Data\Streams\7B\Output\STRM_UPP\EXERGYFL\MIXED\TOTAL").↵
value
EXER9(i,j)=a.Tree.FindNode("\Data\Streams\9\Output\STRM_UPP\EXERGYFL\MIXED\TOTAL").↵
value
EXER4A(i,j)=a.Tree.FindNode("\Data\Streams\4A\Output\STRM_UPP\EXERGYFL\MIXED\TOTAL").↵
value
EXER6A(i,j)=a.Tree.FindNode("\Data\Streams\6A\Output\STRM_UPP\EXERGYFL\MIXED\TOTAL").↵
value
```

```
EXER3(i,j)=a.Tree.FindNode("\Data\Streams\3\Output\STRM_UPP\EXERGYFL\MIXED\TOTAL").value
EXER6(i,j)=a.Tree.FindNode("\Data\Streams\6\Output\STRM_UPP\EXERGYFL\MIXED\TOTAL").value
EXER4(i,j)=a.Tree.FindNode("\Data\Streams\4\Output\STRM_UPP\EXERGYFL\MIXED\TOTAL").value
EXER18(i,j)=a.Tree.FindNode("\Data\Streams\18\Output\STRM_UPP\EXERGYFL\MIXED\TOTAL").value
EXER8(i,j)=a.Tree.FindNode("\Data\Streams\8\Output\STRM_UPP\EXERGYFL\MIXED\TOTAL").value
EXERDMHX(i,j)=EXER17(i,j)+EXER7B(i,j)+EXER9(i,j)+EXER4A(i,j)+EXER6A(i,j)-(EXER3(i,j)+EXER6(i,j)+EXER4(i,j)+EXER18(i,j)+EXER8(i,j))

EXER18(i,j)=a.Tree.FindNode("\Data\Streams\18\Output\STRM_UPP\EXERGYFL\MIXED\TOTAL").value
EXER19(i,j)=a.Tree.FindNode("\Data\Streams\19\Output\STRM_UPP\EXERGYFL\MIXED\TOTAL").value
EXERWWT(i,j)=a.Tree.FindNode("\Data\Streams\WWT\Output\STRM_UPP\EXERGYFL\MIXED\TOTAL").value

EXERDUtility(i,j)=Utility(i,j)

EXER16(i,j)=a.Tree.FindNode("\Data\Streams\16\Output\STRM_UPP\EXERGYFL\MIXED\TOTAL").value
ASU(i,j)=85.45*1000000+EXER18(i,j)-EXER17(i,j)-EXER16(i,j)
%-----

EXERDDISTILATm1

%-----

%%%%%%%%%%%%%%

Combustion1m1

%%%%%%%%%%%%%%

TOTALEXERGYD(i,j)=sum([EXERDTURBINE(i,j),EXERDCOM1(i,j),EXERDCOM2(i,j),EXERDCOM3(i,j),EXERDCOM4(i,j),EXERDCOM5(i,j),EXERDPUMP1(i,j),EXERDPUMP2(i,j),EXERDHEATEX1(i,j),EXERDHEATEX2(i,j),EXERDHEATEX3(i,j),EXERDHEATEX4(i,j),EXERDHEATEX5(i,j),EXERDHEATEX6(i,j),EXERDHEATEX7(i,j),EXERDMHX(i,j),EXER19(i,j),ASU(i,j),(EXERDUtility(i,j)-ASU(i,j))*1.7,EXERDDISTILAT(i,j),EXERGDCOMBUS1(i,j)]/1000000)
%-----

TOTALEXERGYinputm

%-----
```

```
EXEEFF(i,j)=1-(TOTALEXERGYD(i,j)/TOTALEXERGYinput(i,j))

EXEEFFNET(i,j)=((-Network(i,j)-Utility)/1000000)/TOTALEXERGYinput(i,j)

Netwokexer(i,j)=TOTALEXERGYinput(i,j)-TOTALEXERGYD(i,j)

%-----
CO2MASSFLOW=a.Tree.FindNode("\Data\Streams\19\Output\MASSFLOW\MIXED\CO2").value

Co2perKWe=CO2MASSFLOW/(-Network/1000)
%-----
j=j+1;

%end

i=i+1;

%end

% ↙
----- ↘

%a.Close
%a.delete
%Cost
%Zhrsg=Hrsgcost(Qph,Qev,TLMph,TLMev,Msteam,Mgas)
%Zturbine=Turbinecost(pe,pi,Ti,m)
%Zcombustion=Combustioncost(pe,pi,Te,m)
%Zrecuperator=Recuperatorcost(hi,he,TLM,m)
%ZC=Comcost(Pe,Pi,Mai)
%Zintercool=Intercoolcost(hi,he,TLM,m)

%Zsturbine=Sturbinecost(sturbinework)
%Zp=Pumcost(pumpwork)
%Zeva=Evacost(Aarea)
%Zcondr=Condcost(Mstream)
%Zihe=Heatxsteamcost(AIHE)
Zcombustion=Combustioncost(300,305,1147+273,1262.16251158441)
ZCtotal=Comcost(41,33,1329.76369506902)+Comcost(51,41,1329.76369506902)+Comcost ↙
(64,51,1329.76369506902)+Comcost(80,64,1329.76369506902)+Comcost ↙
(305,120,612.070284125462)
Zp=Pumcost(9682.75712)+Pumcost(22212.0632)
ZCgas=Comcost(305,15,16.5171882333334)
```